SIMULATION AND CONTROL OF THICKNESS - MODE PIEZOELECTRIC TRANSDUCERS

Presented by

MERVYN N JACKSON

In the fulfilment of the requirement
for the degree of Doctor of
Philosophy of the University
of Strathclyde

Department of Electronic
and Electrical Engineering

November 1984

Glasgow

CONTENTS

Abstract

A new general three-port systems model of the thickness-mode piezoelectric transducer is proposed. This model is considered to have several substantial advantages over existing modelling techniques. In particular, it may be readily used to explain the underlying physical operation of ultrasonic transducers. The model has been developed in such a manner that the effects of arbitrary electrical load and source elements and mechanical matching layers may be incorporated.

The use of z-transforms in the calculation of the transducer transient response has been investigated. This has resulted in a fast, efficient and accurate method for calculating the transducer response to arbitrary transient excitation.

In the course of this work, the model has been verified extensively by computer simulation and experimental measurement. Excellent agreement was obtained between the theoretical and practical results for a comprehensive range of electrical and mechanical configurations.

Techniques for controlling piezoelectric transmitters electrically have been investigated. This involves the generation of a precisely defined force transient, by exciting the transducer system with a calculated voltage. These methods were verified by simulation and experiment, and it is concluded that they offer a significant improvement over existing transducer control strategies.

Finally, it is considered that the techniques and models proposed have made a significant contribution to the investigation of thickness-mode piezoelectric devices.

Symbol Table

This symbol table contains the more important symbols and indices used in the mathematical expressions and systems diagrams of this thesis. Less common or rarely occurring terms are defined in the text when required.

(i) Transducer Quantities

C_0	Transducer Static Capacitance
h	Piezoelectric Charge Constant
Z_t	Characteristic acoustic impedance of the transducer
R_F	Transducer front-face acoustic reflection coefficient
R_B	Transducer rear-face acoustic reflection coefficient
T_t	Transducer transit period

(ii) Transform Notation

s	Complex Laplace operator
$(\overline{N})$	Bar symbol signifies a Laplace quantity
z	Z-transform operator
N^z	Z superscript indicates a z-transformed

quantity.

(iii) Transformed Quantities

$\overline{F}$	Laplace transform of a forward-travelling force component
$\overline{B}$	Laplace transform of a backward-travelling force component
$\overline{A}_t$	Laplace transform of the particle displacement of a wave travelling in the forward direction
$\overline{A}_b$	Laplace transform of the particle displacement of a wave travelling in the backward direction
$\overline{\xi}$	Laplace transform of total particle displacement
$\overline{\Gamma}$	Laplace transform of total force
$\overline{V}_E$	Laplace transform of the excitation voltage
$\overline{V}_t$	Laplace transform of the transducer voltage
$\overline{Q}_t$	Láplace transform of the total charge on the transducer
$\overline{I}_t(=s\overline{Q}_t)$	Laplace transform of the current flowing in the transducer
$[P]$	Three-port system matrix, (in Laplace transfer function form), describing the no-layer transducer

$\overline{p}_{ij}$ Transfer function element of $[\overline{P}]$

$[\overline{W}]$ Three-port system matrix, (in Laplace transfer function form), describing the layered transducer

$\overline{w}_{ij}$ Transfer function element of $[\overline{W}]$

$[\overline{U}^F]$ Two-port system matrix, describing front-face layers

$\overline{U}^F_{ij}$ Transfer function element of $[\overline{U}^F]$

$[\overline{U}^B]$ Two-port system matrix, describing rear-face layers

$\overline{U}^B_{ij}$ Transfer function element of $[\overline{U}^B]$

$\overline{d}_i$ Differential Laplace polynomial, of the form

$$\sum_{i=0}^{N} a_i s^i$$

$\overline{D}_j$ Delay-only Laplace polynomial of the form

$$\sum_{j=0}^{M} b_j e^{-sT_j}$$

(iv) Layer Index Notation and Parameters

h subscript identifying the layer structure. For the layered transducer system, the following convention is assumed,

n<0 refers to rear-face media

n=0 refers to the transducer

n>0 refers to front-face media

X_n	Defined co-ordinate system for the n^{th} layer
ℓ_n	Thickness of the n^{th} layer
V_n	Velocity of the n^{th} layer
$T_n (= \ell_n/V_n)$	Propagation time of the n^{th} layer
Z_n	Characteristic acoustic impedance of the n^{th} layer

(Note: Occasionally the subscript t is used when referring to transducer terms. This is used either to agree with convention or to avoid confusion which may result from using n=0. These usages are clearly defined in the text).

(v) General Index Notation

N^N	N superscript refers to a numerator polynomial
N^D	D superscript refers to a denominator polynomial
N_D	D subscript refers to a desired quantity

(vi) Miscellaneous Quantities

$[Q]$	Q-matrix used to perform algebraic

z-transform operations.

T_s — Sampling period of a discrete time system.

 — Flow graph symbol used in the systems diagrams. The lines connect quantities and the direction of the flow is shown by the arrow.

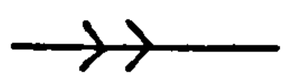 — Double arrow is used to highlight or stress a particular flow-path.

Piezoelectric transducers have found widespread application in the generation and detection of ultrasound. These devices may be manufactured from a wide range of both naturally occurring, (for example, quartz, tourmaline) or synthetic, (lead zirconate-titanate, polyvinylidene fluroride) materials. The transducers may be used as either single, independent devices, or arranged as arrays of individual elements, which radiate together to produce a sound beam of specific characteristics. However, the devices to be considered here are thickness-mode transducrs. These may be defined as thin plates or discs of piezoelectric material which undergo uniform compressional vibration in the thickness direction. Other modes of vibration may occur in practice, but it will be assumed here that these may be safely ignored. It will also be assumed that the devices operate in their fundamental mode, and that this lies in the range 0.1 - 10 MHz. (This range may vary in practice depending upon the material and application considered, but includes most of the commercial devices which are available.)

CHAPTER 1

INTRODUCTION

1.1 Background Review

Thickness-mode piezoelectric transducers have found widespread application in the following main areas.

.Sonar (Underwater navigation, target identification and communication.)

.Ultrasonic non-destructive evaluation (nde) systems

.Medical diagnosis and imaging

.Acoustic emission systems

.Acoustic holography

.Materials and tissue characterisation.

In almost every case, the transducer is a key element in the system. Consequently, it is imperative that the response of the transducer is known sufficiently well to allow optimal design of the system. For example,

(i) That the remainder of the system may be designed to accommodate the transducer for the application considered.

(ii) That the transducer may be constructed to meet specific requirements and performance criteria imposed by the system and application.

(iii) That the system may be designed to control the transducer. That is, the system is designed around the transducer, such that the response of the transducer is pre-defined, hence permitting the generation of specific outputs by mechanical and electrical control.

To these ends, it is highly desirable that a model of the transducer should be available, which accurately predicts both the temporal and spectral characteristics of the transducer system. Clearly, such a model should also include the acoustic and electrical parameters associated with the transducer. Thus, a suitable model must incorporate the following practical features.

a) The electrical source and passive electrical load elements.

b) In many applications, transducers are constructed with front and rear mechanical layers. These should be included, as should the effects of electrodes, bondlines and couplant layers.

c) If possible, the model should reflect the underlying physical principles upon which the transducer operates . This may allow specific cause and effect relationships to be established,

which may aid the design and construction of the devices.

d) The model should be amenable to computer implementation, both in terms of speed and storage. It is also desirable that any computer model should be structured such that the elements of a), b) and c) are readily identified and may be used as design tools.

e) The model should be amenable to mathematical inversion - that is, the describing equations may be manipulated to permit the generation of a mathematically derived excitation function.

The behaviour of piezoelectric transducers, and the development of transducer models has been widely investigated. Among the different methods which have been used to model the devices are:- equivalent circuits, transmission-line analogies, finite-element techniques, functional analysis, and systems modelling techniques. These have had varying degrees of success with each possessing relative advantages and drawbacks. Most of the techniques are well-documented in the literature. However, some of the more important and successful methods are presented now in further detail. Each method is critically assessed using the criteria a) to

e) described previously. Its relative merits are then clearly outlined.

1.2 Present Modelling Techniques

Three main techniques for modelling the thickness-mode piezoelectric transducer are considered. Their merits and drawbacks are then compared with the previously identified desirable model characteristics.

1.2(i) The Equivalent Circuit Approach

These models were developed as an extension of the techniques used to model piezoelectric crystal oscillators. Much of the original work in this area was carried out by W P MASON (42), and his book contains a comprehensive treatment of equivalent circuit modelling for various piezoelectric configurations.

The models are based upon the electro-mechanical analogies of force-voltage and velocity-current. Thus, the mechanical parameters of the transducer correspond to the appropriate electrical parameters in the circuit model. The differential equations which describe the transducer and the equivalent circuit are thus of the same form.

The circuits are derived from the fundamental piezo-

electric relationships (2), (9), (42), and may be represented in several ways. For example, Fig 1.1 shows the lumped parameter model of MASON, while Fig 1.2 shows the KLM model proposed by LEEDOM et al. (36), (37). Both models represent the thickness-mode piezoelectric transducer. Clearly, the models have been formed in quite a different manner, although they are mathematically identical.

Both of these dynamic analogies have found widespread use in transducer modelling. For example, both KOSSOFF (35) and SITTIG (62) use the Mason model as a starting point for their analyses of multilayered transducer structures. However, the KLM model has now largely superseded that of Mason for two reasons. Firstly, it is of a simpler structure - the transmission line is intuitively a better method of representing the transducer propagation delay. Secondly, it separates the electrical and mechanical quantities and is thus more amenable to implementation on a computer. This has resulted in several computerised modelling packages, notably those of SILK (59), KERVEL and THIJSSEN (34), DeSILETS et.al.(14) and SELFRIDGE et.al.(55), which satisfy requirements (a), (b) and (d) as described in the previous section.

However, neither model relates to the underlying physical operation of the transducer. For example, consider Fig 1.2 . It appears from this model that electromechanical interaction occurs at the centre of the transducer. This is not the case, as REDWOOD [51] has shown. Plane wave propagation through a piezoelectric and a non-piezoelectric material is identical with the piezoelectric effect occurring only at the electroded boundaries of the piezoelectric material.

Each model also contains an unreal circuit element. In the Mason model, this is a negative capacitance, and in the KLM model, a frequency-dependent reactance and acousto-electric transformer. These elements are necessary to accurately model the acousto-electric interaction within the transducer, but offer limited physical insight into how these processes occur. Thus the transmission-line models do not fully meet requirement (c) of the preceeding section.

LIU (39) has used the KLM model to derive the generating voltage required to produce a specified force output from a transducer. This involves calculating the spectra of the transducer system and the desired output, and then evaluating the spectrum of the required input. The temporal excitation voltage was then obtained using an Inverse-Fast-Fourier Trans-

form (IFFT) routine. However, this necessitated the use of a window function to render the required input spectrum causal, and hence realisable.

The cases considered by Liu were narrowband and the window function had little discernible effect on the output. For broadband cases, however, it is possible that these functions could distort the required input to such an extent that there may be marked differences between the actual and the desired outputs.

Thus, the mathematical equations which define the equivalent circuit models are not generally suitable for inversion and electronic control of the transducer.

All equivalent circuit models are essentially based upon spectral techniques. In each of the cases considered here, the transient response is obtained by calculating the appropriate spectrum, and using an IFFT procedure. This works well for narrowband cases, but may cause problems for wideband applications. The reason for this is the transit delay of the transducer system which may, for some cases, result in a spectrum with a very large bandwidth. To obtain good resolution with such a spectrum, it is necessary to substantially

increase the total number of sample points used in the IFFT. This is often unacceptable in many cases. If, however, the spectrum is truncated so that fewer sample points are used, then the resultant transient may exhibit severe distortion which is clearly undesirable. One solution to this problem which has been proposed, is to use z-transform techniques, whereby the transit-delay of the transducer is modelled directly in the z-domain, and the differential elements of the system are approximated by z-domain transfer functions.

Rhynne (53) first attempted this by transforming the Mason model into a z-domain model. This was of limited use however, since it proved difficult to include arbitrary electrical load elements.

Stepanishen (63) developed a z-transform model for a length-expansion transducer, based on an equivalent circuit approach. The resultant model provided a simple, accurate method of determining the transient response of the transducer. However, again this was of limited value, since the case considered was not of great practical importance.

CHALLIS and HARRISON (10), (11) have more recently

developed a z-domain equivalent of the Mason model. This has been experimentally verified for several cases, and, like the method of Stepanishen, is a fast, accurate method of calculating the transient response. However, the techniques used there are extremely limited in extent and application.

Hence, it appears that, while z-transform techniques do offer advantages over IFFT methods in calculating the transducer transient response, their applications to date have been limited. Thus, the inherent frequency domain approach of equivalent circuit models may present difficulties in the calculation of the transducer transient response.

1.2(ii) Finite Element Techniques

These techniques have, for the most part, been used to analyse the behaviour of complex vibratory structures. For example, LLOYD and REDWOOD (40) have used a finite element technique to investigate the vibrations of a thin, rectangular piezoelectric plate. KAGAWA et al (24), (25), (26), (27), (28), (29), (30), (31), (69), have used several finite element techniques to analyse a variety of transducer configurations and applications.

This method may be briefly summarised as follows. The transducer or structure under investigation is theoretically broken down into a number of small elements which are connected by a grid or mesh. The describing differential equations are then applied to each element in turn, and the relationships between adjacent elements calculated. This process is repeated using an iterative procedure until a steady state solution is obtained. For most applications, this involves a great deal of repetitive calculation, and a suitable computer is essential.

The major advantage of this method over other modelling techniques is the ability to handle transducers with complex geometries. However, for the application considered here, the thickness-mode transducer, this technique offers no improvement on the equivalent circuit method. It provides no physical insight into the underlying transducer operation, is not well suited to transient analysis, and has limited potential for the investigation of electronic control strategies. Consequently, finite element methods do not merit further investigation in the present context.

1.2(iii) Mathematical Analyses based upon the Laplace Transform

This method involves finding a closed-form Laplace transform solution for the relevant piezoelectric and differential equations which describe the transducer. This solution may then be used to obtain either the spectral or transient response of the device under consideration.

Laplace techniques were first developed by COOK (12) who used the piezoelectric constant e_{11} (9) to relate stress and applied voltage within the transducer. He then solved the relevant system and boundary conditions to develop a model, comprising two stress generators, one at each face of the transducer. While this model is simplistic, (it does not include the effects of electrical load elements), it does show how the voltage-stress relationship occurs physically within the device.

This method was further extended by REDWOOD (51), (52) SINHA (60) and FILIPCZYNSKI (16) who applied Laplace transform techniques to the fundamental transducer equations of Mason (42). Redwood analysed the transducer for both reception and transmission, and,

for each case, he developed transfer functions relating voltage and force. However, he was unable to analyse the transducer completely due to the complexity of the resultant transfer functions. This arises from the negative capacitance, shown in the Mason model of Fig 1.1 , which accounts for secondary piezoelectric action. When this component is included in the Laplace transform analysis, it may produce transfer functions of a mixed differential/delay nature. These are, in many cases, extremely difficult to inverse transform into the time domain.

Instead, Redwood examined a series of specific transmission and reception configurations, and analysed the response of each case. This provided a valuable insight into the transient response of piezoelectric devices. SINHA (60) extended this work by investigating the effects of specific excitation functions on the transducer; for example, step and ramp functions.

FILIPCZYNSKI (16) employed a similar analysis to that of Redwood, however, he examined the effects of the negative capacitance in greater depth. From this, he was able to show that the negative capacitance has a direct effect upon the resonant properties of the

transducer because of its influence on the electrical and mechanical resonances.

More recently, LEWIS (58), HAYWARD (19), (20) and YING (70) have employed Laplace transform techniques to analyse transducer behaviour.

Lewis investigated the effects of both mechanical matching layers, and electrical tuning components upon the transducer response. To do this, he implemented a generalised computer model for the multilayer transducer. However, he did not attempt to develop a physical model nor did he investigate the physical operation of the transducer.

Hayward extended the Redwood technique, and developed the Laplace transfer functions into two block-diagram systems models of the transducer; one for transmission and one for reception. This method has the advantage over other modelling techniques in that the individual blocks within the system may be manipulated into different configurations. From this, it is possible to form physically meaningful relationships between the variables and parameters of the transducer system. By doing this, Hayward was able to analyse fully the oper-

ation of the thickness-mode piezoelectric transducer. He showed that secondary piezoelectric action is essentially a positive feedback effect, and that this is accounted for in the Mason model by the negative capacitance. In (19), Hayward presents a complete analysis of the application of systems modelling techniques to the thickness-mode piezoelectric transducer and concludes that this method is superior in many instances to existing dynamic analogies. This is particularly true of the ability of the systems approach to highlight the underlying physical operation of the transducer.

Ying (70) has analysed the transmitter-only case, by means of a direct Laplace transform approach. While this method is complicated and, in view of the work of Hayward, somewhat clumsy, he reaches the same conclusions as Hayward, regarding secondary piezoelectric action.

Thus, from the work of Lewis and Hayward, it is apparent that Laplace transform techniques and systems modelling in particular, may be used to satisfy criteria a), b), c), and d) of the preceding section. However, some work is still required in the application of these

techniques. For example, the systems-diagrams developed by Hayward are not in a form which readily allows the addition of mechanical layers.

The last criterion, e) - the amenability of the model to mathematical inversion, is well suited to Laplace techniques, and has been investigated by several authors, in particular, KAŽYS and LUKOŠEVIČIUS (33), COURSANT (13), and MEL'KANOVICH (45).Kazys and Lukosevicius employed a mixture of passive and active correction to generate acoustic impulses. Their system was designed using a Laplace transform impedance model of the transducer.

Coursant and Mel'Kanovich both used the transfer function for a piezoelectric transmitter to calculate the Laplace transform of the excitation voltage required to generate a series of desired acoustic pulses. Coursant investigated the use of this technique with low-efficiency devices, where secondary piezo-electric action may be neglected. However, he gener-ated the calculated voltages and confirmed the technique experimentally, thus controlling the transmitter response electronically. Mel'Kanovich analysed the more difficult case, that where secondary action is present.

He also calculated the required excitation voltages for several desired outputs, although it is not clear from (45) whether these were validated experimentally. Thus, Laplace transform techniques are suitable for the development of electronic control strategies.

Finally, the Laplace modelling technique may be used to calculate the transient response of the transducer directly, by inverse transformation into the time domain. However, as was noted earlier, this may present difficulties in certain cases. To this end, several different techniques have been developed to calculate the transient response from the Laplace transform.

Hayward (19) and Lewis (38) have both used the Laplace transform to calculate the spectrum of the system and thence, using an IFFT routine, the transient response. This method is straightforward but suffers from the disadvantages outlined earlier.

Ying (70), Mel'Kanovich (44) and Gitis and Shenker (17), inverse transform the system transfer functions directly, by deriving the describing Laplace transform into a suitable form. The methods used to do this, while mathematically rigorous, tend to be unduly

complicated and are not readily implemented on a computer.

Hayward (19) has investigated the use of z-transformation for the case of a transducer without secondary piezoelectric action. It is apparent from his results, and those discussed earlier, that the z-transform offers considerable scope for calculating the transient response, although some development is still required.

Thus, comparing the three modelling techniques which have been discussed, it is apparent that finite element techniques are inappropriate for the case under consideration. Of the remaining two techniques, equivalent circuit methods are the more widely used. These, however, lack two important points. They give little or no insight into the underlying physical operation of the transdcuer, and they are not well suited for the development of electronic control strategies. They may also present difficulties in the calculation of the transducer transient response.

Laplace transform and systems modelling techniques have been used to satisfy all five of the desirable model criteria. However, these techniques lack coher-

ence - that is, they have been developed independently by several authors to solve specific problems. No one Laplace or systems model has been developed which satisfies all five criteria. Comparing these two methods, it may be observed from section 1.2(i) that the problems with the equivalent circuit methods arise from the dependence of these methods on frequency domain techniques, and the use of frequency dependent components in the models. There is no simple method of overcoming this problem, other than to use an alternative technique to form the equivalent circuits.

The problems with the Laplace and systems modelling techniques are largely due to the manner in which these techniques have been applied and are not fundamental to the method,

Thus, it may be concluded that Laplace transform and systems modelling techniques in particular, offer the greatest scope for the development of a general transducer model which meets the five criteria defined previously.

1.3 Required Improvements in Systems Modelling

It is now possible to identify the improvements which are required in systems modelling techniques to produce a transducer model which meets the requirements of section 1.1 . The systems models proposed by Hayward (19), already meet several of these criteria. In particular, they have been developed to show the underlying physical operation of the transducer; they have been used with a wide range of electrical load and source elements; and they have been implemented on a computer. So, assuming that the systems model already contains these points, the further requirements are:-

The systems approach developed by Hayward results in two separate models. This is inherently unsuitable because the piezoelectric effect should be combined in a unified fashion. Consequently, the fundamental approach of Hayward requires further investigation, particularly for the development of a general three-port systems model encompassing both transmission and reception.

The model must include the effects of mechanical layers. The systems models of Hayward are not developed into a form whereby layers may be readily incorporated. Since many practical transducers and probe assemblies include matching and couplant layers, the systems modelling technique must be extended to allow the inclusion of these.

Further development of techniques for calculating the transducer transient response are required, particularly the z-transform method.

Further investigation and development of inversion techniques for electronic control is required, particularly to deal with the effects of passive electrical load elements and mechanical matching layers. This is necessary before electronic control can become a practical proposition.

minimises the degree of algebraic manipulation normally associated with this method.

4. A strategy has been developed for calculating the optimal acoustic impedance of multiple matching layers.

5. The effects of passive electrical load elements upon the calculation of the inverse voltage has been investigated, and it is shown that these may have a significant influence on the order and realisability of the generated output.

6. The effects of mechanical layers upon the calculation of the inverse control voltage has been investigated, both theoretically and experimentally.

The following chapters present the derivation of the model and its associated techniques. Chapter 2 presents the derivation of the basic transducer model. This is extended in Chapter 3 to include multiple mechanical layers, Chapter 4 investigates z-transform techniques and develops a method suitable for transfer functions

of the transducer type. The model, and the z-transform techniques are verified extensively in Chapter 5 by the comparison of simulated and experimental results. Finally, Chapter 6 investigates the methods and usefulness of electronic control.

CHAPTER 2
A NEW THREE-PORT LATTICE MODEL

2.1 INTRODUCTION

This chapter presents the derivation of a three-port linear systems model of the thickness-mode piezoelectric transducer. Unlike transmission line models, for example, MASON (42), and LEEDOM et al (37), this approach uses Laplace transforms and linear systems techniques. These techniques are based on the methods developed by, principally, REDWOOD (51) and HAYWARD (19).

In a similar manner to the models developed by Hayward, this model also uses a feedback mechanism to account for secondary piezoelectric action. However, acoustical reverberation is modelled by an acoustic lattice, similar to that developed by ROBINSON and TREITEL (54) for modelling multilayered structures in geophysics.

This model has three main advantages:-

1. A single general model may be used for both transmission and reception. (It may be shown that the general model reduces to the models proposed by Hayward, for the cases he considers.)
2. The addition of further mechanical layers

is straightforward (as will be shown in Chapter 3).

3. This model provides a greater insight into the interaction between the electrical and mechanical effects which are inherent in the transducer.

2.2 THE ACOUSTIC LATTICE

Consider the single-layer structure shown in Fig 2.1, in which medium 2 is positioned between media 1 and 3. Each of the media is assumed to be acoustically lossless, so that their associated acoustic impedances Z1, Z2 and Z3 are real.

Media 1 and 3 are considered to be semi-infinite in the negative and positive x-directions respectively, and medium 2 has a finite thickness ℓ_2. All three media are assumed to be infinite in the lateral dimensions. Each medium also has an associated propagation velocity, V_1, V_2 and V_3 respectively.

Then, if it is assumed that only thickness-mode, plane-wave propagation occurs in the system, it may be shown that the equations for particle displacement ($\bar{\xi}$), and force ($\bar{\Gamma}$), in the n^{th} medium, may be expressed in Laplace Transform notation as [38],

$$\bar{\xi}_n = \bar{A}_{fn} e^{-s(x_n/v_n)} + \bar{A}_{bn} e^{+s(x_n/v_n)} \qquad 2.1$$

$$\overline{\Gamma}_n = sZ_n(-\overline{A}_{fn}e^{-s(x_n/v_n)}+\overline{A}_{bn}e^{+s(x_n/v_n)}) \qquad 2.2$$

where $\overline{A}_{fn}$ is the amplitude of the particle displacement of a wave travelling in the positive x-direction, at position x_n,

and $\overline{A}_{bn}$ is the amplitude of the particle displacement of a wave travelling in the negative x-direction, at position x_n. Z_n is the acoustic impedance,

Then, defining the force components at position x_n to be,

$$\overline{F}_n = -sZ_n\overline{A}_{fn} \qquad 2.3$$

$$\overline{B}_n = sZ_n\overline{A}_{bn} \qquad 2.4$$

Equations 2.1 and 2.2 may be rewritten as,

$$\overline{\xi}_n = (-\overline{F}_n e^{-s(x_n/v_n)}+\overline{B}_n e^{+s(x_n/v_n)})/sZ_t \qquad 2.5$$

$$\overline{\Gamma}_n = \overline{F}_n e^{-s(x_n/v_n)} + \overline{B}_n e^{+s(x_n/v_n)} \qquad 2.6$$

Applying the normal boundary conditions, namely continuity of particle displacement, and continuity of force, to the interface between media 1 and 2, and media 2 and 3 gives:-

$$\overline{\xi}_1\big|_{x_1=0} = \overline{\xi}_2\big|_{x_2=0}$$

$$\overline{\xi}_2\big|_{x_2=\ell_2} = \overline{\xi}_3\big|_{x_3=0}$$

$$\overline{\Gamma}_1\big|_{x_1=0} = \overline{\Gamma}_2\big|_{x_2=0}$$

$$\overline{\Gamma}_2\big|_{x_2=\ell_2} = \overline{\Gamma}_3\big|_{x_3=0} \qquad 2.7$$

Next, defining the forward and backward force components inside the n^{th} layer at its boundaries. That is, at $x_n=0$ and $x_n=\ell_n$ to be,

$$\overline{F}_{n0} = \overline{F}_n \; e^{-s(x_n/v_n)}\Big|_{x_n=0}$$

$$\overline{B}_{n0} = \overline{B}_n \; e^{+s(x_n/v_n)}\Big|_{x_n=0}$$

$$\overline{F}_{n\ell_n} = \overline{F}_n \; e^{-s(x_n/v_n)}\Big|_{x_n=\ell_n}$$

$$\overline{B}_{n\ell_n} = \overline{B}_n \; e^{+s(x_n/v_n)}\Big|_{x_n=\ell_n} \qquad 2.8$$

The transit-time for mechanical waves to cross the n^{th} layer may be defined as,

$$T_n = \ell_n \; / \; v_n$$

So, applying this, and equations 2.8 to the system of Fig 2.1, wave propagation through medium 2 is described in matrix form as,

$$\begin{bmatrix} \overline{F}_{2\ell_2} \\ \\ \overline{B}_{2\ell_2} \end{bmatrix} = \begin{bmatrix} e^{-sT_2} & 0 \\ \\ 0 & e^{+sT_2} \end{bmatrix} \begin{bmatrix} \overline{F}_{20} \\ \\ \overline{B}_{20} \end{bmatrix} \qquad 2.9$$

Equations 2.5, 2.6, 2.8 and 2.9 may now be used to solve the boundary conditions 2.7, in force-component form, yielding,

$$(-\overline{F}_{10} + \overline{B}_{10})/Z_1 = (-\overline{F}_{20} + \overline{B}_{20})/Z_2$$

$$(-\overline{F}_{2\ell_2} + \overline{B}_{2\ell_2})/Z_2 = (-\overline{F}_{30} + \overline{B}_{30})/Z_3$$

$$\overline{F}_{10} + \overline{B}_{10} = \overline{F}_{20} + \overline{B}_{20}$$

$$\overline{F}_{2\ell_2} + \overline{B}_{2\ell_2} = \overline{F}_{30} + \overline{B}_{30} \qquad 2.10$$

These may be rearranged into matrix form,

$$\begin{bmatrix} \overline{F}_{20} \\ \\ \overline{B}_{20} \end{bmatrix} = \frac{1}{2} \begin{bmatrix} 1 + \frac{Z_2}{Z_1} & 1 - \frac{Z_2}{Z_1} \\ \\ 1 - \frac{Z_2}{Z_1} & 1 + \frac{Z_2}{Z_1} \end{bmatrix} \begin{bmatrix} \overline{F}_{10} \\ \\ \overline{B}_{10} \end{bmatrix} \qquad 2.11$$

$$\begin{bmatrix} \overline{F}_{30} \\ \\ \overline{B}_{30} \end{bmatrix} = \frac{1}{2} \begin{bmatrix} 1 + \frac{Z_3}{Z_2} & 1 - \frac{Z_3}{Z_2} \\ \\ 1 - \frac{Z_3}{Z_2} & 1 + \frac{Z_3}{Z_2} \end{bmatrix} \begin{bmatrix} \overline{F}_{2\ell_2} \\ \\ \overline{B}_{2\ell_2} \end{bmatrix} \qquad 2.12$$

Equations 2.11 describe wave propagation across the medium 1:2 interface, in force-component form; similarly, equations 2.12 describe the 2:3 interface.

The equations may be be rewritten in terms of the reflection coefficients at the media interfaces. Defining

$$R_{12} = \frac{Z_2 - Z_1}{Z_1 + Z_2} \quad \text{and} \quad R_{23} = \frac{Z_3 - Z_2}{Z_2 + Z_3}$$

Where R_{12} is the reflection coefficient for waves of force travelling from medium 1 to medium 2, and R_{23} the reflection coefficient going from medium 2 to medium 3.

Rearranging equations 2.11 and 2.12 gives,

$$\begin{bmatrix} \overline{F}_{20} \\ \overline{B}_{10} \end{bmatrix} = \begin{bmatrix} 1 + R_{12} & -R_{12} \\ R_{12} & 1 - R_{12} \end{bmatrix} \begin{bmatrix} \overline{F}_{10} \\ \overline{B}_{20} \end{bmatrix} \qquad 2.13$$

$$\begin{bmatrix} \overline{F}_{30} \\ \overline{B}_{2\ell_2} \end{bmatrix} = \begin{bmatrix} 1 + R_{23} & -R_{23} \\ R_{23} & 1 - R_{23} \end{bmatrix} \begin{bmatrix} \overline{F}_{2\ell_2} \\ \overline{B}_{30} \end{bmatrix} \qquad 2.14$$

Equations 2.13 and 2.14 describe waves of force leaving the 1:2 and 2:3 interfaces, in terms of the force waves incident upon them. This is shown in block diagram form in Figs 2.2A and 2.2B.

Equation 2.9 describes wave propagation through medium 2 and is shown in Fig 2.2C.

Combining Figs 2.2A, B and C gives the overall systems diagram Fig 2.3 .

Comparing Figs 2.1 and 2.3 , it may be observed that Fig 2.3 resembles the original system diagram, Fig 2.1, but also contains the mathematical information describing the system. That is, Fig 2.3 clearly shows the relationship between the chosen variables within the system.

This is the major advantage of the acoustic lattice model over the transmission-line analogy. Although transmission line models can be used to obtain the force and particle displacements in a layered system, they do not show the relationships between the variables at the interfaces.

2.3 THE TRANSDUCER LATTICE MODEL

Consider the layered system shown in Fig 2.4, which depicts a piezoelectric slab positioned between two semi-infinite non-piezoelectric media, denoted by -1 and 1 for the rear and front faces respectively. All media are assumed mechanically lossless, possessing real acoustic impedances, Z_{-1}, Z_t and Z_1 , and velocities V_{-1}, V_t and V_1 respectively. The piezoelectric layer has a finite thickness ℓ_t, and it is assumed that electrodes of negligible thickness are positioned at the front and rear faces. All media are assumed to be infinite in the lateral dimensions.

Attached to the electrodes, as shown, is an arbitrary electrical load, consisting of a lumped Thevenin impedance, Z_E, in series with a Thevenin source, V_E. The voltage across the electrodes is designated V_t, as shown.

For plane-wave propagation in the thickness direction, the expressions for particle displacement in the non-piezoelectric media are given by equations 2.1 and 2.2.

The corresponding equations for the piezoelectric medium are given by LEWIS (38) as,

$$\bar{\xi}_t = \bar{A}_{ft}\, e^{-s(x_t/v_t)} + \bar{A}_{bt}\, e^{+s(x_t/v_t)} \qquad 2.15$$

$$\bar{\Gamma}_t = sZ_t(-\bar{A}_{ft}\, e^{-s(x_t/v_t)} + \bar{A}_{bt}\, e^{+s(x_t/v_t)}) - h\bar{Q}_t \qquad 2.16$$

The voltage across the piezoelectric layer is proportional to the difference in particle displacement between the front and rear faces.

This may be expressed as (38),

$$\bar{V}_t = -h((\bar{\xi}_t)\Big|_{x_t=\ell_t} - (\bar{\xi}_t)\Big|_{x_t=0}) + \bar{Q}_t/C_t \qquad 2.17$$

where $\bar{Q}_t$ is the Laplace transform of the total charge on the electrodes, h is the piezoelectric constant h_{33} and C_t is the static capacitance of

the piezoelectric layer (alternatively written as C_0).

Applying the same mechanical boundary conditions as before, namely,

$$\bar{\xi}_{-1}\big|_{x_{-1}=0} = \bar{\xi}_t\big|_{x_t=0}$$

$$\bar{\xi}_t\big|_{x_t=\ell_t} = \bar{\xi}_1\big|_{x_1=0}$$

$$\bar{\Gamma}_{-1}\big|_{x_{-1}=0} = \bar{\Gamma}_t\big|_{x_t=0}$$

$$\bar{\Gamma}_t\big|_{x_t=\ell_t} = \bar{\Gamma}_1\big|_{x_1=0} \qquad 2.18$$

and defining the force components inside the n^{th} layer (whether it is piezoelectric or not) in exactly the same manner as equations 2.8 , then equations 2.1, 2.2, 2.15 and 2.16 may be used to solve equations

2.18, to give,

$$(-\overline{F}_{10} + \overline{B}_{-10})/Z_{-1} = (-\overline{F}_{t0} + \overline{B}_{t0})/Z_t$$

$$(-\overline{F}_{t\ell_t} + \overline{B}_{t\ell_t})/Z_t = (-\overline{F}_{10} + \overline{B}_{10})/Z_1$$

$$\overline{F}_{-10} + \overline{B}_{-10} = \overline{F}_{t0} + \overline{B}_{t0} - h\overline{Q}_t$$

$$\overline{F}_{t\ell_t} + \overline{B}_{t\ell_t} - h\overline{Q}_t = \overline{F}_{10} + \overline{B}_{10} \qquad 2.19$$

where, in a similar manner to equation 2.9,

$$\begin{bmatrix} \overline{F}_{t\ell_t} \\ \\ \overline{B}_{t\ell_t} \end{bmatrix} = \begin{bmatrix} e^{-sT_t} & 0 \\ \\ 0 & e^{+sT_t} \end{bmatrix} \begin{bmatrix} \overline{F}_{t0} \\ \\ \overline{B}_{t0} \end{bmatrix} \qquad 2.20$$

T_t is the transit period of the piezoelectric layer.

Rearranging equations 2.19 gives,

$$\begin{bmatrix} \overline{B}_{-10} \\ \\ \overline{F}_{t0} \end{bmatrix} = \begin{bmatrix} R_{-1} & 1 - R_{-1} \\ \\ 1 + R_{-1} & -R_{-1} \end{bmatrix} \begin{bmatrix} \overline{F}_{10} \\ \\ \overline{B}_{t0} \end{bmatrix} + \frac{h}{2} \begin{bmatrix} R_{-1} - 1 \\ \\ R_{-1} + 1 \end{bmatrix} \overline{Q}_t \qquad 2.21$$

$$\begin{bmatrix} \overline{F}_{10} \\ \\ \\ \overline{B}_{t\ t} \end{bmatrix} = \begin{bmatrix} R_1 & 1 - R_1 \\ \\ \\ 1 + R_1 & -R_1 \end{bmatrix} \begin{bmatrix} \overline{B}_{10} \\ \\ \\ \overline{F}_{t\ t} \end{bmatrix} + \frac{h}{2} \begin{bmatrix} R_1 - 1 \\ \\ \\ R_1 + 1 \end{bmatrix} \overline{Q}_t \qquad 2.22$$

where,

$$R_1 = \frac{Z_t - Z_1}{Z_1 + Z_t} \qquad \text{and} \qquad R_{-1} = \frac{Z_t - Z_{-1}}{Z_{-1} + Z_t}$$

are the reflection coefficients for waves of force travelling into the piezoelectric layer at the l,t and -l,t interfaces respectively.

Equations 2.20, 2.21 and 2.22 describe the systems lattice which is outlined in Fig 2.5 . This is similar to the acoustic lattice of Fig 2.3. However, the system now has an extra input, caused by the charge on the electrodes, Q_t.

It is now required to obtain a relationship between the source voltage and charge, and incorporate this in an overall model.

From Fig 2.4,

$$\overline{I}_t = s\overline{Q}_t \qquad 2.23$$

and,

$$\overline{V}_t = \overline{V}_E - \overline{I}_t.\overline{Z}_E \qquad 2.24$$

So, substituting 2.23 and 2.24 into 2.17 gives,

$$\overline{Q}_t = \left(\frac{C_t}{1+sC_tZ_E}\right)\left(\overline{V}_E + h\left(\left(\overline{\xi}_t\right)\Big|_{x_t=\ell_t} - \left(\overline{\xi}_t\right)\Big|_{x_t=0}\right)\right)$$

2.25

Using equation 2.19, this becomes,

$$\overline{Q}_t = \left(\frac{C_t}{1+sC_tZ_E}\right)\left(\overline{V}_E + \frac{h}{sZ_t}\left(1 - e^{-sT_t}\right)\left(\overline{F}_{tO} + \overline{B}_{t\ell_t}\right)\right)$$

2.26

This is shown in system block diagram form in Fig 2.6

However, it is usually easier to measure the voltage across the transducer, V_t, than the charge on the electrodes, so, substituting equations 2.23 and 2.24 into equation 2.26 and rearranging,

2.27

$$\overline{V}_t = -\frac{h}{sZ_t}\left(1 - e^{-sT_t}\right)\left(\overline{F}_{tO} + \overline{B}_{t\ell_t}\right)\left(\frac{sC_t\overline{Z}_E}{1+sC_t\overline{Z}_E}\right) + \frac{\overline{V}_E}{1+sC_t\overline{Z}_E}$$

This is shown in Fig 2.7 .

Equations 2.21, 2.22 and 2.27 describe the piezoelectric layer system of Fig 2.4 as a three-port system. The three input ports are the incident forces upon the piezoelectric layer, F_{-10} and B_{10}, and the electrical driving voltage, V_E. Similarly, the three output ports comprise the forces leaving the piezoelectric layer F_{10}, B_{-10} and the voltage across the electrodes, V_t. As a result, the general lattice block diagram outlined in Fig 2.8 may be constructed.

Physical interpretation of the lattice block diagram may be carried out in a relatively straightforward fashion.

Consider firstly, the device acting as a receiver, with waves of force, B_{10} and F_{-10} incident on the front and rear faces respectively. With reference to Fig 2.8, a portion of each incident force is reflected, and a portion, $(1+R_1)B_{10}$, $(1+R_1)F_{-10}$, is transmitted into the transducer material, whereupon the transmitted portions reverberate back and forth, as indicated by

the lattice structure. A component of charge, proportional to the difference in particle displacement between the front and rear faces, is also generated via the blocks h/sZ_t and $C_t/(1+sC_t\bar{Z}_E)$. The latter may be regarded as a charge modification factor due to the external electrical load. This charge component is responsible for the generation of secondary forces, which propagate into the transducer and the surrounding media. The secondary piezoelectric action is generated by the two positive feedback loops, as indicated in Fig 2.8 by the double arrow symbols.

It may also be observed that, as Z_E approaches zero, (that is, a short-circuit), the generated charge, and hence the feedback, become maximised. The received voltage, V_t, is of course, zero under these conditions. However, as Z_E increases, the received voltage increases and the feedback (and hence the secondary action) decreases. The amount of feedback also depends on the piezoelectric properties and mechanical load conditions. This has been investigated by Hayward, and full details of these effects are given in (20).

For the device acting as a transmitter, the input to the system is the electrical excitation voltage, V_E.

The resulting deposition of charge generates waves of force travelling into the transducer and the load media at each interface. The nett forces acting on each face of the device also generate secondary components of charge, via the feedback voltage quantity, V_F. Once again, secondary piezoelectric action is represented by a positive feedback section. However, in this case, the forward and feedback paths are reversed in comparison to the piezoelectric receiver. That is, the transmission forward path corresponds to the reception feedback path. Furthermore, as Z_E approaches zero, transmission efficiency increases, along with the influence of secondary action. However, as Z_E approaches infinity, the forward path becomes zero and no transmission takes place.

As with most block systems diagrams, it is possible to rearrange the blocks to obtain alternative structures. Such alternatives may enhance the physical understanding, or simplify the relationships within the model.

The previous systems model of Fig 2.8 was derived from equations 2.21, 2.22 and 2.27. Equations 2.26 and 2.27 may be rearranged into the form,

$$\overline{Q}_t = \frac{(\frac{C_t}{1+sC_tZ_E})(\overline{V}_E+\frac{h}{sZ_t}((1+R_1)(\overline{B}_{10}-\overline{F}_{t\ell_t})+(1+R_{-1})(\overline{F}_{-10}-\overline{B}_{t0}))}{(1-(\frac{C_t}{1+sZ_EC_t})(\frac{h^2}{2sZ_t}(2+R_1+R_{-1})))} \qquad 2.28$$

$$\overline{V}_t = \{(1-(\frac{C_t}{1+sZ_EC_t})(sZ_E+\frac{h^2}{2sZ_t}(2+R_1+R_{-1})))\overline{V}_E+(\frac{C_t}{1+sC_tZ_E})*$$

$$*(\frac{h}{sZ_t})((1+R_1)(\overline{B}_{10}-\overline{F}_{t\ell_t})+(1+R_{-1})(\overline{F}_{-10}-\overline{B}_{t0}))\}$$

$$/\ (1-(\frac{C_t}{1+sZ_EC_t})(\frac{h^2}{2sZ_t}(2+R_1+R_{-1}))) \qquad 2.29$$

These equations may then be used to form the alternative block diagram shown in Fig 2.9 . This differs from Fig 2.8 in two important respects. Firstly, charge generation is now a function of the force components incident upon the interfaces of the system. This reduced to the nett particle displacement within the layer. However, the system of Fig 2.9 is simpler to manipulate mathematically.

Secondly, secondary action has now been reduced to a single positive charge feedback block. Positive feedback is often associated with unstable or oscill - atory systems. In this case, the system is stable, but a general stability analysis is extremely difficult because of the mixed differential/delay nature of the system. In a later chapter, it will be shown that z-transform techniques provide a simple mehtod for analysing the stability of the system. However, a qualitative explanation is as follows.

Any excitation of the system of Fig 2.9 (either by an incident force, or an electrical source), has two effects. Firstly, it generates two waves of force travelling into the layer from each interface, $\overline{F}_{t0}$ and $\overline{B}_{t\ell_t}$. Secondly, it produces a charge on the electrodes. (This charge may partially or wholly generate the force waves.) The waves of force take a finite time, T_t to cross the piezoelectric layer. During this time, the charge on the electrodes increases, due to positive feedback. However, when the

force waves reach the opposite electrodes, a portion of each wave generates charge. This charge has a 180° phase shift, with respect to the charge on the electrodes, and consequently disrupts the positive feedback process.

This mechanism repeats every T_t seconds, thus the positive charge feedback does not cause instability within the system. Hayward (19) and Ying et. al. (70) reach similar conclusions for their analyses.

2.4 MATHEMATICAL ANALYSIS

The transducer lattice models of Figs 2.8 and 2.9 represent three-port systems. It is convenient to express the transducer system as a mathematical transfer function of the form,

$$\begin{bmatrix} \overline{F}_{10} \\ \overline{B}_{-10} \\ \\ \overline{V}_t \end{bmatrix} = \begin{bmatrix} \overline{P} \end{bmatrix} \begin{bmatrix} \overline{B}_{10} \\ \overline{F}_{-10} \\ \\ \overline{V}_E \end{bmatrix} \qquad 2.30$$

where $\overline{P}$ is a 3 x 3 system matrix, given by:-

$$\begin{bmatrix} \overline{P} \end{bmatrix} = \begin{bmatrix} \overline{P}_{11} & \overline{P}_{12} & \overline{P}_{13} \\ \overline{P}_{21} & \overline{P}_{22} & \overline{P}_{23} \\ \overline{P}_{31} & \overline{P}_{32} & \overline{P}_{33} \end{bmatrix} \qquad 2.31$$

and the $\overline{p}_{ij}$ elements define the precise input/output relationships.

Consider the lattice model shown in Fig 2.9. In the present notation, $\overline{p}_{33}$ defines the relationship between the voltage across the electrodes, $\overline{V}_t$, and the driving voltage, $\overline{V}_E$. Assuming that the system is driven by $\overline{V}_E$ only, and that the forces leaving the transducer into the load media, $\overline{F}_{10}$, $\overline{B}_{10}$, may be neglected, then the system reduces to that of Fig 2.10.

Thus, using equations 2.20, 2.21, 2.22, 2.24 and 2.28, (or directly from Fig 2.10), the following relationships are apparent,

$$\overline{F}_{tO} = -R_{-1}e^{-sT_t}\overline{B}_{t\ell_t}+(\frac{R_1+1}{2})h\overline{Q}_t \qquad 2.32$$

$$\overline{B}_{t\ell_t} = -R_1e^{-sT_t}\overline{F}_{tO} \ +(\frac{R_1+1}{2})h\overline{Q}_t \qquad 2.33$$

thus,

$$\bar{Q}_t = \frac{\left(\frac{C_t}{1+s\bar{Z}_E C_t}\right)\left(\bar{V}_E - \frac{he^{-sT_t}}{sZ_t}\left((1+R_1)\bar{F}_{t0} + (1+R_{-1})\bar{B}_{t\ell_t}\right)\right)}{\left(1 - \left(\frac{C_t}{1+s\bar{Z}_E C_t}\right)\left(\frac{h^2}{sZ_t}(2+R_1+R_{-1})\right)\right)} \qquad 2.34$$

and,

$$\overline{V}_t = \overline{V}_E - s\overline{Z}_E\overline{Q}_t \qquad 2.35$$

From 2.32 and 2.33,

$$\overline{F}_{tO} = \frac{\frac{h}{2}((R_{-1}+1)-R_{-1}(R_1+1)e^{-sT_t})\overline{Q}_t}{1 - R_1R_{-1}e^{-2sT_t}} \qquad 2.36$$

$$\overline{B}_{t\ell_t} = \frac{\frac{h}{2}((R_1+1)-R_1(R_{-1}+1)e^{-sT_t})\overline{Q}_t}{1 - R_1R_{-1}e^{-2sT_t}} \qquad 2.37$$

and then, from 2.34, 2.36 and 2.37,

(see next page) 2.38

$$\bar{Q}_t = \frac{\left(\frac{C_t}{1+s\bar{Z}_E C_t}\right)\bar{V}_E}{1 - \left(\frac{C_t}{1+s\bar{Z}_E C_t}\right)\left(\frac{h^2}{2sZ_t}\right)(1-e^{-sT_t})(1+R_{-1})(1-R_1 e^{-sT_t})+(1+R_1)(1-R_{-1}e^{-sT_t})\left(\frac{}{1 - R_1 R_{-1} e^{-2sT_t}}\right)}$$

2.38

$$\bar{V}_t = \frac{\left(\frac{1}{1+s\bar{Z}_E C_t}\right)\left(1 - \left(\frac{h^2 C_t}{2sZ_t}\right)(1-e^{-sT_t})\left(\frac{(1+R_{-1})(1-R_1 e^{-sT_t})+(1+R_1)(1-R_{-1}e^{-sT_t})}{1 - R_1 R_{-1} e^{-2sT_t}}\right)\right)\bar{V}_E}{1 - \left(\frac{C_t}{1+s\bar{Z}_E C_t}\right)\left(\frac{h^2}{2sZ_t}\right)(1-e^{-sT_t})\left(\frac{(1+R_{-1})(1-R_1 e^{-sT_t})+(1+R_1)(1-R_{-1}e^{-sT_t})}{1 - R_1 R_{-1} e^{-2sT_t}}\right)}$$

2.39

Equation 2.38 is the Laplace Transform of the charge on the electrodes, $\overline{Q}_t$, produced by the driving voltage $\overline{V}_E$.

Thus, combining equations 2.35 and 2.38 gives,

(see page before) 2.39

which is the Laplace Transform of the voltage across the electrodes, $\overline{V}_t$, in terms of the driving voltage, $\overline{V}_E$.

This procedure may be applied to each successive input/output pair to obtain each $\overline{p}_{ij}$ value of equation 2.31. The resultant expressions are given as follows.

To reduce the complexity of the expressions, define,

$$\overline{U} = \frac{h^2 C_t}{2sZ_t(1+sC_t\overline{Z}_E)} \qquad 2.40$$

$$\overline{G} = \frac{hC_t}{2(1+sC_t\overline{Z}_E)} \qquad 2.41$$

$$\overline{P}_{11} = ((R_1 - R_{-1}e^{-2sT_t}) + \overline{U}(1-e^{-sT_t})((e^{-sT_t}-1)(1+R_1R_{-1}) + 2(R_{-1}e^{-sT_t}-R_1))) \; / \; \overline{P}_D \qquad \text{(i)}$$

$$\overline{P}_{12} = ((1-R_1)(1+R_1)e^{-sT_t} + \overline{U}(1-e^{-sT_t})(1+e^{-sT_t})(R_1-1)(R_{-1}+1)) \; / \; \overline{P}_D \qquad \text{(ii)}$$

$$\overline{P}_{13} = \overline{G}(1-e^{-sT_t})(R_1-1)(1-R_{-1}e^{-sT_t}) \; / \; \overline{P}_D \qquad \text{(iii)}$$

$$\overline{P}_{21} = ((1-R_{-1})(1+R_{-1})e^{-sT_t} + \overline{U}(1-e^{-sT_t})(1+e^{-sT_t})(R_{-1}+1)*(R_1+1)) / \overline{P}_D \qquad \text{(iv)}$$

$$\overline{P}_{22} = ((R_{-1} - R_1e^{-2sT_t}) + \overline{U}(1-e^{-sT_t}) ((e^{-sT_t}-1)(1+R_1R_{-1}) + 2(R_1e^{-sT_t}-R_{-1}))) \; / \; \overline{P}_D \qquad \text{(v)}$$

$$\overline{P}_{23} = \overline{G}(1-e^{-sT_t})(R_{-1}-1)(1-R_1e^{-sT_t}) \; / \; \overline{P}_D \qquad \text{(vi)}$$

$$\overline{P}_{31} = \overline{G}(-2\overline{Z}_E/Z_t)(1+R_1)(1-e^{-sT_t})(1-R_{-1}e^{-sT_t}) \; / \; \overline{P}_D \qquad \text{(vii)}$$

$$\overline{P}_{32} = \overline{G}(-2\overline{Z}_E/Z_t)(1+R_{-1})(1-e^{-sT_t})(1-R_1e^{-sT_t}) \; / \; \overline{P}_D \qquad \text{(viii)}$$

$$\overline{P}_{33} = ((1-R_1R_{-1}e^{-2sT_t})/(1+sC_t\overline{Z}_E) \qquad 2.42 \qquad \text{(ix)}$$
$$-\overline{U}(1-e^{-sT_t})((1+R_1)(1-R_{-1}e^{-sT_t})+(1+R_{-1})(1-R_1e^{-sT_t})))$$

where $\overline{P}_D$ is a common denominator term, given by,

$$\overline{P}_D = ((1-R_1R_{-1}e^{-2sT_t})-\overline{U}(1-e^{-sT_t})*$$
$$* ((1+R_1)(1-R_{-1}e^{-sT_t})+(1+R_{-1})(1-R_1e^{-sT_t})))$$

2.43

Equations 2.42 and 2.43 form the complete set of Laplace transform solutions for the original piezoelectric layer system of Fig 2.4 . Since the system is linear, the system matrix of equations 2.30 and 2,31 may be used for multiple input/output cases.

From equations 2.40 and 2.41 it may be observed that the expression for $\overline{G}$ contains the term h , while that for $\overline{U}$ contains the term h^2 . This indicates that $\overline{G}$ is associated with a single electro-acoustic (or acousto-electric) conversion, while $\overline{U}$ is associated with a double conversion, that is electro-acousto-electric or vice-versa. From this, it may be concluded that the $\overline{U}$ term relates to secondary piezoelectric action.

When this is considered in relation to equations 2.42 and 2.43, it is apparent that the four $\overline{p}_{ij}$ terms with a single piezoelectric conversion, namely $\overline{p}_{13}$, $\overline{p}_{23}$ (voltage to force), and $\overline{p}_{31}$,$\overline{p}_{32}$ (force to voltage),

contain the term $\overline{U}$ in the denominator ($\overline{p}_D$) only. Thus the secondary action is caused by the charge feedback due to the output term only.

However, the other five $\overline{p}_{ij}$ terms, $\overline{p}_{11}$, $\overline{p}_{12}$, $\overline{p}_{21}$, $\overline{p}_{22}$ (force to force conversion) and $\overline{p}_{33}$ (voltage to voltage conversion) contain the $\overline{U}$ term in both the numerator and the denominator. This indicates that secondary action is caused by charge feedback which is due to both the input and output. Thus, in these cases, there are two sources of secondary action. Although this complicates the feedback system, this point may be observed directly from the lattice models of Fig 2.8 and 2.9 . However, this is not always apparent in other transducer models. Consider again the KLM model of Fig 1.2. Assume that the system is initially at rest, with an electrical load, $\overline{Z}_E$, connected across the electrodes but with no electrical source. Then, if a wave of force is incident on one face of the device, it appears from the KLM model that the wave must travel through the transducer until it encounters the electro-acoustic transformer before any piezoelectric action can occur. This is not the case.

Acousto-electric interaction will occur instantaneously when the force wave is incident on the electrode, and the charge generated will also instantaneously produce force waves leaving both faces of the opposite electrode. This effect is certainly not apparent from either the KLM (37) or MASON (42) models. (These effects are accounted for by the frequency dependent electrical terms in these models.)

Thus, it is possible using the lattice model and its associated system matrix not only to model the interaction of the system with any input/output configuration, but also to break the model down to examine the relationship between any chosen variables within the system.

2.5 SUMMARY

This chapter has presented the derivation of a new three-port systems model of the thickness-mode piezoelectric transducer. The resultant model makes use of Laplace Transforms to model the differential components, and acoustic lattices to model acoustic propagation through the piezoelectric layer.

As indicated during the derivation, this type of model has several major advantages over conventional transmission-line models.

Firstly, the use of systems block diagrams allows the exact relationships between the physical elements of the transducer to be examined. Secondly, the systems diagrams clearly indicate the mechanisms which are responsible for the response of the piezoelectric system. For example, the effects of primary and secondary piezoelectric action may be considered separately. Thirdly, the model is an accurate representation of the physical processes involved (unlike a centre-tapped transmission line, for example).

Finally, since the system is linear, the appropriate elements of equations 2.42 and 2.43 may be combined to model multiple input/output cases. Or, correspondingly, the effect of each input/output may be considered separately.

However, in its present form, the lattice model does not allow the addition of multiple mechanical layers. This is considered in the next chapter,

CHAPTER 3

EXTENSION OF THE LATTICE MODEL TO GENERAL MULTILAYER CASES

3.1 INTRODUCTION

The previous chapter presented the derivation of a three-port model of the thickness-mode piezoelectric transducer. In this form, the cases covered by the model may include complex electrical loads, but do not permit the inclusion of layered mechanical loads. Multilayered acoustic structures, however, form an important part of any practical transducer system. There are two main areas of application which necessitate the use of a multilayered system model.

Firstly, in the study and design of acoustic matching layers. In these cases, multiple acoustic layers are added to the front, and/or rear faces of the transducer. The layers are usually designed to improve the mechanical energy transfer from the transducer to the load medium. For example, the piezoelectric material PZT-5A is often used in the manufacture of transducers because of its high electromechanical conversion efficiency. In cases where such a transducer is to be used with a water load, there is a 20:1 difference ratio between

the acoustic impedances of the PZT-5A and water, and consequently, energy transmission from the transducer to the load is poor. The addition of one or more matching layers to the front face of the transducer can greatly improve the efficiency of energy transmission to the load. In Continuous Wave, (CW), transducers, the addition of matching layers may greatly improve the resonant properties of the transducer. (This is analogous to stub matching in transmission lines.)

Mechanical matching techniques have received considerable attention in the literature and some of the more important works are covered by SITTIG (61), KOSSOFF (35), DeSILETS et al. (14), SELFRIDGE (55), KERVEL et al. (34) and SILK (59).

In addition, multiple acoustic layers may also be used to model the media through which the sound propagates after leaving the transducer. Some examples are ultrasound propagation through metallic samples in non-destructive testing and analysis of composite material structures.

LOW (41) describes a multiple-layer non-destructive testing application, in which both the transducer matching layers and target media are modelled. However, the transducer model employed is extremely limited, and does not cover all the types of transducer which are used in practical cases. Thùs the major application of this method is the modelling of the layered propagation path.

Thus it is clear that the maximum benefit of the acoustic lattice model will be achieved only with the addition of multiple front and rear face layers to the model.

This chapter extends the previous model to incorporate multiple mechanical layers.

3.2 THE MULTILAYERED ACOUSTIC LATTICE

Consider the multiple layer system of Fig 3.1 which is an extension of the single layer system of Fig 2.2 . As with the single layer case, the layers are assumed to be semi-infinite in the lateral directions, lossless in the thickness direction and to possess the acoustic impedance, thickness and velocity as shown. Defining, as before, the transit-time for mechanical waves to cross the i^{th} layer, T_i, as,

$$T_i = \ell_i / v_i \qquad 3.1$$

the system may be solved in a similar manner to the one-layer case. Consider the interface between the i^{th} and the $i + 1^{th}$ layers. Using a similar notation to the single layer case, the force-components in the i^{th} and $i + 1^{th}$ layers at the i:i + 1 interface may be related in an analogous manner to equations 2.11 and 2.12.

$$\begin{bmatrix} \overline{F}_{(i+1)0} \\ \\ \overline{B}_{(i+1)0} \end{bmatrix} = \frac{1}{2} \begin{bmatrix} 1 + \frac{Z_{i+1}}{Z_i} & 1 - \frac{Z_{i+1}}{Z_i} \\ \\ 1 - \frac{Z_{i+1}}{Z_i} & 1 + \frac{Z_{i+1}}{Z_1} \end{bmatrix} \begin{bmatrix} \overline{F}_{i\ell_i} \\ \\ \overline{B}_{i\ell_i} \end{bmatrix} \qquad 3.2$$

also, mechanical wave propagation through the i^{th} layer is given by:-

$$\begin{bmatrix} \overline{F}_{i\ell_i} \\ \\ \overline{B}_{i\ell_i} \end{bmatrix} = \begin{bmatrix} e^{-sT_i} & 0 \\ \\ 0 & e^{+sT_i} \end{bmatrix} \begin{bmatrix} \overline{F}_{i0} \\ \\ \overline{B}_{i0} \end{bmatrix} \qquad 3.3$$

which is analogous to equation 2.9 .

Equations 3.2 and 3.3 may now be combined,

$$\begin{bmatrix} \overline{F}_{(i+1)0} \\ \\ \overline{B}_{(i+1)0} \end{bmatrix} = \frac{1}{2} \begin{bmatrix} (1 + \frac{Z_{i+1}}{Z_i})e^{-sT_i} & (1 - \frac{Z_{i+1}}{Z_i})e^{+sT_i} \\ \\ (1 - \frac{Z_{i+1}}{Z_i})e^{-sT_i} & (1 + \frac{Z_{i+1}}{Z_i})e^{+sT_i} \end{bmatrix} \begin{bmatrix} \overline{F}_{i0} \\ \\ \overline{B}_{i0} \end{bmatrix} \qquad 3.4$$

This expression relates the force-components at the origin of the layer i co-ordinate system to the force components at the origin of the layer i+1 co-ordinate system.

Defining

$$\left[\frac{\overline{T}_{i+1}}{i}\right] = \begin{bmatrix} \frac{1}{2}\left(1 + \frac{Z_{i+1}}{Z_i}\right)e^{-sT_i} & \frac{1}{2}\left(1 - \frac{Z_{i+1}}{Z_i}\right)e^{+sT_i} \\ \frac{1}{2}\left(1 - \frac{Z_{i+1}}{Z_i}\right)e^{-sT_i} & \frac{1}{2}\left(1 + \frac{Z_{i+1}}{Z_i}\right)e^{+sT_i} \end{bmatrix} \qquad 3.5$$

as the transmission matrix for the i:i+1 interface, several layers may now be combined by multiplying the transmission matrices in cascade, giving:-

$$\left[\frac{T_{n+1}}{1}\right] = \left[\frac{T_{n+1}}{n}\right] x \left[\frac{T_n}{n-1}\right] x \ldots x \left[\frac{\overline{T}_{i+1}}{i}\right] x \ldots . x \left[\frac{\overline{T}_3}{2}\right] x \left[\frac{\overline{T}_2}{1}\right] \qquad 3.6$$

where $\left[\frac{T_{n+1}}{1}\right]$ relates the force components $\overline{F}_{(n+1)0}$, $\overline{B}_{(n+1)0}$, to $\overline{F}_{10}$, $\overline{B}_{10}$.

Defining

$$\begin{bmatrix} \\ \overline{T}_{\underline{n+1}} \\ \\ \overline{1} \end{bmatrix} = \begin{bmatrix} \overline{T}_{11} & \overline{T}_{12} \\ \overline{T}_{21} & \overline{T}_{22} \end{bmatrix} \qquad 3.7$$

gives

$$\begin{bmatrix} \overline{F}_{(n+1)0} \\ \overline{B}_{(n+1)0} \end{bmatrix} = \begin{bmatrix} \overline{T}_{11} & \overline{T}_{12} \\ \overline{T}_{21} & \overline{T}_{22} \end{bmatrix} \begin{bmatrix} \overline{F}_{10} \\ \overline{B}_{10} \end{bmatrix} \qquad 3.8$$

In a similar manner to the one layer case, force components $\overline{F}_{10}$ and $\overline{B}_{(n+1)0}$ may be considered as the input's to the layer system. Correspondingly, force-components $\overline{B}_{10}$ and $\overline{F}_{(n+1)0}$ become the outputs. This is expressed as follows:-

$$\begin{bmatrix} \overline{F}_{(n+1)0} \\ \overline{B}_{10} \end{bmatrix} = \begin{bmatrix} \\ \overline{U}_{\underline{n+1}} \\ \\ \overline{1} \end{bmatrix} \begin{bmatrix} \overline{F}_{10} \\ \overline{B}_{(n+1)0} \end{bmatrix} \qquad 3.9$$

where,

$$\begin{bmatrix} \overline{U}_{n+1} \\ \overline{1} \end{bmatrix} = \begin{bmatrix} \overline{U}_{11} & \overline{U}_{12} \\ \overline{U}_{21} & \overline{U}_{22} \end{bmatrix} \qquad 3.10$$

and, solving equations 3.8 and 3.9 gives,

$$\overline{U}_{11} = \overline{T}_{11} - (\overline{T}_{21} \cdot \overline{T}_{12}) / \overline{T}_{22}$$

$$\overline{U}_{12} = \overline{T}_{12} / \overline{T}_{22}$$

$$\overline{U}_{21} = -\overline{T}_{21} / \overline{T}_{22}$$

$$\overline{U}_{22} = 1 / \overline{T}_{22} \qquad 3.11$$

The T_{ij} terms of equation 3.7 comprise scalar constants and both e^{-sT} and e^{+sT} terms. Since this is a causal, linear system, the $\overline{U}_{ij}$ terms of equations 3.10 and 3.11 must comprise only scalar and e^{-sT} terms. The presence of e^{+sT} terms would render the system non-

causal. It may be shown that $\overline{U}_{ij}$ terms do represent a causal system as follows.

Each $\overline{T}_{ij}$ in equation 3.7 is a polynomial function, while each $\overline{U}_{ij}$ term in equations 3.11 is a ratio of polynomials. It may be shown by evaluating several $\left[\overline{T}_{\frac{i+1}{1}}\right]$ products in equation 3.6 for general layer configurations that polynomial $\overline{T}_{22}$ will always contain the largest e^{+sT} term, and that this has the value,

$$e^{+(sT_{max})} = e^{+(s\sum_{i=1}^{n} T_i)} \qquad 3.12$$

Thus the e^{+sT} terms may be cleared from the $\overline{U}_{ij}$ terms by multiplying the numerator and denominator polynomials by $e^{-sT_{max}}$.

It may also be shown that the term $\overline{U}_{11}$, when expressed as,

$$\overline{U}_{11} = \frac{\overline{T}_{11}\cdot\overline{T}_{22} - \overline{T}_{21}\cdot\overline{T}_{12}}{\overline{T}_{22}} \qquad 3.13$$

reduces to

$$\overline{U}_{11} = K/\overline{T}_{22} \qquad 3.14$$

where K is a scalar constant. The value of K is given by:-

$$K = Z_{n+1}/Z_1 \qquad 3.15$$

that is, K is the ratio of the acoustic impedances of the $n+1^{th}$ layer to the 1^{st} layer in Fig 3.1.

Equation 3.15 may be proved by induction, as follows. The transmission matrix for mechanical waves travelling between layer 1 and layer i+1, $\begin{bmatrix} \overline{T}_{\frac{i+1}{1}} \end{bmatrix}$ is

$$\begin{bmatrix} \overline{T}_{\frac{i+1}{1}} \end{bmatrix} = \begin{bmatrix} \overline{T}_{\frac{i+1}{i}} \end{bmatrix} \times \begin{bmatrix} \overline{T}_{\frac{i}{1}} \end{bmatrix} \qquad 3.16$$

where $\left[\overline{T}_{\frac{i+1}{i}}\right]$ is defined by equation 3.5, thus,

$$\begin{bmatrix} \overline{T}_{11} & \overline{T}_{12} \\ \overline{T}_{21} & \overline{T}_{22} \end{bmatrix}_{\frac{i+1}{1}} = \left[\overline{T}_{\frac{i+1}{i}}\right] * \begin{bmatrix} \overline{T}_{11} & \overline{T}_{12} \\ \overline{T}_{21} & \overline{T}_{22} \end{bmatrix}_{\frac{i}{1}} \qquad 3.17$$

and substituting from equation 3.5 gives,

$$\overline{T}_{11}\left(\frac{i+1}{1}\right) = \frac{1}{2}\left(\left(1+\frac{Z_{i+1}}{Z_i}\right)\overline{T}_{11}\left(\frac{i}{1}\right)e^{-sT_i} + \left(1-\frac{Z_{i+1}}{Z_i}\right)\overline{T}_{21}\left(\frac{i}{1}\right)e^{+sT_i}\right)$$

$$\overline{T}_{21}\left(\frac{i+1}{1}\right) = \frac{1}{2}\left(\left(1-\frac{Z_{i+1}}{Z_i}\right)\overline{T}_{11}\left(\frac{i}{1}\right)e^{-sT_i} + \left(1+\frac{Z_{i+1}}{Z_i}\right)\overline{T}_{21}\left(\frac{i}{1}\right)e^{+sT_i}\right)$$

$$\overline{T}_{12}\left(\frac{i+1}{1}\right) = \frac{1}{2}\left(\left(1+\frac{Z_{i+1}}{Z_i}\right)\overline{T}_{12}\left(\frac{i}{1}\right)e^{-sT_i} + \left(1-\frac{Z_{i+1}}{Z_i}\right)\overline{T}_{22}\left(\frac{i}{1}\right)e^{+sT_i}\right)$$

$$\overline{T}_{22}\left(\frac{i+1}{1}\right) = \frac{1}{2}\left(\left(1-\frac{Z_{i+1}}{Z_i}\right)\overline{T}_{12}\left(\frac{i}{1}\right)e^{-sT_i} + \left(1+\frac{Z_{i+1}}{Z_i}\right)\overline{T}_{22}\left(\frac{i}{1}\right)e^{+sT_i}\right) \qquad 3.18$$

The product terms, $\overline{T}_{11(\frac{i+1}{1})}$ $\overline{T}_{22(\frac{i+1}{1})}$ and $\overline{T}_{12(\frac{i+1}{1})}$ $\overline{T}_{21(\frac{i+1}{1})}$ may be evaluated from equations 3.18 to give, (see next page). 3.19

3.20

Subtracting equation 3.20 from equation 3.19 and factorising gives:-

$$(\overline{T}_{11}\overline{T}_{22} - \overline{T}_{12}\overline{T}_{21})_{(\frac{i+1}{1})} = (\overline{T}_{11}\overline{T}_{22} - \overline{T}_{12}\overline{T}_{21})_{(\frac{i}{1})} *$$

$$* \frac{1}{4}((1+\frac{Z_{i+1}}{Z_i})^2 - (1-\frac{Z_{i+1}}{Z_i})^2) \qquad 3.21$$

and thus,

$$(\overline{T}_{11}\overline{T}_{22} - \overline{T}_{12}\overline{T}_{21})_{(\frac{i+1}{1})} = (\overline{T}_{11}\overline{T}_{22} - \overline{T}_{12}\overline{T}_{21})_{(\frac{i}{1})}(\frac{Z_{i+1}}{Z_i})$$

3.22

This equation may now be evaluated as follows. From equation 3.5 , the $\overline{T}_{ij}$ matrix for a two layer

$$\overline{T}_{11}\left(\frac{i+1}{1}\right)\overline{T}_{22}\left(\frac{i+1}{1}\right) = \frac{1}{4}\left(\left(1-\left[\frac{\overline{Z}_{i+1}}{Z_i}\right]^2\right)e^{-2sT_i}\overline{T}_{11}\left(\frac{i}{1}\right)\overline{T}_{12}\left(\frac{i}{1}\right)+\left[1-\frac{Z_{i+1}}{Z_i}\right]^2\overline{T}_{12}\left(\frac{i}{1}\right)\overline{T}_{21}\left(\frac{i}{1}\right) +\right.$$

$$\left. + \left[1+ \frac{Z_{i+1}}{Z_i}\right]^2\overline{T}_{11}\left(\frac{i}{1}\right)\overline{T}_{22}\left(\frac{i}{1}\right) + \left(1-\left[\frac{\overline{Z}_{i+1}}{Z_i}\right]^2\right)e^{+2sT_i}\overline{T}_{21}\left(\frac{i}{1}\right)\overline{T}_{22}\left(\frac{i}{1}\right)\right)$$

3.19

$$\overline{T}_{12}\left(\frac{i+1}{1}\right)\overline{T}_{21}\left(\frac{i+1}{1}\right) = \frac{1}{4}\left(\left(1-\left[\frac{\overline{Z}_{i+1}}{Z_i}\right]^2\right)e^{-2sT_i}\overline{T}_{11}\left(\frac{i}{1}\right)\overline{T}_{12}\left(\frac{i}{1}\right)+\left[1- \frac{Z_{i+1}}{z_i}\right]^2\overline{T}_{12}\left(\frac{i}{1}\right)\overline{T}_{21}\left(\frac{i}{1}\right) +\right.$$

$$\left. + \left[1- \frac{Z_{i+1}}{Z_i}\right]^2\overline{T}_{11}\left(\frac{i}{1}\right)\overline{T}_{22}\left(\frac{i}{1}\right) + \left(1-\left[\frac{\overline{Z}_{i+1}}{Z_i}\right]^2\right)e^{+2sT_i}\overline{T}_{21}\left(\frac{i}{1}\right)\overline{T}_{22}\left(\frac{i}{1}\right)\right)$$

3.20

system is,

$$\begin{bmatrix} \overline{T}_{2} \\ \overline{1} \end{bmatrix} = \frac{1}{2} \begin{bmatrix} (1 + \frac{Z_2}{Z_1})e^{-sT_1} & (1 - \frac{Z_2}{Z_1})e^{+sT_1} \\ (1 - \frac{Z_2}{Z_1})e^{-sT_1} & (1 + \frac{Z_2}{Z_1})e^{+sT_1} \end{bmatrix} \qquad 3.23$$

Thus evaluating the expresssion,

$$\overline{T}_{11}\overline{T}_{22} - \overline{T}_{12}\overline{T}_{21} \qquad 3.24$$

gives,

$$\overline{T}_{11}\overline{T}_{22} - \overline{T}_{12}\overline{T}_{21} = \frac{1}{4}\left((1 + \frac{Z_2}{Z_1})^2 - (1 - \frac{Z_2}{Z_1})^2\right) \qquad 3.25$$

which reduces to,

$$\overline{T}_{11}\overline{T}_{22} - \overline{T}_{12}\overline{T}_{21} = Z_2 \,/\, Z_1 \qquad 3.36$$

Thus equation 3.15 has been proved for the two layer case. This may be extended to cover any number of layers by the method of induction, using equation 3.22.

Thus equations 3.6, 3.9, 3.10, 3.11 and 3.15 show how a general multilayered system may be reduced to a simple acoustic lattice system. This is shown in Fig 3.2.

This method is similar to that proposed by ROBINSON and TREITEL (54), to obtain the spectral function of a layered system. However, in this application, the resultant polynomials must be developed in Laplace transforms to comply with the transducer model of Chapter 2.

From reference 9, it is apparent that the polynomial pairs, $\overline{T}_{11}$, $\overline{T}_{22}$ and $\overline{T}_{12}$,$\overline{T}_{21}$ are reverse polynomials. That is,

if $\overline{T}_{11}$ is a polynomial of the form,

$$\overline{T}_{11} = t_1 e^{-sD_1} + t_2 e^{-sD_2} + \ldots\ldots + t_n e^{+sD_n} \qquad 3.27$$

where t_i are scalar coefficients, and D_i are delays resulting from the multiplicative combinations of the layer propagation delays, $\overline{T}_i$; then,

$$\overline{T}_{22} = t_n\, e^{-sD_n} + \ldots\ldots\ldots + t_2\, e^{+sD_2} + t_1\, e^{+sD_1} \qquad 3.28$$

and similarly for $\overline{T}_{12}$, $\overline{T}_{21}$.

This condition is useful in reducing the degree of calculation required to generate the $\overline{T}_{ij}$ polynomials and hence the $\overline{U}_{ij}$ transfer functions. Consider the following case;

Let $\left[\begin{matrix}\overline{T}_i \\ \overline{1}\end{matrix}\right]$ be the transmission matrix for mechanical waves propagating between layers 1 and i. Then, from equation 3.6, the transmission matrix for waves travelling between layers 1 and i+1, $\left[\begin{matrix}\overline{T}_{i+1} \\ \overline{1}\end{matrix}\right]$ is given by equations 3.16 and 3.17. The recurrence relationships between the $\left[\begin{matrix}\overline{T}_i \\ \overline{1}\end{matrix}\right]$ and $\left[\begin{matrix}\overline{T}_{i+1} \\ \overline{1}\end{matrix}\right]$ transmission matrices are given in equations 3.18.

From equations 3.18, it may be seen that the polynomial pairs, $\bar{T}_{11}$, $\bar{T}_{21}$ and $\bar{T}_{12}$, $\bar{T}_{22}$ are generated independently. Thus, either polynomial pair may be generated for a multilayer system, without generating the other pair. The reverse-polynomial property, given in equations 3.27 and 3.28, may then be used to generate the second polynomial pair directly from the first pair. This method approximately halves the amount of calculation required to generate the T-matrix for a multilayer system.

Thus, any multilayer system of the form shown in Fig 3.1 may be modelled by the appropriate T and U matrices, and may be represented by the system of Fig 3.2.

The relationships presented in equations 3.12, 3.14, 3.15, 3.17, 3.18 and 3.28 may be used to significantly reduce the amount of calculation required to generate these matrices.

3.3 THE MULTILAYERED TRANSDUCER MODEL

Consider the general multilayered transducer system shown in Fig 3.3. The assumptions regarding acoustic impedance, losses and propagation delays, which were made in Chapter 2 and the preceding section, also apply to this case. Thus, the system of Fig 3.3 may be re-drawn by combining Figs 2.11 and 3.3 as shown in Fig 3.4.

To reduce the complexity of the diagram, the following assumptions are made:-

1. The positive charge feedback section has been replaced by the single block $\bar{Y}$.
2. Superscripts F and B have been adopted for the $\bar{U}$-matrix components, $\bar{U}_{ij}$ to distinguish between front and rear face layers.
3. The positive/negative subscript notation has been extended for the layers, so that layers with a positive subscript are assumed to be front face layers and those with a negative subscript are rear face layers. Thus, for example, the $+i^{th}$ layer is the i^{th} layer from the front face of the transducer and similarly, the $-i^{th}$ layer is

the i^{th} layer from the rear face of the transducer. (This notation also applies to the properties of each layer.)

Thus, equations describing the system may be written as follows:-

$$\begin{bmatrix} \bar{F}_{10} \\ \bar{B}_{-10} \\ \\ \bar{V}_t \end{bmatrix} = \begin{bmatrix} \bar{P}_{11} & \bar{P}_{12} & \bar{P}_{13} \\ \bar{P}_{21} & \bar{P}_{22} & \bar{P}_{23} \\ \bar{P}_{31} & \bar{P}_{32} & \bar{P}_{33} \end{bmatrix} \begin{bmatrix} \bar{B}_{10} \\ \bar{F}_{-10} \\ \\ \bar{V}_E \end{bmatrix} \qquad 3.29$$

$$\begin{bmatrix} \bar{F}_{(n+1)0} \\ \bar{B}_{10} \end{bmatrix} = \begin{bmatrix} \bar{U}^F_{11} & \bar{U}^F_{12} \\ \bar{U}^F_{21} & \bar{U}^F_{22} \end{bmatrix} \begin{bmatrix} \bar{F}_{10} \\ \bar{B}_{(n+1)0} \end{bmatrix} \qquad 3.30$$

$$\begin{bmatrix} \bar{B}_{-(m+1)0} \\ \bar{F}_{-10} \end{bmatrix} = \begin{bmatrix} \bar{U}^B_{11} & \bar{U}^B_{12} \\ \bar{U}^B_{21} & \bar{U}^B_{22} \end{bmatrix} \begin{bmatrix} \bar{B}_{-10} \\ \bar{F}_{-(m+1)0} \end{bmatrix} \qquad 3.31$$

where equation 3.29 is given by equations 2.30 and 2.31 in Chapter 2, and equations 3.30 and 3.31 come from the preceding section.

Clearly, the multilayer system of Fig 3.4 may be considered as a 3-port system, with a describing matrix of the form,

$$\begin{bmatrix} \overline{F}_{(n+1)0} \\ \overline{B}_{-(m+1)0} \\ \overline{V}_t \end{bmatrix} = [\overline{W}] \begin{bmatrix} \overline{B}_{(n+1)0} \\ \overline{F}_{-(m+1)0} \\ \overline{V}_E \end{bmatrix} \qquad 3.32$$

where $\overline{B}_{(n+1)0}$, $\overline{F}_{-(m+1)0}$, and $\overline{V}_E$ are the inputs to the system, and $\overline{F}_{(n+1)0}$, $\overline{B}_{-(m+1)0}$ and $\overline{V}_t$ the outputs, and,

$$[\overline{W}] = \begin{bmatrix} \overline{W}_{11} & \overline{W}_{12} & \overline{W}_{13} \\ \overline{W}_{21} & \overline{W}_{22} & \overline{W}_{23} \\ \overline{W}_{31} & \overline{W}_{32} & \overline{W}_{33} \end{bmatrix} \qquad 3.33$$

where the $\overline{W}_{ij}$ elements are obtained by solving equations 3.29, 3.30 and 3.31.

Firstly, equations 3.30 and 3.31 are expanded and the terms $\overline{F}_{10}$, $\overline{B}_{-10}$ are substituted from equation 3.29,

$$\overline{F}_{(n+1)0} = \overline{U}^{F}_{11}(\overline{P}_{11}\cdot\overline{B}_{10}+\overline{P}_{12}\cdot\overline{F}_{-10}+\overline{P}_{13}\cdot\overline{V}_{E}) + \overline{U}^{F}_{12}\cdot\overline{B}_{(n+1)0} \quad (i)$$

$$\overline{B}_{10} = \overline{U}^{F}_{21}(\overline{P}_{11}\cdot\overline{B}_{10}+\overline{P}_{12}\cdot\overline{F}_{-10}+\overline{P}_{13}\cdot\overline{V}_{E}) + \overline{U}^{F}_{22}\cdot\overline{B}_{(n+1)0} \quad (ii)$$

$$\overline{B}_{-(m+1)0} = \overline{U}^{B}_{11}(\overline{P}_{21}\cdot\overline{B}_{10}+\overline{P}_{22}\cdot\overline{F}_{-10}+\overline{P}_{23}\cdot\overline{V}_{E}) + \overline{U}^{B}_{12}\cdot\overline{F}_{-(m+1)0} \quad (iii)$$

$$F_{-10} = U^{B}_{21}(\overline{P}_{21}\cdot\overline{B}_{10}+\overline{P}_{22}\cdot\overline{F}_{-10}+\overline{P}_{23}\cdot\overline{V}_{E}) + \overline{U}^{B}_{22}\cdot\overline{F}_{-(m+1)0} \quad (iv)\ 3.34$$

Next, equations 3.34, (ii) and (iv) are substituted into each other, giving,

$$\bar{B}_{10} = \frac{((\bar{U}^F_{21}\bar{P}_{12}\bar{U}^B_{22})\bar{F}_{-(m+1)0} + \bar{U}^F_{21}(\bar{P}_{12}\bar{U}^B_{21}\bar{P}_{23} + \bar{P}_{13}(1 - \bar{U}^B_{21}\bar{P}_{22}))\bar{V}_E + (\bar{U}^F_{22}(1 - \bar{U}^B_{21}\bar{P}_{22}))\bar{B}_{(n+1)0})}{((1 - \bar{U}^F_{21}\bar{P}_{11})(1 - \bar{U}^B_{21}\bar{P}_{12}) - \bar{U}^F_{21}\bar{P}_{12}\bar{U}^B_{21}\bar{P}_{21})} \quad \text{(i)}$$

$$\bar{F}_{-10} = \frac{((\bar{U}^B_{21}\bar{P}_{21}\bar{U}^F_{22})\bar{B}_{(n+1)0} + \bar{U}^B_{21}(\bar{P}_{21}\bar{U}^F_{21}\bar{P}_{13} + \bar{P}_{23}(1 - \bar{U}^F_{21}\bar{P}_{11}))\bar{V}_E + (\bar{U}^B_{22}(1 - \bar{U}^F_{21}\bar{P}_{11}))\bar{F}_{-(m+1)0})}{((1 - \bar{U}^F_{21}\bar{P}_{11})(1 - \bar{U}^B_{21}\bar{P}_{22}) - \bar{U}^F_{21}\bar{P}_{12}\bar{U}^B_{21}\bar{P}_{21})} \quad \text{(ii)}$$

3.35

Now, equations 3.35 (i) and (ii) may be substituted into equations 3.34 (i) and (iii) and 3.29 to give the $\overline{W}_{ij}$ terms, thus,

$$\overline{W}_{11} = (\overline{U}^B_{21}(\overline{U}^F_{11}\overline{U}^F_{22}-\overline{U}^F_{12}\overline{U}^F_{21})(\overline{P}_{12}\overline{P}_{21}-\overline{P}_{11}\overline{P}_{22})+\overline{P}_{11}\overline{U}^F_{11}\overline{U}^F_{22}+ + \overline{U}^F_{12}(1-\overline{P}_{22}\overline{U}^B_{21}-\overline{P}_{11}\overline{U}^F_{21})) / \overline{W}_D \quad \text{(i)}$$

$$\overline{W}_{12} = \overline{U}^F_{11}\overline{U}^B_{22}\overline{P}_{12} / \overline{W}_D \quad \text{(ii)}$$

$$\overline{W}_{13} = \overline{U}^F_{11}(\overline{U}^B_{21}(\overline{P}_{12}\overline{P}_{33} - \overline{P}_{13}\overline{P}_{22}) + \overline{P}_{13}) / \overline{W}_D \quad \text{(iii)}$$

$$\overline{W}_{21} = \overline{U}^B_{11}\overline{U}^F_{22}\overline{P}_{21} / \overline{W}_D \quad \text{(iv)}$$

$$\overline{W}_{22} = (\overline{U}^F_{21}(\overline{U}^B_{11}\overline{U}^B_{22}-\overline{U}^B_{12}\overline{U}^B_{21})(\overline{P}_{12}\overline{P}_{21}-\overline{P}_{11}\overline{P}_{22})+\overline{P}_{22}\overline{U}^B_{11}\overline{U}^B_{22}+ + \overline{U}^B_{12}(1-\overline{P}_{11}\overline{U}^F_{21}-\overline{P}_{22}\overline{U}^B_{21})) / \overline{W}_D \quad \text{(v)}$$

$$\overline{W}_{23} = \overline{U}^B_{11}(\overline{U}^F_{21}(\overline{P}_{21}\overline{P}_{13} - \overline{P}_{11}\overline{P}_{23}) + \overline{P}_{23}) / \overline{W}_D \quad \text{(vi)}$$

$$\overline{W}_{31} = (\overline{P}_{31}\overline{U}^F_{22}(1 - \overline{U}^B_{21}\overline{P}_{22})+ \overline{P}_{31}\overline{U}^B_{21}\overline{P}_{21}\overline{U}^F_{22}) / \overline{W}_D \quad \text{(vii)}$$

$$\overline{W}_{32} = (\overline{P}_{32}\overline{U}^B_{22}(1-\overline{U}^F_{21}\overline{P}_{11}) + \overline{P}_{32}\overline{U}^F_{21}\overline{P}_{12}\overline{U}^F_{22}) / \overline{W}_D \quad \text{(viii)}$$

3.36

$$\bar{W}_{33} = (\bar{P}_{33}+\bar{U}^F_{21}(\bar{P}_{31}\bar{P}_{13}-\bar{P}_{11}\bar{P}_{33}) + \bar{U}^B_{21}(\bar{P}_{23}\bar{P}_{32}-\bar{P}_{22}\bar{P}_{33})+$$

$$+ \bar{U}^F_{21}\bar{U}^B_{21}(\bar{P}_{31}(\bar{P}_{12}\bar{P}_{23}-\bar{P}_{13}\bar{P}_{22}) + \bar{P}_{32}(\bar{P}_{21}\bar{P}_{13}-\bar{P}_{23}\bar{P}_{11})+$$

$$+ \bar{P}_{33}(\bar{P}_{11}\bar{P}_{22}-\bar{P}_{12}\bar{P}_{21})))/ \bar{W}_D \qquad \text{(ix)}$$

3.36

where $\bar{W}_D$ is a common denominator term, given by:-

$$\bar{W}_D = (1-\bar{U}^F_{21}\bar{P}_{11})(1-\bar{U}^B_{21}\bar{P}_{22}) - \bar{U}^F_{21}\bar{U}^B_{21}\bar{P}_{12}\bar{P}_{21} \qquad 3.37$$

Equations 3.36 and 3.37 are the complete solution for the multilayered transducer system of Fig 3.1 . The procedure adopted in this and the preceding section may be directly compared with that of LEWIS (38).

Lewis considers a piezoelectric transducer with multiple front-face layers only. However, the basic transducer configuration is identical to the case considered in Chapter 2. The major difference between the methods is in the manipulation of the layers. Lewis does not attempt to model the layers independ-

ently and consequently produces a system matrix with dimensions which depend on the number of layers considered. It is necessary to invert the system matrix to obtain the desired system response. This is a straightforward procedure for only a few layers, but becomes increasingly complex as the number of layers increases. It is thus necessary to revert to numerical inversion techniques. This does not however, allow the formation of the system transfer functions, with a consequent loss of information.

The method of section 3.2 avoids this problem by considering the transducer and layer systems independently, and then relating the system inputs and outputs algebraically. However, for cases with several layers, the degree of algebraic manipulation required is excessive. It is possible to simplify equations 3.36 and 3.37 for the more important system transfer functions. This is dealt with in the next section.

3.4 REDUCTION OF THE MULTILAYER SYSTEM TRANSFER FUNCTIONS

The $\overline{W}_{ij}$ transfer functions of equations 3.36 and 3.37 describe the general multilayer transducer system. However, in practice, only three cases are of great importance. These are the transmitter, $\overline{W}_{13}$, the receiver, $\overline{W}_{31}$, and the voltage across the transmitter $\overline{W}_{33}$. It may be observed from equations 3.36 and 3.37 that these three cases require substantial manipulation of the $\overline{P}_{ij}$, $\overline{U}^{F}_{ij}$ and $\overline{U}^{B}_{ij}$ transfer functions to obtain the $\overline{W}_{ij}$ transfer functions in mixed differential/delay format. In particular, products of the form, $\overline{P}_{ij} \cdot \overline{P}_{ke}$ involve complicated algebraic manipulations.

This may, however, be simplified by rederiving the multilayer transducer transfer functions from a simpler level.

Consider the multilayer diagram shown in Fig 3.5. This uses the acoustic lattice of Fig 2.8 to model the transducer. It is assumed that the input at the rear acoustic port, $F_{-(m+1)0}$ is zero, and that the rear

acoustic output, $\overline{B}_{-(m+1)0}$ is not required. Further, for transmitter cases, it is assumed that the front-face input force, $\overline{B}_{(n+1)0}$ is zero, and that in reception, the electrical excitation, $\overline{V}_E$ is zero and the front face output force, $\overline{F}_{(m+1)0}$ is not required.

The complexity of Fig 3.5 may be reduced by incorporating the $\overline{U}^F_{21}$ and $\overline{U}^B_{21}$ transfer function blocks into the transducer lattice. Fig 3.6A shows the part lattice section for the rear acoustic port. From this figure the following relationships are apparent.

$$\overline{F}_{-10} = \overline{U}^B_{21}\overline{B}_{-10} \qquad 3.38$$

$$\overline{B}_{-10} = R_{-1}\overline{F}_{-10} + (1-R_{-1})\overline{B}_{t0} + \left(\frac{R_{-1}+1}{2}\right)h\overline{Q}_t \qquad 3.39$$

Combining these gives:-

$$\overline{F}_{-10} = \left[\frac{\overline{U}^B_{21}}{1-R_{-1}\overline{U}^B_{21}}\right]\left((1-R_{-1})\overline{B}_{t0} + \left(\frac{R_{-1}+1}{2}\right)h\overline{Q}_t\right) \qquad 3.40$$

This is shown in Fig 3.6B.

Thus the rear port of the acoustic lattice has been simplified.

This method may also be applied to the front-face as shown in Fig 3.7A . In this case, the relevant describing equations are

$$\overline{F}_{(n+1)0} = \overline{U}^{F}_{11}\overline{F}_{10} \qquad 3.41$$

$$\overline{B}_{10} = \overline{U}^{F}_{21}\overline{F}_{10} + \overline{U}^{F}_{22}\overline{B}_{(n+1)0} \qquad 3.42$$

$$\overline{F}_{10} = R_1\overline{B}_{10} + (1-R_1)\overline{F}_{t\ell_t} + (\frac{R_1-1}{2})h\overline{Q}_t \qquad 3.43$$

Combining equations 3.42 and 3.43 gives:-

$$\overline{F}_{10} = \frac{R_1\overline{U}^{F}_{22}\overline{B}_{(n+1)0} + (1-R_1)\overline{F}t\ell_t + (\frac{R_1-1}{2})h\overline{Q}_t}{1 - R_1\overline{U}^{F}_{21}} \qquad 3.44$$

$$\overline{B}_{10} = \frac{(\overline{U}^F_{22}\overline{B}_{(n+1)0}+\overline{U}^F_{21}((1-R_1)\overline{F}_{t\ell_t}+(\frac{R_1-1}{2})h\overline{Q}_t))}{1 - R_1\overline{U}^F_{21}} \qquad 3.45$$

Equations 3.41, 3.44 and 3.45 are shown in Fig 3.7B . The complete modified lattice system is shown in . Fig 3.8 .

From this diagram, the following equations relating the force components and the charge are apparent.

$$\overline{F}_{t0} =((\frac{R_{-1}+1}{2})+(1+R_{-1})(\frac{R_{-1}-1}{2})(\frac{\overline{U}^B_{21}}{1-R_{-1}\overline{U}^B_{21}}))h\overline{Q}_t +$$
$$+((\frac{\overline{U}^B_{21}}{1-R_{-1}\overline{U}^B_{21}})(1-R_{-1})(1+R_{-1}) - R_{-1})e^{-sT_t}\overline{B}_{t\ell_t}$$
$$3.46$$

$$\overline{B}_{t\ell_t} = ((\frac{R_1+1}{2})+(1+R_1)(\frac{R_1-1}{2})(\frac{\overline{U}^F_{21}}{1-R_1\overline{U}^F_{21}}))h\overline{Q}_t +$$
$$+ ((\frac{\overline{U}^F_{21}}{1-\overline{R}_1\overline{U}^F_{21}})(1+R_1)(1-R_{-1}) - R_1)e^{-sT}\overline{F}_{t0} +$$
$$+ (1+R_1)(\frac{\overline{U}^F_{22}}{1-R_1\overline{U}^F_{21}})\overline{B}_{(n+1)0} \qquad 3.47$$

$$\overline{F}_{(n+1)0} = \left(\frac{\overline{U}^F_{11}\cdot\overline{U}^F_{22}}{1-R_1\overline{U}^F_{21}}\right)\left(R_1\overline{B}_{(n+1)0} + (1-R_1)e^{-sT_t}\overline{F}_{t0} + \right.$$

$$\left. + \left(\frac{R_1-1}{2}\right)h\overline{Q}_t\right) \qquad 3.48$$

However, only three cases will be considered; the force output from a transmitter, the voltage across a transmitter and the voltage across a receiver.

Thus several of the blocks of Fig 3.8 become redundant. For the transmitter, it was assumed earlier that the force input $\overline{B}_{(n+1)0}$ is zero. This corresponds to removing the last terms in equations 3.47 and 3.48 and the blocks labelled 2 and 3 in Fig 3.8 . In the receiver, the force output from the transducer $\overline{F}_{(n+1)0}$, is neglected. So, equation 3.48 does not apply and the blocks labelled 1 and 2 in Fig 3.8 may be omitted. To generalise the analysis, these terms will be included for the present and the appropriate terms set to zero when the specific transfer functions are considered.

Equations 3.46 and 3.47 may be rearranged to give:-

$$\begin{bmatrix} \overline{F}_{t0} \\ \\ \overline{B}_{t\ell_t} \end{bmatrix} = \begin{bmatrix} \overline{Y}_{11} & \overline{Y}_{12} \\ \\ \overline{Y}_{21} & \overline{Y}_{22} \end{bmatrix} \begin{bmatrix} h\overline{Q}_t \\ \\ \overline{B}_{(n+1)0} \end{bmatrix} \qquad 3.49$$

where

$$\overline{Y}_{11} = \left(\left(\frac{R_{-1}+1}{2}\right)+(1+R_{-1})\left(\frac{R_{-1}-1}{2}\right)\left(\frac{\overline{U}^B_{21}}{1-R_{-1}\overline{U}^B_{21}}\right)+\right.$$

$$+ \left(\left(\frac{\overline{U}^B_{21}}{1-R_{-1}\overline{U}^B_{21}}\right)(1-R_{-1})(1+R_{-1}) - R_{-1}\right) *$$

$$\left. * \left(\left(\frac{R_1+1}{2}\right)+(1+R_1)\left(\frac{R_1-1}{2}\right)\left(\frac{\overline{U}^F_{21}}{1-R_1\overline{U}^F_{21}}\right)\right)e^{-sT_t}\right) / \overline{Y}_D \qquad (i)$$

$$\overline{Y}_{12} = \left(\left(\frac{\overline{U}^B_{21}}{1-R_{-1}\overline{U}^B_{21}}\right)(1-R_{-1})(1+R_{-1}) - R_{-1}\right)e^{-sT_t}\ (1+R_1) *$$

$$* \left(\frac{\overline{U}^F_{22}}{1-R_1\overline{U}^F_{22}}\right) / \overline{Y}_D \qquad (ii)$$

$$\bar{Y}_{21} = \left(\left(\frac{R_1+1}{2}\right)+(1+R_1)\left(\frac{R_1-1}{2}\right)\left(\frac{\bar{U}^F_{21}}{1-R_1\bar{U}^F_{21}}\right)+\right.$$

$$+\left(\left(\frac{\bar{U}^F_{21}}{1-R_1\bar{U}^F_{21}}\right)(1+R_1)(1-R_1) - R_1\right) *$$

$$\left. * \left(\left(\frac{R_{-1}+1}{2}\right)+(1+R_{-1})\left(\frac{R_{-1}-1}{2}\right)\left(\frac{\bar{U}^B_{21}}{1-R_{-1}\bar{U}^B_{21}}\right)\right)e^{-sT_t}\right) / \bar{Y}_D$$

(iii)

$$\bar{Y}_{22} = (1+R_1)\left(\frac{\bar{U}^F_{22}}{1-R_1\bar{U}^F_{21}}\right) / \bar{Y}_D \qquad \text{(iv)}$$

3.50

and

$$\bar{Y}_D = 1 -\left(\left(\frac{\bar{U}^F_{21}}{1-R_1\bar{U}^F_{21}}\right)(1+R_1)(1-R_1) - R_1\right) *$$

$$* \left(\left(\frac{\bar{U}^B_{21}}{1-R_{-1}\bar{U}^B_{21}}\right)(1+R_{-1})(1-R_{-1}) - R_{-1}\right)e^{-2sT_t} \qquad 3.51$$

These equations may be further reduced by substituting for the $\bar{U}_{ij}^{F/B}$ terms from equation 3.11 .

Thus defining $[\bar{T}^F]$ and $[\bar{T}^B]$ as the front and rear face layer matrices respectively, the following relationships are apparent.

$$\frac{\bar{U}_{21}^B}{1-R_{-1}\bar{U}_{21}^B} = \frac{-\bar{T}_{21}^B}{\bar{T}_{22}^B+R_{-1}\bar{T}_{21}^B} \qquad 3.52$$

$$\frac{\bar{U}_{21}^F}{1-R_1\bar{U}_{21}^F} = \frac{-\bar{T}_{21}^F}{\bar{T}_{22}^F+R_1\bar{T}_{21}^F} \qquad 3.53$$

So, substituting into equation 3,50 and 3.51 and rearranging the terms gives:-

$$\bar{Y}_{11} = ((\bar{T}_{22}^F+R_1\bar{T}_{21}^F)((\frac{R_{-1}+1}{2})(\bar{T}_{22}^B+R_{-1}\bar{T}_{21}^B)-(I+R_{-1})(\frac{R_{-1}-1}{2})*$$

$$\bar{T}_{21}^B)- (\bar{T}_{21}^B(1-R_{-1})(1+R_{-1}) + R_{-1}(\bar{T}_{22}^B+R_{-1}\bar{T}_{21}^B)) *$$

$$*((\frac{R_1+1}{2})(\bar{T}_{22}^F+R_1\bar{T}_{21}^F) - (1+R_1)(\frac{R_1-1}{2})\bar{T}_{21}^F)e^{-sT_t}) /$$

$$/ Y_D \qquad (i)$$

$$\overline{Y}_{12} = -(\overline{T}^B_{21}(1-R_{-1})(1+R_{-1})+R_{-1}(\overline{T}^B_{22}+R_{-1}\overline{T}^B_{21}))e^{-sT_t}(1+R_1)/\overline{Y}_D$$

(ii)

$$\overline{Y}_{21} = ((\overline{T}^B_{22}+R_{-1}\overline{T}^B_{21})((\frac{R_1+1}{2})(\overline{T}^F_{22}+R_1\overline{T}^F_{21})-(1+R_1)(\frac{R_1-1}{2})\overline{T}^F_{21})-$$

$$-(\overline{T}^F_{21}(1-R_1)(1+R_1)+R_1(\overline{T}^F_{22}+R_1\overline{T}^F_{21})) *$$

$$* ((\frac{R_{-1}+1}{2})(\overline{T}^B_{22}+R_{-1}\overline{T}^B_{21})-(1+R_{-1})(\frac{R_{-1}-1}{2})\overline{T}^B_{21})e^{-sT_t}) / \overline{Y}_D$$

(iii)

$$\overline{Y}_{22} = (1+R_1)(\overline{T}^B_{22}+R_{-1}\overline{T}^B_{21}) / \overline{Y}_D \qquad \text{(iv)}$$

3.54

and

$$\overline{Y}_D = ((\overline{T}^F_{22}+R_1\overline{T}^F_{21})(\overline{T}^B_{22}+R_{-1}\overline{T}^B_{21})-(\overline{T}^B_{21}(1+R_{-1})(1-R_{-1})+$$

$$+R_{-1}(\overline{T}^B_{22}+R_{-1}\overline{T}^B_{21})) *(\overline{T}^F_{21}(1+R_1)(1-R_1)+R_1(\overline{T}^F_{22}+R_1\overline{T}^F_{21}))e^{-2sT_t})$$

3.55

These equations may be further reduced, to give:-

$$\overline{Y}_{11} = \frac{1}{2}((\overline{T}^F_{22}+R_1\overline{T}^F_{21})(1+R_{-1})(\overline{T}^B_{22}+\overline{T}^B_{21})-$$

$$- (1+R_1)(\overline{T}^F_{22}+\overline{T}^F_{21})(\overline{T}^B_{21}+R_{-1}\overline{T}^B_{22})e^{-sT_t}) \; / \; \overline{Y}_D \qquad (i)$$

$$\overline{Y}_{12} = -(1+R_1)(\overline{T}^B_{21}+R_{-1}\overline{T}^B_{22})e^{-sT_t} \; / \; \overline{Y}_D \qquad (ii)$$

$$\overline{Y}_{21} = \frac{1}{2}((\overline{T}^B_{22} + R_{-1}\overline{T}^B_{21})(1+R_1)(\overline{T}^F_{22}+\overline{T}^F_{21}) -$$

$$-(1+R_{-1})(\overline{T}^B_{22}+\overline{T}^B_{21})(\overline{T}^F_{21}+R_1\overline{T}^F_{22})e^{-sT_t}) \; / \; \overline{Y}_D \qquad (iii)$$

$$\overline{Y}_{22} = (1+R_1)(\overline{T}^B_{22}+R_{-1}\overline{T}^B_{21}) \; / \; \overline{Y}_D \qquad (iv)$$

3.56

and

$$\overline{Y}_D = ((\overline{T}^F_{22}+R_1\overline{T}^F_{21})(\overline{T}^B_{22}+R_{-1}\overline{T}^B_{21})-(\overline{T}^B_{21}+R_{-1}\overline{T}^B_{22})(\overline{T}^F_{21}+R_1\overline{T}^F_{22})*$$

$$e^{-2sT_t}) \qquad 3.57$$

Thus each of the $\overline{Y}_{ij}$ transfer functions is a ratio of discrete polynomials which may be formed directly from the $\overline{T}^{F}_{ij}$ and $\overline{T}^{B}_{ij}$ polynomials given in section 3.2 .

Now, from Chapter 2, the relationships between voltage, charge and force in the lattice are:-

$$\overline{Q}_t = \left[\frac{C_t}{1+s\overline{Z}_E C_t}\right]\left(\overline{V}_E + \frac{h}{sZ_t}(1-e^{-sT_t})(\overline{F}_{t0} + \overline{B}_{t\ell_t})\right) \qquad 3.58$$

$$\overline{V}_t = \overline{V}_E - s\overline{Q}_t\overline{Z}_E \qquad 3.59$$

Thus from equations 3.49, 3.58 and 3.59, the transfer functions for the three cases under consideration may be formed.

Firstly, $\overline{W}_{13}$ which relates the output force $\overline{F}_{(n+1)0}$ to the driving voltage $\overline{V}_E$. In this case, the input force, $\overline{B}_{(n+1)0}$ is assumed to be zero and equations 3.48 and 3.49 reduce as follows:-

$$\overline{F}_{(n+1)0} = \left(\frac{\overline{U}^F_{11}}{1-R_1\overline{U}^F_{21}}\right)\left(\left(\frac{R_1-1}{2}\right)h\overline{Q}_t+(1-R_1)e^{-sT}t\overline{F}_{t0}\right) \qquad 3.60$$

$$\begin{bmatrix}\overline{F}_{t0}\\ \\ \overline{B}_{t\ell_t}\end{bmatrix} = \begin{bmatrix}\overline{Y}_{11}\\ \\ \overline{Y}_{12}\end{bmatrix}(h\overline{Q}_t) \qquad 3.61$$

Equation 3.60 may be rewritten as:-

$$\overline{F}_{(n+1)0} = \left(\frac{Z_{n+1}/Z_1}{\overline{T}^F_{22}+R_1\overline{T}^F_{21}}\right)\frac{(1-R_1)}{2}(2\overline{F}_{t0}e^{-sT}t-h\overline{Q}_t) \qquad 3.62$$

Thus substituting equation 3.61 into equation 3.58 gives:-

$$\overline{Q}_t = \frac{\left(\frac{C_t}{1+s\overline{Z}_EC_t}\right)\overline{V}_E}{1-\left(\frac{h^2C_t}{sZ_t(1+s\overline{Z}_EC_t)}\right)(1-e^{-sT}t)(\overline{Y}_{11}+\overline{Y}_{21})} \qquad 3.63$$

Also, from equation 3.61, equation 3.62 becomes:-

$$\overline{F}_{(n+1)0} = \left(\frac{Z_{n+1}/Z_1}{\overline{T}^F_{22}+R_1\overline{T}^F_{21}}\right)\left(\frac{1-R_1}{2}\right)\left(2\overline{Y}_{11}e^{-sT_{t-1}}\right)h\overline{Q}_t \qquad 3.64$$

and thus,

$$\overline{F}_{(n+1)0} = \frac{\left(\frac{Z_{n+1}/Z_1}{\overline{T}^F_{22}+R_1\overline{T}^F_{21}}\right)\left(\frac{1-R_1}{2}\right)\left(2\overline{Y}_{11}e^{-sT_{t-1}}\right)\left(\frac{hC_t}{1+s\overline{Z}_EC_t}\right)\overline{V}_E}{1-\left(\frac{h^2C_t}{sZ_t(1+s\overline{Z}_EC_t)}\right)(1-e^{-sT_t})(\overline{Y}_{11}+\overline{Y}_{21})} \qquad 3.65$$

Similarly, from equation 3.59 and 3.63, the voltage across the transmitter, $\overline{V}_t$ is given by:-

$$\overline{V}_t = \left(\frac{1}{1+s\overline{Z}_EC_t}\right)-\left(\frac{h^2C_t}{sZ_t(1+s\overline{Z}_EC_t)}\right)(1-e^{-sT_t})(\overline{Y}_{11}+\overline{Y}_{21})$$

$$1-\left(\frac{h^2C_t}{sZ_t(1+s\overline{Z}_EC_t)}\right)(1-e^{-sT_t})(\overline{Y}_{11}+\overline{Y}_{21}) \qquad 3.66$$

and, for the receiver voltage, assuming $\overline{V}_E$ is zero, and $\overline{F}_{(n+1)0}$ is not required, equation 3.58 becomes:-

$$\overline{Q}_t = \left(\frac{C_t}{1+s\overline{Z}_E C_t}\right)\left(\frac{h}{sZ_t}(1-e^{-sT_t})(\overline{Y}_{11}+\overline{Y}_{21})h\overline{Q}_t+(\overline{Y}_{12}+\overline{Y}_{22})*\right. \qquad 3.67$$
$$\left. * \quad \overline{B}_{(n+1)0}\right)$$

whence

$$\overline{Q}_t = \frac{\left(\frac{hC_t}{sZ_t(1+s\overline{Z}_E C_t)}\right)(1-e^{-sT_t})(\overline{Y}_{12}+\overline{Y}_{22})\overline{B}_{(n+1)0}}{1-\left(\frac{h^2 C_t}{sZ_t(1+s\overline{Z}_E C_t)}\right)(1-e^{-sT_t})(\overline{Y}_{11}+\overline{Y}_{21})} \qquad 3.68$$

and thus from equation 3.58,

$$\overline{V}_t = \frac{-\left(\frac{hC_t\overline{Z}_E}{Z_t(1+s\overline{Z}_E C_t)}\right)(1-e^{-sT_t})(\overline{Y}_{12}+\overline{Y}_{22})\overline{B}_{(n+1)0}}{1-\left(\frac{h^2 C_t}{sZ_t(1+s\overline{Z}_E C_t)}\right)(1-e^{-sT_t})(\overline{Y}_{11}+\overline{Y}_{22})} \qquad 3.69$$

Equations 3.65, 3.66 and 3.69 give the alternative expressions for $\overline{W}_{13}$, $\overline{W}_{33}$ and $\overline{W}_{31}$ respectively. These may be compared with the expressions given in equations 3.36 . Clearly, the expressions of equations 3.65, 3.66 and 3.69 are simpler. The reason for this is the absence of common factor terms which are present in equations 3.36 . If these equations were expanded, then the common factors could be eliminated but this generally requires a great deal of algebraic manipulation. Also, even if only a few layers are considered, the complexity of the expanded transfer functions is so great that mistakes and inaccuracies may easily occur. The alternative derivation presented in this section produces the reduced transfer functions in their simplest forms directly.

This analysis has been carried out for only three of the $\overline{W}_{ij}$ transfer functions. It may be extended for the remaining terms but the three cases dealt with here are the most useful and also, the most likely to be implemented in practical applications, as will be shown later.

3.5 SINGLE LAYER EXAMPLE

Consider the single system shown in Fig 3.9, where the previous assumptions about acoustic impedance, losses and index notation all apply. The layer is assumed to have a transit-time of T_1 seconds. Then, since there are no rear face layers, equations 3.11, 3.30 and 3.31 give:-

$$\left[\overline{T}^B\right] = \begin{bmatrix} 1 & 0 \\ 0 & 1 \end{bmatrix} \qquad 3.70$$

$$\left[\overline{U}^B\right] = \begin{bmatrix} 1 & 0 \\ 0 & 1 \end{bmatrix} \qquad 3.71$$

$$\left[\overline{T}^F\right] = \frac{1}{2}\begin{bmatrix} (1+\frac{Z_2}{Z_1})e^{-sT_1} & (1-\frac{Z_2}{Z_1})e^{+sT_1} \\ (1-\frac{Z_2}{Z_1})e^{-sT_1} & (1+\frac{Z_2}{Z_1})e^{+sT_1} \end{bmatrix} \qquad 3.72$$

$$\overline{U}^F = \begin{bmatrix} (\frac{2Z_2}{Z_1+Z_2})e^{-sT_1} & (\frac{Z_1-Z_2}{Z_1+Z_2}) \\ (\frac{Z_2-Z_1}{Z_1+Z_2})e^{-2sT_1} & (\frac{2Z_1}{Z_1+Z_2})e^{-sT_1} \end{bmatrix} \quad 3.73$$

Thus, using the multilayer analysis method of section 3.2, equations 3.36 and 3.37 yield:-

$$\overline{W}_{13} = \frac{(\frac{2Z_2}{Z_1+Z_2})e^{-sT_1}\overline{P}_{13}}{1-(\frac{Z_2-Z_1}{Z_1+Z_2})e^{-2sT_1}\overline{P}_{11}} \quad 3.74$$

$$\overline{W}_{31} = \frac{(\frac{2Z_1}{Z_1+Z_2})e^{-sT_1}\overline{P}_{31}}{1-(\frac{Z_2-Z_1}{Z_1+Z_2})e^{-2sT_1}\overline{P}_{11}} \quad 3.75$$

$$\overline{W}_{33} = \frac{\overline{P}_{33}+(\frac{Z_2-Z_1}{Z_1+Z_2})e^{-2sT_1}(\overline{P}_{31}\overline{P}_{13}-\overline{P}_{11}\overline{P}_{33})}{1-(\frac{Z_2-Z_1}{Z_1+Z_2})e^{-2sT_1}\overline{P}_{11}} \quad 3.76$$

Alternatively, equations 3.65, 3.66 and 3.69 give the above transfer functions in their reduced forms directly. Firstly, equations 3.70 and 3.72 may be used to reduce the $\overline{Y}_{ij}$ terms of equations 3.56 and 3.57 as follows,

$$\overline{Y}_{11} = \frac{1}{2}((1+R_{-1})(1-R_1R_{12}e^{-2sT1})-(1+R_1)R_{-1}e^{-sTt} *$$

$$* (1-R_{12}e^{-2sT1})) / \overline{Y}_D \qquad \text{(i)}$$

$$\overline{Y}_{12} = -(1+R_1)R_{-1}e^{-sT}(1-R_{12})e^{-sT1} / \overline{Y}_D \qquad \text{(ii)}$$

$$\overline{Y}_{21} = \frac{1}{2}((1+R_1)(1-R_{12}e^{-2sT1})-(1+R_{-1})e^{-sTt} *$$

$$* (R_1-R_{12}e^{-2sT1})) / \overline{Y}_D \qquad \text{(iii)}$$

$$\overline{Y}_{22} = (1+R_1)(1-R_{12})e^{-sT1} / \overline{Y}_D \qquad \text{(iv)}$$

3.77

and

$$\overline{Y}_D = 1-R_1R_{12}e^{-2sT1}-R_{-1}e^{-2sT_t}(R_1-R_{12}e^{-2sT1}) \qquad 3.78$$

where

$$R_{12} = \frac{Z_2-Z_1}{Z_1+Z_2} \qquad 3.79$$

Then substituting the $\overline{Y}_{ij}$ terms into equations 3.65, 3.66 and 3.69 and clearing the $\overline{Y}_D$ denominator gives:-

$$\overline{W}_{13} = (1+R_{12})e^{-sT1}(R_1-1)(1-e^{-sT_t})(1-R_{-1}e^{-sT_t}) *$$

$$* \left(\frac{hC_t}{2(1+s\overline{Z}_EC_t)}\right) / \overline{W}_D \qquad 3.80$$

$$\overline{W}_{31} = -\left(\frac{hC_t\overline{Z}_E}{Z_t(1+s\overline{Z}_EC_t)}\right)(1-e^{-sT_t})(1+R_1)(1-R_{12})(1-R_{-1}e^{-sT_t})$$

$$* e^{-sT_t} / \overline{W}_D \qquad 3.81$$

$$\overline{W}_{33}=((\frac{1}{1+s\overline{Z}_E C_t})(1-R_1R_{12}e^{-sT_1}-R_{-1}e^{-2sT_t}(R_1-R_{12}e^{-2sT_1})-$$

$$-(\frac{h^2C_t}{Z_t s(1+s\overline{Z}_E C_t)})(\frac{1-e^{-sT_t}}{2})(2+R_1+R_{-1}-R_{12}(1+R_1+R_{-1}+R_1R_{-1})*$$

$$*e^{-2sT_1})-e^{-sT_t}(R_1+R_{-1}+2R_1R_{-1}-R_{12}(1+2R_{-1}+R_1R_{-1})e^{-2sT_1})))$$

$$/\ \overline{W}_D \qquad 3.82$$

and

$$\overline{W}_D+(1-R_1R_{12}e^{-2sT_1}-R_{-1}e^{-sT_t}(R_1-R_{12}e^{-2sT_1})-(\frac{h^2C_t}{Z_t s(1+s\overline{Z}_E C_t)})$$

$$*(\frac{1-e^{-sT_t}}{2})(2+R_1+R_{-1})-R_{12}(1+R_1+R_{-1}+R_1R_{-1})e^{-2sT_1})-$$

$$-e^{-sT_t}(R_1+R_{-1}+2R_1R_{-1}-R_{12}(1+2R_{-1}+R_1R_{-1})e^{-2sT_1}))) \qquad 3.83$$

Equations 3.80 to 3.83 give the $\overline{W}_{13}$, $\overline{W}_{31}$ and $\overline{W}_{33}$ transfer functions in their reduced form. This result may alternatively be obtained by expanding equations 3.74 to 3.76. In this case, where only one front face layer is present, the degree of algebra required for the two methods is approximately equal. However, if more layers are added to either the front or rear face, the complexity of the first method (that is equations 3.36 and 3.37) increases

to such an extent that it is not feasible. For these cases, the second method must be used.

(It will also be shown in a later chapter that the second method is better suited to computer implementation than the first.)

The second method also retains the simplest form for identifying secondary piezoelectric action. For example, in equations 3,36 and 3,37, there are several cross-product $\overline{P}_{ij}$ terms. This implies that there will be some dependence on the powers of h higher than h^2. In fact, these terms will always cancel out and the transfer functions will reduce to h and h^2 terms only. However, this is not apparent from the first method. Consequently, it is difficult to identify the underlying mechanisms (especially secondary action), from equations 3.36 and 3,37.

This difficulty is avoided in the second method by analysing the lattice diagram with the multilayered faces added. This allows the internal force-components to be related to the force-components at the layer faces, and also to the electrical voltage and charge.

When these are combined, the result is in the form of equations 3.65, 3.66 and 3.69 . These equations clearly show the dependence of the system on primary and secondary piezoelectric action.

This method may be extended to provide a general three-port system, having terms similar to equations 3.36 . However, this has not been done, since the remaining terms have little practical application and are not relevant to the remainder of this thesis.

When these are combined, the result is in the form of equations 3.65, 3.66 and 3.69 . These equations clearly show the dependence of the system on primary and secondary piezoelectric action.

This method may be extended to provide a general three-port system, having terms similar to equations 3.36 . However, this has not been done, since the remaining terms have little practical application and are not relevant to the remainder of this thesis.

3.6 SUMMARY

This chapter has presented two general procedures for analysing multilayered piezoelectric transducer systems.

Firstly, a procedure for analysing non-piezoelectric multilayered systems was derived. This produced similar results to those obtained in geophysical modelling (54), as was expected. However, the more general application which is considered here, produced several extra results, notably those of equations 3.14 and 3.15.

The non-piezoelectric multilayered analysis was then applied to a piezoelectric system. Firstly, the general multilayered system was analysed using the equations for a single piezoelectric layer, presented in Chapter 2. This analysis took the form of a 2-port:2-port:3-port analysis and produced the general systems equations 3.36 and 3.37. However, these equations were then shown to be difficult to handle, especially for cases with several front and rear face layers. It was also indicated that a substantial

degree of algebraic reduction was required to reduce the equations to a form where primary and secondary piezoelectric effects could be easily identified. To this end, an alternative set of systems equations was derived.

The starting point for this analysis was the extended lattice model of Fig 3.5 . The procedure adopted was similar to that of Chapter 2, however the lattice diagram now incorporates front and rear face layers. The lattice was remodelled as shown in Fig 3.8 and then analysed directly. The resulting equations relate the initial force components to the force components at the layer faces and the charge on the transducer. This allows the system transfer functions to be derived in such a way that primary and secondary piezoelectric action are apparent.

The second method was not developed into a general 3-port system but was used to generate the most useful system transfer functions, that is, those for transmission and reception. To illustrate the methods, a simple one-layer example was considered. This shows the difference between the methods and clearly indicates how the second method produces the transfer

functions in their reduced form directly (that is, with little extra reduction). It will be shown in a later chapter that the second method is also more amenable to computerisation than the first.

Thus, both these methods provide a complete mathematical description for a multilayered piezoelectric transducer.

CHAPTER 4

THE APPLICATION OF Z-TRANSFORMATION TO MIXED DIFFERENTIAL - DELAY TRANSFER FUNCTIONS

4.1 INTRODUCTION

The systems models of the preceding chapters provide Laplace transform solutions of the general 3-port transducer. These equations may be used to obtain the response of the transducer to a variety of input functions, in several ways.

If the input function is known explicitly as a Laplace transform, then it may be convolved with the system transfer function to give the Laplace transfer function of the desired output. However, this method has two drawbacks. Firstly, the input function is frequently unobtainable in Laplace form. If sufficient information is available about the input, it may be possible to approximate it by a Laplace transform but this introduces an extra source of error. Secondly, inversion of the resultant Laplace transform into the time-domain is compounded by the differential delay nature of the transfer functions. This problem has been studied by several authors, notably, GITIS and SHENKER (17), MEL'KANOVICH (44) and YING (70), as mentioned previously.

The general method adopted by these authors involves expanding the transfer function into an infinite series. This procedure becomes increasingly complicated as the expansion proceeds, and requires a great deal of calculation to evaluate even a few terms. Thus, although this method is direct, it is feasible only for either simply loaded transducers (that is, transducers with only a single electrical load element and no layers) or with the aid of a large computer. (Even with a computer, the complexity of the algebraic manipulation involved requires very complex algorithms which, consequently, take a long time to evaluate, or require a large portion of the computer resources.)

An alternative method is to evaluate the complex frequency spectrum of the transducer directly from the Laplace transform. The complex frequency spectrum of the input may then be convolved with that of the transducer to obtain the output. This method has the major advantage over the previous method, in that even if little is known about the input, it may be measured using a spectrum analyser. Inversion of the complex frequency spectrum into the time-domain may be achieved using a standard Inverse-Fast-Fourier Transform, (IFFT) routine which is

available for most computers. This is the most widely used method of modelling the transducer response, as indicated by DESILETS et. al. (14), LEWIS (38), KERVEL and THIJSSEN (34) and SILK (59). The application of IFFT routines requires the original spectrum to be bandlimited. The normal assumption that the spectrum is orginally periodic will produce aliasing effects if this is not the case. This does not pose any problems for most Continuous Wave, (CW), operations, where the spectrum of the transducer is such that the majority of the spectral energy is concentrated near the resonant frequency. The addition of transducer matching layers and electrical tuning elements also serves to bandlimit the spectrum, and hence the results of (14) - (59) are usually independent of errors introduced by the IFFT routines.

However, when this method is applied to transient analysis, or cases where the transducer is lightly loaded mechanically, the energy in the spectrum becomes spread out and is no longer concentrated near a single frequency. To obtain results in these cases, it is necessary either to truncate the spectrum using a window function or to use a larger spectral bandwidth. Both of these methods have severe disadvantages. Using the

window functions can introduce distortion into the transient response, to the extent that the actual and predicted responses differ significantly. Utilising a much larger bandwidth greatly increases the amount of computation required. This may be reduced by increasing the frequency sampling interval for the spectrum (that is, spacing the frequency samples further apart, so that a given number of samples covers a larger bandwidth), but this is limited by the nature of the transducer spectrum. There is also a direct trade-off between the temporal and spectral sampling intervals, such that, as the temporal sampling period is reduced, the frequency sampling interval increases. Thus, if the entire impulse response of a particular transducer is required in the time-domain, then, for a given number of samples, there is a minimum sampling period which can be used. Below this, only a portion of the impulse response will be reproduced. This problem may be resolved only by using more samples. HAYWARD (19) describes some of these problems, and the degree of error introduced by the IFFT for several specific cases.

So the spectral model, while useful for narrowband and highly tuned transducers, can present difficulties for wideband analysis.

The final method which has been used to solve the inverse-Laplace transform problem is that of numerical analysis, whereby the Laplace Transform is approximated by a difference equation. This technique may be applied in two ways:-

1. The system transfer functions of the preceding chapters are transformed into a difference equation, whose input is the sampled version of the input function.

or

2. The Laplace transform of the output is solved directly using a numerical method.

Clearly the second case requires information concerning the explicit Laplace transform of the input function. The first case has the same advantage as the spectral method, that is, the input fuction may be measured explicitly. This is the method which will be considered here.

There are a large number of numerical methods which may be used to solve Laplace transforms. Several of these are given by JURY (22) but one of the most widely used, and most flexible, is the z-transform. A comprehensive

discussion of the z-transform and its properties may be found in Reference (22).

Several authors have applied the z-transform to the solution of the transducer Laplace transforms. It is particularly suited to this case since it accurately models the delay terms. HAYWARD (19) gives a rigorous derivation of the application of z-transforms to transducers and presents some simple examples. STEPANISHEN (63) applies the method of BOXER and THALER (6) to the lateral vibrations of the transducer. His paper highlights several of the difficulties encountered with the z-transform method, notably that of algebraic manipulation. CHALLIS (11) used the bilinear transform (22) to model several specific transducer examples. This method is less involved than that of Stepanishen, but has a serious drawback which will be investigated later in this chapter.

It is apparent from the results of these authors that the use of the z-transform provides an accurate method of obtaining the temporal solution of the transducer Laplace transforms. The method also avoids some of the problems discussed previously with the IFFT and hence it may be applied to both transient and narrowband cases but it does have some disadvantages.

Firstly, the differential Laplace terms are approximated by difference equations. This requires a judicious choice of sampling rate to avoid aliasing and other truncation errors. Secondly, the method as applied in References (19)-(63) has been applied only to specific transducer transforms. Each different transform requires a re-application of the method. Thus there is no general z-transform model for the transducer.

This chapter will present a technique for obtaining a general z-transform model of differential/delay type Laplace transfer functions. The method largely avoids problems with algebraic manipulation. The different z-transforms considered by Challis and Stepanishen will be compared and it will be shown that these tend to the same solution as the sampling period is reduced to zero. Several other problems which may occur, and their possible consequences, will also be discussed.

4.2 DIFFERENTIAL/DELAY FUNCTIONS AND Z—TRANSFORMS

There are four basic types of mixed differential/delay transfer function, which may be summarised as follows:-

$$H(s) = \frac{\sum_{i=0}^{I} a_i s^i}{\sum_{j=0}^{J} b_j s^j} \quad ; \; J>I \qquad 4.1$$

$$H(s) = \frac{\sum_{n=0}^{N} a_n e^{-sT_n}}{\sum_{m=0}^{M} b_m e^{-sT_m}} \qquad 4.2$$

$$H(s) = \left[\frac{\sum_{i=0}^{I} a_i s^i}{\sum_{j=0}^{J} b_j s^j}\right] * \left[\frac{\sum_{n=0}^{N} c_n e^{-sT_n}}{\sum_{m=0}^{M} d_m e^{-sT_m}}\right] \quad ; \; J>1 \qquad 4.3$$

$$H(s) = \frac{\sum_{n=0}^{N} \left[\sum_{i=0}^{I} a_{in} s^i\right] e^{-sT_n}}{\sum_{m=0}^{M} \left[\sum_{j=0}^{J} b_{jm} s^j\right] e^{-sT_m}} \qquad 4.4$$

Equation 4.1 represents a normal Laplace transfer function. The condition J>I has been imposed to render the transfer function low-pass, since this is the simplest type of Laplace function to transform into the z-domain. (The procedure for high-pass, band-pass and band-stop transfer functions is slightly more involved and is discussed in References (22) and (48).)

Equation 4.2 represents a delay only system. There is no requirement for the degree of the numerator and denominator in this case.

Equation 4.3 describes a cascaded differential and delay system, where the differential and delay terms may be separated. Once again, the condition J>I is imposed to render the differential term low-pass.

Finally, equation 4.4 represents a general mixed differential/delay system. No condition has been placed on the degree of the numerator and denominator differential terms, since the inclusion of the delay terms renders consideration of the differential terms as low-pass inappropriate.

References (22) and (48) give a comprehensive discussion of the different methods of z-transformation which exist and their applicability. From them, it is apparent that to preserve accurately the temporal characteristics of the original Laplace transfer functions, only the Impulse Invariance Method, (IIR), may be used. The bilinear and other methods will introduce various errors (as outlined in (22) and (48)), and will not generally preserve the original temporal response.

The general procedure for IIR transformation is fully detailed in (22) and (48) but may be briefly summarised as follows:-

Defining

$$z^{-1} = e^{-sT_s} \qquad 4.5$$

where z^{-1} is the delay operator and T_s the sampling period in the z-domain,

then, functions of the type given in equation 4.1 may be transformed into the z-domain, as follows.

Firstly, it is convenient to express the transfer function in partial fraction form, that is:-

$$H(s) = \sum_{j=1}^{J} \frac{\beta_j}{s+\alpha_j} \qquad 4.6$$

(α_j and β_j are generally complex.)

Each partial fraction is then transformed into the z-domain to give:-

$$H(z^{-1}) = \sum_{j=1}^{J} \frac{\nabla_j}{z^{-1}+\delta_j} \qquad 4.7$$

(again, ∇_j and δ_j are generally complex.)

These partial fractions may be recombined,

$$H(z^{-1}) = \frac{\sum_{i=0}^{I} e_i z^{-1}}{\sum_{j=0}^{J} f_j z^{-1}} \quad ; \quad J>I \qquad 4.8$$

(The coefficients e_i and f_j will be real if the coefficients of equation 4.1 were originally real because any complex partial-fraction will exist in complex-conjugate pairs.)

Functions of the type described by equation 4.2 may be transformed directly to the z-domain as follows:-

Firstly, T_s is chosen such that,

$$k = T / T_s \qquad 4.9$$

where k is an integer. Then substituting directly from equation 4.5, equation 4.2 becomes:-

$$H(z^{-1}) = \frac{\sum_{n=0}^{N} a_n z^{-kn}}{\sum_{m=0}^{M} b_m z^{-km}} \qquad 4.10$$

(Note that the coefficients, a_n and b_m are unchanged.)

Thus functions of the type described by equation 4.3 may be transformed into the z-domain by combining the methods used for equations 4.1 and 4.2 . In this case, the choice of the sampling period, T_s is restricted by both the aliasing criterion for the differential part, and the integer sub-multiple criterion from the delay part. This may result in the value of T_s being lower than for either part individually

Thus transforming each section of equation 4.3 gives:-

$$H(z^{-1}) = \left[\frac{\sum_{i=0}^{I} e_i z^{-1}}{\sum_{j=0}^{J} f_j z^{-j}}\right] * \left[\frac{\sum_{n=0}^{N} c_n z^{-kn}}{\sum_{m=0}^{M} d_m z^{-km}}\right]; \quad J>I \qquad 4.11$$

This may be written as

$$H(z^{-1}) = \frac{\sum_{\ell_i=0}^{I+KN} e_{\ell_i} z^{-\ell_i}}{\sum_{\ell_j=0}^{J+KM} f_{\ell_j} z^{-\ell_j}} \qquad 4.12$$

which is similar to equation 4.8.

Functions of the type shown in equation 4.4 however, cannot be z-transformed by simply combining the IIR methods for equations 4.1. and 4.2, since in this case the differential terms in 4.4 cannot be expanded into partial fractions. Challis (11) solved this problem by using the bilinear transform

$$s = \frac{2}{T_s}\left[\frac{1 - z^{-1}}{1 + z^{-1}}\right] \qquad 4.13$$

The delay terms are now transformed using the method applied to equation 4.2 whereas the differential terms are transformed by using the substitution given

in equation 4.13. This method of mixing transforms is not generally valid, although, as will be shown later, it may be used in certain special cases. Equation 4.4 may be rewritten in the following manner:-

$$H(s) = \sum_{\ell=0}^{\infty} H\ell(s)\ e^{-sT} \qquad 4.14$$

where each block $H_\ell(s)$ is a transfer function similar to that of equation 4.1 . (Although it does not necessarily follow that all, or indeed any of the $H_\ell(s)$ transfer-functions will be low-pass.)

This is essentially the method used by Mel'Kanovich (44), to invert the Laplace transfer functions directly into the time-domain. Each block $H_\ell(s)$ may be transformed into the z-domain, by using the method of equation 4.1 and the resultant $H_\ell(z^{-1})$ transfer functions combined to give the overall function, $H(z^{-1})$. However, the series given by equation 4.14 is infinite, therefore realistic calculation of $H(z^{-1})$ will comprise a finite number of terms only. The degree of calculation involved

in forming $H(z^{-1})$ is actually more than that required to invert the Laplace transform, so the only advantage of z-transformation in this case, is the ability of the $H(z^{-1})$ system to use sampled input data.

Thus, if z-transformation is to be applied to systems of the type given by equation 4.4, an alternative method of performing IIR z-transforms must be used. Such a method is the z-form method of Boxer and Thaler.

4.3 THE IMPULSE INVARIANCE METHOD OF BOXER AND THALER

The method developed by Boxer and Thaler (6) is an approximation to the impulse invariance method whereby a power-series expansion is employed to provide a mapping between s and z domain functions.

The rigorous derivation of the method is given in (6) and for the present context may be briefly summarised as follows,

$$z = e^{sT_s} \tag{4.15}$$

where T_s is, as before, the sampling period in the time-domain. Then,

$$s = \left[\frac{1}{T_s}\right] \ell n(z) \tag{4.16}$$

ℓn may be approximated by the following polynomial expansion,

$$\ell n(z) = 2(u+\frac{1}{3}u^3+\frac{1}{5}u^5+\ldots\ldots\ldots) \qquad 4.17$$

where,

$$u = \frac{1-z^{-1}}{1+z^{-1}} \qquad 4.18$$

An expansion for s^{-1},may now be obtained from equations 4.16 and 4.17,

$$s^{-1} = \frac{T_{s/2}}{(u+\frac{1}{3}u^3+u^5+\ldots\ldots\ldots)} \qquad 4.19$$

By means of synthetic division, the following Laurent series is obtained.

$$s^{-1} = \frac{T_s}{2}(\frac{1}{u} - \frac{1}{3}u - \frac{4}{45}u^3 + \frac{44}{945}u^5+ \ldots\ldots\ldots) \qquad 4.20$$

Series expansions of higher powers of s^{-1} may

be obtained by raising both sides of equation 4.20 to the desired power. For example:-

$$s^{-2} = \left[\frac{T_s}{2}\right]^2\left[\frac{1}{u^2} - \frac{2}{3} - \frac{1}{15}u^2 - \frac{32}{945}u^4 \ldots\ldots\right] \qquad 4.21$$

Boxer and Thaler show that only the principal part and constant terms of the Laurent series need be retained, therefore equations 4.20 and 4.21 become,

$$s^{-1} = \frac{T_s}{2}\left[\frac{1}{u}\right] \qquad 4.22$$

$$s^{-2} = \left[\frac{T_s}{2}\right]^2\left[\frac{1}{u^2} - \frac{2}{3}\right] \qquad 4.23$$

Substituting equation 4.18 into equations 4.22 and 4.23 gives:-

$$s^{-1} = \frac{T_s}{2}\left[\frac{1 + z^{-1}}{1 - z^{-1}}\right] \qquad 4.24$$

$$s^{-2} = \left[\frac{T_s}{2}\right]^2 \left[\frac{\frac{1}{3} + \frac{1}{3}0z^{-1} + \frac{1}{3}z^{-2}}{(1 - z^{-1})^2}\right] \qquad 4.25$$

Thus the general expression for s^{-k} is given by:-

$$s^{-k} = \left[\frac{T_s}{2}\right]^k \left[\frac{N_k(z^{-1})}{(1 - z^{-1})^k}\right] \qquad 4.26$$

where N_k is a polynomial in z^{-1} of order k. The coefficients of s^{-k}, for $1 \leqslant k \leqslant 3$ are shown in Table 1.

(see next page.)

s^{-k}	$F_k(z^{-1})$
s^{-1}	$\left[\frac{T_s}{2}\right]\left[\frac{1+z^{-1}}{1-z^{-1}}\right]$
s^{-2}	$\left[\frac{T_s}{2}\right]^2\left[\frac{\frac{1}{3}+\frac{10}{3}z^{-1}+\frac{1}{3}z^{-2}}{(1-z^{-1})^2}\right]$
s^{-3}	$\left[\frac{T_s}{2}\right]^3\left[\frac{0+4z^{-1}+4z^{-2}+0}{(1-z^{-1})^3}\right]$

TABLE 1

The application of this method to differential/delay transfer functions is best illustrated by a simple example.

Consider the differential/delay expression given by:-

$$H(s) = \frac{1 + s\,e^{-sT} + s^2\,e^{-2sT}}{s + e^{-sT}} \qquad 4.27$$

Firstly, this is rewritten in negative powers of s, giving:-

$$H(s^{-1}) = \frac{s^{-2} + s^{-1}\,e^{-sT} + e^{-2sT}}{s^{-1} + s^{-2}\,e^{-sT}} \qquad 4.28$$

Next, the negative powers of s are replaced by the appropriate expressions from Table 1, giving:-

(see next page.)

4.29

$$H(z^{-1}\ e^{-sT}) = \frac{\left[\frac{T_s}{2}\right]^2 \frac{1}{3}+\frac{10}{3}z^{-1}+\frac{1}{3}z^{-2} + \left[\frac{T_s}{2}\right](1+z^{-1})(1-z^{-1})e^{-sT}+(1-z^{-1})^2\ e^{-2sT}}{\left[\frac{T_s}{2}\right](1+z^{-1})(1-z^{-1})+\left[\frac{T_s}{2}\right]^2(\frac{1}{3}+\frac{10}{3}\ z^{-1}+\frac{1}{3}z^{-2})e^{-sT}}$$

4.29

$$H(z^{-1}) = \frac{\left[\frac{T_s^2}{12}\right]+\left[\frac{5T_s^2}{6}\right]z^{-1}+\left[\frac{T_s^2}{12}\right]z^{-2}+\left[\frac{T_s}{2}\right]z^{-3}-\left[\frac{T_s}{2}\right]z^{-5}+z^{-6}-2z^{-7}+z^{-8}}{\left[\frac{T_s}{2}\right]-\left[\frac{T_s}{2}\right]z^{-2}+\left[\frac{T_s^2}{12}\right]z^{-3}+\left[\frac{5T_s^2}{6}\right]z^{-4}+\left[\frac{T_s^2}{12}\right]z^{-5}}$$

4.31

Now, if T_s is chosen such that,

$$T / _T = 3 \qquad 4.30$$
$$s$$

Then equation 4.29 becomes:-

(see page before) 4.31

This form shows clearly the dependence of the coefficients on the value of T_s. However, it may be observed from equations 4.29 and 4.30 that the order of $H(z^{-1})$ depends on T_s. This demonstrates how a judicious choice of T_s is required with this type of function.

In their paper, Boxer and Thaler use the method to invert Laplace Transforms. This requires the z-transform $H(z^{-1})$ to be divided by the sampling period T_s, before the z-transform is inverted. If, however, $H(z^{-1})$ is to be implemented as a digital filter, this is not required, since the input to the filter will be in sampled form.

In the applications considered here, $H(z^{-1})$ will always be implemented as a digital filter, so $H(z^{-1})$ in equation 4.31 is in its final form.

This example has illustrated the method developed by Boxer and Thaler. However, it still needs a degree of algebraic manipulation. It is also necessary to re-apply the method for each individual case. This is tedious and time consuming.

However, these problems which are also common to the bilinear transform in digital filtering may be substantially reduced by application of the Q-matrix method, (23) - (50).

4.4 Q-MATRIX TECHNIQUES FOR THE BILINEAR TRANSFORM

Matrix techniques for the bilinear transformation of single and multivariable polynomials are well known, (4), (23), (47), (50). The basis of the method may be described briefly, as follows:-

Consider a transfer function of the form,

$$H(s) = \frac{a_0 + a_1 s^1 + a_2 s^2 + \ldots\ldots\ldots a_n s^n}{b_0 + b_1 s^1 + b_2 s^2 + \ldots\ldots\ldots b_n s^n} \qquad 4.32$$

where any of the a or b coefficients may be zero as required.

This may be z-transformed using the bilinear transform of equation 4.13, to give:- (see next page.)

4.33

Clearing the denominator terms $\frac{2}{T}(1 + z^{-1})^n$ gives, (see next page again).

4.34

$$H(z^{-1}) = \frac{a_0+a_1\left[\frac{2}{T_s}\left(\frac{1-z^{-1}}{1+z^{-1}}\right)\right]+a_2\left[\frac{2}{T_s}\left(\frac{1-z^{-1}}{1+z^{-1}}\right)\right]^2+\cdots\cdots+a_n\left[\frac{2}{T_s}\left(\frac{1-z^{-1}}{1+z^{-1}}\right)\right]^n}{b_0+b_1\left[\frac{2}{T_s}\left(\frac{1-z^{-1}}{1+z^{-1}}\right)\right]+b_2\left[\frac{2}{T_s}\left(\frac{1-z^{-1}}{1+z^{-1}}\right)\right]^2+\cdots\cdots+b_n\left[\frac{2}{T_s}\left(\frac{1-z^{-1}}{1+z^{-1}}\right)\right]^n}$$

4.33

$$H(z^{-1}) = \frac{a_0\left[\frac{T_s}{2}(1+z^{-1})\right]^n+a_1\left[\frac{T_s}{2}(1+z^{-1})\right]^{n-1}(1-z^{-1})+\cdots\cdots+a_n(1-z^{-1})^n}{b_0\left[\frac{T_s}{2}(1+z^{-1})\right]^n+b_1\left[\frac{T_s}{2}(1+z^{-1})\right]^{n-1}(1-z^{-1})+\cdots\cdots+b_n(1-z^{-1})^n}$$

4.34

This equation may be rewritten in the form,

$$H(z^{-1}) = \frac{c_0+c_1z^{-1}+c_2z^{-2}+\ldots\ldots\ldots\ldots c_nz^{-n}}{d_0+d_1z^{-1}+d_2z^{-2}+\ldots\ldots\ldots\ldots d_nz^{-n}} \qquad 4.35$$

where the values of the c and d coefficients are obtained from equation 4.34 . By comparing equations 4.34 and 4.35, it may be seen that each of the c and d coefficients comprises a portion of all the a and b coefficients respectively. Thus,

$$c_0 = \left[\frac{T_s}{2}\right]^n a_0+\left[\frac{T_s}{2}\right]^{n-1} a_1+\left[\frac{T_s}{2}\right]^{n-2} a_2+\ldots\ldots+a_n \qquad 4.36$$

$$c_1 = \left[\frac{T_s}{2}\right]^n a_0+\left[\frac{T_s}{2}\right]^{n-1} a_1(n-2)+\ldots\ldots+a_n(-n) \qquad 4.37$$

$$c_n = \left[\frac{T_s}{2}\right]^n a_0+(-1)\left[\frac{T_s}{2}\right]^{n-1} a_1+\left[\frac{T_s}{2}\right]^{n-2} a_2+\ldots+(-1)^n a_n \qquad 4.38$$

and similarly for the d coefficients.

Equations 4.34 - 4.38 may be interpreted as follows,

$$\left]a\right] = \left[a_0,\ a_1,\ldots\ldots\ldots a_n\right]^t \qquad 4.39$$

$$\left]b\right] = \left[b_0,\ b_1,\ldots\ldots\ldots b_n\right]^t \qquad 4.40$$

$$\left]c\right] = \left[c_0,\ c_1,\ldots\ldots\ldots c_n\right]^t \qquad 4.41$$

$$\left]d\right] = \left[d_0,\ d_1,\ldots\ldots\ldots d_n\right]^t \qquad 4.42$$

where $\left]a\right]$, $\left]b\right]$, $\left]c\right]$, and $\left]d\right]$ are column vectors containing all of the a, b, c, and d coefficients of equations 4.32 and 4.35, where t denotes the transpose operation.

Then equations 4.39 and 4.40 may be directly related to equations 4.41 and 4.42, as follows,

$$\left]c\right] = \left]Q\right]\left]T\right]\left]a\right] \qquad 4.43$$

$$\left]d\right] = \left]Q\right]\left]T\right]\left]b\right] \qquad 4.44$$

where, $\boxed{T}$ is given by,

$$\boxed{T} = \begin{bmatrix} \left[\frac{T_s}{2}\right]^n, & 0, & \cdot & \cdot & \cdot & 0 \\ 0, & \left[\frac{T_s}{2}\right]^{n-1}, & 0, & \cdot & \cdot & \cdot \\ \cdot & \cdot & \cdot & \cdot & \cdot & \cdot \\ \cdot & \cdot & \cdot & \cdot & \cdot & \cdot \\ \cdot & \cdot & \cdot & \cdot & \cdot & \cdot \\ \cdot & \cdot & \cdot & \cdot & \left[\frac{T_s}{2}\right] & 0 \\ 0, & \cdot & \cdot & 0, & 0, & 1 \end{bmatrix} \qquad 4.45$$

and $\boxed{Q}$ is defined by its column vectors.

The first column of $\boxed{Q}$ is comprised of the coefficients of the expression $(1 + z^{-1})^n$, that is,

$$\boxed{Q}\ i,j = \boxed{1,n,\ \ldots\ldots\ldots\ldots\ldots\ n,1}^{t} \qquad 4.46$$

the second column by the expansion $(1-z^{-1})(1+z^{-1})^{n-1}$,

$$\boxed{Q}\ i,2 = \boxed{1,(n-1)\ldots\ldots(-1)^{n-1}(n-1),(-1)^{n}}^{t} \qquad 4.47$$

continuing until the final column which comprises the coefficients of $(1-z^{-1})^{n}$,

$$\boxed{Q}\ i,n+1 = \boxed{1,-n,\ \ldots\ldots\ldots\ldots(-1)^{n-1}n,(-1)^{n}}^{t} \qquad 4.48$$

Thus, $\boxed{Q}$ is an (n+1)x(n+1) matrix, whose columns are defined by equations 4.46 - 4.48 . The method used here to define the coefficients of $\boxed{Q}$ was chosen to highlight the underlying structure of the Q-matrix. References (4)and (50) contain

algorithms which may be used to generate the coefficients of the Q-matrix directly, given only the highest power of s in the transfer function H(s). Alternatively, the individual Q-matrices for a range of indices may be stored and used as required.

This method allows direct bilinear transformation of the s-domain coefficients of equation 4.32 into the z-domain coefficients of equation 4.35. The Q-matrix itself is independent of the sampling period T_s, which is contained in the square matrix T . Thus, a particular Q-matrix may be generated and used with a variety of different sampling periods.

This method is thus flexible, simple and easy to use being particularly suited for computer implementation. It will now be demonstrated that a similar approach may be developed for the IIR method of Boxer and Thaler.

4.5 A Q-MATRIX TECHNIQUE FOR THE IIR METHOD OF BOXER AND THALER

Consider the Laplace transfer function defined by equation 4.32. If this is to be transformed into the z-domain using the z-form method, it must first be rewritten in negative powers of s,

$$H(s^{-1}) = \frac{a_0 s^{-n} + a_1 s^{(1-n)} + \ldots\ldots a_{n-1} s^{-1} + a_n}{b_0 s^{-n} + b_1 s^{(1-n)} + \ldots\ldots b_{n-1} s^{-1} + b_n} \qquad 4.49$$

Each of the negative powers of s in equation 4.49 may now be replaced by the appropriate z-form giving, (see next page).

4.50

Clearing the $(1 - z^{-1})^n$ denominators, yields

(see next page again)

4.51

$$H(z^{-1}) = \frac{\left[\frac{T_s}{2}\right]^n (N_n(z^{-1}))a_0 + \left[\frac{T_s}{2}\right]^{n-1} (N_{n-1}(z^{-1}))(1-z^{-1})a_1 + \ldots\ldots + a_n(1-z^{-1})^n}{\left[\frac{T_s}{2}\right]^n (N_n(z^{-1}))b_0 + \left[\frac{T_s}{2}\right]^{n-1} (N_{n-1}(z^{-1}))(1-z^{-1})b_1 + \ldots\ldots + b_n(1-z^{-1})^n}$$

4.51

$$H(z^{-1}) = \frac{\left[\frac{T_s}{2}\right]^n \left(\frac{N_n(z^{-1})}{(1-z^{-1})^n}\right)a_0 + \left[\frac{T_s}{2}\right]^{n-1} \left(\frac{N_{n-1}(z^{-1})}{(1-z^{-1})^{n-1}}\right)a_1 + \ldots\ldots + a_n}{\left[\frac{T_s}{2}\right]^n \left(\frac{N_n(z^{-1})}{(1-z^{-1})^n}\right)b_0 + \left[\frac{T_s}{2}\right]^{n-1} \left(\frac{N_{n-1}(z^{-1})}{(1-z^{-1})^{n-1}}\right)b_1 + \ldots\ldots + b_n}$$

4.50

This equation may be manipulated into the form of equation 4.35, in a similar manner to the previous section. However, in this case, the polynomials are no longer simple power series expansions, but are defined by the Laurent series of equation 4.20.

It may be observered from Table 1 and equation 4.51 that the product terms,

$$N_{n-k}\,(z^{-1})\ .\ (1 - z^{-1})^{k} \qquad 4.52$$

produce polynomials of order z^{-n}, hence the relationship between the a, b and c, d coefficients which was noted for the bilinear transform, will also apply here. Consequently, it should be possible to form a Q-matrix for the IIR z-transform.

Three procedures have been developed to generate the IIR Q-matrix.

The first two methods may be conveniently separated into two distinct parts. Firstly, a

look-up table, which corresponds to the Boxer and Thaler transformation, is generated. Then the coefficients from this table are manipulated to form the appropriate Q-matrix.

The third method stores each Q-matrix (which is generated by either of the first two methods) in a larger look-up table and simply reads the required Q-matrix from the table, with no extra computation.

4.5 (i) GENERATION OF THE LOOK-UP TABLE

Two methods have been developed for generating the z-form look-up table; their relative merits depending on available storage space and calculation time. Both algorithms possess a common starting point, the generation of the $\ell n(z)$ series of equation 4.17. If it is assumed that N is the largest power of s in the mixed differential/delay transfer function, it is readily shown that:-

$$T_{MIN} = \begin{cases} N + 1 , & N \text{ odd} \\ N + 2 , & N \text{ even} \end{cases} \qquad 4.53$$

where T_{MIN} is the minimum number of terms of the $\ell n(z)$ series required to provide the principal part and constant term of the Laurent series in equation 4.20.

Thus, a vector containing the $\ell n(z)$ series may be generated and stored as follows:-

$$L_n] = \{0,\ 1,\ \frac{1}{3},\ 0,\ \frac{1}{5},\ 0, \ldots\ldots\}$$

up to T_{MIN} terms

4.54

Furthermore, equation 4.20 may be rewritten as,

$$s^{-1} = (\frac{T_s}{2})(\frac{1}{u})(1 - \frac{u^2}{3} - \frac{4u^4}{45} - \ldots\ldots)$$

4.55

This is in turn generated and stored as the following vector,

$$L_v] = \{1,\ 0,\ \frac{-1}{3},\ 0,\ \frac{-4}{45},\ \ldots\ldots\}$$

4.56

This equation contains the minimum number of terms required to generate the largest power of s. However, the coefficients for the preceding indices of s must also be generated with, for each case,

only the principal part and constant term being retained.

It is readily shown that for any given k, where k is an index of s, such that $1 \leqslant k \leqslant N$, the minimum number of terms required in the Laurent vector to generate the correct principal part and constant term is given by,

$$E_{MIN} = \begin{cases} k & , \text{ k odd} \\ k+1 & , \text{ k even} \end{cases} \qquad 4.57$$

The specified number of terms in the Laurent vector, $\lceil L_v \rceil$, may then be raised to the k^{th} power to produce the following general expression,

$$s^{-k} = \left(\frac{T_s}{2}\right)^k \left[\sum_{\ell=0}^{k} \frac{a_\ell}{u^\ell}\right] \qquad 4.58$$

where $1 \leqslant k \leqslant N$

The a_ℓ terms are coefficients which result from raising the Laurent vector to the k^{th} power.

(Note: for k odd, $a_0 = 0$).

The a_ℓ coefficients are stored in a matrix, A, as follows:-

$$\left[A\right] = \begin{bmatrix} a_{10} & a_{11} & 0 & 0 & \cdot & \cdot & \cdot & \cdot \\ a_{20} & a_{21} & a_{22} & 0 & \cdot & \cdot & \cdot & \cdot \\ a_{30} & a_{31} & a_{32} & a_{33} & \cdot & \cdot & \cdot & \cdot \\ \cdot & \cdot & \cdot & \cdot & \cdot & \cdot & \cdot & \cdot \\ \cdot & \cdot & \cdot & \cdot & \cdot & \cdot & \cdot & \cdot \\ \cdot & \cdot & \cdot & \cdot & \cdot & \cdot & \cdot & \cdot \end{bmatrix} \qquad 4.59$$

where A has dimensions N x (N + 1) and the coefficients $a_{k\ell}$ correspond to the ℓ^{th}.

coefficient of the k^{th} expansion in equation 4.58.

From equation 4.58, the s^{-k} terms are pre-multiplied by the scalar term, $\left[\overline{T_s} / \overline{2}\right]^k$. For the majority of the applications, the sampling period depends on the characteristics of the transfer function. Consequently, to maintain the generality of the method, the scaling factors are included in the algorithm at a later stage. (This is similar to the T-vector of equation 4.45.)

The coefficients of matrix A may be stored sequentially in the following manner:-

$$a_{10}, a_{11}; a_{20}, a_{21}, a_{22}; a_{30}\cdots\cdots\cdots \qquad 4.60$$

The second method for generating the look-up table uses the coefficients of the A-matrix, along with equation 4.18, to generate the coefficients of Table 1, according to the following

equation,

$$s^{-k} = \left[\frac{T_s}{2}\right]^k \frac{\left[\sum_{\ell=0}^{k} (1 + z^{-1})^{(k-\ell)} \cdot (1 - z^{-1})^{\ell} \cdot a_{\ell}\right]}{(1 - z^{-1})^k} \qquad 4.61$$

where equation 4.61 is obtained by substituting equation 4.18 into equation 4.58.

As before, to retain generality, the $\left[T_s / 2\right]^k$ scaling terms are omitted, giving,

$$s^{-k} = \frac{\sum_{\ell=0}^{k} (1 + z^{-1})^{(k-\ell)} \quad (1 - z^{-1})^{\ell} \cdot a_{\ell}}{(1 - z^{-1})^k} \qquad 4.62$$

where s^{-k} is the unscaled s-term. (The terms $(1 + z^{-1})^k$ and $(1 - z^{-1})^k$ may be generated using a Pascal-triangle method, and stored in an array P, up to the largest expansion required, N. However,

recursive generating procedures for each application of equation 4.62 provide an alternative if an extra storage array is not desirable.

The z-domain coefficients thus generated may now be stored in sequential pairs, for both numerator and denominator. For example, consider the first few expansions of equation 4.62, expressed as follows:-

$$\underbrace{1,1}_{N1};\underbrace{1,-1}_{D1}:\underbrace{3,3,3;}_{N2}\underbrace{1,-2,1}_{D2}:\underbrace{0,4,4,0;}_{N3} \qquad 4.63$$

where,

N1 = coefficients of s^{-1} numerator

D1 = " " s^{-1} denominator

N2 = " " s^{-2} numerator

D2 = " " s^{-2} denominator

.
.
.
etc.

These coefficients are directly comparable with the z-coefficients of Table 1.

4.5 (ii) Q-MATRIX GENERATION

METHOD 1

The first method for Q-matrix generation assumes that the look-up table contains the A-matrix coefficients of equation 4.59, stored in the form of equation 4.60.

The required number of terms are read from the look-up table into an (N + 1) x (N + 1) transition matrix, P, and stored as follows:-

$$
\left[P \right] = \begin{bmatrix}
1 & 0 & \cdots & \cdots & \cdots & \cdots & \cdots & \cdots & \cdots & 0 \\
a_{10} & a_{11} & & & & & & & & \vdots \\
a_{20} & a_{21} & a_{22} & & & & & & & \vdots \\
a_{30} & a_{31} & a_{32} & a_{33} & \cdots & \cdots & \cdots & \cdots & \cdots & 0 \\
\vdots & & & & & & & & & \vdots \\
\cdots & \cdots & \cdots & \cdots & \cdots & \cdots & \cdots & \cdots & a_{(N+1)(N+1)} &
\end{bmatrix}
$$

4.64

These coefficients may now be used to generate the desired Q-matrix in the following manner.

Let,

$$
\left[R_k \right] = \{ q_{k,1} \; ; \; q_{k,2} \; ; \; q_{k,3} \cdots\cdots q_{k,n+1} \}
$$

4.65

be the k^{th} row of the desired Q-matrix, and $P_{k,i}$ be the elements of the P-matrix described by the equation 4.64 .

The desired row vector, R_k, may then be generated from the $P_{k,i}$ elements in the k^{th} row of P by the following expression, which is derived directly from equation 4.62,

$$\underline{R_k} = \sum_{\ell=1}^{K} P_{k,\ell} \cdot (1+z^{-1})^{(k-\ell)} (1-z^{-1})^{(\ell-1)} (1-z^{-1})^{(N+1-K)} \qquad 4.66$$

which yields,

$$\underline{R_k} = \sum_{\ell=1}^{k} P_{k,\ell} \cdot (1+z^{-1})^{(k-\ell)} (1-z^{-1})^{(N+\ell-K)} \qquad 4.67$$

This generates the Q-matrix, but, as stated previously, the time-scale terms have been omitted.

METHOD 2

The method for Q-matrix generation assumes that the look-up table contains the coefficients of Table 1, stored in the form of equation 4.63 . As before, the required number of terms are read from the look-up table into the P-matrix. However, there are both numerator and denominator coefficients in this case, and inspection of the look-up table shows that the number of coefficients exceeds (N+1)x(N+1). In fact, there are (N+1)x(N+2) coefficients and hence P is defined to be an (N+1)x(N+2) matrix for this method. These coefficients are then stored as follows:-

Numerator terms in the lower triangular portion of P, denominator terms in the upper triangular portion of P.

That is,

$$\underline{\underline{P}} = \begin{bmatrix} & \text{DENOMINATOR} \\ & \text{TERMS} \\ \text{NUMERATOR} & \\ \text{TERMS} & \end{bmatrix} \qquad 4.68$$

This is best illustrated by considering the first few terms of equation 4.63 which are stored in the following manner:-

$$P] = \begin{bmatrix} 1 & 0 & \cdots & 0 \\ 1 & 1 & & \\ \frac{1}{3} & \frac{10}{3} & \frac{1}{3} & \\ 0 & 4 & 4 & 0 \\ & & & \\ 0 & & 0 & 1 & -3 & 3 & -1 \\ \vdots & & & & & & \\ & & & & 1 & -2 & 1 \\ \vdots & & & & & & \\ 0 & \cdots & & & 0 & 1 & -1 \end{bmatrix} \qquad 4.69$$

If, for example, N = 3, then P is a 4 x 5 matrix, given by,

$$P] = \begin{bmatrix} 1 & 1 & -3 & 3 & -1 \\ 1 & 1 & 1 & -2 & 1 \\ \frac{1}{3} & \frac{10}{3} & \frac{1}{3} & 1 & -1 \\ 0 & 4 & 4 & 0 & 1 \end{bmatrix} \qquad 4.70$$

Once the data has been read into P in this form, each row of the desired P-matrix is obtained by operating on the existing rows of P, as follows:-

Let,

$$R_k] = \{q_{k,1} \; ; \quad q_{k,2} \; ; \ldots\ldots\ldots q_{k,N+2}\} \qquad 4.71$$

where R_k is the desired row-vector, as before,

Then each element of R_k is given by,

$$q_{k,i} = \sum_{j=1}^{k} \sum_{n=k+1}^{N+2} P_{k,j} \cdot P_{k,n} \qquad 4.72$$

where,

$P_{k,j}$ are the existing elements of the k^{th} row in the interval $1 \leqslant j \leqslant k$. (These correspond to the numerator terms of row k.)

$P_{k,n}$ are the existing elements of the k^{th} row in the interval $k+1 \leqslant n \leqslant N+2$. (These correspond to the denominator terms of row k.)

$$i = j + n - (k + 1) ; \quad \boxed{1 \leqslant i \leqslant N+1}$$

and, $q_{k,n+2} = 0$ always.

This operation corresponds to the creation of a common denominator for the a coefficients in equation 4.62. The Q-matrix thus generated has a zero final column, that is,

$$\boxed{Q} = \begin{bmatrix} q_{11} & q_{12} \ldots\ldots\ldots q_{1,N+1} & 0 \\ \cdot & & \cdot \\ \cdot & & \cdot \\ \cdot & & \cdot \\ \cdot & & \cdot \\ \cdot & & \cdot \\ q_{n+1,1} & q_{n+2,2} \ldots\ldots\ldots q_{n+1,n+1} & 0 \end{bmatrix}$$

4.73

This final column may be omitted, reducing the dimensions of Q to (N+1) x (N+1).

The operation described above is best illustrated by an example. Consider the example matrix of equation 4.70. Performing the above operation on this matrix, and dropping the final

zero column gives,

$$\boxed{Q} = \begin{bmatrix} 1 & -3 & 3 & -1 \\ 1 & -1 & -1 & 1 \\ \frac{1}{3} & 3 & -3 & -\frac{1}{3} \\ 0 & 4 & 4 & 0 \end{bmatrix} \qquad 4.74$$

This matrix must now be scaled with the sampling terms $\boxed{T_s / 2}^k$. In this case, the Q-matrix was derived to transform negative powers of s, unlike the previous bilinear Q-matrix which was derived to transform positive powers of s. Thus each row of equation 4.73 must be multiplied by $\boxed{T_s / 2}^{k-1}$, where k is the row number such that $1 \leqslant k \leqslant N+1$.

Alternatively, Q may be premultiplied by the matrix T, where T is now an (N+1) x (N+1) matrix, of the form,

$$\left[T\right] = \begin{bmatrix} 1 & 0 & 0 & \cdot & \cdot & \cdot & \cdot & \cdot & \cdot & 0 \\ 0 & \left[T_s/2\right] & 0 & \cdot & \cdot & \cdot & \cdot & \cdot & \cdot & \cdot \\ 0 & 0 & \left[T_s/2\right]^2 & \cdot & \cdot & \cdot & \cdot & & & \cdot \\ \cdot & & & & & & & & & \cdot \\ \cdot & & & & & & & & & \cdot \\ \cdot & & & & & & & & & \cdot \\ \cdot & & & & & & & & & \cdot \\ \cdot & & & & & & & & & \cdot \\ \cdot & & & & & & & & & 0 \\ 0 & \cdot & \cdot & \cdot & \cdot & \cdot & \cdot & 0 & \left[T_s/2\right]^n & \end{bmatrix} \qquad 4.75$$

To illustrate this, consider the following examples,

(i) Let $T_s=2$, then $\left[T_s/2\right]=1$. Applying this to equation 4.74 leaves the Q-matrix unaltered.

(ii) $T_s=1$, then $\lceil T_s/2 \rceil = \frac{1}{2}$, and equation 4.74 becomes:-

$$\lceil Q \rceil = \begin{bmatrix} 1 & -3 & 3 & -1 \\ \frac{1}{2} & -\frac{1}{2} & -\frac{1}{2} & \frac{1}{2} \\ \frac{1}{12} & \frac{3}{4} & -\frac{3}{4} & -\frac{1}{12} \\ 0 & \frac{1}{2} & \frac{1}{2} & 0 \end{bmatrix} \qquad 4.76$$

(iii) Finally, $T_s=\frac{1}{2}$, then $\lceil T_s/2 \rceil = \frac{1}{4}$, and,

$$\lceil Q \rceil = \begin{bmatrix} 1 & -3 & 3 & -1 \\ \frac{1}{4} & -\frac{1}{4} & -\frac{1}{4} & \frac{1}{4} \\ \frac{1}{48} & \frac{3}{16} & \frac{-3}{16} & \frac{-1}{48} \\ 0 & \frac{1}{16} & \frac{1}{16} & 0 \end{bmatrix} \qquad 4.77$$

METHOD 3

The third method of generating the Q-matrix is much simpler. Each Q-matrix, for each index of s is generated using either of the first two methods. These Q-matrices are then stored sequentially, either row by row or column by column, in a simple large look-up table. Then, given N for a specific case, and knowing that the Q-matrix for any given value N has (N+1) x(N+1) elements, the first m elements of the look-up table will be the coefficients of the preceding Q-matrices, where,

$$m = \sum_{i=1}^{N-1} (i+1)^2 \quad ; \quad 2 \leqslant N \leqslant N_{max} \qquad 4.78$$

$$m = 0 \; ; \; N = 1$$

N_{max} is the largest index of s in the look-up table.

Thus, the first m elements may be omitted before reading the next (N+1) x (N+1) elements directly into the desired Q-matrix.

This matrix must then be scaled with the $\left[T_s/2\right]^k$ row multipliers.

The only drawback with this method, is that the look-up table will have a maximum size. Thus there will be a maximum value, N_{max}, of the s-indices, above which the table cannot be used.

4.5 (iii) COMPARISON OF THE ALGORITHMS

The algorithms may be compared in terms of both the storage required for the look-up tables, and the degree of calculation required to generate the final Q-matrix. In comparing the amount of calculation used by each method, the $\left[T_s/2\right]^k$ scaling is omitted, since this is common to each method.

The first method requires least storage, but involves a rather complex coefficient evaluation procedure. For small Q-matrices, for example, $N<5$, the degree of calculation is trivial, and the method may be readily applied. However, for these same cases, the degree of storage required is also very small, and the degree of extra calculation required to generate a Q-matrix directly from the initial Laurent vector so little, that the method has few or no advantages over direct generation. For large Q-matrices, $N>10$, the amount of calculation required increases approximately with N^3. This does not compare favourably with the two alternative methods, and hence the first method should only be considered for Q-matrices with $5 \leqslant N \leqslant 10$.

The second method requires approximately twice the storage of the first for its look-up table. The same criticism for N<5 may also be applied to this case. However, for N>10, the degree of calculation now increases with N^2 and this method is acceptable for the range $5 \leqslant N \leqslant 20$. For N>20, the degree of calculation required does not compare favourably with the third method which involves essentially no calculation, simply the access time of the look-up table. This increases with N^2 but is still significantly less than the time required to perform the calculations of the second method.

The amount of storage required for the third method is substantially more than that required for either the first two methods. For any given N_{max}, the total number of elements, N_{TOT}, in the required look-up table is given by:-

$$N_{TOT} = \sum_{i=1}^{N_{max}} (i+1)^2 \qquad 4.79$$

Applying this to several values of N_{max} gives,

N_{max} = 10 , N_{TOT} = 505

" = 20 , " = 3310

" = 30 , " = 10415

From this, it is apparent that the look-up table increases in size at a rate greater than N^2.

Consequently, an acceptable maximum size must be chosen, based on equation 4.79.

For the applications considered in this chapter, a maximum size of 20 was regarded as acceptable. For Q-matrices with N_{max} greater than 20, it was necessary to generate the matrix from the initial Laurent vector, using the second method.

Finally, it should be noted that the transition matrix P, used in methods 1 and 2 may be avoided by careful programming as follows:-

1. The elements of the look-up tables are read directly into the Q-matrix which takes the place of

the P-matrix.

2. The algorithms of equations 4.67 and 4.72 are modified to operate on the rows of the Q-matrix. Thus, each row of the Q-matrix is replaced by a new row, defined by either 4.67 or 4.72.

This was the method used in implementing the algorithms of methods 1 and 2. It approximately halves the amount of storage which would otherwise be required. However, the P-matrix was retained in deriving these methods to clarify the procedure.

4.6 COMPARISON OF THE BILINEAR AND Z-FORM Q-MATRICES

The bilinear Q-matrix of section 4.4 was derived to transform s-domain coefficients into z-domain coefficients under bilinear transformations. The s-domain coefficients are arranged into vectors in ascending positive powers of s. Regarding the z-form Q-matrix of the preceding section, it is a consequence of Boxer and Thaler's method that the s-coefficients must be arranged in descending negative powers of s. It is also important to note that the z-form Q-matrix is premultiplied by the s-vector, in the following manner:-

Let,

$$\left]a\right] = \{a_n, a_{n-1}, \ldots\ldots\ldots a_1, a_0\} \qquad 4.80$$

$$\left]b\right] = \{b_n, b_{n-1}, \ldots\ldots\ldots b_1, b_0\} \qquad 4.81$$

Defining the matrices $\left]c\right]$ and $\left]d\right]$, as in equations 4.41 and 4.42, then

$$c\rceil = a\rceil \cdot T\rceil \cdot Q\rceil \qquad 4.82$$

$$d\rceil = b\rceil \cdot T\rceil \cdot Q\rceil \qquad 4.83$$

Although this method is rather cumbersome, the algorithms for generating the Q-matrix are in their simplest form.

If the $a\rceil$ and $b\rceil$ vectors are redefined as column vectors, then,

$$a\rceil = \{a_n,\ a_{n-1},\ \ldots\ldots\ldots a_1,\ a_0\}^t \qquad 4.84$$

$$b\rceil = \{b_n,\ b_{n-1},\ \ldots\ldots\ldots b_1,\ b_0\}^t \qquad 4.85$$

and equations 4.82 and 4.83 become:-

$$c\rceil = (Q\rceil)^t\ T\rceil \cdot a\rceil \qquad 4.86$$

$$d\rceil = (Q\rceil)^t\ T\rceil \cdot b\rceil \qquad 4.87$$

However, the $\underline{a}\rceil$ and $\underline{b}\rceil$ vectors are now in an inverted form compared to that for the bilinear transform. Defining the operator r to represent row inversion, and redefining vectors $\underline{a}\rceil$ and $\underline{b}\rceil$ and matrix $\underline{\underline{T}}\rceil$, as given in equations 4.39, 4.40 and 4.45 respectively, then equations 4.86 and 4.87 may be rewritten as,

$$\underline{c}\rceil = (\underline{Q}\rceil)^{t\,r}\,\underline{\underline{T}}\rceil \,.\, \underline{a}\rceil \qquad 4.88$$

$$\underline{d}\rceil = (\underline{Q}\rceil)^{t\,r}\,\underline{\underline{T}}\rceil \,.\, \underline{b}\rceil \qquad 4.89$$

This may be illustrated by considering the Q-matrices of equation 4.74, 4.76 and 4.77, which, under this operation, become:-

$$\underline{Q}\rceil = \begin{bmatrix} 0 & \frac{1}{3} & 1 & 1 \\ 4 & 3 & -1 & -3 \\ 4 & -3 & -1 & 3 \\ 0 & \frac{1}{3} & 1 & -1 \end{bmatrix} \qquad 4.90$$

$$\underline{\underline{Q}} = \begin{bmatrix} 1 & \frac{1}{2} & \frac{1}{2} & 1 \\ \frac{1}{2} & \frac{3}{4} & -\frac{1}{2} & -3 \\ \frac{1}{2} & -\frac{3}{4} & -\frac{1}{2} & 3 \\ 0 & -\frac{1}{2} & \frac{1}{2} & -1 \end{bmatrix} \qquad 4.91$$

$$\underline{\underline{Q}} = \begin{bmatrix} 1 & \frac{1}{48} & \frac{1}{4} & 1 \\ \frac{1}{16} & \frac{3}{16} & -\frac{1}{4} & -3 \\ \frac{1}{16} & \frac{-3}{16} & -\frac{1}{4} & 3 \\ 0 & \frac{-1}{48} & \frac{1}{4} & -1 \end{bmatrix} \qquad 4.92$$

Thus, now the operations for bilinear and IIR transformation are performed in the same manner.

It is possible to rearrange the algorithms of the preceding section to generate the Q-matrices directly in this form. However, it is more difficult

to relate the algorithm derivation to the method of Boxer and Thaler. The algorithms themselves are also slightly more complicated. For these reasons, the derivations chosen here were adopted.

There is, at first, no apparent reason to compare these transformation methods. However, from equations 4.34 and4.51, it is apparent that, as the term $\boxed{T_s/2}$, tends to zero, the dominant s-domain coefficients are the same for both cases, namely, a_{n-1} and a_n (and also b_{n-1}, b_n). Thus as,

$$\frac{T_s}{2} \longrightarrow 0 \qquad 4.93$$

then

$$H(z^{-1}) \longrightarrow \frac{\frac{T_s}{2}(1+z^{-1})(1-z^{-1})^{n-1}\cdot a_{n-1}+(1-z^{-1})^n a_n}{\frac{T_s}{2}(1+z^{-1})(1-z^{-1})^{n-1}\cdot b_{n-1}+(1-z^{-1})^n b_n} \qquad 4.94$$

Thus, in the limit, both methods reduce to very nearly the same transformation.

This effect explains why Challis 4.13 obtained good results when apparently using an incorrect transform. This result also shows that the warping which is usually associated with the Bilinear transform may be neglected if T_s is chosen to be sufficiently small.

Finally, there is a potentially serious drawback to this method, which, in view of the above result may also apply to the Bilinear transform. If the transfer function of equation 4.32 has common factors in the numerator and denominator which have not been eliminated, then the resulting z-domain transfer function will be of a higher order than is necessary. This can lead to instability problems, therefore each differential transfer function considered here was first reduced to its simplest form. (For further discussion, see APPENDIX A).

4.7 SUMMARY

This chapter has presented the derivation of a Q-matrix for Impulse Invariance z-transforms, based on the method of Boxer and Thaler. Although the derivation was performed for differential-only transfer functions, it is apparent that it may also be applied to transfer functions of the type given by equation 4.4 . The specific application of this method to the transducer system equations is discussed in the following chapter.

Three alternative procedures for generating the Q-matrix were derived. It was concluded that the third method (storing the Q-matrices for each index of s in a large look-up table) appeared to be the best choice for index values up to 20. Above this, it is probably best to generate the specific Q-matrix required for each application.

The procedure used to derive the Q-matrix was chosen so as to highlight the method of Boxer and Thaler. It also emphasises how the structure of the Q-matrix replaces the otherwise necessary

algebraic manipulation. It was then shown that some further manipulation is required to obtain the z-form Q-matrix in the same form as the bilinear Q-matrix. This could be performed before the look-up table is generated, or the generating algorithms for methods one and two rederived to include this factor. However, since the main aim of this chapter was to illustrate the method, this feature was left until the end.

Once in a compatible form, the bilinear and z-form Q-matrices were compared. It was shown that as the sampling period reduces to zero, the two methods become identical. This result was unexpected, since the bilinear and z-form methods are dissimilar transforms.

However, this explains the results obtained by Challis, who appeared initially, to be mixing two unrelated transforms. (It should be noted that if the sampling period is not chosen sufficiently small, the results will be different, therefore this restricts the method used by Challis.)

No attempt has been made to analyse the errors associated with the Boxer and Thaler method. This is covered by WASOW (67).

Several possible sources of error which may arise in applying the method have been identified, and are described in Appendix A.

Finally, this method allows the IIR z-transform to be applied to transfer functions which cannot or have not been expanded into partial fractions. It avoids the majority of the algebraic manipulation usually associated with substitution transforms, and is ideally suited to computerisation.

The Q-matrices formed by this method are independent of the sampling period T_s, hence one Q-matrix may be used with several different sampling periods, without reforming the matrix. Thus this method is also highly flexible.

CHAPTER 5
A GENERAL Z-DOMAIN MODEL OF THE THICKNESS-MODE PIEZOELECTRIC TRANSDUCER

5.1 INTRODUCTION

Chapters 2 and 3 presented the derivation of the general Laplace transform solution for the vibrations of a thickness-mode piezoelectric transducer. The resultant describing equations are of the mixed differential/delay type. These equations may be readily used to obtain the spectrum of the transducer system. However, they present certain difficulties when applied to the solution of transient, or broadband excitation problems. Chapter 4 outlined these problems and presented an alternative method for inverting the Laplace transforms - the z-form method of Boxer and Thaler.

Before this method may be applied however, some further manipulation of the system equations of Chapters 2 and 3 is required.

This chapter will show how the system equations may be manipulated into a single general form which may then be transformed into the z-domain using the procedure of Chapter 4. The general z-transform system will then be used to model a variety of practical cases. A series of

experimental results is included and these serve to validate the analytical approach.

5.2 MANIPULATION OF THE SYSTEMS EQUATIONS INTO A GENERAL DIFFERENTIAL/DELAY FORMAT

Consider the transducer system equations of Chapter 2, equations 2.42 and 2.43 . Each of these equations is in a mixed differential/delay form. It may be observed from the equations that the order of the delay terms is constant, (that is, $1, e^{-sT_t}$ and e^{-2sT_t}), while for the differential terms, the order depends on the particular electrical load selected.

For the more general system equations of Chapter 3, (equations 3.65, 3.66 and 3.69), the order of the delay terms now depends on the particular layer configuration selected.

To generalise the z-transform procedure, it was necessary to develop a general format for the equations. This is best illustrated by considering the simple no-layer equations first and extending the method to the multilayer case, once the basic procedure has been established. The required general differential/delay format is given in Chapter 4 by equation 4.4 .

Firstly, it is assumed that the electrical load term, $\overline{Z}_E$ is composed of differential elements only, and may be expressed in the form,

$$\overline{Z}_E = \frac{\sum_{i=0}^{N_1} c_i s^i}{\sum_{j=0}^{N_2} d_j s^j} \qquad 5.1$$

where, usually $N_1 \neq N_2$.

This may be further simplified by selecting,

$$N_{max} = N_1 \quad N_1 > N_2$$
$$\{$$
$$N_{max} = N_2 \quad N_2 > N_1$$

and inserting the appropriate zero-coefficients for the extra c_i or d_j coefficients as required. Thus, the electrical load becomes,

$$\overline{Z}_E = \frac{\sum_{i=0}^{N_{max}} c_i s^i}{\sum_{i=0}^{N_{max}} d_i s^i} \qquad 5.2$$

It is convenient to make the following definitions:-

$$\overline{Z}_E^N = \sum_{i=0}^{N_{max}} c_i s^i \qquad 5.3$$

$$\overline{Z}_E^D = \sum_{i=0}^{N_{max}} d_i s^i \qquad 5.4$$

so that,

$$\overline{Z}_E = \frac{\overline{Z}_E^N}{\overline{Z}_E^D} \qquad 5.5$$

where $\overline{Z}_E^N$ and $\overline{Z}_E^D$ are the numerator and denominator polynomials of the electrical load, $\overline{Z}_E$.

Using this notation, each of the equations 2.42 and 2.43 may be manipulated into the form of 4.4. This may be demonstrated by considering transfer function $\overline{P}_{33}$. That is, from equations 2.42 and 2.43,

(see next page) 5.6

Substituting for $\overline{U}$ from equation 2.40, and rearranging gives,

(see next page) 5.7

where,

$$X_k \cdot= \frac{h^2 C_t}{2Z_t} \qquad 5.8$$

This procedure may be applied to each of the $\overline{P}_{ij}$ transfer functions in equations 2.42 and 2.43.

$$\bar{P}_{33} = \frac{\left(\left(\frac{1-R_1R_{-1}e^{-2sT_t}}{1+sC_t\bar{Z}_E}\right) - \bar{U}(1-e^{-sT_t})((1+R_1)(1-R_{-1}e^{-sT_t})+(1+R_{-1})(1-R_{-1}e^{-sT_t}))\right)}{(1-R_1R_{-1}e^{-2sT_t}) - \bar{U}(1-e^{-sT_t})((1+R_1)(1-R_{-1}e^{-sT_t})+(1+R_{-1})(1-R_1e^{-sT_t}))}$$

5.6

$$\bar{P}_{33} = \frac{\left[\begin{array}{l}(s.\bar{Z}_E^D - X_k.\bar{Z}_E^D(2+R_1+R_{-1})+ \\ \quad +(2\bar{Z}_E^D.X_K(1+R_1)(1+R_{-1}))e^{-sT_t} - \\ \quad -(s\bar{Z}_E^D.R_1R_{-1}+\bar{Z}_E^D.X_K(R_1+R_{-1}+2R_1R_{-1}))e^{-2sT_t}\end{array}\right]}{\left[\begin{array}{l}(s^2C_t\bar{Z}_E^N + \bar{Z}_E^D(s-X_K(2+R_1+R_{-1}))+ \\ \quad +(2\bar{Z}_E^DX_K(1+R_1)(1+R_{-1}))e^{-sT_t} - \\ \quad -(R_1R_{-1}s^2C_t\bar{Z}_E^N + \bar{Z}_E^D(sR_1R_{-1}+X_K(R_1+R_{-1}+2R_1R_{-1}))e^{-2sT_t}\end{array}\right]}$$

5.7

However, for the practical experiments of this chapter, only the terms $\overline{p}_{31}$, $\overline{p}_{13}$ and $\overline{p}_{33}$ are required. So, adopting a similar procedure, these may be re-written as,

$$\overline{p}_{13} = \left(\frac{hC_t}{2}\right)\left((s\overline{Z}_E^D(R_1-1))+((1+R_{-1})(1-R_1)s\overline{Z}_E^D)e^{-sT}t_+\right.$$

$$\left.+(s\overline{Z}_E^D\ R_{-1}(R_1-1))e^{-2sTt}\right) \cdot / \ \overline{p}_D \qquad 5.9$$

$$\overline{p}_{31} = \left(\frac{-hC_t}{Z_t}\right)\left((s\overline{Z}_E^N(1+R_1))-((1+R_1)(1+R_{-1})s\overline{Z}_E^N)e^{-sT}t_+\right.$$

$$\left.+(R_{-1}(1+R_1)s\overline{Z}_E^N e^{-2sTt}) \ / \ \overline{p}_D\right) \qquad 5.10$$

$$\overline{p}_{33} = ((s\overline{Z}_E^D - \overline{Z}_E^D.X_k(2+R_1+R_{-1}))+(2\overline{Z}_E^D.X_k(1+R_1)(1+R_{-1}))*$$

$$*e^{-sT}t \ -(s\overline{Z}_E^D.R_1R_{-1}+\overline{Z}_E^D.X_k.(R_1+R_{-1}+2R_1R_{-1}))e^{-2sTt}) \ / \ \overline{p}_D$$

$$5.11$$

where,

$$\overline{P}_D = (s^2 C_t \overline{Z}_E^N + \overline{Z}_E^D (s - X_k(2+R_1R_{-1}))) + (2\overline{Z}_E^D X_k(1+R_1)(1+R_{-1}))*$$

$$*e^{-sT_t} - (R_1R_{-1}s^2C_t\overline{Z}_E^N + \overline{Z}_E^D(sR_1R_{-1} + X_k(R_1+R_{-1}+2R_1R_{-1})))*$$

$$*e^{-2sT_t} \qquad 5.12$$

is the common denominator term.

These equations have been arranged into the differential/delay format of equation 4.4. The differential polynomials are composed of combinations of the electrical load polynomials, $\overline{Z}_E^N$ and $\overline{Z}_E^D$ together with the parameters of the transducer. It may be observed from equations 5.9 - 5.12 that each $\overline{p}_{ij}$ transfer function comprises six differential polynomials; three for the numerator and three for the denominator. From this, it may be deduced that with the addition of layers, the total number of differential vectors will increase substantially . This is both inefficient and unnecessary since further study of equations 5.9 - 5.12 shows that several of the differential vectors are simple scalar multiples of each other. Thus, equations $\overline{p}_{13}$ $\overline{p}_{3I}$ and $\overline{p}_{33}$ may be rewritten in terms of the products

of differential-only and delay-only vectors, giving,

$$\overline{P}_{13}=\left(\frac{hC_t}{2}\right)(R_1-1).s\overline{Z}_E^D)(1-(1+R_{-1})e^{-sT_t}+R_1e^{-2sT_t})\ /\ \overline{P}_D$$

5.13

$$\overline{P}_{31}=(\frac{-hC_t}{Z_t}(1+R_1)s\overline{Z}_E^N)(1-(1+R_{-1})e^{-sT_t}+R_{-1}e^{-2sT_t})\ /\ \overline{P}_D$$

5.14

$$\overline{P}_{33} .= ((s\overline{Z}_E^D)(1-R_1R_{-1}e^{-2sT_t})-(X_k.\overline{Z}_E^D)((2+R_1R_{-1})-$$
$$-2(1+R_1)(1+R_{-1})e^{-sT_t}+(R_1+R_{-1}\pm 2R_1R_{-1})e^{-2sT_t}))\ /\ \overline{P}_D$$

5.15

and,

$$\overline{P}_D=(s(\overline{Z}_E^D+sC_t\overline{Z}_E^N))(1-R_1R_{-1}e^{-2sT_t})-(X_k.\overline{Z}_E^D)\ *$$
$$*\ ((2+R_1R_{-1})-2(1+R_1)(1+R_{-1})e^{-sT_t}+(R_1+R_{-1}+2R_1R_{-1})$$
$$*\ e^{-2sT_t})$$

5.16

Thus, defining $\overline{d}_i$ vectors as differential-only vectors, and $\overline{D}_i$ vectors as delay-only vectors, then for $\overline{p}_{33}$,

Let,

$$\overline{d}_1 = s\overline{Z}_E^D$$

$$\overline{d}_2 = (X_k.\overline{Z}_E^D)$$

$$\overline{d}_3 = s(\overline{Z}_E^D+sC_t\overline{Z}_E^N) \qquad 5.17$$

and,

$$\overline{D}_1 = (1-R_1R_{-1}e^{-2sT_t})$$

$$\overline{D}_2 = ((2+R_1+R_{-1})-2(1+R_1)(1+R_{-1})e^{-sT_t}+(R_1+R_{-1}+2R_1R_{-1})*$$

$$* e^{-2sT_t}) \qquad 5.18$$

then,

$$\overline{P}_{33} = \frac{\overline{d}_1.\overline{D}_1 - \overline{d}_2.\overline{D}_2}{\overline{d}_3.\overline{D}_1 - \overline{d}_2.\overline{D}_2} \qquad 5.19$$

This form is not as general as that of equation 4.4, but requires substantially less storage, and is clearly simpler.

In a similar manner, $\overline{P}_{13}$ and $\overline{P}_{31}$ become:-

$$\overline{P}_{13} = \frac{\overline{d}_4.\overline{D}_3}{\overline{d}_3.\overline{D}_1 - \overline{d}_2\overline{D}_2} \qquad 5.20$$

$$\overline{P}_{31} = \frac{\overline{d}_5.\overline{D}_3}{\overline{d}_3.\overline{D}_1 - \overline{d}_2.\overline{D}_2} \qquad 5.21$$

where,

$$\overline{d}_4 = \frac{hC_t(R_1-1)s\overline{Z}^D_E}{2} \qquad (i)$$

$$\overline{d}_5 = \frac{-hC_t(1+R_1)s\overline{Z}_E^N}{2} \qquad \text{(ii)}$$

5.22

$$\overline{D}_3 = (1 - (1+R_{-1})e^{-sT_t} + R_{-1}e^{-2sT_t}) \qquad 5.23$$

Thus, the three transfer functions, $\overline{P}_{13}$, $\overline{P}_{31}$ and $\overline{P}_{33}$ are completely described by five differential-only polynomials and three delay-only polynomials. (In fact, the differential-only polynomial $\overline{d}_4$ is simply $\overline{d}_1$ multiplied by a scalar, and only four distinct differential polynomials are required.)

This method may be readily applied to the corresponding multilayer transfer functions, $\overline{W}_{13}$, $\overline{W}_{31}$ and $\overline{W}_{33}$ given in equations 3.65, 3.66 and 3.69.

Firstly, clearing the electrical load polynomials and rearranging the differential terms gives,

$$\overline{W}_{13} = \left(\frac{hC_t}{2}\ (R_1-1)s\overline{Z}_E^D\right)(1 - 2\overline{Y}_{11}e^{-sT_t})\left(\frac{Z_{n+1}/Z_1}{\overline{T}_{22}^F+R_1\overline{T}_{21}^F}\right) / \overline{W}_D$$

5.24

$$\overline{W}_{31} = \left(\frac{-hC_t}{Z_t}\ s\overline{Z}_E^N\right)(1 - e^{-sT_t})(\overline{Y}_{12}+\overline{Y}_{22}) / \overline{W}_D \qquad 5.25$$

$$\overline{W}_{33} = ((s\overline{Z}_E^D) - (X_k.\overline{Z}_E^D)(1 - e^{-sT_t})(\overline{Y}_{11}+\overline{Y}_{21})) / \overline{W}_D$$

5.26

and,

$$\overline{W}_D = s(\overline{Z}_E^D+sC_t\overline{Z}_E^N)-(X_k.\overline{Z}_E^D)(1-e^{-sT_t})(\overline{Y}_{11}+\overline{Y}_{21}) \qquad 5.27$$

Clearly the differential components of these transfer functions are, with one exception, identical to those for the no-layer case. The exception, equation 5.25 does not contain the factor $(1+R_1)$, in equation 5.22.

This results from the inclusion of this factor in the formation of the delay term, $\overline{Y}_{ij}$.

The delay transfer functions $\overline{Y}_{ij}$, have a common denominator, $\overline{Y}_D$ as was shown in Chapter 3. It is thus possible to split each $\overline{Y}_{ij}$ transfer function into a numerator and denominator polynomial, where the polynomials are delay only. Thus, using the superscript N to indicate the numerator polynomial, (in a similar fashion to the electrical load), and defining:-

$$\overline{D}_1 = \overline{Y}_D \qquad 5.28$$

$$\overline{D}_2 = (\overline{Y}^N_{11}+\overline{Y}^N_{21})(1-e^{-sT_t}) \qquad 5.29$$

$$\overline{D}_3 = \frac{(1-e^{-sT_t})(\overline{Y}^N_{12}+\overline{Y}^N_{22})}{(1+R_1)} \qquad 5.30$$

and,

$$\overline{D}_4 = \frac{\overline{Z}_{N+1}}{Z_1}\left(\frac{\overline{Y}_D - 2\overline{Y}^N_{11}e^{-sT_t}}{\overline{T}^F_{22}+R_1\overline{T}^F_{21}}\right) \qquad 5.31$$

(The denominator term, $\overline{T}^F_{22}+R_1\overline{T}^F_{21}$ will always cancel with the numerator in equation 5.31, thus $\overline{D}_4$ is always a discrete polynomial. The general proof of this is tedious, and has been omitted here. However, the one-layer example of Chapter 3, section 5 gives the procedure for a specific case, This may be readily extended to the general case.)

The general multilayer transfer functions may now be rewritten as,

$$\overline{W}_{13} = \frac{\overline{d}_4.\overline{D}_4}{\overline{d}_3.\overline{D}_1 - \overline{d}_2.\overline{D}_2} \qquad 5.32$$

$$\overline{W}_{31} = \frac{d_5.D_3}{\overline{d}_3.\overline{D}_1 - \overline{d}_2.\overline{D}_2} \qquad 5.33$$

$$\overline{W}_{33} = \frac{\overline{d}_1.\overline{D}_1 - \overline{d}_2.\overline{D}_2}{\overline{d}_3.\overline{D}_1 - \overline{d}_2.\overline{D}_2} \qquad 5.34$$

Comparing equations 5.17, 5.19. 5.20 and 5.21 with equations 5.32, 5.33 and 5.34, it is apparent that the general form of the no-layer and multilayer transfer functions is the same. In fact, the differential polynomials are the same in both cases, and the delay-polynomials of the multilayer cases, as defined by equations 5.28 to 5,31, reduce to those for the no-layer case, when no layers are present. This is to be expected.

The remaining $\overline{p}_{ij}$ and $\overline{W}_k$ transfer functions can be broken down and formed into mixed differential/delay polynomial form in a similar manner. This has been omitted here, since these will not be used for experimental verification.

Equation 4.4 gives the most general form for a mixed differential/delay transfer function. For reasons of efficiency and storage, equations 5.32, 5.33 and 5.34 have been written in a slightly modified form. As will

be shown in the next section, the manipulation and storage of differential/delay systems is simpler when they reduce to the form of equations 5.32 to 5.34.

5.3 Z-TRANSFORMATION OF DIFFERENTIAL/DELAY TRANSFER FUNCTIONS

Equations 5.32, 5.33 and 5.34 are now in a suitable form to be transformed into the z-domain, using the Q-matrix technique of Chapter 4. This method is applied in two stages. Firstly, the differential polynomials are transformed into z-domain polynomials using the Q-matrix, as described in Chapter 4. Secondly, the delay polynomials are transformed by a direct application of the Impulse-Invariance method. The resultant z-domain polynomials may then be combined into the form of a digital filter.

However, before transformation can be carried out, the sampling period, T_s must be chosen. There are two conditions which the sampling period must meet. Firstly, T_s must be sufficiently small to avoid possible aliasing effects, and secondly, T_s must be an integer sub-multiple of each delay in the delay-only polynomials. Since these transfer functions are of the mixed differential/delay type, it is difficult to define an exact method for choosing T_s to avoid aliasing. However, the follow-

ing procedure worked well for all the applications considered:-

1. Choose an initial value of T_s which avoids aliasing with the electrical load, Z_E, alone. T_s must also be an integer sub-multiple of all the delays in the $\bar{D}_i$ polynomials. That is, T_s must correspond to an integer sub-multiple of the transit-times of all the layers in the system, (including the transducer.) This may be very difficult to achieve in practice, (for example, if the transit-times correspond to different prime numbers), and it is possible that some layers will have to be assumed slightly thicker or thinner than they actually are. So, the second step is as follows:-

2. Choose a second value of T_s which meets the sub-multiple criterion, approximating the layer thickness as required.

Both criteria 1 and 2 must be met, so:-

3. Choose between the two values of T_s, such that; if the second value of T_s is less than the first value, use the second value. If the first

value is less then the second, divide the second value by an integer constant to render the second value less than the first and then use this value.

If aliasing occurs, then the simplest method of re-evaluating T_s is to repeatedly halve the value of T_s, trying the new value at each stage until aliasing is no longer apparent.

In some broadband cases, it was sometimes useful to evaluate the spectrum of the system and from this obtain an estimate of the highest frequency component in the system. T_s may then be chosen in accordance with the sampling theorem, but it is still necessary that T_s is a sub-multiple of the transit-times.

Once a suitable form of T_s has been selected, the differential polynomials may be transformed.

However, as may be seen from equations 5.17 and 5.22, the differential polynomials are not all of the same order. If the electrical load polynomials, $\overline{Z}_E^N$

and $\bar{Z}_E^D$ are assumed to be of order N_{max}, then the order of the differential polynomials in equations 5.17 and 5.22 is,

$\bar{d}_1$ has order $N_{max}+ 1$

$\bar{d}_2$ has order N_{max}

$\bar{d}_3$ has order $N_{max}+ 2$

$\bar{d}_4$ has order $N_{max}+ 1$

$\bar{d}_5$ has order $N_{max}+ 1$

From Chapter 4, however, it may be seen that the z-form method, when applied in its simplest form, (direct substitution), requires the differential polynomials to be expressed as negative powers of s. The $\bar{d}_i$ polynomials may be rewritten in this form by dividing throughout by the highest index of s in each transfer function. It may be observed from equations 5.32, 5.33 and 5.34 that the highest index of s is

given by polynomial $\overline{d}_3$, and is $N_{max}+ 2$. Thus each of the $\overline{d}_i$ polynomials must be of order $N_{max}+ 2$. The Q-matrix method does not require the $\overline{d}_i$ polynomials to be written in negative powers of s, as was explained in Chapter 4, but for the correct application of the method, the $\overline{d}_i$ polynomials must all have the same order, $N_{max}+ 2$. This is easily achieved by inserting coefficients of zero value into each polynomial as required.

Once the $\overline{d}_i$ polynomials are in the correct form, the required Q-matrix may be formed. Defining $\overline{d}_i^z$ as the polynomial of the z-transformed coefficients, the $\overline{d}_i$ polynomials are transformed into the z-domain according to,

$$\overline{d}_i^z = ((Q\ )^t)^r . \underline{\overline{T}} . \overline{d}_i \qquad 5.35$$

where Q and T are the Q and T-matrices, as defined in the previous chapter.

The delay polynomials are transformed directly into the z-domain, so defining $\overline{D}_i^z$ as the z-transform of the $\overline{D}_i$ polynomial, equations 5.32, 5.33 and 5.34 become:-

$$\overline{W}_{13}^z = \frac{\overline{d}_4^z.\overline{D}_4^z}{\overline{d}_3^z.\overline{D}_1^z - \overline{d}_2^z.\overline{D}_2^z} \qquad 5.36$$

$$\overline{W}_{31}^z = \frac{\overline{d}_5^z.\overline{D}_3^z}{\overline{d}_3^z.\overline{D}_1^z - \overline{d}_2^z.\overline{D}_2^z} \qquad 5.37$$

$$\overline{W}_{33}^z = \frac{\overline{d}_1^z.\overline{D}_1^z - \overline{d}_2^z.\overline{D}_2^z}{\overline{d}_3^z.\overline{D}_1^z - \overline{d}_2^z.\overline{D}_2^z} \qquad 5.38$$

where $\overline{W}_{ij}^z$ is the z-domain transfer function $\overline{W}_{ij}$. These equations may then be resolved into the digital-filter format, described by:-

$$\overline{W}_{ij}^z = \frac{\sum_{i=0}^{MAX} e_i z^{-i}}{\sum_{j=0}^{MAX} f_j z^{-i}} \qquad 5.39$$

The order of the transfer function (MAX), depends on both the differential and delay polynomials. For large values of T_s, this value may be in the range,

$$40 \leqslant MAX \leqslant 100.$$

However, for small values of T_s, when several layers are present, the value of MAX may become unacceptably large. For example, MAX may exceed 1000. This can lead to excessive and unnecessary calculation.

It is important to note that, regardless of the value of T_s, the number of non-zero coefficients in the $\overline{W}^z_{ij}$ transfer function is constant. As T_s is reduced, although the order of the transfer function is increased no new coefficients are introduced (the values and locations of the existing coefficients are merely altered). This highlights the need to choose T_s with care, and not to specify an arbitrarily small value.

5.4 SIMULATION AND EXPERIMENTAL RESULTS FOR A TRANSDUCER WITH NO LAYERS

This section presents the corresponding simulation and experimental results for a transducer operating into semi-infinite real media at each face. A variety of electrical load conditions are considered for three different cases, viz: the voltage measured across a transmitter; the force output from a transmitter; and the voltage measured across a receiver.

Experimental details and data on the transducers employed are provided in Appendix B, along with a description of the excitation circuitry.

5.4.(i) Transmitter Voltage

This is described by the transfer function $\overline{W}_{33}$. The transducer used (designated 'A' in Appendix B), com-

prised a free 20 mm diameter 1MHz PZT-5A ceramic disc. The electrical firing circuit comprised a VMOS switching FET, as described in Appendix B, Experimental Setup 1. The firing circuit may be modelled according to the methods described by Hayward (19), and this data is presented alongside the simulation and experimental results. To unify the results, a sampling period equivalent to one hundredth of the transducer transit-time was selected for all the simulations. Thus, from Appendix B, T_s has value 4.35 n.s. This value is smaller than that required for some of the cases, however, it avoids aliasing, and allows the simulation results to be compared on an equal basis.

CASE 1

The electrical configuration is shown in Fig 5.1A. In this example, the electrical load is a blocking capacitor of 2nF. The input voltage was observed to be a 50 V ramp of duration 30 n$, so, HT = 50 V and t = 30 ns.
on

To demonstrate the differential and delay polynomials of the previous section, this case may be

expanded as follows:-

From Fig 5.1A

$$\overline{Z}_E = \frac{1}{sC_B} \qquad 5.40$$

Hence,

$$\overline{Z}_E^N = 1$$

$$\overline{Z}_E^D = 0 + sC_B \qquad 5.41$$

where C_B is the value of the blocking capacitor, in this case, 2 nF.

Hence, the $\overline{d}_i$ polynomials become,

$$\overline{d}_1 = 0 + 0.s + C_B s^2 \qquad (i)$$

$$\overline{d}_2 = X_k(0 + s.C_B) \qquad \text{(ii)}$$

$$\overline{d}_3 = 0 + 0 + s^2(C_t + C_B) \qquad \text{(iii)}$$

5.42

($\overline{d}_4$ and $\overline{d}_5$ are not required for this case).

It may be observed from equations 5.42, that the first term of each $\overline{d}_i$ polynomial is zero. This indicates that the polynomials have a common factor and, removing this,

$$\overline{d}_1 = 0 + s.C_B$$

$$\overline{d}_2 = X_k.C_B + 0.s$$

$$\overline{d}_3 = 0 + s(C_B + C_t) \qquad 5.43$$

The value of X_k may be obtained from the data in Appendix B, and the equations 5.43 may be transformed

using the Q-matrix technique of Chapter 4.

The differential vectors, $\overline{D}_1$ and $\overline{D}_2$ become, for this case:-

$$\overline{D}_1 = 1 - e^{-2sT}$$

$$\overline{D}_2 = (4 - 8e^{-sT} + 4e^{-2sT}) \qquad 5.44$$

since it is valid to approximate R_1 and R_{-1} by unity for an air-backed, air-loaded transducer.

Also,

$$T/T_s = 100 \qquad 5.55$$

where T is the transit-period of the transducer. So $\overline{D}_1$ and $\overline{D}_2$ may be z-transformed directly, to give:-

$$\overline{D}_1^z = 1 - Z^{-200}$$

$$\overline{D}_2^z = 4(1 - 2Z^{-100} + Z^{-200}) \qquad 5.56$$

Thus the overall z-transform of the transducer system may be formed.

The simulation and experimental responses for this case, are shown in Figs 5.1B and 5.1C respectively.

CASE 2

This case is identical to CASE 1 but the value of the blocking capacitor has been reduced to 100 pF. The electrical load configuration is shown in Fig 5.2A and the simulation and experimental results in Figs 5.2B and 5.2C respectively.

CASE 3

In this case, the electrical load comprises a 2 nF blocking capacitor in parallel with a 1 $K\Omega$ resistor. The electrical driving voltage and trans-

ducer are identical to those of CASE 1. The electrical load, simulation and experimental results are shown in Figs 5.3A, B and C respectively.

CASE 4

The final transducer voltage case is shown in Figs 5.4. Now the electrical load comprises a 1 nF blocking capacitor with a 100 Ω resistor and 1 μH inductor in parallel. The electrical excitation and transducer are identical to CASE 1. As before, the electrical load, configuration, simulation and experimental results are shown in Figs 5.4A, B and C respectively.

Comparing results in Figs 5.1, 5.2, 5.3 and 5.4, it may be seen that there is generally excellent agreement between the simulation and experimental results. There are however, several possible sources of error which may account for minor differences between the plots.

In Figs 5.1C and 5.2C, it may be observed that there is an upward trend to the experimental voltages which does not appear in the simulation results. This is caused by radial vibrations within the transducer which

are not covered by the model. This may also be observed in Fig 5.3C, where the slope of the experimental result decreases as the voltage returns to zero. The simulation plot does not predict this. However, in all three cases, the portion of the experimental voltages which is caused by the thickness vibrations of the transducer agrees very well with that predicted by the simulation results.

In Fig 5.4C, there is a minor difference in the precise nature of the first phase change. This is most likely caused by minor differences in the values of the electrical components which were used for the experimental results and the assumed values which were used for the simulation plots.

Finally, it may be concluded that there is generally excellent agreement between the simulation and experimental results and that both the model and Q-matrix technique are valid for the transfer function $\overline{W}_{33}$.

5.4 (ii) Transmitter Output Force

This is described by transfer function $\overline{W}_{13}$. The transducer used, (designated 'B' in Appendix B) comprised a 20mm diameter, 1 MHz, PZT-5A disc, backed with an epoxy compound of known acoustic impedance. The electrical firing circuit used was similar to that of the preceding section.

The transducer was positioned in a water tank, and aligned co-axially with a PVDF membrane hydrophone. Hayward (19) has shown that the bandwidth of the hydrophone is large enough to have no effect on the force output from the transducer, other than a scaling factor.

A complete description of the firing circuit and experimental configuration are given in Appendix B, Experimental Setup 2.

CASE 5

In this case, the electrical load configuration is identical to CASE 1. However, the firing voltage has now been increased from 50 V to 300 V. The electrical

load, simulation and experimental results are shown in Fig 5.5A, B and C respecticely.

CASE 6

This case is identical to CASE 5, with the addition of a parallel 100 Ω resistor. The electrical configuration, simulation and experimental plots are given in Figs 5.6A, B and C respectively.

CASE 7

This case uses an electrical load which consists of a 2 nF blocking capacitor, in series with a 100 Ω resistor and 2.4 μH conductor in parallel, as shown in Fig 5.7A . The electrical driving voltage is 300 V, but the ramp-on-time has been increased to 500 ns. As before, the simulation and experimental results are shown in Figs 5.7B and C respectively.

When comparing the simulation and experimental results in Figs 5.5, 5.6 and 5.7, it may be seen that, while there is still generally good agreement between the results, this is not as good as that obtained with the transducer voltage measurements. There are several reasons for this.

Firstly, the hydrophone, although aligned co-axially with the transducer, is subject to the diffracted field of the transducer. Great care was taken in positioning the hydrophone to minimise diffraction effects, however this cannot be neglected. Since the simulation plots do not account for diffraction, this effect is the most likely cause of discrepancies between the simulation and experimental results. Secondly, all three experimental results show marked rounding when compared with the simulation results. This is partially due to diffraction, but also to attenuation in the water channel. This has not been included in the model.

Thus it may be concluded that there is good general agreement between the simulation and experimental results for cases 5, 6 and 7. When physical effects which are not included in the model are accounted for, it may be observed that the model predicts accurately the portion of response due to thickness-mode piezoelectric action. Hence transfer function $\overline{W}_{13}$ is valid.

5.4(iii) Receiver Voltage

This section deals with transfer function $\overline{W}_{31}$. For this set of experiments, the transducer used, (designated 'C' in Appendix B) was a 20 mm diameter, 1 MHz, PZT-5A disc, mounted in a Perspex holder. This probe was air-backed.

The experimental equipment and configuration are described in Appendix B, Experimental Setup 3.

To model the receiving transducer experimentally, it was necessary to excite the transducer with a known force input. Since it was not possible to generate specific forces in the water tank, the force outputs of cases 6 and 7 were used instead.

CASE 8

In this case, the receiver had an electrical load of 100 Ω connected across the transducer. The force i/p, incident upon the receiver, was the force generated by Case 6. Figs 5.8A, B and C show the electrical load, the simulation and experimental measurements respectively.

CASE 9

This case is identical to Case 8 except that an inductor of 4.7 μH has now been added in parallel with the 100 Ω resistor. As before, Figs 5.9A, B and C show the electrical load, the simulation voltage and the experimental voltage respectively.

CASE 10

This case is identical to the preceding case. However the 4.7 μH inductor is replaced by a 2.4 μH inductor. Figs 5.10A, B and C show the electrical load, the simulation result and the experimental measurements respectively.

CASE 11

In this case, the force generating transducer is that of Case 7. The receiving transducer had a 100 Ω parallel electrical load. Figs 5.11A, B and C show the electrical configuration, simulation result and experimental result respectively.

CASE 12

This case is identical to the preceding case except that an inductor of 2.4 μH has now been added, in parallel with the 100 Ω resistor. Figs 5.12A, B and C

give the electrical load, the simulation voltage and the experimental result respectively.

Comparing the simulation and experimental results of Figs 5.8, 5.9, 5.10, 5.11 and 5.12, it may be observed that there is generally very good agreement between the results. However, there are several small discrepancies which may be explained as follows.

Firstly, the receiving transducers have a much larger active area than the PVDF hydrophone. Consequently, these devices are exposed to a substantial part of the diffracted field of the transmitter. However, the diffracted field varies across the face of the receiving transducer, and the transducer has the effect of averaging out the diffracted field. This has two main effects on the receiver voltage.

(i) The experimental voltage will be smoother than the simulation result; so any sharp spikes in the simulation plots will become rounded in the experimental result.

(ii) Phase differences in the diffracted field will essentially cancel out in the averaging process, so, the envelope of the experimental result will

decay faster than that of the simulated result.

Secondly, attenuation of the force wave will occur in the water channel, (as was noted with Cases 5, 6 and 7), so that the experimental voltage will be smoother than the simulation.

Finally, it was assumed for the simulation results that the receiving transducer, transducer C, was air-backed. However, as is explained in Appendix B, this transducer is mounted in a Perspex holder which clamps the transducer laterally. This will have the effect of apparently increasing the acoustic impedance of the backing material. As the acoustic impedance of the backing increases, so the envelope of the received voltage decays faster.

Thus when these effects are considered, it may be concluded that there is excellent agreement between the simulation and experimental results of Figs 5.8 to 5.12 . Hence transfer function $\bar{W}_{31}$ is proved to be valid.

(iv) Conclusion

This section has presented twelve results covering three different transducer configurations. In general,

it may be concluded that, when the physical effects not included by the simulation model are considered, there is excellent agreement between the simulation and experimental results. Thus transfer functions $\overline{W}_{33}$, $\overline{W}_{13}$ and $\overline{W}_{31}$ may be assumed to be generally valid for the no-layer case.

The cases covered here have considered only simple mechanical loads with reasonably complex electrical loads. The next section will deal with some layered cases.

5.5 SIMULATION AND EXPERIMENTAL RESULTS FOR A TRANSDUCER WITH FRONT AND REAR FACE LAYERS.

This section presents the corresponding simulation and experimental results for a piezoelectric transducer with front and rear face mechanical layers. The preceding section dealt with the effects of various electrical loads on the response of a thickness mode transducer. To highlight the effects of the mechanical layers, only simple electrical loads will be used in this section.

As before, three cases are dealt with; the force output and voltage across a transmitter, and the voltage across a receiver. The experimental setups are similar to those of the preceding section and the results are presented in the same manner. A brief description of the experiment, and of the transducer used, is followed by a detailed analysis and comparison of the simulation and experimental results. Full details of the equipment used, the experimental setup and the transducer construction are given in APPENDIX B.

5.5(i) Force Output from a Transmitter

This case corresponds to transfer function $\overline{W}_{13}$.

Transducers D and E were used for these experiments. Each transducer was manufactured using a two-stage process, and experimental and simulation results were taken at each stage for both transducers. The transducers are broadly similar, and are made up as follows;

Transducer D consists of a lead plug glued to the rear of a 1 MHz, 20 mm PZT-5A ceramic, with an aluminium layer cemented to the front face. The rear bondline glue was Silver-loaded Araldite, while the front bondline was commercial Araldite.

Transducer E consists of a lead plug glued to the rear of a 1 MHz, 30 mm PTZ-5A ceramic, with a steel layer glued to the front face.

In both cases, the lead plug is assumed to be sufficiently thick to act as a semi-infinite medium. The major difference between the transducers is the thickness of the front layers. The aluminium layer was chosen to be 2.5 mm thick; this gives it a transit period of approximately 0.4 μs which is close to the

transit period of the ceramic (0,434 μs). The steel layer was chosen to be 0.035 mm thick. This results in a transit period of approximately 0.06 μs which is about an order of magnitude smaller than that of the ceramic.

Full details of the construction and the materials used in manufacturing the transducers are given in APPENDIX B.

Experimental and simulation results were carried out for each transducer, before and after the addition of the front face layers. This allowed some quantitative measurements of the rear bondline thickness to be made.

The oscilloscope settings for all the experimental results in this section were:- 0.5 μs/large div (x-axis)
5 mv/large div (y-axis)

CASE 13

This measurement was made for transducer D, before the addition of the front layer. The electrical firing circuit (shown in Fig 5,13A) comprised a series 2 nF

blocking capacitor. The electrical source voltage was a 300 V, 60 ns ramp. As with the previous results, the PVDF hydrophone was aligned co-axially with the transducer. This is detailed in experimental setup 2.

Fig 5.13B shows the simulation result for this case, when the rear bondline thickness was taken as 10 μm. Fig 5.13C shows the corresponding experimental result. Figs 5.13D and E show simulation results for bondline thicknesses of 5 μm and 20μm respectively.

CASE 14

This is identical to Case 13, with the addition of a 100 Ω parallel resistor in the firing circuit. Fig 5.14A shows the electrical configuration; Fig 5.14C shows the experimental result, and Figs 5.14B, D and E give the simulated response for rear bondlines of 10μm, 5μm and 20μm respectively.

Comparing the results of Cases 13 and 14,it may be observed that there is generally good agreement between the simulated and experimental results. By comparing the relative amplitudes of the spikes and the main pulse for each case, it may be concluded that the best agreement is achieved for a rear bondline

thickness of 10μm. However, it is apparent from the 5μm simulation plots (D in each case) that the true bondline thickness lies somewhere between 5 and 10μm. There is some corruption of the main pulse shape in both cases. This is most likely due to cabling effects. The sharpness of the spikes in both cases is much less in the experimental result than in the simulated results. This is caused by attenuation in the water column between the transducer and the hydrophone which is not modelled. Also, there is an edge-wave visible at the extreme right-hand edge of each experimental result.

Finally, it may be concluded that the rear bondline thickness for transducer D lies between 5 and 10μm and it will be assumed, for later plots to be 10μm.

CASE 15

This case is identical to Case 14 but transducer D now has a front face aluminium layer. The co-axial cable attached to the transducer was shortened in an attempt to avoid the effects noted for Cases 13 and 14. Fig 5.15A shows the electrical circuit; Fig 5.14C shows the experimental results and Figs 5.14B, D and

E show simulation plots for an aluminium layer of thickness 2.5 mm, 2.48 mm and 2.52 mm respectively. (These correspond to the measured thickness and the minimum and maximum likely thicknesses respectively.) (It was assumed that the front bondline was also 10 μm thick. To check this, several simulations were plotted for a variety of front bondline thicknesses and compared with Fig 5.15C. The best results were for 10μm., so the assumption was valid. These plots have not been included here.)

Comparison of Figs 5.15B, D and E with the experimental result of Fig 5.15C shows that the simulation results are generally in very good agreement with the experimental ones. There is very little difference between the simulated plots which is to be expected, since the tolerance in the measured thickness is small. Thus it may be concluded that the multilayered model accurately models the force output from a transmitter and hence, transfer function $\overline{W}_{13}$ is valid for multi-layered cases.

It is interesting to note that there is no disruption of the main pulse in this case, which seems to confirm that these effects were caused by the co-axial

cable in Cases 13 and 14.

Finally, the aluminium layer is sufficiently thick to cause some attenuation of the force waves as they pass through it. This adds an extra source of error which may also account for some of the small discrepancies between the experimental and simulation results.

CASE 16

This case deals with transducer E, before the addition of the steel layer. The electrical firing circuit comprised a 2 nF blocking capacitor and is sketched in Fig 5.16A . Electrical excitation was a 300 V, 60 ns ramp. The experimental setup was identical to Cases 13,14 and 15.

Fig 5.16B shows the simulation plot for 10 μm rear bondline and Fig 5.16C shows the corresponding experimental result. Several other simulations were carried out for 5 and 20 μm bondlines but the best agreement was for 10 μm. These results are not included here.

CASE 17

This case is identical to Case 16, with the addition of a parallel 100 Ω resistor in the electrical firing circuit (as shown in Fig 5.17A).

Figs 5.17B and C show the simulation result for a 10 μm rear bondline, and the corresponding experimental result.

Comparing the simulation and experimental results for Cases 16 and 17, it is apparent that there is good agreement between them in both cases, However, both the experimental results show some distortion at the right-hand side. This is due to edge waves which are not included in the model. There are also some minor differences between the simulation and experimental plots, most noticeably slight distortion of the main pulse. These are most probably due to cabling effects, and may be ignored.

Thus cases 16 and 17 indicate that the rear bondline thickness of transducer E is of the order of 10μm.

CASE 18

This case deals with transducer E, after the addition of the front steel layer. The experimental setup is identical to Case 16. Figs 5.18A and C show the electrical configuration and experimental results respectively. Figs 5.18B, D and E show the simulation results for front layer thicknesses of 0.345, 0.0370 and 0.40 mm. (The measured layer thickness was 0.355 mm.) The front bondline was assumed to be 10 μm.

CASE 19

This case deals with transducer E, after the addition of the front steel layer. The experimental setup is identical to Case 17. Figs 5.19A and C show the electrical configuration and experimental result respectively. Figs 5.19B, D and E show the simulation results for the front layer thicknesses given in Case 18. Again, the front bondline was assumed to be 10 μm.

When comparing the experimental and simulation results for Cases 18 and 19, it may be observed that the best agreement is with simulation plot E in each case. This is unexpected, since this case corresponds to a layer with thickness 0.40 mm, approximately 50 μm thicker

than the measured thickness of the layer, and well outside the error tolerance of the measurement.

This may be explained as follows;

In the simulation, the defining criteria for each layer are its acoustic impedance and its transit time (the time taken for mechanical waves to cross the layer). The acoustic impedance determines the relative reflectivity of the layer boundaries and minor variations in this affect only the relative amplitudes of the spikes in the simulation responses. Thus, the simulation is comparatively insensitive to minor variations in acoustic impedance.

However, variations in the transit time affect the location of the spikes and hence, the shape of the simulation response.

Each of the layers in plots B, D and E of Cases 18 and 19 was specified by layer thickness in mm. It is more accurate to specify these layers in terms of their transit times, which are 0.0565 μs, 0.0608 and 0.0652 μs for plots B, D and E respectively. Now, the transit time of each layer is given by the quotient of its thickness and velocity. The velocity assumed for

the steel layer is given in Table B3 and was 6.1 mm /μs. From the results of Cases 18 and 19, and assuming the measured layer thickness of 0.355 mm to be correct, then if the layer transit time is taken to be 0.0652 μs, the velocity of mechanical waves in the layer must be 5.4 mm/μs. This value is substantially lower than the initially assumed value. The assumed value of 6.1 mm/μs was for the longitudinal velocity in a steel bar. Similarly, the velocity for the aluminium layer (6.3 mm/μs) was for an aluminium bar. In fact, the aluminium layer was made from a 20 mm rod of aluminium and the results of Case 15 agree well with this assumed velocity. However, the steel layer was made from a thin steel plate and it is possible that the manufacture of the steel plate could have affected the longitudinal velocity in this manner.

Another possible reason for this discrepancy may be attenuation in either the steel layer or the water tank. This would smooth out the experimental result in which case, either simulation plots B or D of Cases 18 and 19 could be correct. These give calculated longitudinal velocities of 6.3 mm/μs and 5.8 mm/μs respectively. The value 6.3 mm/μs is

slightly high for steel, whereas that of 5.8 mm/us falls within the range of values given by the source of Table B1 (Ref 15). Thus, it may be concluded that the best agreement in Cases 18 and 19 is between plot D in both cases, if attenuation is considered, and between plot E in both cases, if attenuation is ignored. (In both cases, several simulations were carried out for a variety of front bondline thicknesses. As with the previous cases, best agreement was around 10 μm, and the other plots are not presented here.)

Finally, the presence of edge waves may be observed in several of the results of Cases 13 to 19. HAYWARD has proposed a simple model to predict these effects, on the transducer axis. This is derived in APPENDIX C.

CASE 20

Identical to Case 19, but with the hydrophone positioned 200 mm from the transducer, on axis. Fig 5.20A shows the simulation plot and Fig 5.20B the corresponding experimental result. There is reasonable agreement between the results, although at this distance, attenuation in the water column has a

significant effect. The simulation was carried out for a steel layer thickness of 0.37 mm (Fig 5.19D). However, at this distance, small variations in the layer thickness have little effect on the simulation. This experiment was repeated for distances of 100 mm and 150 mm but agreement in these cases was poor. This is probably because these points lie within the near-field of the transducer (calculated as 150 mm). The physical size of the water tank restricted the maximum distance to 200 mm so more distant far-field measurements could not be made.

Thus, the experimental and simulation results of Cases 13 to 20 have generally shown good agreement between the predicted responses of the transducers and the experimentally measured responses. When the factors not included in the model, namely diffraction and attenuation are considered, the small discrepancies between the results may be explained. It is thus possible, using this method, to both model and estimate the effects and dimensions of front and rear mechanical layers on the transducer. It may therefore be concluded that the model and z-form methods are correct for transfer function $\overline{W}_{33}$.

5.5 Receiver Voltage

This case corresponds to transfer function $\overline{W}_{31}$. Transducers B and E were used for these results. In the case of transducer E, no results were taken during the intermediate construction stages, and the transducer was assumed to have the dimensions given in Case 19.

Experimental setup 3 (detailed in Appendix B), was used for the experimental measurements. Oscilloscope settings for the experimental results were 0.5 μs/large division (x-axis) and 0.5 V/ large division (y-axis), unless otherwise stated.

CASE 21

In this case, transducer B was the transmitter, and transducer E the receiver with a 100 Ω electrical load. (This is sketched in Fig 5.21A). Both transducers were aligned co-axially, as detailed in Appendix B.

The force output from transducer B is that of Case 5, shown in Figs 5.5A, B and C. Fig 5.21C shows the experimentally measured receiver voltage. Figs 5.21B, D and E show the corresponding simulation plots for steel layer transit periods of 0.0565 μs, 0.0608 μs and 0.0652 μs respectively. Clearly,

there is generally very good agreement between the experimental and simulation plots, although there is a slight difference in the envelope shapes.

CASE 22

This case is identical to that of Case 21, but now the force output from transducer B is that of Case 6, detailed in Figs 5.6A, B and C. (The y-axis oscilloscope setting is 0.2 V/large division, here.)

Again there is very good agreement between the simulation and experimental results.

Comparing the simulation and experimental results of Case 21 and 22, it may be observed that there is generally very good agreement between the simulated and experimental results, in both cases.

This contradicts the results of Cases 18 and 19, where the best agreement was for simulation plots D or E, depending upon whether attenuation was included or not. It is most likely that there is some attenuation in both the steel layer and the

water column. Then the transmitter force experiments of Cases 13 to 20 will highlight this effect, since the hydrophone measures a specific portion of the plane wave component generated by the transducer. The reception experiments of Cases 21 and 22 measure the entire plane wave component of the transmitter, and the receiver voltage is a function of this. Thus, since the receiver has a substantial integrating effect, any small discontinuities will be averaged out, and the resultant voltage will not highlight attenuation effects.

Thus, the best conclusion which may be drawn from these experiments is that the transit period of the steel layer lies between 0.0565 μs and 0.0608 μs, and has a velocity range of 5.8 mm/μs to 6.3mm/μs. Several different bondline thicknesses were simulated for Cases 21 and 22 but their effects were not apparent. The simulation results of Figs 5.21B and 5.22B assumed 10μm bondlines. These could have been zero or as much as 25 μm, with little or no discernible difference.

CASE 23

This is identical to Case 21, with the transmitter

and the receiver reversed. The transmitter (now transducer E), is shown in Case 18, Fig 5.18. Again, the receiver had a 100 Ω electrical load, as sketched in Fig 5.23A. Fig 5.23C shows the experimental result, and Figs 5.23B, D and E, the simulation plots for a transmitter steel layer with transit times of 0.0565 μs, 0.0608 μs and 0.0652 μs respectively.

There is generally good agreement between the simulation and experimental results, however, there is some smoothing of the experimental response.

CASE 24

This is identical to Case 22, with the transmission and reception transducers reversed. The transmitter output force corresponds to Case 19, and, as with Case 22, the receiver has a 100 Ω electrical load. This is sketched in Fig 5.24A. The experimental result is shown in Fig 5.24C . Figs 5.24B, D and E show the received voltage corresponding to a transmitter front steel layer of transit times 0.0565 μs, 0.0608 μs and 0.0652 μs respectively.

There is generally good agreement between the

simulated and experimental responses, although, as with Case 23, there is some smoothing of the experimental result.

Comparing the simulation and experimental results of Cases 23 and 24, it is apparent that the best agreement is with plot B. This reinforces the result of Cases 21 and 22. However, in Cases 23 and 24, both the experimental results exhibit substantial smoothing. There is also a scale factor difference in the relative amplitudes of the simulation and experimental results. This may be explained as follows;

In Cases 21 and 22, the receiving transducer E has a diameter of 30 mm, while the transmitter B has a diameter of 20 mm, thus the receiver is subject to the entire plane wave component of the transmitter. When the transmitter and receiver are reversed, the receiver is subjected to only 4/9 ths of the transmitter plane wave component, hence, the receiver voltage will be approximately half the value predicted by the simulation.

This effect may have contributed to the smoothing of the received voltages in Cases 23 and 24 since,

although there is some smoothing in Cases 21 and 22, it is a lot less then that of Cases 23 and 24.

From this, it may be concluded that the method of Cases 21 and 22, (that is, using the layered probe as a receiver), gives better results than that of Cases 23 and 24. Thus, if the parameters of a layered probe are to be determined using two transducers of similar dimensions, it is best to use the layered probe as a receiver,

Finally, it may be concluded that the results of this section verify the accuracy of transfer function $\overline{W}_{31}$, for a transducer with mechanical layers.

5.5(iii) Transmitter Voltage

This case corresponds to transfer function $\overline{W}_{33}$. Only transducer E was used for these results, since it is the aim of this section to demonstrate the accuracy and applicability of the model, and not to analyse all the transducers in depth. Experimental setup 1 (detailed in Appendix B), was used for the

experimental results. The oscilloscope settings for the experimental results were 0.5 μs/large division (x-axis) and 20 V/large division (y-axis).

CASE 25

In this case, transducer E was setup as shown in Fig 5.25A. The electrical load was a 2 nF blocking capacitor, and the electrical excitation a 300 V, 60 ns ramp. Fig 5.25B shows the experimental result and Fig 5.25C shows the simulation result. The transducer parameters were assumed to be:-

Front Bondline, 10 μm
Rear Bondline, 10 μm
Front Layer, 0.0608 μs.

Clearly, there is poor agreement between the experimental and simulated results.

Fig 5.25D shows another simulation result, this time for a rear bondline thickness of 50 μm. There is much better agreement between the experimental result and Fig 5.25D.

CASE 26

This is identical to Case 25, with the inclusion of a 100 Ω parallel resistor in the firing circuit,

as shown in Fig 5.26A. Fig 5.26B shows the experimental result and Figs 5.26C and D, the corresponding simulation results for a rear bondline thickness of 10 μm and 50 μm respectively. There is poor agreement between Figs 5.26B and C, but reasonably good agreement between Figs 5.26B and D.

Comparing the experimental and simulation results for Cases 25 and 26, it is apparent that the best agreement is with plot D in both cases. This plot corresponds to a rear bondline of 50 μm - a result which disagrees with the results of the two preceding sections. To check this, several simulations were carried out for each of Cases 25 and 26, with a variety of front and rear bondline thicknesses, as well as several steel layer thicknesses. These are not included here, but it was apparent from them, that the major factor in producing the experimental results of Cases 25 and 26 was the rear bondline thickness, and that the best agreement was reached when this was assumed to be 50 μm.

This result may be explained as follows:

the modelling programs assume the layers to have infinite lateral dimensions, and to be smooth and

parallel. For transducer E, (dia. 30 mm), it is valid to assume the lateral dimensions to be infinite, since the diameter/thickness ratio of the crystal is 16:1 . For the bondline, if it has an assumed thickness of 10 μm, the diameter/ thickness ratio is 3000:1 which falls to 600:1 for a 50 μm thickness. This is sufficiently large to assume the lateral dimensions are infinite.

However, the other requirements for the layers are more difficult to measure, Although both the backing and crystal were cleaned and polished before joining, it is possible that there were air bubbles near the surface of the lead backing. It is also possible that the bondline thickness was non-uniform, especially near the edges where the backing plug was roughest.

Comparing the method used in Cases 25 and 26 with those used to measure the transmitted force and the received voltage, there are fundamental differences in these techniques which could mask the effects of a non-uniform bondline. For the measurement of the transmitted force, the hydrophone was aligned co-axially with the transducer. Thus the plane wave

component incident upon the hydrophone was generated at or near the centre of the transducer and, if the bondlines are of 10 μm thickness in this vicinity, this will be reflected in the hydrophone measurement.

For the received voltage measurement, the transducer is subject to the entire plane wave component, and the edge components of the transmitter. From the experimental results, it is apparent that the edge waves have little or no effect on the receiving transducer, so it seems likely that minor fluctuations in the shape of the plane wave component due to localised backing irregularities, will also have little effect.

However, for the voltage measurement across the transmitter, it may be observed, from Figs 5.25C and 5.26C, that a uniform bondline produces a smooth plot. Any irregularity in the bondline will disrupt the plot. Thus, this method is useful for analysing the overall quality and integrity of the bondlines.

Finally, bearing in mind the above factors, it may be concluded that Cases 25 and 26 prove the validity and accuracy of the model for the transfer function $\overline{W}_{33}$.

5.5(iv) Conclusion

This section has presented 14 experimental cases covering three different transducer configurations. It was the aim of this section to show that the $\overline{W}_{ij}$ transfer functions of Chapter 3, and the z-form techniques of Chapter 4, could be applied to the modelling of piezoelectric transducers with mechanical matching layers. When the factors not included in the model are acoounted for, it is reasonable to conclude that the transfer functions $\overline{W}_{13}$, $\overline{W}_{31}$ and $\overline{W}_{33}$ are valid for the layered transducer case.

5.6 SUMMARY

This chapter has shown how the general multilayered transducer model of Chapters 2 and 3 may be combined with the z-transform techniques of Chapter 4 to produce a general z-domain model of the thickness-mode piezoelectric transducer. The validity and accuracy of this model were then tested by comparing simulation results, produced by the model, with the corresponding experimental results.

Section 5.4 presented a series of results for a transducer with no mechanical layers but with a variety of electrical loads. Three different experimental configurations were tested:-

(i) the voltage across a transmitter, corresponding to transfer function $\overline{W}_{33}$,

(ii) the force output from a transmitter; $\overline{W}_{13}$,

(iii) the voltage across a receiver; $\overline{W}_{31}$.

In the first experimental configuration, agreement between the simulated and experimental results was generally very good. The only major factor which influenced the results and was not included in the model, was lateral vibration of the transducer.

In the second experimental case, it became apparent that both diffraction and attenuation had a significant effect on the response of the transducer. However, these effects could be explained, and were generally not serious.

Finally, in the third case, agreement between the experimental and simulation results was very good, and it became apparent that the receiving transducer averaged out the received signal, thereby significantly reducing the effects of the diffracted edge waves from the transmitter.

Thus, it was concluded from these results that transfer functions $\overline{W}_{13}$, $\overline{W}_{31}$ and $\overline{W}_{33}$ were all valid, and that the z-form techniques of Chapter 4 could be used to accurately model the transient response of a thickness-mode piezoelectric transducer.

Section 5.5 presented a corresponding set of experimental results for two layered transducers. This section concentrated on one particular transducer, (transducer E), since it became apparent that at least one of the parameters of the transducer was

subject to some doubt.

In experimental cases 5.5(i), it was shown that the force ouput from the transducer could be used to accurately estimate the thickness of the layers over a localised area of the transducer surface, in this case, the area near the axis.

Experimental cases 5.5(ii) broadened this method to show that, by using the layered transducer as a receiver, it was possible to obtain a good estimate of the overall effective thickness.

Finally, experimental cases(iii) showed that the transmitter voltage gives an indication of the severity of any irregularities in the layers, in this case, particularly the rear bondline. Diffracted edge waves and the effects of attenuation were also observed in several of these results, and their effect on each individual result noted. Another possible source of error which may have affected the results is the propagation of shear waves in the backing material or the layers. However, no effects which were directly attributable to this were observed, so the possibility

was ignored.

Thus, it was concluded from the results of Section 5.5, that transfer functions $\overline{W}_{13}$, $\overline{W}_{31}$ and $\overline{W}_{33}$ were valid for the case of a transducer with multiple mechanical layers.

It was not possible to test all the $\overline{W}_{ij}$ transfer functions for practical reasons. However, from the symmetry of the equations, the validity of $\overline{W}_{13}$ implies the validity of $\overline{W}_{23}$, and the validity of $\overline{W}_{31}$ implies the validity of $\overline{W}_{32}$.

Finally, this chapter has shown the models of Chapters 2 and 3 to be valid, and the z-transform methods of Chapter 4 to be accurate. It has also investigated the use of these models in determining the properties of multilayered transducers.

The next chapter will investigate methods of improving and controlling the responses of these transducers.

CHAPTER 6
METHODS FOR CONTROLLING AND OPTIMISING THE PERFORMANCE OF TRANSDUCERS

6.1 INTRODUCTION

This chapter investigates methods for improving, controlling and optimising the performance of thickness mode piezoelectric transducers.

A great deal of work has been carried out in this field, by a number of authors, However, the techniques and solutions which have been presented to date may be conveniently divided into two broad categories: passive techniques and active techniques.

Passive techniques, as their name suggests, are concerned with the addition of passive electrical and mechanical elements to the transducer. There are two principal aims of such methods.

Firstly, to improve the power transmission from the transducer to the load. This is often a major problem in areas such as non-destructive testing and biomedicine, where the acoustic impedance of the transducer material can be up to 25 times greater than that of the load medium.

Secondly, passive techniques are employed to improve the spectral characteristics of the transducer system. The transducer usually exhibits a narrowband spectrum, and consequently generates transient outputs which are subject to severe ringing. By adding electrical and mechanical elements to the transducer, it is possible to broaden the spectral response, thereby producing sharper transient outputs with a corresponding improvement in system resolution.

The addition of mechanical layers to the transducer may improve both the power transmission, and the spectrum. To increase the efficiency of the power transmission, mechanical layers of decreasing acoustic impedance are inserted between the transducer and the load material. This effectively presents a smoother transition in acoustic impedance profile between the transducer and the load.

The transducer spectrum may be improved by careful choice of layer thickness. This is usually based on stub-matching techniques used for transmission lines or microwaves. However, there are several different strategies which may be adopted.

Mechanical matching techniques have been investigated by many authors, for example, SITTIG (61), KOSSOFF (24), LEWIS (38), DeSILETS et. al. (14) and SELFRIDGE et. al. (55).

Electrical tuning, using R-L-C networks may also enhance both the efficiency and spectral characteristics of the transducer. By matching the impedance of the transducer to that of the driving source, considerable improvements in power transmission efficiency may be obtained. The resonant nature of some R-L-C networks may also be used to effectively broadband the transducer spectrum. Examples of such techniques are discussed by Lewis (38) and Selfridge et. al. (55).

A combination of mechanical and electrical tuning techniques may lead to substantial improvements in transducer efficiency and response. However, these methods are, by their very nature, restricted to a narrow bandwidth centred around the design frequency. The selected design frequency is invariably the mechanical resonance of the ansducer. This restricts the duration of the generated transient response, such that it must be greater than the transit period of the transducer. Some applications, particularly in non-destructive testing, require narrow pulses of shorter

duration than the transit period. This has led to the development of active transducer control.

There are two main aims of active transducer control. Either to generate pulses of shorter duration than the transit period, or to generate a precisely defined ouput transient. The techniques which have been developed in connection with active control, usually require detailed knowledge of either the impulse response of the transducer system, or the transfer function of the system.

Two fundamentally different methods which illustrate the generation of short pulses have been developed by BØRJESSEN et. al. (3), and KAŽYS and LUKOŠEVIČIUS (33). The method of (3) uses a weighted least squares filter procedure, in conjunction with a knowledge of the transducer impulse response to evaluate an optimal excitation voltage. When the voltage is applied to the transducer system, a very short spiked waveform is generated.

The method used by KAŽYS and LUKOŠEVIČIUS employs active electrical correction circuits to cancel secondary piezoelectric action. The transfer function

of the resultant system may then be inverted (or deconvolved), in a relatively straightforward manner, to allow the generation of a single short spike.

The second aim of active control, to generate a desired waveform, has been attempted in several ways. LIU (39) uses the spectral impulse response, with the spectrum of the desired output, to obtain the spectrum of the required input. This method has a disadvantage, in that the use of window functions may be required to render the input spectrum causal. These functions may alter the required input to such a degree that marked distortion occurs in the desired output. Thus this method is of limited use.

COURSANT (13) adopts a similar approach to that of Kažys and Lukoševičius. However, the method differs in two important aspects. Firstly, he generates a triangular pulse of known shape and width, not a single spike. Secondly, he assumes that secondary action is sufficiently small to be ignored. This assumption of zero secondary action cannot be extended to the high-efficiency ceramic transducers. The method is thus limited in application to less efficient transducer systems.

Finally, Mel'kanovich (45) uses the Laplace transfer function of the transducer system, in conjunction with the Laplace transform of the output, to calculate the Laplace transform of the required input. His method is rather complicated and deals only with cases where the electrical load is zero, (that is, the generating source is assumed to have zero impedance). Nevertheless, it does include the effects of secondary action.

When comparing passive and active control of transducers, it is apparent that, while passive control is much simpler to achieve in practice, the results which may be obtained with this method are limited, in terms of bandwidth and duration. Conversely, active control offers the ability to generate specific outputs. However, generation of the required excitation voltage may involve sophisticated apparatus (13) due to the complexity of the waveform. It is also important to note that active control offers no improvements in power transmission efficiency.

This chapter extends the inversion method developed by Mel'Kanovich and it will be shown that the complexity of his method may be substantially reduced by using the modelling techniques of the preceding

chapters. This allows the inclusion of non-zero electrical elements and their effects will be investigated. The effects of multiple layers will also be investigated, both in terms of power efficiency transmission, and on the nature of the inversion techniques.

6.2 MECHANICAL MATCHING LAYERS

Mechanical matching layers are often used in transducer construction to increase the efficiency of acoustic energy transfer from the transducer to the load medium. Consider Fig 6.1, which shows the interface between two media, of acoustic impedances Z_T and Z_L respectively. If a wave of force, F_t, encounters this boundary, then a portion is transmitted, according to the expression,

$$\bar{F}_L = \frac{2Z_L}{Z_L+Z_T} \bar{F}_t \qquad 6.1$$

If, Z_L is substantially smaller then Z_t, then, from equation 6.1, there will be little energy transfer across the boundary, and most of the energy in F_t will be reflected. This situation occurs frequently in ultrasonic transducer systems where the acoustic impedance of the transducer may be substantially higher than that of the load. This problem may be partially solved by placing intermediate layers, of varying acoustic impedance between the transducer and the load

medium, as shown in Fig 6.2.

However, the acoustic impedances of the various matching layers are not defined. Several authors have proposed methods for calculating the optimum values of the matching layers. DeSilets et al. (14), and Selfridge et al. (55) use values derived from transmission line matching techniques. Lewis (38) however, proposes a method whereby each layer has an impedance which is a fixed percentage lower than the preceding one. These methods are different.

Consider the single layer system of Fig 6.3. If the finite width of the layer and reflections at both the interfaces are ignored, then the relationships between the transmitted and incident forces are, from equation 6.1,

$$\frac{\overline{F}_1}{\overline{F}_t} = \frac{2Z_1}{Z_1+Z_T} \qquad 6.2$$

$$\frac{\overline{F}_L}{\overline{F}_1} = \frac{2Z_L}{Z_L+Z_1} \qquad 6.3$$

and hence,

$$\frac{\overline{F}_L}{\overline{F}_t} = C \qquad 6.4$$

where,

$$C = \frac{2Z_1}{Z_1+Z_T} \; \frac{2Z_L}{Z_L+Z_1} \qquad 6.5$$

is defined as the transmission factor.

Now, both Z_t and Z_L are assumed to be known, so Z_1 is the only unknown in equation 6.5 . Thus differentiating 6.5, with respect to Z_1 gives,

$$\frac{dC}{dZ_1} = \frac{4Z_L(Z_TZ_L - Z_1^2)}{((Z_1+Z_T)(Z_L+Z_1))^2} \qquad 6.6$$

Equating 6.6 to zero gives:-

$$Z_1 = \sqrt{Z_TZ_L} \qquad 6.7$$

This is the optimum value of Z_1 which maximises the transmission coefficient.

Now, consider the multiple layer system of Fig 6.2 . The result of equation 6.7 is true for any single layer system, and if each layer is assumed to have the optimum impedance value, with respect to the adjacent layers, then,

$$Z_{iOPT} = (Z_T \cdot Z_{2OPT})^{1/2}$$

$$Z_{2OPT} = (Z_{1OPT} \cdot Z_{3OPT})^{1/2}$$

$$\vdots$$

$$Z_{nOPT} = (Z_{(n-1)OPT} \cdot Z_L)^{1/2} \qquad 6.8$$

and for the i^{th} layer,

$$Z_{iOPT} = (Z_{(i-1)OPT} \cdot Z_{(i+1)OPT})^{1/2} \qquad 6.9$$

The layers i-1 and i+1 are also optimal, and hence, equation 6.9 may be rewritten as,

$$Z_{iOPT} = ((Z_{(i-2)OPT} \cdot Z_{iOPT})^{1/2} \cdot (Z_{iOPT} \cdot Z_{(i+1)OPT})^{1/2})^{1/2}$$

6.10

which becomes,

$$Z_{iOPT} = (Z_{(i-2)OPT} \cdot Z_{(i+2)OPT})^{1/2} \qquad 6.11$$

Also,

$$Z_{(i+1)OPT} = (Z_{iOPT} \cdot Z_{(i+2)OPT})^{1/2} \qquad 6.12$$

and by substitution, since $Z_{(i+2)OPT}$ is also optimal,

$$Z_{(i+1)OPT} = (Z^2_{iOPT} \cdot Z_{(i+3)OPT})^{1/3} \qquad 6.13$$

Repeating this process several times, it is readily shown that the following general expression applies,

$$Z_{(i+1)OPT} = (Z_{iOPT}^{(\ell-1)} . Z_{(i+\ell)OPT})^{1/\ell} \qquad 6.14$$

Similarly,

$$Z_{(i-1)OPT} = (Z_{iOPT}^{(j-1)} . Z_{(i-j)})^{1/j} \qquad 6.15$$

In Fig 6.2, the known layers correspond to layers $Z_0(Z_T)$ and $Z_{n+1}(Z_L)$. Extending equations 6.14 and 6.15 to the known layers gives,

$$Z_{(i+1)OPT} = (Z_{iOPT}^{(n-1)} . Z_{(n+1)})^{1/(n+1-i)} \qquad 6.16$$

$$Z_{(i-1)OPT} = (Z_{iOPT}^{(i-1)} . Z_0)^{1/i} \qquad 6.17$$

where $\ell = n+1-i$.

Now, substituting equations 6.16 and 6.17 into equation 6.9 gives:-

$$Z_{iOPT} = ((Z_{iOPT}^{(n-i)} . Z_{n+1})^{1/(n+1-i)} . (Z_{iOPT}^{(i-1)} . Z_0)^{1/i})^{1/2} \qquad 6.18$$

This reduces to,

$$Z_{iOPT} = (Z_0^{(n+1-i)} . Z_{n+1}^{i})^{1/(n+1)} \qquad 6.19$$

which becomes,

$$Z_{iOPT} = (Z_T^{(n+1-i)} . Z_L^{i})^{1/(n+1)} \qquad 6.20$$

This expression gives the optimal acoustic impedance of the i^{th} layer of an n-layer matching set, in terms of the known acoustic impedances, Z_T and Z_L.

The ratio of any two optimal impedances is given by,

$$\frac{Z_{(i+1)OPT}}{Z_{iOPT}} = \frac{Z_T^{(n-i)} . Z_L^{(i+1)}}{Z_T^{(n+1-i)} . Z_L^{i}}^{1/(n+1)} \qquad 6.21$$

which becomes,

$$\frac{Z_{(i+1)OPT}}{Z_{iOPT}} = \frac{Z_L}{Z_T}^{1/(n+1)} \qquad 6.22$$

This is the same solution as that obtained by Lewis. Defining C_{TOT} as the total energy transmission factor in the multilayered system of Fig 6.2, Lewis has shown that when the acoustic impedances of the matching layers are chosen to be optimal,

$$C_{TOT} = \frac{Z_L}{Z_T} \quad \frac{2^{n+1}}{\left(1+\left[\frac{Z_L}{Z_T}\right]^{1/(n+1)}\right)^{n+1}} \qquad 6.23$$

He also presents the result,

$$\lim_{n\to\infty} \quad \frac{Z_L}{Z_T} \quad \frac{2}{\left(1+\left(\frac{Z_L}{Z_T}\right)^{1/(n+1)}\right)} \quad ^{n+1} \rightarrow \sqrt{\frac{Z_L}{Z_T}} \qquad 6.24$$

The usefulness of this result depends on the impedance ratio, Z_L/Z_T. For example, consider the case of a transducer operating into a water load. If the transducer active element is a ceramic (of the type discussed in Appendix B) then, typically it will have an acoustic impedance of

n	C_{TOT} Z_L ($\frac{Z_L}{Z_T}$=0.0455)	$\frac{C_{TOT(n)}}{C_{TOT(\infty)}}$%	C_{TOT} Z_L ($\frac{Z_L}{Z_T}$=0.375)	$\frac{C_{TOT(n)}}{C_{TOT(\infty)}}$%
0	0.0869	40%	0.545	89%
1	0.1235	58%	0.5770	94%
2	0.1456	68%	0.5884	96%
3	0.1593	75%	0.5943	97%
4	0.1685	79%	0.5978	97.6%
5	0.1751	82%	0.6002	98%
6	0.1800	84%	0.6019	98.3%
7	0.1838	86%	0.6032	98.5%
8	0.1868	87.5%	0.6042	98.7%
9	0.1893	88.7%	0.6051	98.8%
∞	0.2133		0.6124	

TABLE 6.1

$$Z_T = 33 * 10^6 kg/m^2\text{-}s \qquad 6.25$$

The acoustic impedance of water is,

$$Z_L = 1.5 * 10^6 kg/m^2\text{-}s \qquad 6.26$$

Thus,

$$\frac{Z_L}{Z_T} = 0.0455 \qquad 6.27$$

Substituting this value into equation 6.23, and evaluating the expression for n ranging from 0 to 9, gives the values of C_{TOT} shown in Column 2 of Table 6.1 . Column 3 shows the percentage ratio of C_{TOT} to the maximum possible value of C_{TOT}, for each value of n.

Clearly, even the addition of only one optimal matching layer significantly improves the efficiency of acoustic energy transmission to the load. However, the addition of more matching layers does not have such a significant effect, with the percentage increase gradually reducing per layer, for each

additional layer added. For example, four layers increase the transmission factor by a factor of two. Nine layers however, only increase the transmission factor by a factor of 2.25 .

If the transducer material was made of PVDF (a plastic compound, from which the hydrophone of Appendix B was manufactured), then, typically, it would have an acoustic impedance of,

$$Z_T = 4*10^6 kg/m^2\text{-}5 \qquad 6.28$$

and thus,

$$\frac{Z_L}{Z_T} = 0.375 \qquad 6.29$$

The corresponding values of C_{TOT} and its ration to $C_{TOT(MAX)}$ are given in columns four and five of Table 6.1 .

Comparing these results, it is apparent that PVDF is well matched to water without matching layers. Consequently, the addition of a single layer increases

the energy transmission factor by only 5%, and subsequent layers have a lesser effect.

Thus, comparing the results for the PZT transducer and the PVDF transducer, it is apparent that the addition of optimal layers in the PZT case may offer a significant improvement in energy transmission. However, in the PVDF case, the benefit of adding layers is doubtful, since any increase in energy transmission will be small. So, Table 6.1 demonstrates the usefulness of equations 6.23 and 6.24 in comparing the effects of optimal matching layers, when the optimum impedances are specified by equation 6.22 .

This section has presented the derivation of the optimal acoustic impedances of a set of matching layers. It was hoped that some practical results could have been presented at this stage, to demonstrate the effects highlighted in Table 6.1 . However, due to a lack of equipment and materials, it was not possible to manufacture layers with accurate acoustic impedances, and no experiments of any significance were carried out.

6.3 ELECTRONIC CONTROL OF A PIEZOELECTRIC TRANSMITTER.

This section presents the derivation of a technique which allows the generation of precisely defined transient force pulses from a piezoelectric transmitter. The basis of this technique is the inversion of the forward transmitter transfer function ($\overline{W}_{13}$ in the preceding chapters) to calculate the required excitation voltage. MEL'KANOVICH (45) performs a similar analysis, but the case dealt with is limited to a transducer system with zero driving impedance, and no matching layers. The technique he derives is also rather complicated mathematically.

This section will show how the transducer model of the preceding chapters lends itself to inversion and how the complexity of Mel'Kanovich's technique may be substantially reduced.

Consider firstly, the no-layer transducer transfer function, $\overline{P}_{13}$, specified by equation 5.13,

$$\overline{P}_{13} = \left(\frac{hC_t}{2}(R_1-1)s\overline{Z}_E^D\right).\left(1-(1+R_{-1})e^{-sT_t}+R_{-1}e^{-2sT_t}\right) / \overline{P}_D \qquad 6.30$$

where,

$$\overline{P}_D = (s(\overline{Z}_E^D + sC_t\overline{Z}_E^N)).(1-R_1R_{-1}e^{-2sT_t})-(X_k.\overline{Z}_E^D)((2+R_1+R_{-1})$$

$$-2(1+R_1)(1+R_{-1})e^{-sT_t}+(R_1+R_{-1}+2R_1R_{-1})e^{-2sT_t}) \qquad 6.31$$

The basis of the inversion technique may be described as follows.

Given that $\overline{P}_{13}$ is the forward Laplace transfer function of the transducer system, then, for an input, $\overline{I}$, the output is defined as:-

$$\overline{O} = \overline{I}.\overline{P}_{13} \qquad 6.32$$

where $\overline{O}$ is the Laplace transform of the output.

Now, for a specific output, equation 6.33 defines the required input as,

$$\overline{I} = \frac{\overline{O}}{\overline{P}_{13}} \qquad 6.33$$

which becomes,

$$\overline{I} = \overline{O}.\ \frac{1}{\overline{p}_{13}} \qquad 6.34$$

Substituting from equation 6.30 gives,

$$\overline{I} = \overline{O}.\ (s(\overline{Z}_E^D + sC_t\overline{Z}_E^N))(1-R_1R_{-1}e^{-2sT_t}) - (X_k).\overline{Z}_E^D((2+R_1+R_{-1}) -$$

$$-2(1+R_1)(1+R_{-1})e^{-sT_t} + (R_1+R_{-1}+2R_1R_{-1})e^{-2sT_t}) \ /$$

$$/\ ((\frac{hC_t}{2}(R_1-1)s\overline{Z}_E^D)(1-(1+R_{-1})e^{-sT_t}+R_{-1}e^{-2sT_t})) \qquad 6.35$$

Using the notation of the preceding chapter, and making the following definitions,

$$Y_{.k} = \frac{hC_t}{2}(R_1-1)$$

$$\overline{d}_1 = s\overline{Z}_E^D$$

$$\overline{d}_2 = X_k.\overline{Z}_E^D$$

$$\overline{d}_3 = s(\overline{Z}_E^D + sC_t\overline{Z}_E^N)$$

$$\overline{D}_1 = (1-R_1R_{-1}e^{-2sT}t)$$

$$\overline{D}_2 = ((2+R_1+R_{-1})-2(1+R_1)(1+R_{-1})e^{-sT}t+(R_1+R_{-1}+2R_1R_{-1})*$$
$$*e^{-2sT}t)$$

$$\overline{D}_3 = (1-(1+R_{-1})e^{-sT}t+R_{-1}e^{-2sT}t) \qquad 6.36$$

where, as before the $\overline{d}_i$ terms represent differential polynomials, and the $\overline{D}_j$ terms delay polynomials,

then, equation 6.35 may be rewritten as,

$$\overline{I} = \overline{O}.\ \frac{1}{Y_k}\left[\frac{\overline{d}_3.\ \overline{D}_1}{\overline{d}_1.\ \overline{D}_3} - \frac{\overline{d}_2.\ \overline{D}_2}{\overline{d}_1.\ \overline{D}_3}\right] \qquad 6.37$$

This may be rearranged to give,

$$\overline{I} = \overline{O}\ \ \frac{1}{Y_k}\left[\left(\frac{\overline{d}_3}{\overline{d}_1}\right)\left(\frac{\overline{D}_1}{\overline{D}_3}\right) - \left(\frac{\overline{d}_2}{\overline{d}_1}\right)\left(\frac{\overline{D}_2}{\overline{D}_3}\right)\right] \qquad 6.38$$

In this form, the first differential/delay product term

in 6.38 represents primary piezoelectric action and the second block represents secondary piezoelectric action. Coursant (13) proceeded in a similar manner to this, but at this stage, the terms arising due to secondary action were ignored.

In the analysis of Mel'Kanovich (45), equation 6.38 is essentially expressed as,

$$\bar{I} = \bar{O}\,\frac{1}{Y_k}\left[\left(\frac{\bar{d}_3}{\bar{d}_1}\right).\bar{D}_1 - \left(\frac{\bar{d}_2}{\bar{d}_1}\right).\bar{D}_2\right].\left(\frac{1}{\bar{D}_3}\right) \qquad 6.39$$

The term $(1/\bar{D}_3)$ is then expanded into an infinite power series, such that,

$$\frac{1}{1-(1+R_{-1})e^{-sT_t}+R_{-1}e^{-2sT_t}} = \sum_{n=1}^{\infty}(1-R_{-1}^{n}).e^{-sT_t(n-1)} \qquad 6.40$$

Now, for the input $\bar{I}$ to be of any practical importance, $\bar{I}$ must be stable, and for a real output, so must $\bar{O}$. Using the method of Mel'kanovich for the present, equation 6.39 reduces to,

$$\overline{I} = \overline{O}\,\frac{1}{Y_k}\left[\left(\frac{\overline{d}_3}{\overline{d}_1}\right).\ \overline{D}_4 - \left(\frac{\overline{d}_2}{\overline{d}_1}\right).\overline{D}_5\right] \qquad 6.41$$

where

$$\overline{D}_4 = \overline{D}_1.\ \frac{1}{\overline{D}_3}$$

$$\overline{D}_5 = \overline{D}_2.\ \frac{1}{\overline{D}_3} \qquad 6.42$$

are infinite discrete polynomials.

The delay polynomials may be ignored for the present as may Y_k, since these have no effect on the stability of the system.

A simple condition which is necessary for the inversion of the system may be established as follows.

Defining,

$$\overline{O} = \frac{\overline{d}^N_o}{\overline{d}^D_o}\ .\ \overline{D}_o \qquad 6.43$$

where $\overline{d}_o^N$ and $\overline{d}_o^D$ are numerator and denominator differential polynomials, and $\overline{D}_o$ a delay polynomial.

Again, ignoring the delay polynomial for the moment, the differential component of $\overline{I}$ is now made up of two differential only Laplace Transfer functions,

$$\left(\frac{\overline{d}_o^N}{\overline{d}_o^D}\right)\left(\frac{\overline{d}_3}{\overline{d}_1}\right) \; ; \quad \left(\frac{\overline{d}_o^N}{\overline{d}_o^D}\right)\left(\frac{\overline{d}_2}{\overline{d}_1}\right) \qquad 6.44$$

Now, for $\overline{I}$ to be realised, each of these differential only transfer functions must be such that the order of their denominators is at least the same as the order of their numerators. That is,

$$\begin{aligned} &\text{order } (\overline{d}_o^D.\overline{d}_1) \geq \text{order}(\overline{d}_o^N.\overline{d}_3) \\ &\text{order } (\overline{d}_o^D.\overline{d}_1) \geq \text{order}(\overline{d}_o^N.\overline{d}_2) \end{aligned} \qquad 6.45$$

In its simplest form, the differential component of the desired output is of the form,

$$\frac{\overline{d}_o^N}{\overline{d}_o^D} = \frac{1}{s^k} \qquad 6.46$$

Now, to meet the condition stated above, the order of k must be least the maximum of the differences in order between $\overline{d}_3$ and $\overline{d}_1$, and, $\overline{d}_2$ and $\overline{d}_1$, assuming that one of $\overline{d}_2$, $\overline{d}_3$ is of greater order than $\overline{d}_1$. This assumption is not always true, as may be observed from equatons 6.36, where three conditions may be imposed on the electrical load:-

(i) order $\overline{Z}_E^N >$ order $\overline{Z}_E^D$.

For example, if Z_E is an inductor, then the order of $\overline{d}_3$ is greater than $\overline{d}_1$.

(ii) order $\overline{Z}_E^N =$ order $\overline{Z}_E^D$.

For example, if Z_E is a pure resistance, then the order of $\overline{d}_3$ is greater than $\overline{d}_1$.

(iii) order $\overline{Z}_E^N <$ order $\overline{Z}_E^D$.

Then the order of $\overline{d}_3$ is at least equal to the order of $\overline{d}_1$.

In the final case, it is well known from electrical circuit theory, that the difference in order between the numerator and the denominator of any real impedance function cannot be greater than one, thus, for example, if Z_E is a blocking capacitor then,

$$\overline{Z}_E^N = 1$$

$$\overline{Z}_E^D = sC_B \qquad 6.47$$

and hence,

$$\overline{d}_1 = s^2 C_B$$

$$\overline{d}_2 = X_k . s . C_B$$

$$\overline{d}_3 = s^2 C_B + s^2 C_t \qquad 6.48$$

Here, both $\overline{d}_1$ and $\overline{d}_3$ have the same order, and $\overline{d}_1$ is of greater order than $\overline{d}_2$, so the assumption is not always valid.

Another exception to this rule is the case dealt with by Mel'kanovich, where the electrical load has zero impedance. In this situation,

$$\overline{Z}_E^N = 0$$

$$\overline{Z}_E^D = 1 \qquad 6.49$$

and hence,

$$\overline{d}_1 = s$$

$$\overline{d}_2 = X_k$$

$$\overline{d}_3 = s \qquad 6.50$$

These two examples show that, for at least two cases, k may take the value zero. That is, the differential component of the output may be a Dirac delta function. However, consider the $\overline{d}_3/\overline{d}_1$ and $\overline{d}_2/\overline{d}_1$ transfer functions for each case. These are, respectively,

$$\frac{\overline{d}_2}{\overline{d}_1} = \frac{X_k}{s} \; ; \; \frac{\overline{d}_3}{\overline{d}_1} = 1 + \frac{C_t}{C_B} \qquad 6.51$$

and,

$$\frac{\overline{d}_2}{\overline{d}_1} = \frac{X_k}{s} \; ; \; \frac{\overline{d}_3}{\overline{d}_1} = 1 \qquad 6.52$$

In both examples, the transfer function $\overline{d}_3/\overline{d}_1$ has a constant value. This implies that if the output differential component is a delta function, then the input voltage must also contain delta functions. Clearly, this is actually impossible to achieve in practice, since the bandwidth of a Dirac function is infinite, and all electronic apparatus has a finite bandwidth, even if it is very large. To avoid this problem, the order of k may be re-stated, such that the following constraint applies.

The order of k must be at least one more than the maximum of the differences in order between $\overline{d}_3,\overline{d}_1$ and $\overline{d}_2,\overline{d}_1$, where the order of at least one of $\overline{d}_2,\overline{d}_3$ must be at least equal to the order of $\overline{d}_1$.

This condition defines the differential component of the desired output, such that the differential component of the required input is realisable, and may therefore be generated in practice.

Next, consider the delay polynomials, $\overline{D}_1$, $\overline{D}_2$ and $\overline{D}_3$. The numerator polynomials $\overline{D}_1$ and $\overline{D}_2$ pose no

problems, and do not affect the stability of the system. However, the denominator term, $\overline{D}_3$,

$$(1-e^{-sT}t) \qquad 6.53$$

may give rise to instability in certain cases, and steps must be taken to exclude such a possibility occurring in the inverted system.

Several solutions to this problem have been proposed. For example, Mel'kanovich (45) incorporates the delay term of equation 6.53 in the infinite expansion of equation 6.40. This series may be truncated after N' terms. However, truncation of the series does not present a solution itself - it merely limits the problem to those terms of the series greater than N - that is, those not included in the expansion.

Coursant (13) eliminates this factor by considering an output function of the form,

$$\overline{O} = \frac{\overline{d}_o^N}{\overline{d}_o^D} .(1-e^{-sT}t) \qquad 6.54$$

so that the delay term in the output function cancels the unstable part of the delay term in the denominator. This technique is well-known in digital filtering.

Kažys and Lukoševičius (33) analyse the zeroes of the denominator delay polynomial. They then move any unstable zeroes from the right half s-plane so that they are just inside the left half of the s-plane. The modified delay polynomial is thus stable.

In the present case, it is advantageous to first rewrite the polynomial $\overline{D}_2$ in the form,

$$\overline{D}_2 = (1-e^{-sT}t)((1+R_1)(1-R_{-1}e^{-sT}t)+(1+R_{-1})(1-e^{-sT}t)) \qquad 6.55$$

From this, it is apparent that the term $(1-e^{-sT}t)$ is a factor of $\overline{D}_2$ and consequently, cancels with the identical factor in $\overline{D}_3$ of the denominator. Thus, the component of $(1/\overline{p}_{13})$ associated with secondary piezo-electric action does not pose a stability problem, since the remaining denominator factor

$$(1-R_{-1}e^{-sT_t}) \qquad 6.56$$

is always stable.

This may be demonstrated using a similar method to Kažys and Lukoševičius. However, instead of evaluating the zeroes of $\overline{D}_3$ directly, consider the z-transform of $\overline{D}_3$,

$$\overline{D}_3^Z = 1-(1+R_{-1})Z^{-M} + R_{-1}Z^{-2M} \qquad 6.57$$

where,

$$M = T_t/T_s \qquad 6.58$$

and T_s is the sampling period, as detailed in Chapter 4. The zeroes of this function are,

$$Z^{-M} = 1$$

$$Z^{-M} = \frac{1}{R_{-1}} \qquad 6.59$$

Thus, there are M zeroes on the unit circle in the Z-plane and M zeroes on a circle of radius:-

$$M\sqrt{R_{-1}} \qquad 6.60$$

The range of values which R_{-1} may take is defined by :-

$$R_{-1} = \frac{Z_t - Z_{-1}}{Z_t + Z_{-1}} \qquad 6.61$$

Where Z_t is the acoustic impedance of the transducer material, and Z_{-1} the acoustic impedance of the backing material. If it is assumed that Z_t is a known constant then Z_{-1} may take the range of values:-

$$0 \leqslant Z_{-1} \leqslant \infty \qquad 6.62$$

Consequently, R_{-1} may take the range of values given by

$$-1 \leqslant R_{-1} \leqslant 1 \qquad 6.63$$

where the value -1 occurs when R_{-1} is ∞ , and +1 when R_{-1} is zero.

Thus, since no practical material may possess an infinite acoustic impedance, the following condition must hold:-

$$-1 < R_{-1} \qquad 6.64$$

Furthermore, R_{-1} cannot be zero, since the transducer electrodes, although very thin in most applications, present a non-zero acoustic impedance to the transducer. Consequently,

$$R_{-1} < 1 \qquad 6.65$$

Hence,

$$|R_{-1}| < 1 \qquad 6.66$$

This yields the condition,

$$|M\sqrt{R_{-1}}| < 1 \qquad 6.67$$

Thus, the roots of the discrete polynomial $\bar{D}_3^Z$, due to the factor,

$$(1-R_{-1}Z^{-M}) \qquad 6.68$$

lie inside the unit-circle in the z-plane, and are stable. Thus the portion of the inverse transfer function due to secondary action does not pose any stability problems.

Returning to the unstable factor problem with the first portion of the inverse transfer function (that is, that corresponding to primary piezoelectric action), Coursant's (13) solution is clearly the simplest, since it does not require any modification of the transfer function. However, it is limited to certain output shapes, since each desired output must contain the factor:-

$$(1-e^{-sT}t) \qquad 6.69$$

Kažys and Lukoševičius (33) present a more flexible solution to the unstable factor problem. However,

they move the unstable zeroes in an arbitrary fashion. An alternative to this, is to consider the transducer as slightly lossy (a valid physical assumption), such that the transducer delay term,

$$e^{-sT_t} \qquad 6.70$$

then becomes,

$$(1-\varepsilon)e^{-sT_t} \qquad 6.71$$

where ε is a small number.

Thus, polynomial $\bar{D}_E^Z$ may be expressed as:-

$$1-(1+R_{-1})(1-\varepsilon)e^{-sT_t}+R_{-1}(1-\varepsilon)^2e^{-2sT_t} \qquad 6.72$$

This possesses the following roots:-

$$Z = {}^{M}\!/\,(1-\varepsilon)$$

$$Z = {}^{M}\!/\,R_{-1} \qquad 6.73$$

These now lie inside the unit circle in the z-domain and are consequently stable. This method is more flexible than Coursant's and is more physically valid than that of Kažys and Lukoševičius.

The methods which have been developed for the no-layer transfer function $\overline{p}_{13}$ may be extended to the general multilayered transfer function $\overline{W}_{13}$, with the following modifications.

Firstly, the inverse system for $\overline{W}_{13}$ may be written in exactly the same manner as equation 6.38 . However, now the discrete polynomials D_1, D_2 and D_3 are functions of the front and rear layer structures, as well as of the transducer. In particular, it may be shown that the term:-

$$1-e^{-sT_t} \qquad 6.74$$

is a factor of polynomials $\overline{D}_2$ and $\overline{D}_3$, such that,

$$\overline{D}_2 = (1-e^{-sT_t})\overline{D}_6 \qquad 6.75$$

$$\overline{D}_3 = (1-e^{-sT}t)\overline{D}_7 \qquad 6.76$$

where polynomials $\overline{D}_6$ and $\overline{D}_7$ are residual delay polynomials. From this, it may be observed that the unstable factor cancels, as before, in the portion of the inverse transfer function which is due to secondary action. The stability of the residual polynomial $\overline{D}_7$ may be analysed by evaluating the roots of $\overline{D}_7^Z$. This produces an interesting result. $\overline{D}_7^Z$ is of the form:-

$$\overline{D}_7^Z = Y_j.Z^{-N}.\overline{D}_8^Z \qquad 6.77$$

where Y_j is a scalar constant, and Z^{-N} a delay. $\overline{D}_8^Z$ is a further delay polynomial.

In fact, Y_j is the product of the transmission factors of the front layers and Z^{-N}, the total delay associated with a wave of force leaving the transducer and propagating through the front layers.

The term Y_j is unimportant as regards the inversion of the transfer function, and may be grouped with the

scale factor, Y_k. The term Z^{-N}, however, presents a serious problem. In this form, it renders any calculated input function non-causal, implying that the input must exist before t=0. This problem occurs because of the finite time delay between the generated wave of force leaving the transducer and the same wave of force leaving the last layer and propagating into the load. This situation is obviously due to the physical construction of the device and cannot be overcome. Therefore, the delay term, Z^{-N} must be removed from the polynomial $\overline{D}_7^Z$. This has the effect that there is a delay of Z^{-N} between the application of the electrical excitation and the generated wave of force leaving the transducer. It has no other effect on the stability of the system.

The stability of the residual polynomial, $\overline{D}_8^Z$, may be analysed by calculating its zeroes in the same manner as before. Several attempts were made to formulate a closed-form expression for the zeroes of $\overline{D}_8^Z$, but a general solution for the multilayered case proved to be intractable as a result of mathematical complexity. However, the values of the zeroes were calculated for a wide range of multilayer structures and, in each case, the zeroes were found to lie inside the unit circle of the z-domain.

Thus it would appear that the polynomial $\overline{D}_8^Z$ does not have unstable zeroes, at least for most practical layer configurations. (This can, of course, be checked numerically for any particular example.) Hence, the general inverse equation may be expressed in the following format:-

$$\overline{I} = \overline{O}\,\frac{1}{Y_k \cdot Y_j}\left[\left(\frac{\overline{d}_3}{\overline{d}_1}\right)\left(\frac{\overline{D}_1}{\overline{D}_8}\right) - \left(\frac{\overline{d}_2}{\overline{d}_1}\right)\left(\frac{\overline{D}_2}{\overline{D}_8}\right)\right] \cdot \frac{1}{1-e^{-sT_t}} \qquad 6.78$$

It should be noted that the multilayer case imposes no further restrictions on the stability of the differential polynomials, over those which were developed for the no-layer case. Thus the restrictions which were placed on the differential components of the desired output for the no-layer case also apply to equation 6.78.

It appears from the numerical analysis of several cases, that $\overline{D}_8^Z$ is always stable, thus the limiting factor in the stability of the delay polynomials is the denominator factor of equation 6.74 . This may be removed by either of the methods described for the no-layer transducer. (In fact, should a case arise where $\overline{D}_8^Z$ has unstable zeroes, these could be removed by either of the

methods described.)

Thus, in conclusion, this section has presented an analysis of the inversion of the forward transfer function, $\overline{W}_{13}$. This anlysis has highlighted the factors which restrict the invertibility, stability and causality of the system and placed suitable constraints upon them. It should thus be possible to generate a range of precisely defined output transients from a practical transducer system.

The next section investigates some of the practical and physical limitations which must also be considered.

6.4 PRACTICAL INVERSION CONSIDERATIONS

This section investigates some of the practical limitations of generating the desired outputs which were discussed theoretically in the preceding section. There are three areas of major practical importance associated with the inversion of piezoelectric systems.

(i) The calculation and generation of the required input voltage.

(ii) The hardware required to generate the excitation voltage.

and (iii) The period and shape of the excitation voltage.

These three areas are now discussed in detail.

6.4.(i) Calculation and Generation of the Excitation Voltage.

The desired excitation voltages discussed in section 6.3 have been specified in such a manner that they are causal and realiseable. However, it is apparent from the work of MEL'KANOVICH (45), and equation 6.78 that the delay terms in the two transfer function elements give the required voltage a very complex transient shape. In fact, such a voltage cannot be generated by

a simple passive electrical network. KAŽYS and LUKOŠEVIČIUS reduce the complexity of the input voltage by using a second transducer which effectively eliminates the effects of the second transfer function in 6.78 . This reduces the complexity of the input voltage but does not eliminate the first transfer function. In their application, the first block was filtered out by using a digital filter to pre-shape the excitation voltage.

Such a solution is not practicable in this context for two reasons.

Firstly, the effects of the second block transfer function are to be included and secondly the more complex differential/delay equations specified here would require a filter of such complexity that it would not function at the required speed in real time.

The alternative solution is to calculate the required input voltage as a temporal transient response. This may then be digitized and stored in a suitable digital memory. When the digitized signal is clocked out of the memory at a suitable speed, it may be converted back to an analogue signal using a digital to analogue converter (DAC), and then amplified accordingly. This is shown

schematically in Fig 6.4 .

This method requires the calculated voltage to be specified in a sampled form, a method particularly suited to the z-domain.

If it is assumed that the desired output is written in the form of equation 6.43, where the numerator and denominator polynomials, $\bar{d}_o^N$ and $\bar{d}_o^D$ meet the requirement of the preceding section. Then, if the output delay polynomial , $\bar{D}_0$ is of the form:-

$$\bar{D}_0 = (1-e^{-sT}t)\bar{D}_{oR} \qquad 6.79$$

the required input voltage is specified as:-

$$I = \left[\frac{1}{Y_k Y_j}\right]\left[\left(\frac{\bar{d}_o^N}{\bar{d}_o^D}\cdot\frac{\bar{d}_3}{\bar{d}_1}\right)\left(\frac{\bar{D}_{oR}\cdot\bar{D}_1}{\bar{D}_8}\right)-\left(\frac{\bar{d}_o^N}{\bar{d}_o^D}\cdot\frac{\bar{d}_2}{\bar{d}_1}\right)\left(\frac{\bar{D}_{oR}\cdot\bar{D}_2}{\bar{D}_8}\right)\right] \qquad 6.80$$

The differential/delay transfer functions in this case, correspond to those of equation 4.3 . That is, they are separate functions, and may be inverse-transformed in several different ways.

For example, each of the differential only blocks,

$$\frac{\overline{d}_o^N}{\overline{d}_o^D}.\frac{\overline{d}_3}{\overline{d}_1} \; ; \; \frac{\overline{d}_o^N}{\overline{d}_o^D}.\frac{\overline{d}_2}{\overline{d}_1} \qquad 6.81$$

may be inverse-transformed using the conventional partial fraction expansion method. The temporal responses so obtained could then be sampled and passed through a synthetic digital filter (that is not a real time filter but one programmed on the computer), corresponding to their respective delay transfer functions.

$$\frac{\overline{D}_{oR}.\overline{D}_1}{\overline{D}_8} \; ; \; \frac{\overline{D}_{oR}.\overline{D}_2}{\overline{D}_8} \qquad 6.82$$

After scaling, the required excitation voltage may be generated in sampled form.

Alternatively, each of the differential/delay transfer functions in equation 6.80 may be transformed into the z-domain using either the normal z-transform, or Boxer and Thaler's method. The resultant transfer functions may then be combined to form a single synthetic filter. The impulse response of this filter is then the required input voltage.

However, both of these methods require the input to be expressed as a Laplace transform in the form of equation 6.43.

Another method is to specify the desired output as a sampled temporal response. If the inverse transfer function of $\overline{W}_{13}$ is then implemented as a synthetic digital filter, then the response of the filter to the desired output will be the required input. To eliminate instability problems, the desired output must include the delay factor of equation 6.74 . This method has the advantage that complex outputs may be considered without having to obtain their Laplace transforms beforehand.

Each of these methods was implemented and tested as a computer algorithm. The object of the tests was to determine whether any particular method was noticeably better or worse than the others. (The results are not presented here, although some are included in Appendix A, to highlight the problems of the Boxer and Thaler method.)

From these tests, the following points were noted. The first method, inversion by partial fraction expansion, provides a mathematically correct solution

with no approximation errors. However, except for the simplest cases, the algorithms which were developed to calculate the partial fractions became increasingly complex as the order of the differential transfer functions increased. This was most noticeable for cases involving multiple poles. The major drawbacks of this method are twofold.

Firstly, the complexity of the algorithms takes an appreciable amount of the computer resources, and consequently, a fairly long time to evaluate, to the extent that this section became the slowest part of the program.

Secondly, for cases with several or multiple poles, the accuracy of the calculated partial fractions is reduced, since computer round-off errors increase with increasing complexity of the transfer functions.

As a result, this technique is unsuitable for computer implementation, and may only be used for simple transfer functions (those with not more than three single-order poles.)

The second method, inversion of the complete transfer function, by Boxer and Thaler's z-form method, contains inherent errors due to coefficient rounding. For most applications however, these errors may be safely ignored and the method is both quick and efficient in terms of computer resources. However, it was observed that, when the difference in order between the numerator and the denominator exceeded 3, that is:-

$$\text{order } (\bar{d}_o^D . \bar{d}_1) > \text{order } (\bar{d}_o^N . \bar{d}_3) + 3$$

or

$$\text{order } (\bar{d}_o^D . \bar{d}_1) > \text{order } (\bar{d}_o^N . \bar{d}_2) + 3 \qquad 6.83$$

round-off errors in the algorithm increased exponentially, and quickly led to an unstable result. This was initially rectified by performing the arithmetic calculation using double-precision coefficients. This solved the instability problem for some cases but in others only had the effect of delaying the onset of instability. Since a finite number of input samples are being calculated for any one case, this problem may be overcome by repeatedly increasing the accuracy of the arithmetic calculations, until a stable solution is obtained. However, this is very costly in terms of

resources, and takes a great deal of user interaction to determine the best solution. Thus, this technique is only suited to cases where the difference in order between the numerator and denominator polynomials is three or less.

The third technique, implementation of the inverse transfer function $\overline{W}_{13}$ (using Boxer and Thaler's method), as a synthetic digital filter, possesses an inherent drawback. Considering only the differential transfer functions for those cases where,

$$\text{order } \overline{d}_3 > \text{order } \overline{d}_1$$

or

$$\text{order } \overline{d}_2 > \text{order } \overline{d}_1 \qquad 6.84$$

such cases represent differential transfer functions of the form:-

$$\frac{\overline{d}^N}{\overline{d}^D} \quad ; \quad \text{order } \overline{d}^N > \text{order } \overline{d}^D \qquad 6.85$$

This may be rewritten as:-

$$\frac{\bar{d}^N}{\bar{d}^D} = \underbrace{\frac{\bar{d}^{NO}}{\text{differential polynomial}}}_{} + \underbrace{\frac{\bar{d}^{NR}}{\bar{d}^D}}_{\text{reduced order transfer function}} \quad ; \text{ order } \bar{d}^D > \text{order } \bar{d}^{NR} \qquad 6.86$$

where $\bar{d}^{NO}$ is a differential polynomial and $\bar{d}^{NR}$ and $\bar{d}^D$ form a differential transfer function where the order of the denominator is greater than the order of the numerator. If Boxer and Thaler's z-form method is applied to a transfer function of the form of equation 6.85, then the resultant z-transform will, when implemented as a filter, be at best oscillatory and at worst unstable. This problem is discussed by Boxer (5) but occurs because the method of Boxer and Thaler develops the z-forms as integrating operators. In this form, when applied to a differential polynomial of the form of equation 6.86, the resultant z-transform is unstable.

One solution to the problem is to use a differential operator to take the z-transform of the differential polynomial. For example, the first order backward difference operator discussed in Chapter 4. (Note the bilinear operator is not suitable as a differential operator since it is the first z-form derived by Boxer and Thaler.) The reduced order transfer function may be

transformed using the Boxer and Thaler method, as before. This solution has the disadvantage that it produces two synthetic filter structures when applied to transfer functions of this type. It also mixes two z-transform techniques which is not strictly valid.

However, the test results of this method were excellent. There were no appreciable discrepancies due to arithmetic round-off errors or to the mixed z-transform solution.

The increased complexity of the algorithm caused by the need for two synthetic digital filter structures, added little or no extra cost in terms of either resources or calculation speed.

Thus, comparing the results of the three methods considered, it may be concluded that the third method was best suited to computer implementation. This method also has the advantage that it requires only the sampled output transient, not the Laplace transform of the output. Consequently, it is more flexible than the preceding methods and was adopted as the practical inversion technique.

6.4.(ii) Hardware Considerations

Consider the schematic diagram of Fig 6.4 . From this, it may be observed that there are three key elements in the practical inversion hardware; the digital memory, the DAC and the amplifier. The limiting factors of these components are bandwidth and gain.

In the simulations of Chapter 5, it was noted that the sampling period, T_s, was required to be an integer sub-multiple of the transit periods of the transducer and all the matching layers. This requirement also applies to electronic control. Thus, the sampling period of the sampled excitation voltage must also be an integer sub-multiple of the transducer and layer transit periods. To obtain the maximum benefit from electronic control, it is also desirable that the sampling rate should be as large as possible, so that maximum definition of the excitation voltage is achieved.

From Appendix B, the transit period of the 1 MHz transducers is 0.435 μs. Thus, the sampling period for calculation of the excitation voltage must be considerably less than this value.

The fastest digital memory which was available for storing the excitation voltages, was an Emitter Coupled Logic (ECL), array. This was originally part of an array control system and is detailed in Appendix B. Initially, this memory operated at a clock rate of 33 MHz, corresponding to a sampling period of 30 ns. This was later updated to operate at 50 MHz, (20 ns sampling period.) At this frequency, it is apparent that the thinnest layer which the system can cater for must have a transit period of 20 ns. In the layered transducers of Chapter 5, the bondline thicknesses were estimated to be of the order of 10 μm. From the data in Appendix B, it is apparent that the transit period of the bondlines is thus of the order of 5 ns. That is, a factor of four less than the minimum required. The only solution in such cases was to ignore the bondlines and the corresponding simulation and exprimental results are presented in the next section.

The DAC which was used for the experimental trials had a maximum operating frequency of 100 MHz and did not restrict the operation of the system.

Finally, the driving amplifier presented limitations of both bandwidth and gain. From the apparatus data

given in Appendix B, the chosen amplifier had a gain-bandwidth product of 600 MHz. The output signal of the DAC had a peak to peak swing of ± 0.5 V, while the amplifier peak to peak swing was ± 10 V (maximum). Clearly, to achieve the maximum amplifier output swing requires a gain of 20 . With this gain, however, the amplifier bandwidth reduces to 30 MHz - considerably lower than that of the ECL memory. This problem was partially overcome by reducing the amplifier gain, and using a second stage, although the second stageincreased the noise level of the system.

Comparing the driving voltages used in the experiments of Chapter 5, (approximately 300 V peak), it may be observed that there is a thirty to one scale difference between the driving voltages. Thus, the force outputs generated by the transducer are very small, and in fact, could not be detected by the hydrophone alone. This problem was partially overcome by using a hydrophone charge amplifier, but this of course againincreased the noise level of the system.

There are two solutions to this problem, either use a driving amplifier with a larger output swing, or reduce the amplitude of the required excitation voltage (for

example, by the addition of mechanical matching layers.) The first solution was not viable at the time the experimental measurements were made so the second solution was investigated in more detail.

Consider the no-layer inverse transfer function of equation 6.35 . If the desired output is assumed to be of unity magnitude, and the differential terms are ignored for the present, then the limiting factor which determines the magnitude of the required excitation voltage is the constant term,

$$\frac{2}{hC_t(R_1-1)} \qquad 6.87$$

This has a minimum value when R_1 is zero. That is, when the acoustic impedances of the load and the transducer are the same. In many applications, for example, those considered in section 6.2 , this is not the case.

Consider the multi-layered inverse transfer function of equation 6.78 . The limiting constant term in this case, is given by,

$$\left[\frac{1}{Y_k \cdot Y_j}\right] \qquad 6.88$$

which becomes,

$$\frac{-2}{hC_t(1-R_1)} \cdot \frac{1}{Y_j} \qquad 6.89$$

The term $(1-R_1)$ is the transmission coefficient from the transducer to the first layer. The term Y_j is the product of the remaining layer transmission coefficients. Thus the term,

$$(-R_1)Y_j \qquad 6.90$$

is the overall transmission coefficient of the layered system, C_{TOT} of equation 6.23 . From equation 6.24, this has a maximum value of,

$$\sqrt{\frac{Z_L}{Z_T}} \quad n \to \infty \qquad 6.91$$

The minimum magnitude of the excitation voltage is thus given by:-

$$|I|_{min} = \frac{2}{hC_t}\sqrt{\frac{Z_T}{Z_L}} \qquad 6.92$$

In practice of course, this value cannot be achieved, but a measure of the decrease in the magnitude of the excitation voltage with the addition of matching layers may be obtained from Table 6.1 . Taking the reciprocal of the percentage transmission gives the scale factor increase required in the magnitude of the excitation voltage to generate a given output, as compared with the theoretical minimum of equation 6.92 . For example, with a PZT-5A transducer and a water load, the percentage transmission factor is 40%. This corresponds to an excitation of 2.5 times the theoretical minimum. Unfortunately, as was stated at the end of section 6.2 , it proved difficult to manufacture layers with a sufficiently accurate acoustic impedance to test these results experimentally. If, however, multiple matching layers were used with electrical control, then it is clear that the thickness of the layers must be such that the layer transit time is an integer multiple of the sampling period. This greatly increases the flexibility of the matching layer system, since any layers which were manufactured from a lossy material could be made only a few samples thick - thereby minimising

attenuation.

6.4.(iii) Excitation Voltage Considerations

The absolute magnitude of the excitation voltage, and its influence on the generating hardware were considered in the previous section. From this section, the desired output was defined in a manner which ensured that the required generating voltage is both causal and stable. However, there is no guarentee that the input voltage will always converge to zero. The digital memory has a finite size and if the stored waveform converges to a non-zero value, then, when the last sample is clocked out of the memory, there will be a discontinuity after the last sample, when the output from the DAC jumps back to zero. This will act like a step function and the transducer will be excited accordingly. If the last value in the digital memory is small, this will have little effect, but if it is large, the force output generated by the transducer may be of comparable magnitude to that generated electronically. Clearly, this is not desirable. Two solutions are proposed.

Firstly, the digital memory was modified slightly, so that the last sample could be clocked out continuously. Thus when the last sample was reached, further

increments of the clock continued to generate the last sample. This method was successful for single waveforms of the type shown in Fig 6.5 . However, for certain cases, particularly sinusoidal generation, the voltage trace does not converge - the envelope of the trace converges. This is sketched in Fig 6.6 . In these cases, holding the last sample is pointless, it now requires a complete cycle of the waveform to be repeated. The complexity of designing a system to detect and repeat a cycle of the stored waveform was prohibitive, so an alternative solution was developed, thatof forced convergence.

The second method essentially forces a waveform to converge using an exponential multiplier of the form,

$$e^{-at} \qquad 6.93$$

This was applied in the following manner.

The digital memory has a finite number of samples, N, as an example. At the last sample, the value of the multiplier should be very small, for example K. Given the total number of samples, and assuming that the value of the multiplier is unity at the first sample, yields the following conditions:-

$$e^{-at} = 1 - \text{first sample}$$

$$e^{-at} = k - \text{last sample} \qquad 6.94$$

If T_s is the sampling period, then at the last sample,

$$e^{-a(N-1)T_s} = K \qquad 6.95$$

where the first sample is assumed to be t=0. Consequently,

$$a = \frac{1}{T_s(N-1)} \cdot \ell n\left[\frac{1}{k}\right] \qquad 6.96$$

In fact, this was modified in practice so that the exponential operator could be delayed until the M^{th} sample, that is,

$$e^{-at} = 1 \qquad \text{for all samples up to the } M^{th} \qquad 6.97$$

hence,

$$a = \frac{1}{T_s(N-M-1)} \cdot \ell n\left[\frac{1}{k}\right] \qquad 6.98$$

The effect of this operator is shown in the sketch of Fig 6.7 .

This method was used in practice and a comparison between the simulated and experimental results, with and without forced exponential convergence is included in the next section.

This section has analysed the basic practical limitations of electronically controlling a piezoelectric transducer. Full details of the circuits and hardware used in the experimental tests are contained in Appendix B. The results of some of the inversion methods which were tested are given in Appendix A. Finally, the next section contains a comparison of simulated and experimental transducer control which highlights some of the limitations discussed in this section.

6.5 COMPARISON OF SIMULATED AND EXPERIMENTAL INVERSION RESULTS

This section presents the corresponding simulation and experimental results for the electronic control of a piezoelectric transmitter. The techniques described in the two preceding sections were used to generate the required excitation voltages for several desired outputs. The sampled voltages were then stored in an ECL digital memory and used to drive the selected transducer, as described in Appendix B. Two transducers were used for these results; the 1 MHz devices, B and E, described in Appendix B.

Two electrical load configurations were used to form the differential polynomials of transfer function $\overline{W}_{13}$.

These were :-

(i) A series 50Ω resistor.

This resulted in the following differential polynomials:-

$$\overline{d}_1 = s \qquad \text{(i)}$$

$$\overline{d}_2 = X_k \qquad \text{(ii)}$$

$$\overline{d}_3 = s+50.C_t.s^2 \qquad \text{(iii)}$$

6.99

From this, it is apparent that the maximum difference in the order of the numerator and denominaTs is 1. Consequently, the differential component of the desired output must be such that the order of the denominator is at least 2 greater than the order of the numerator to satisfy the conditions of section 6.3 .

(ii) A series 2nF blocking capacitor (C_B), and a parallel 100Ω resistor (R_E), similar to that used for the firing circuits of Chapter 5. This resulted in the following differential polynomials.

$$\overline{d}_1 = s^2C_BR_E$$

$$\overline{d}_2 = X_k(1+sR_EC_B)$$

$$\overline{d}_3 = s + s^2R_E(C_B+C_t) \qquad 6.100$$

In this case, it is apparent that the maximum difference between the numerator and denominator polynomials is the zero, that is, one pair of polynomials are of equal

order ($\overline{d}_1$,$\overline{d}_3$), and the other pair are such that the numerator is of lower order than the denominator ($\overline{d}_1$,$\overline{d}_2$). Thus, the differential component of the desired output must be such that the order of the denominator is at least one more than the order of the numerator.

A similar case to this one was considered in section 6.3, that of a blocking capacitor without the parallel resistance. However, when this was attempted in practice, some distortion of the generated voltage occurred. The precise reason for this is not known but may be due to the fact that the amplifier was not designed to drive large capacitative loads. The case described above presented a better result, and was used for the experimental results instead, Both the electrical load configurations were used with transducer B, while only the first was used with transducer E. The behaviour of these load/transducer configurations is shown in Figs 6.8, 6.9 and 6.10 .

Fig 6.8 shows the impulse response of transducer B, with a series 50 Ω electrical load,

Fig 6.9 shows the impulse response of transducer B,

with a parallel 100Ω resistor and a 2nF blocking capacitor.

Fig 6.10 shows the impulse response of transducer E with a series 50Ω electrical load.

Clearly there are significant difference between the three responses. However, these configurations have defined the conditions which determine the order of the differential polynomials of the desired outputs.

For the case (i) electrical load, two differential outputs were considered,

$$\frac{\bar{d}_o^N}{\bar{d}_o^D} = \frac{1}{s^2} \qquad 6.101$$

This corresponds to a unit ramp function.

$$\frac{\bar{d}_o^N}{\bar{d}_o^D} = \frac{a}{s^2+a^2} \qquad 6.102$$

That is, a unit sine-wave function.

For the case (ii) electrical load, one differential output was considered:-

$$\frac{\overline{d}_o^N}{\overline{d}_o^D} = \frac{1}{s} \qquad 6.103$$

This corresponds to a unit step function.

In section 6.3, it was stated that the desired output must contain the delay factor,

$$(1-e^{-sT_t}) \qquad 6.104$$

Applying this to the unit step and unit ramp functions of equations 6.103 and 6.101 produces a unit square pulse of width T_t and the function sketched in Fig 6.11. Clearly, this function is a rather strange output, so a unipolar triangular function was considered instead, as shown in Fig 6.12 . This function has the following delay term,

$$(1-2e^{-sb}+e^{-2sb}) \qquad 6.105$$

This factorises to give:-

$$(1-e^{-sb})^2 \qquad 6.106$$

Thus, if $b=T_t$, the required condition is satisfied.

Applying the condition of equation 6.105 to the sine-wave function is more difficult. If the half-period of the sine-wave is not equal to T_t, then application of the delay factor of equation 6.104 produces an output function with a discontinuity. This is not desirable, since it may upset the stability of the inverse filter. Consequently, for this case, only sine-waves of a specific frequency were chosen. This frequency was selected such that an integer multiple of the half-period of the sine-wave equalled T_t. Thus the delay multiplier of equation 6.104 produced an output with an integer number of half-cycles.

To test these selected outputs, three simulations were carried out with transducer B.

(i) Using the blocking capacitor and parallel resistor, the required excitation voltage for the unit square pulse was calculated.

(ii) With the series 50Ω load the excitation

voltage for the unipolar triangular pulse was calculated.

(iii) The excitation voltage for a half-sine cycle (half period equal to T_t), was calculated.

In each case, the calculated voltage proved to be divergent. This was unexpected, particularly since the rate of divergence appeared to be exponential. Case (ii) above is similar to that presented by Coursant (13); however, it differs in two respects. Firstly, the voltage derived by Coursant converges, and secondly, his calculation ignores secondary action.

Case (i) is dealt with by Mel'Kanovich (45), for a transmitter with zero source impedance. Again, the derived voltage converges, this time to a non-zero constant value.

Thus, considering these results, it would appear that either the electrical load, or the inclusion of secondary action, or a combination of both, is responsible for the divergent results. On closer analysis of the case dealt with by Coursant, it is apparent that no information is given about the electrical load. Combining this with the fact that

Mel'Kanovich includes the effect of secondary action in his inverse calculations, suggests that secondary action alone is not the cause of the divergence.

Now, since practical transducer applications will contain some degree of electrical impedance, it was decided to investigate further the shape and nature of possible outputs. To this end, each of the three previous unipolar outputs was now considered to be bipolar, (the sine-wave output was now defined to be a finite number of whole sine-cycles, such that an integer multiple of the period equalled T_t).

The delay multipliers are now,

$$1-2e^{-bs}+e^{-2bs}$$

$$1-2e^{-bs}+2e^{-3bs}-e^{-4bs}$$

$$1-e^{-2bs} \qquad 6.107$$

for the bipolar square, ramp and sine-wave respectively. These factorise to give:-

$$(1-e^{-bs})^2 \qquad (i)$$

$$(1-e^{-bs})^2(1-e^{-2bs}) \qquad \text{(ii)}$$

$$(1-e^{-bs})(1+e^{-bs}) \qquad \text{(iii)}$$

6.108

Again, substituting T_t for b gives delay polynomials which meet the initial delay condition.

These were then applied to the defined differential outputs, and used to calculate the required excitation voltages. In each case, the calculated voltage converged to zero.

Thus, six defined outputs were chosen to test the feasibility of using electronic methods to control a piezoelectric transmitter.

Figs 13A, B and C show three bipolar ramp functions of varying width. The respective output delay polynomials are, for each case; Fig 13A

$$(1-e^{-2sT_t})(1-e^{-4sT_t})(1+e^{-sT_t})\underline{(1-e^{-sT_t})} \quad b=2T_t \quad 6.109$$

Fig 13B

$$\underline{(1-e^{-sT_t})}(1-e^{-sT_t})(1-e^{-2sT_t}) \quad b=T_t \qquad 6.110$$

Fig 13C

$$(1-e^{-sT_t/2})^2\underline{(1-e^{-sT_t})} \qquad b=T_t/2 \qquad 6.111$$

where the required factor is underlined for each case.

Fig 14 shows a single sine-cycle, where the period of the cycle is twice the transit period of the transducer, (thus the frequency of the sine-wave is the same as the mechanical resonance of the transducer). This has the following output delay polynomial:-

$$(1+e^{-sT_t})(1-e^{-sT_t}) \qquad b=T_t \qquad 6.112$$

Fig 15 shows a second sine-cycle, this time of period equal to the transit period of the transducer (thus it is of frequency twice the mechanical resonance.) This has the delay multiplier,

$$(1-e^{-sT_t}) \qquad b=T_t/2 \qquad 6.113$$

Apparently, this is identical to the first test sine-wave but in this case, the output is a whole sine-cycle, whereas in the initial test, it was a half-cycle.

Finally, Fig 16 shows a bipolar square pulse

with delay factor,

$$\frac{(1-e^{-sT_t})}{}(1+e^{-sT_t}) \qquad 6.114$$

These six defined outputs were used with transducers B and E, to derive the required excitation voltages. These voltages were then used to fire transducers B and E and the generated force-waves compared with the original defined outputs.

CASE 1

Transducer B was set up in experimental configuration 4, (specified in Appendix B). The bipolar triangular output of Fig 6.13A was then used to calculate the required excitation voltage for the case where the electrical load was a series 50Ω resistor. Figs 6.17A and B show the calculated voltage, and the generated voltage respectively. There is good agreement between the two, (apart from a vertical scale difference). Figs 6.17C and D show the desired force output shape, and the achieved output shape, measured in a water tank. Again, there is very good agreement between the results, although there is a degree of noise in the measured result. This result was carried out for a hardware clock frequency of 33 MHz.

CASE 2

This is identical to Case 1 but now the desired output is that of Fig 6.13B and the hardware clock frequency has been increased to 50 MHz.

Figs 6.18A and B show the calculated and generated voltage respectively, (oscilloscope settings: x - 1 μs; y - 2 V, both per large division). Figs 6.18C and D show the desired and obtained force outputs respectively, (oscilloscope settings: x - 1 μs; y - 5 mV, both per large division). Again, there is very good agreement between the simulated and experimental results. (The electrical noise on the force measurement was reduced by using a different amplifier with the receiving hydrophone).

CASE 3

This is identical to Case 2 but the desired force output is now that of Fig 6.13C. Figs 6.19A and B show the calculated and generated voltages respectively, (oscilloscope settings: x -0.5 μs; y - 2 V, both per large divisions). Figs 6.19C and D show the desired and the measured force outputs, (oscilloscope settings: x - 0.5 μs; y - 5 mV, both per large division).

There is good agreement between both the simulated and the experimental results. However, there is some distortion of the generated voltage, most probably due to a bandwidth limitaton in one of the amplifier stages. This has the effect of rounding the generated force outputs.

CASE 4

This is also identical to Case 2 with the desired output now that of Fig 6.14, a single sine cycle, with the same frequency as the mechanical resonance of the transducer. Figs 20A and B show the calculated and the generated voltages respectively, (oscilloscope: x - 0.5 us; y - 2 V; both per large division.) Figs 20C and D show the desired and the measured force output, (oscilloscope: x - 0.2 us; y - 5 mV.)

There is reasonable agreement between the voltage simulation and the generated voltage, and excellent agreement between the desired and measured forces. The minor differences in the voltage responses are again probably due to bandwidth limitations. However, it is apparent that this has had little effect on the generated force output.

CASE 5

Again, this is identical to Case 2 with the desired output now the plot of Fig 6.15, a single sine cycle of twice the mechanical resonance of the transducer. As before, Fig 6.21A and B show the calculated and measured voltages respectively, (oscilloscope: x - 0.5 μs; y - 5 V, both per large division). Figs 6.21C and D show the desired and measured force outputs respectively, (oscilloscope: x - 0.2 us; y - 5 mV).

There is reasonable agreement between the voltage simulation and the generated voltage, and excellent agreement between the desired and measured force outputs. It is apparent from Fig 6.21B that the sharp spikes of the calculated voltage have again been smoothed out due to the finite bandwidth of the system. However, as before, this appears to have had little effect on the measured force output. This case is an example of the failure of convergence which was discussed in section 6.4 . The calculated voltage has an envelope which converges to a constant value, but the voltage itself does not converge to zero.

CASE 6

This is identical to Case 5 but now the excitation voltage has been forced to converge to zero by using the exponential multiplier discussed in section 6.4 . From equation 6.98 the value of the exponential constant, a, is given as:-

$$a = \frac{1}{T_s(N-M-1)} \cdot \ell n\left[\frac{1}{k}\right] \qquad 6.115$$

In this case, the following values were selected for K, N and M,

$$\begin{aligned} N &= 512 \\ M &= 100 \\ K &= 0.1 \end{aligned} \qquad 6.116$$

Thus a had the value (for T_s = 20 ns) given by,

$$a = 280*10^3 \qquad 6.117$$

Figs 6.22A and B show the calculated and measured voltages respectively (oscilloscope: x - 0.5 μs; y - 5 V; both per large division). Figs 6.22C and D show the predicted and the generated force outputs, (oscilloscope: x - 0.2 μs; y - 5 mV; both per large division.)

Clearly there is excellent agreement between the simulated and experimental results. Once again, the amplifier bandwidth has truncated the sharp spikes which occurred in the calculated excitation voltage. However, this appears to have had little effect on the generated force output. The slight after-ringing which was predicted on the desired output force simulation has also largely disappeared from the measured force output. This is probably due to attenuation in the water column. Finally, comparing the measured force output with that of Case 5, (Figs 21D and 22D), there is excellent agreement between the two results which shows that the exponential convergence factor has little effect on the generated force output.

CASE 7

This is identical to Case B with the desired output the bipolar step function of Fig 6.16 . Figs 6.23A and B show the calculated and generated excitation voltages respectively, (oscilloscope: x - 0.5 μs; y - 0.5 V, both per large division). There is excellent agreement between these results. However, the generated voltage is approximately a factor of ten less than the calculated voltage. This was necessary since the amplifier stages of the generating equipment would not reproduce the volt-

age accurately with a large gain, due to the reduced bandwidth. Consequently, the amplifier gain was reduced until the generated and calculated voltages were in good agreement. However, this had a marked effect upon the amplitude of the generated force output. Figs 6.23C and D show the desired and the measured force outputs, (oscilloscopes: x-0.5 μs: y- 5 mV; both per large division). There is reasonable agreement between these results but it is apparent that the generated force output is close to the limit of detectability of the receiving hydrophone apparatus. The generated voltage in this case is a second example of a waveform which does not converge to zero. However, since the voltage converges to a constant value, the last sample latch technique of section 6.4(ii) was used to hold the last sample value and maintain the constant offset.

CASES 8 and 9

These examples both used the layered device, transducer E to generate the force outputs. The hardware clock frequency used for these results was 50 MHz but as was discussed in section 6.4(ii), this is not high enough to include the effects of the bondline layers in the calculated voltage. Consequently, the required excitation voltages were calculated for a transducer

with no bondlines. The effects of this assumption are discussed below.

CASE 8

The desired output for this example was the bipolar triangular pulse of Fig 6.13C. Figs 6.24A and B show the calculated and generated excitation voltages respectively, (oscilloscopes: x-0.2 μs; y-1 V; both per large division). There is good agreement between these results. Figs 6.24C and D show the calculated and the measured force outputs respectively, (oscilloscope x-0.5 μs; y- 5 mV; both per large division). Again, there is good agreement between the results. However, it is again apparent that the generated output is close to the detectability limit of the receiving apparatus. Thus it is difficult to establish whether ignoring the bondlines has had any effect on the response. Fig 6.24E shows the simulated force output for the case where the voltage was calculated without the bondlines but the transmitter model included them. It is apparent that there is a slight overshoot after the generated force output and this is just visible in Fig 6.25D. So the agreement between the simulated and calculated results is reasonably good.

CASE 9

This is identical to the previous case but the desired force output is now that of Fig 6.14, a single cycle sine wave. Again, the excitation voltage was calculated with the bondlines omitted. Figs 6.25A and B show the calculated and the generated excitation voltages respectively, (oscilloscope: x - 0.2 μs; y - 1 V; both per large division.) There is good agreement between these results. Figs 6.25C and D show the desired and the generated force outputs respectively, (oscilloscope: x - 0.5 μs; y - 5 mV; both per large division.) As with Case 8, it is difficult to compare these results because of the low amplitude of the measured output. Fig 6.25E shows the simulated force output with the bondlines included. Comparing this simulation to the measured output, it is apparent that the slight after-ringing is present in both cases. Thus it may be concluded that there is reasonable agreement between the simulated and the desired force outputs.

This section has presented simulated and experimental results which show that electronic control of the piezoelectric transducer may be used to generate precisely defined force transients in a water tank. The experimental results were generally in very good agreement

with the desired outputs, although some minor differences did occur. These were mainly attributable to the limited bandwidth of the driving amplifiers. However, a second possible error source is the chosen sampling period. Theoretically, the sampling period of the digital electronics should be an integer submultiple of the transducer and layer transit periods. However, this is virtually impossible to achieve in practice and consequently, there will be some minor differences in the calculated and generated driving voltages. For example, the transit period of transducers B and E is 0,435 μs, from Appendix B. With a 50 MHz driving frequency, the sampling period is 20 ns. Thus the nearest integer multiples of the sampling period to the transducer transit time are 21 (0.42 μs) and 22 (0.44 μs). In this case, the required voltage was calculated for 22 samples per transit. This will produce a slight cumulative error in the generated output force, and this may account for the slight discrepancies in some of the results. Obviously, this effect is compounded in transducer E which has a front layer as well.

Another problem with the experimental results was the magnitude of the generated voltages. This problem arose because of the inverse relationship between the gain

and the bandwidth of the amplifier. For some cases, particularly Case 7, it was necessary to reduce the gain substantially, to obtain sufficient bandwidth for the amplifier to reproduce the driving voltage accurately. This led to a generated force output with such a small magnitude that it was just detectable by the receiving apparatus.

A similar problem arose in Cases 8 and 9, however the low amplitude of the generated force outputs was now due to the poor match between the steel layer and the water load.

Thus a detailed comparison of some of these results really requires a better driving amplifier, so that the strength of the received signals can be boosted well above the noise level.

The results of Cases 6 and 7 demonstrated that the techniques of exponentially forcing the voltage envelope to converge, and of holding the last sample, both worked well. This offers a great deal of scope for generating more complex output shapes.

Cases 8 and 9 produced results which showed that,

although the bondlines are comparatively thin, they do influence the response . With better driving electronics, it may be possible to analyse the precise effects of the bondlines and develop techniques for compensating or reducing the after-ringing of the generated output.

The apparent theoretical anomaly over the generation of uni-polar pulses has not been resolved. As stated earlier, this appears to be caused by a combination of the non-zero electrical load and secondary action, but no quantitative solution has been found. It was initially suspected that this may have been caused by round-off errors in the inverse filter structures, similar to those reported in section 6.4 . This was investigated fully, and does not appear to be the cause of the voltage divergence. A qualitative explanation of this effect may be derived as follows.

Assuming that the inverse direct piezoelectric function produces a stable, convergent voltage which it appears to do, then, in some cases, the secondary piezoelectric function may produce a divergent voltage. With the initial theory, the required output delay multiplier should ensure that the voltage does not diverge. Apparently, this is not the case with a unipolar pulse. How-

ever, with the bipolar pulses, the secondary function will generate a second divergent voltage of opposite sign to the first, delayed by the half period of the pulse. This may partially cancel out the first divergent voltage to produce a net voltage which converges to some constant value. However, this explanation has not been verified and there is scope for a great deal more work in this area.

Finally, this section has shown that electronic control of piezoelectric transducers is feasible in a real situation. It has also shown that this method has several advantages over alternative methods. This is demonstrated in Case 6, where the generated waveshape has a frequency twice that of the mechanical resonance of the transducer. Clearly, while electronic control still requires a great deal of investigation, it offers results and improvements in the transducer response which are not available with passive methods alone.

6.6 CONCLUSIONS

This chapter has investigated both mechanical and electronic methods for controlling and optimising the performance of the thickness mode piezoelectric transducer.

In section 6.2, an expression was derived which gives the optimum acoustic impedances for an arbitrary set of matching layers. This was then used to compare the increase in energy transmission into the load as additional layers are added to a transducer. From this, it was concluded that, while matching layers provide a significant improvement in the efficiency of energy transmission, this increase decreases per layer as more layers are added. Consequently, the optimum number of layers for a particular case depends upon the acoustic impedance mismatch between the transducer and the load.

The next section investigated the theoretical basis of electronically controlling the transducer response. From this, it was concluded that precisely defined output force transients may be generated by inverting the forward piezoelectric transfer function,

$\overline{W}_{13}$. The analysis of this section produced conditions defining the order and nature of the differential and delay portions of both the inverse transfer function and the desired output. When these conditions are met, the system may be theoretically inverted and the required input should be stable, causal and realiseable.

Section 6.4 investigated the practical limitations of performing the inversion and generating the required voltage. It was concluded that the only realistic method of generating the excitation voltage was with digital hardware. Consequently, the voltage must be expressed in sampled form.

Several methods of inverting the transfer function were considered and tested. It was concluded that the optimum method was to implement the inverse transfer function as a synthetic digital filter. This allowed the desired output to be specified in sampled form, which offers distinct advantages in terms of the number and type of outputs which may be considered.

It was shown that even the best digital memories were not fast enough to cope with the bondlines of a real transducer. There is, as yet, no complete solution

to this problem, and it was decided to ignore the bond-lines when calculating the inverse driving voltage. The magnitudes of several calculated voltages were then compared and were found to be greater than the system could produce. Reducing the magnitude of the voltage also reduced the magnitude of the generated force output leading to detectability problems. This problem was investigated and it was shown that the addition of matching layers could substantially reduce the magnitude of the required voltage. This is analogous to increasing the transmission efficiency of the system discussed in section 6.2 .

Finally, several methods of forcing the required input voltage to converge to zero were considered. This is necessary in some applications.

Section 6.5 presented a comparison of simulated and experimental inversion results. Initially, attempts were made to generate unipolar force transients. However, these cases all produced diverging excitation voltages. A qualitative explanation for this effect was presented but this has not been verified and further work requires to be done in this area. This led to an investigation of the desired output waveshapes and it

was discovered that bipolar pulses produced converging excitation voltages. These were used for the experimental cases.

It had been hoped to use transducers with multiple, optimal matching layers for the experiments, but it proved impossible using the facilities available, to manufacture layers of sufficient accuracy. Thus two of the transducers which were used for the experimental results of Chapter 5 were used instead.

Nine experiments were performed and six different output transients were generated. By comparing the simulated and experimental results, it was concluded that they were generally in very good agreement. Several interesting points were also noted. Firstly, for some applications, it was necessary to reduce the amplifier gain substantially to achieve good reproduction of the excitation waveform. This led, as predicted, to detectability problems with the generated force transient.

Secondly, the technique for forcing the voltage envelope to converge to zero worked very well and thus offers scope for the generation of further, more complicated outputs.

Finally, ignoring the bondlines in the layered transducer resulted in output force transients with some after-ringing. This was predicted, and agreement between the simulated and experimental results was very good.

Thus, it may be concluded that, while a great deal of work remains to be done in this field, electronic control of transducers offers substantial advantages over alternative methods of improving the transducer response. In particular, it allows the generation of precisely defined output force transients which, in some cases, have a period equal to that of the transducer. It should be possible to extend this method to generate pulses which are shorter than this. However, this has not been considered in the present context.

CHAPTER 7
CONCLUSIONS AND SUGGESTIONS FOR FURTHER WORK

7.1 CONCLUDING SUMMARY

A general three-port systems model of the thickness-mode piezoelectric transducer has been developed. This model may be used to examine both the CW and transient modes of transducer operation. However, since transducer transient analysis has proved difficult for many applications, this area has been considered in detail.

By developing the describing equations into a single lattice-type system, the resultant model is considered to be a significant improvement on prior work. The main advantages of both the model and the modelling techniques used, may be summarised as follows.

1. The model clearly reflects the underlying physical operation of the transducer. Both primary and secondary piezoelectric effects have been identified for both transmission and reception. This allows a direct comparison of transducer behaviour for different operating modes.
2. Arbitrary electrical load and source elements are readily incorporated.
3. Both front and rear mechanical layers may be modelled

The techniques described in Chapter 3, whereby the lattice model is extended using lattice techniques, to include layers, have been compared with the coventional 2-port;3-port;2-port method. From this, it is apparent that the lattice technique is superior.

4. The use of z-transforms in evaluating the transducer transient response has been investigated. This resulted in a suitable Q-matrix technique, whereby the transient response may be calculated quickly and accurately without resorting to a great deal of algebraic manipulation and calculation.

5. The model has been used successfully for electronic transducer control. This required inversion of the system transfer function, and both techniques for, and the effects of this, were investigated.

6. The model is readily implemented on a computer.

Thus the model and its associated techniques are considered to satisfy the five requirements of a transducer model which were identified in Chapter 1.

In the course of this work, the model and the techniques used, have been extensively verified by simulation and experimentation. This has resulted in several additional

contributions, notably,

a) The development of a transient technique for accurately estimating layer thickness without the use of physical measuring apparatus.

b) The effects of the transducer configuration on layer analysis has been investigated. This was shown to have a significant effect upon the measurement of layer parameters. Particularly, overall layer integrity and specific layer thickness.

c) The Q-matrix technique which was developed for z-transformation of differential/delay functions may be applied to a wide range of other functions.

d) A strategy has been developed, whereby the optimal acoustic impedance of a set of mechanical matching layers may be calculated.

e) The effects of electrical load elements and mechanical matching layers upon transfer function inversion has been investigated. These were shown to have a significant effect upon the order and stability of the desired output.

f) A simple technique for calculating the on-axis diffracted field was derived and verified by experimentation, in the far field.

Thus, it is considered that the work presented in this thesis, represents a significant contribution to the fields of piezoelectric transducer modelling and transducer design. However, it is also apparent that several of the areas investigated leave scope for further work. These are indicated in the following section.

7.2 SUGGESTIONS FOR FURTHER WORK

The suggestions for further work may be conveniently divided into two categories, improvements to the model, and applications of the modelling techniques.

7.2.(i) Improvements to the Model.

In the development of the lattice model, it was assumed that the transducer, and the associated mechanical layers, were lossless and had lateral dimensions much greater than their thicknesses. However, in many practical transducers this is not the case.

Munk (46) has investigated the radial vibrations of disc transducers. It is apparent from his work, that for devices where the lateral and thickness dimensions are of the same order of magnitude, lateral vibrations have a significant effect on the transducer response. This is of great importance in ultrasonic array design, where the array elements are often rectangular or square in cross-section. Consequently, the element response may be dominated by lateral vibrations.

The solutions obtained by Munk for radial vibrations were developed into Bessel functions. As such, these are not well suited for systems modelling. It is not known whether this problem can be solved in a similar form to that developed here, but if so, the resultant model would certainly increase the knowledge and understanding of transducer behaviour.

In the array case, the problem is compounded by mechanical coupling between the array elements. Clearly, the first step in developing a general array model is to analyse the behaviour of small elements. Some work has been done in this area, using finite element techniques, but, as was indicated in Chapter 1, these methods do not give much insight into the physical operation of the devices. Thus the development of a small element systems model would greatly increase the understanding of small element behaviour and may lead to improved array design.

From some of the experimental results of Chapters 5 and 6, it is apparent that attenuation in the mechanical layers does occur. Attenuation may also occur in certain transducer materials, (for example quartz). However, it is not a serious problem with the ceramic (PZT-5A) used here. Some work has been done on modelling losses

(for example, SILK (57)), but most of this seems to be based on rather arbitrary adjustment factors. A rigorous solution for attenuation in a lossy material requires a solution of the modified wave equation, where the loss mechanism is included in the initial derivation. Since it is often difficult to identify the precise mechanism which causes the attenuation, this may prove difficult. It is also possible that the solution of the modified wave equation may not be well suited to systems modelling.

However, one simple approach may be to extend the existing model as follows. The transducer and mechanical layers were modelled as simple delays,

$$e^{-sT}$$

where T is the layer transit period. It may be possible for some lossy cases to model the layers with functions of the form

$$L(s)e^{-sT} \quad \text{or} \quad L(s,e^{-sT})$$

This does however require substantial investigation.

The model which has been developed in this thesis predicts the plane-wave component at the transducer surface. It does not include the effects of diffraction in the ultrasonic sound field.

Several of the experimental results of Chapter 5 exhibit marked distortion which may be partially due to diffraction effects. Consequently, to obtain an accurate estimate of the system performance, the overall diffracted transducer field must be accounted for.

Appendix C contains a simple method for calculating the on-axis diffracted field of the transducer. However, when this was verified experimentally, it was found to work well only in the far field. It is also apparent from the derivation of Appendix C, that there is no simple closed-form solution to the equation describing the sound field. Nevertheless, a great deal of work has been done in the area of calculating the transient diffracted field. Notably, by Kazina and Makarov (32), and more recently by Stepanishen (64) and Weight (68). It may be possible to extend the transducer model to include some of the techniques developed by these authors and hence obtain a good estimate of the transducer diffracted field.

Such an extended model would have several advantages, but, principally, it would allow the design of transducers with either desired, or at least well-known beam characteristics. It may eventually be possible to use electronic control to generate a series of desired beam profiles.

Thus there are three main improvements which could greatly enhance the usefulness of the lattice model:

a) The extension of the model to include radial and lateral vibrations.

b) The inclusion of loss and attenuation mechanisms in the model.

c) The development of techniques for predicting the ultrasonic sound field.

7.2.(ii) Applications of the Modelling Techniques

The practical experiments which were carried out in the course of this thesis were designed to verify specific portions of the lattice model, and the modelling techniques. From these results, it is apparent that one area to which the techniques may be applied is the analysis of multilayered structures. This encompasses both the design of

optimal matching layers and the estimation of unknown layer parameters. Thus, the model may be used to test the efficiency and construction of practical optimally layered probes. It may also be extended to the analysis of layered materials, although, since in most cases these layers will not be physically attached to the probe, this may require some experimental investigation. Examples include non-destructive testing of composite structures and general thickness measurement in NDT and biomedicine.

The Q-matrix technique of Chapter 4 has been widely used for bilinear transformation. Recently, several authors, (for example, O'Connor and Huang (47)), have used this method to transform multivariable polynomials. So far, this has been restricted to bilinear transformation but the z-form Q-matrix of Chapter 4 extends this to IIR transformation. It is apparent from (47), that even with the simpler bilinear Q-matrix, some work is required to extend the technique to the multidimensional case. It is likely that some investigation of the IIR case will be required. However, the development of a suitable technique would offer substantial reductions in algebraic manipulation and coefficient calculation.

Chapter 6 investigated techniques for inverting the transmitter transfer function and controlling the transmitter electronically. These techniques were verified experimentally. However, it is apparent from the practical results that further investigation is required if these techniques are to be fully developed. The following areas in particular, require further investigation.

It was shown in Chapter 6 that theoretically, unipolar pulses could be generated. In practice, this proved impossible because the required excitation voltage diverged rapidly. A qualitative explanation for this suggested that the reason for the divergence was a function of the combined effects of the electrical load and secondary piezoelectric action. There are two possible solutions to this problem. Firstly, if the precise effects of the electrical load can be established, it may be possible to identify cases where instability does not occur. Secondly, for some applications, it may be possible to simply ignore secondary effects entirely. Although this would produce some distortion of the desired output, it may still be acceptable. This area is certainly worth further investigation.

Although a variety of desired outputs were generated in Chapter 6, the choice was arbitrary. It is therefore suggested that an experimental investigation into the usefulness of each pulse shape should be carried out. Once the most useful cases have been identified, a more concentrated effort could be made on the problems associated with generating these shapes. This may be particularly important in the design of the electronic driving apparatus, where the system gain and bandwidth were the limiting factors. For example, the bandwidth required to generate the bipolar triangular pulses was less than that required for the corresponding single sine cycles.

Finally, the practical considerations of electronic control warrant further investigation, particularly the design and manufacture of the memory and driving amplifier stages. The equipment used here was based on an ECL array controller (as detailed in Appendix B). It is likely that a customised memory system would reduce costs and operate more reliably. The major limiting factor in generating the driving voltages however, was the amplifier. The devices used here were the best available at the time but it should be possible to design a system with a larger voltage output swing. This should improve the pulse shape definition and the detectability

of the signals.

Thus there is substantial scope for further work in the area of electronic transmitter control.

In a similar manner to the inversion of the transmitter transfer function, it is possible to invert the receiver transfer function. However, the problem under consideration is somewhat different.

For the transmitter, the object of system inversion was to calculate a stable, causal and realisable excitation voltage which would produce a desired force output. Assuming that the calculated voltage for any particular case meets these requirements, it should, on application to the transducer, generate the desired output. Any discrepancy in this output is due to a combination of the following factors:

a) Poor voltage generation.

b) Incorrect system model.

c) System noise.

The first two factors may be corrected by either, improving the generation equipment, or correcting the

system model. There is no solution to the third factor and this forms the basic difference between the transmitter and the receiver. For the receiver, the object of system inversion may be defined as the calculation of the exciting force wave, from the measured receiver voltage. In the transmitter, the deconvolved signal is applied to the system to produce the desired output. In the receiver, the received signal is deconvolved to obtain the exciting force wave. Consequently, system noise is not involved in the transmitter calculation. However, the measured voltage in the receiver will almost certainly contain noise. The techniques developed in Chapter 6 are generally not suitable for the inversion of systems containing noise. Thus the receiver case must be inverted using different techniques, for example, stochastic methods, or least mean square techniques. These methods were considered to be beyond the scope of this thesis and were not investigated here. However, this area is certainly worth further investigation.

Thus four main areas for the further development and application of the modelling techniques have been identified.

a) The characterisation and analysis of mechanical

layer structures.

b) The extension of the Q-matrix technique to multivariable polynomials.

c) The theoretical and experimental extension of system inversion for practical electronic transmitter control.

d) The investigation of receiver inversion techniques.

Acknowledgements

I would like to thank the following persons within the Department of Electronic and Electrical Engineering.

Special thanks are due to DR G HAYWARD (Lecturer) who both supervised the development of the present work and provided much useful advice and many suggestions.

The author would also like to thank the Heads of Department, Professors T S DURRANI and A M ROSIE for providing all of the facilities required to carry out this work.

Thanks are also due to DR E OLCAYTO (Lecturer) for useful discussions and advice on the development of the z-transform techniques and to DR C J MACLEOD (former Departmental Reader) for introducing the author to this area of research.

The author gratefully acknowledges the financial support given to this work by the SERC Marine Technology Directorate.

Finally, I would like to thank MISS L STEWART for

typing this thesis; MR A BASHIR for supplying the typing equipment; and all of my friends and colleagues within the department for their support and encouragement.

REFERENCES

The following abbreviations have been used in the list of References and Bibliography.

ASSP - Institute of Electrical and Electronic Engineers, Transactions on Acoustics, Speech and Signal Processing.

GSU - Institute of Electrical and Electronic Engineers, Transactions on Sonics and Ultrasonics.

IEE - Institute of Electrical Engineers.

IEEE - Institute of Electrical and Electronic Engineers.

JASA - Journal of the Acoustical Society of America.

JASJ Journal of the Acoustical Society of Japan.

PIRE Proceedings of the Institute of Radio

Engineers.

SP-A Soviet Physics Acoustics.

References and Bibliography

1. BACON, D.R. "Characteristics of a PVDF membrane hydrophone for use in the range 1-100 MHz, IEEE, GSU SU 29, pp18-25.

2. BERLINCOURT, D.A., CURRAN D.R., JAFFE, H. "Piezoelectric and Piezomagnetic materials and their function in transducers." PHYSICAL ACOUSTICS, I, PART A, pp 170-267. (Edited by W. P. MASON), Academic Press, London, 1964

3. BÖRJESSON, P.O., HOLMER, N.G., LINDSRÖM, K., MANDERSSON, B., SALOMONSSON, G. "Digital Preshaping of Ultrasonic signals; Equipment and applications." IEEE ULTRASONICS SYMPOSIUM PROCEEDINGS, 1982, pp 696-699

4. BOSE, N.K., JURY, E.I., "Positivity and stability tests for multidimensional filters, (discrete-continuous)", IEEE ASSP-22, pp174-180, JUNE 1974.

5. BOXER, R. "A note on numerical transform calculus". PIRE, VOL 45, 1957, pp1401-1406.

6. BOXER, R., THALER, S., "A simplified method of solving linear and nonlinear systems." PIRE, VOL 44, 1956, pp89-101.

7. BRIGHAM, O., The Fast Fourier Transform. Prentice-Hall, 1974.

8. BURR-BROWN, Product Data Book, Burr-Brown Research Corporation Ltd, International Airport Industrial Park, PO BOX 11400 TUCSON, Arizona, USA.

9. CADY, W.G. Piezoelectricity, Mc Graw-Hill Book Company, London, 1946.

10. CHALLIS, R.E., HARRISON, J.A., "Transient response of Piezoelectric transducer elements derived by z-transform technique." Proceedings of the Institute of Acoustics, Department of Biophysics and Bioengineering, Chelsea College, London, SW3.

11. CHALLIS, R.E., HARRISON, J.A., "Rapid solutions to the transient response of piezoelectric elements by z-transform techniques", JASA, VOL 74(6), December 1983, pp1673-1680.

12. COOK, E.G., "Transient and steady-state response of ultrasonic Piezoelectric transducers" Schlumberger Well Surveying Corporation, Ridgefield, Connecticut, USA.

13. COURSANT, R.H., "Piezoelectric transducer design and generation of simple ultrasonic waveshapes via transducer transfer functions". Laboratories d'Electronique et de Physique, Appliquee, 3 avenue Descartes, 94450 Luneil-Prevannes, France.

14. DeSILETS, C.S., FRASER, J.D., KINO, G., "The design of efficient broad-band Piezoelectric transducers", IEEE GSU, SU -25, MAY 1978, p115

15. ENGSMINGER, D., "Ultrasonics, the Low and High Intensity Applications", MARCEL DEKKER INC. NEW YORK, 1973.

16. FILIPCZYNSKI, L., "Transients, Equivalent circuits and negative capacitance of a Piezoelectric transducer performing thickness vibrat-

ions.", Journal of Technical Physics, VOL 16, No 2, 1975, pp 121-135.

17, GITIS, M.B., SCHENKER, A.A., "Pulsed operation of a flat Piezolectric transducer." SP-A VOL 27(6), November/December 1981, p469.

18 HARRIS, S., "Analog Linear Data Acquistion", Matra-Harris Semiconducteurs, Harris GmbH, Semiconductor Group, D-8000 MUNICH 80, West Germany.

19. HAYWARD, G., "Time and frequency domain modelling of the piezoelectric transducer." PhD Thesis, University of Strathclyde, Glasgow, U.K. 1981.

20. HAYWARD, G., MAC LEOD, C.J., DURRANI, T.S., "A Systems model of the thickness-mode piezoelectric transducer." JASA, VOL 76(2), August 1984.

21. HAYWARD, G., JACKSON, M.N., "A study of Electronic Switching Devices for the characterisation of ultrasonic probe assemblies." IEEE ULTRASONICS SYMPOSIUM PROCEEDINGS, 1983, pp 752-756.

22. JURY, E.I., Theory and Application of the Z-Transform Method. Kreiger, 1973, reprint of 1964 edition.

23. JURY, E.I., CHAN, O.W.C., "Combinatorial rules for some useful transformations". IEEE CT-20(5), September 1973, pp476-480.

24. KAGAWA, Y., GLADWELL, G.M.L., "Finite Element Analysis of flexure-type vibrators with

Electrostrictive Transducers", IEEE GSU - SU 17, January 1970, pp41-49.

25. KAGAWA, Y., GLADWELL, G.M.L., "Application of a Finite Element method to vibrational problems in which Electrical and Mechanical systems are coupled." JASJ, VOL 26(3), 1970, pp117-128.

26. KAGAWA, Y., "A new approach to analysis and design of Electromechanical filters by the Finite Element technique." JASJ, VOL 49(5), 1971, pp1348-1356.

27. KAGAWA, Y., "Analysis and design of Electro-mechanical filters by Finite Element technique" JASJ, VOL 27(4), 1971, pp201-214.

28. KAGAWA, Y., YAMABUCHI, T., "Finite-element simulation of 2-D Electromechanical filters". IEEE GSU - SU 21, October 1974, pp275-283.

29. KAGAWA, Y., YAMABUCHI, T., "A finite element approach to Electromechanical problems with an application to energy trapped and surface wave devices". IEEE, GSU -SU 23, JULY 1976, pp263-272.

30. KAGAWA, Y., YAMABUCHI, T., "Finite Element approach for a Piezoelectric circular rod." IEEE GSU -SU 23 November 1976, pp376-385.

31. KAGAWA, Y., YAMABUCHI, T., "Finite Element simulation of a composite piezoelectric transducer". IEEE, GSU -SU 26, March 1979, pp81-88.

32. KAZINA, O. G., MAKAROV, G. I., "Transient processes in the acoustic fields generated by

a piston membrane of arbitrary shape." SP-A - Vol 7, 1961, pp 39-43.

33. KAŽYS, R., LUKOŠEVIČIUS, A., "Optimization of the Piezoelectric Transducer response by means of Electrical correcting circuits." ULTRA-SONICS, MAY 1977, pp 111-116.

34. KERVEL, S.J.H., THIJSSEN, J.M., "A calculation scheme for the optimum design of ultrasonic transducers," ULTRASONICS, MAY 1983, p134.

35. KOSSOFF, G., "Backing and Matching effects on transducer performance." IEEE, GSU -SU 13 March 1966, p20.

36. KRIMHOLTZ, R., LEEDOM, D.A., MATTHEI, G.L., "New equivalent circuits for elementary piezo-electric transducers." IEE - Electronics Letters, VOL 6 No 13, 25 June 1970.

37. LEEDOM, D.A., KRIMHOLTZ, R., MATTHEI, G.L. "Equivalent circuits for transducers having abitrary even-odd symmetry Piezoelectric Excitation." IEEE GSU -SU 18, July 1971, p128

38. LEWIS, G.K., "Matrix technique for analysing multilayered piezoelectric transducers." Acoustical Imaging, 8, pp395-416. Plenum New York, (1980).

39. LIU, R.Y., "The design of electric excitations for the formation of desired temporal responses of highly efficient transducers." Acoustical Imaging, 12, p293, Plenum New York, (1982).

40. LLOYD, P., REDWOOD, M., "Finite-difference method for the investigation of the vibrations of solids and the evaluation of the equivalent

circuit characteristics of piezoelectric resonators, I, II, III". JASA, VOL 39(2), 1966, p346.

41. LOW, G.C., "A simple computer method for predicting the transient response of ultrasonic ndt probes." NDT International VoL 13, pp285-290.

42. MASON, W.P., Electromechanical Transducers and Wave Filters." D. Van Nostrand Company LTD, London, 2nd Edition, 1958.

43. MARTIN, R.W., SIGELMANN, R.A., "Force and Electrical Thevenin equivalent simulations for thickness-mode Piezoelectric Transducers". JASA, VOL 58(2), August 1975, p475.

44. MEL'KANOVICH, A.F., "Calculation of transient processes in a plane piezoelectric transducer" SP-A VOL 24, September/October 1978, p402.

45. MEL'KANOVICH, A.F., "Generation of acoustic pulses having a prescribed shape by means of a piezoelectric transducer". SP-A VOL 25, 1979, pp515 - 517.

46. MUNK, E.C., "The equivalent circuit for radial modes of a piezoelectric ceramic disc with concentric electrodes." Philips Research Reports, 20, 1965, pp170-189.

47. O'CONNOR, B., HUANG, T.S., "An efficient algorithm for Bilinear transformation of multivariable polynomials." IEEE ASSP 26, pp380-381, AUGUST 1978.

48. OPPENHEIM, A.V., SCHAFER, R.W., Digital Signal Processing, Prentice-Hall, London, 1975.

49. PRESTON, R.C., BACON,D.R. LIVETT, A.J., RAJENDRAN, K., "PVDF membrane hydrophone performance properties and their relevance to acoustics," Journal of Physics E, Instrumentation VOL 16, 1983, pp786-796.

50. RAO, V.V.B., AARTE, V.K., "Transformation matrices for Bilinear transformation of multivariable polynomials." IEEE ASSP 24, pp266-267, June 1976.

51. REDWOOD, M., "Trnasient performance of a piezoelectric transducer." JASA VOL 33(4), April 1961, p527.

52. REDWOOD,M., "Experiments with the electrical analogue of a piezoelectric transducer," JASA VOL 36(10), October 1964, p1872.

53. RHYNNE, L., "An improved interpretation of Mason's model for piezoelectric plate transducers." IEEE GSU -SU 25(2), March 1978, pp98-103.

54. ROBINSON, E.A., TREITEL, S., "The spectral function of a layered system and the determination of the waveforms at depth." Geophysical Prospecting, VOL 25, pp434-459.

55. SELFRIDGE, A.R., BAER, R., KHURI-YAKUB, B.I., KINO, G.S., "Computer-optimized design of quarter-wave acoustic matching and electrical matching networks for acoustic transducers," IEEE Ultrasonics Symposium Proceedings 1981, p644.

56. SILICONIX VMOS Power FET Design Catalogue, January 1979.

57. SILK, M.G., "An extended model of the ultrasonic transducer." Journal of Physics E, Scientific Instruments, VOL 16, 1983, pp879-887.

58. SILK, M.G., "NDT using Ultrasound", International Metals. Review, 1982, No 1, pp29-30.

59. SILK, M.G., "Calculations on the Effect of some constructional variables on ultrasonic transducer performance," Materials Physics Division, AERE Harwell, Report, JUNE 1980 (UK)

60. SINHA, D.K., "Note on Electrical and Mechanical responses with ramp-type input signal in piezoelectric plate transducer". Indian Journal of Theoretical Physics, VOL 11 (1963), pp93-99.

61. SITTIG, E.K., "Transmission parameters of thickness-driven piezotransducers in multilayer configuration." IEEE GSU -SU 14(4), October 1967, p167.

62. SITTIG, E.K., "Effects of bonding and electrode layers on the transmission parameters of piezotransducers used in ultrasonic delay lines." IEEE GSU -SU 16(1), January 1969, p2.

63. STEPANISHEN, P.R., "Transient analysis of lumped and distributed parameter systems using an approximate z-transform technique." JASA VOL 52(1), 1972, p270 .

64. STEPANISHEN, P.R., "Transient radiation from pistons in an infinite planar baffle." JASA VOL 49(5). 1971, p1629.

65. "ULTRA-HIGH SPEED ECL HYBRID D/A CONVERTER". HDS 0810E Datasheet, Analog Devices.

66. VERNITRON APPLICATIONS BULLETINS (Southampton Ltd), 66047/A, 66011/F, 66017/B.

67. WASOW, W., "Discrete approximations to the Laplace transform." Z. ANGEW MATHEMATICAL PHYSICS (1957), VOL 8, pp401-407.

68. WEIGHT, J.P., HAYMAN, A.J., "Observations of the propagation of very short ultrasonic pulses and their reflection by small targets." JASA VOL 32, 1976, pp751-757.

70. YING, C.F., LI, M.X., ZHANG, H.L., "Complete solutions of the transient behaviour of a transmitting thickness-mode piezoelectric transducer, and thier physical interpretations." JASA, VOL 74(4) October 1983, pp1105-1114.

Publications Associated with this Thesis.

HAYWARD, G., JACKSON, M.N., "A study of Electronic Switching Devices for the Characterisation of Ultrasonic Probe Assemblies."
IEEE Ultrasonics Symposium, November 1983, Atlanta, USA.

JACKSON, M.N., HAYWARD, G., "A New Three-Port Model of the Thickness-Mode Piezoelectric Transducer."
IEEE Ultrasonics Symposium, November 1983, Atlanta, USA.

HAYWARD, G., JACKSON,M.N., "The use of Z-Transforms in Modelling Piezoelectric Transducers".
IEEE Ultrasonics Symposium, November 1983, Atlanta, USA.

HAYWARD, G., JACKSON,M.N., "Discrete-time Modelling of the Thickness-Mode Piezoelectric Transducer."
IEEE Transactions on Sonics and Ultrasonics, VOL SU 31(3), May 1984.

JACKSON, M.N., HAYWARD, G., "Inversion Methods for the Generation of Ultrasonic Wave Profiles."
IEEE Ultrasonics Symposium, November 1984, Dallas, USA.

HAYWARD, G., JACKSON, M.N., "A Lattice Model for the Discrete-Time Simulation of a Multilayered Piezo-electric Transducer System."
IEEE Ultrasonics Symposium, November 1984, Dallas, USA.

Under Review

HAYWARD, G., JACKSON,M.N., "A Lattice Model of the Thickness-Mode Piezoelectric Transducer."
IEEE Transactions on Sonics and Ultrasonics.

JACKSON, M.N., HAYWARD, G., "A Q-Matrix Algorithm for the Transformation of Mixed Differential/Delay Transfer Functions."
IEEE Transactions on Circuits and Systems.

APPENDIX A

Some Practical Considerations of the Boxer and Thaler Method

APPENDIX A

This appendix discusses in detail, some of the problems which were described in Chapters 4, 5 and 6 regarding the z-form method of Boxer and Thaler. Three areas are investigated, namely, the common factor problem, the numerical error round-off problem and the use of the z-forms as differential operators. These cases arise from the application of the z-form technique rather than the underlying method. A comprehensive analysis of the error associated with the z-form method is given by WASOW (67).

(i) The Common-Factor Problem

The electrical configuration of the transducer system has so far been assumed to be of the form shown in Fig A1. In this form, any common factors which occur in the differential polynomials of the transducer transfer function will also exist in the load term $\overline{Z}_E$. These may be removed by expressing $\overline{Z}_E$ in the form,

$$\overline{Z}_E = \frac{\prod_{i=1}^{I}(s+\alpha_i)}{\prod_{j=1}^{J}(s+\beta_j)} \quad ; \quad J \geq I \qquad \text{A1}$$

A1

and eliminating the common terms from the numerator and denominator. The reduced form of $\overline{Z}_E$ may then be used with the required system transfer function, with the assurance that no common factors exist.

However, consider the electrical configuration of Fig A2. If this is rewritten in its Thevenin equivalent form and related to Fig A1, then,

$$\overline{Z}_E = \frac{\overline{Z}_1.\overline{Z}_0}{\overline{Z}_1+\overline{Z}_0}$$

$$\overline{V}_E = \left(\frac{\overline{Z}_1}{\overline{Z}_1+\overline{Z}_0}\right).\overline{V}_s = \overline{Z}_s.\overline{V}_s \qquad \text{A2}$$

Assuming $\overline{Z}_0$ and $\overline{Z}_1$ are of the form,

$$\overline{Z}_0 = \frac{\overline{Z}_0^N}{\overline{Z}_0^D} \; ; \quad \overline{Z}_1 = \frac{\overline{Z}_1^N}{\overline{Z}_1^D} \qquad \text{A3}$$

then,

$$\overline{Z}_E = \frac{\overline{Z}_1^N.\overline{Z}_0^N}{\overline{Z}_1^N\overline{Z}_0^D+\overline{Z}_0^N\overline{Z}_1^D} \qquad \text{(i)} \quad \text{A4}$$

$$\overline{V}_E = \left(\frac{\overline{Z}_1^N \cdot \overline{Z}_0^D}{\overline{Z}_1^N \cdot \overline{Z}_0^D + \overline{Z}_0^N \cdot \overline{Z}_1^D}\right) \cdot \overline{V}_s \qquad \text{(ii)}$$

A4

These may be rewritten as,

$$\overline{Z}_E = \frac{\overline{Z}_E^N}{\overline{Z}_E^D} \; ; \qquad \overline{V}_E = \frac{\overline{Z}_s^N}{\overline{Z}_s^D} \cdot \overline{V}_s \qquad \text{A5}$$

where,

$$\overline{Z}_E^N = \overline{Z}_1^N \cdot \overline{Z}_0^N$$

$$\overline{Z}_s^N = \overline{Z}_1^N \cdot \overline{Z}_0^D$$

$$\overline{Z}_E^D = \overline{Z}_s^D = \overline{Z}_1^N \cdot \overline{Z}_0^D + \overline{Z}_0^N \overline{Z}_1^D \qquad \text{A6}$$

If the general z-transform model is to be used, then the excitation voltage, $\overline{V}_s$ must be specified in sampled form.

Consequently, the additional Laplace term, $\overline{Z}_s$, must be included in the differential polynomials of the transducer transfer function.

From chapters 5 and 6, these are, for the system of Fig A1,

$$\overline{d}_1 = s\overline{Z}_E^D$$

$$\overline{d}_2 = X_k.\overline{Z}_E^D$$

$$\overline{d}_3 = s(\overline{Z}_E^D+sC_t\overline{Z}_E^N) \qquad \text{A7}$$

For a system of the type shown in Fig A2, these become,

$$\overline{d}_1 = s\overline{Z}_E^D.\overline{Z}_s^N$$

$$\overline{d}_2 = X_k.\overline{Z}_E^D.\overline{Z}_s^D$$

$$\overline{d}_3 = s(\overline{Z}_E^D+sC_t\overline{Z}_E^N).\overline{Z}_s^D \qquad \text{A8}$$

Comparing these equations with equation A6, it may be obseved that the differential polynomials now all have a common factor,

$$\overline{Z}_1^N\overline{Z}_0^D+\overline{Z}_0^N\overline{Z}_1^D \qquad \text{A9}$$

Removing the common factor reduces the differential

terms thus,

$$\overline{d}_1 = s\overline{Z}_s^N$$

$$\overline{d}_2 = X_k.\overline{Z}_E^D$$

$$\overline{d}_3 = s(\overline{Z}_E^D+sC_t\overline{Z}_E^N) \qquad \text{A10}$$

which may be rewritten as,

$$\overline{d}_1 = s.\overline{Z}_1^N.\overline{Z}_0^D$$

$$\overline{d}_2 = X_k.(\overline{Z}_1^N.\overline{Z}_0^D+\overline{Z}_0^N.\overline{Z}_1^D)$$

$$\overline{d}_3 = s(\overline{Z}_1^N\overline{Z}_0^D+\overline{Z}_0^N\overline{Z}_1^D+sC_t\overline{Z}_1^N.\overline{Z}_0^N) \qquad \text{A11}$$

Assuming that $\overline{Z}_0$ and $\overline{Z}_1$ have had any common factors removed, then equations A11 will also have no common factors.

An example of this case is the widely used firing circuit shown in Fig A3. For this example, $\overline{Z}_0$ and $\overline{Z}_1$ take the values,

$$\overline{Z}_0 = \frac{1}{sC_B}$$

$$\overline{Z}_1 = \frac{R_E}{1}$$

A12

and the differential polynomials become,

$$\overline{d}_1 = s^2 C_B R_E$$

$$\overline{d}_2 = X_k(1+sC_B R_E)$$

$$\overline{d}_3 = s(1+sR_E(C_t+C_B))$$

A13

Clearly, these do not have a common factor. This method may appear rather cumbersome at first, but in fact this technique is readily computerised and has been successfully extended to include both T and TT networks. Thus this procedure guarentees that there will be no common factor in the differential polynomials of the transducer transfer functions.

The effect of common factors on the response of the transducer system was investigated by deliberately including common terms in several cases. This results

in differential polynomials of a higher order than the minimum required. Consequently, the digital filters produced by the Q-matrix technique are also of a higher order than the minimum required.

In some cases, this led to an unstable response with an oscilliatory output. However, for most applications, the differences between the correct and the higher order responses were slight. Several attempts were made to quantify the cases where an unstable output occurred but no general link between them could be found. There are two possible explanations for this.

(i) The inclusion of certain common factors apparently renders the system z-transform unstable. The nature of these common factors may depend upon both the order factors of the differential polynomials, and the factors of the discrete polynomials.

(ii) The inclusion of certain common factors may render the system z-transform more susceptible to computer round-off errors. If the first explanation is correct, then it should be possible to quantify the instances when instability occurs and identify the undesirable common factors. If the second explanation is corect, it may be solved by adopting alternative programming techniques to minimise the effects

of round-off errors.

Since neither of these explanations could be conclusively linked to the common factor problem, the programs used for the simulations of this thesis were designed to eliminate common factors, and thereby avoid the problem.

(ii) Numerical Round-Off Errors

In chapter 6, it was noted that, for certain cases, when the order of the denominator of a differential transfer function is larger than the order of the numerator, the z-form technique becomes susceptible to computer round-off errors. One solution to this problem was to increase the accuracy with which the calculations were made. However, for large differences in order, the accuracy required becomes very large, and is soon unacceptable. This problem was investigated further, and two interesting points were noted.

Firstly, the problem also depends upon the coefficients of the numerator and denominator terms. For some cases, slight alterations of one or two coefficients in either

the numerator or denominator produced instability.

Secondly, increasing the calculated accuracy of the Q-matrix appeared to have little or no effect on the results.

This is interesting because the problem now appears to be similar to that of the cases with common factors. Again, no link could be found between the cases where instability occurred, but this does increase the likelihood that the common factor problem is caused by computer round-off errors. No solution to this problem was found. In conclusion, there exist cases where the coefficients of the differential transfer function are ill-conditioned such that, when the z-form technique is applied, the resultant digital filter is susceptible to computer round-off errors. In this event, the only solution at present, is to increase the accuracy of the calculations until the response becomes stable.

(iii) The Use of z-forms as Differential Operators

Boxer (5) has considered the use of the z-forms as differential operators. This was discussed in Chapter 6,

where it was stated that the z-forms resulted in unstable differentiators, and consequently, could not be used. For cases where it was required to use the z-forms as differentiators, the technique described in Chapter 6, was used to re-form the transfer function, such that, another differential operator could be used. This section presents a simple example which shows the effects of using both the z-form and the alternative operator techniques.

Consider the differential system of Fig A4, whose input is a unit-ramp. The output of this system is given by,

$$O(s) = \frac{1}{s^2}(1+s) \qquad A14$$

which is, in the time domain,

$$O(t) = 1+t \qquad A15$$

This is sketched in Fig A5.

Now, if the exciting ramp had been a sampled function, the response of this system may have been evaluated as follows.

Take the z-transform of the system using the z-form method; implement the resultant z-transform as a digital filter; and excite the filter with the sampled ramp.

This was carried out, and Fig A6 shows the calculated output. Clearly, this technique has produced an output which exhibits bounded oscillations about the correct solution.

An alternative method of calculating the system response is that outlined in Chapter 6. In this case, the alternative method produces an output which it considers to be the sum of the sampled ramp and its differential. (The differential was obtained numerically, using the first order backward difference method.) This is shown in Fig A7. Thus the alternative method produces the correct result.

When comparing Figs A6 and A7, it is apparent that the z-from method cannot be used for cases which require differential operators.

This appendix has outlined three problems which may occur with the z-form method of Boxer and Thaler and presented the solutions which were used to overcome them.

For the common factor problem, no satisfactory method was found for identifying the common terms which caused instability. Consequently, a technique for removing the common factors was adopted.

In the second case, no solution to the round-off error exists, other than increasing the accuracy of the calculations until they become stable. It was also noted that this may be linked to the common factor problem.

Finally, it was shown that the use of the z-form as differential operators produces unstable results. A method which allows alternative differential operators to be used was described in Chapter 6. This was compared with the z-form method and was shown to give the correct solution for a particular case.

APPENDIX B

Transducer and Experimental Data

APPENDIX B

This appendix gives a detailed account of the experimental apparatus and the transducers which were used in Chapters 5 and 6. It has been subdivided into 3 sections. The first section covers the transducer and probe assemblies. Section 2 describes the general experimental layouts and section 3, the specific pieces of equipment which were used.

(i) Transducer and Probe Assemblies

To maintain compatibility among the transducers and probes which were used, it was decided to use a single crystal type for each transducer. The crystal selected was a 1 MHz Lead Zirconate Titanate ceramic, (PZT5-A) supplied by VERNITRON (66). The data supplied by the manufacturer are given in Table B1.

It may be noted from the relevant chapters, that some of the parameters used by the models are not supplied by the manufacturer, namely, the static capacitance, C_t, and the transducer transit time T_t. Both of these

quantities may be established by experimental measurement, or in the case of C_t, calculated from the physical size of the ceramic, and the relevant constants from Table B1.

HAYWARD (19) has measured the static capacitance and mechanical frequency of the crystal used in Transducer B. The methods used by him were also used to measure the parameters of the crystals used in Transducer D and Transducer E.

The ceramics of Transducers A and C were not measured. However, since the measurements for B and D agreed closely, and all four ceramics had approximately the same physical dimensions, these values were assumed for A and C. (Transducer E is larger than the other 4 transducers and has correspondingly different physical properties.)

Table B2 compares the calculated and the measured values for the ceramics of the transducers B, D and E. The bottom row of the Table gives the values which were used in the simulation programs.

The probe assemblies in which the ceramics were mounted may be briefly described as follows.

TRANSDUCER A

This was a free crystal, mounted at the centre of its faces by the clamping apparatus, shown in Fig B1.

TRANSDUCER B

This transducer was manufactured by HAYWARD (19). It consists of a ceramic crystal backed with a plastic-lead compound, DEVCON-L. The backing material has a measured acoustic impedance of:-

$$9.11 \times 10^6 \text{ kg/m}^2\text{-s}$$

The crystal and backing are not housed, and the nature of the backing material, (self-adhesive), avoids an intermediate glue layer between the ceramic and the backing material. Connections to the front and rear electrodes were made at the edge of the front electrode and at the centre of the rear electrode. It is assumed that the backing material is of sufficient thickness to behave as a semi-infinite medium, not a finite-thickness layer. This transducer is sketched in Fig B2.

After prolonged use, it was observed that the front silver electrode began to deteriorate. The deterioration continued, with the silver apparently dissolving (perhaps due to electrolytic action), until the probe could not be used. It is possible that this effect

could have degraded some of the experimental results in Chapter 6. However, the probe was carefully monitored and the worst deterioration occurred during some experiments after the results presented here had been completed.

TRANSDUCER C

This transducer was also manufactured by Hayward (19). It consists of a ceramic crystal mounted in a Perspex holder, as shown in Fig B3. The crystal protrudes from the holder, as shown, and is sealed at its edges by a small quantity of Araldite. As with Transducer B, the front and rear electrodes are connected at the edge and centre of the front and rear faces respectively. The Perspex holder is sealed, so that the transducer is effectively air-backed, and may be used in a water-tank.

TRANSDUCER D

This transducer was manufactured by the author. It consists of a ceramic crystal, backed by a cast lead plug, with a front layer of aluminium. The lead plug was attached to the ceramic with silver- loaded Araldite (available from RS Components Ltd). As with Transducer B, it was assumed that the plug was of sufficient thick-

ness to behave as a semi-infinite medium. The aluminium layer was attached to the front of the ceramic using ordinary raldite. Fig B4 shows a sketch of the transducer, and Table B3 gives the properties of all the materials used in the probe construction.

The transducer was made in two stages. Firstly, the lead plug was glued to the ceramic. After the glue had been applied, the assembly was placed in a vice, to compress the glue layer. Once the glue had set, the lead plug was varnished, to provide insulation, and the backed probe was tested in a water tank, as is detailed in Chapter 5, cases 13 and 14. From these experiments, it was determined that the bondline was approximately 10 μm thick. Secondly, the aluminium layer was glued in place, using a similar procedure, and the transducer re-varnished. From case 15, Chapter 5, the measured thickness of the front bondline was also approximately 10 μm.

Since the lead plug was glued to the crystal using a conductive adhesive, the rear electrode was connected to the lead plug. The front electrode was soldered to the edge of the ceramic, before the aluminium layer was attached. It was originally intended to remove this

electrode, and re-attach it to the aluminium, once the layer was in place. However, it was not possible to remove the solder completely from the electrode, and since it was necessary that the front electrode should have a smooth, flat surface, the connection was left in place. A small notch was cut in the edge of the aluminium to compensate for the soldered connection.

TRANSDUCER E

This transducer was also manufactured by the author. It consists of a 30 mm diameter crystal, backed by a cast lead plug, with a front layer of steel. The probe was manufactured in an identical manner to Transducer D, with measurements being made before and after the addition of the front layer. (These are detailed in Chapter 5, cases 16, 17, 18 and 19.) The transducer is sketched in Fig B5. Both the front and rear bondlines were measured to be approximately 10 μm thick, . The electrodes were connected in an identical manner, (rear connection to the lead plug, front connection to the crystal), and a small notch was cut at the side of the steel layer to accommodate the front electrode connection.

During the attachment of the front layer, some

skewing of the layer occurred. Thus the layer did not cover the entire surface of the crystal. As is explained in Chapter 5, this effect may account for the discrepancies which arose between the force and voltage measurements. However, this effect did not otherwise seem to affect the performance of this transducer.

Finally, it is also possible, (again from the discrepancies between the force and voltage measurements), that areas of the rear bondline were thicker than 10 μm. Great care was taken to minimise the bondline thicknesses, but it is possible that small air bubbles or irregularities in the lead plug could produce areas where the bondline was much thicker than the measured values. The reasons as to why this would affect the measurements, are given in Chapter 5, section 5.5 .

(ii) Experimental Procedures

Four basic experimental procedures were used, as follows.

Experimental Setup 1

This was the method used to measure the voltage across the free, undamped transducer A. This device was clamped, as shown in Fig B1. The general firing circuit (detailed on a later page), and a suitable oscilloscope were then connected as shown in Fig B6. To minimise cabling effects, the clamping device was built on the same board as the firing circuit.

Experimental Setup 2

This describes the method used to measure the force output from the front face of a transducer. The selected transducer was co-axially aligned with the receiving hydrophone in a water tank, as shown in Fig B7. The length of cable connecting the firing circuit to the transmitting transducer was kept as short as possible, (10-15 cms, approximately), by mounting the firing circuit on an insulating tile directly above the transducer. The position of the hydrophone, in relation to the transducer, was carefully adjusted before each result

and the distance, d, was in the range 15 - 25 mm.

Experimental Setup 3

This setup is very similar to the previous case. However, now the hydrophone is replaced by a receiving transducer, as shown in Fig B8, Again, the distance d, was approximately 15-25 mm and both transducers were carefully aligned before each measurement. The receiving transducer was connected to the electrical load board by a short length of cable and thence to the oscilloscope, as shown.

Experimental Setup 4

This was identical to Setup 2, with the exception that the firing circuit was replaced with the amplifiers which are described at a later stage. For practical reasons, it was not possible to mount the amplifiers in near proximity to the firing transducer. Thus, the cabling which connected the amplifier to the transducer was sufficiently long to produce some distortion of the generated firing pulse. This was minimised by connecting the electrical load elements in line, approximately halfway between the amplifier and the transducer.

(iii) Hardware and Apparatus.

General Firing Circuit

The general firing circuit which was used for the results of Chapter 5, is shown schematically in Fig B9. This circuit was built by Hayward (19) and centred around an IRF 830 VMOS switching power FET. The technical data for this device is given in reference (56).

The firing circuit consists of the IRF 830, connected as shown via a 330 KΩ limiting resistor to an HT supply. For the results of Chapter 5, the HT supply was taken from a BRANDENBURG TYPE 475 R power supply. The electrical load elements were connected to the drain of the MOSFET as shown, and consisted of a series blocking capacitor, C_B, and a parallel resistor and inductor, R_E and L_E, (shown dotted.) The blocking capacitor was used for all of the experimental results but the resistor and inductor were included only in the cases where their presence is indicated.

This circuit was driven by a 10 μs pulse, via a MOSFET driver. The application of this pulse caused the IRF 830 to conduct, effectively shorting the drain and source to

ground. In some applications, the source resistor, R_s, was connected. This had a value of approximately 1 Ω and was used to either enhance or degrade the switching speed of the device, depending upon the electrical load. For the fastest applications, the device switched from 300 V to zero in approximately 30 ns. However, this was degraded in some cases to as much as 500 ns. The precise details of the switching speed used, are given in the experiments of Chapter 5.

The circuit was connected to the transmitting transducer via a short length of co-axial cable. For the measurements of Experimental Setup 1, the firing circuit was connected to the transducer clamp. This was mounted on the board, in close proximity to the circuit.

Several IRF 830 devices were used with this circuit, and it was observed that there was a noticeable spread in their characteristics. Consequently, the turn-on time of the circuit was measured for each experiment, and checked against the desired value.

On the whole, this circuit performed well, although when it was operated at its fastest speed, considerable care had to be taken to ensure that distortion, due to

the co-axial cable, was minimised. It may be possible to include these effects into the modelling program at a later stage., This was not attempted here.

Receiving Hydrophone.

The receiving hydrophone used for the experimental results of Chapters 5 and 6 was a Polyvinylidene fluoride (PVDF) device, supplied by MARCONI Instruments Ltd, (serial number Y-33-7611-B701). This device has been analysed in detail by BACON (1) and Hayward (19). It has a sufficiently large bandwidth to have a negligible effect on the shape of the detected signals, (other than a scaling factor.) However, it was noticed that some slight distortion of the received waveforms did occasionally occur. This is probably due to the directionality of the device, rather than its physical response. These effects were noted but were small enough to be ignored.

For the results of Chapter 6, the hydrophone was connected to a membrane hydrophone amplifier, also supplied by Marconi Instruments Ltd. This device is detailed in reference (49). It is essentially a low noise, high gain, small signal amplifier, designed specifically for use with PVDF hydrophones. This device had a bandwidth of approximately 10 MHz which was rather low for these experiments. Thus it may have contributed to the minor distortions of some of the results of Chapter 6.

Electronic Control Equipment

The equipment .. used for the electronic control of the transducers was shown schematically in Fig 6.4 . It consists of three parts.

(i) ECL digital memory

(ii) Digital to Analogue Converter

(iii) Amplifier stage

The ECL memory originally comprised part of a digital array controller and was the most expensive part of the apparatus. To save costs, it was decided to modify the array controller, rather than re-build a new memory. The array controller was controlled by a TEXAS 9900 micro-processor. By re-writing the control software, it was possible to adapt the array controller without making any major modifications to the hardware.

The operation and data transfer procedure for the ECL memory is shown in Fig B10. The required excitation voltage was initially calculated, in sampled form, on a Honeywell H6640 mainframe computer. This data was next transferred via a serial RS 232 link to a TEKTRONIX 4051 intelligent graphics terminal, where it was stored on tape. The data was then modified into 8-bit binary form, and scaled to allow maximum use of the range of the DAC.

Next, the modified data was transferred to the ECL memory via a General-Purpose Interface Bus, (GPIB). Once loaded into the memory, the stored data was read back to the 4051 and checked. Assuming that no errors occurred, the ECL control program would next copy the last sample word to be transferred into the memory latch

Finally the stored data was clocked out of the ECL memory onto an 8-bit data bus and sent to the DAC. When the clock/counter reached the last sample, the memory latch was triggered, such that, after the last sample was written to the data bus, the latch retained this sample on the bus. This technique was discussed in Chapter 6.

It was impracticable to hold the last sample of the bus for extended periods, so the entire process of generating the sampled waveform from the ECL memory was repeated at a rate of 50 Hz. This rate was chosen for two reasons. Firstly re-freshing the generated voltage allowed time to build up a good image of the waveform on the oscilloscope. For the applications used here, the ECL memory size was 1024, 8-bit words. At the 50 MHz sampling rate, this corresponded to a time length of

$$\frac{1024}{50*10^6} = 20\,\mu s \qquad \text{B1}$$

In fact, for the results of Chapters 6, only 512 words were required and the time length of the waveform was 10 μs. Thus, the maximum refresh rate of the generated voltage was 10 kHz. This is too fast for the storage oscilloscopes, so a lower value of refresh rate was required.

Now, the memory latch was designed to hold the last value of the sampled data string forever, to avoid corruption of the generated waveshape. At a refresh rate of 50 Hz, the time length of the window was 20 ms, clearly this is much larger than the digitized time length, and is sufficiently long to avoid corruption of the generated waveform. So, 50 Hz was chosen as the refresh rate.

However, now the end of the generated waveform may interfere with that of the next cycle. Clearly, this is not desirable. The solution to this problem is shown schematically in Fig B11.

After the 10 μs of generated waveform, the latch is enabled. The latch remained enabled for half the refresh period, and was then switched off. The output from the ECL memory remained at zero until the next refresh cycle began.

This satisfied all of the required generation conditions - the latch held any non-convergent waveforms for an apparently infinite time, and, when switched off, the dead-period before each refresh cycle ensured that the system was at rest before each new refresh cycle. In fact, most of the waveforms generated converged to zero within the period of the generating voltage and the memory latch was required only in one case.

However, the digital memory did produce one unexpected result. Due to the software modifications, it transpired that the first word of the ECL memory could not be loaded with the proper sample value. In fact, this word held a constant value - all but the least significant bit of the word remained at zero. Thus, when this word was clocked out of memory, it generated an unwanted glitch, This initially caused problems, since it distorted the generated waveform. However, a simple solution provided an unexpected benefit.

Ignoring the first sample, the next 100 samples were set to zero and then the digitized generating voltage was loaded into the next 411 memory locations. That is, the generating voltage was effectively delayed by 100 samples. This is shown in Fig B12. The 100 sample buffer after the glitch gave the system enough time to rest before the excitation voltage was applied. This allowed the glitch to be used as a convenient trigger pulse for each cycle of the refreshed voltage. While this did reduce the amount of storage available for the digitized waveform, it did not have a significant effect, and this was used successfully with all of the experimental measurements.

The DAC circuit is shown in Fig B13. This circuit is built in accordance with the manufacturer's specifications (65). The device itself, is a 100 MHz ECL convertor, designed to work with composite video signals. It worked to its specifications and did not cause any problems. Finally, the output of the DAC was connected to an amplifier stage.

Initially, the Harris amplifier, HA 2539 was used and is shown in Fig B14. This circuit was again designed to meet the manufacturer's specified layout conditions (18).

All of the component values were as specified in the diagram, except for the gain resistance, R_G. The 1 kΩ potentiometer was required to level-shift the output of the DAC which was offset since the DAC is an ECL device. This offset was measured and the potentiometer set, such that, when the output of the DAC was zero, the output of the amplifier was zero. After setting, this did not require to be altered.

The gain resistor, R_G, was initially chosen to be 27 KΩ - giving the amplifier a gain of 15. From (18), it is apparent that the full swing of the amplifier is ± 10 V, and from (65), the output swing of the DAC is ±0.5 V, therefore this value of gain will, with maximum DAC output, generate a swing of ±7.5 V. This avoids saturating the amplifier. However, it may also be observed from (18) that the gain bandwidth product of the amplifier is 600 MHz. So, with this gain, the device has a bandwidth of 40 MHz - less than the DAC output. In some of the examples of Chapter 6, it was necessary to increase the bandwidth to that of the memory, 50 MHz. This requires a gain of 12 and R_G was correspondingly reduced to 22 KΩ . Under these conditions, the full gain swing of the amplifier reduced to ±6 V. This was

rather low for some applications, (particularly the bipolar step pulse.) Thus a second amplifier stage was added for some cases.

The second amplifier is shown schematically in Fig B15. It consisted of a Burr-Brown 3554 op-amp, and again, the circuit was laid out and built to the manufacturer's specifications (8). This device is designed to be a high-gain, low noise, small signal amplifier. In this case, it was used as a power amplifier with a gain of 1.5 - 2. Under these conditions, the exceptional bandwidth of this device is dramatically reduced and the noise level of the generated signal rose appreciably. However, the increase in signal strength justified the application and the results taken with this second stage were reasonably good. This amplifier is not designed for the application considered here, but it was the only solution available at the time.

In general, the first amplifier stage performed as it was designed to. It had not been anticipated that a second stage would be required, since the initial calculations suggested that the maximum voltage swing of the first stage would generate acoustic pulses of sufficient amplitude to be readily detected by the receiving

apparatus. In practice, the noise level of the system made the smaller signals almost indistinguishable from the noise, and so the second stage was required. Although this also increased the noise level, the increase in the signal strength was sufficient and the generated acoustic transients were detected. The last three cases of Chapter 6 are examples of voltage generation using the two-amplifier system.

If more time had been available, it should have been possible to build a second stage with a larger voltage swing of, for example 20 - 30 V. Assuming that no significant increase in the noise level occurs, this would produce acoustic outputs of reasonably good intensity - certainly enough to avoid any detectability problems. It may also be possible to increase the gain of the receiving hydrophone amplifier, although this in itself would not solve the problem, since most of the signal noise appears to be generated on the transmission side. Thus, the development of better amplifiers is certainly worth further investigation.

Ancillary Apparatus

Finally, all of the experimental measurements were made using TEKTRONIX storage oscilloscopes,

TEKTRONIX 466

and TEKTRONIX 7633.

The latter had the screen-writing facility which is apparent in some results. However, the first was more sensitive and had a better storage facility.

APPENDIX C

Calculation of the on-axis Field Profile

APPENDIX C

This appendix presents the derivation of a simple expression for the on-axis field of a circular transducer.

Consider the arbitrary surface, s, shown in Fig C1. The velocity potential at the field point, P, is obtained by integrating a number of Huygens' radiators over the surface, s. For harmonic radiators, this is expressed as Rayleigh's equation,

$$\phi = \frac{1}{2\Pi} \iint_s V_m \frac{e^{-ikr}}{r} \, ds \qquad C1$$

where V_m is the normal velocity, with respect to the surface, s.

When the piston motion is not simple harmonic,

$$\phi = \frac{1}{2\Pi} \int\int_s V(t-r/c) \frac{ds}{r} \qquad C2$$

where c is the velocity of sound in the medium. The term V(t-r/c) is the normal velocity for the element-ary radiator ds, and time (t-r/c).

The pressure, P, at the desired field point is given by,

$$P = \rho \frac{d\phi}{dt} \qquad C3$$

where ρ is the density of the medium.

Applying equation C2 to a circular transducer, results in Fig C2. The device is circular, with radius R, and lies in the y-z plane, such that the x-axis is normal to the transducer and passes through its centre.

Two points in the field are shown - P (off-axis) and P' (on-axis). For the geometry shown,

$$ds = \beta d\beta d\psi \qquad C4$$

The impulse velocity potential at the general point P is, from equation C2,

$$\phi_{ip} = \iint_S \frac{\delta(t-r^1/c)\beta d\beta d\psi}{2\Pi r^1} \qquad C5$$

where ,

$$r^1 = (r^2+\beta^2)^{1/2}\left(1-\frac{2r\beta\sin\theta\cos\psi}{(r^2+\beta^2)}\right) \qquad C6$$

There is no simple closed-form solution for this integral. However, consider the impulse velocity potential as P_1. This is given by,

$$\phi_{ip_1} = \int_0^R \int_0^{2\Pi} \frac{\delta\left(t-\frac{(r^2+\beta^2)^{1/2}}{C}\right)\beta d\beta d\psi}{2\Pi(r^2+\beta^2)1/2} \qquad C7$$

This simplifies to give,

$$\theta_{ip_1} = \int_0^R \frac{\delta\left(t-\frac{(r^2+\beta^2)^{1/2}}{C}\right)}{2\Pi(r^2+\beta^2)^{1/2}} \beta d\beta \int_0^{2\Pi} d\psi \qquad C8$$

which becomes,

$$\phi_{ip_1} = \int_0^R \frac{\delta\left(t-\frac{(r^2+\beta^2)^{1/2}}{C}\right)}{(r^2+\beta^2)^{1/2}} \beta d\beta \qquad C9$$

This integral may be solved by substitution as follows:-

Let,

$$W = \left(\frac{r^2+\beta^2}{C^2}\right)^{1/2} \qquad C10$$

and,

$$Y = W^2 \qquad C11$$

Then, from C10 the limits of integration are,

$$\frac{r}{C} \ , \ \left(\frac{r^2+R^2}{C^2}\right)^{1/2} \qquad C12$$

and,

$$\frac{dw}{d\beta} = \frac{dy}{d\beta} \cdot \frac{dw}{dy} \qquad C13$$

thus,

$$d\beta = (wC^2/\beta)\ dw \qquad C14$$

Substituting these terms into equation C9 gives,

$$\phi_{ip_1} = C \int_{r/c}^{(\frac{r^2+R^2}{C^2})1/2} \delta(t-w)dw \qquad C15$$

This is the straightforward integration of a delta function, and, by the sifting property gives,

$$\phi_{ip_1} = C\left[u_{-1}(t-r/C) - u_{-1}(t-(\frac{r^2+R^2}{C^2})^{1/2})\right] \qquad C16$$

where u_{-1} is the unit-step function. This is sketched in Fig C3.

Thus, the pressure impulse response , given by equation C3 becomes, for this case,

$$h_{p_1} = \rho C\left[\delta(t-r/C) - \delta(t-(\frac{r^2+R^2}{C^2})^{1/2})\right] \qquad C17$$

This is sketched in Fig C4.

Thus the pressure profile at any point on the axis may be obtained by convolution,

$$P_1 = h_p * f_p \qquad C18$$

where f_p is the plane-wave output from the discrete-time (z-domain) model.

This result may be explained simply as follows.

The first impulse in equation C17 is delayed by an amount r/c. From Fig C2, this is just the time delay for the plane-wave component to travel from the transducer surface to the measuring point, P_1. The second impulse is delayed by the term $(r^2+R^2)^{1/2}$ /C. This is the time for wave-components to travel to P_1 from the edge of the transducer. These wave-components are, in fact, of exactly the same shape as the plane-wave components, in this case. These correspond to the edge waves which were noted in Chapter 5.

The second impulse has a negative sign, so the edge-wave component is subtracted from the plane-wave component, as specified by equation C17.

This technique was used to model the response of case 20 in Chapter 5. For cases where r>>R, that is, in the far field, the results were reasonably good. However, this method did not work as well in the near field area. There are two possible reasons for this.

Firstly, the edge-components may be partially generated by radial vibrations. Thus, the assumption that the shape of the edge and plane components is the same is not valid. Secondly, the position of the hydrophone is more critical in the near field then the far field. So, small variations in position would have little effect when r>>R but could be critical in the near field region.

This method was originally proposed by Hayward, and is included here to show how the basic z-domain transducer model may be extended to include field effects.

APPENDIX D

Description of Computer Programmes

APPENDIX D

The transducer modelling techniques developed in this thesis were implemented as an interactive computer modelling package. The programmes were written in FORTRAN IV plus and ran on a Honeywell H6060 mainframe. Unfortunately, the programmes were too large to include listings in this Appendix, so only a brief description of the programme structures follows. Listings may be obtained either from the author or from DR G HAYWARD at Strathclyde University.

Three main programmes and a shared library form the basis of the interactive modelling package. These were designed in a structured manner to avoid duplicating routines and algorithms, but it should be appreciated that, since most of the software was undergoing continual development, there exists scope for improvement.

The first programme FMOD, uses the IFFT technique discussed in the introduction, to calculate the transient response of transducer systems from their complex frequency spectra. The three-port system matrices, $[p]$ and $[w]$, of Chapters Two and Three form the basis of the programme. These were implemented using normal program-

ming methods with a simple interactive menu. This allows the user to select the appropriate transfer function. Once the spectrum has been calculated, the user has the option to view both the amplitude and phase plots. Alternatively, he may use the IFFT to calculate the transient response which may then be displayed. Several IFFT routines were tested, including the three available NAG, (Numerical Analysis Group), packages. Unfortunately, these require all I/O to be specified in double-precision format. This is costly, in terms of storage, so a single-precision IFFT was used instead, based on the Sand-Tukey Algorithm. This programme was supplied as a BASIC option for the 4051 intelligent graphics terminal and was rewritten in FORTRAN by the author. It worked as expected and was used for all subsequent calculations.

This programme was not used for any of the plots presented in this thesis, but as a benchmark technique. That is, the results produced by FMOD were known to be correct, (by comparison with, for example, the KLM model). Thus, when the z-form techniques were being developed, FMOD provided a standard solution with which each new algorithm could be compared.

The development time of FMOD was comparatively short- approximately four weeks-although later modifications probably account for this much time again. Hence FMOD contains approximately eight man weeks work. This programme has now been largely superceded by the z-form algorithm.

The second programme ZMOD, uses the z-form technique of Chapter Four. This programme is considerably more complex than FMOD, since it is necessary to manipulate the differential and delay terms as separate vectors, (as discussed in the first section of Chapter Five). The programme is similar to FMOD in one respect - it is also menu-driven. Several versions of ZMOD have been developed, generally with each successive version operating faster than its predecessor. At present, ZMOD is approximately an order of magnitude faster than FMOD, (when both programmes calculate a comparable case).

The development of ZMOD may be conveniently divided into two section - the main programme manipulation and the z-form Q-matrix. Development of the polynomial manipulation routines took approximately three man months to perfect. However, it was this section which was subject to repeated improvement, since there is not necess-

arily a 'best' solution to the problem of storing and handling several variable multi-dimensional polynomials. At present, a compromise method is used, such that the total number of storage vectors required is not excessive. The manipulation algorithms have taken several generations to perfect but those in use at present are the fastest implemented so far.

Development of the Q-matrix algorithms followed the path described in Chapter Four, where several algorithms were implemented and tested, their various merits and drawbacks then being compared. These algorithms were used to form a sub-section of the shared library, such that the implemented software does not form a part of any specific programme. It is used and accessed via a multiple subroutine system. This method was adopted for several reasons but principally because, once implemented, the z-form package was complete, that is, no further development or improvement was likely. Thus, by creating a separate Q-matrix sub-library, the technique became a standard package which may be independently accessed from multiple programmes without any danger of corruption. It also avoids duplication of software and the possible danger of several different versions of the same algorithm existing at the same time.

Thus the ZMOD is a two-level programme which makes extensive use of the shared library.

At present, further development of ZMOD itself seems inlikely, since the current version more than out-performs FMOD. ZMOD was used to generate all of the synthetic plot results of Chapter Five.

The third programme is ZINV, the inversion programme used in Chapter Six. ZINV is a further development of ZMOD and was originally intended to supercede ZMOD. However, there was insufficient time to develop ZINV into a comprehensive interactive package.

At present, it consists of the core of ZMOD with a variety of extra routines added at appropriate places to allow the inversion calculations to be made. Unlike FMOD and ZMOD, ZINV has not been developed into a complete menu-driven package. Thus, at places the user is required to have an extensive knowledge of exactly what is happening to allow the programme to proceed properly. This is unfortunate but leaves scope for substantial future development.

ZINV (in several different versions) was used to

produce the synthetic inversion plots of Chapter Six. So far, this programme has involved approximately six to eight man weeks of development time.

Finally, the shared library contains areas of software which are common either to all, or to one particular programme. The library has been sub-divided into several sections which may be briefly summmarised as follows.

The Q-matrix section occupies approximately one-fifth of the library, together with its associated subroutines. The common input/output subroutines occupy approximately a quarter of the library. These routines were designed such that a user familiar with one of the three main programmes would quickly be able to use either of the other two. As mentioned earlier, this has yet to be extended to ZINV but has proved successful with FMOD and ZMOD. It is also an efficient programming method, since it avoids unnecessary duplication. At present, three levels of interaction exist, although this is subject to modification.

The polynomial manipulation routines occupy about half of the total library space. These routines are largely unrelated, although they all perform the broadly

similar function of manipulating a set of data into a desired form. Approximately half of these routines are final versions, while the remainder are subject to occasional modification.

The remainder of the library space is taken up by a set of useful routines which are only used within the library. For example, polynomial multiplication.

The routines within the library were, without exception, originally developed as part of a master programme (usually ZMOD). Thus, it is inappropriate to estimate the development time of the library itself, although construction and modification themselves probably took about three man months.

Further description of any of the main software is rather pointless without a detailed examination of the programme listings. However, some general points regarding the software development should be considered.

(i) Most of the implemented algorithms are developments of equations given in the main part of this thesis. Particular details are not of great importance, since there are usually

several methods of implementing the same algorithm. The author has attempted, as far as possible, to develop each algorithm into a form that is appropriate for the language and computer used.

(ii) Approximately 40% of the software and 20% of of the algorithms, (particularly those concerned with input/output), are machine or machine-interface related. Thus, if the software were to be trasferred to another computer, these would require modification.

(iii) While a structured development was carried out as far as possible, it should be remembered that these programmes were largely original. Consequently, some of the subroutines and algorithms are not quite as efficient as they could be.

This concludes the description of the software. As mentioned earlier, programme listings are available from the author or DR G HAYWARD at Strathclyde University.

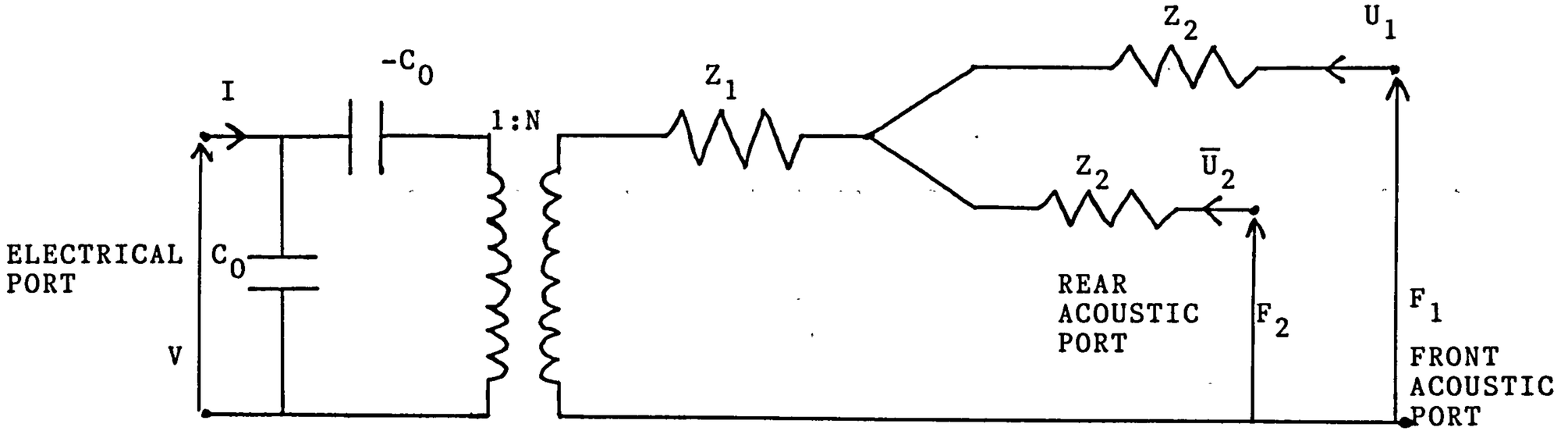

LUMPED PARAMETER MASON MODEL

FIG 1.1

$$Z_1 = \frac{Z_0}{j \sin \frac{\omega \ell}{V_t^D}} \quad ; \quad N = C_0 h_{33}$$

$$Z_2 = j Z_0 \tan \frac{\omega \ell}{2V_t^D}$$

C_0 = STATIC CAPACITANCE

ℓ = TRANSDUCER THICKNESS

h_{33} = PIEZOELECTRIC CONSTANT

V_t^D = COMPRESSIONAL WAVE VELOCITY

Z_0 = ACOUSTIC IMPEDANCE

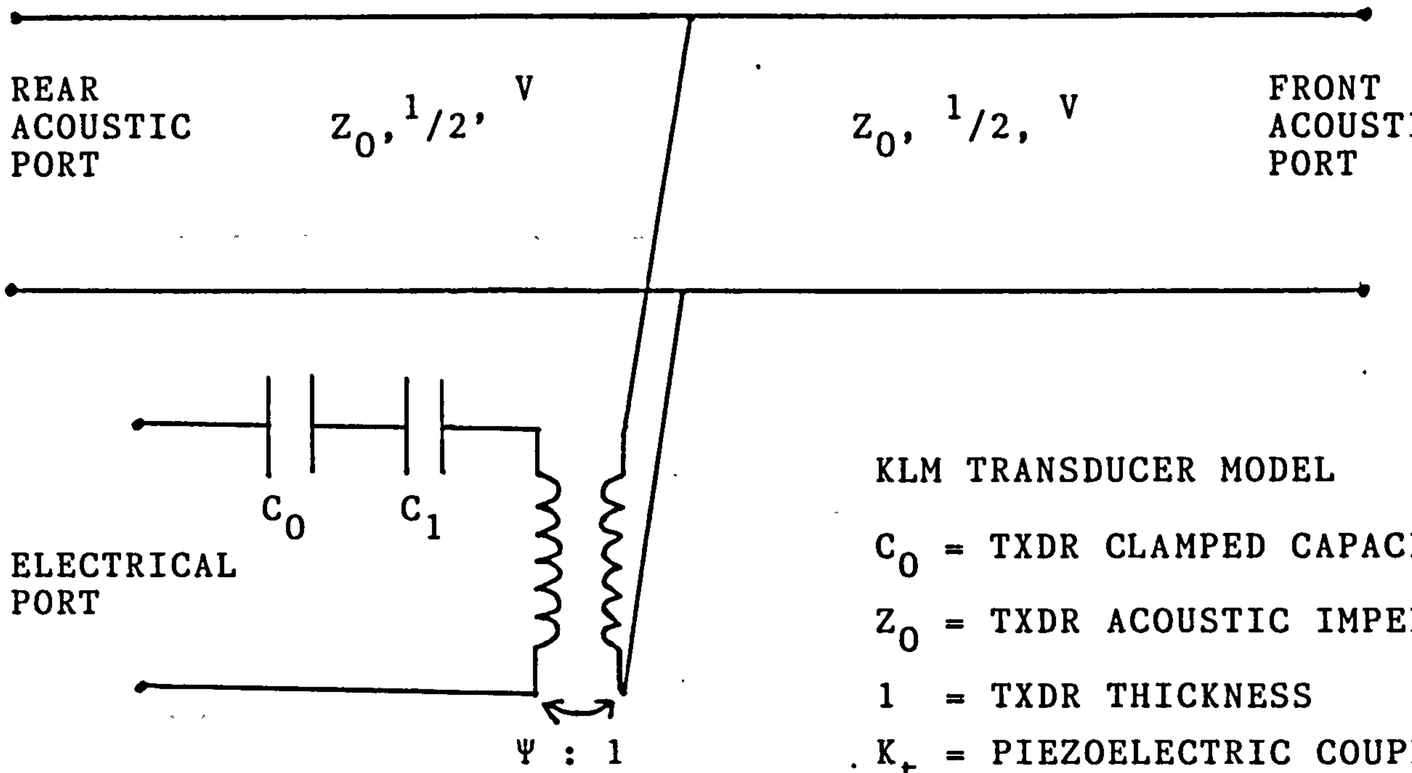

FIG 1.2

KLM TRANSDUCER MODEL

C_0 = TXDR CLAMPED CAPACITNACE

Z_0 = TXDR ACOUSTIC IMPEDANCE

1 = TXDR THICKNESS

K_t = PIEZOELECTRIC COUPLING COEFFICIENT

V = ACOUSTIC PROPAGATION VELOCITY IN TXDR

$$\Psi = K_t\left(\frac{\pi}{\omega_0 C_0 Z_0}\right)^{1/2} * \text{SIN C}\left(\frac{\omega}{2\omega_0}\right) ; \quad C_1 = \frac{-C_0}{\left(K_t^{\,2} * \text{SIN C}\left(\frac{\omega}{\omega_0}\right)\right)} ; \text{ where } \omega_0 = \frac{\pi V}{1}$$

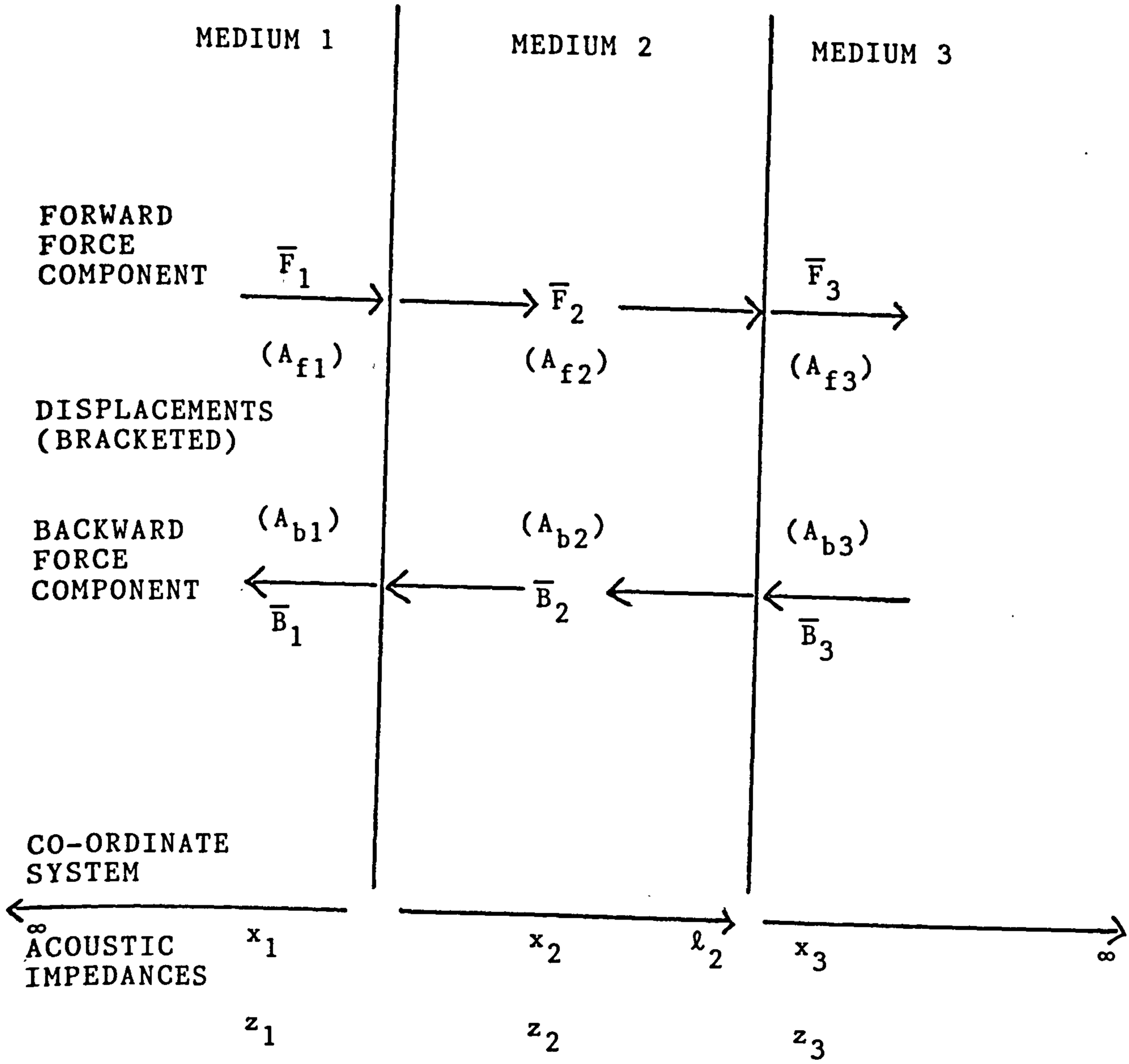
MEDIUM 1
MEDIUM 2
MEDIUM 3
FORWARD FORCE COMPONENT
$\overline{F}_1$
$\overline{F}_2$
$\overline{F}_3$
(A_{f1})
(A_{f2})
(A_{f3})
DISPLACEMENTS (BRACKETED)
BACKWARD FORCE COMPONENT
(A_{b1})
(A_{b2})
(A_{b3})
$\overline{B}_1$
$\overline{B}_2$
$\overline{B}_3$
CO-ORDINATE SYSTEM
$-\infty$
x_1
x_2
ℓ_2
x_3
∞
ACOUSTIC IMPEDANCES
z_1
z_2
z_3

FIG 2.1

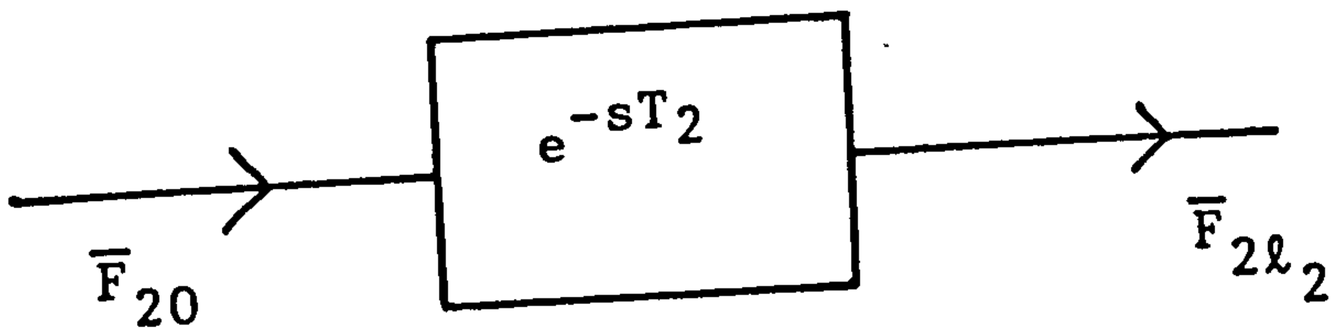

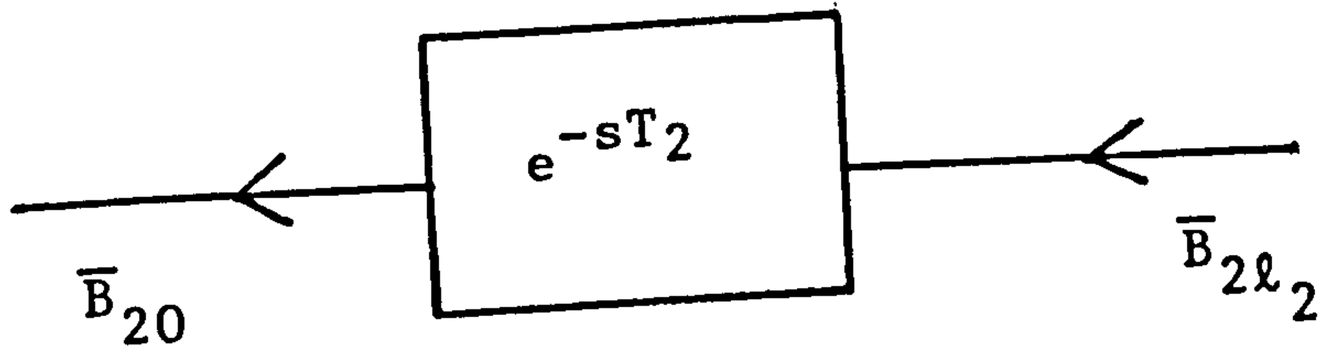

LAYER 2 PROPAGATION

FIG 2.2C

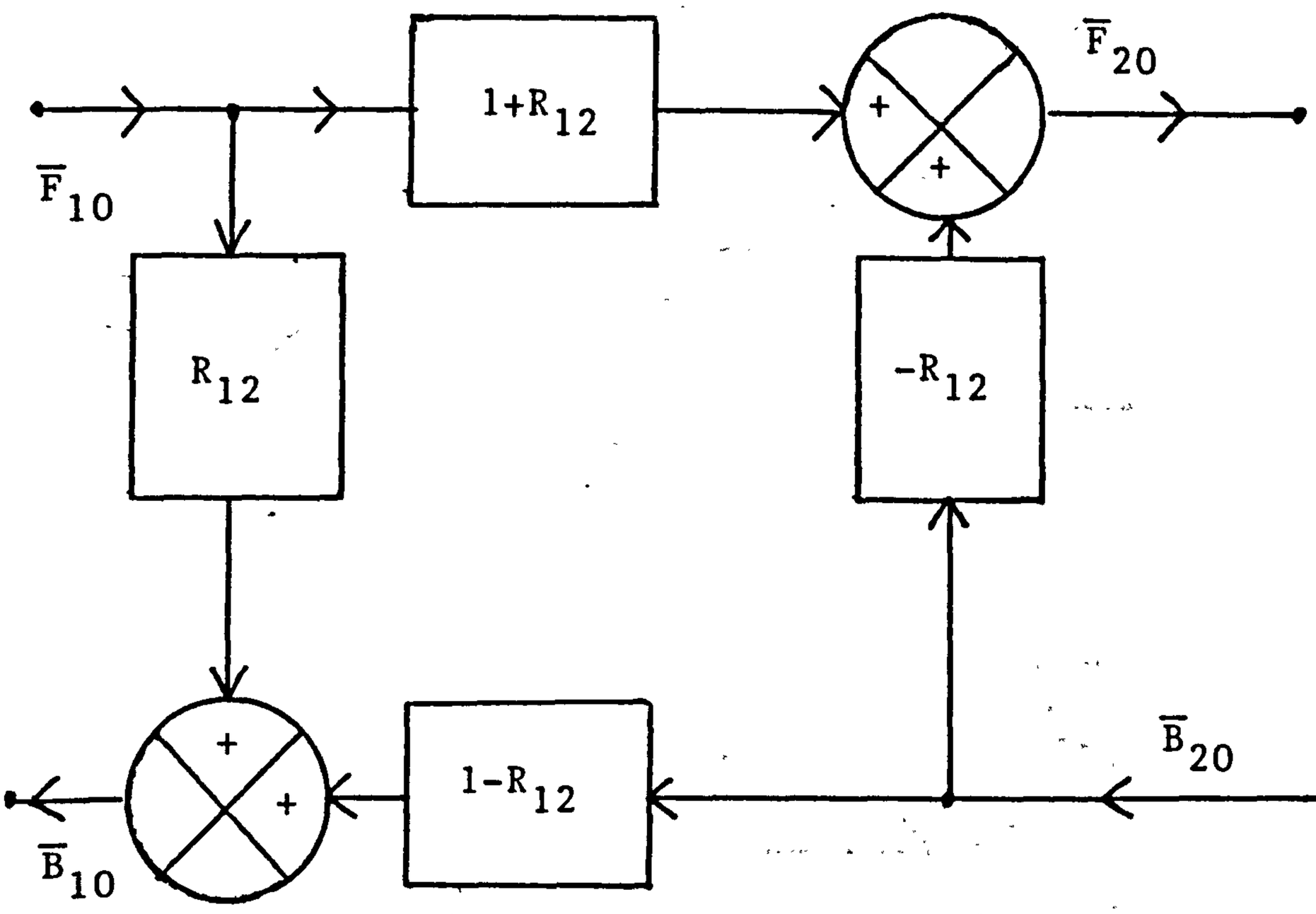

1:2 LAYER INTERFACE

FIG 2.2 A

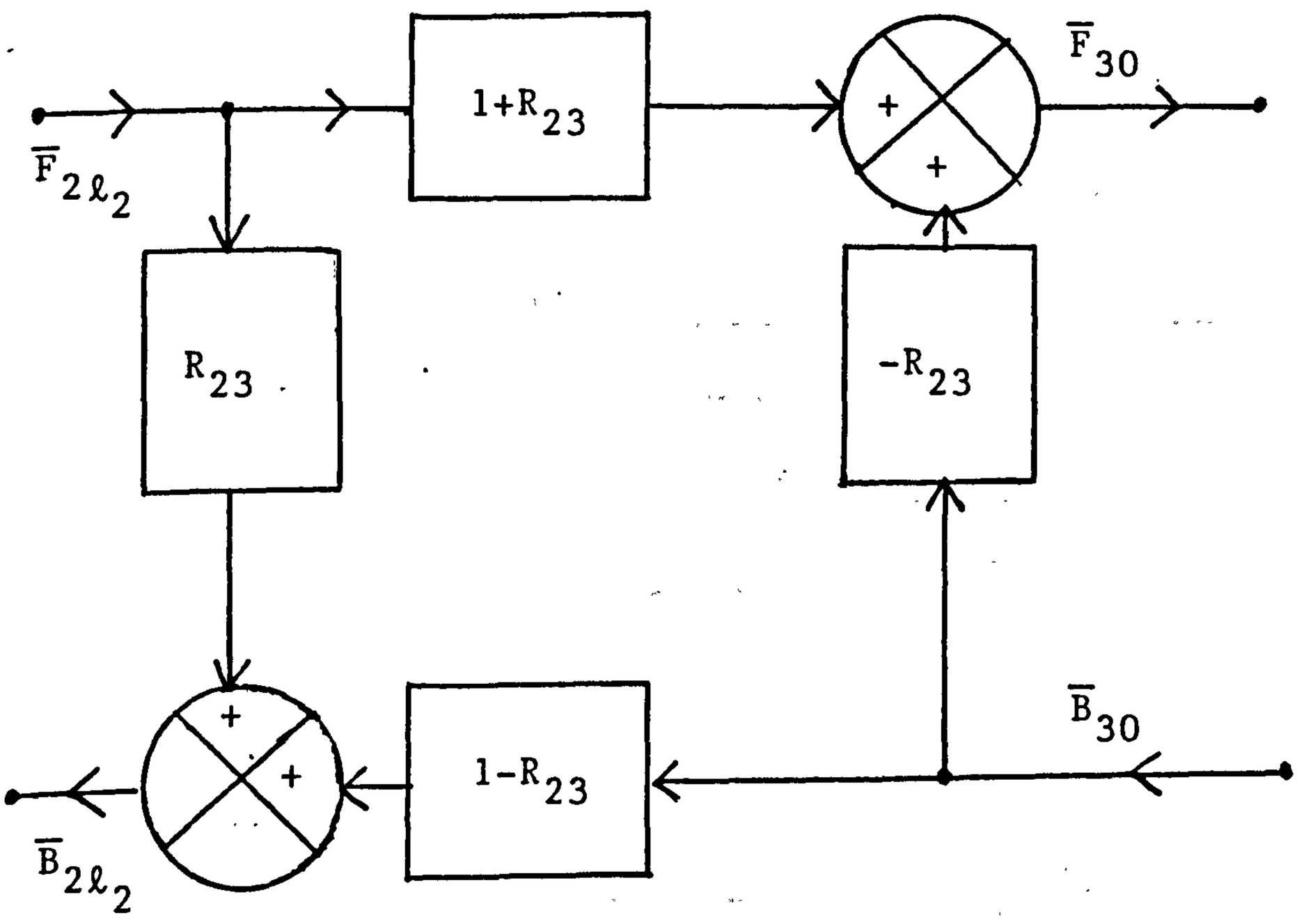

2:3 LAYER INTERFACE

FIG 2.2B

FIG 2.3

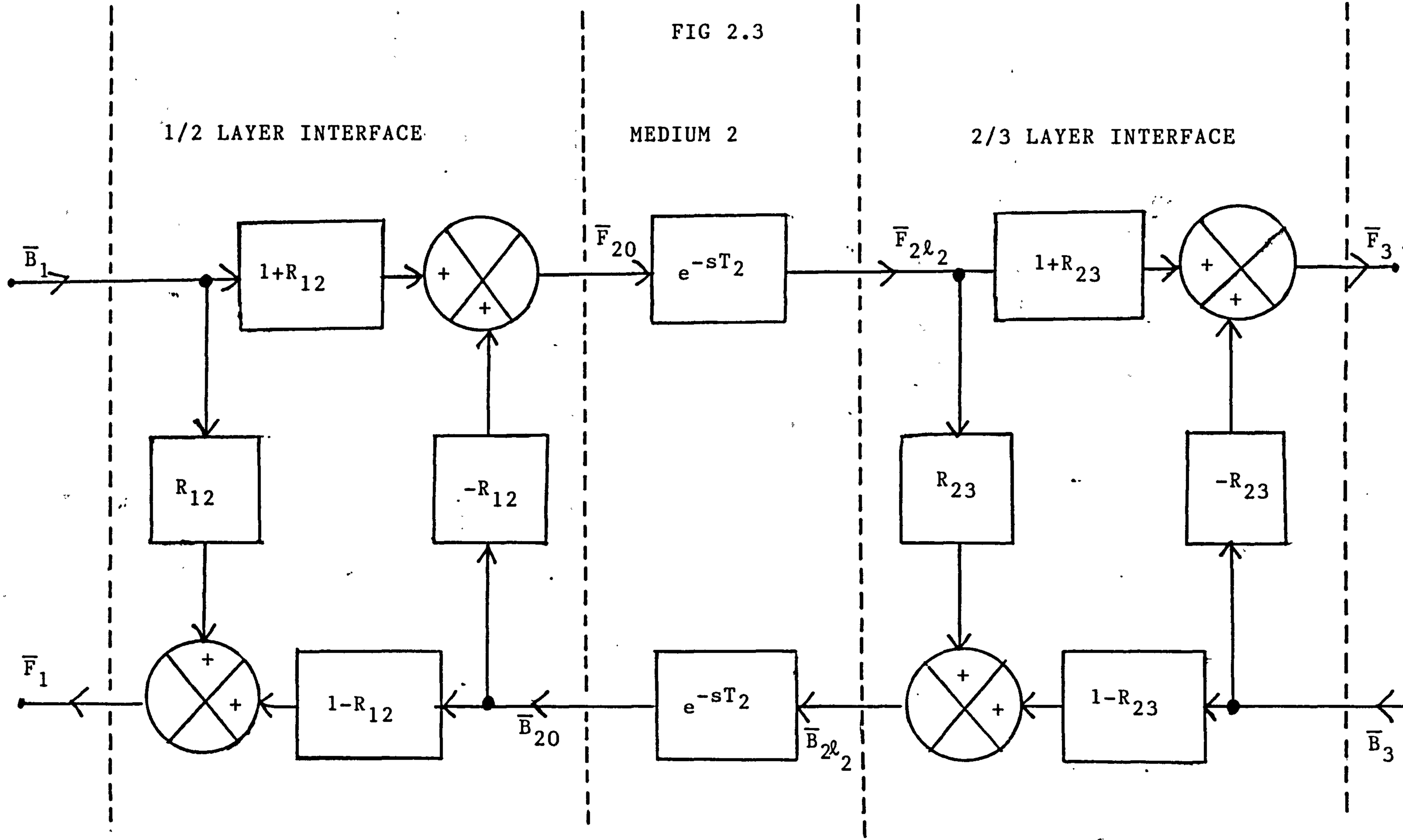
1/2 LAYER INTERFACE
MEDIUM 2
2/3 LAYER INTERFACE
$\overline{B}_1$
$1+R_{12}$
$\overline{F}_{20}$
e^{-sT_2}
$\overline{F}_{2\ell_2}$
$1+R_{23}$
$\overline{F}_3$
R_{12}
$-R_{12}$
R_{23}
$-R_{23}$
$\overline{F}_1$
$1-R_{12}$
$\overline{B}_{20}$
e^{-sT_2}
$\overline{B}_{2\ell_2}$
$1-R_{23}$
$\overline{B}_3$

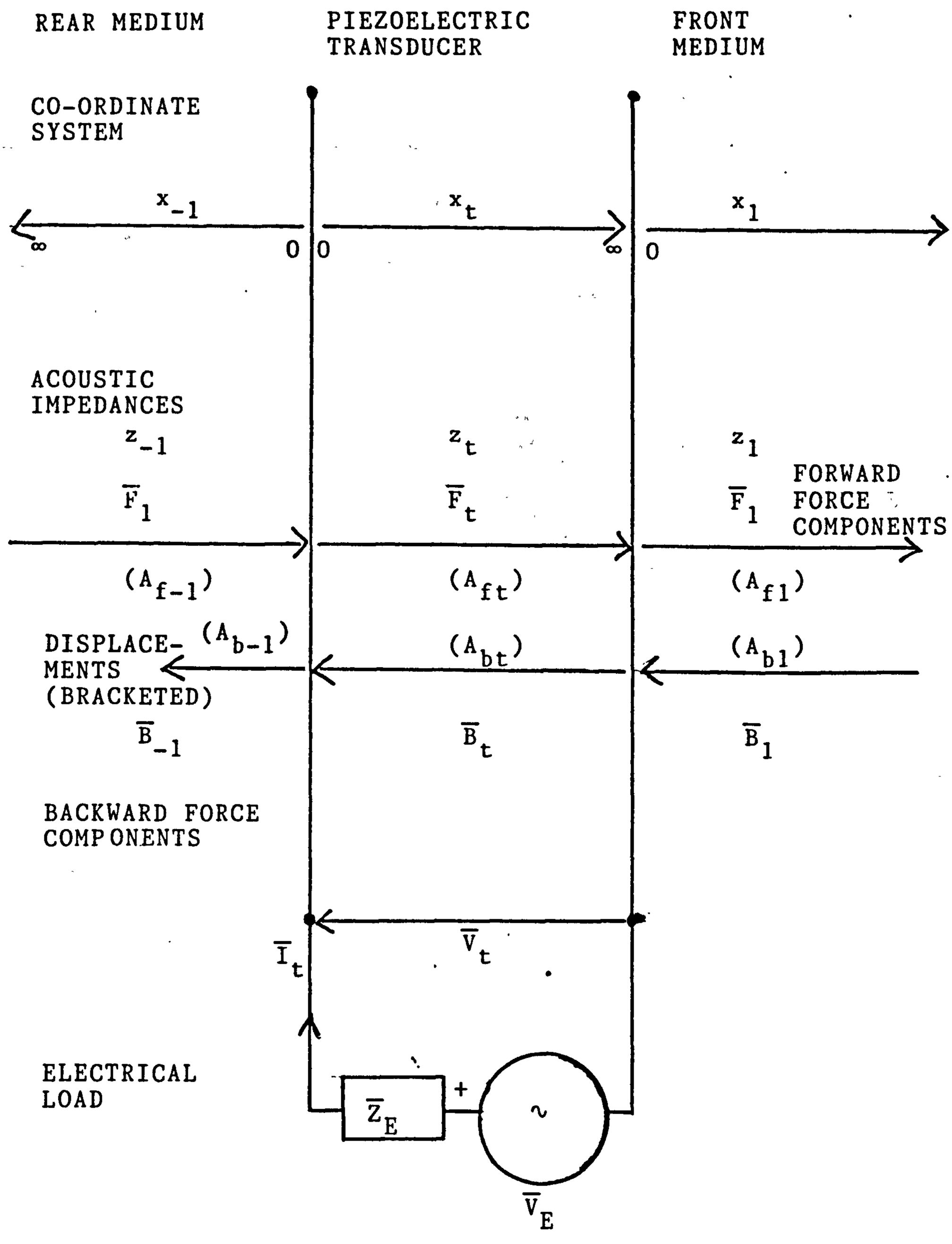

FIG 2.4

PIEZOELECTRIC LAYER SYSTEM

FIG 2.5

ACOUSTIC LATTICE SECTION OF THE PIEZOELCTRIC LAYER SYSTEM

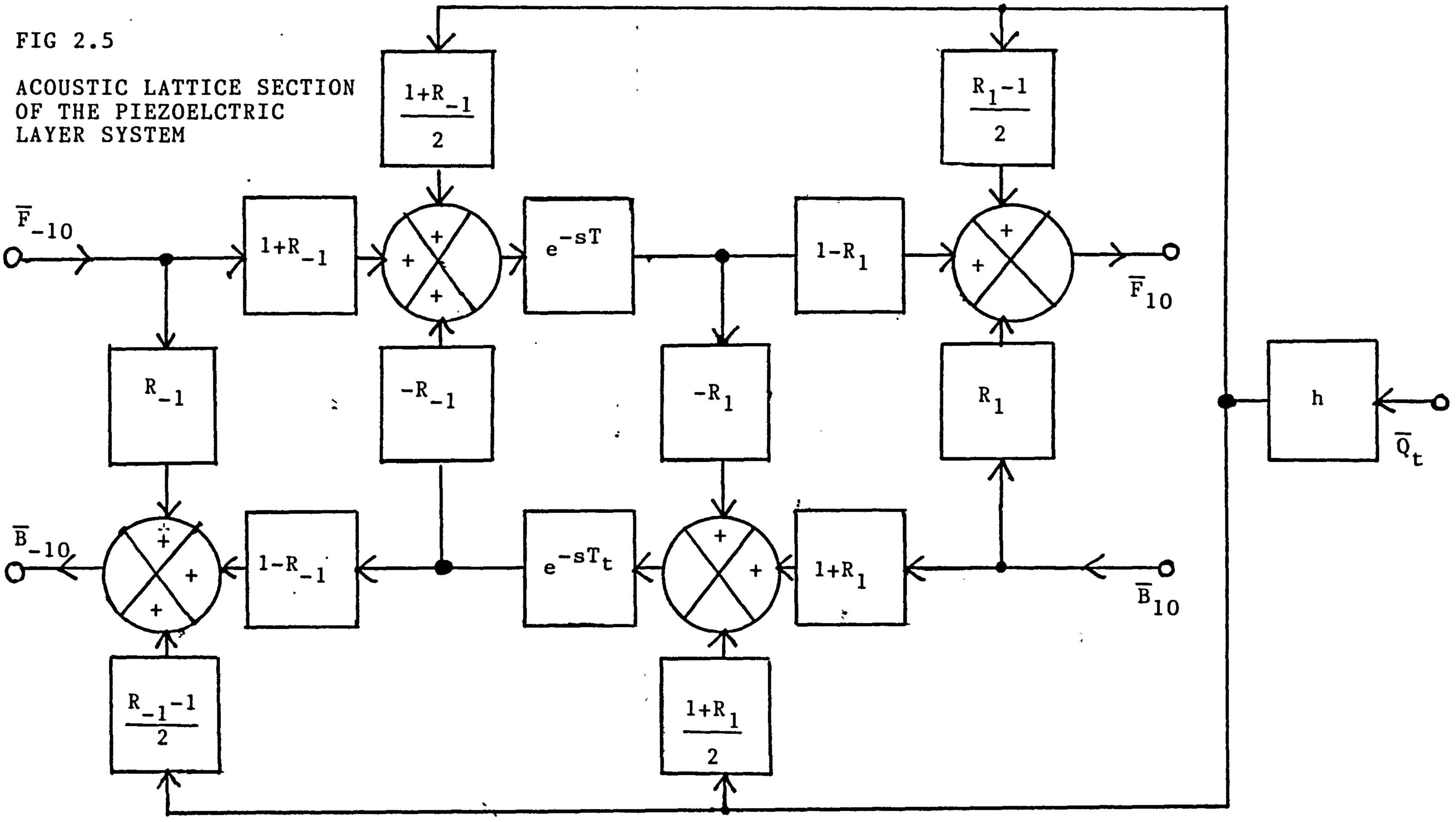

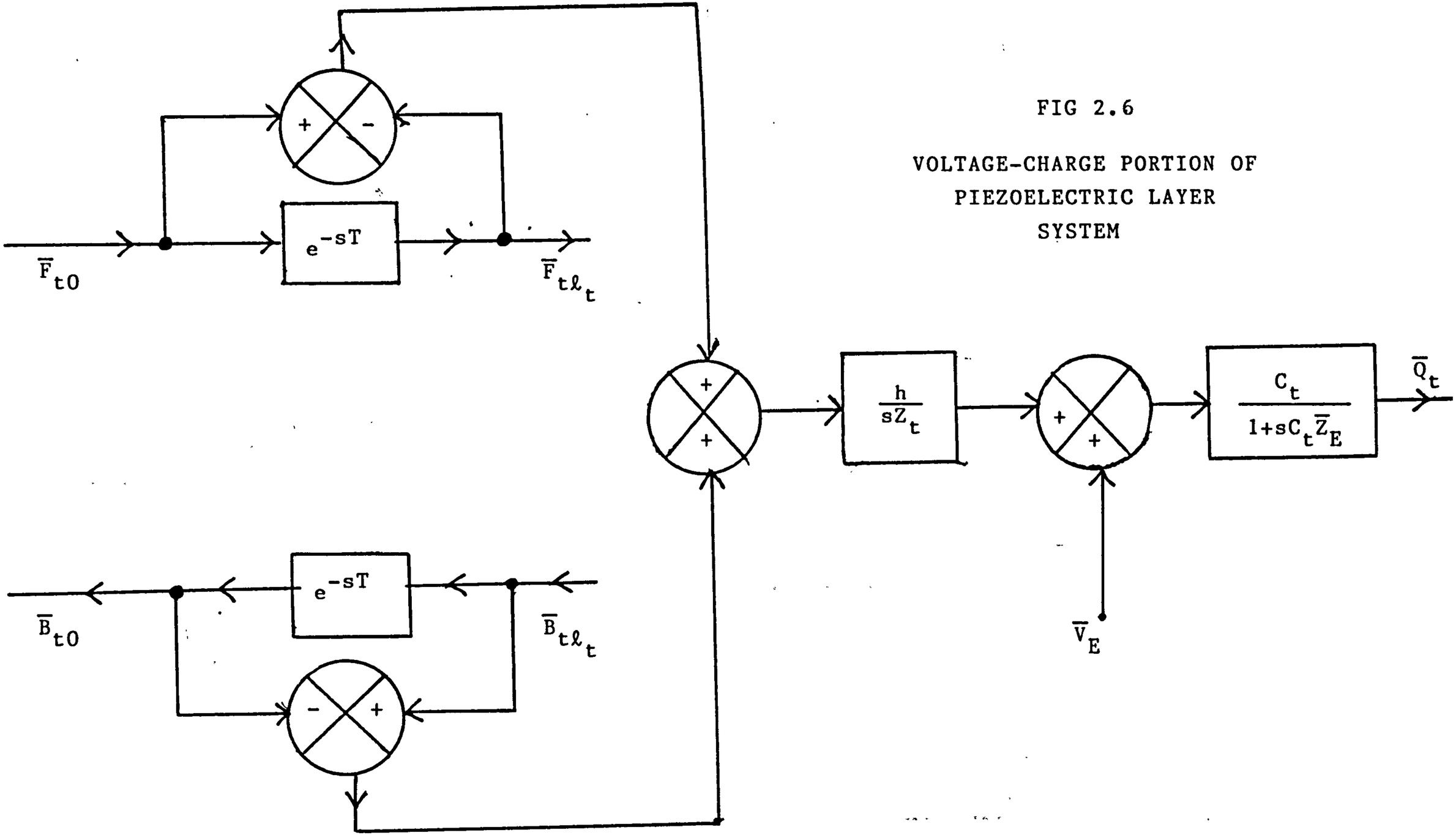

FIG 2.6

VOLTAGE-CHARGE PORTION OF PIEZOELECTRIC LAYER SYSTEM

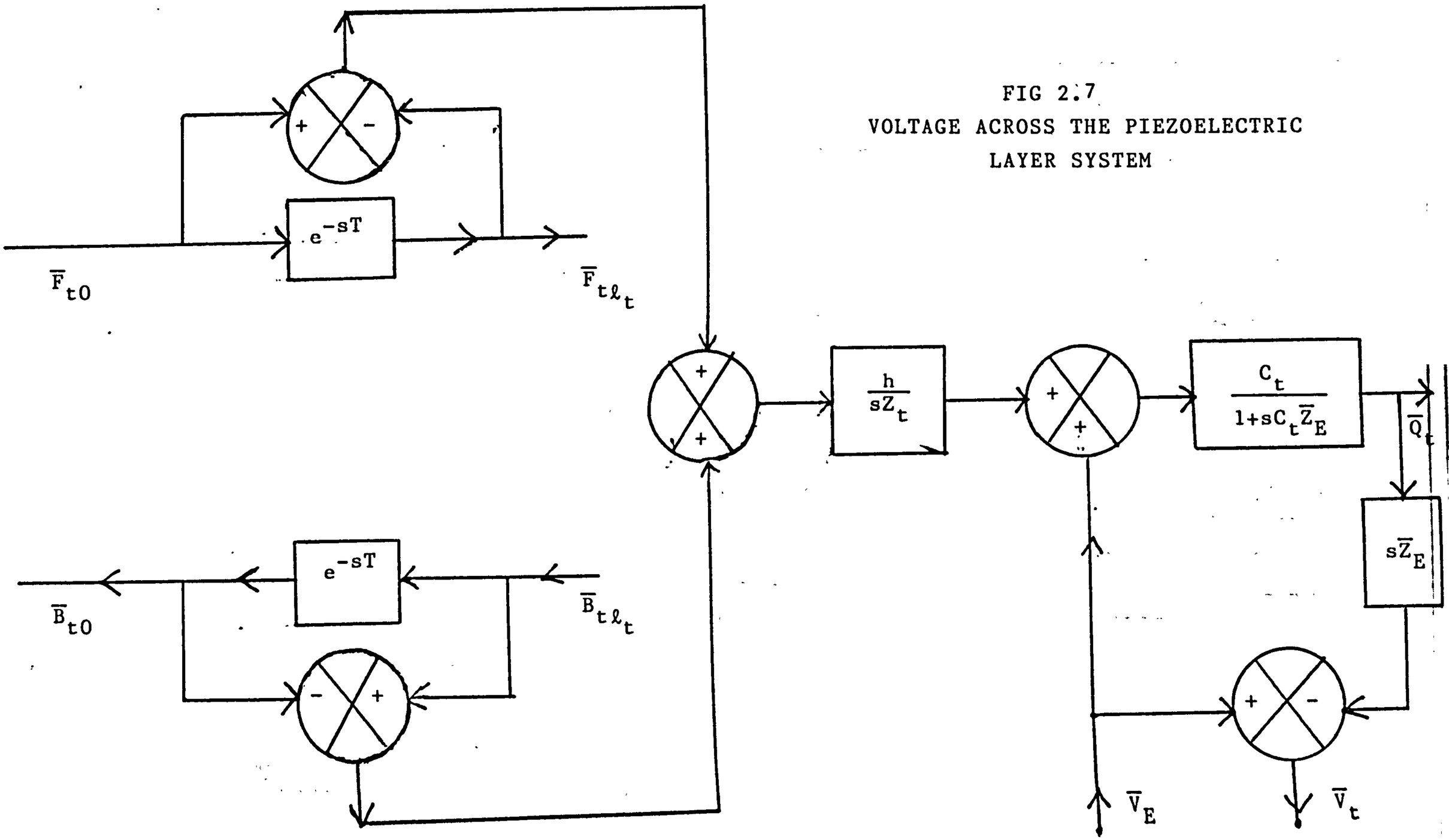

FIG 2.7
VOLTAGE ACROSS THE PIEZOELECTRIC LAYER SYSTEM

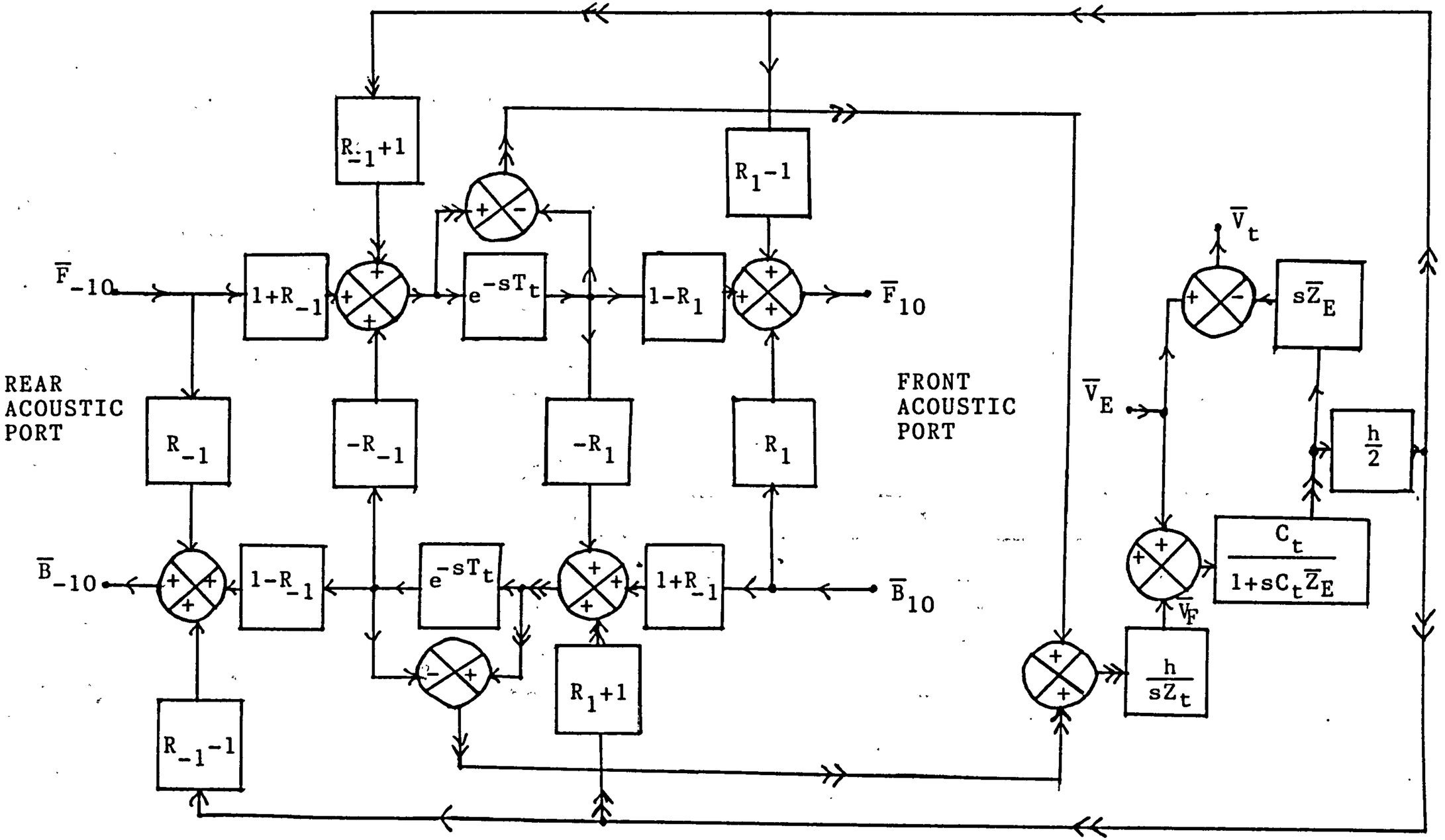

FIG 2.8 PIEZOELECTRIC LATTICE DIAGRAM

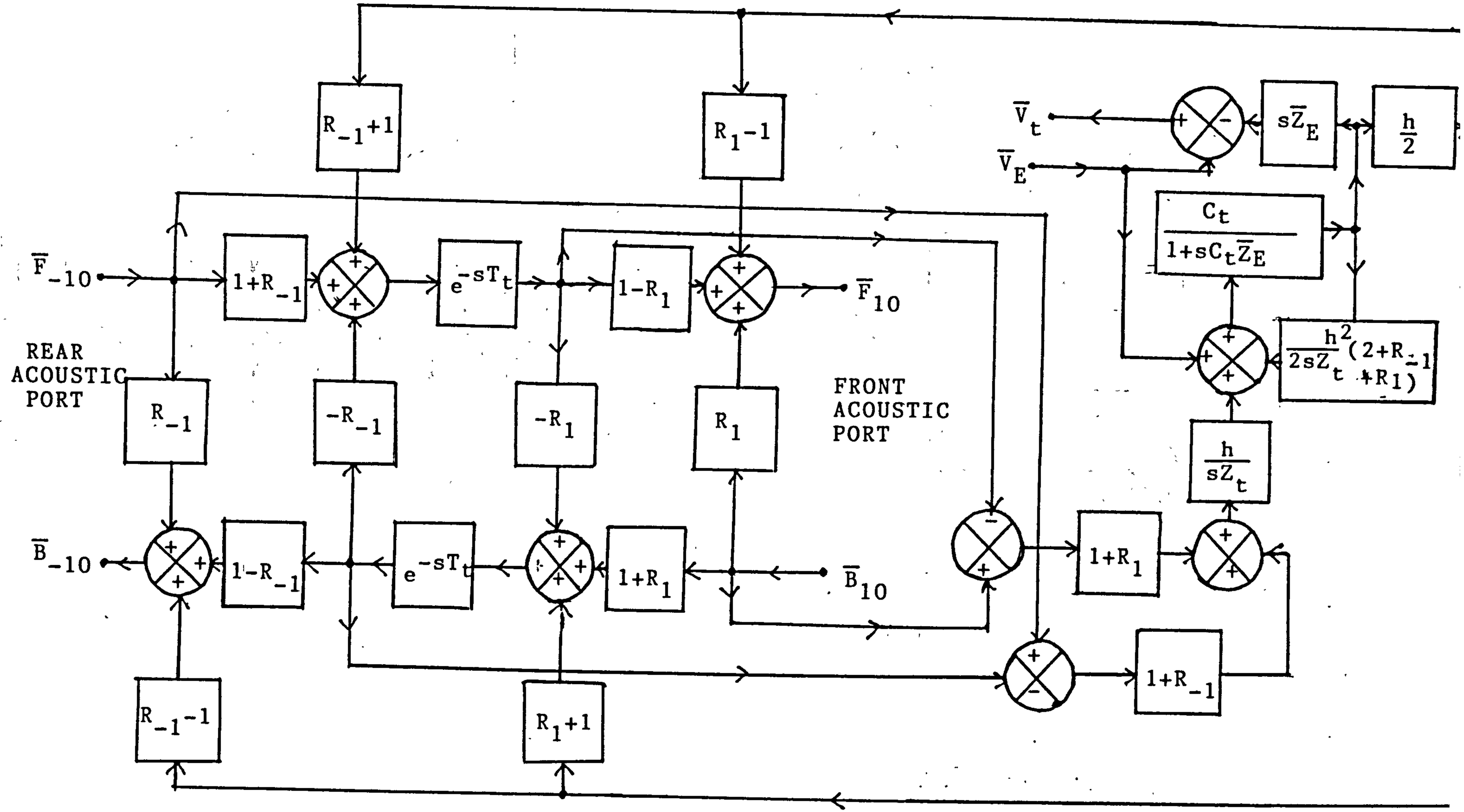

FIG 2.9 ALTERNATIVE PIEZOELECTRIC LATTICE DIAGRAM

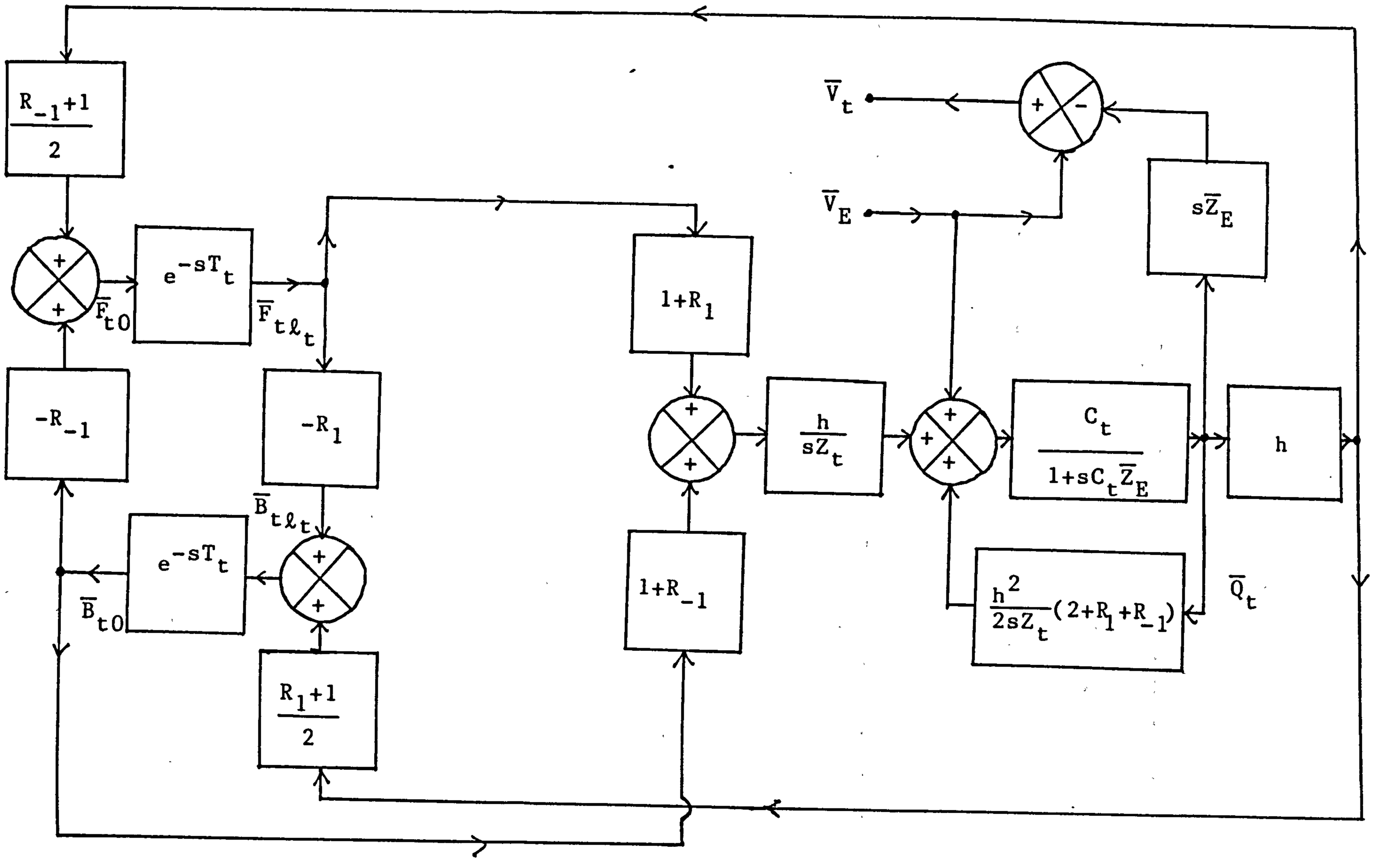
$\frac{R_{-1}+1}{2}$
e^{-sT_t}
$\overline{F}_{t0}$
$\overline{F}_{t\ell_t}$
$1+R_1$
$-R_{-1}$
$-R_1$
$\overline{B}_{t\ell_t}$
e^{-sT_t}
$\overline{B}_{t0}$
$\frac{R_1+1}{2}$
$1+R_{-1}$
$\overline{V}_t$
$\overline{V}_E$
$s\overline{Z}_E$
$\frac{h}{sZ_t}$
$\frac{C_t}{1+sC_t\overline{Z}_E}$
h
$\overline{Q}_t$
$\frac{h^2}{2sZ_t}(2+R_1+R_{-1})$

FIG 2.10

FIG 3.1 GENERAL MULTILAYER SYSTEM

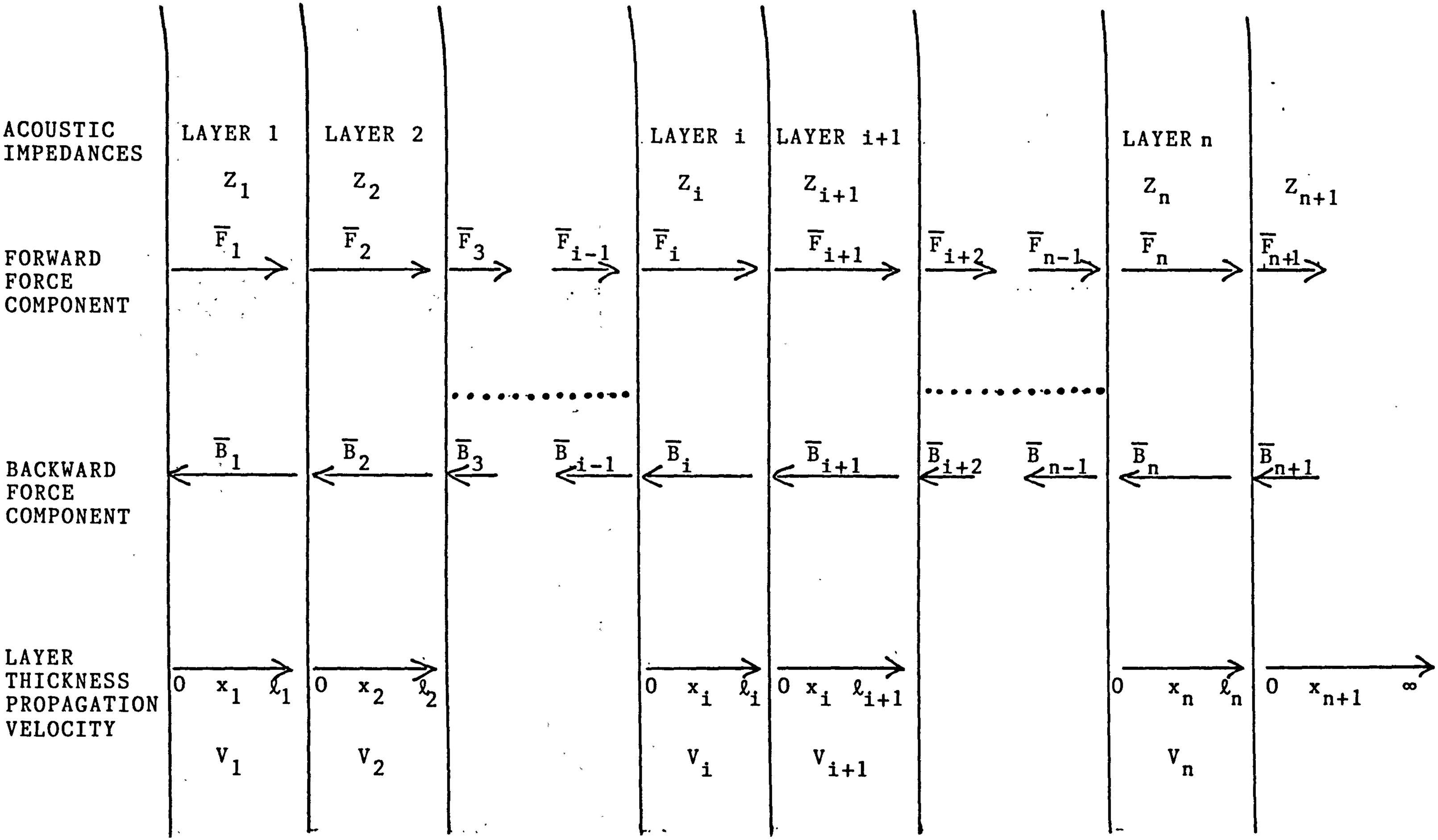

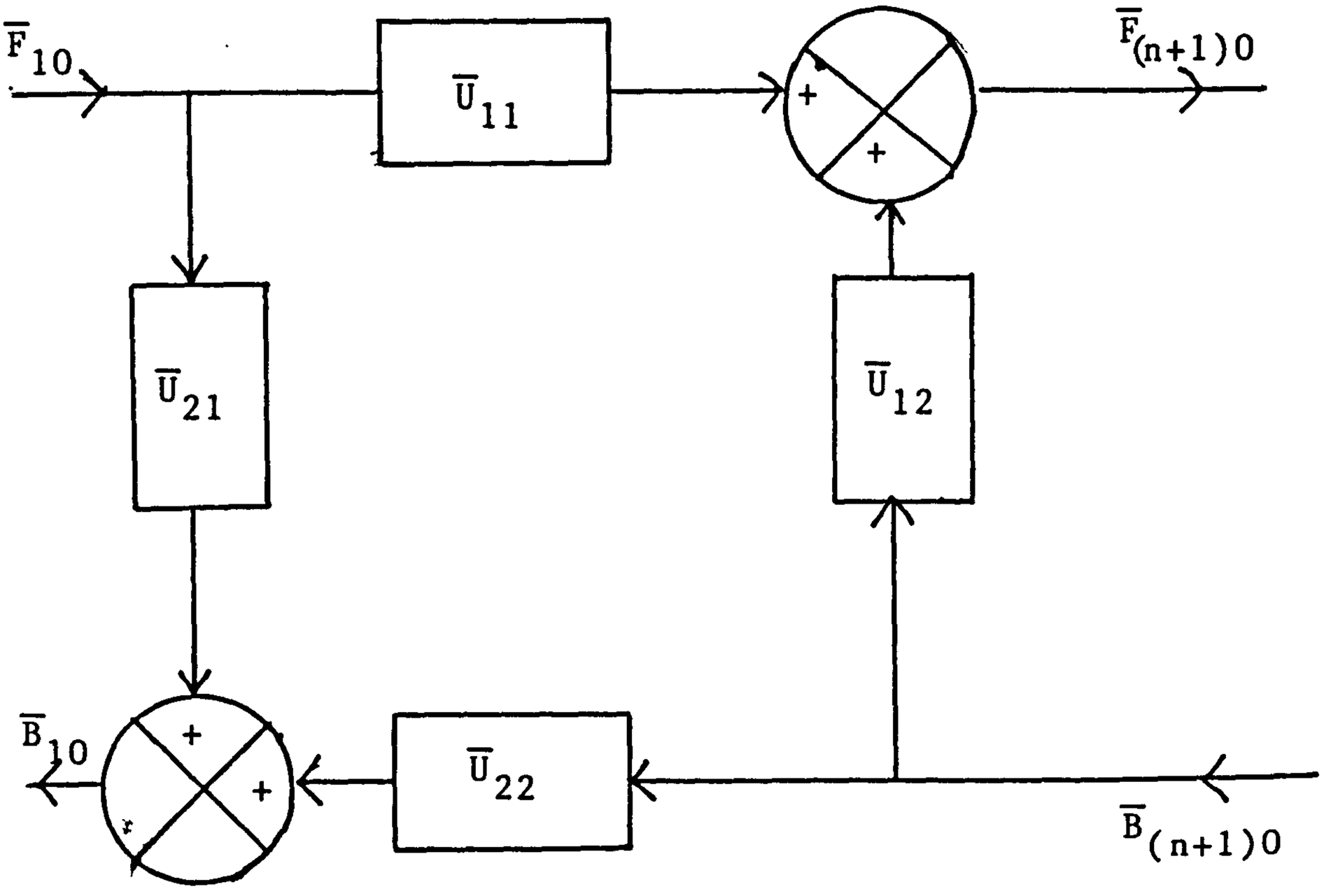

MULTILAYER SYSTEM IN REDUCED
ACOUSTIC LATTICE FORM

Fig 3.2

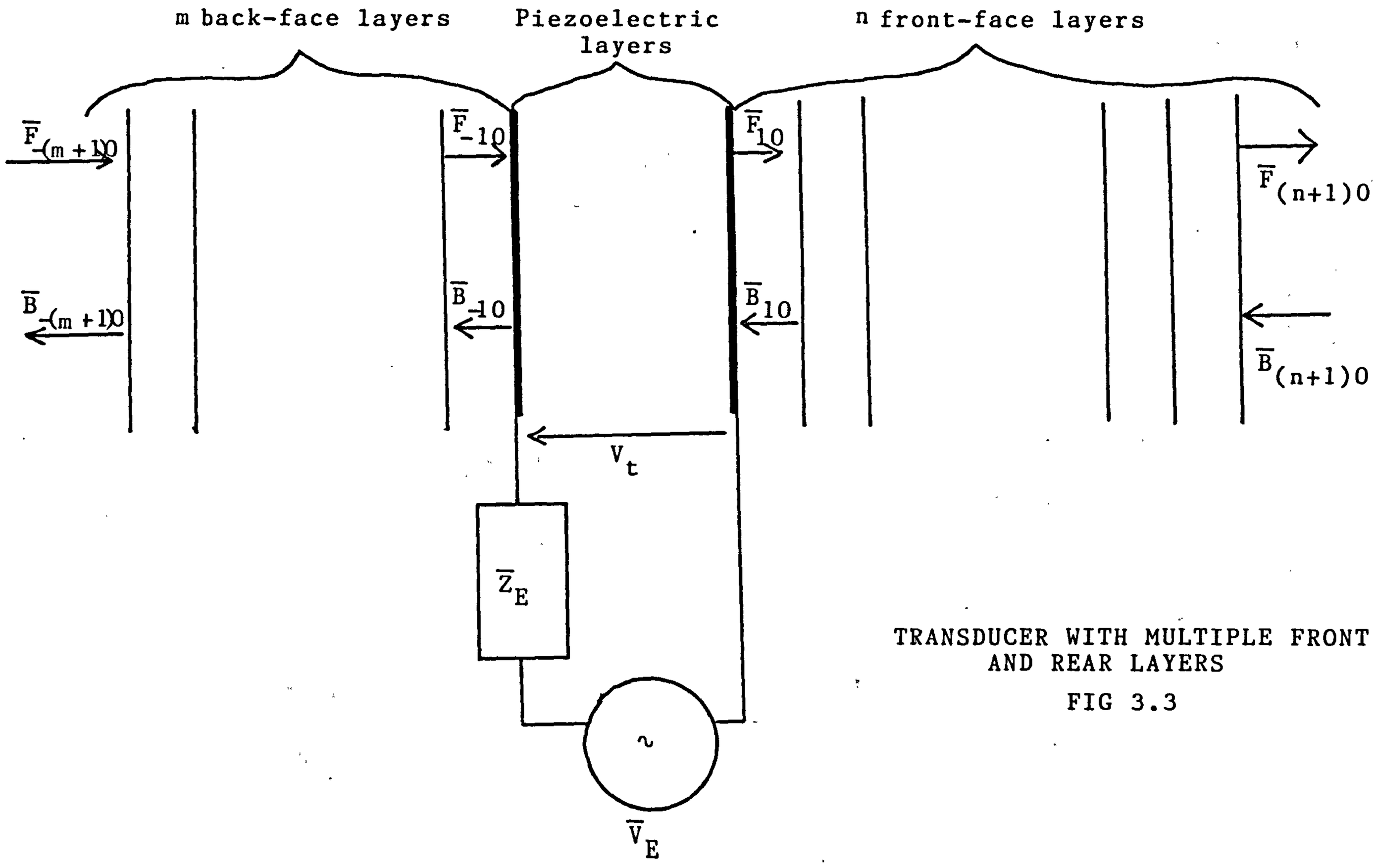

TRANSDUCER WITH MULTIPLE FRONT AND REAR LAYERS

FIG 3.3

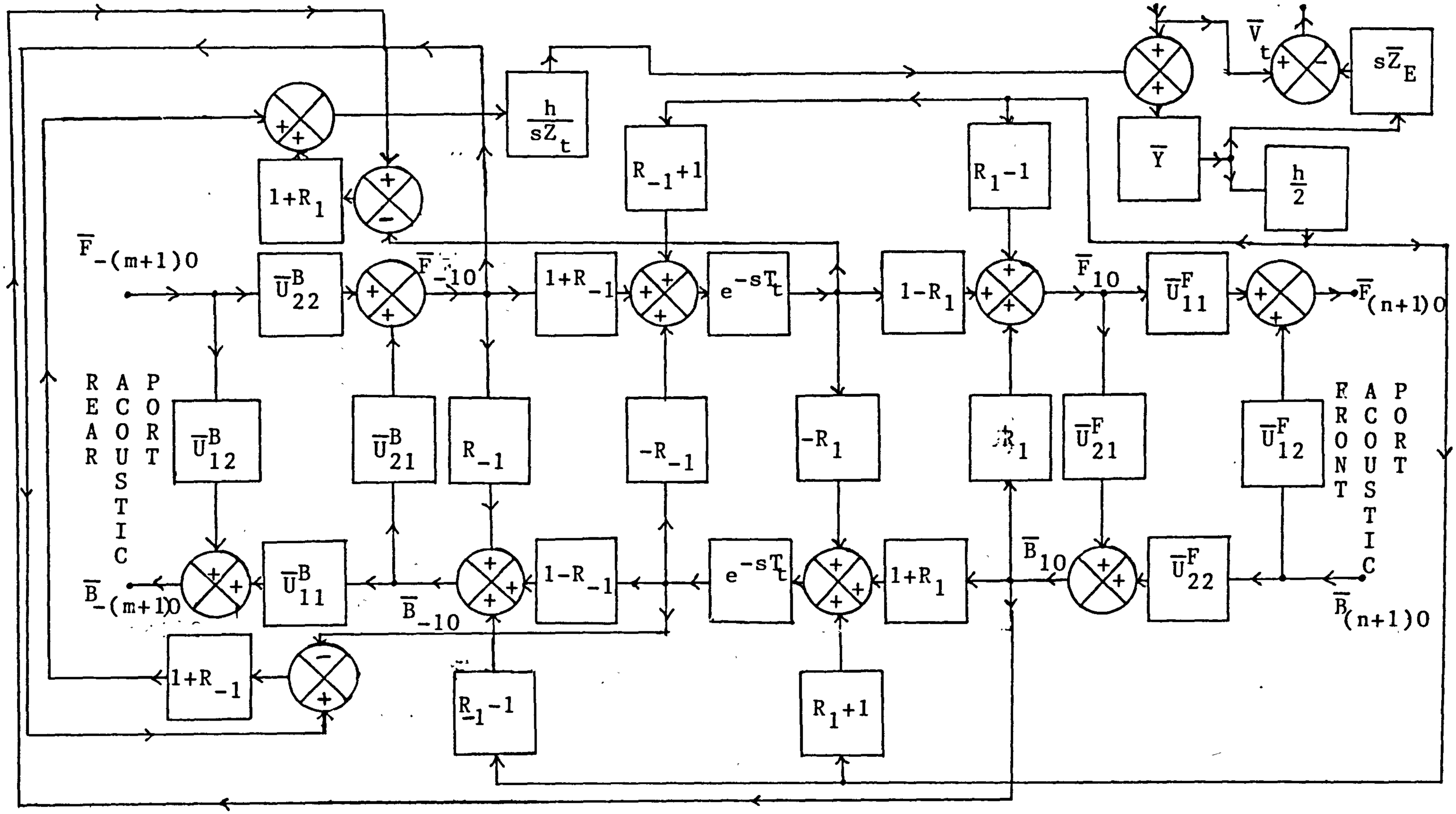

FIG 3.4 SYSTEMS DIAGRAM OF THE MULTILAYERED TRANSDUCER

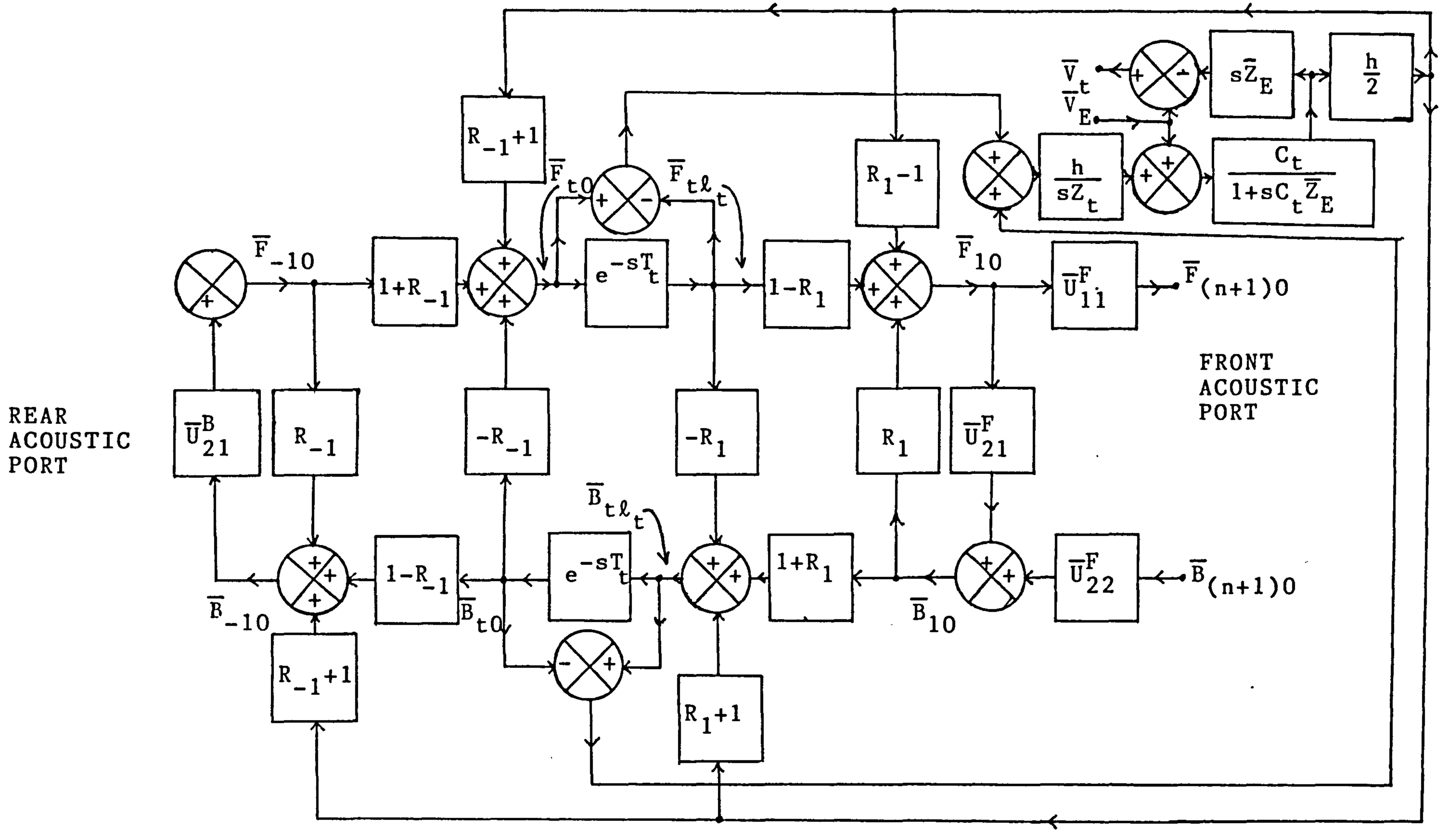

FIG 3.5 MODIFIED MULTILAYER LATTICE

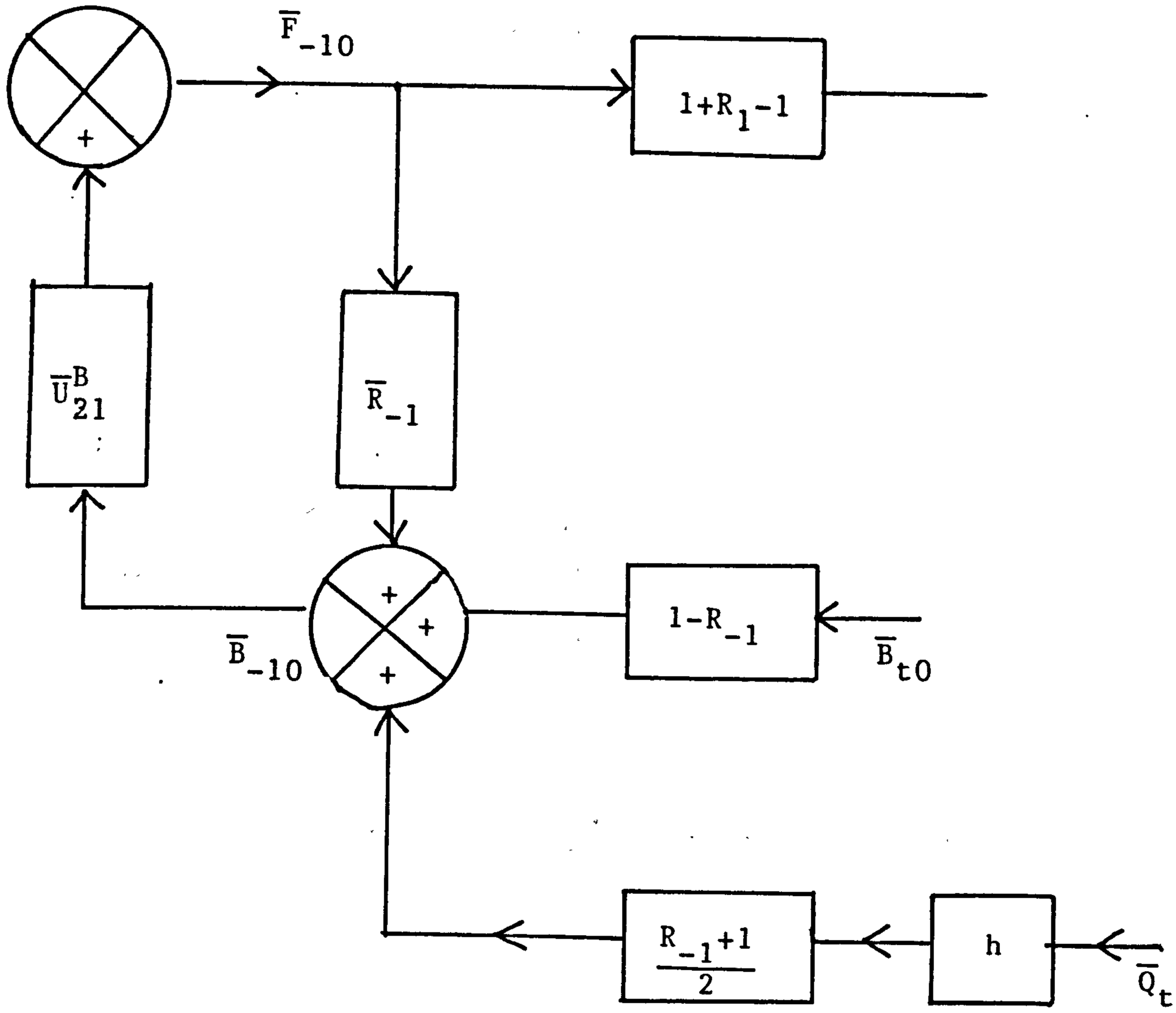

FIG 3.6A

REAR ACOUSTIC PORT LATTICE SECTION

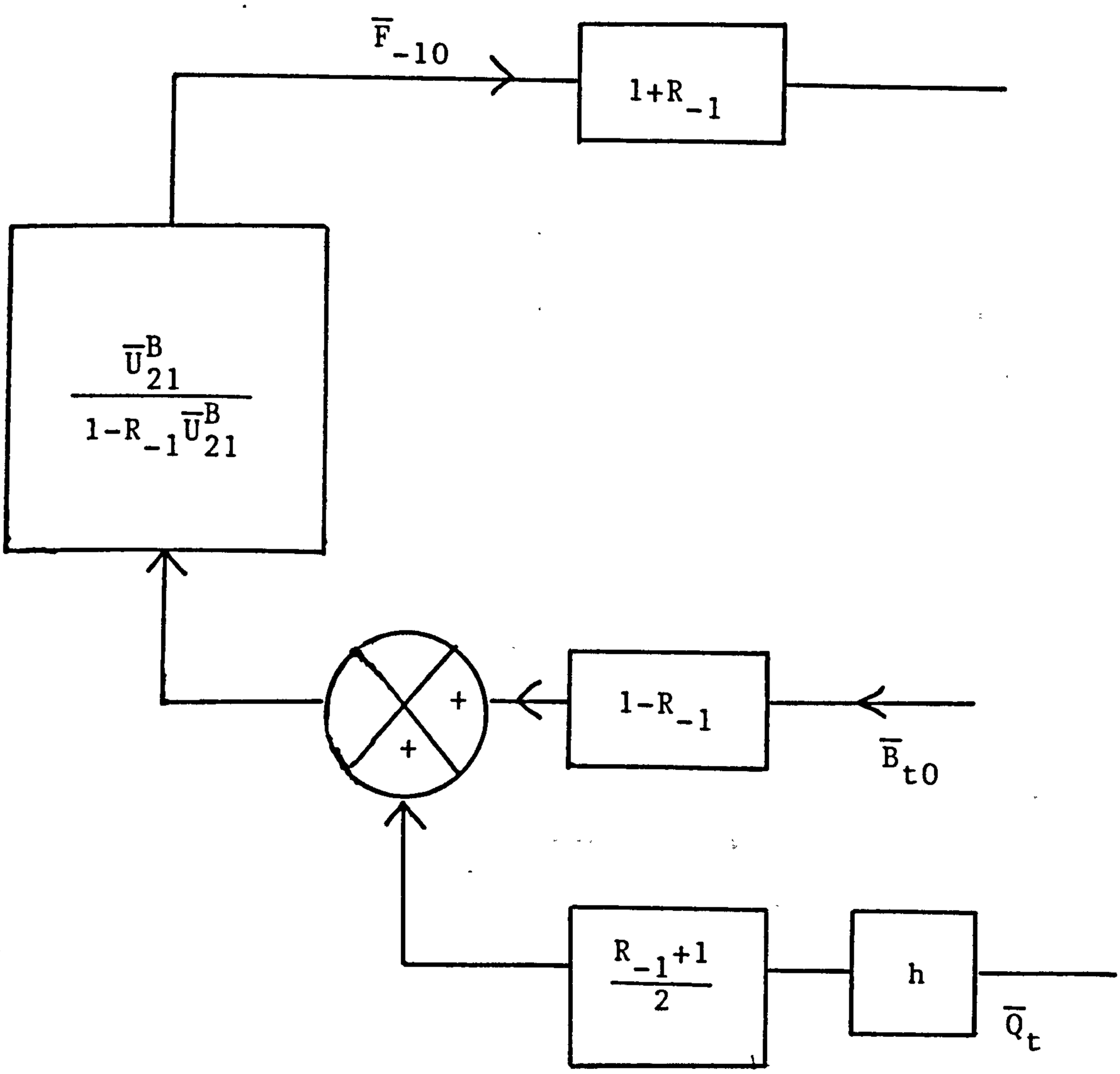

Fig 3.6B

MODIFIED REAR-PORT SECTION

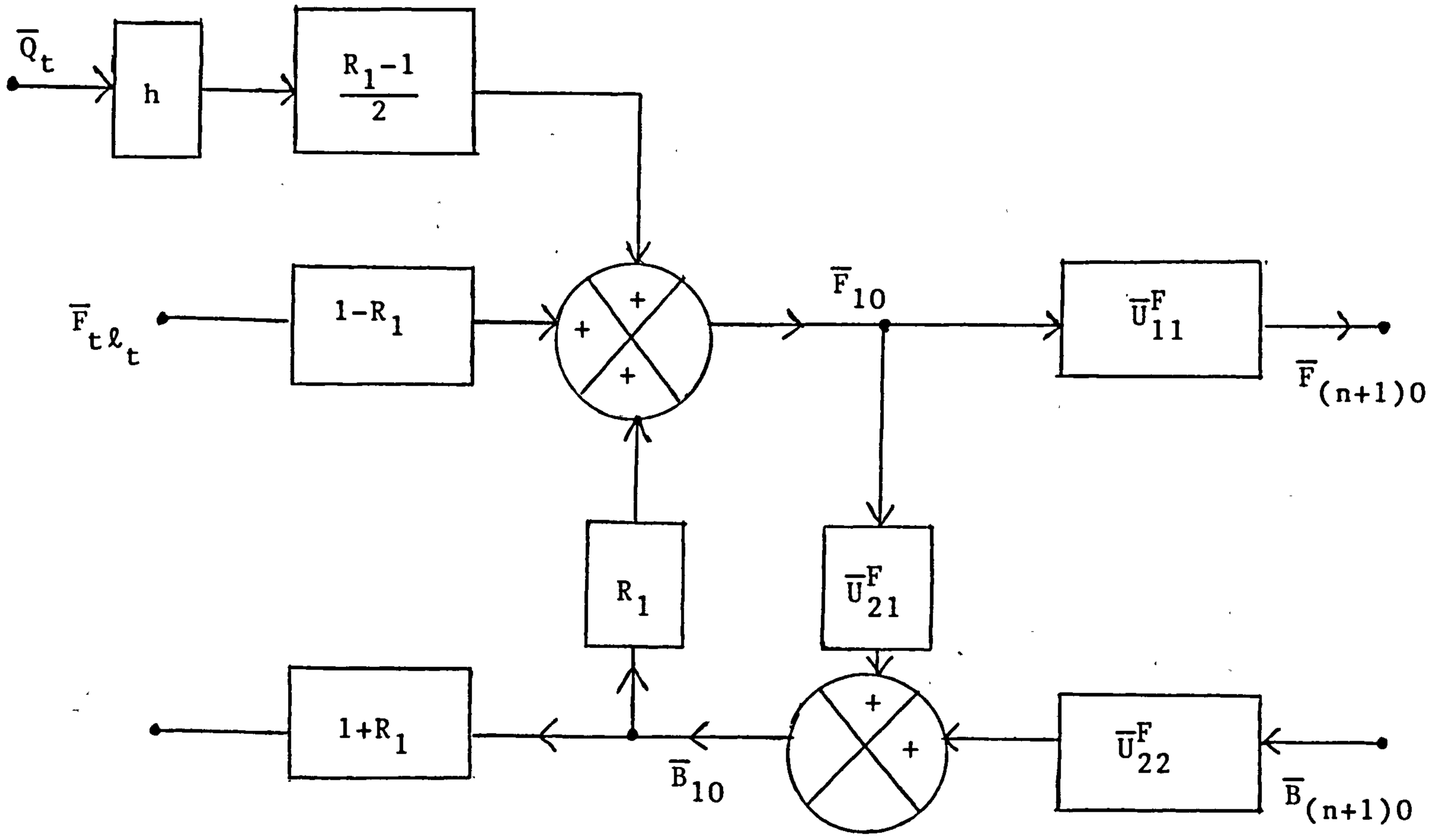

FRONT ACOUSTIC PORT LATTICE SECTION

FIG 3.7A

FIG 3.7B MODIFIED FRONT-PORT SECTION

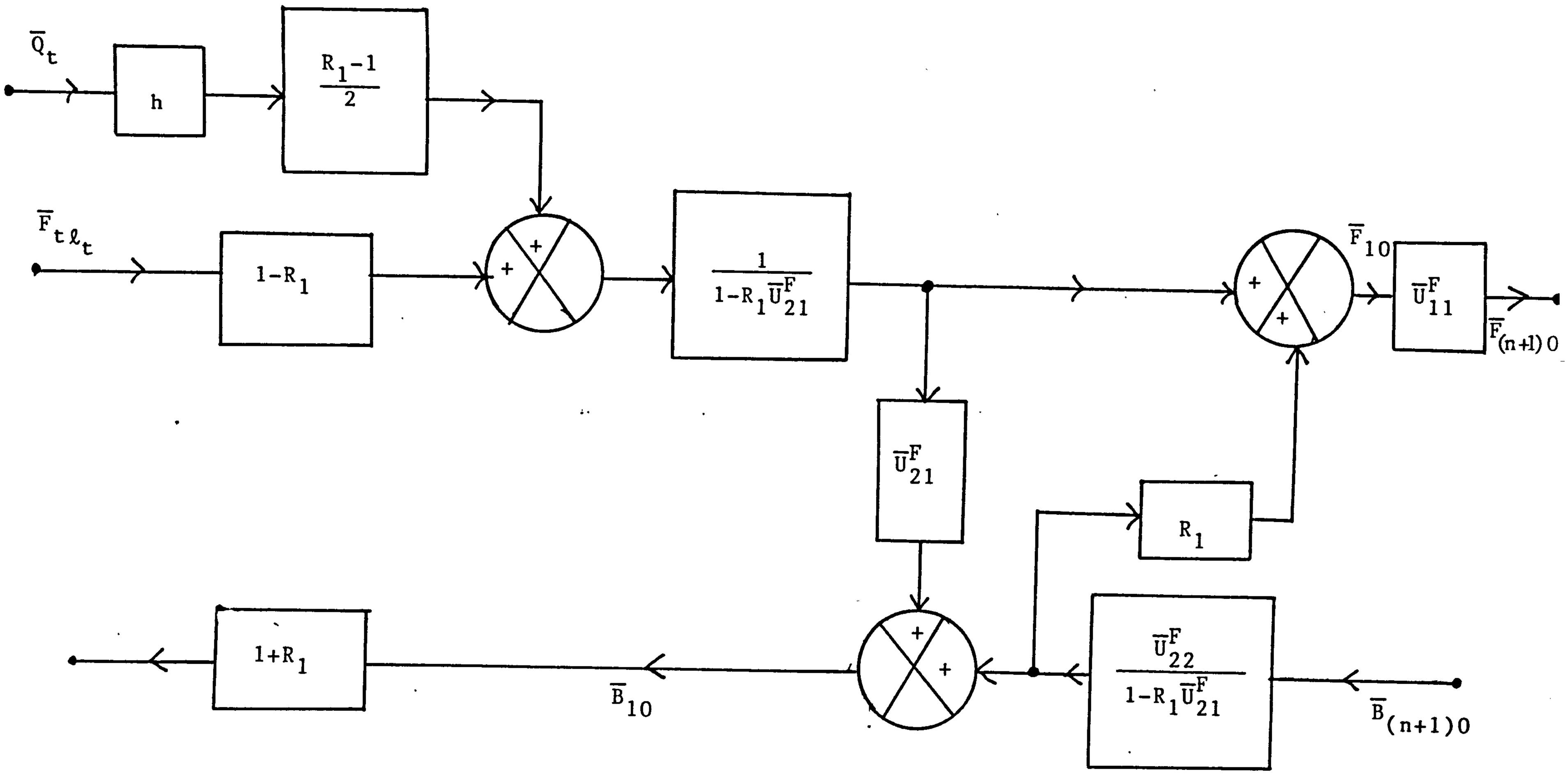

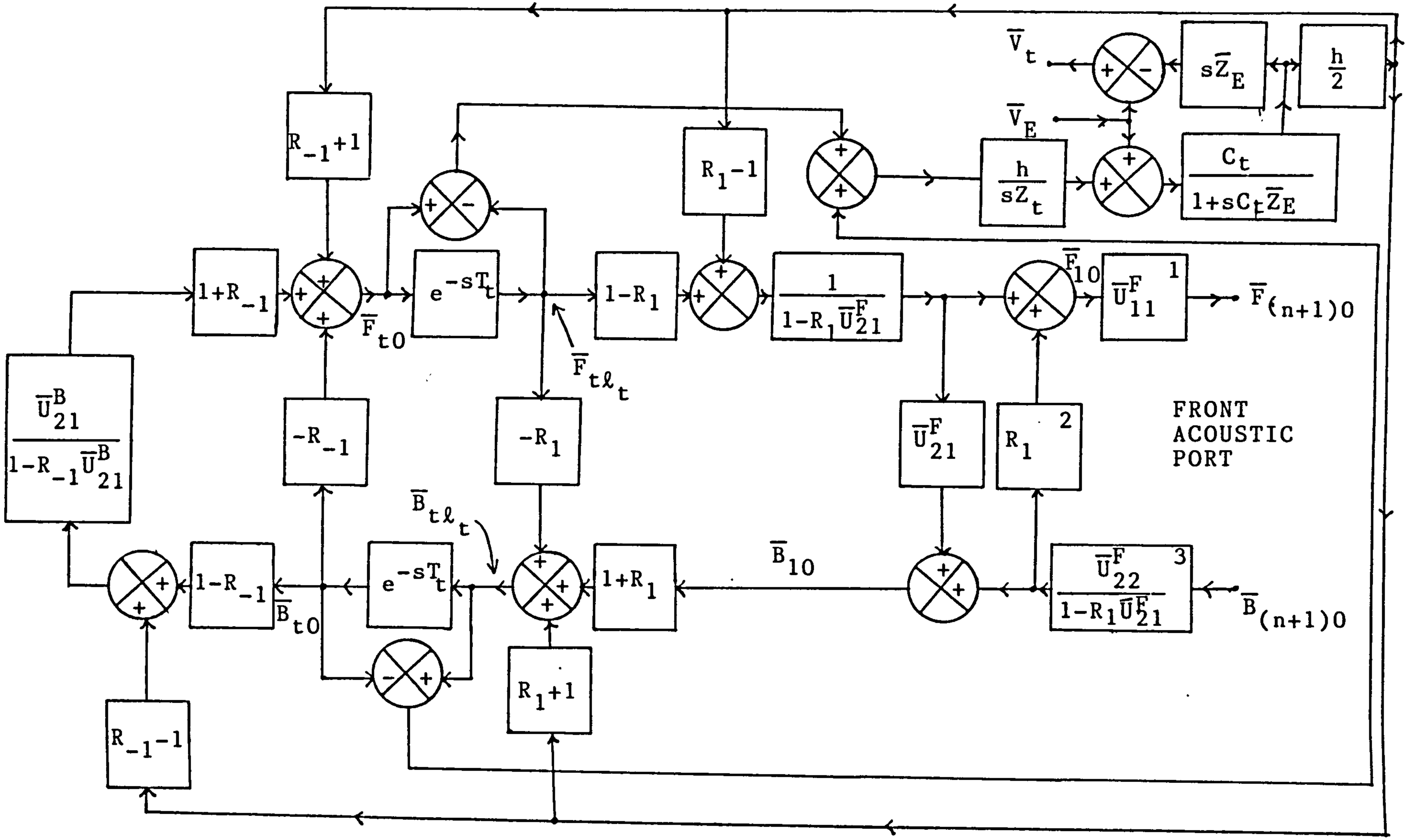

KEY
1 - TRANSMITTER ONLY
2 - NOT REQUIRED
3 - RECEIVER ONLY

FIG 3.8 COMPLETE MODIFIED LATTICE DIAGRAM

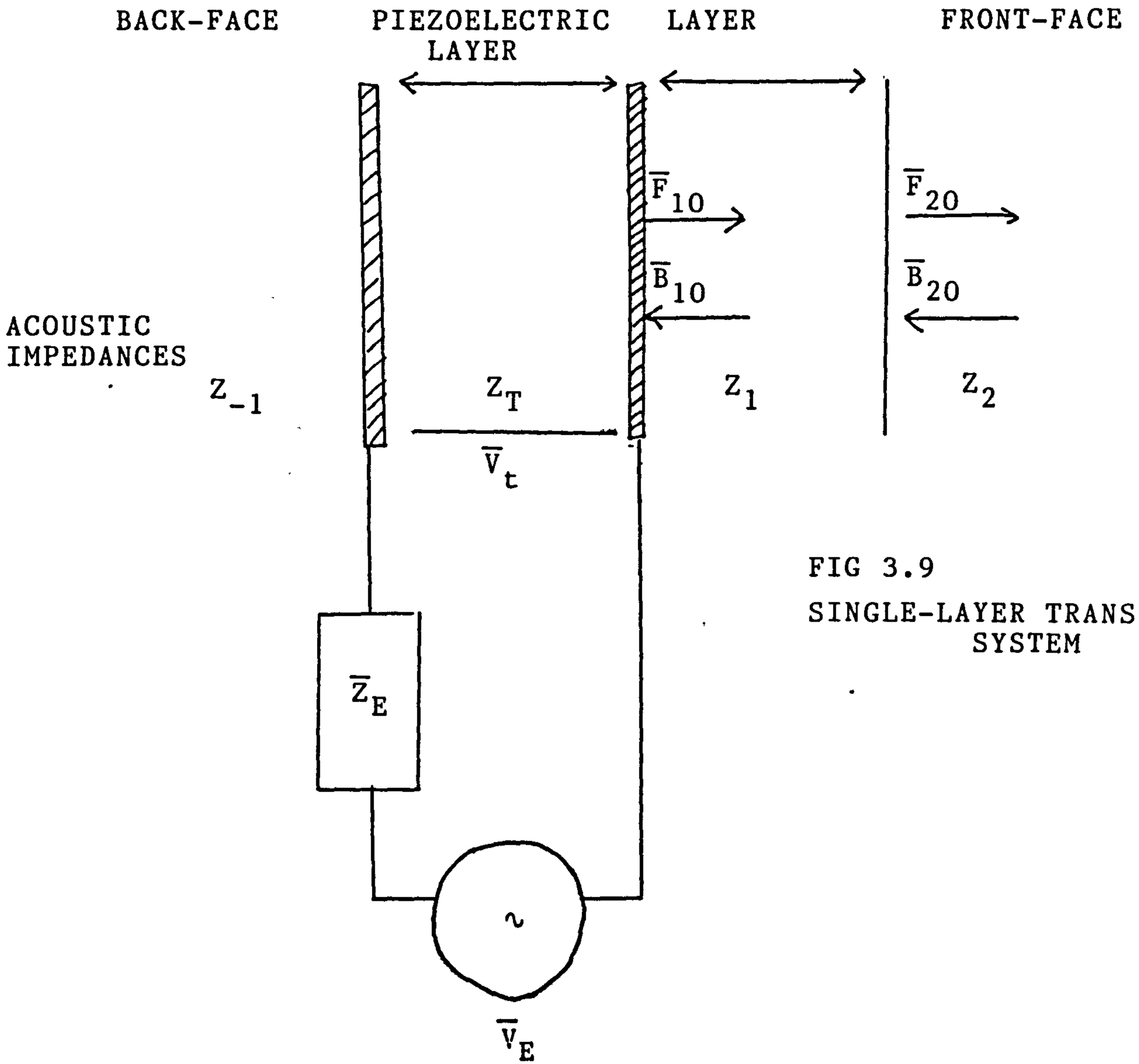

FIG 3.9

SINGLE-LAYER TRANSDUCER SYSTEM

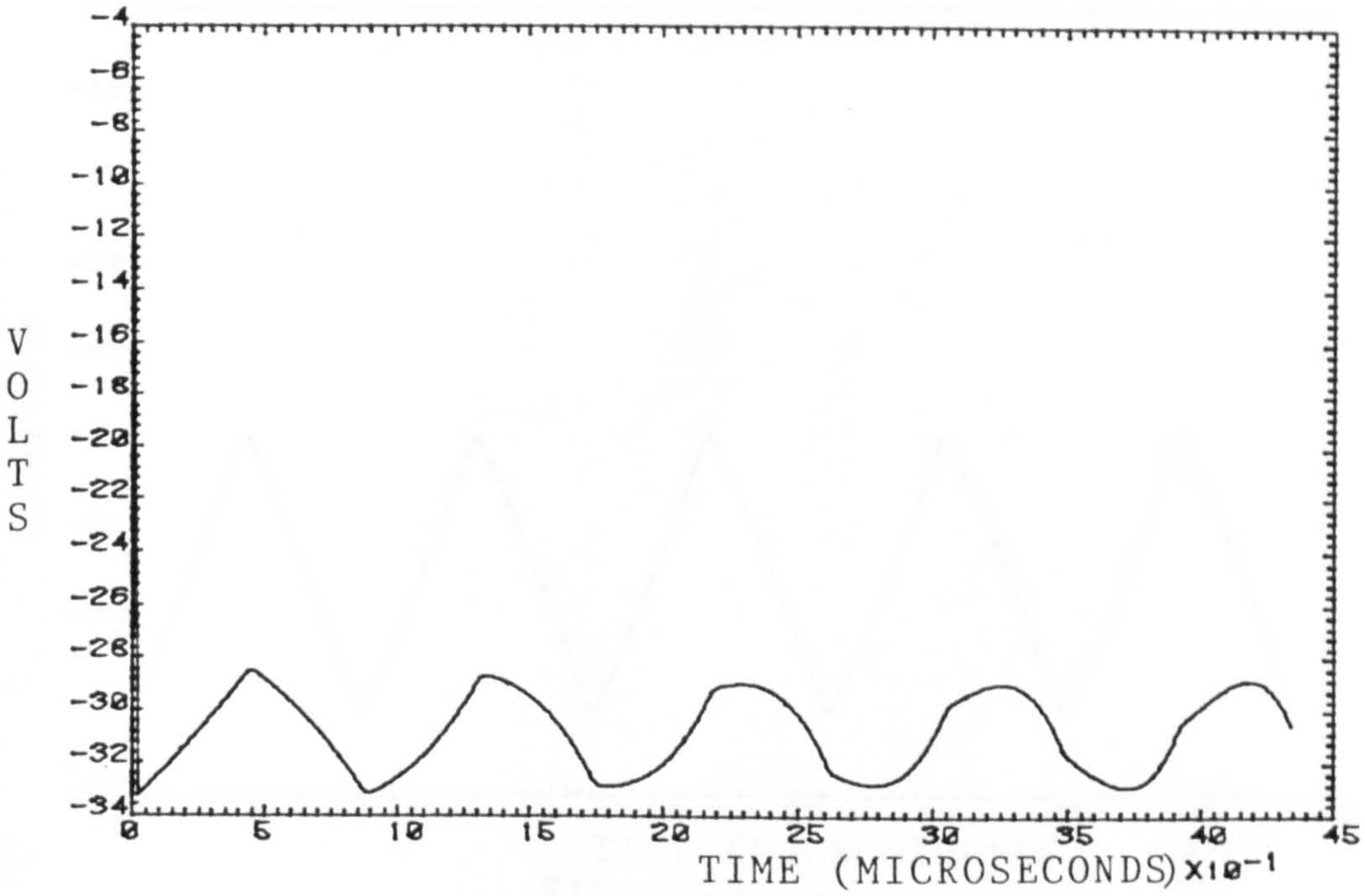

FIG 5.1B

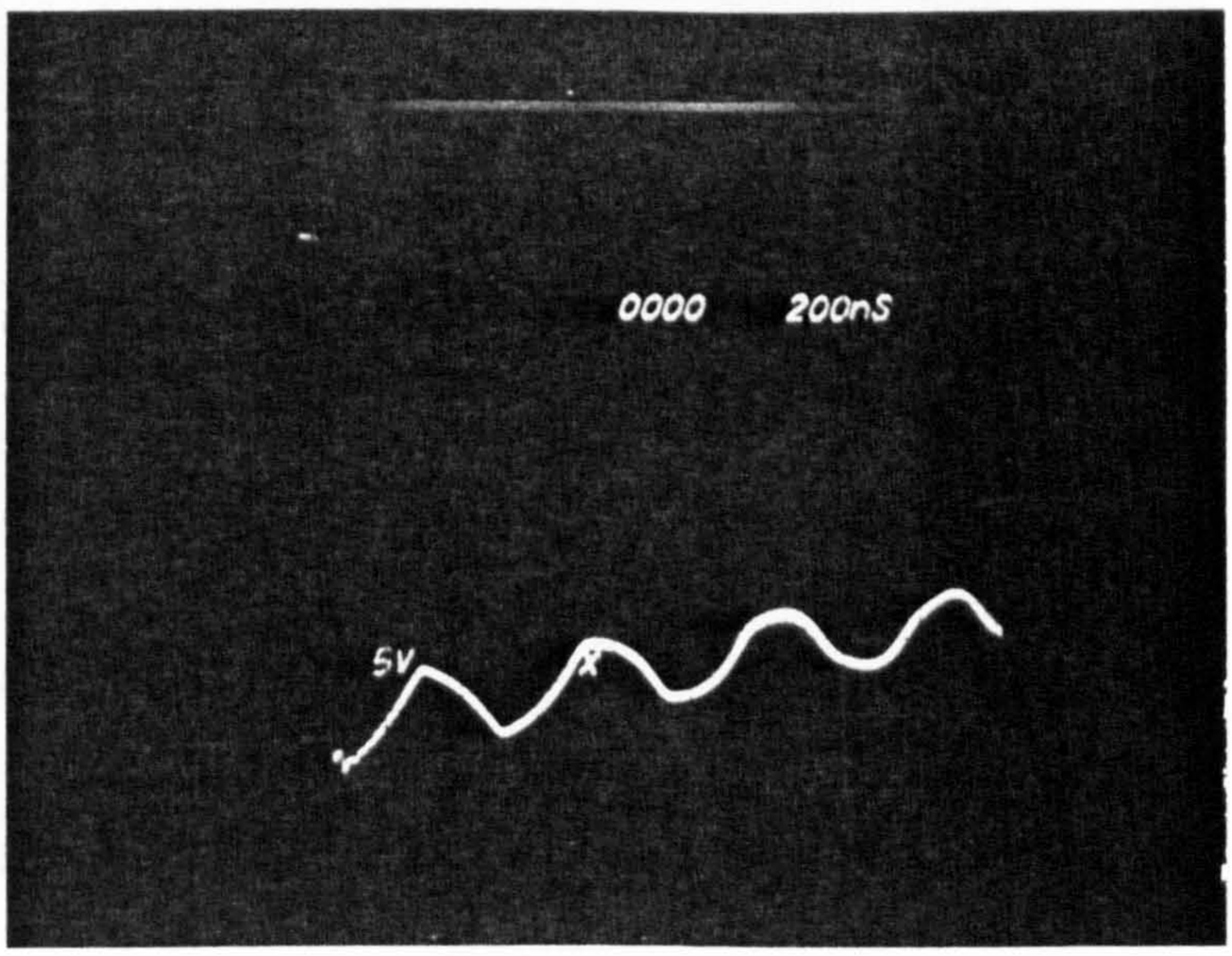

FIG 5.1C

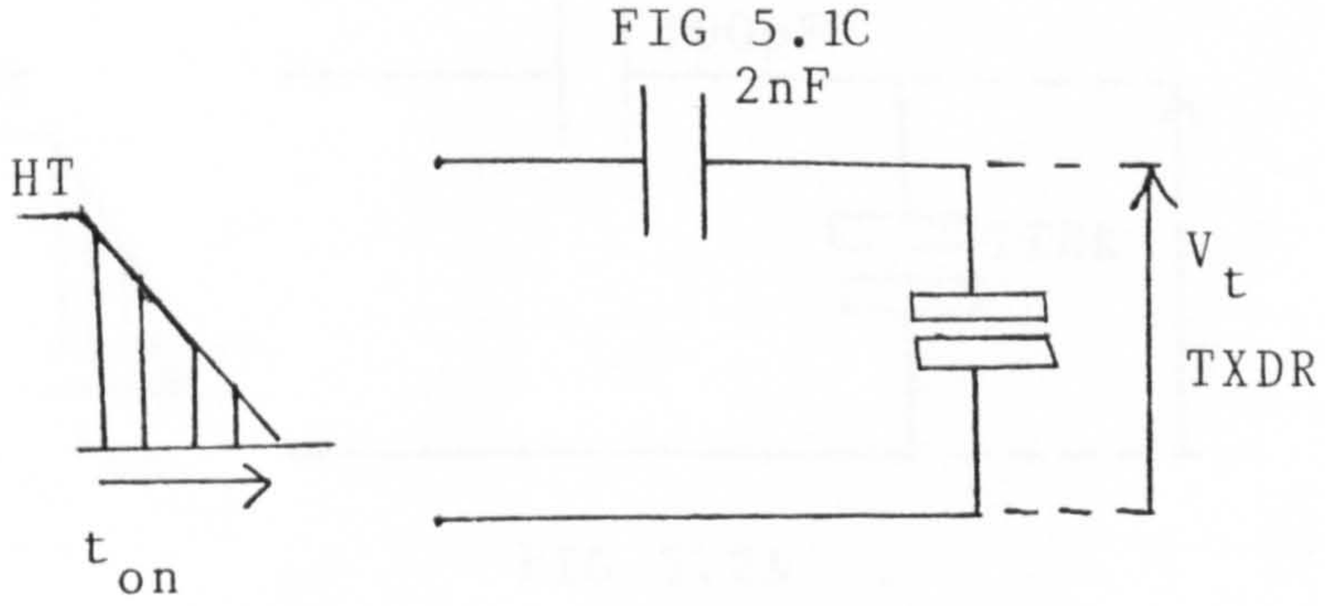

FIG 5.1A

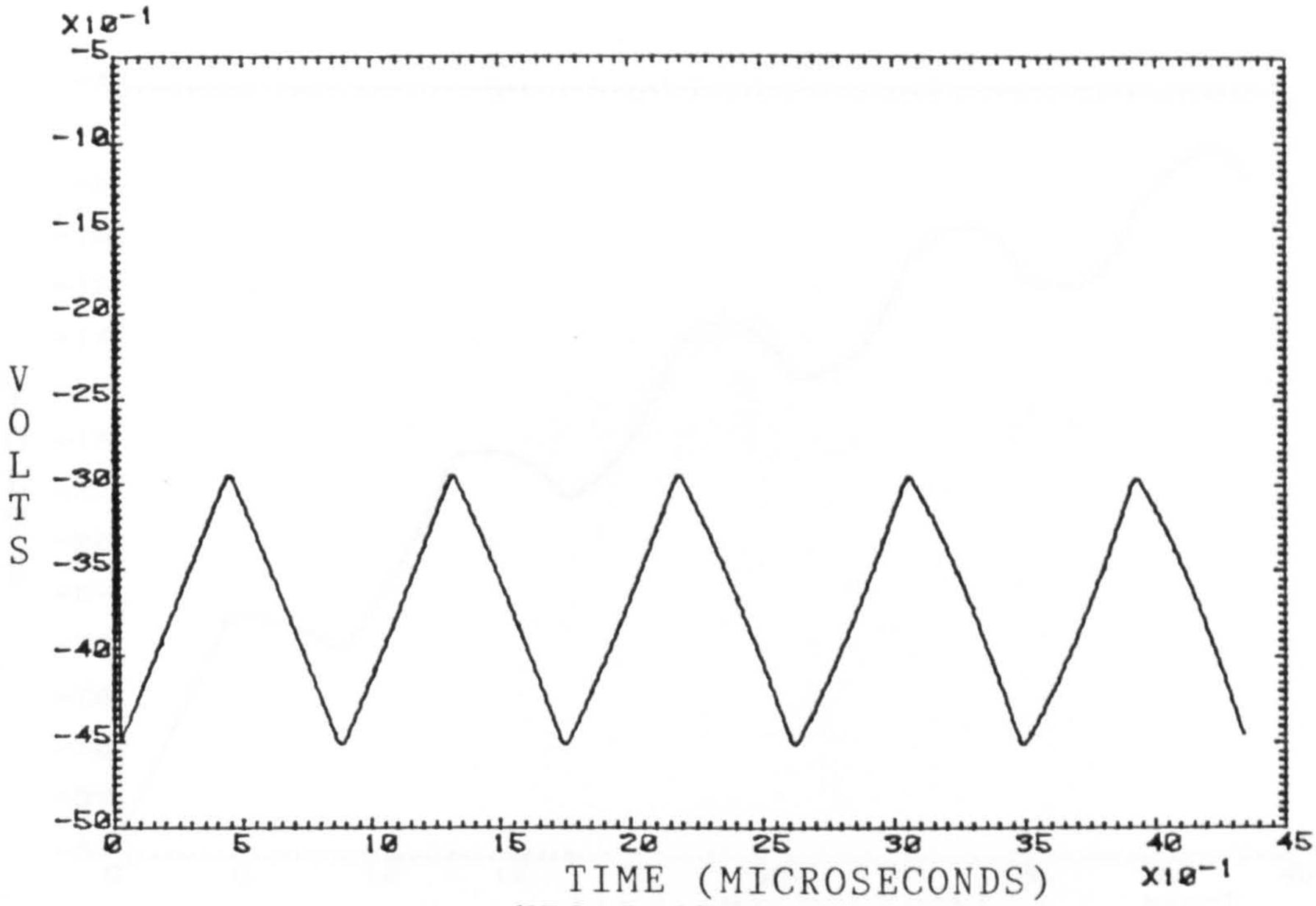

FIG 5.2B

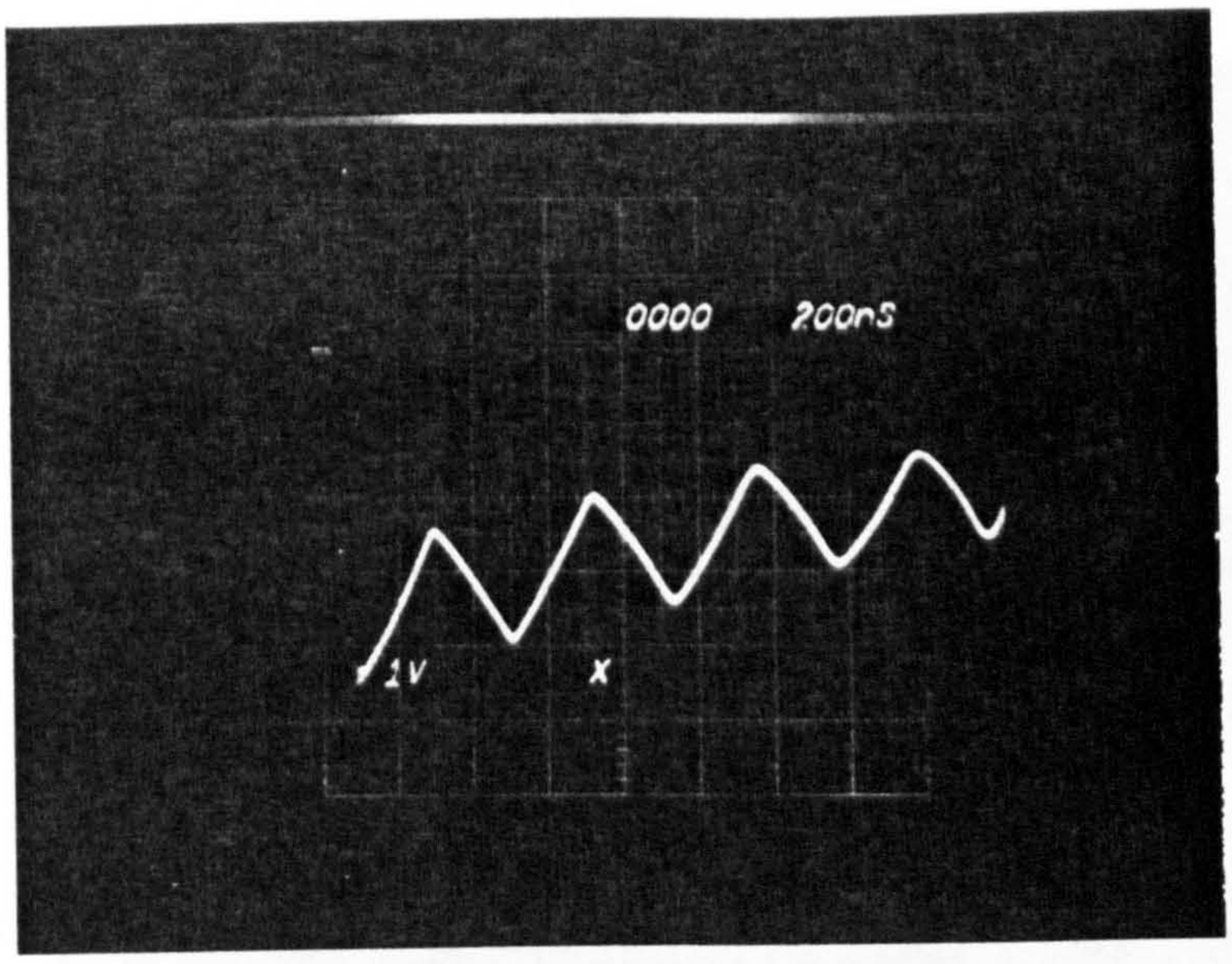

FIG 5.2C

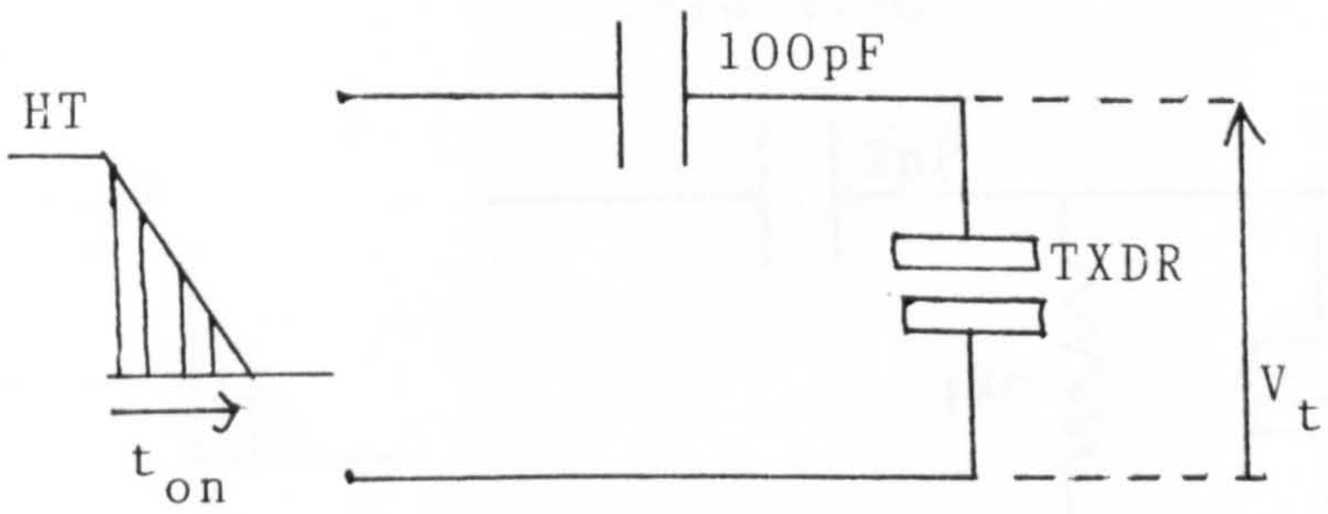

FIG 5.2A

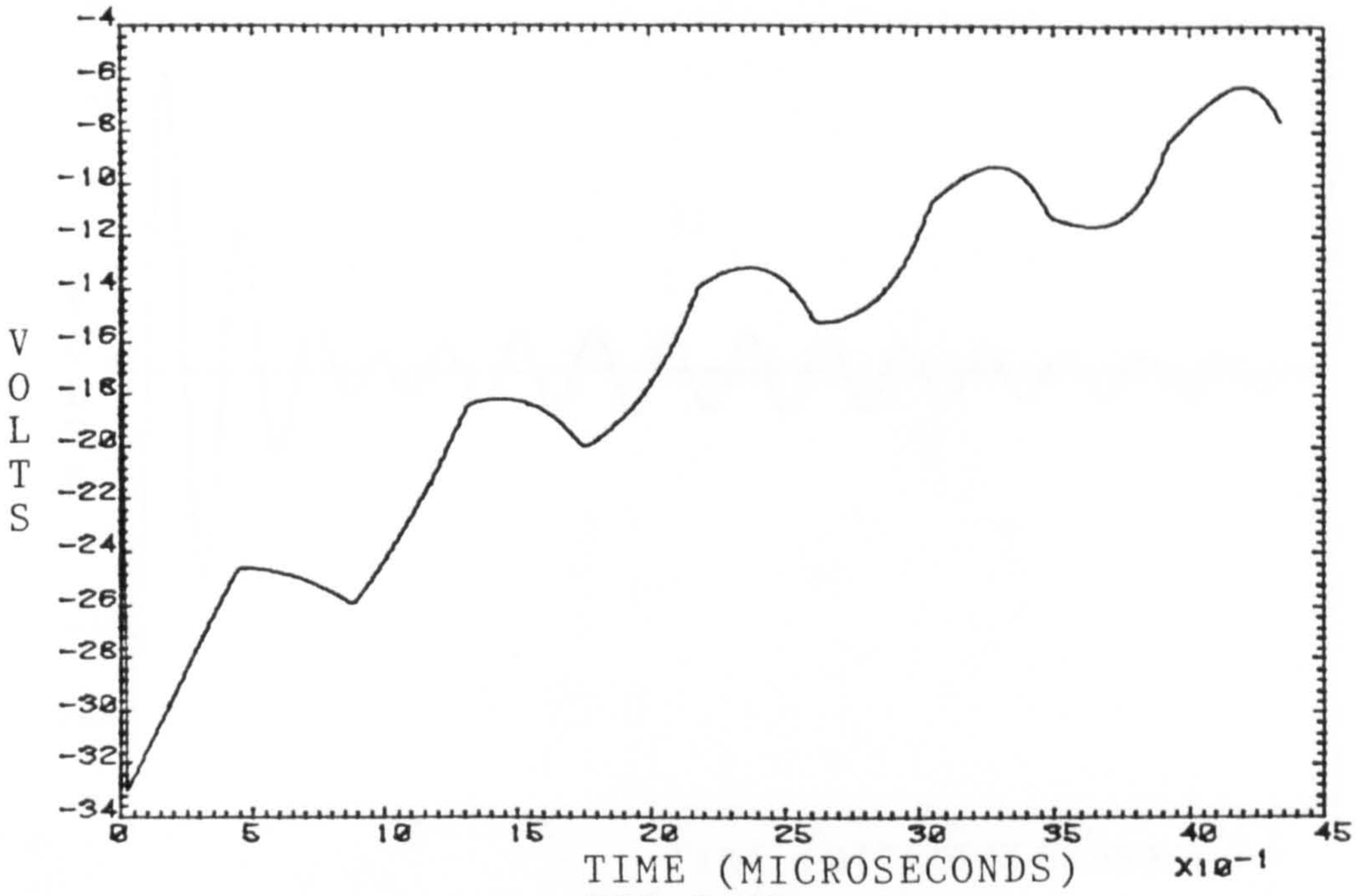

FIG 5.3B

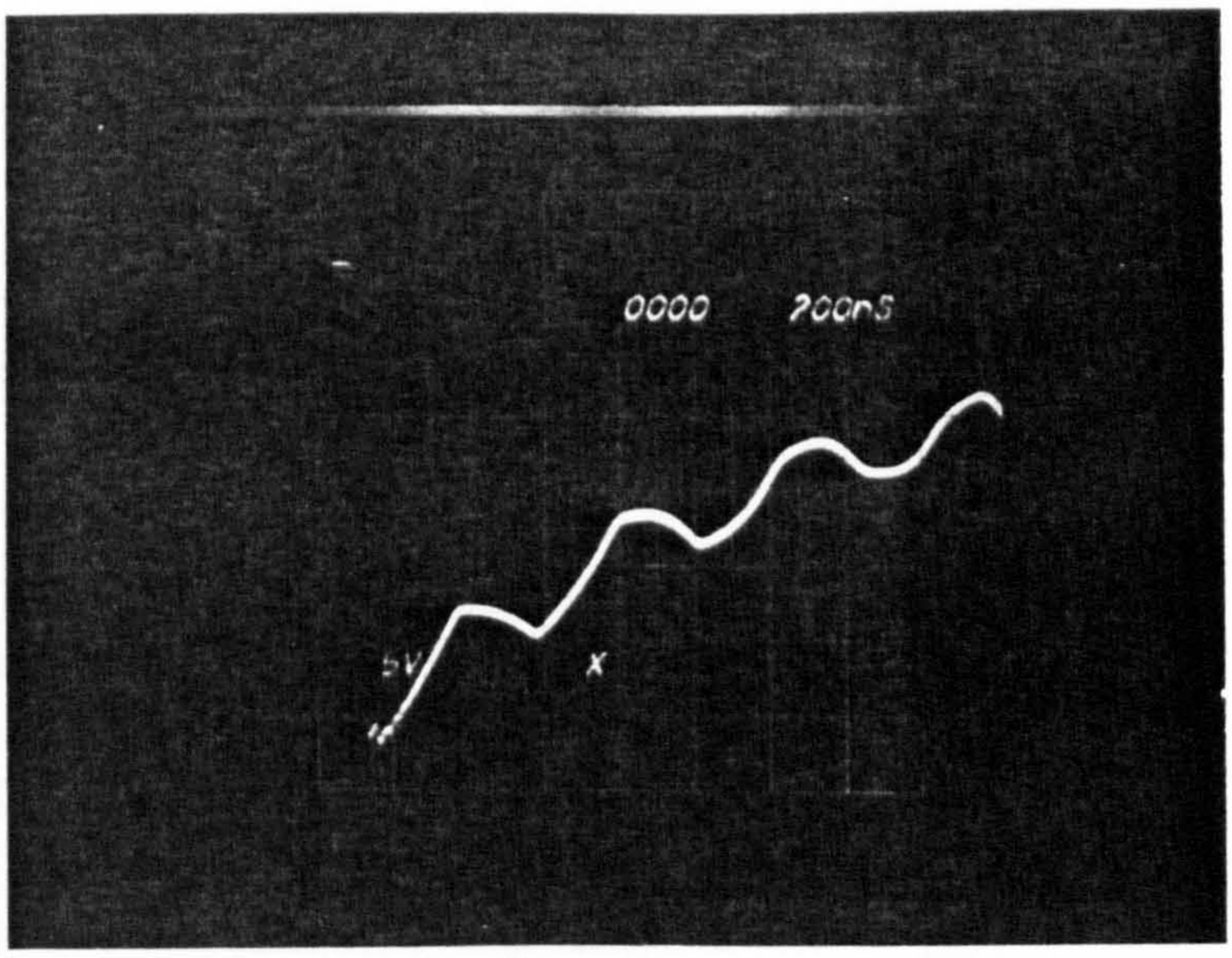

FIG 5.3C

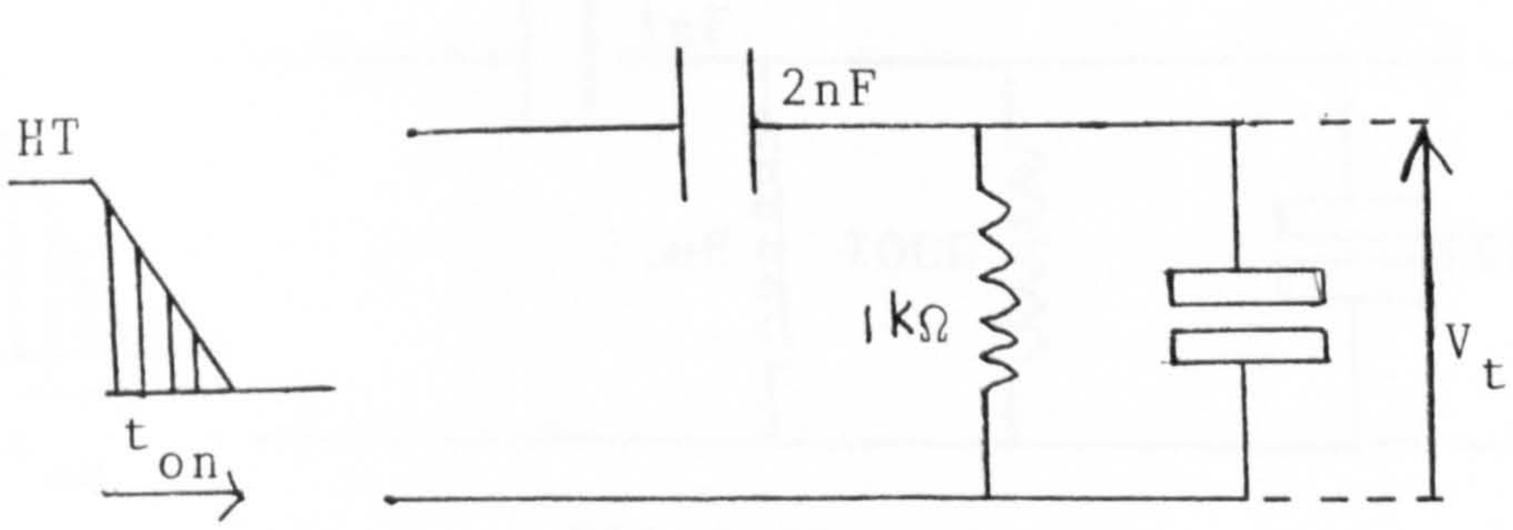

FIG 5.3A

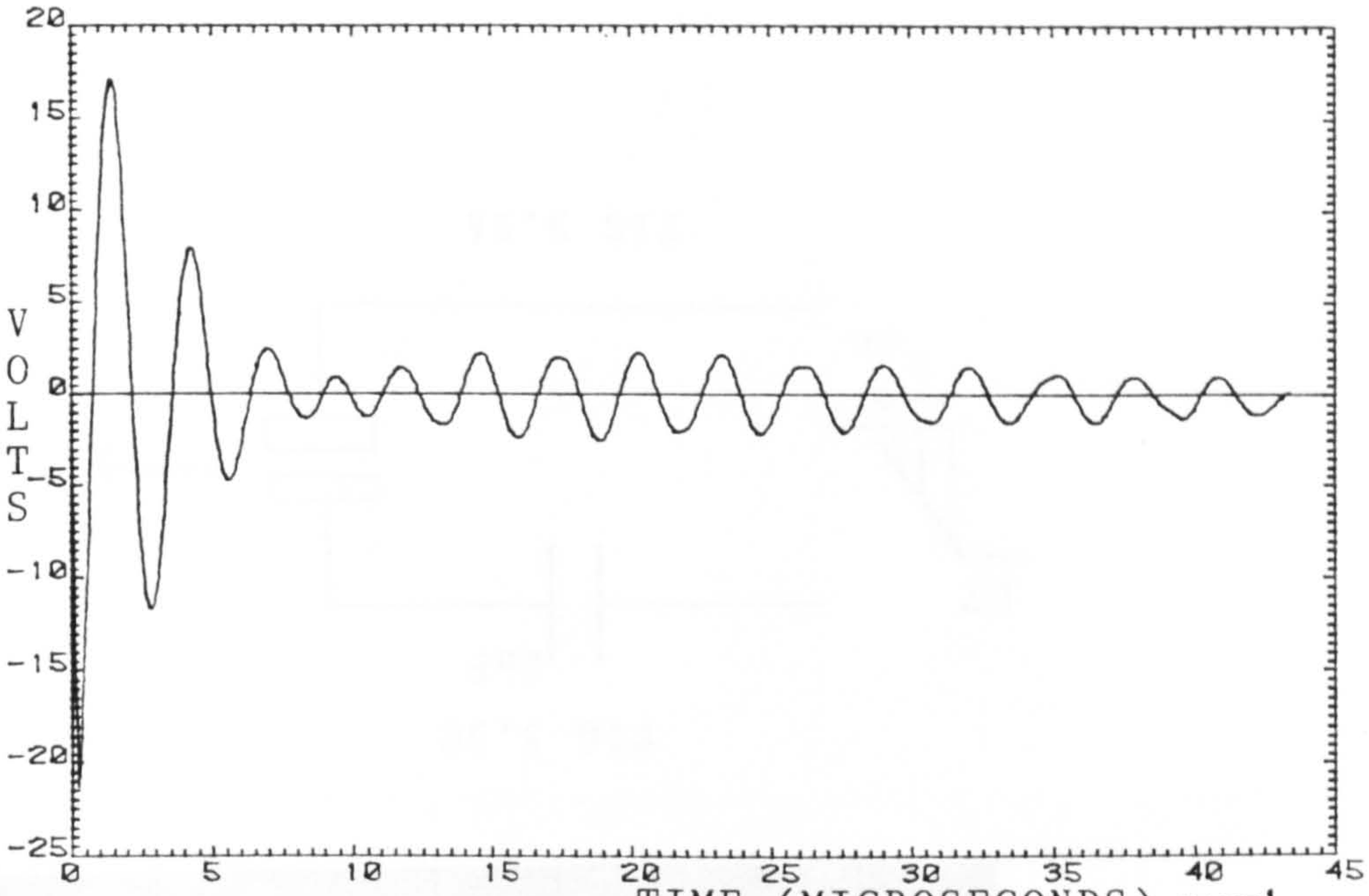

FIG 5.4B

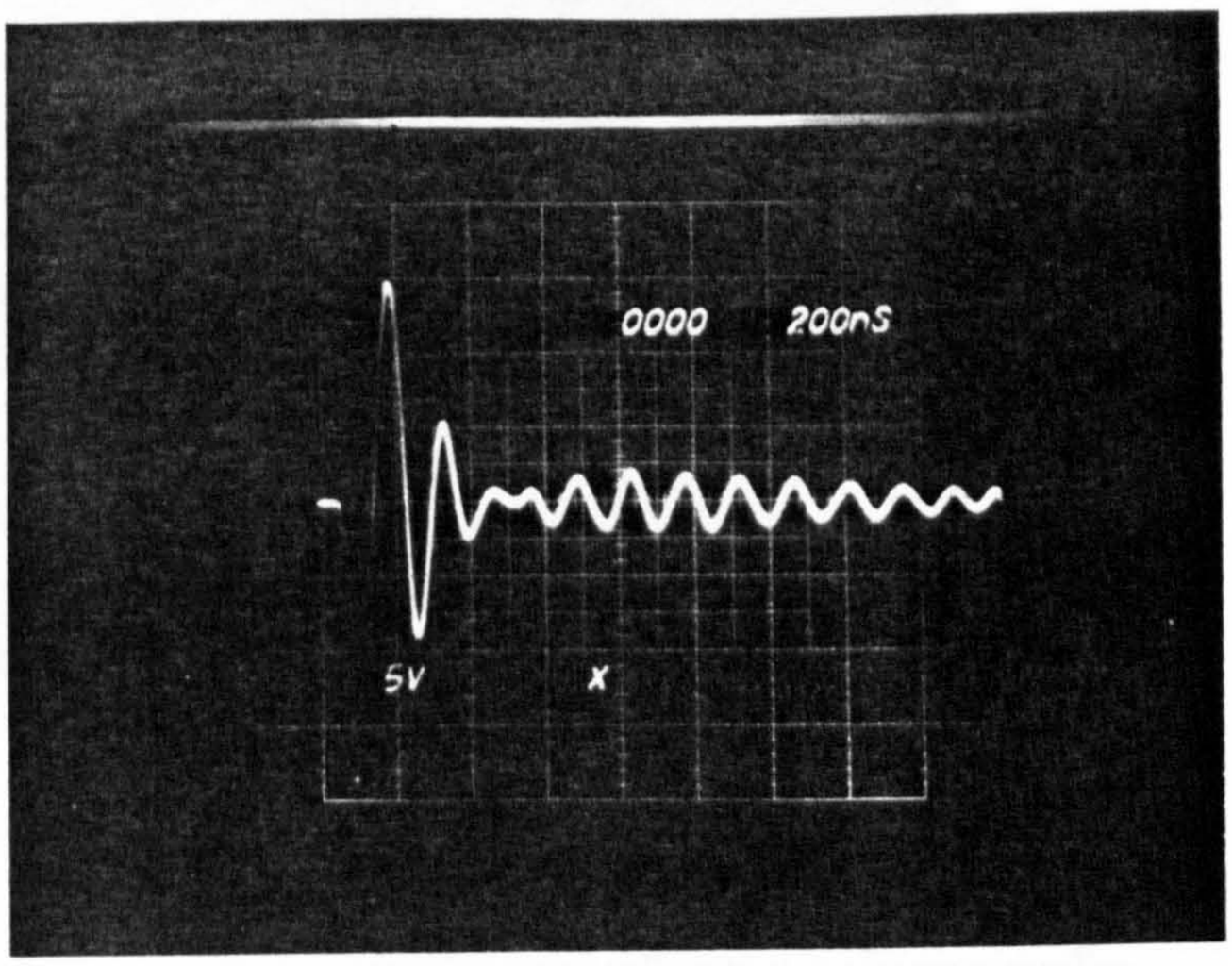

FIG 5.4C

FIG 5.4A

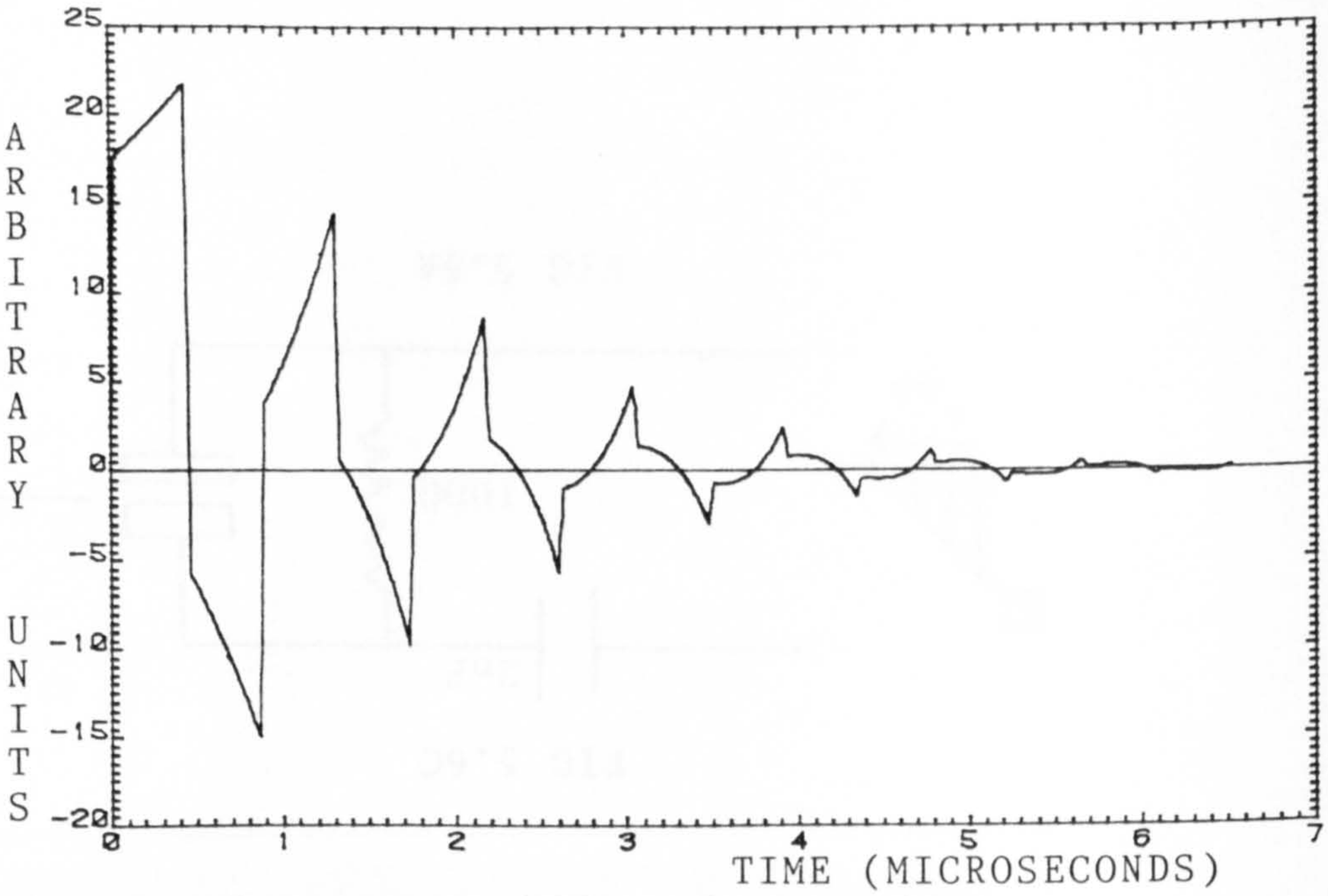

FIG 5.5B

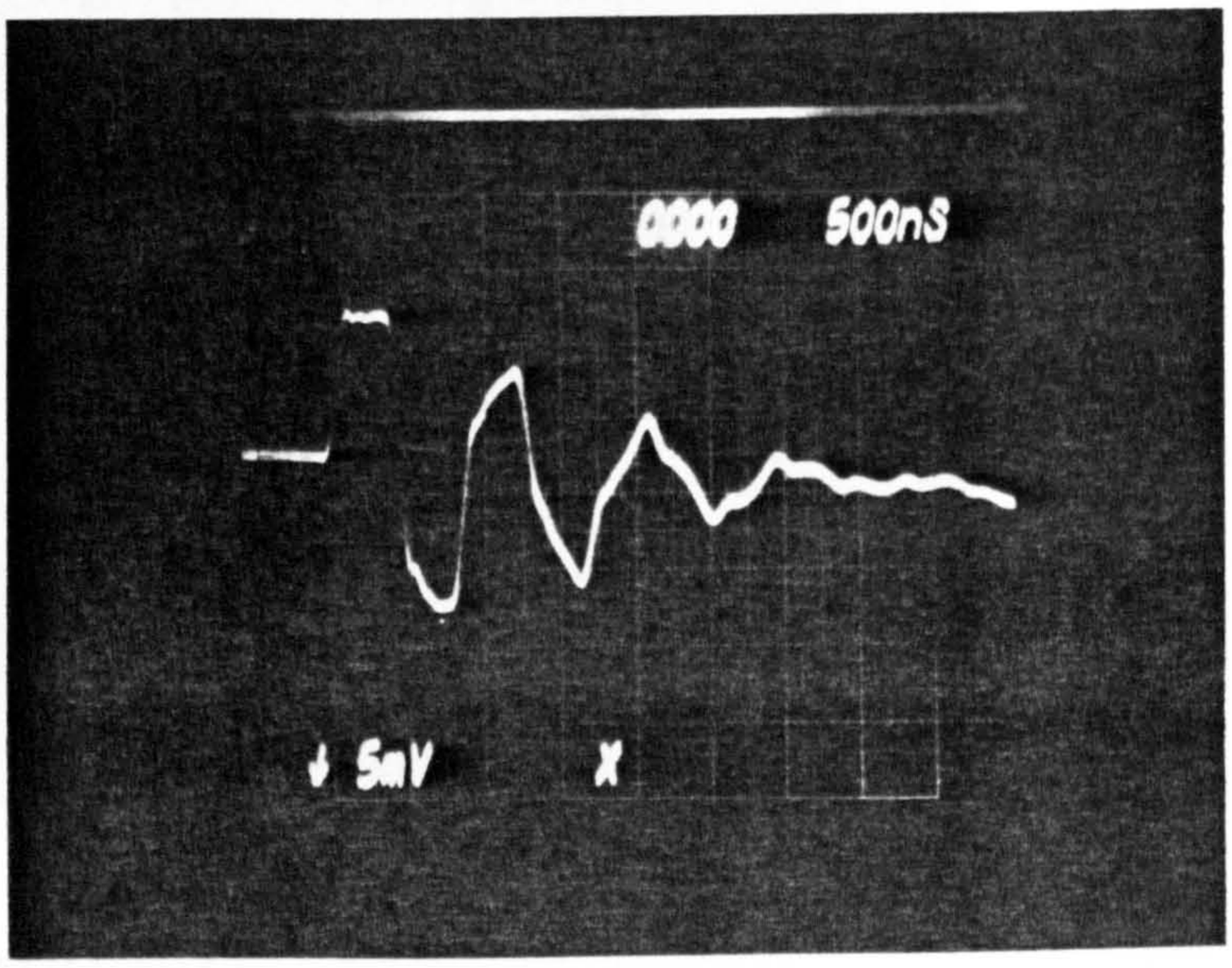

FIG 5.5C

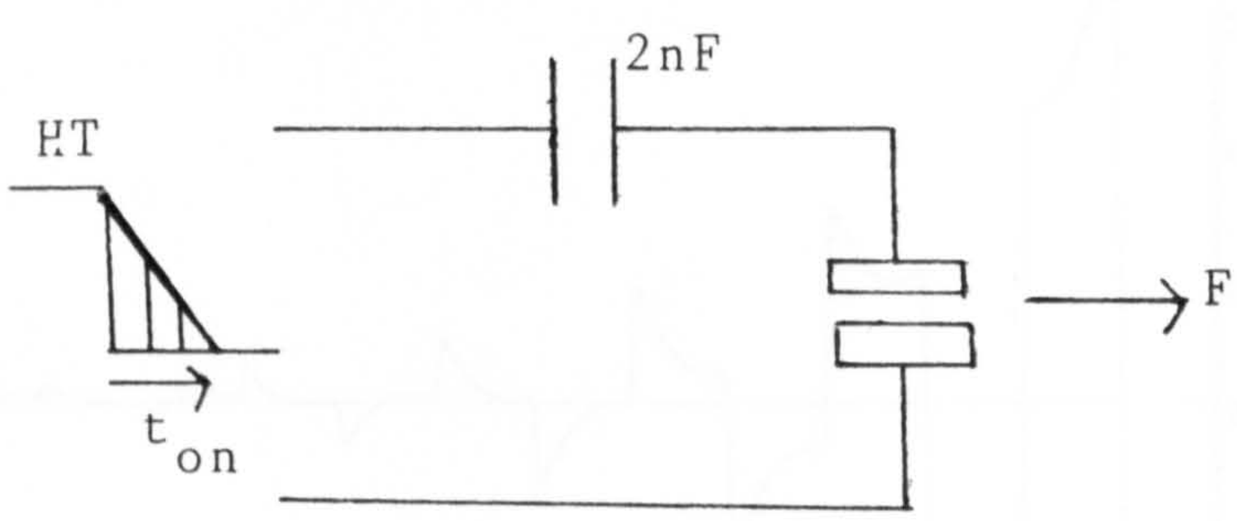

FIG 5.5A

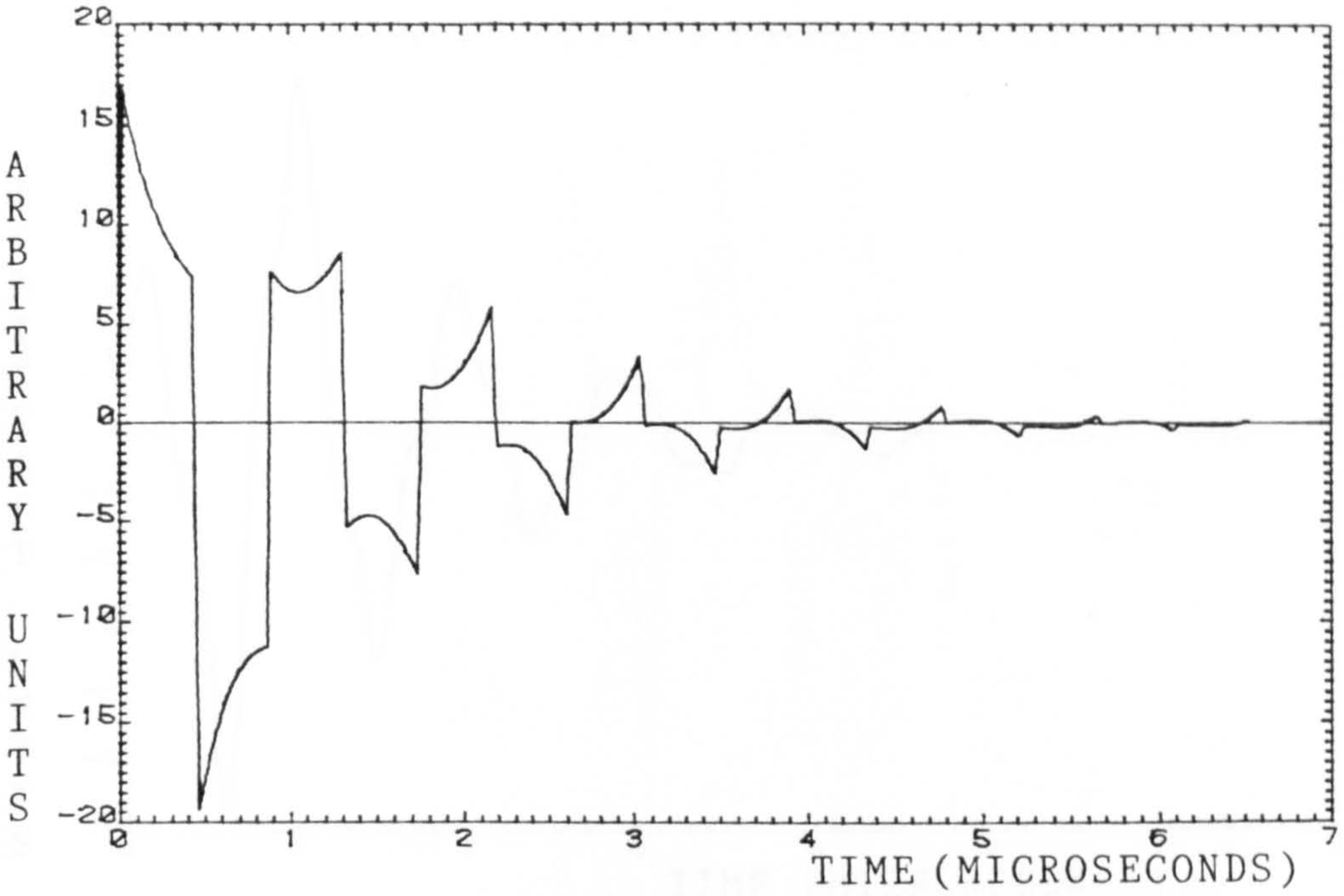

FIG 5.6B

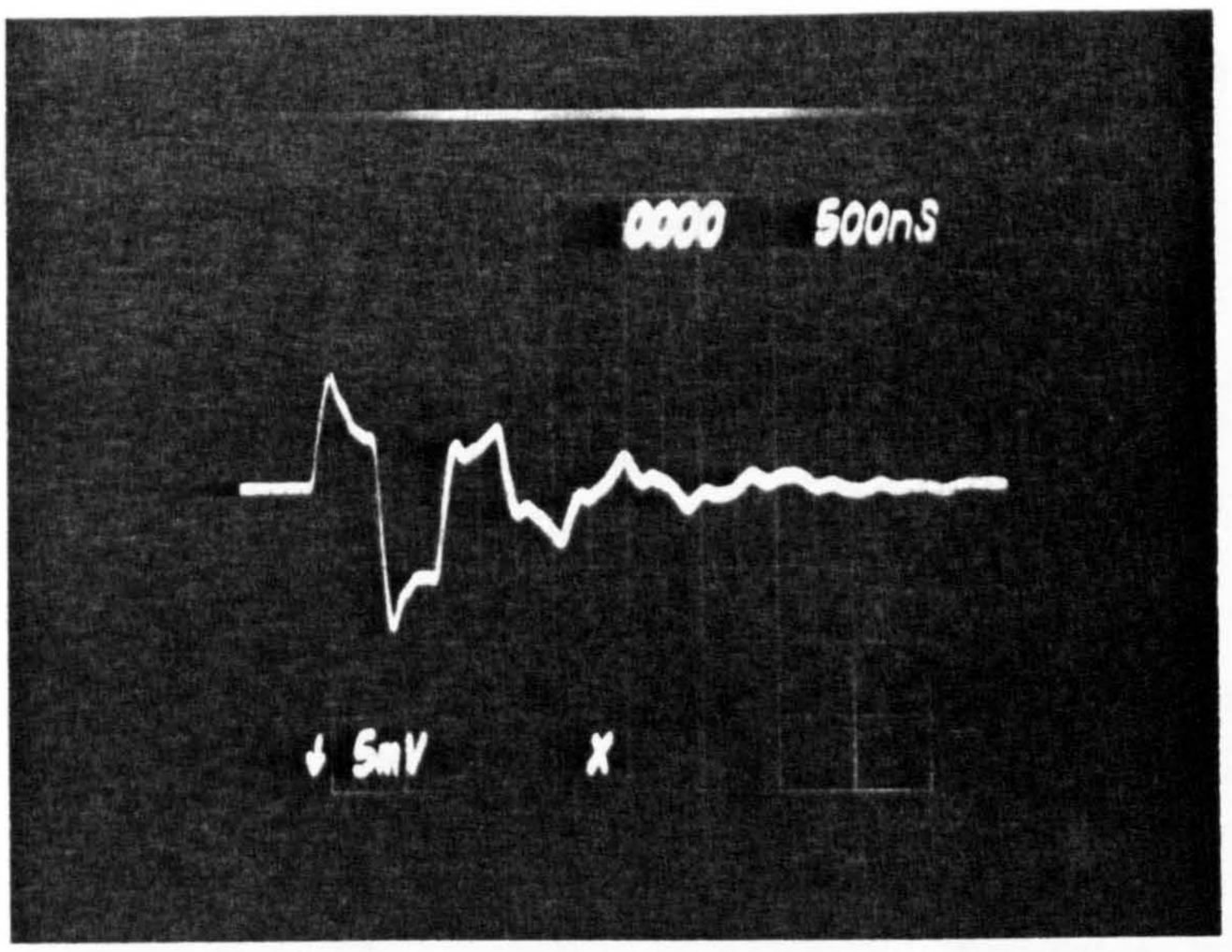

FIG 5.6C

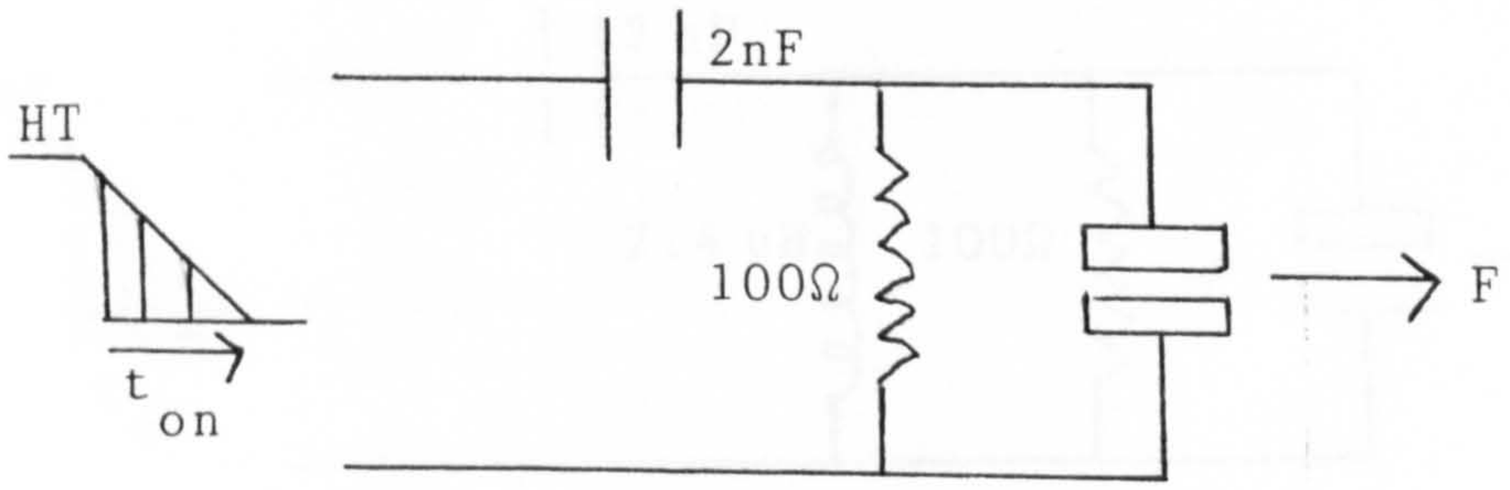

FIG 5.6A

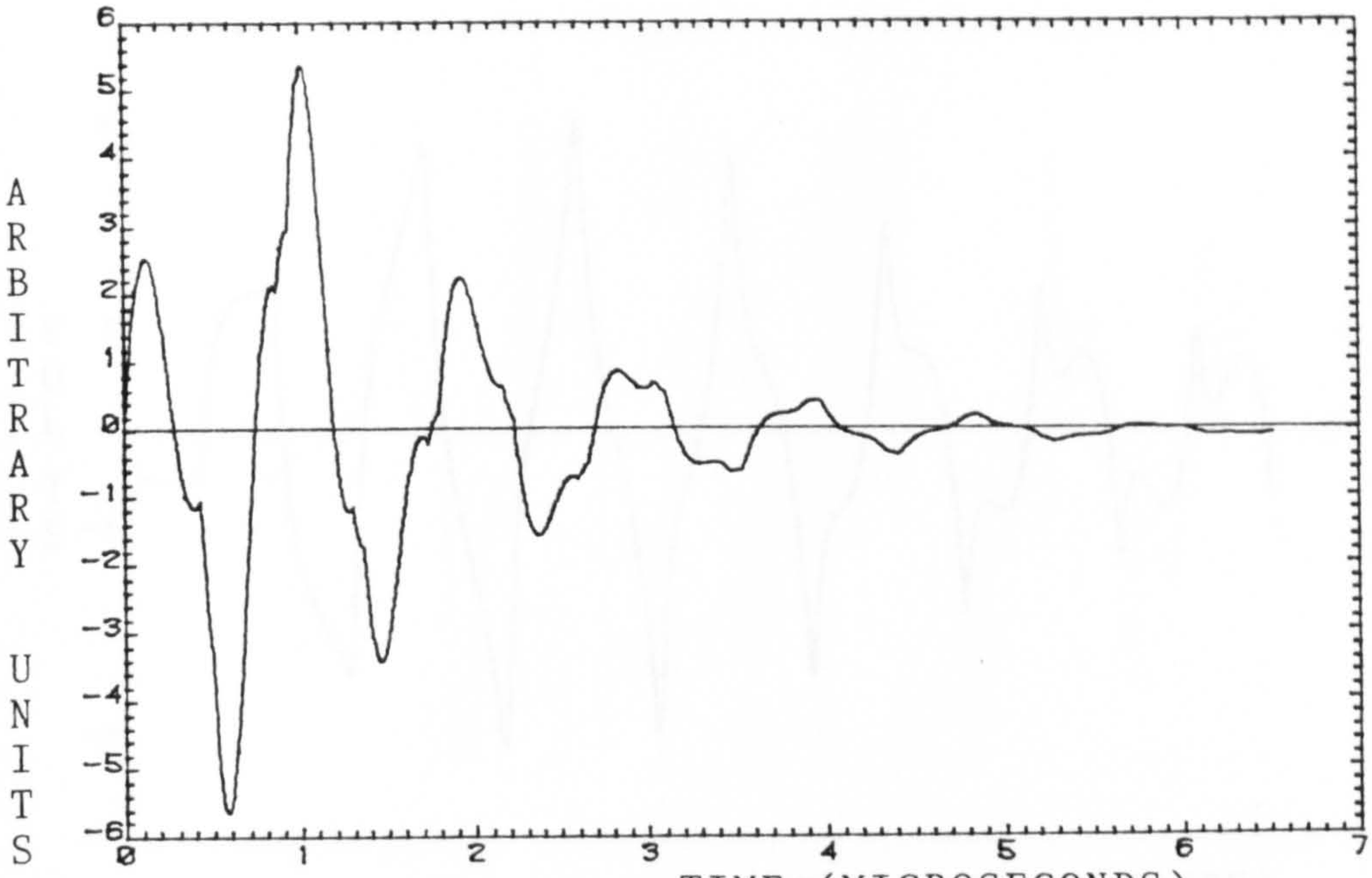

FIG 5.7B

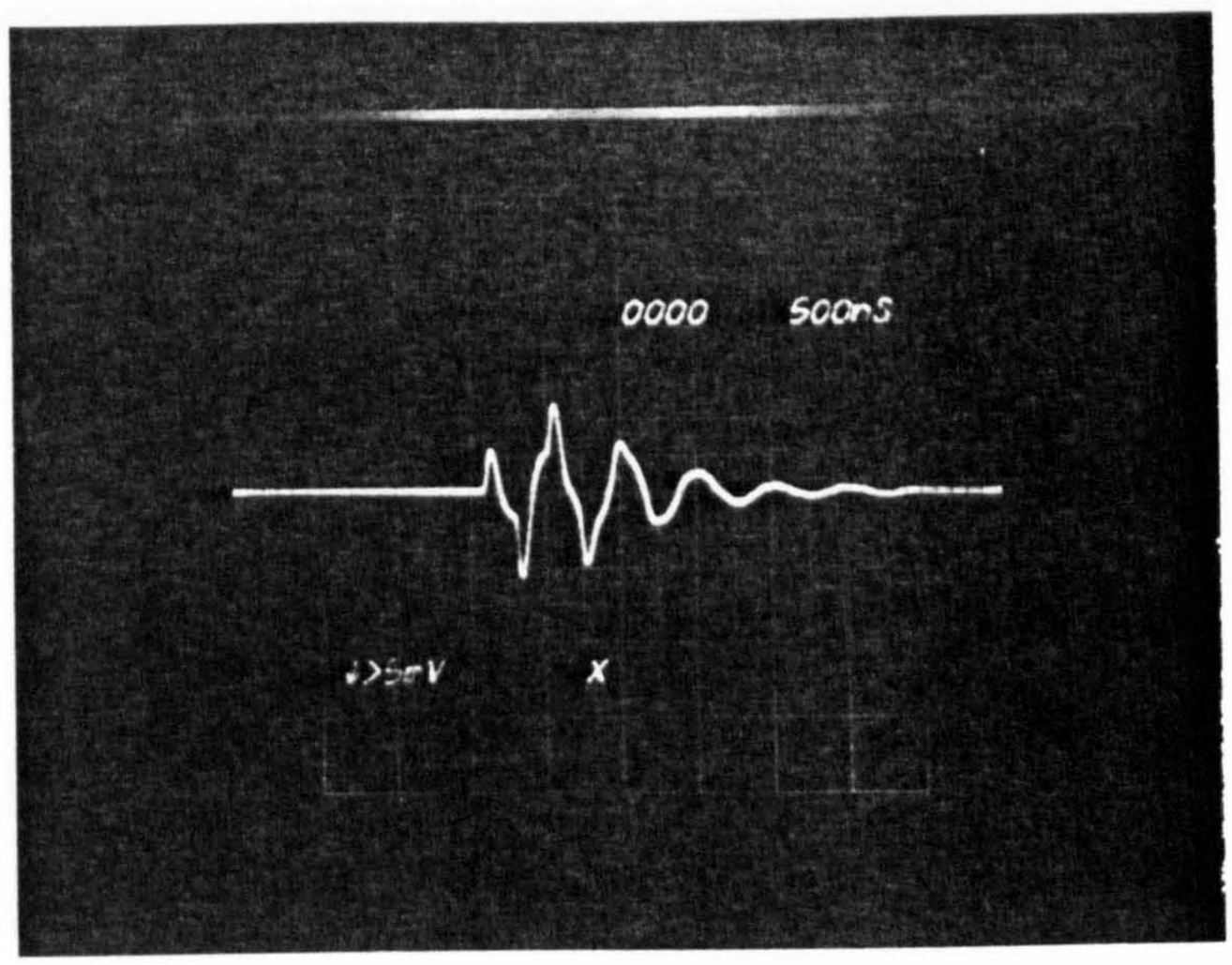

FIG 5.7C

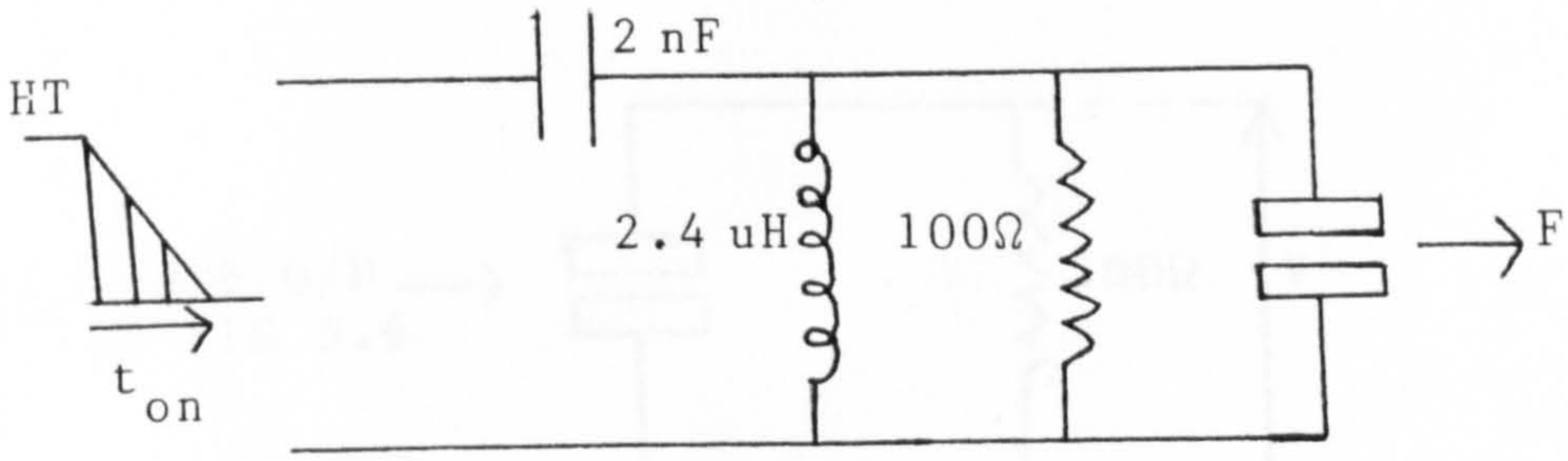

FIG 5.7A

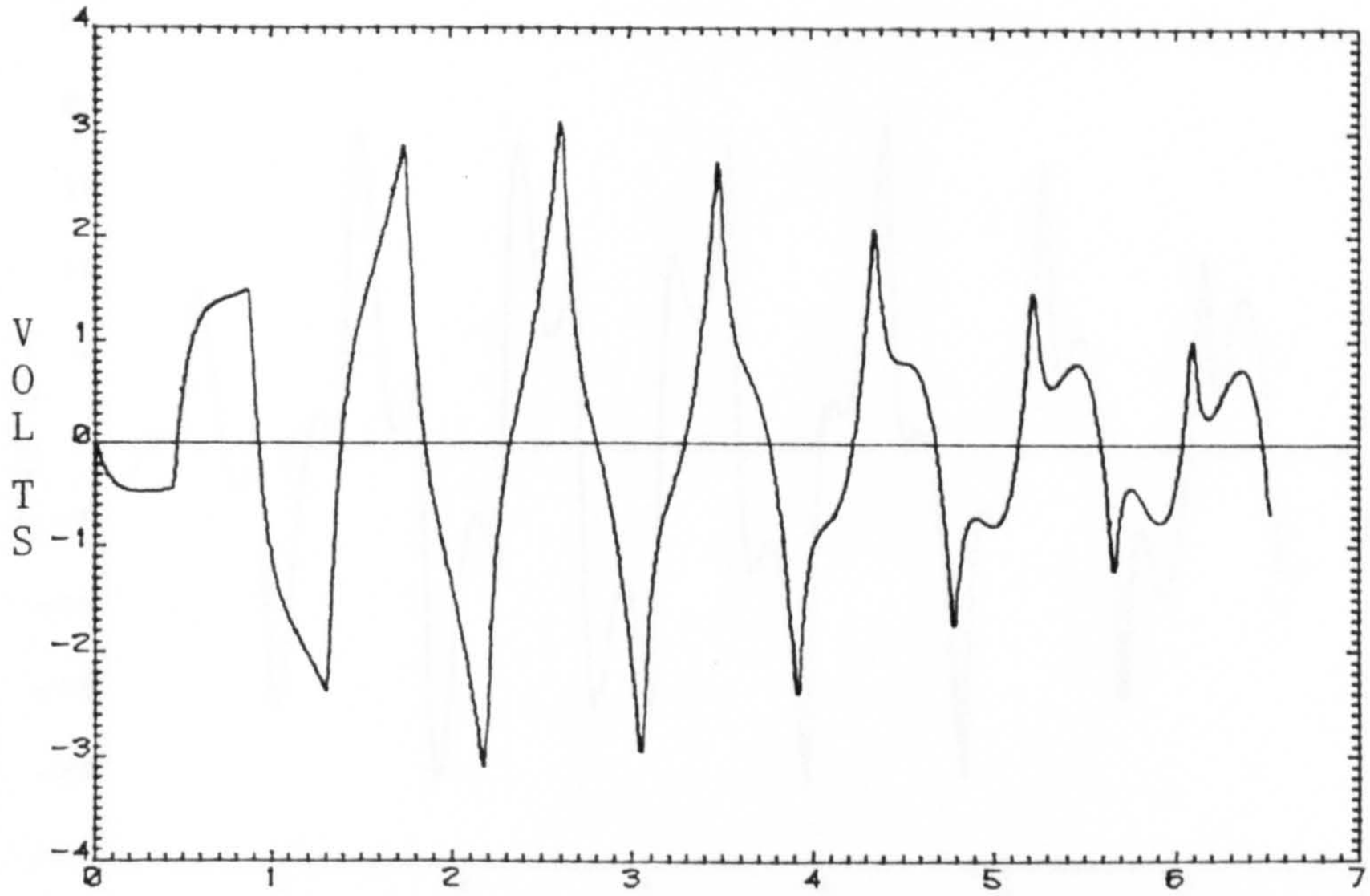

FIG 5.8B

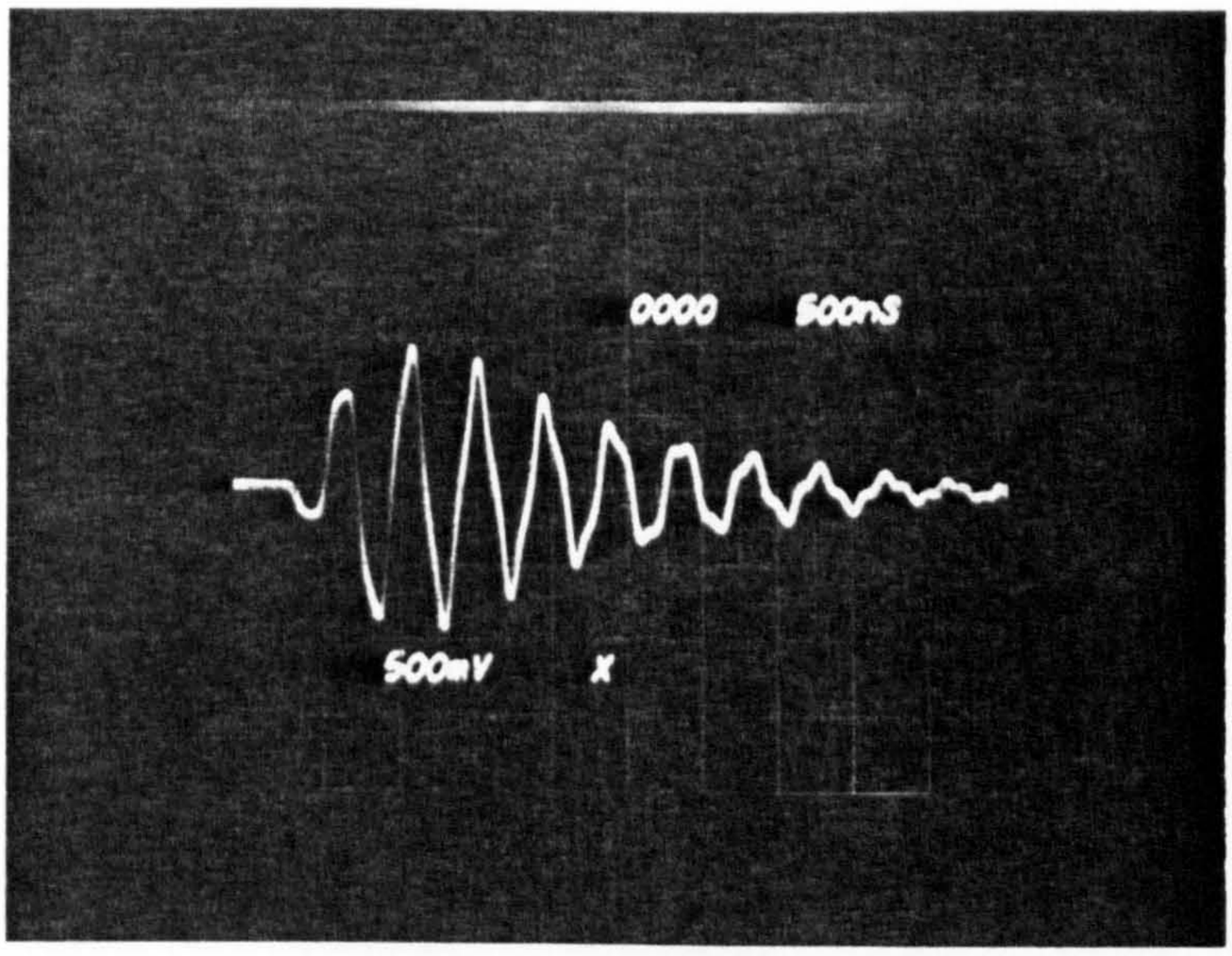

FIG 5.8C

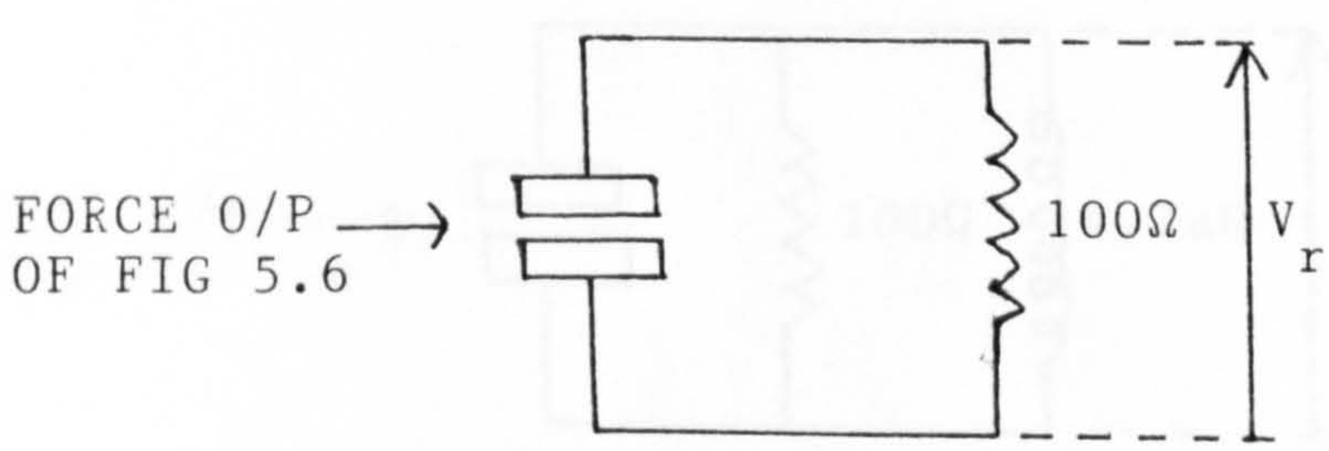

FIG 5.8A

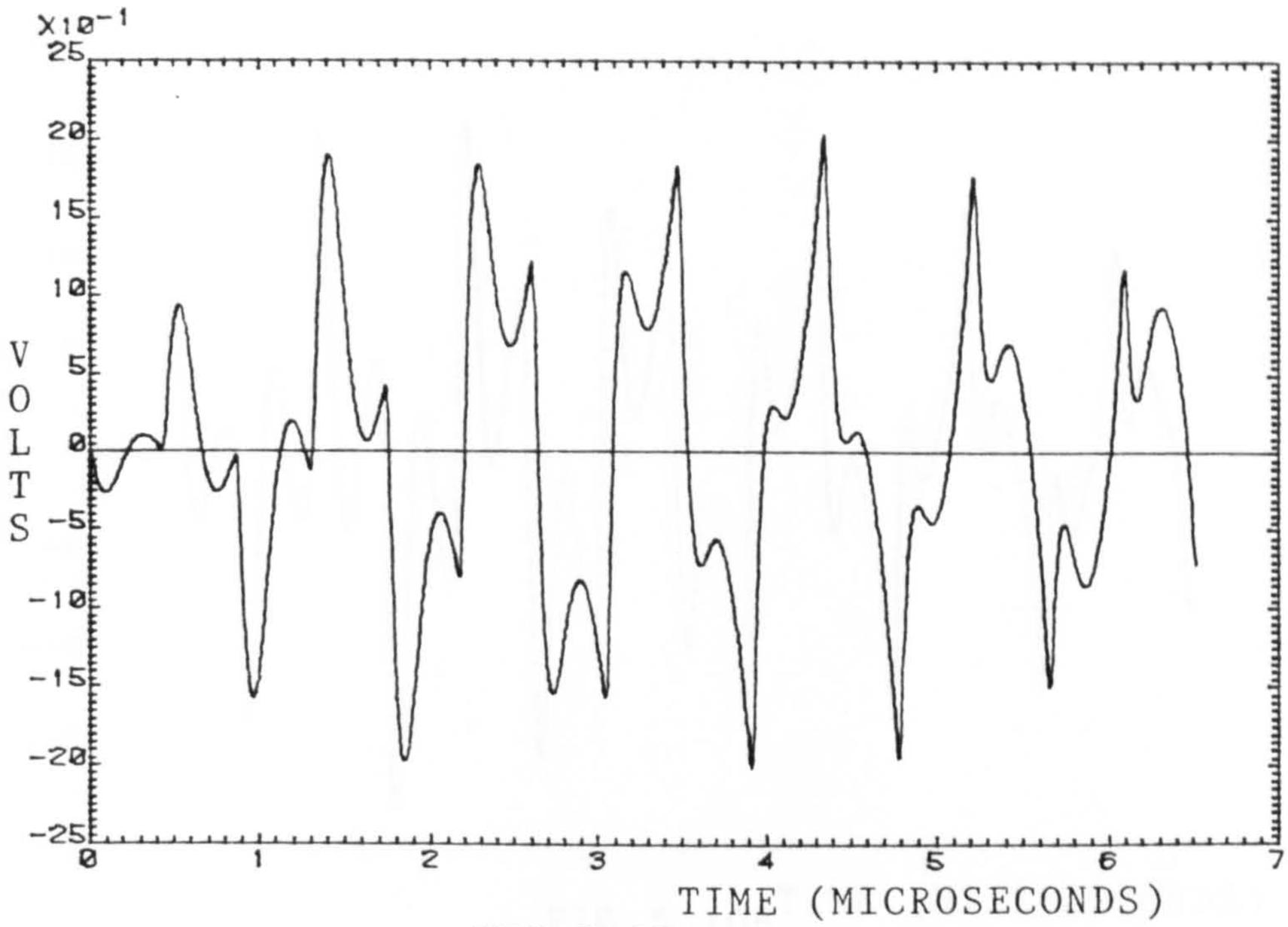

FIG 5.9B

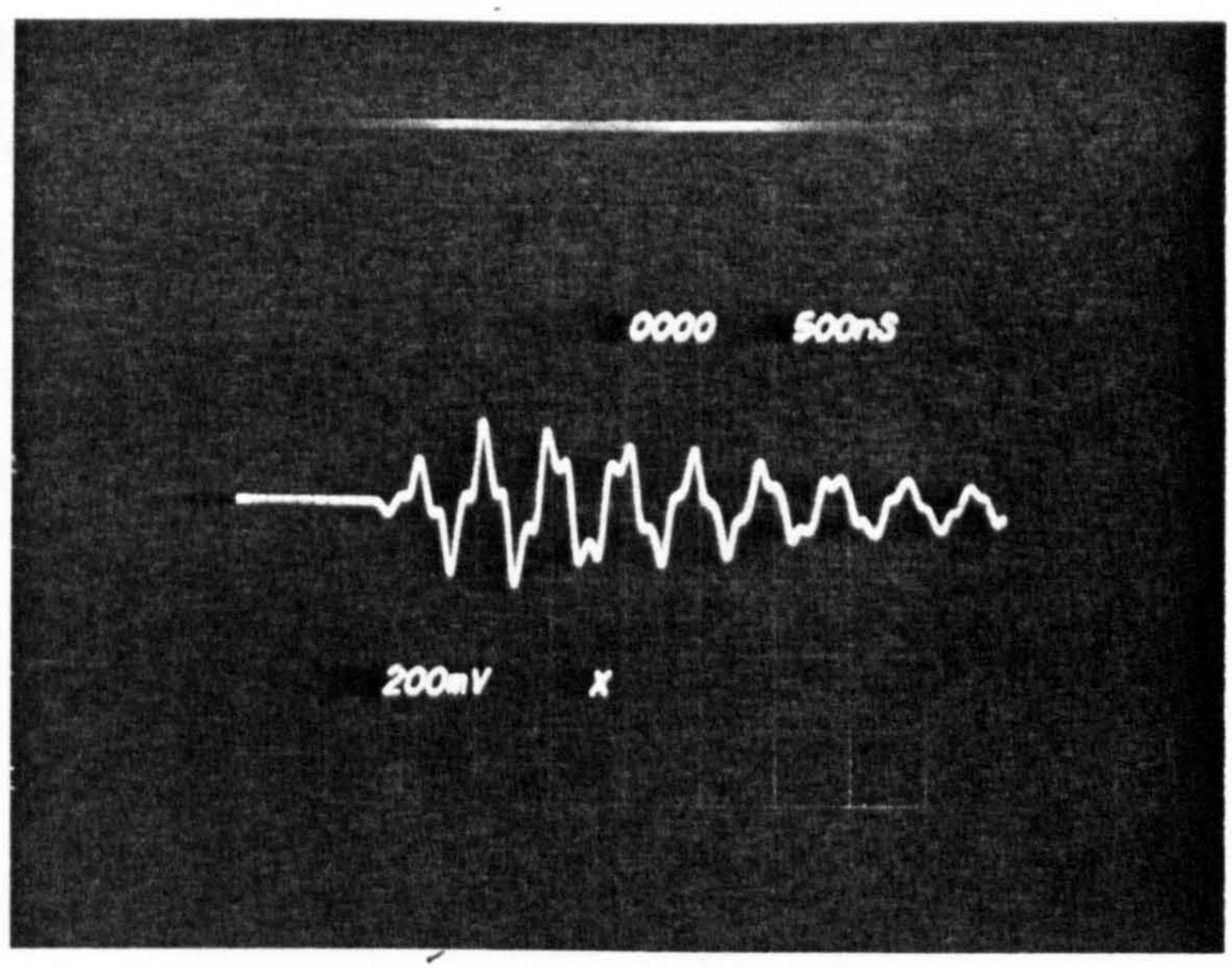

FIG 5.9C

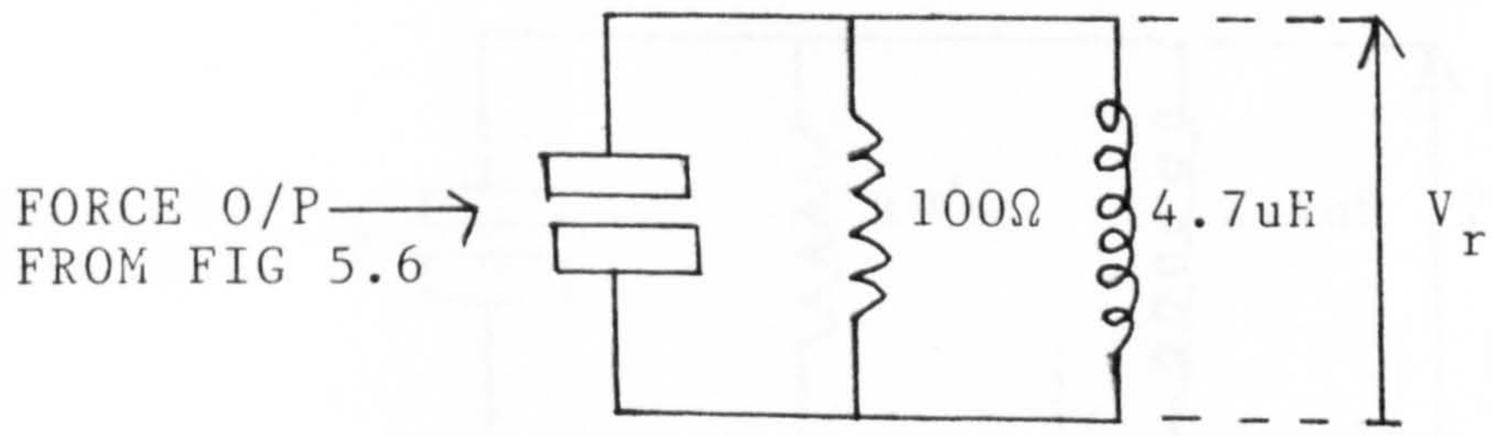

FIG 5.9A

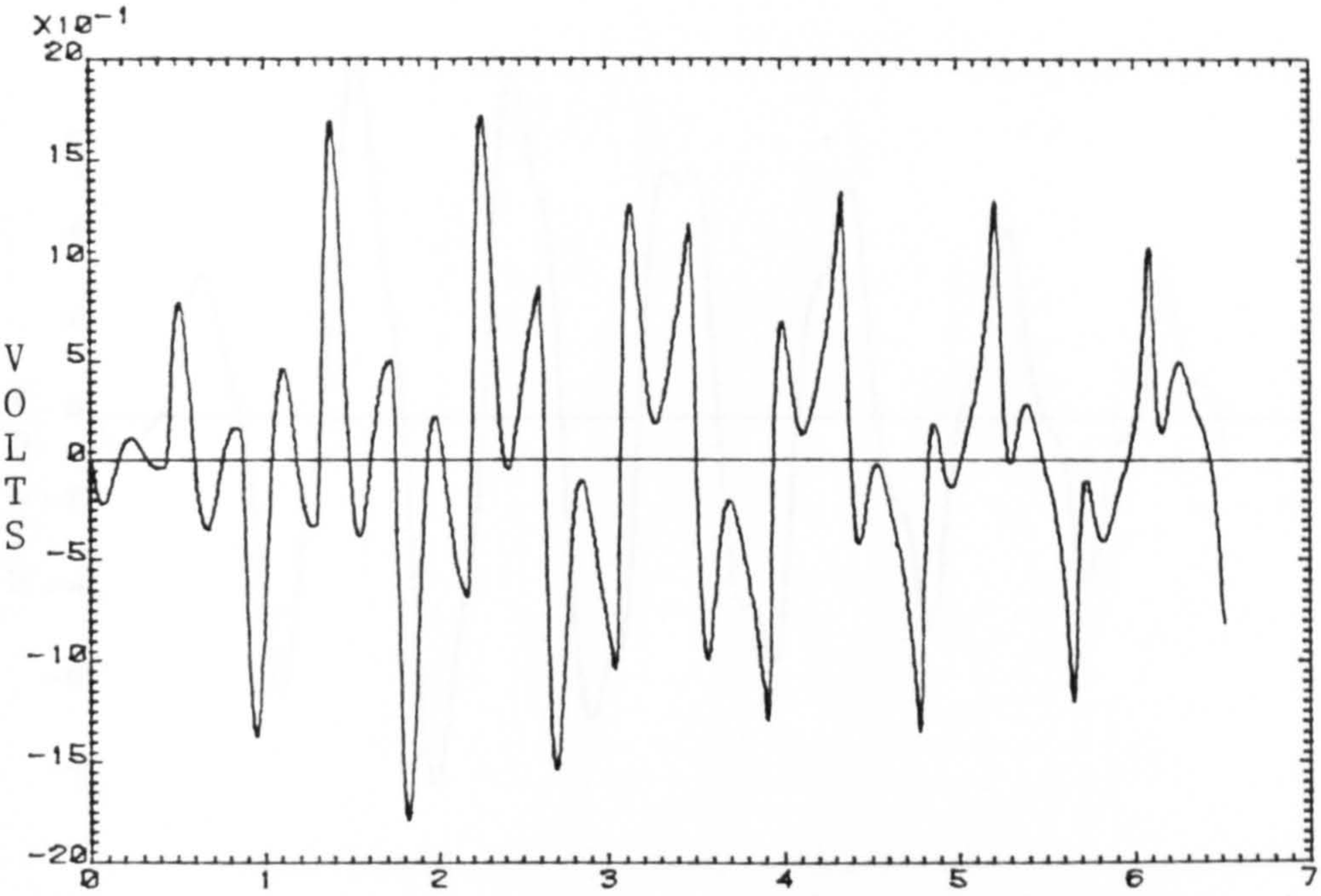

FIG 5.10B

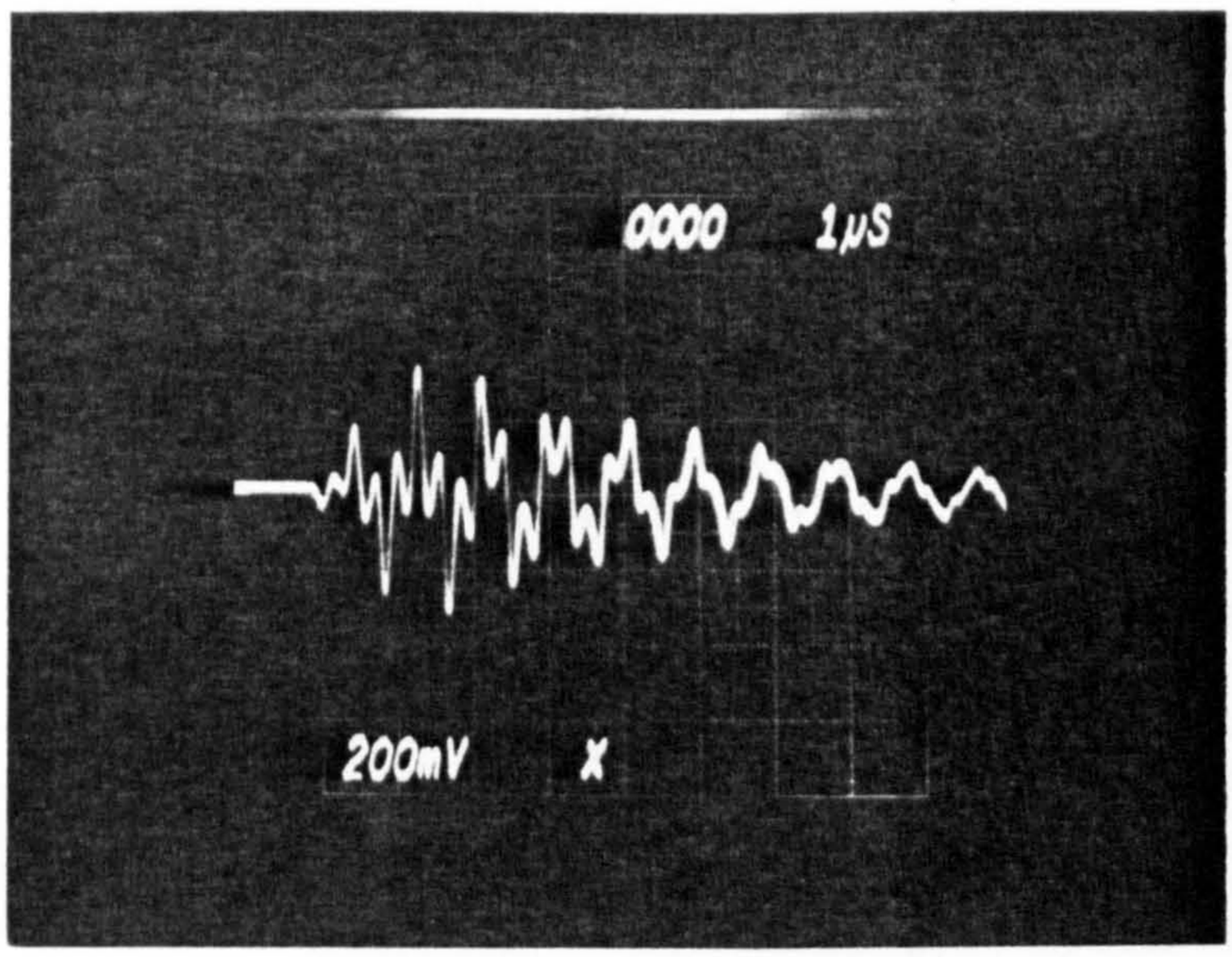

FIG 5.10C

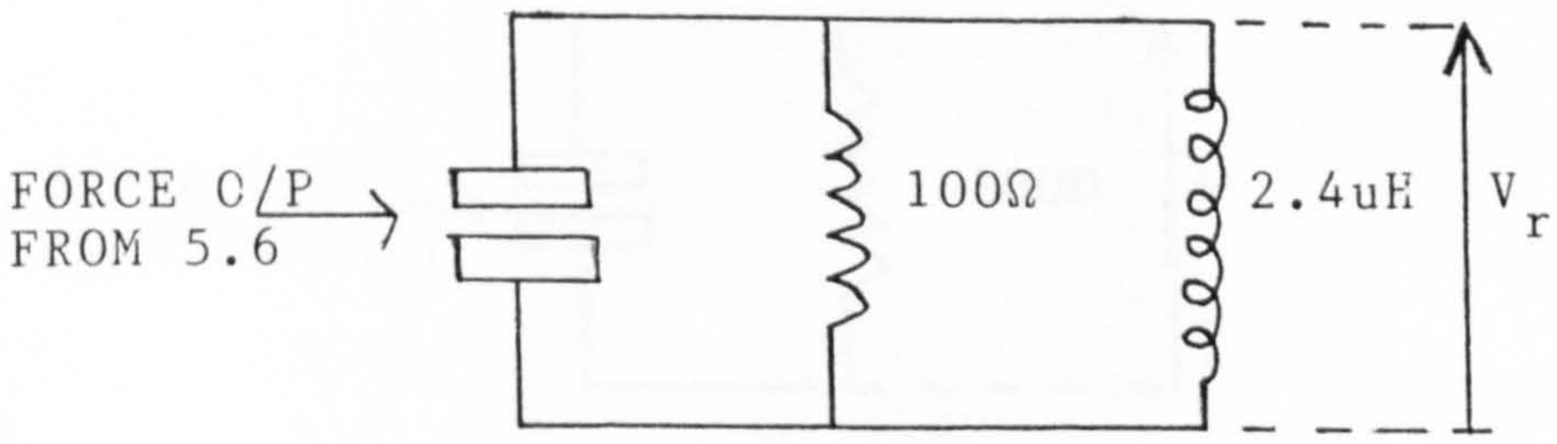

FIG 5.10A

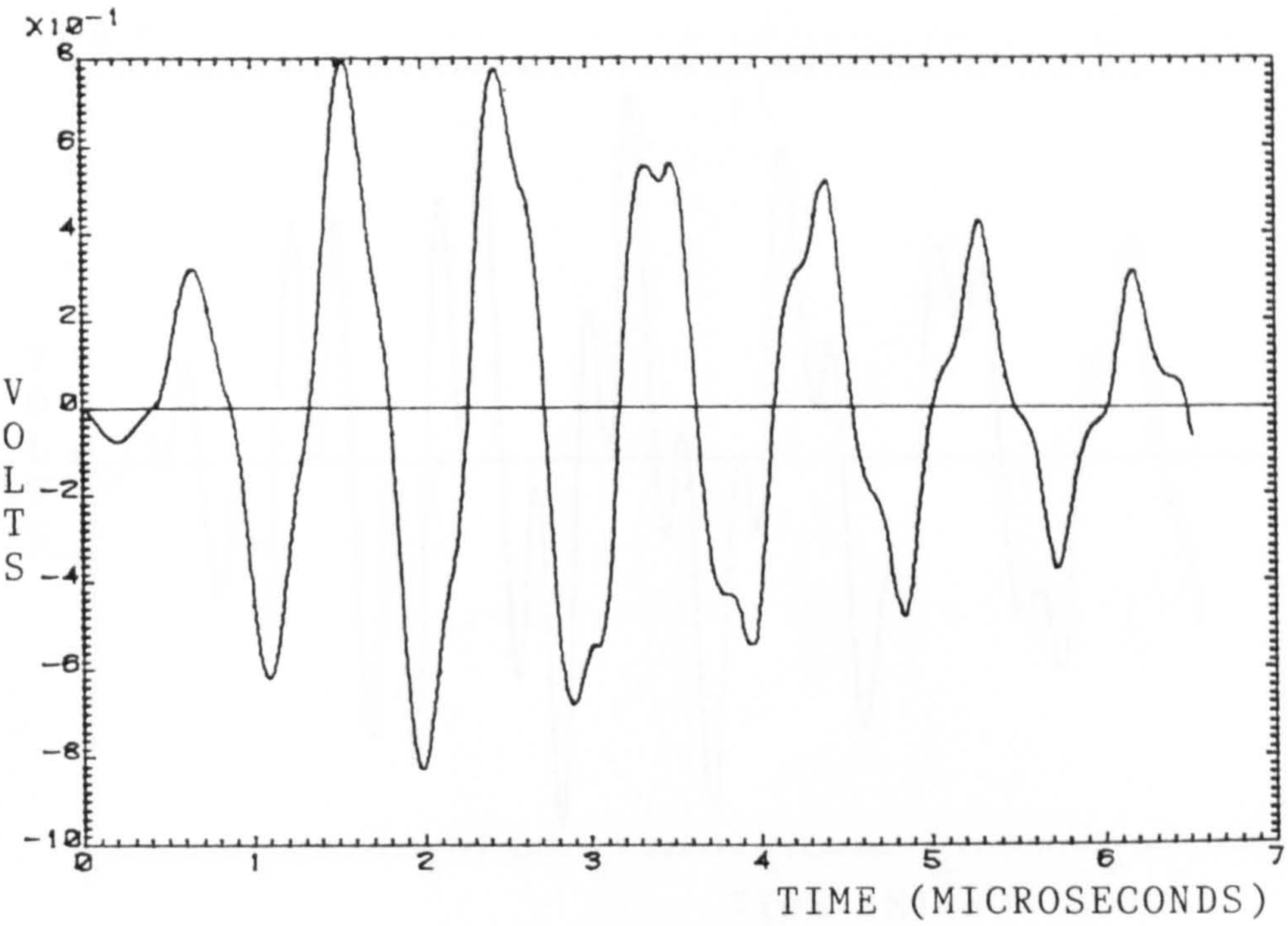

FIG 5.11B

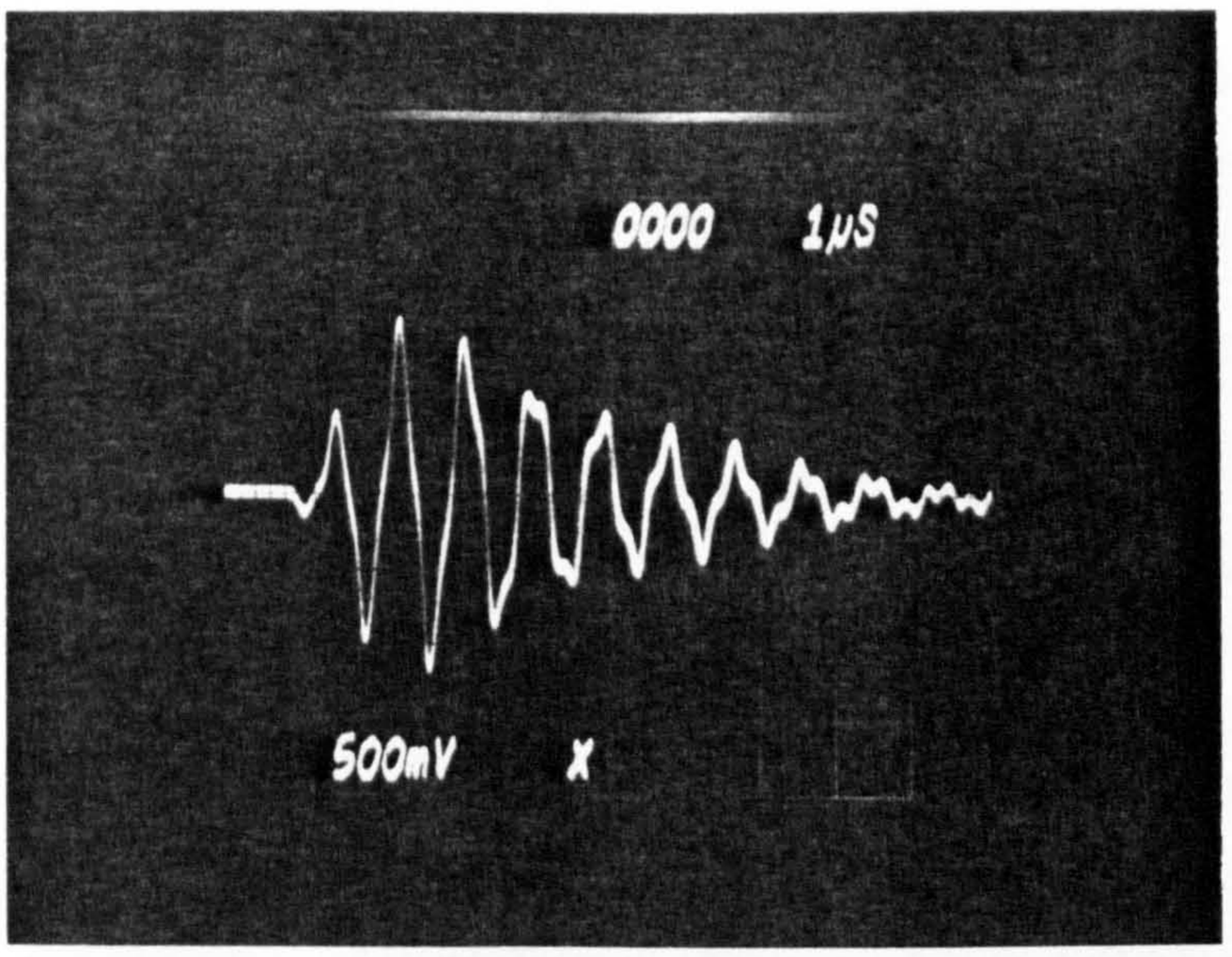

FIG 5.11C

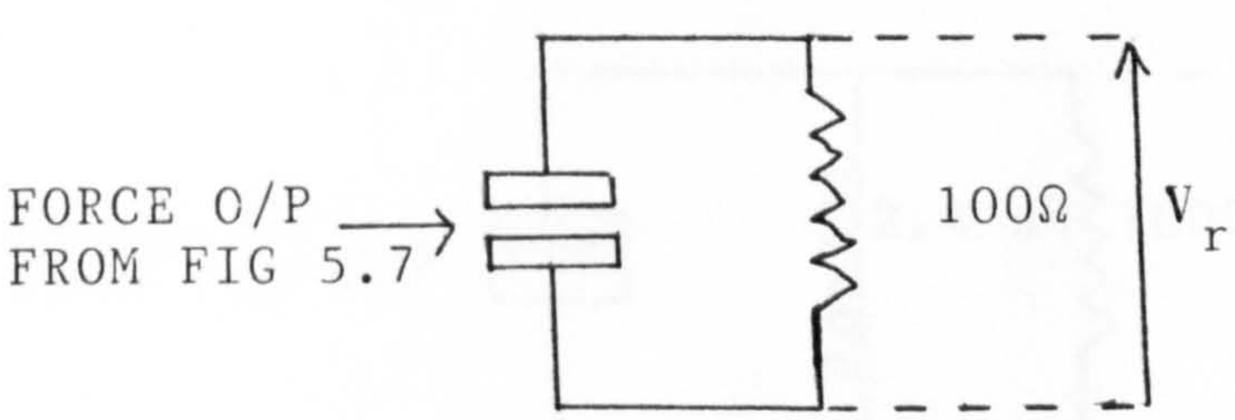

FIG 5.11A

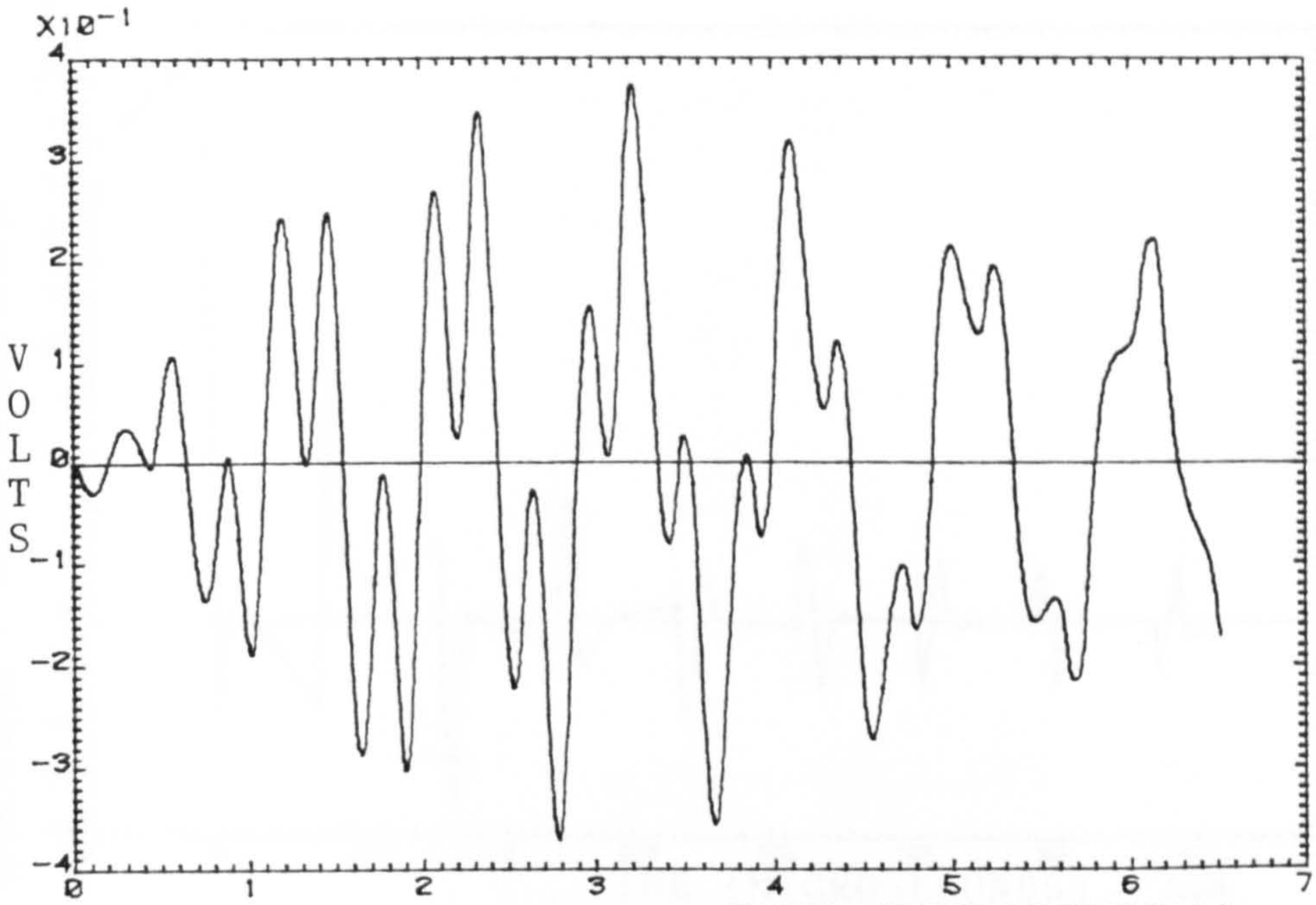

FIG 5.12B

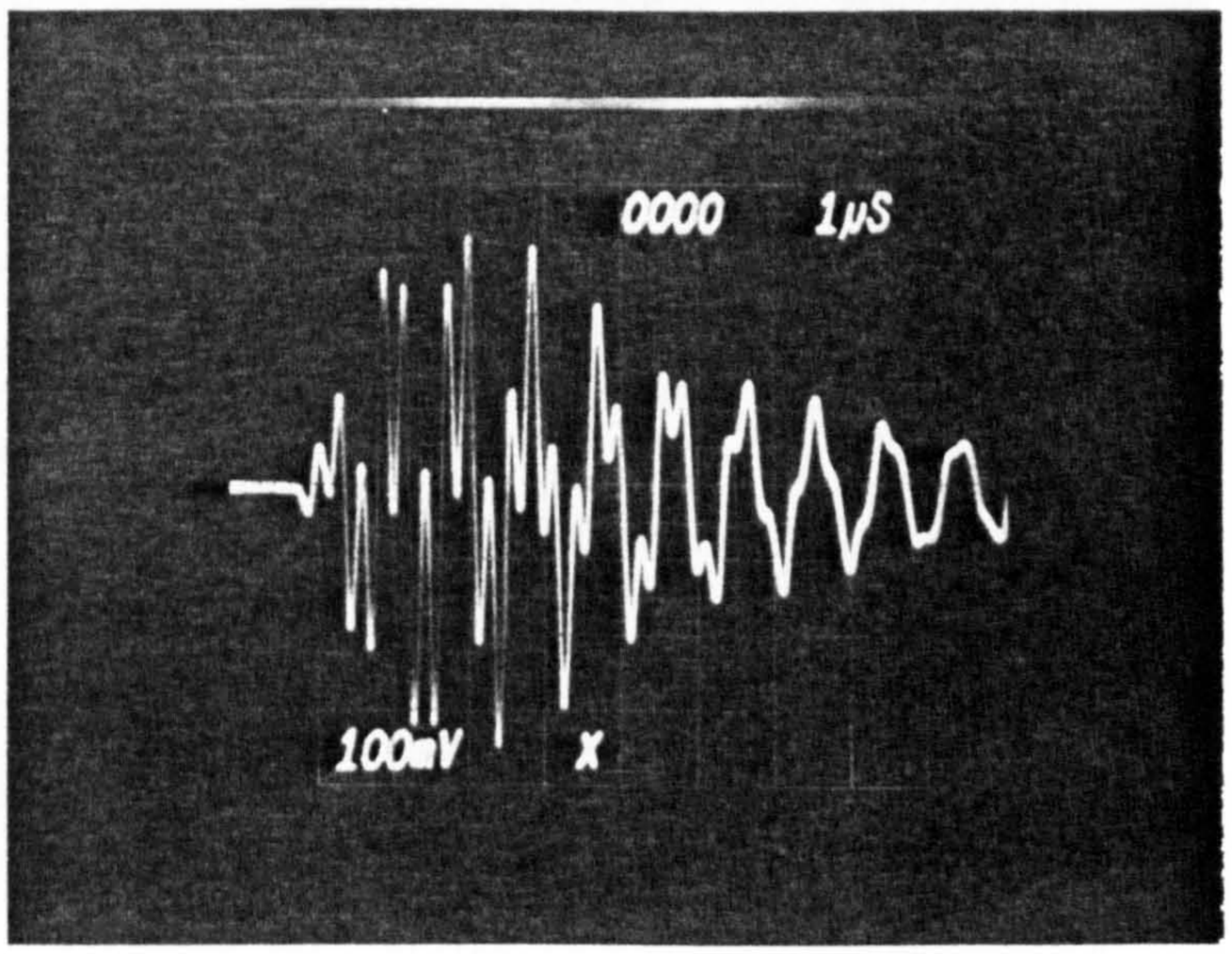

FIG 5.12C

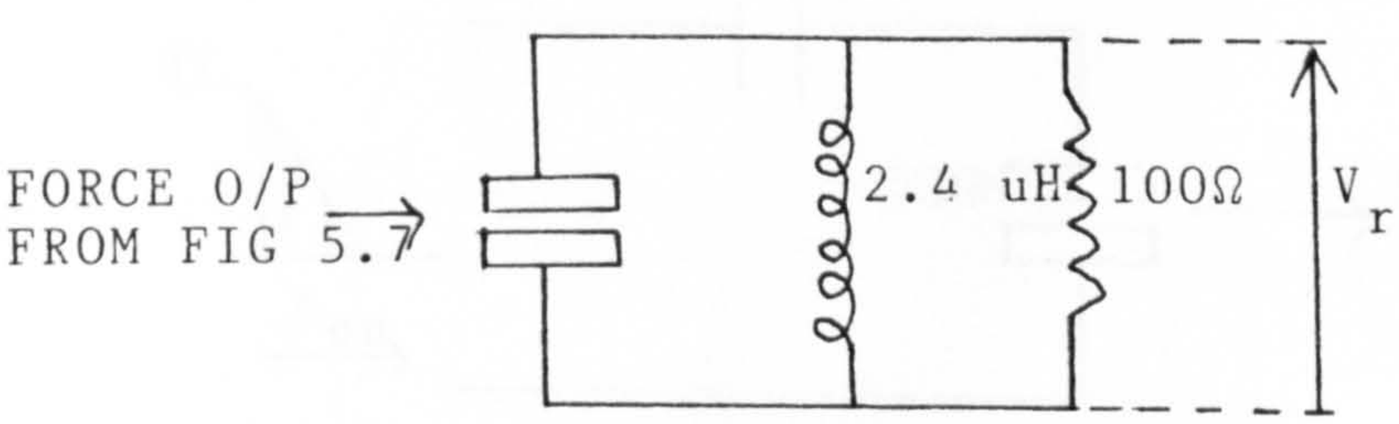

FIG 5.12A

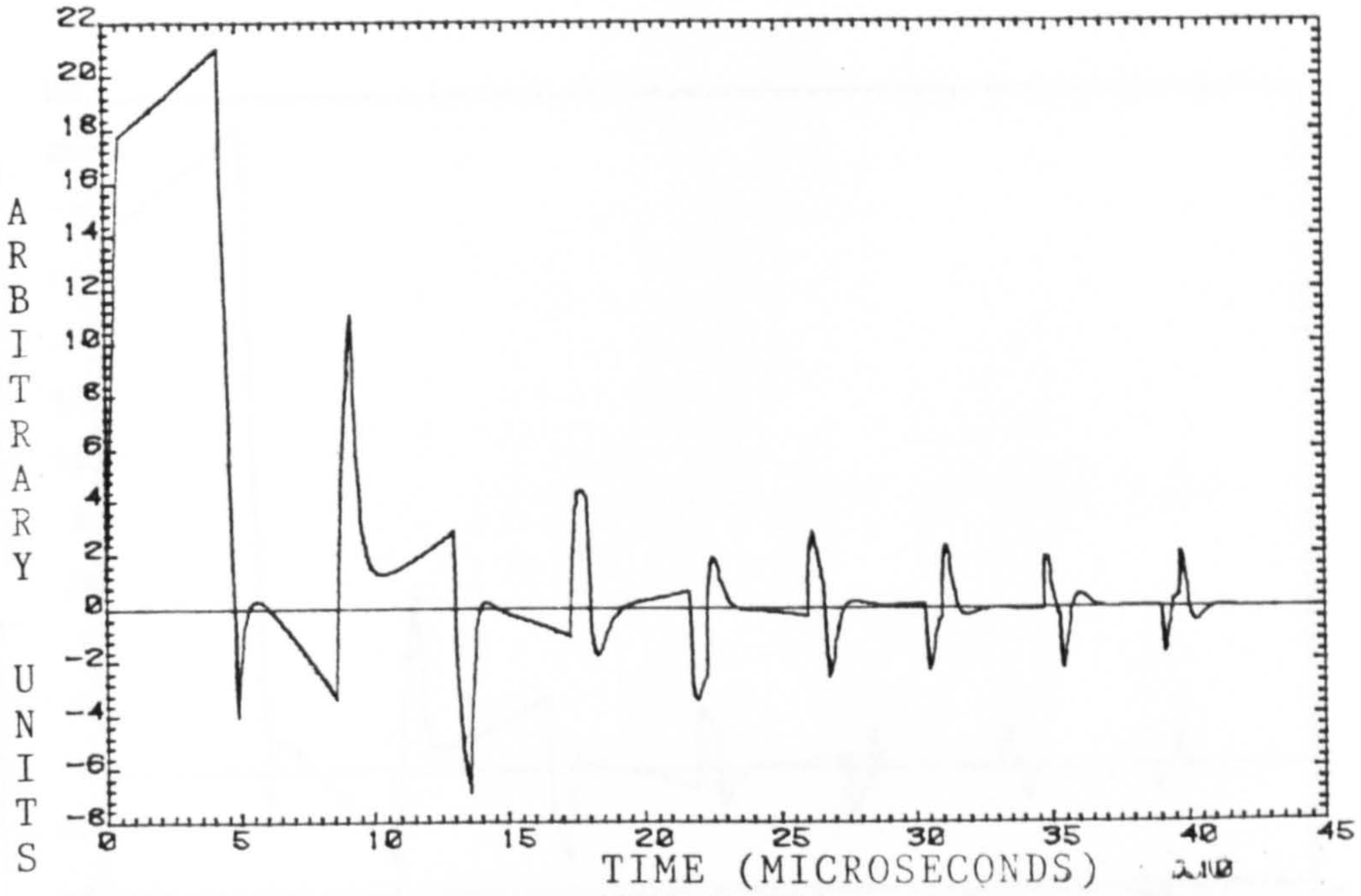

FIG 5.13B

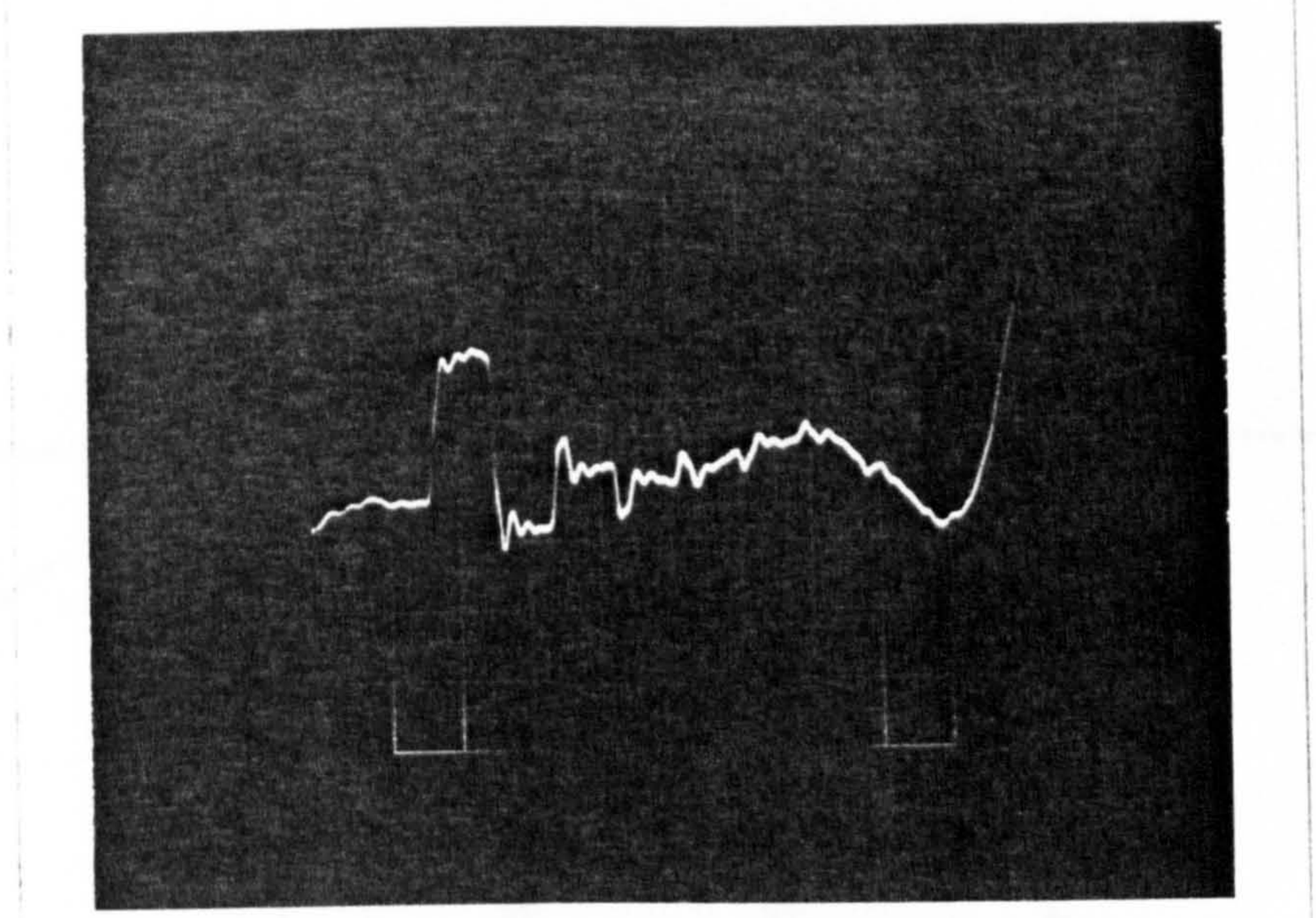

FIG 5.13C

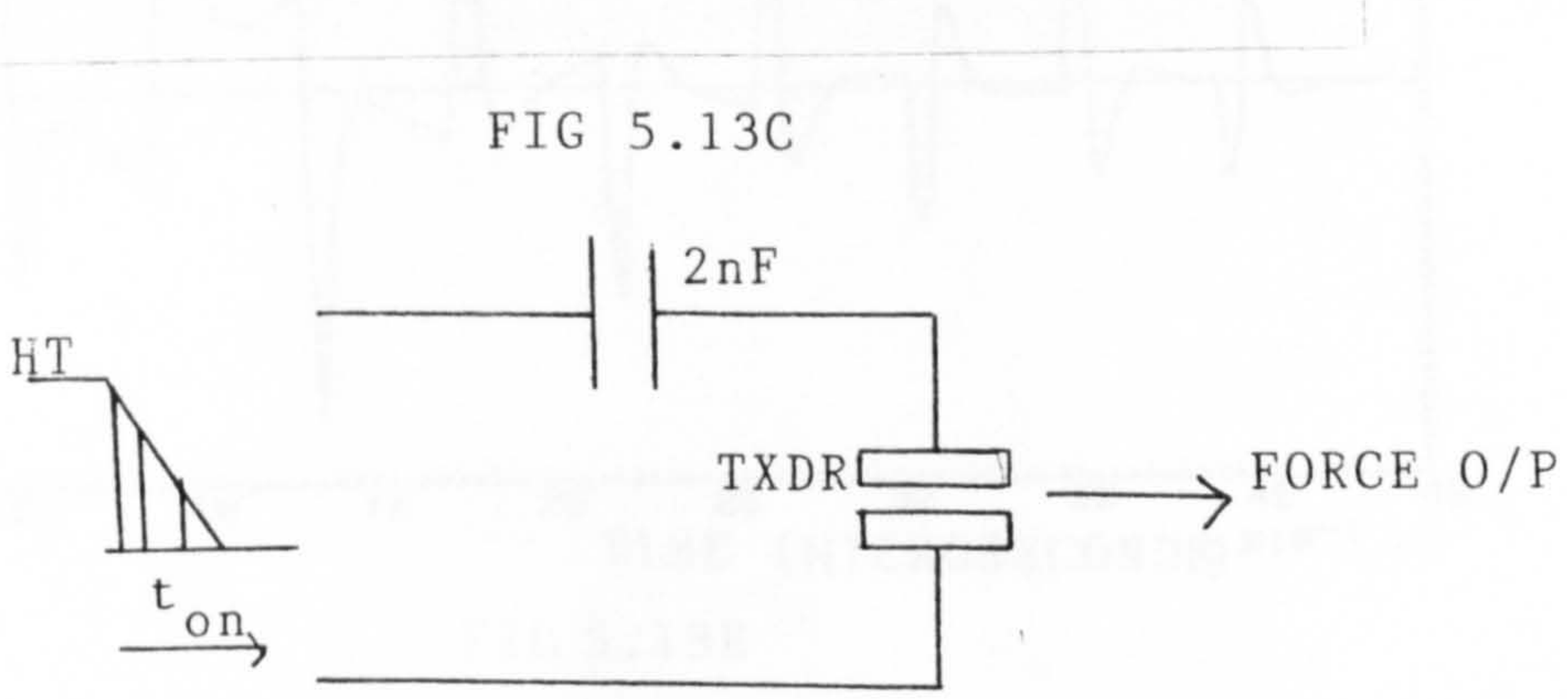

FIG 5.13A

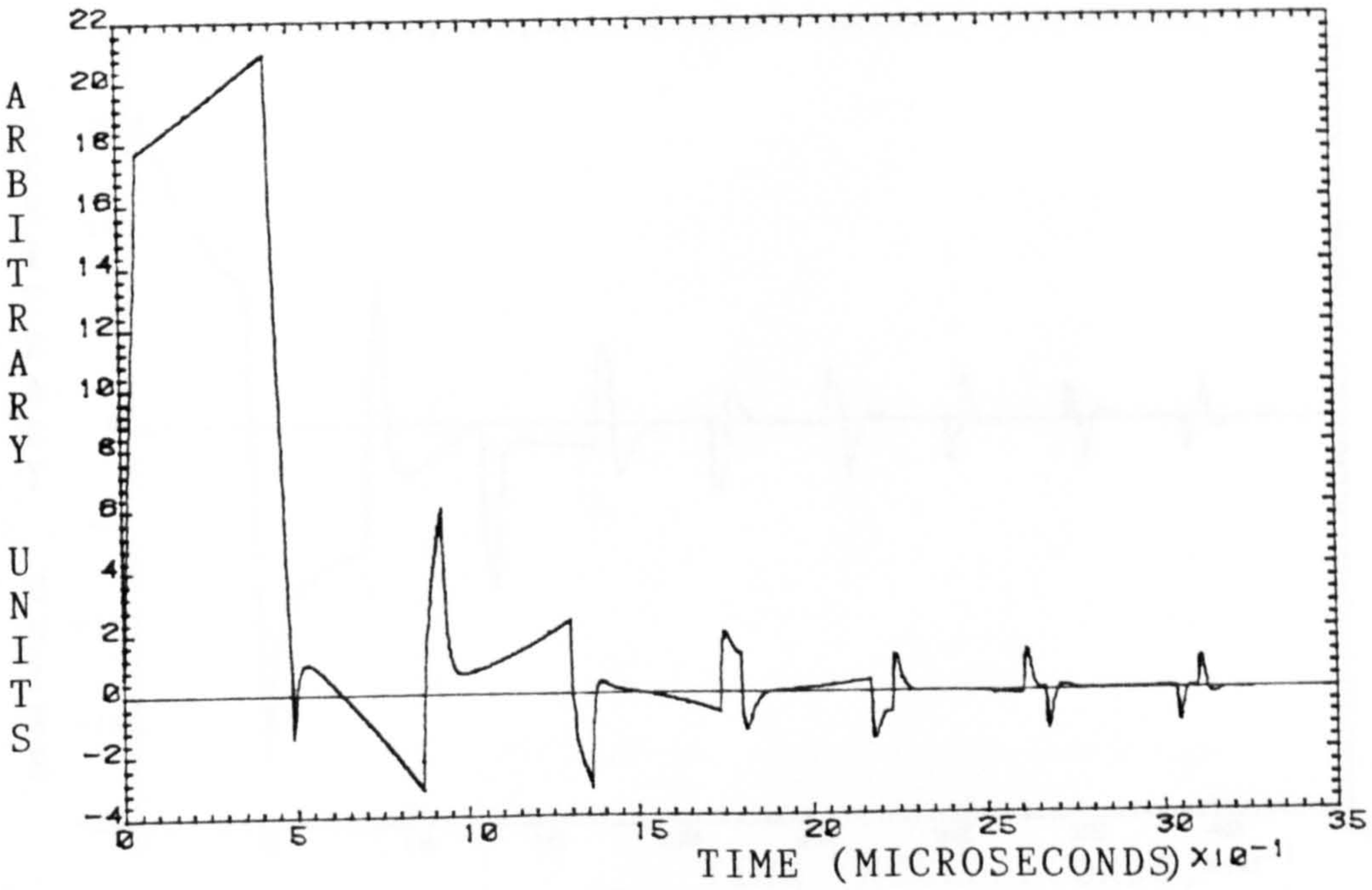

FIG 5.13D

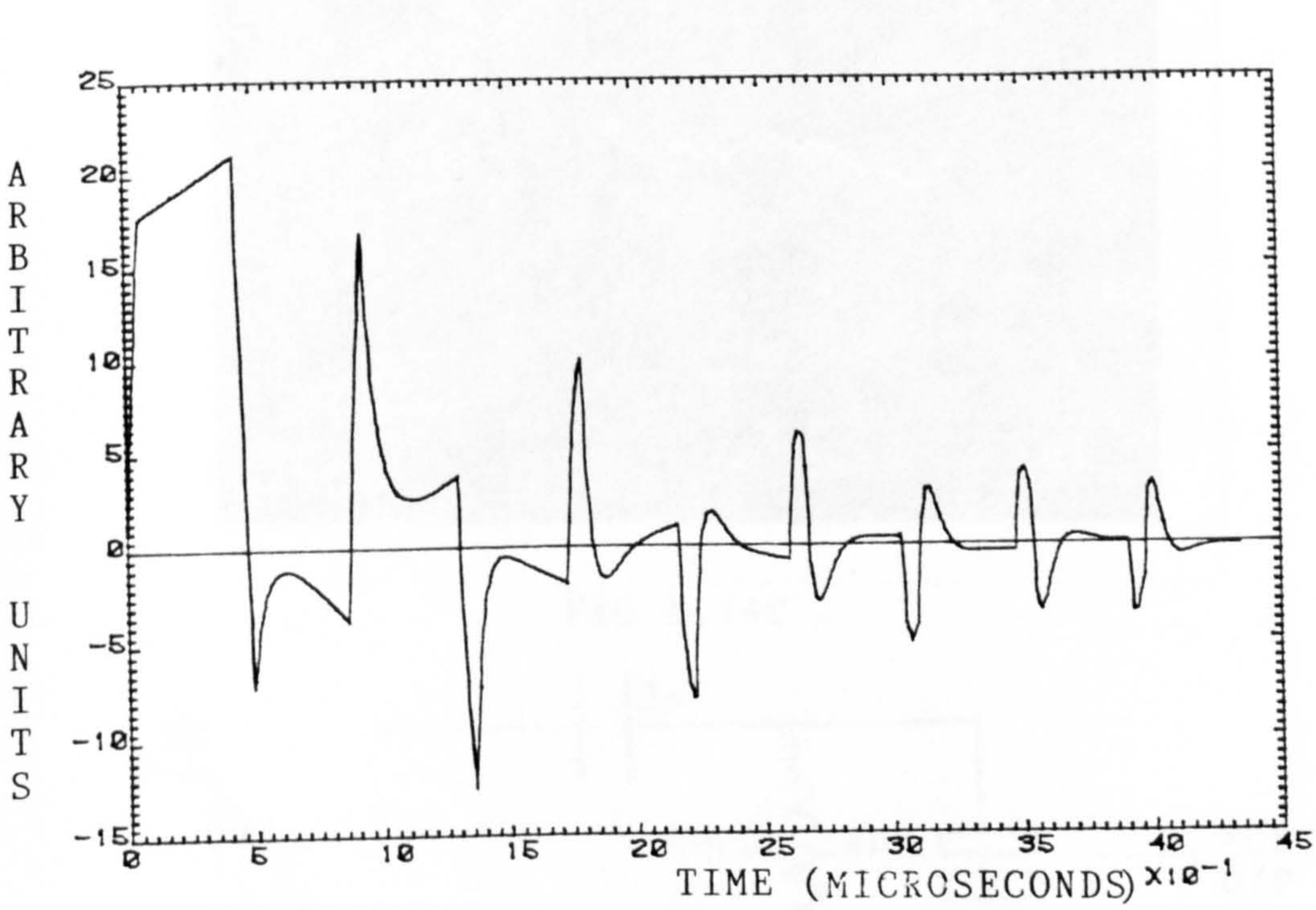

FIG 5.13E

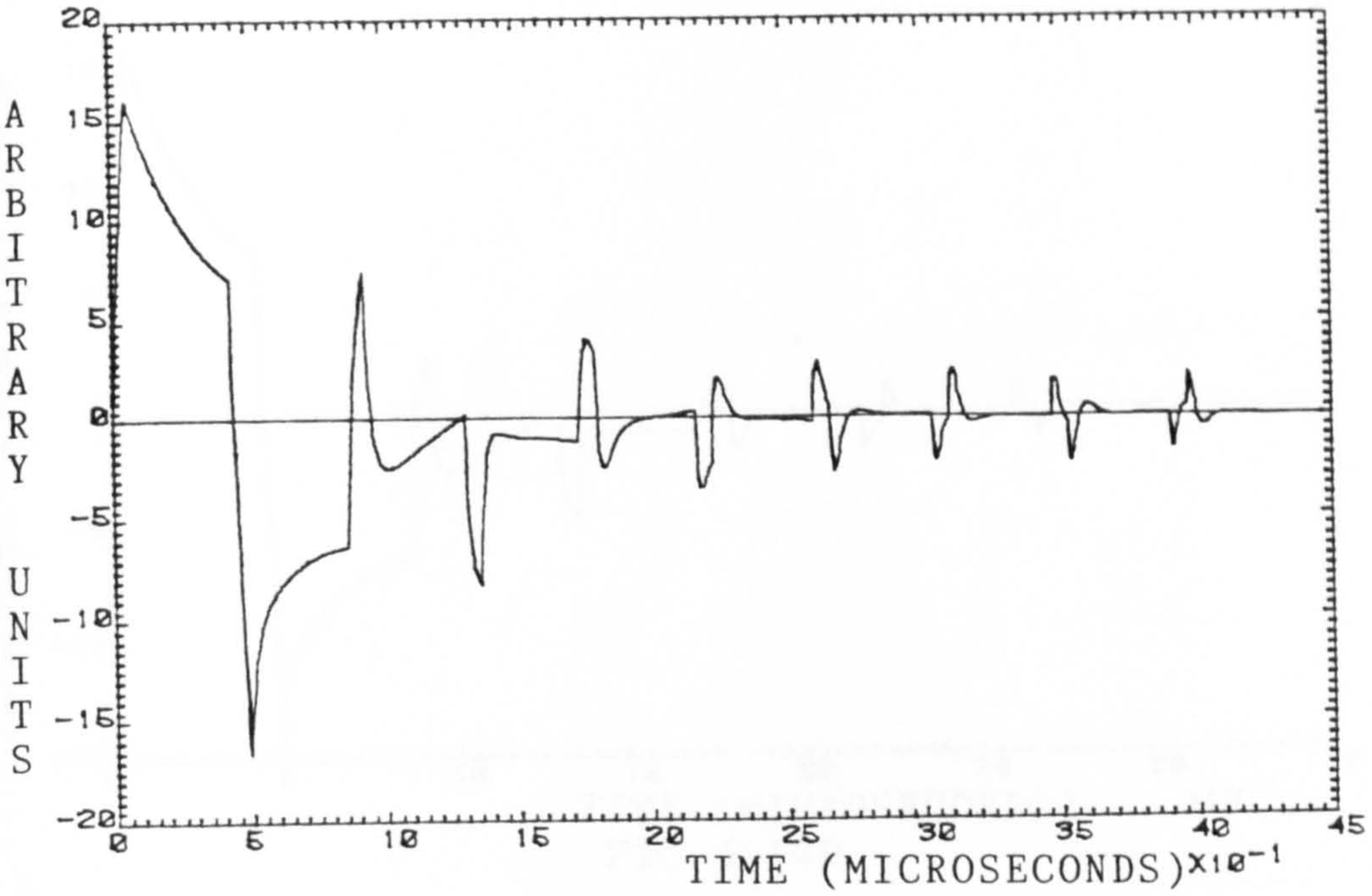

FIG 5.14B

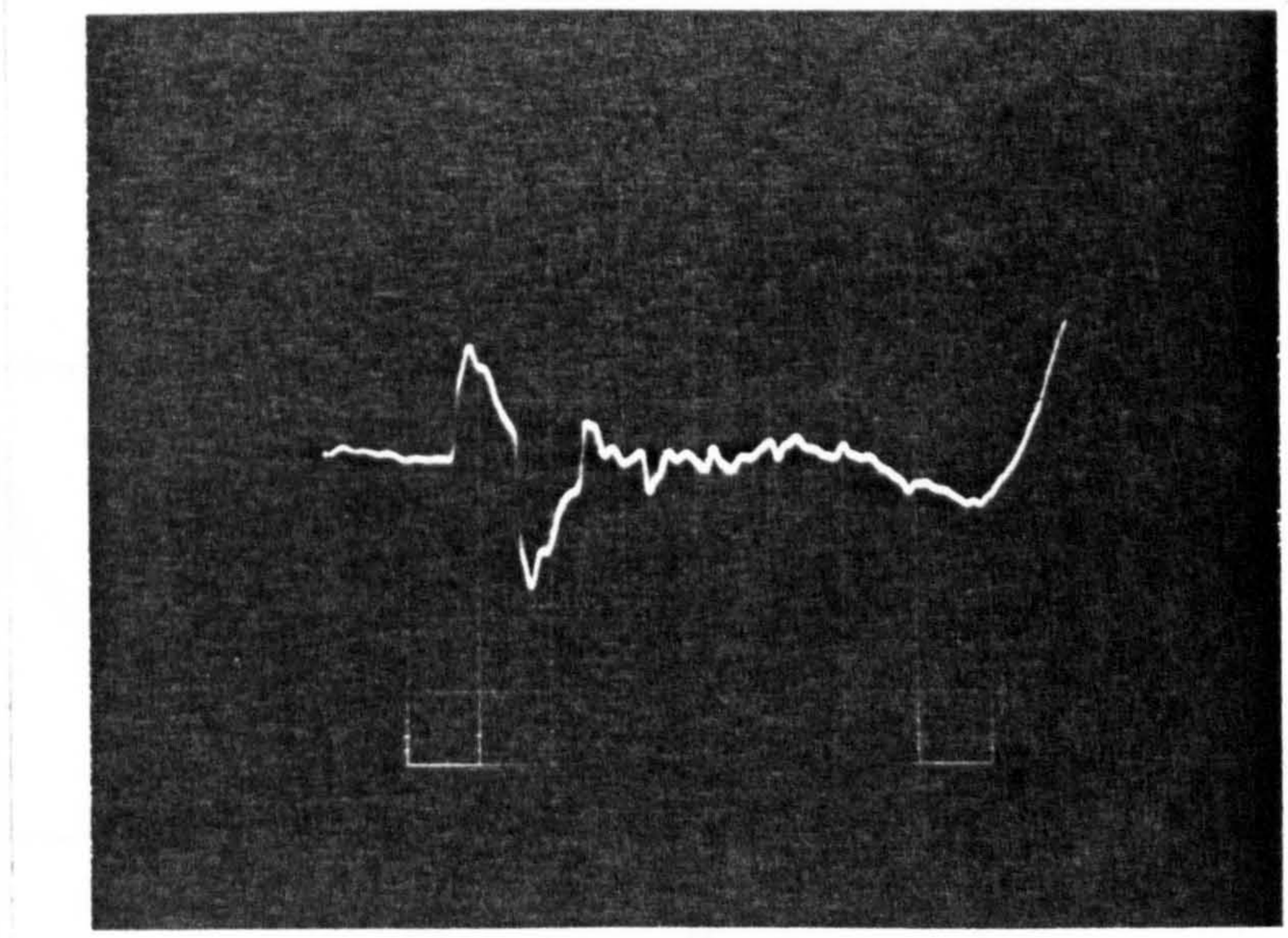

FIG 5.14C

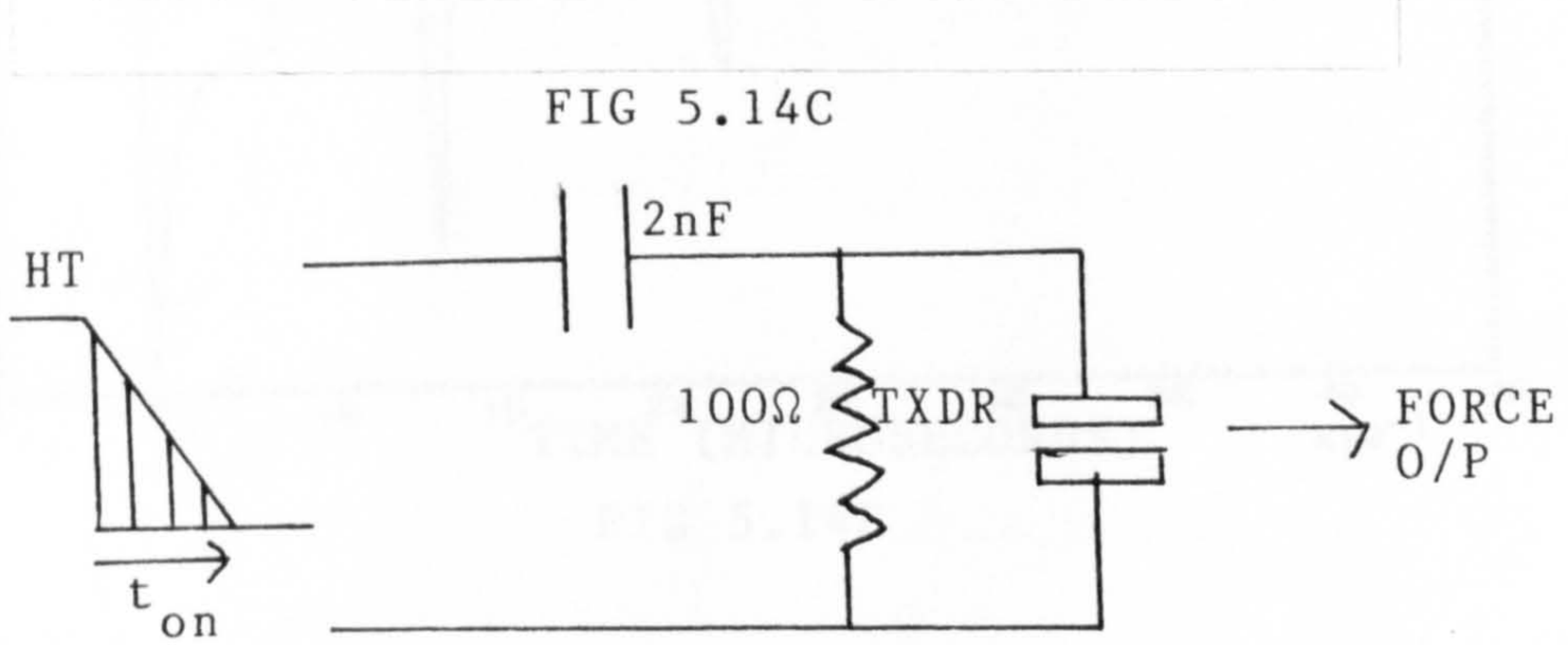

FIG 5.14A

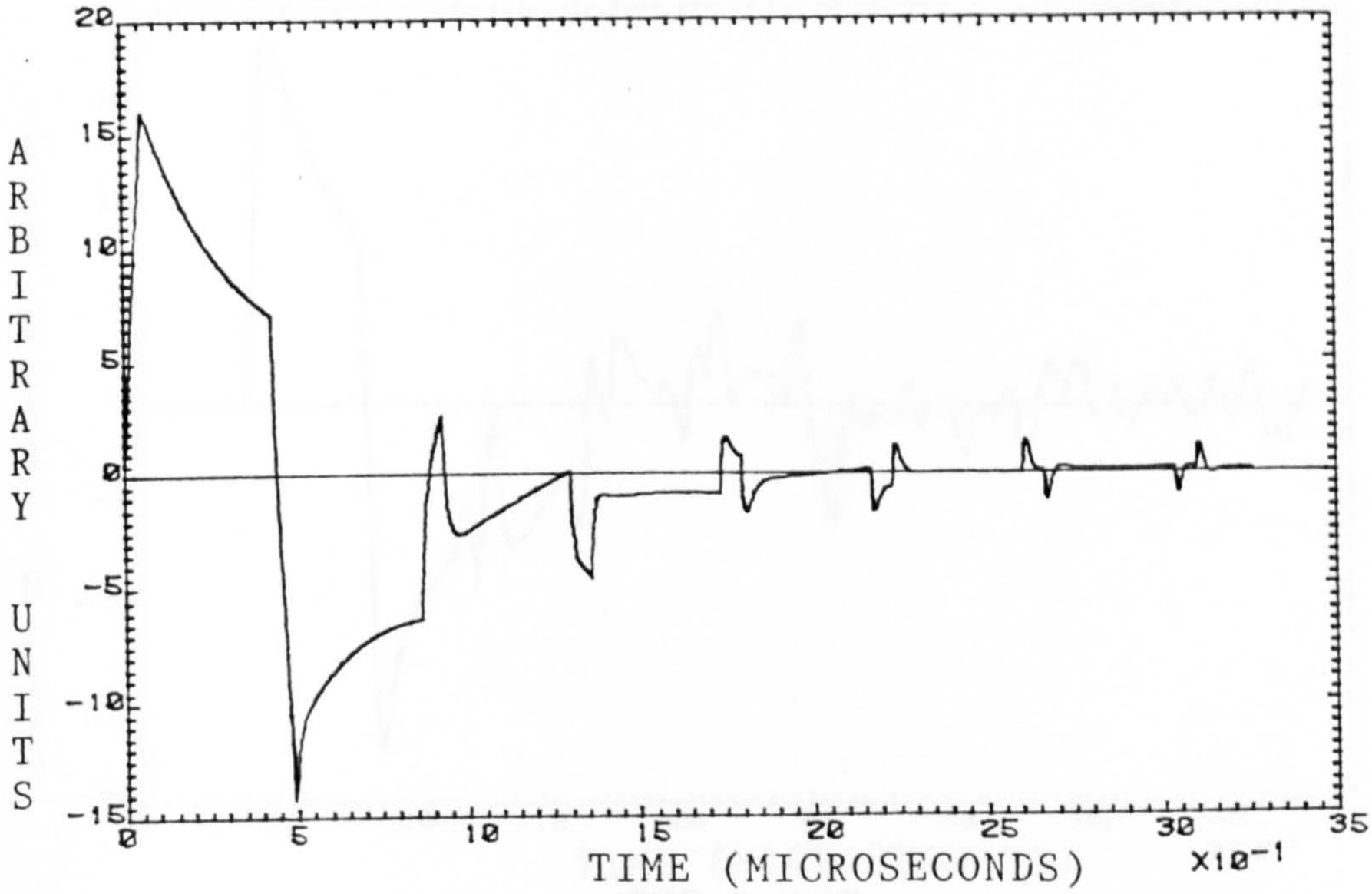

FIG 5.14D

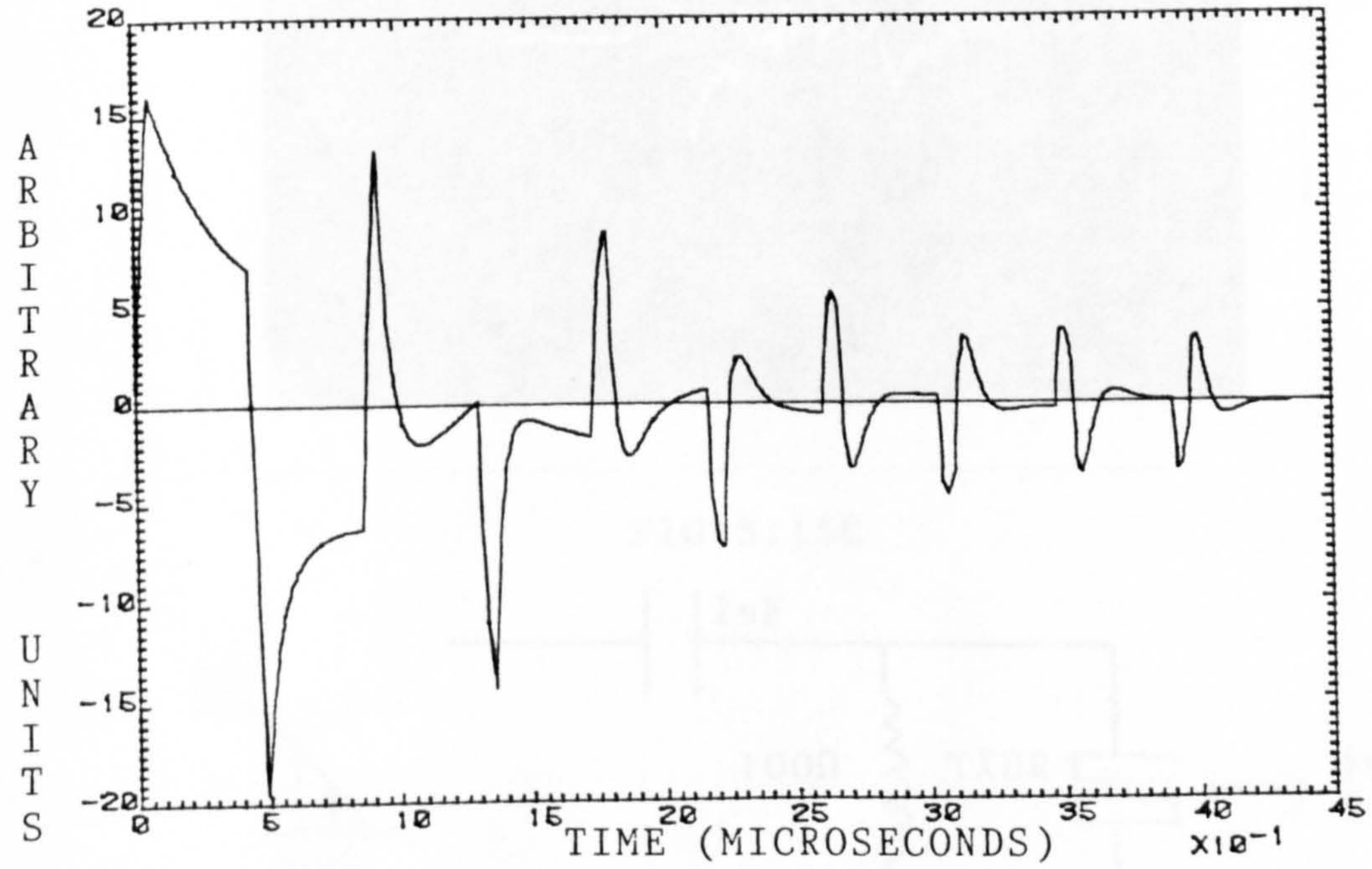

FIG 5.14E

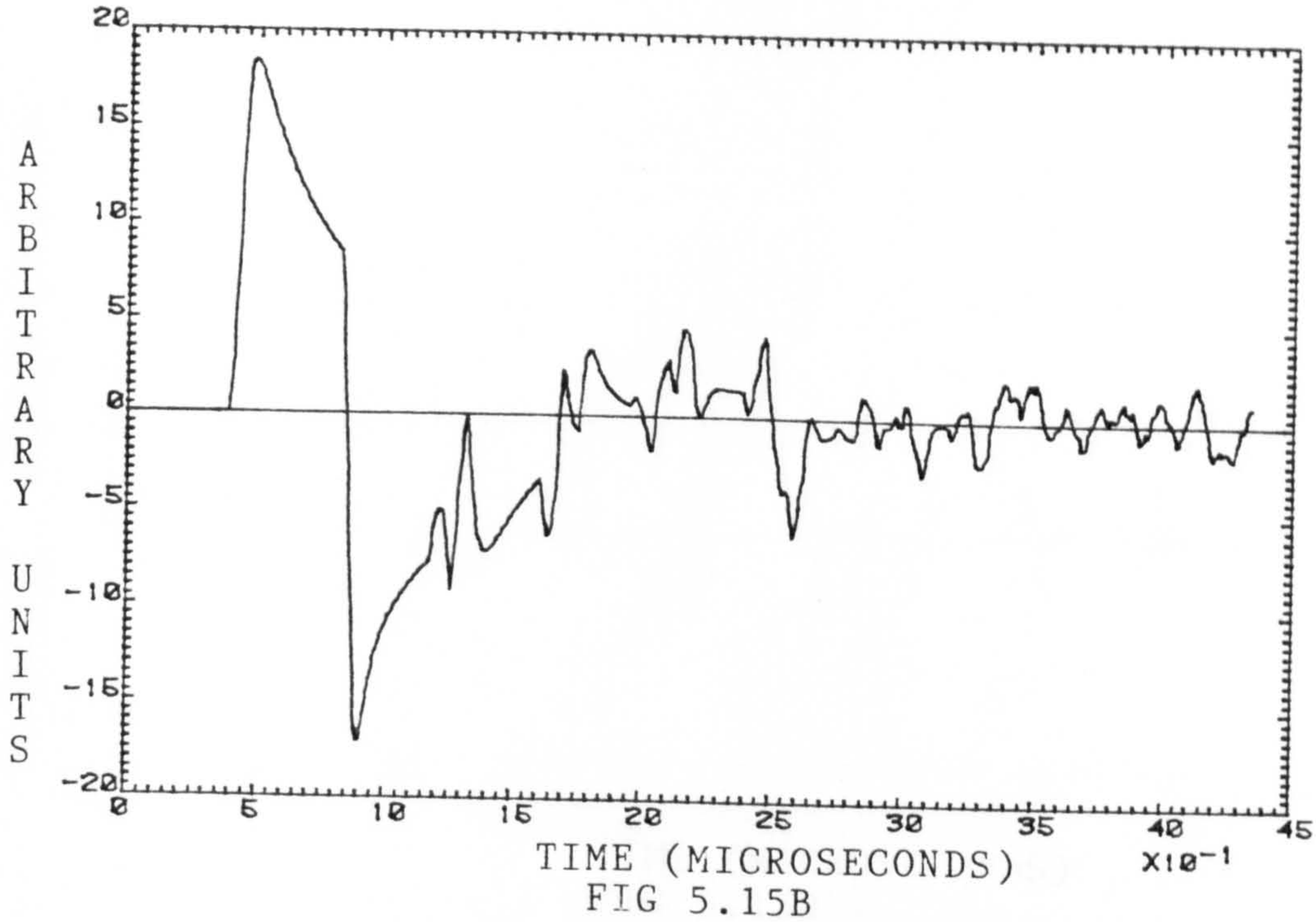

FIG 5.15B

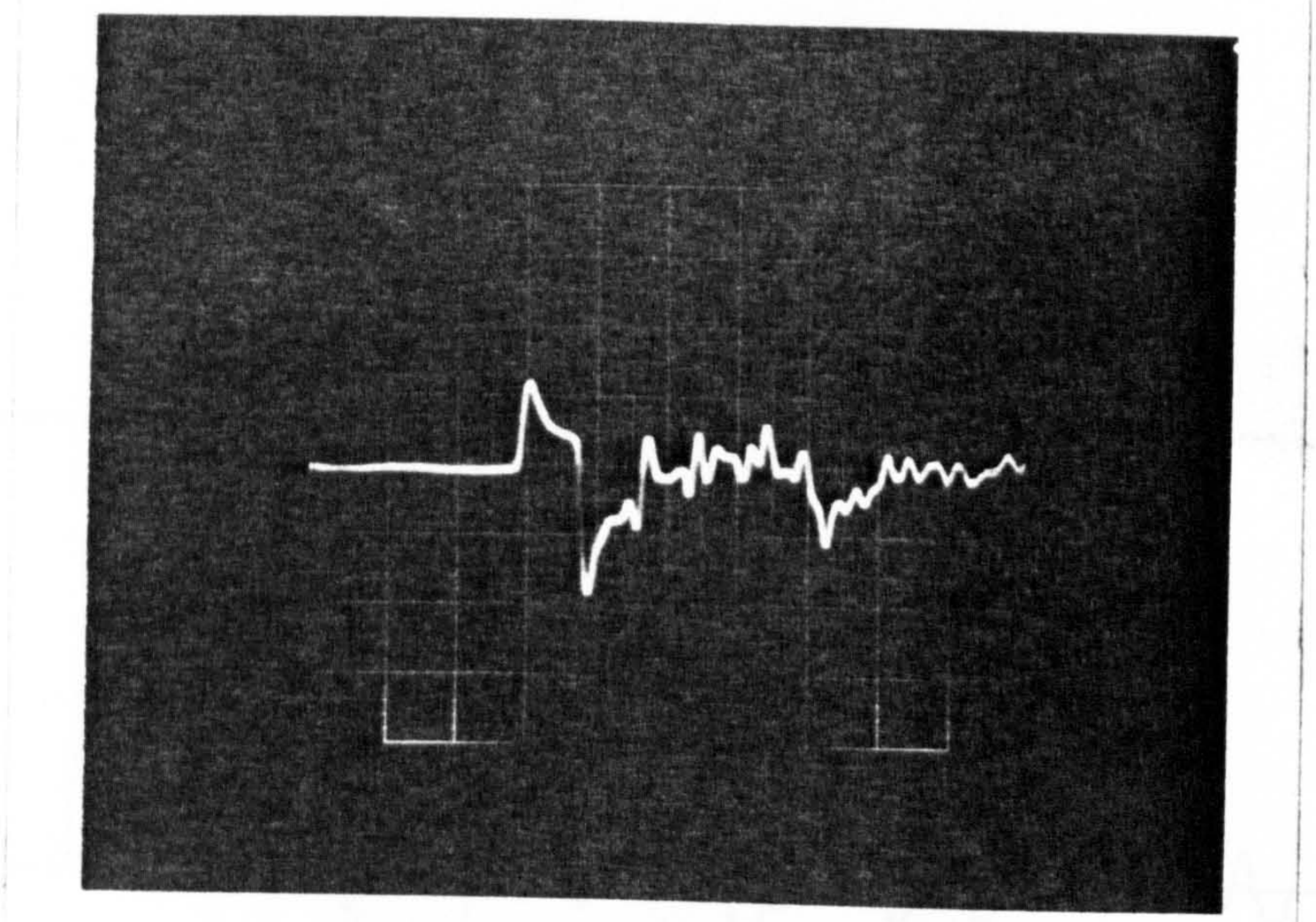

FIG 5.15C

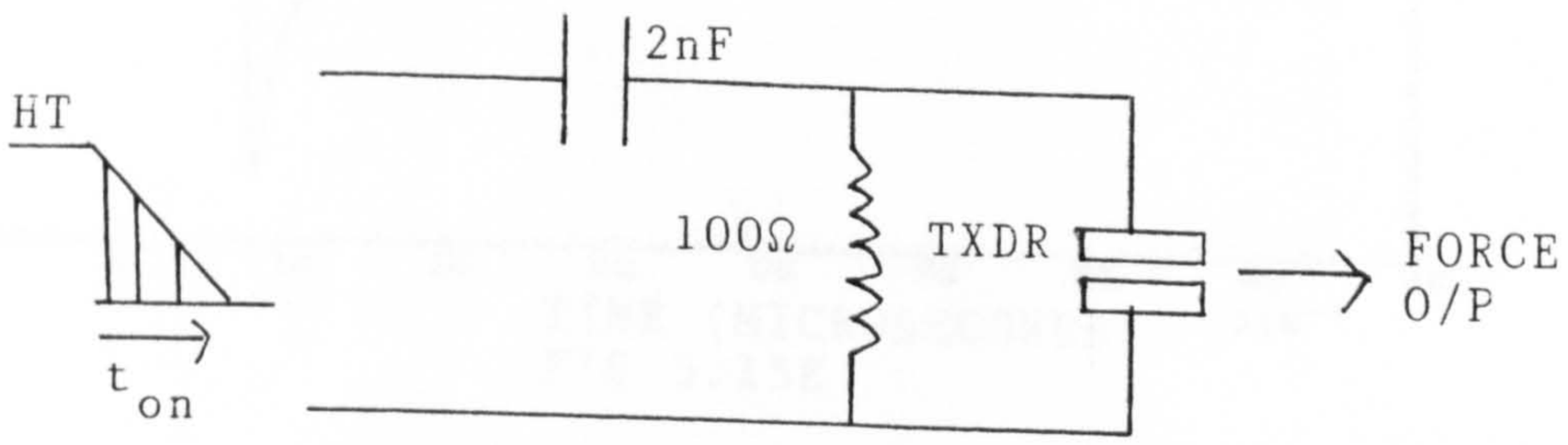

FIG 5.15A

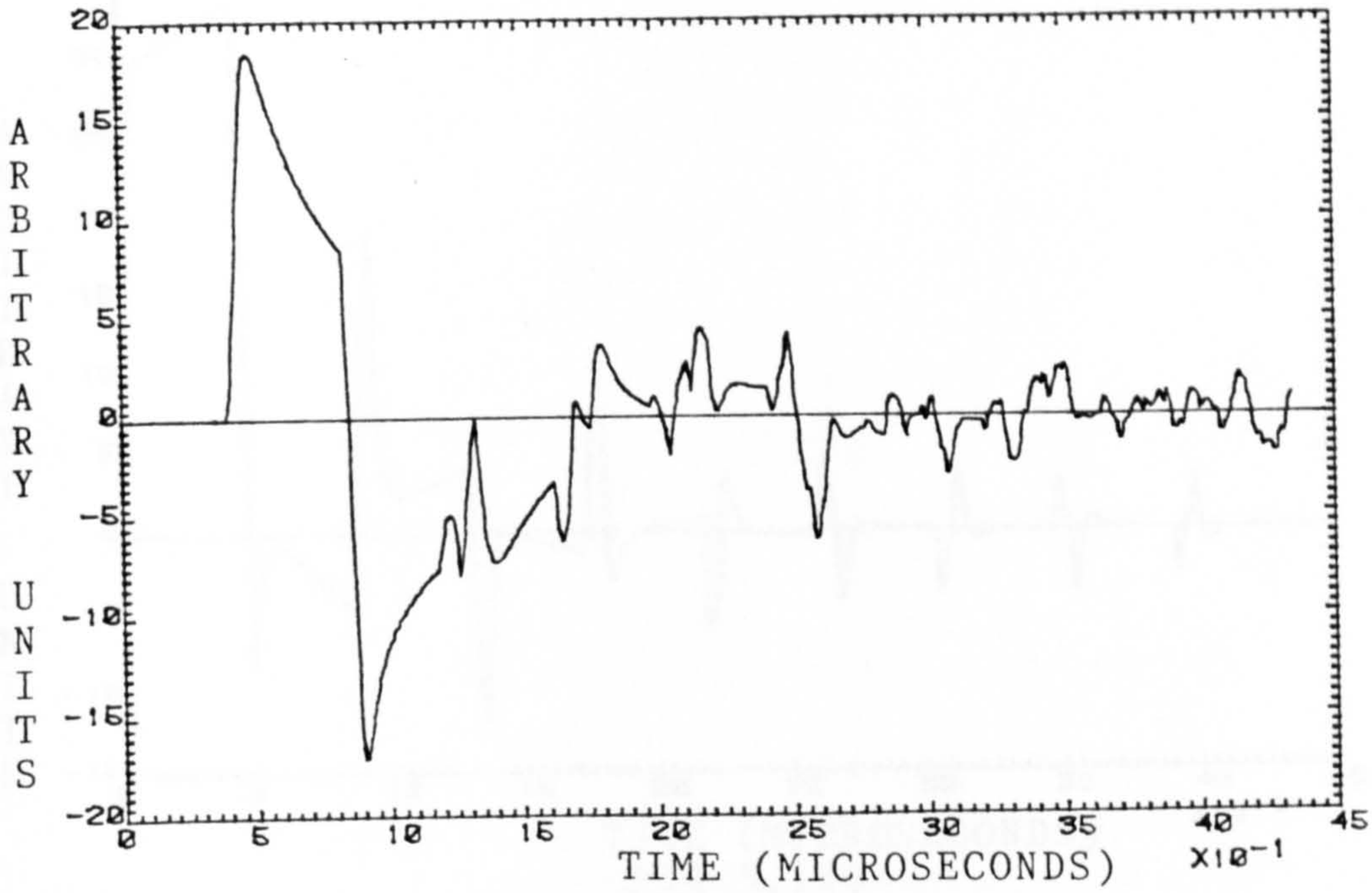

FIG 5.15D

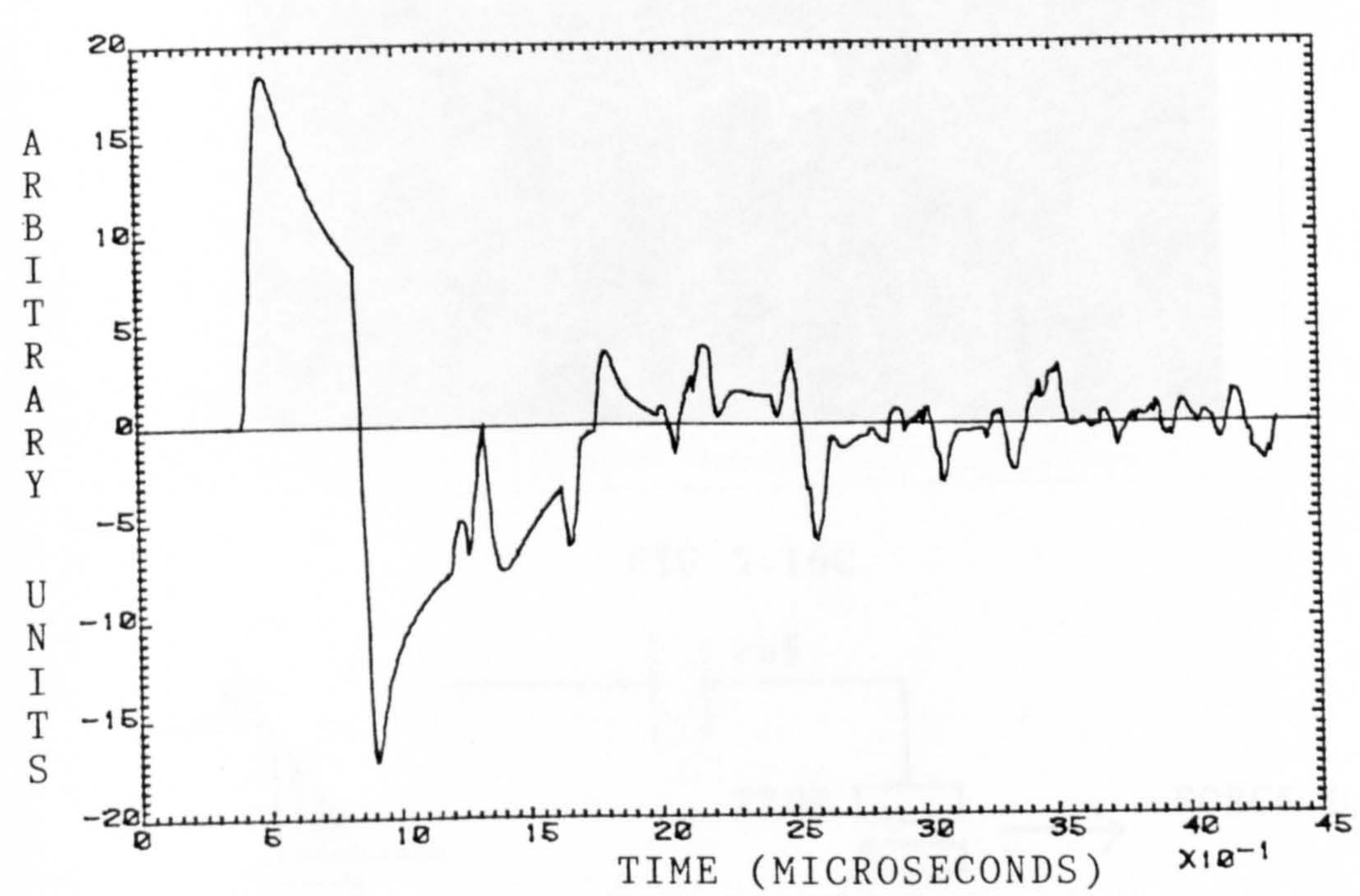

FIG 5.15E

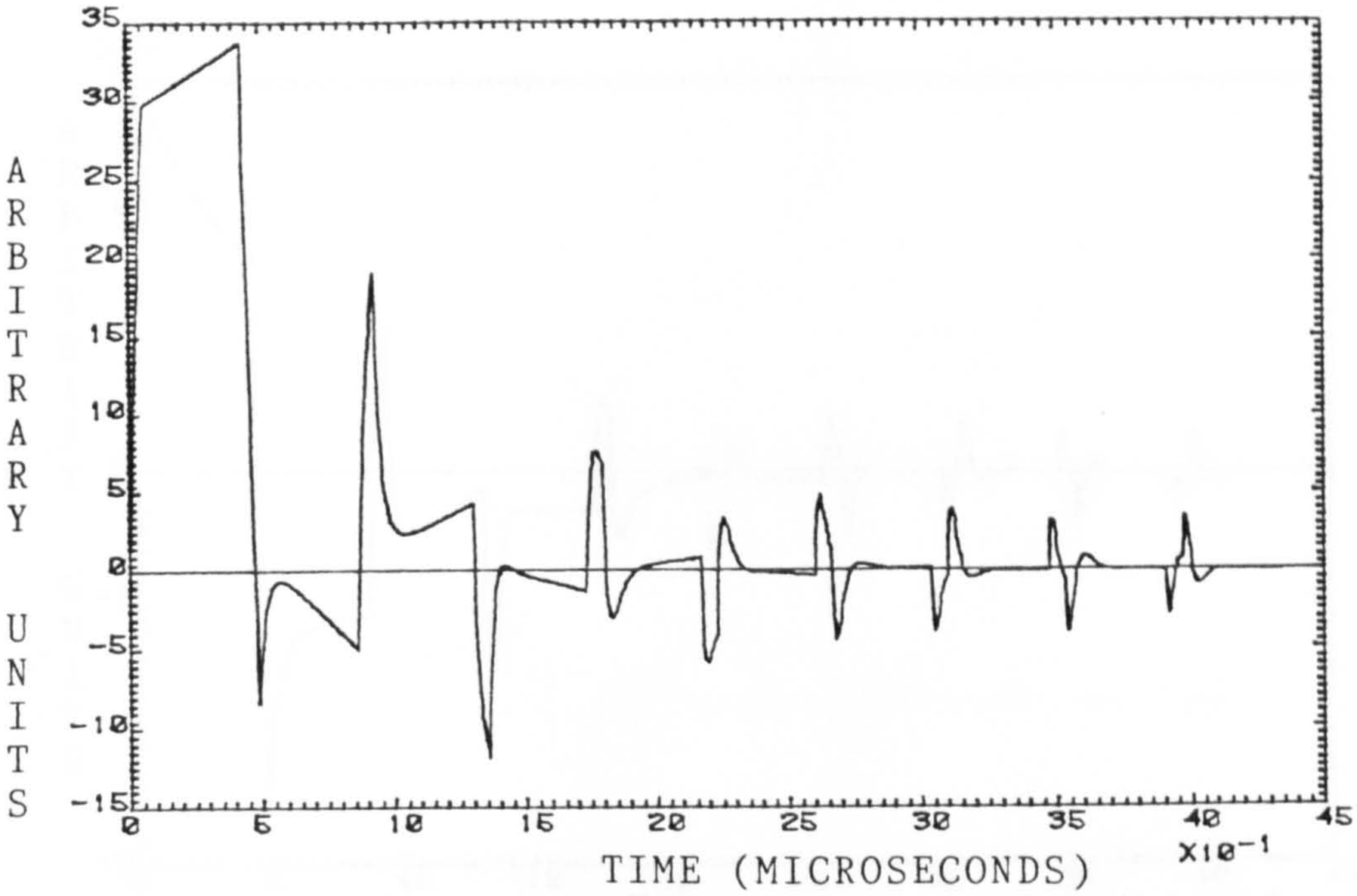

TIME (MICROSECONDS)

FIG 5.16B

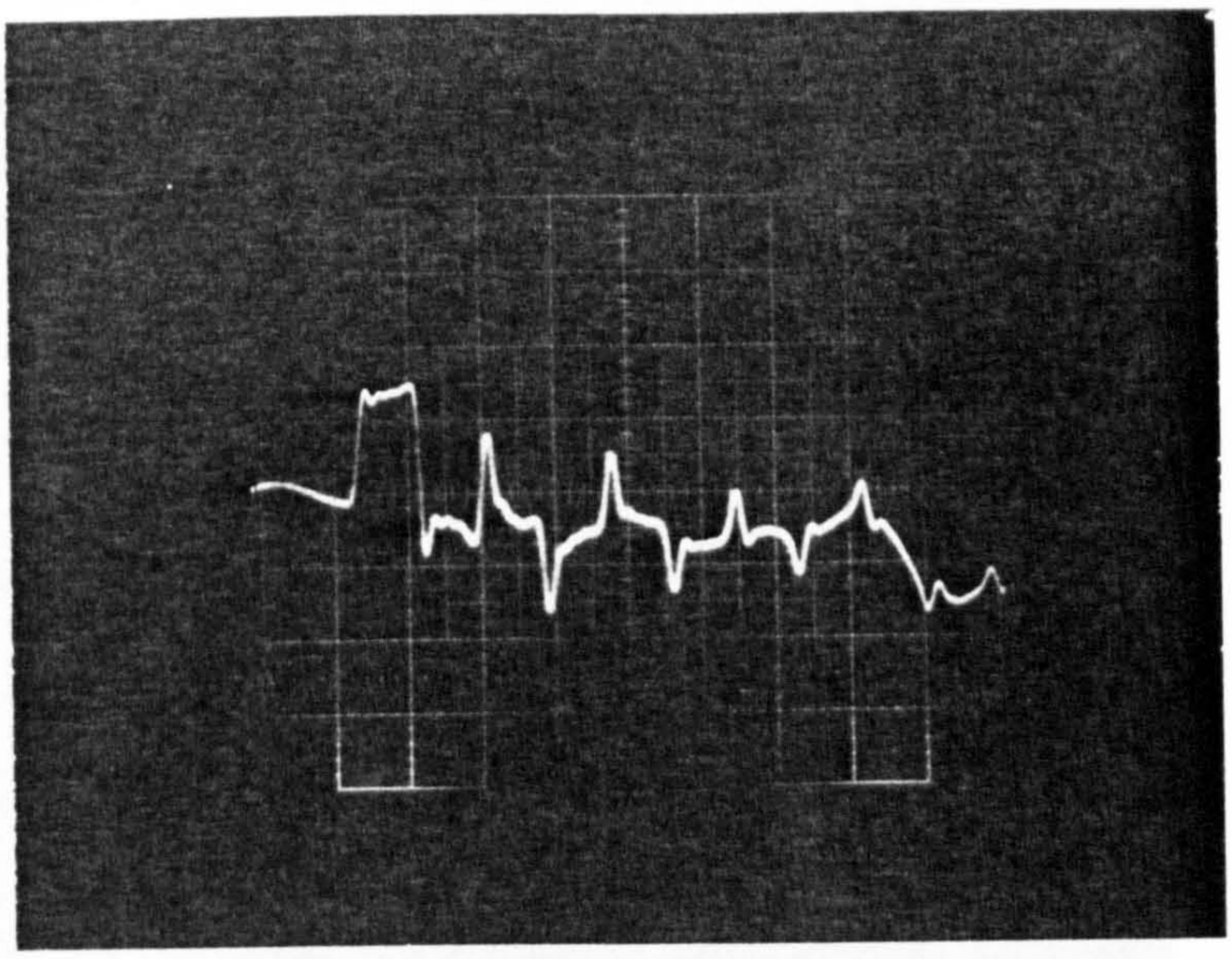

FIG 5.16C

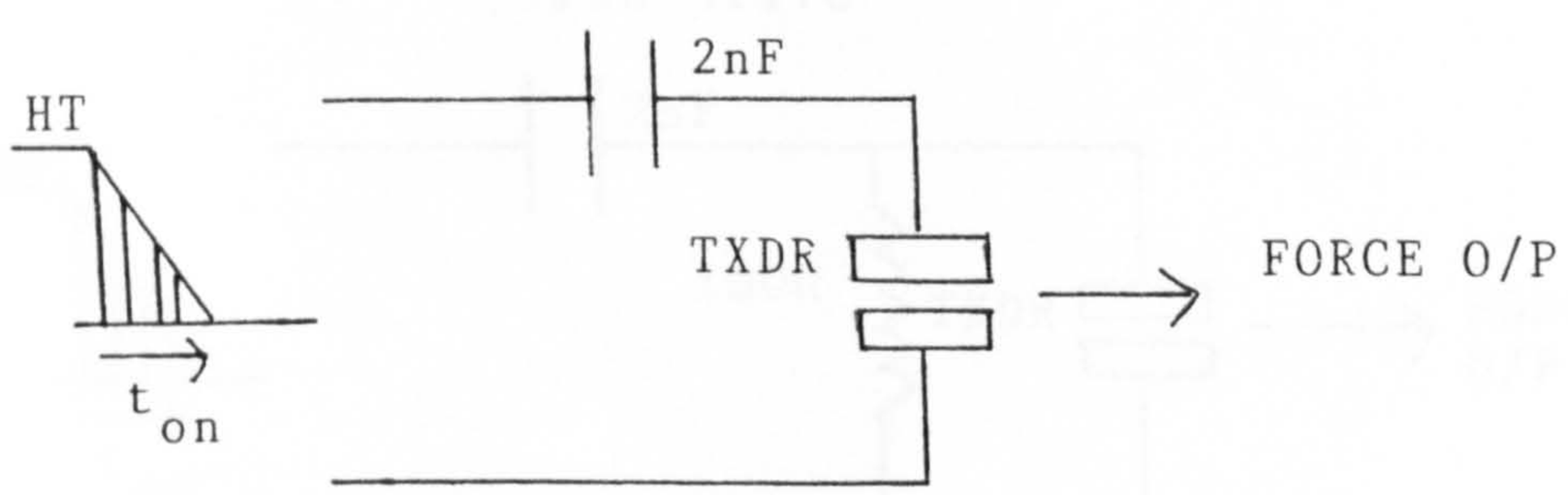

FIG 5.16A

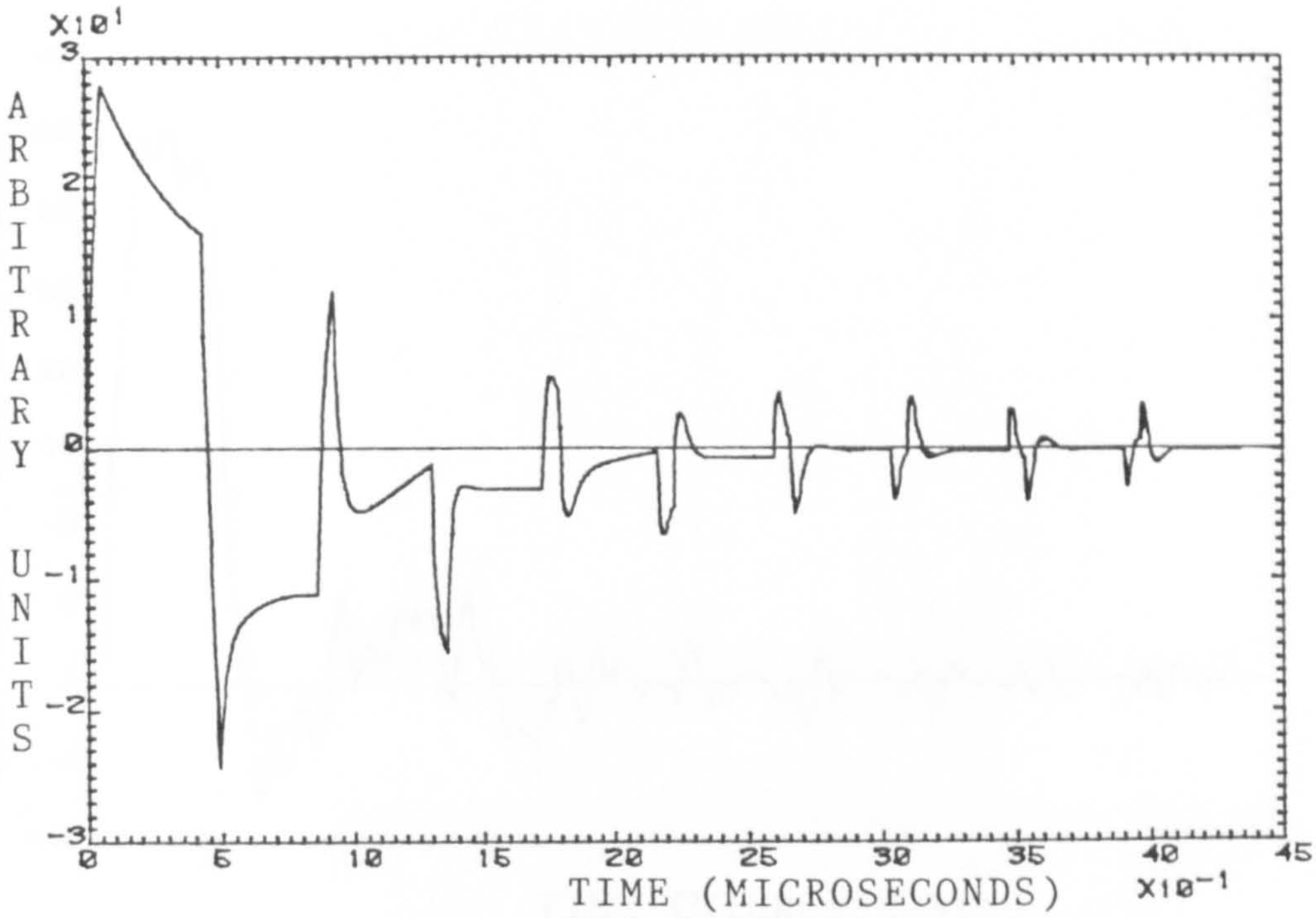

FIG 5.17B

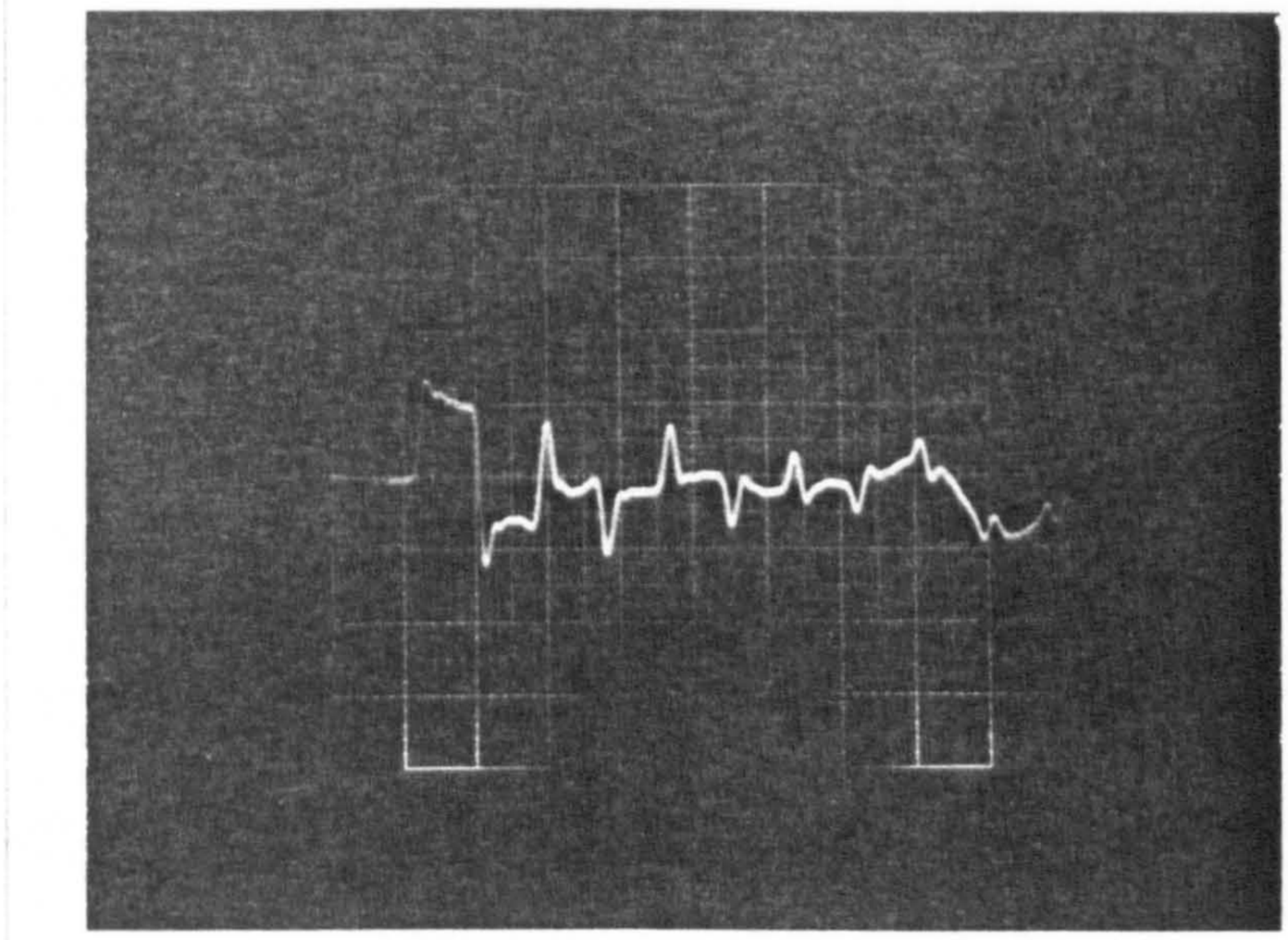

FIG 5.17C

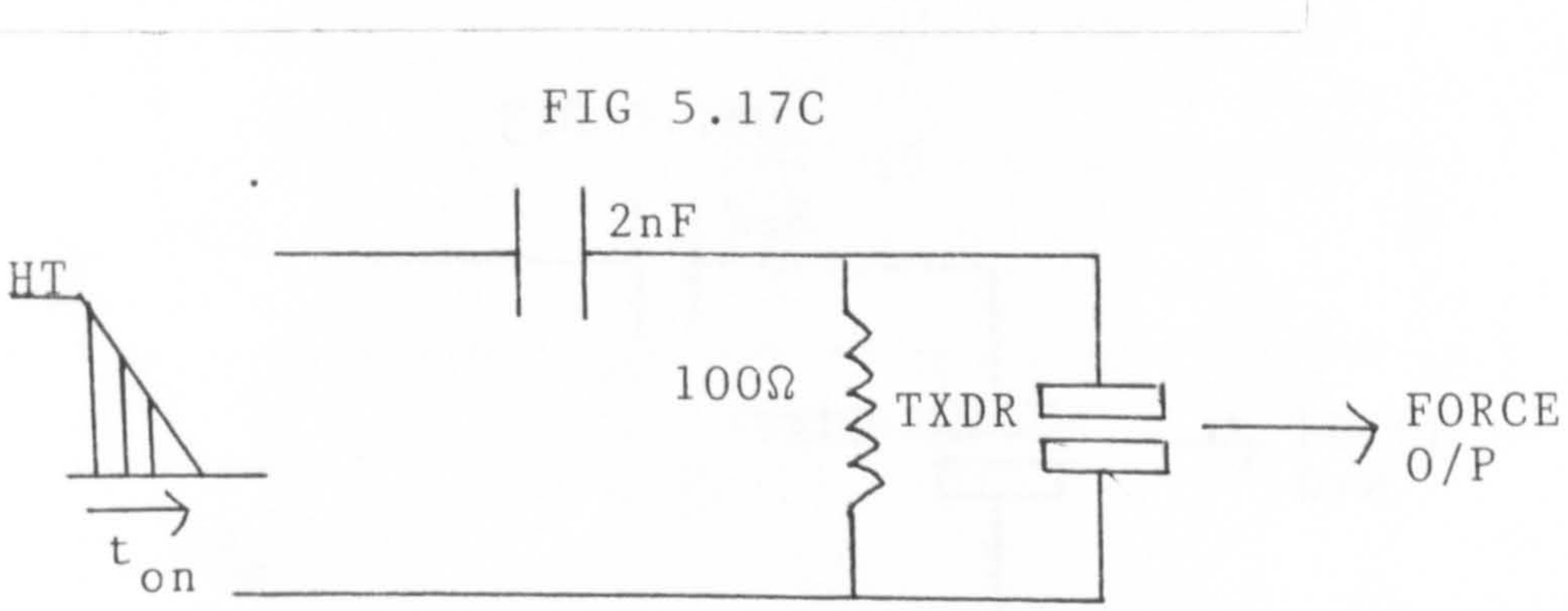

FIG 5.17A

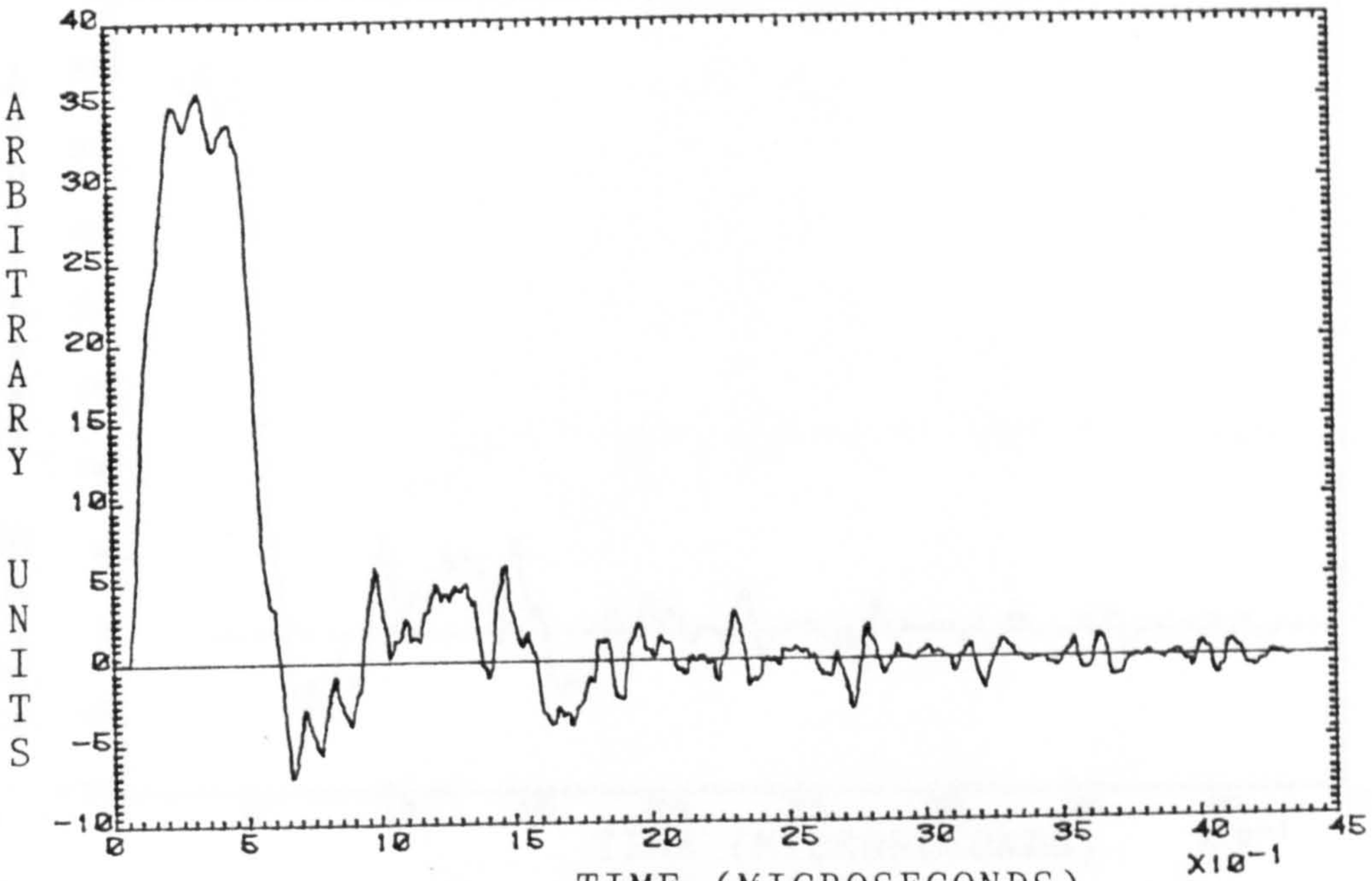

FIG 5.18B

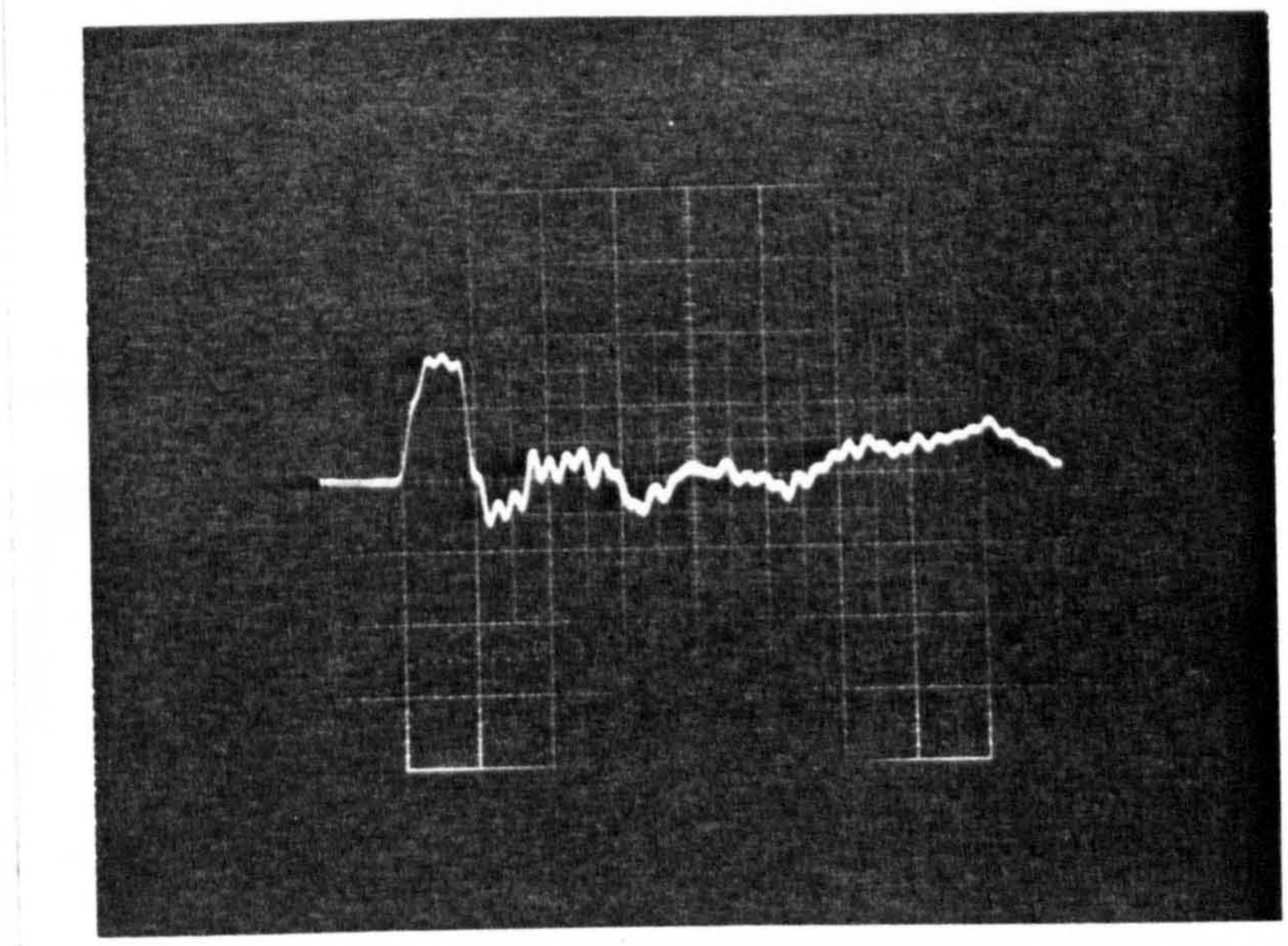

FIG 5.18C

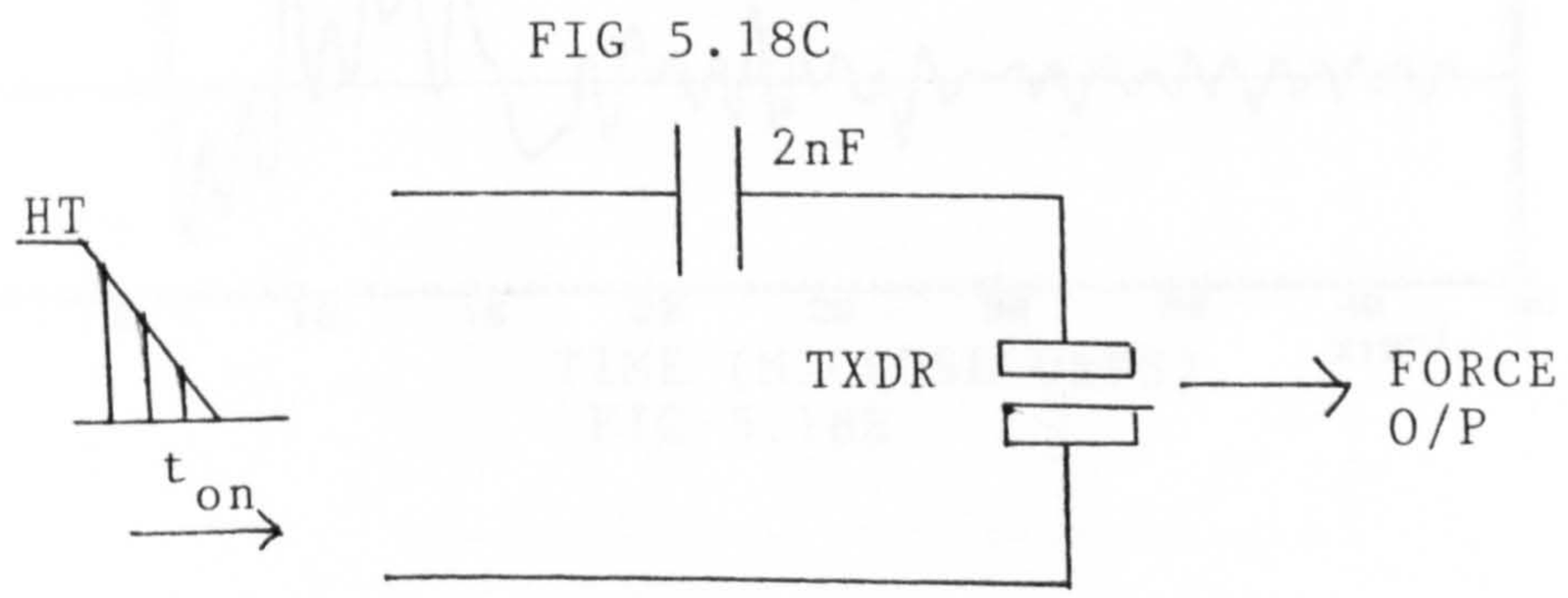

FIG 5.18A

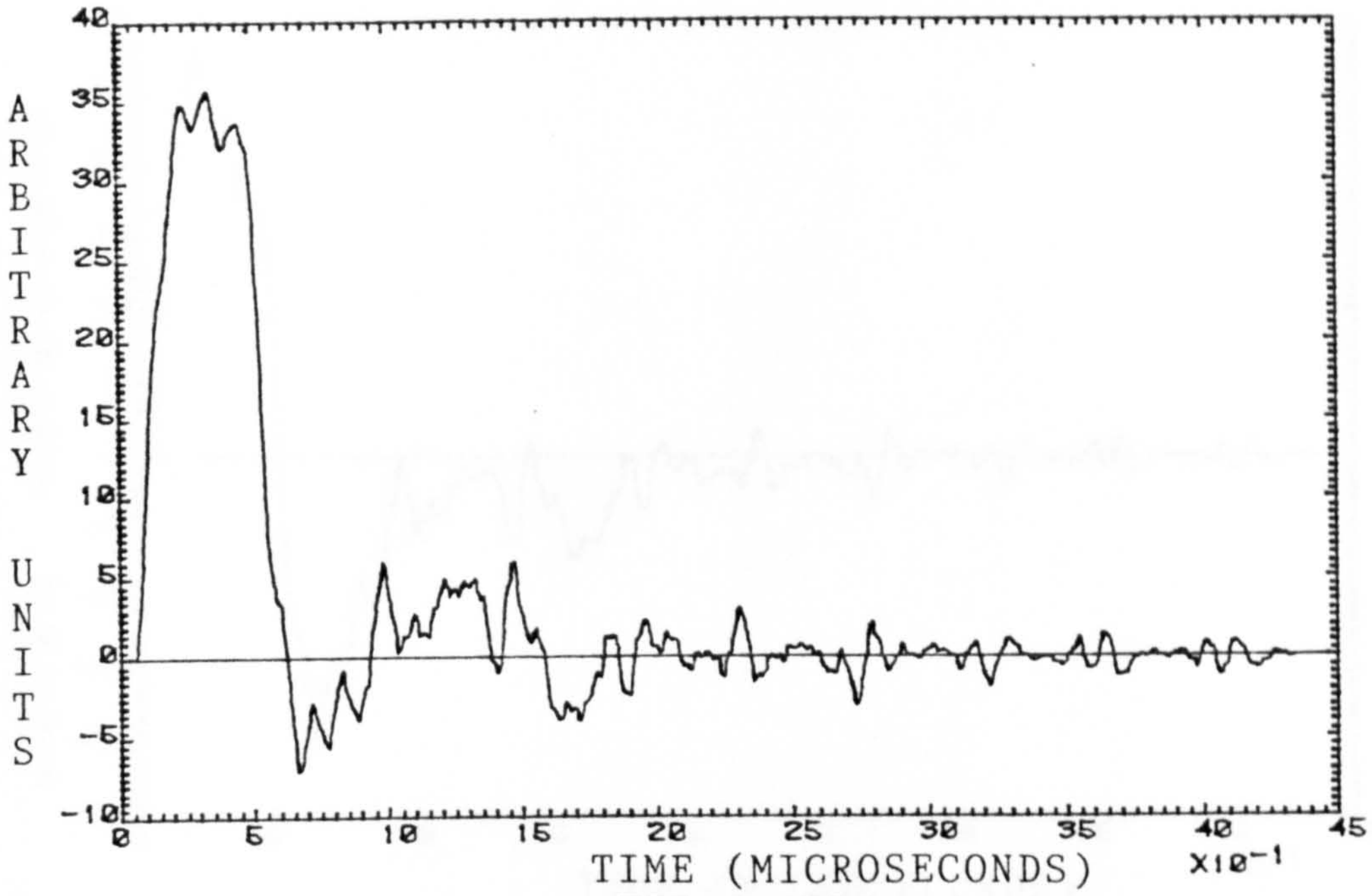

FIG 5.18D

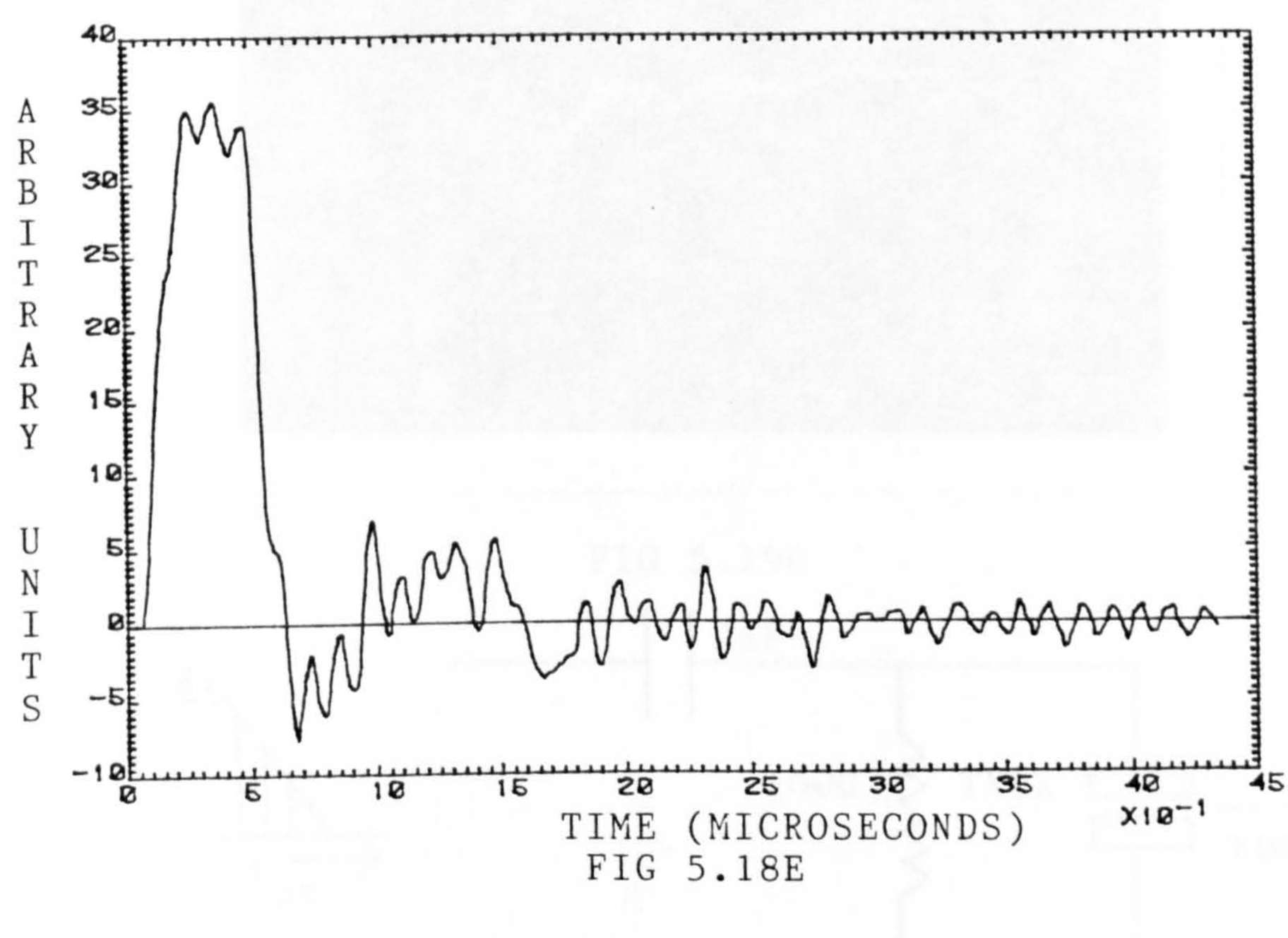

FIG 5.18E

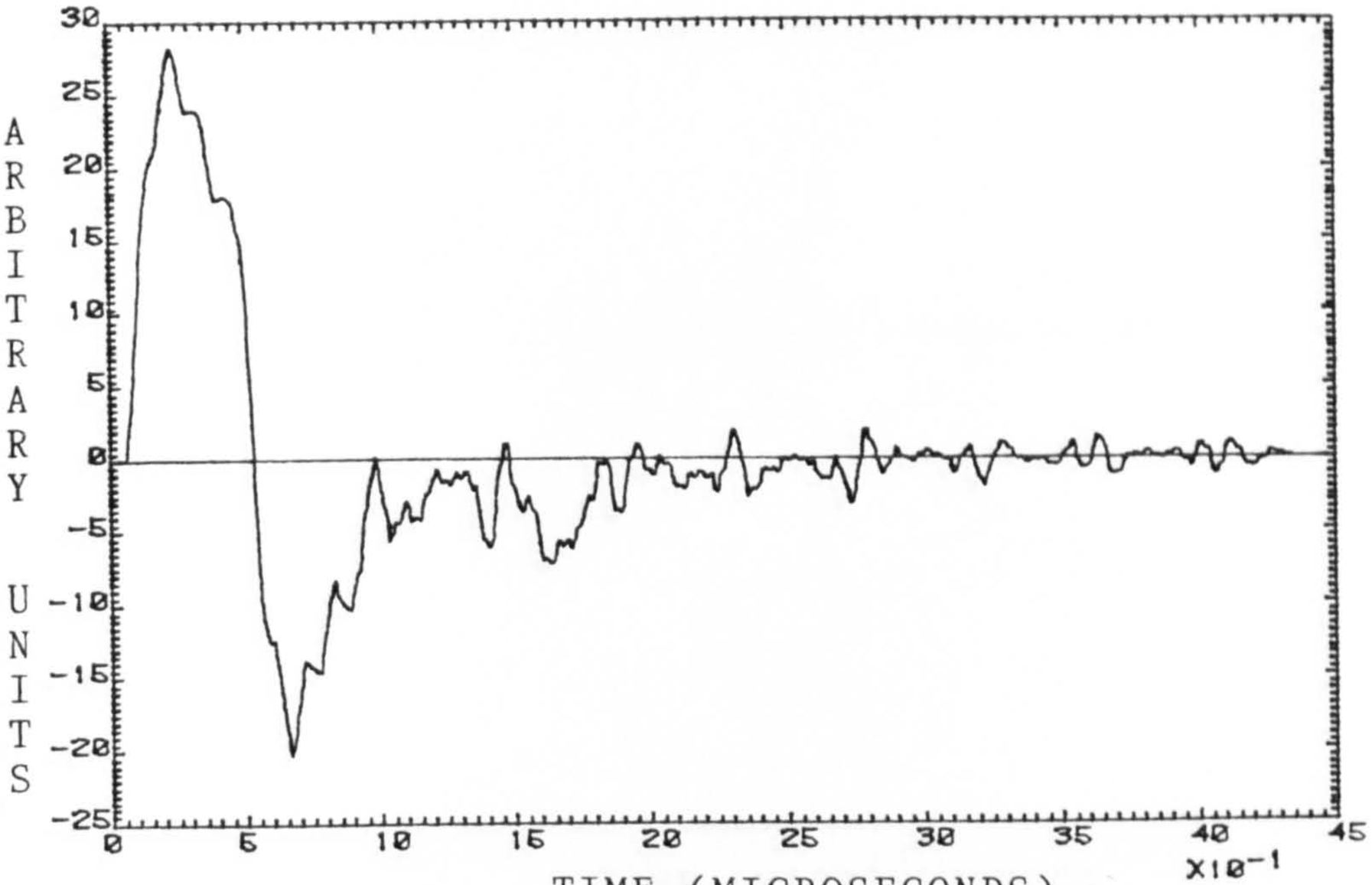

TIME (MICROSECONDS)

FIG 5.19B

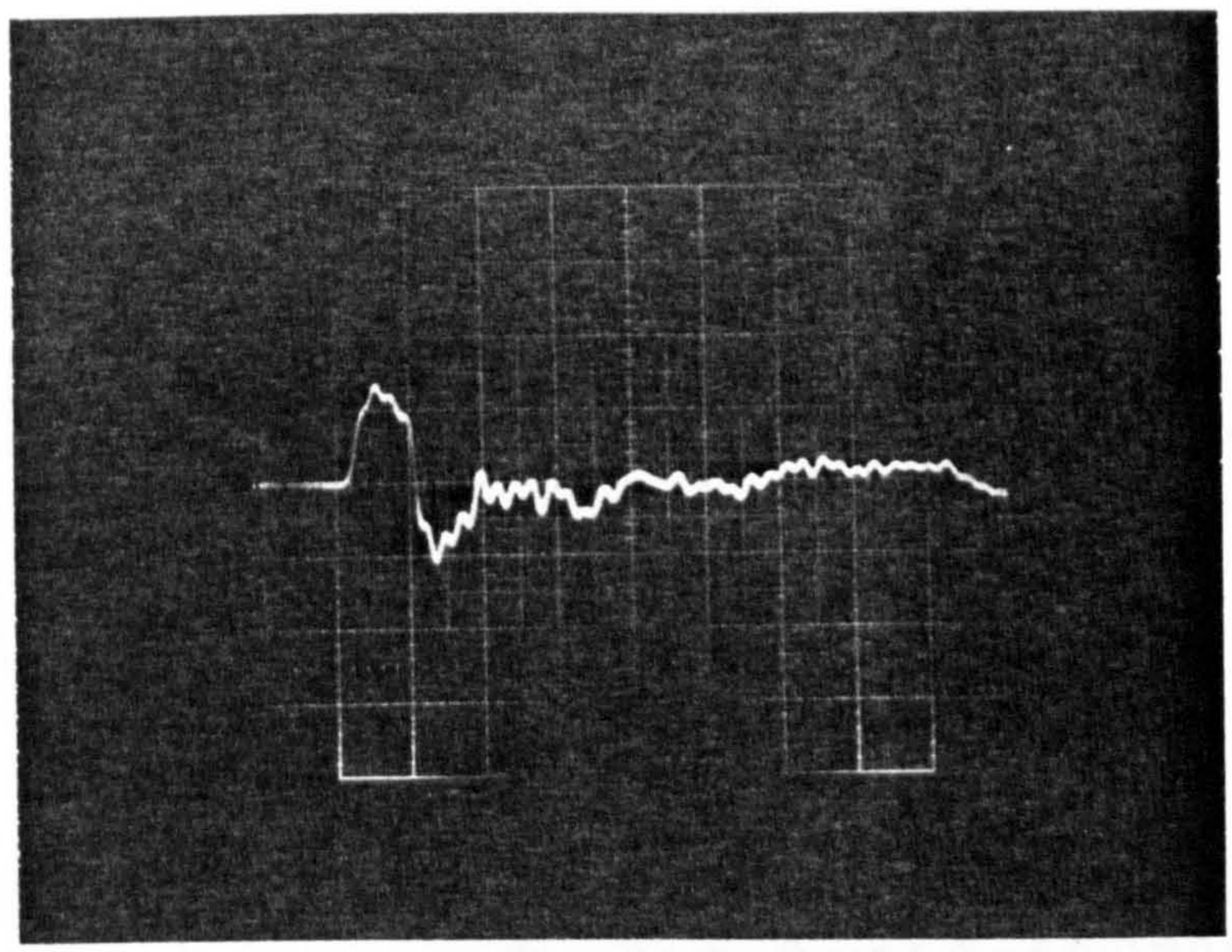

FIG 5.19C

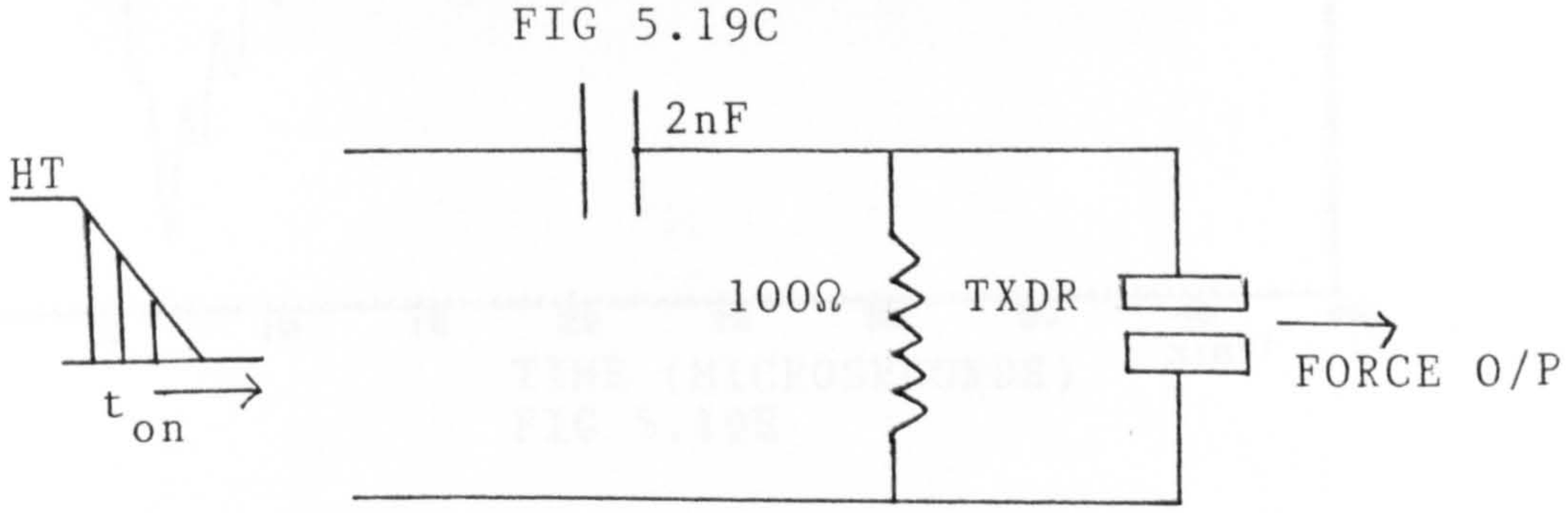

FIG 5.19A

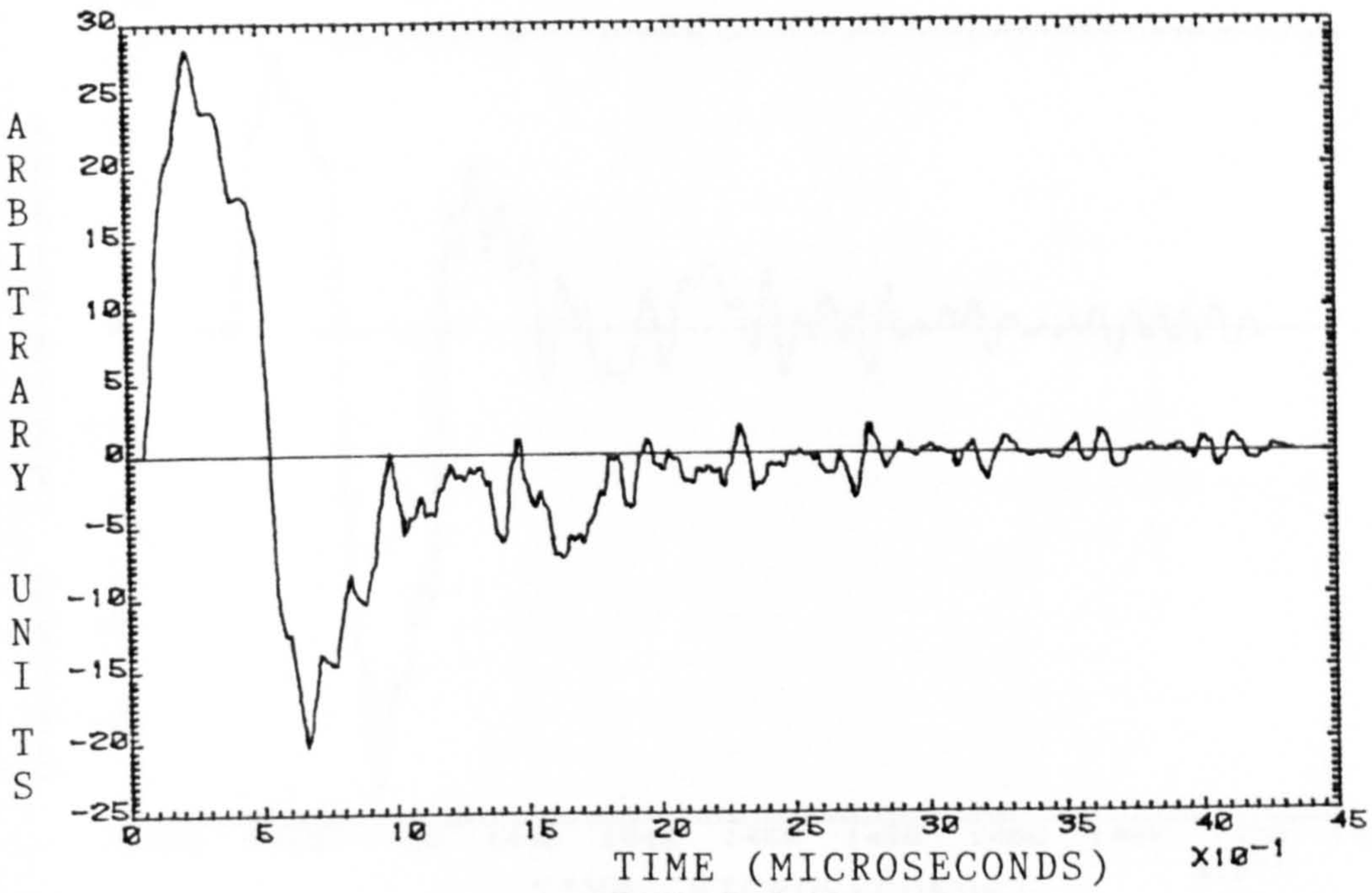

TIME (MICROSECONDS)

FIG 5.19D

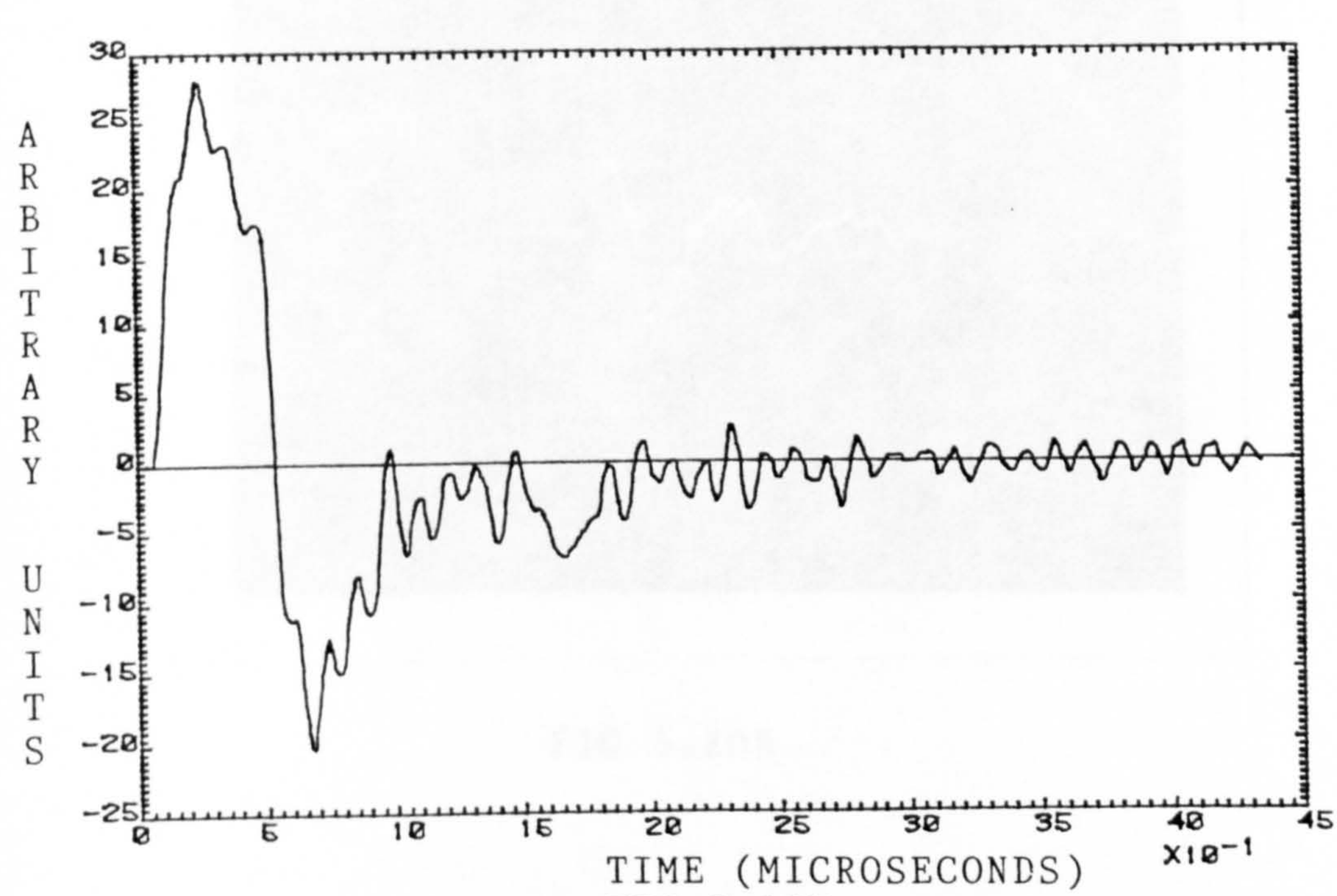

TIME (MICROSECONDS)

FIG 5.19E

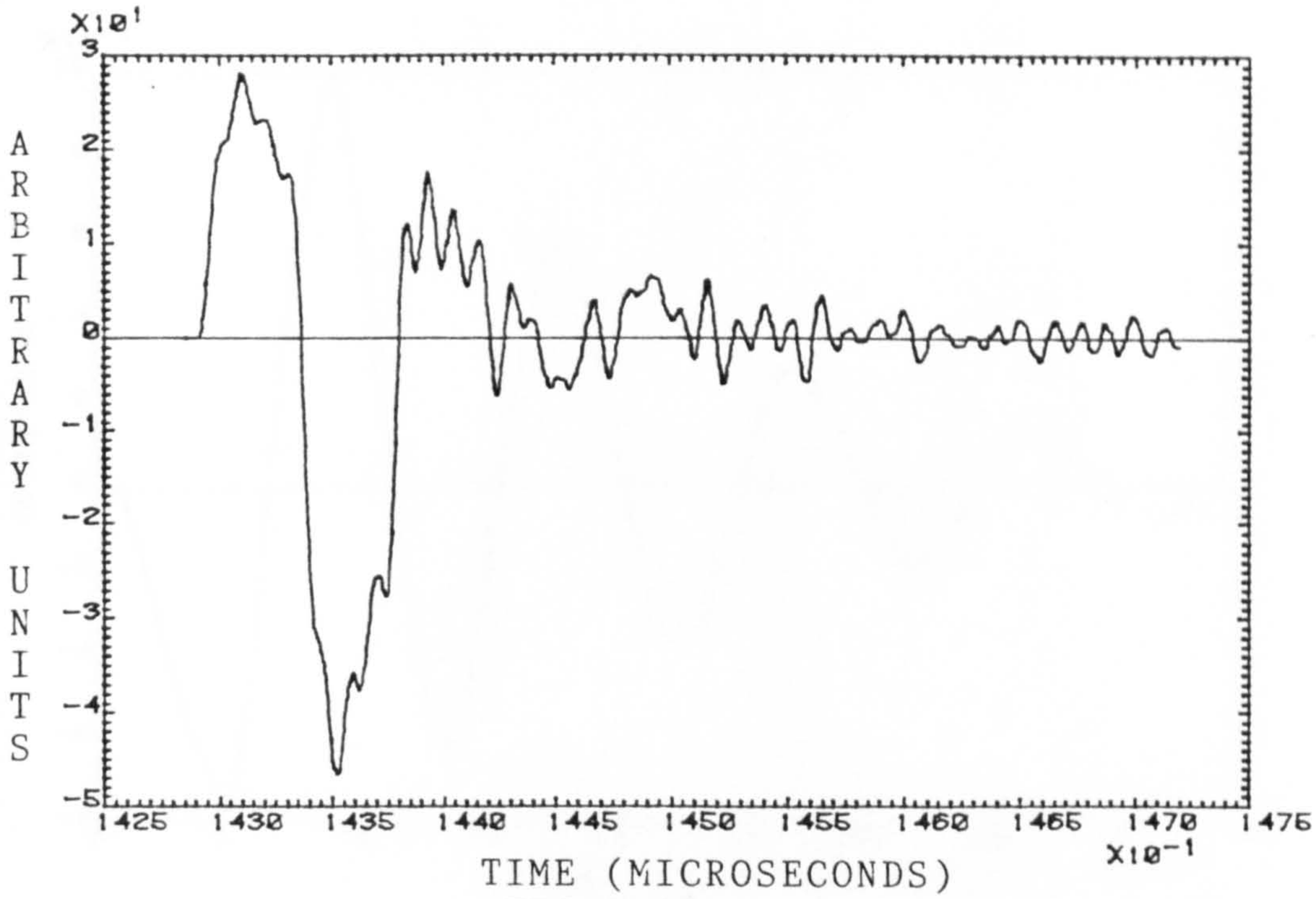

FIG 5.20A

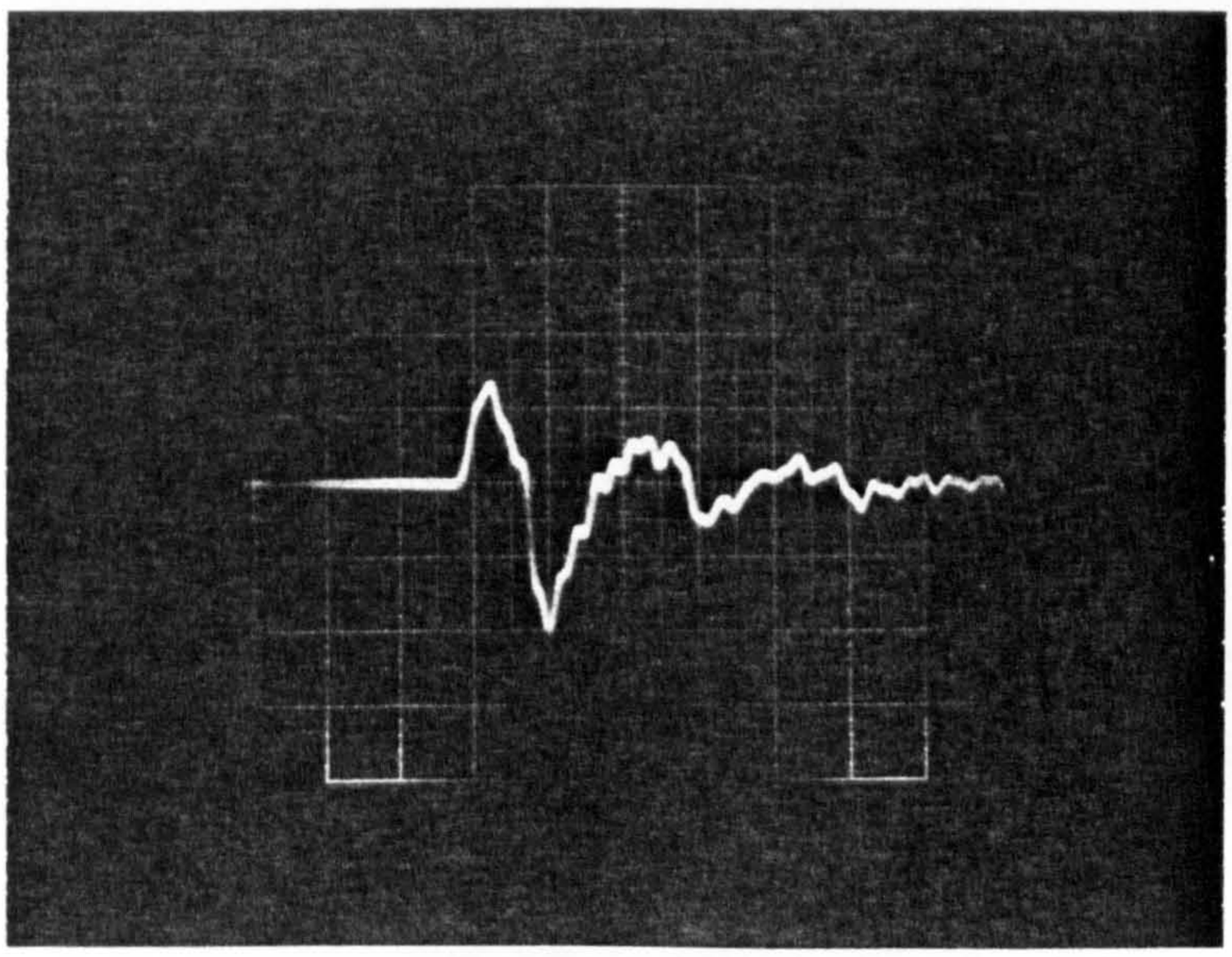

FIG 5.20B

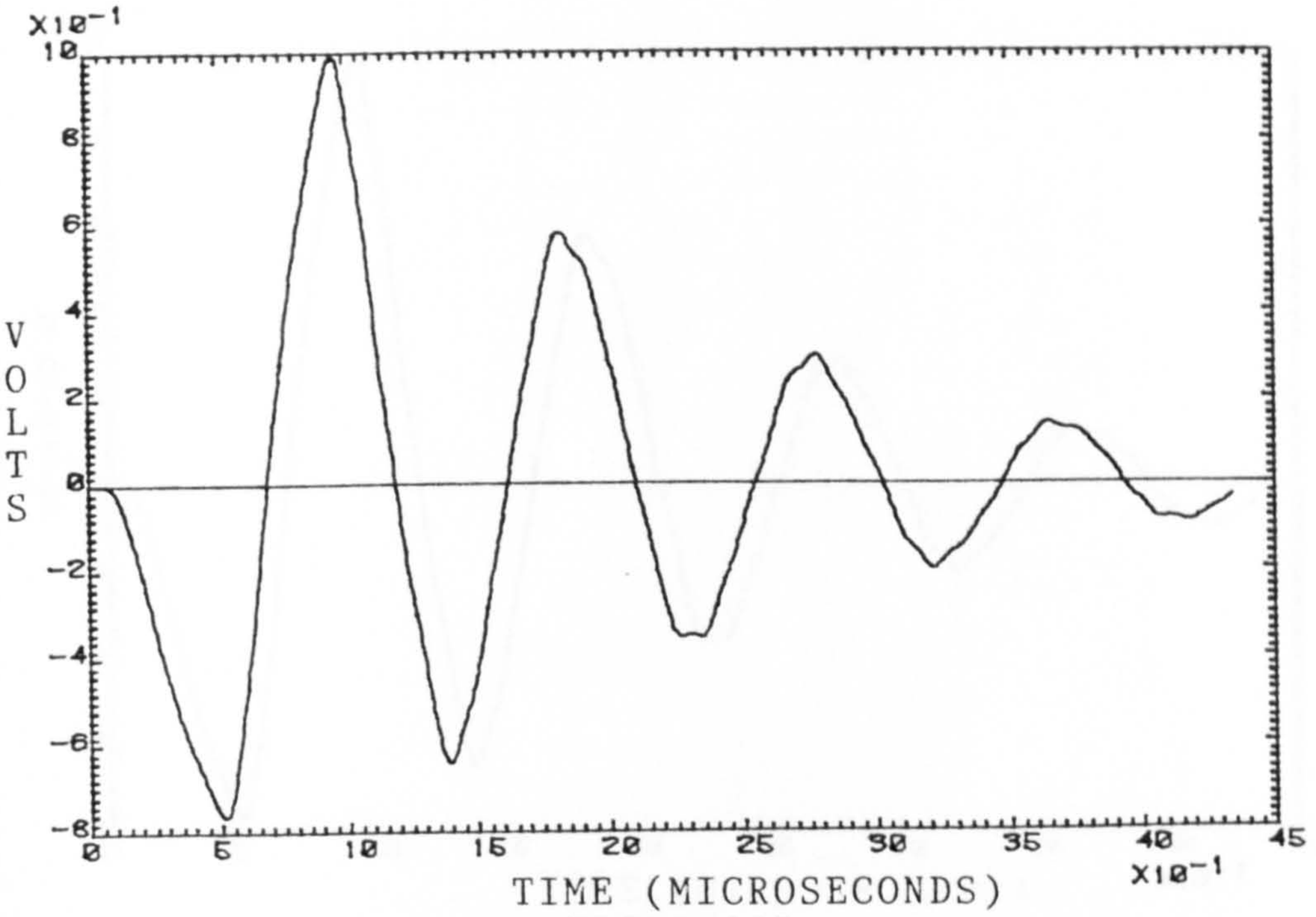

FIG 5.21B

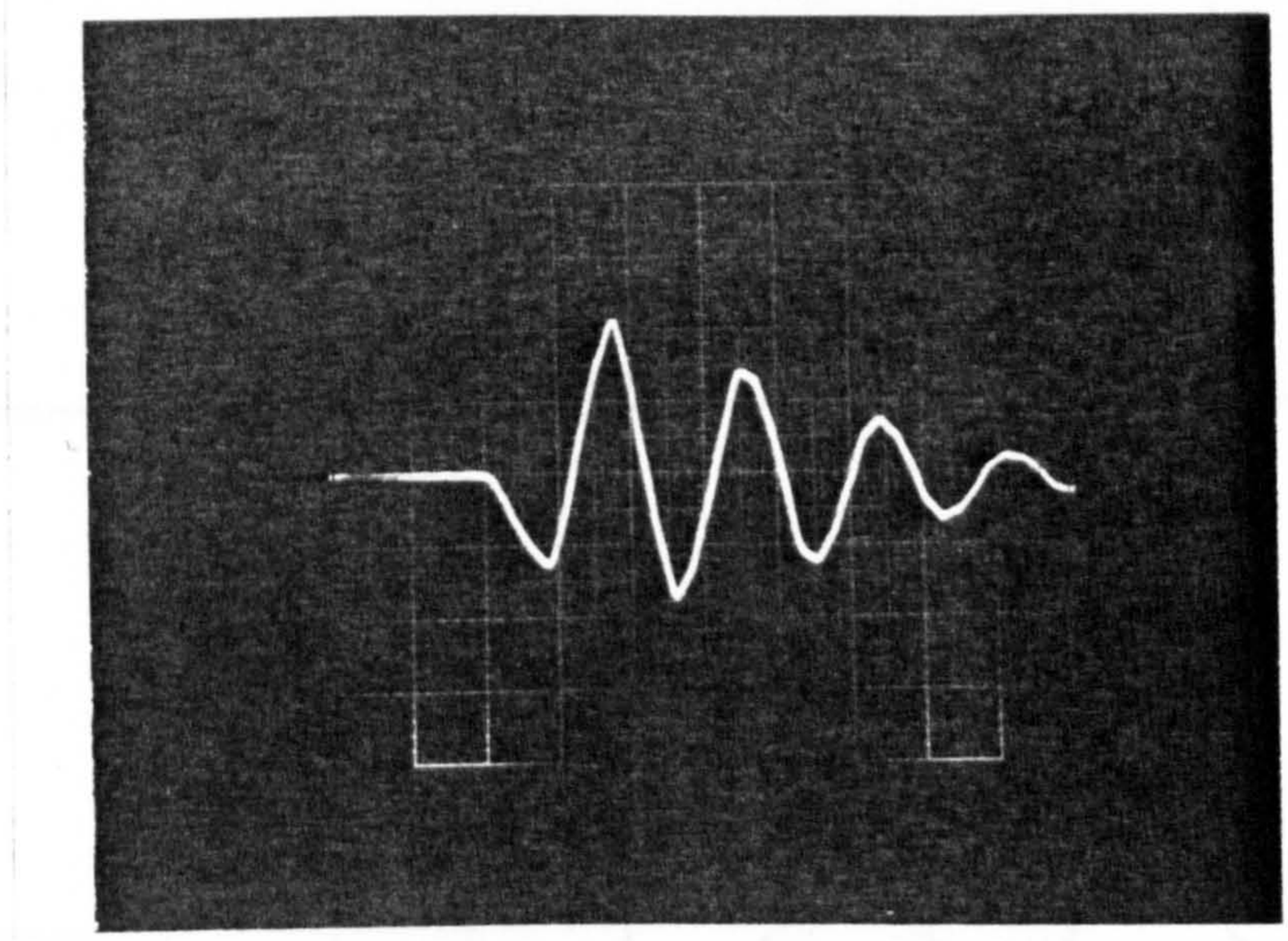

FIG 5.21C

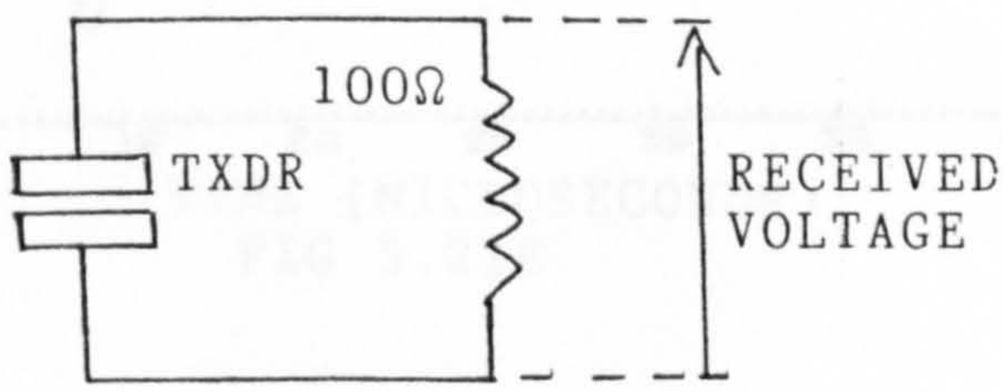

FIG 5.21A

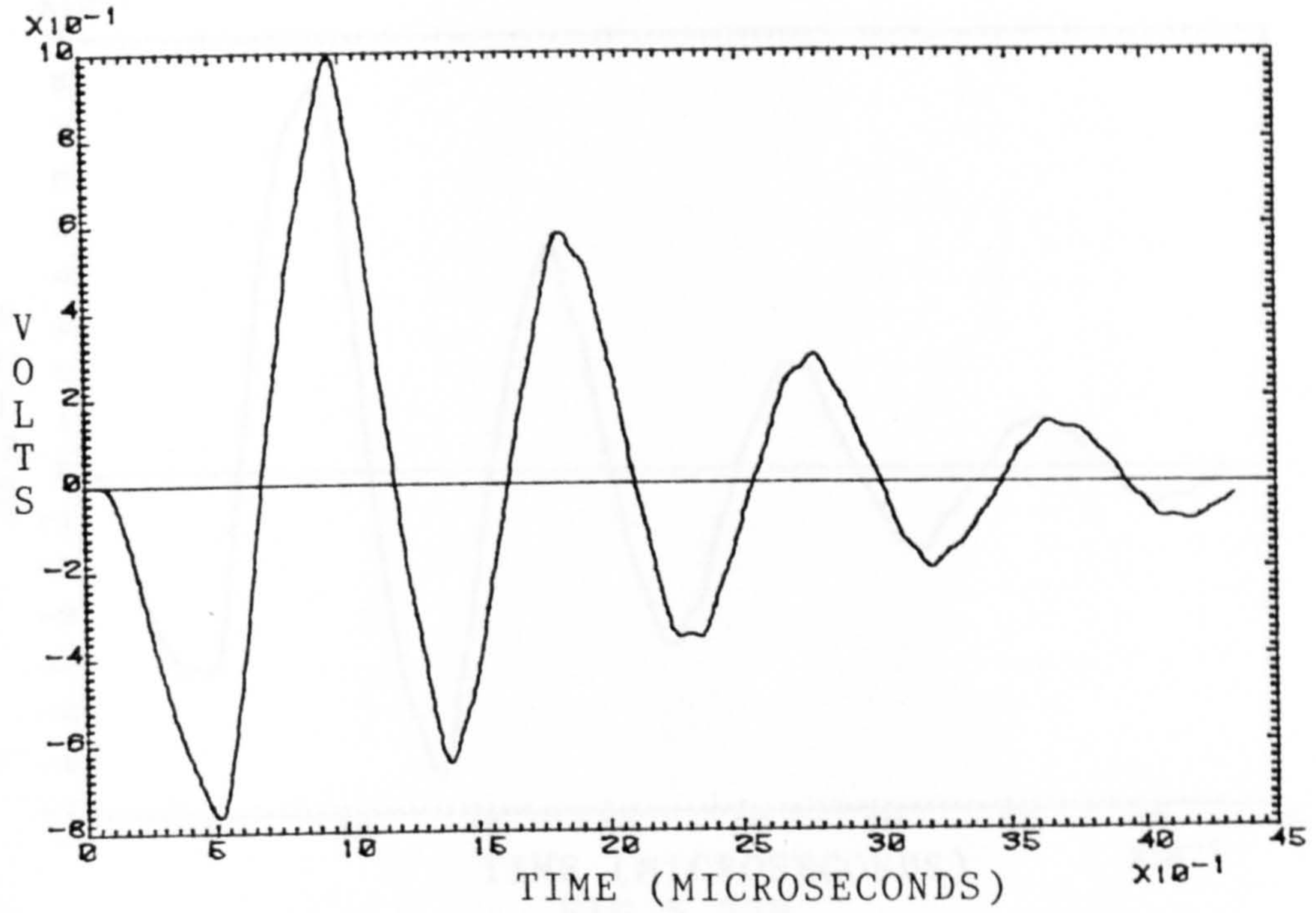

TIME (MICROSECONDS)

FIG 5.21D

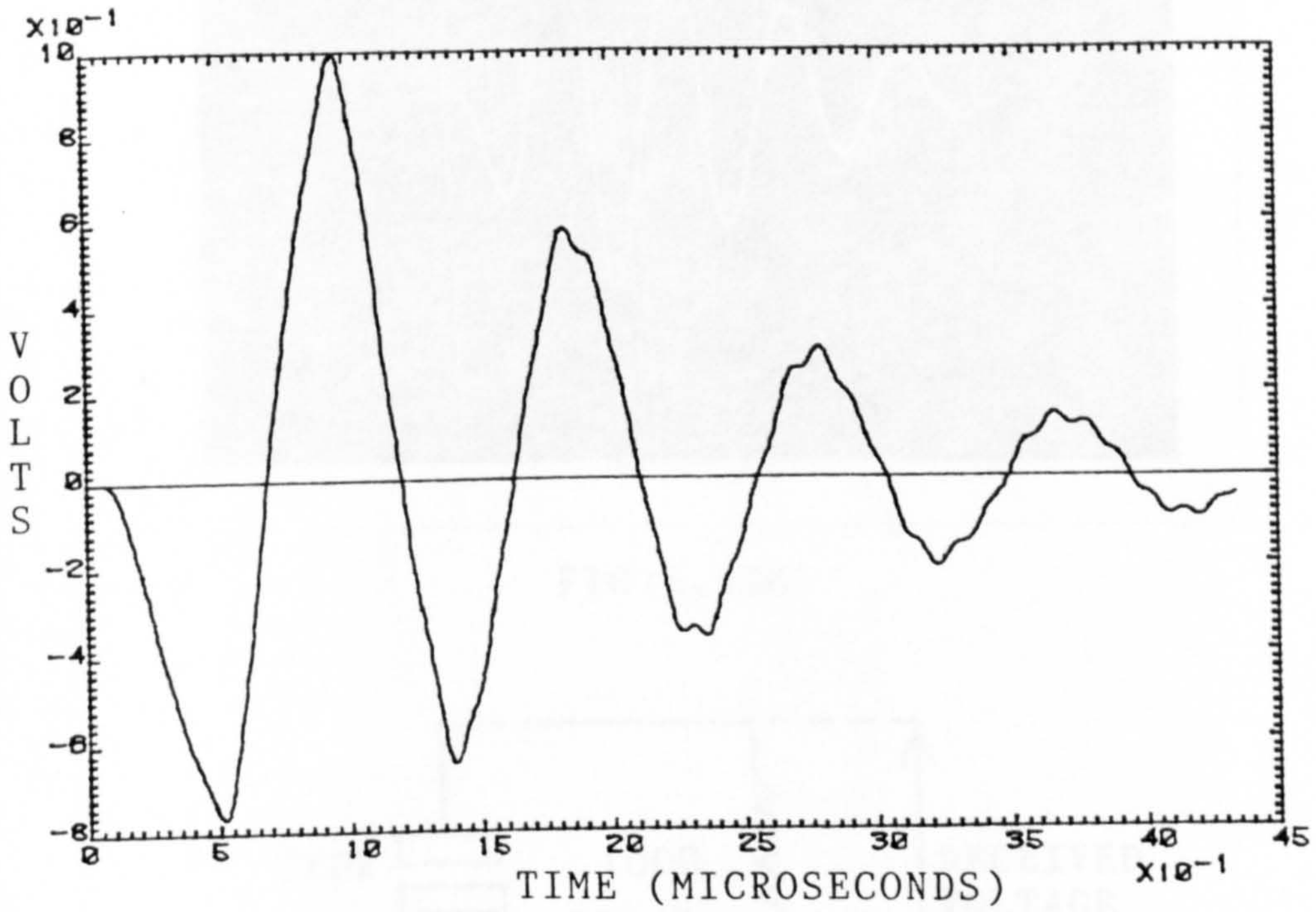

TIME (MICROSECONDS)

FIG 5.21E

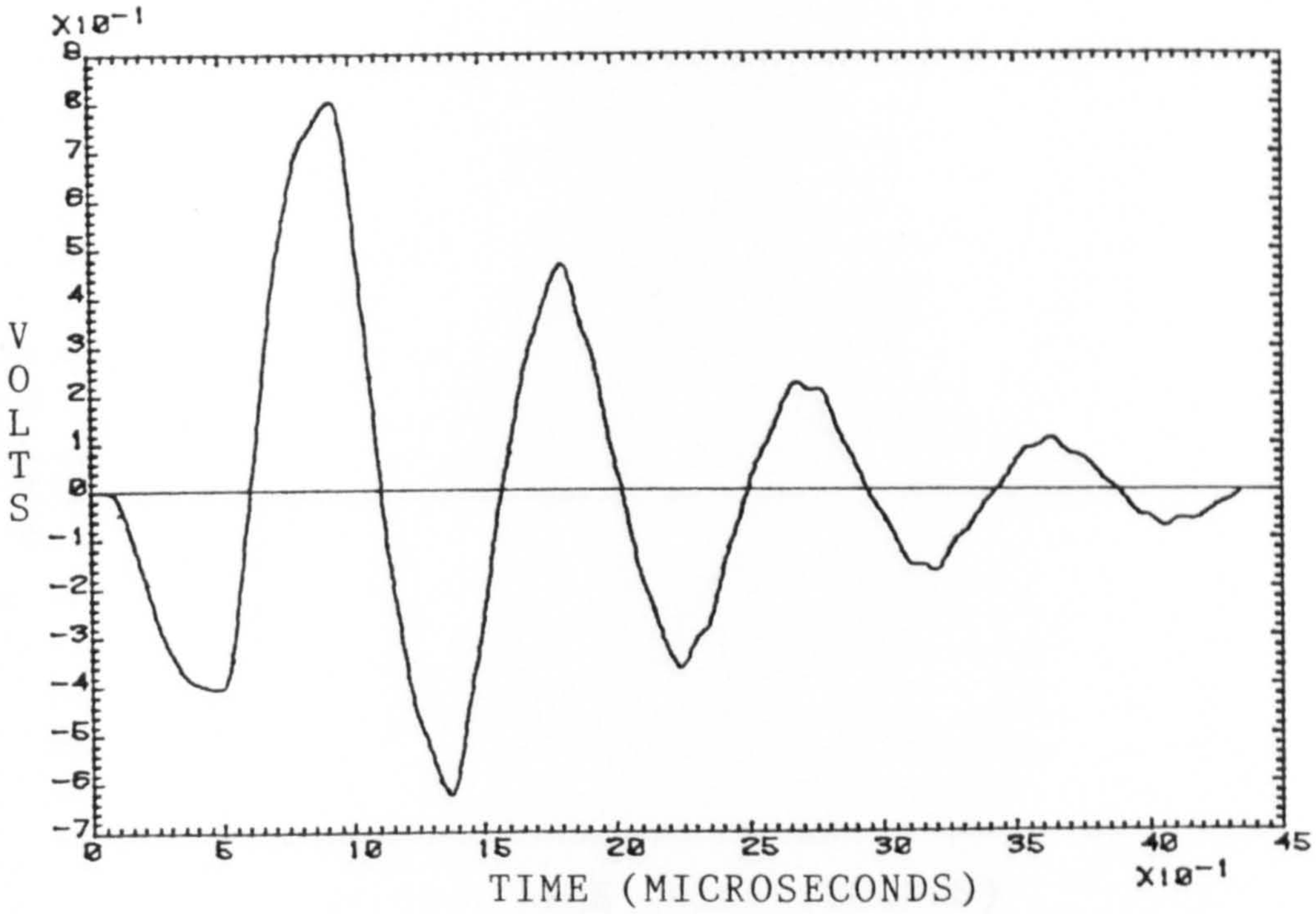

FIG 5.22B

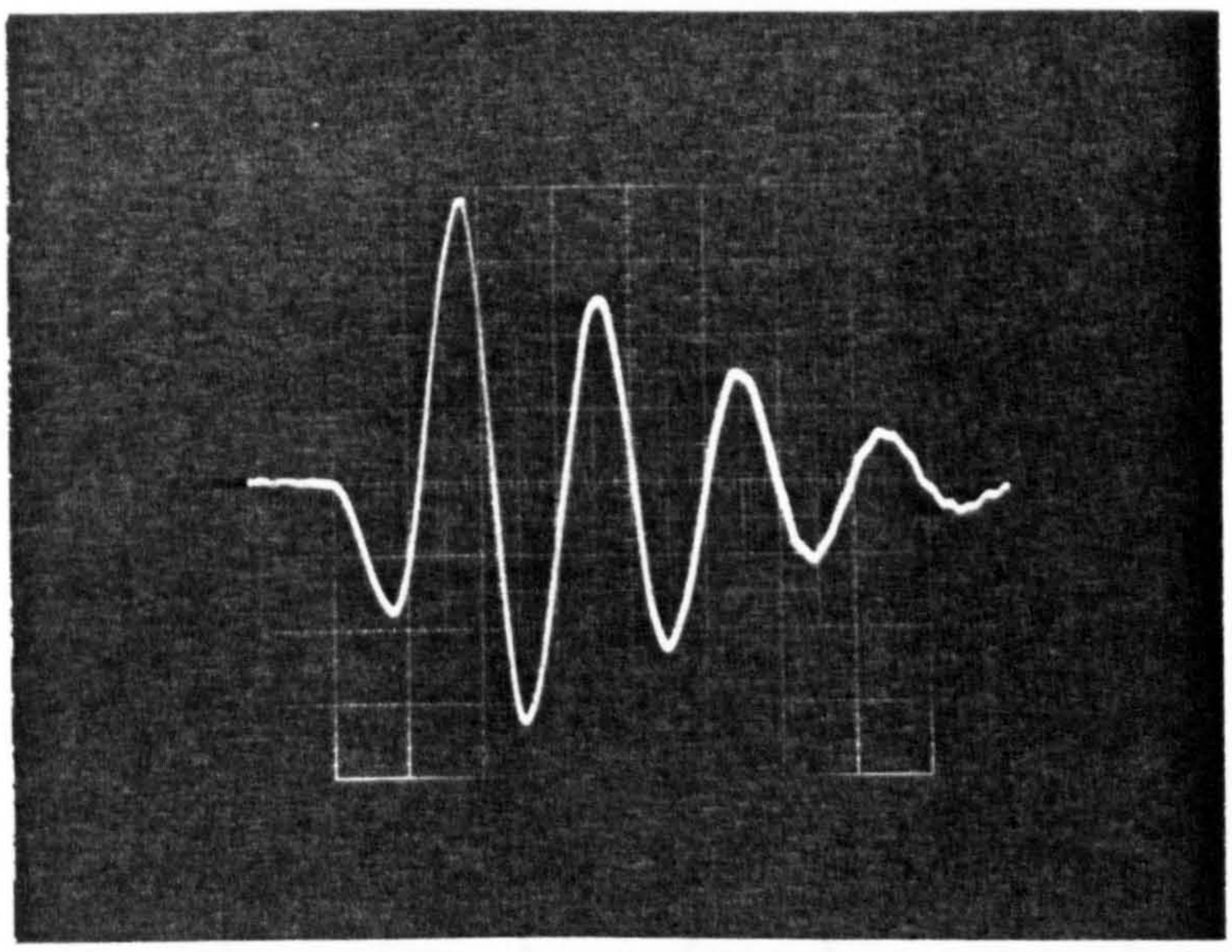

FIG 5.22C

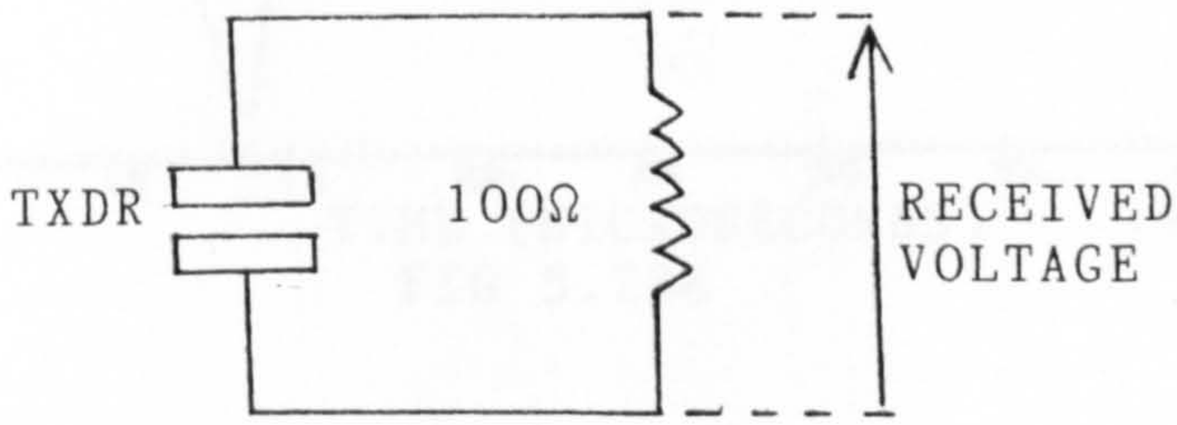

FIG 5.22A

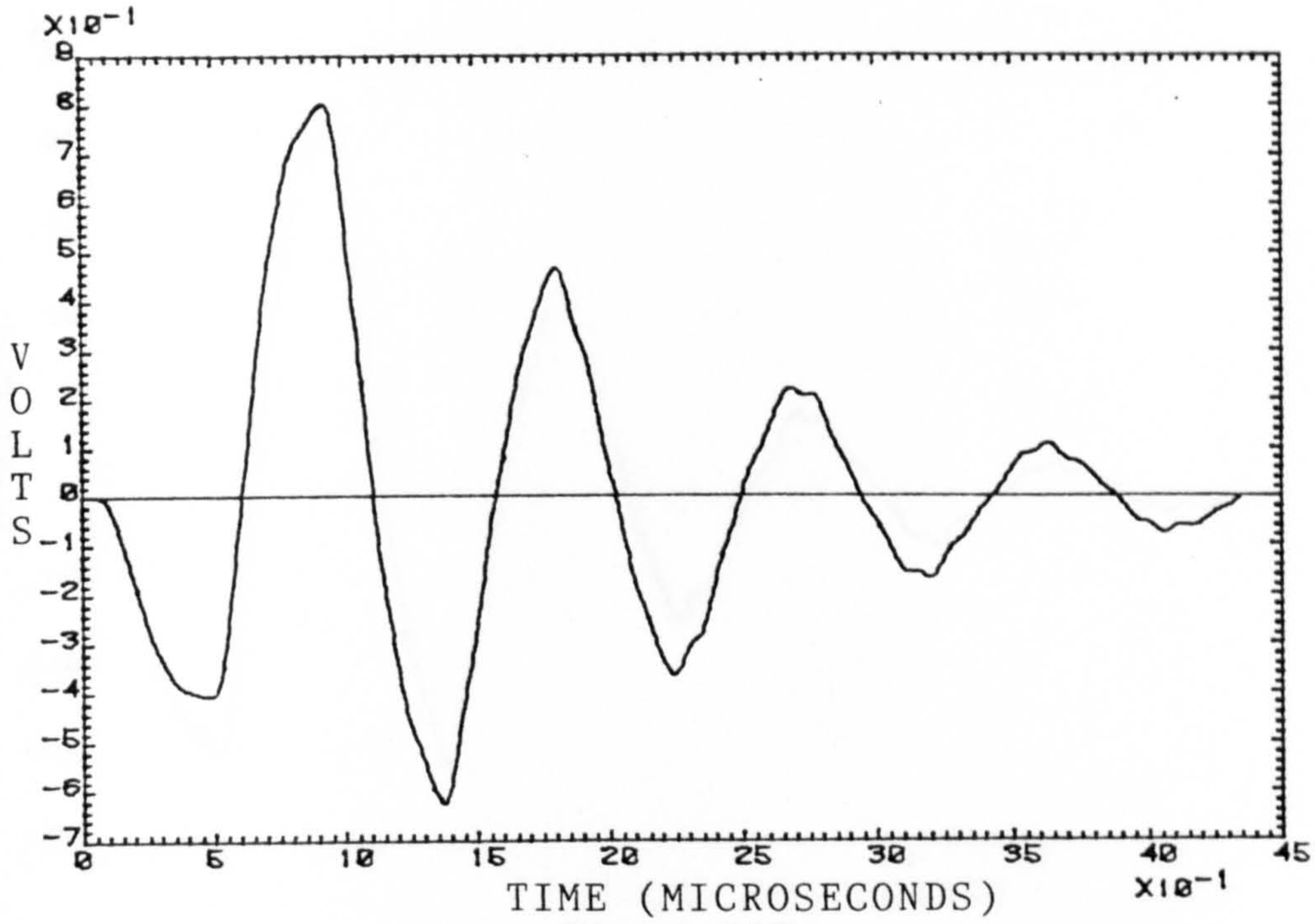

FIG 5.22D

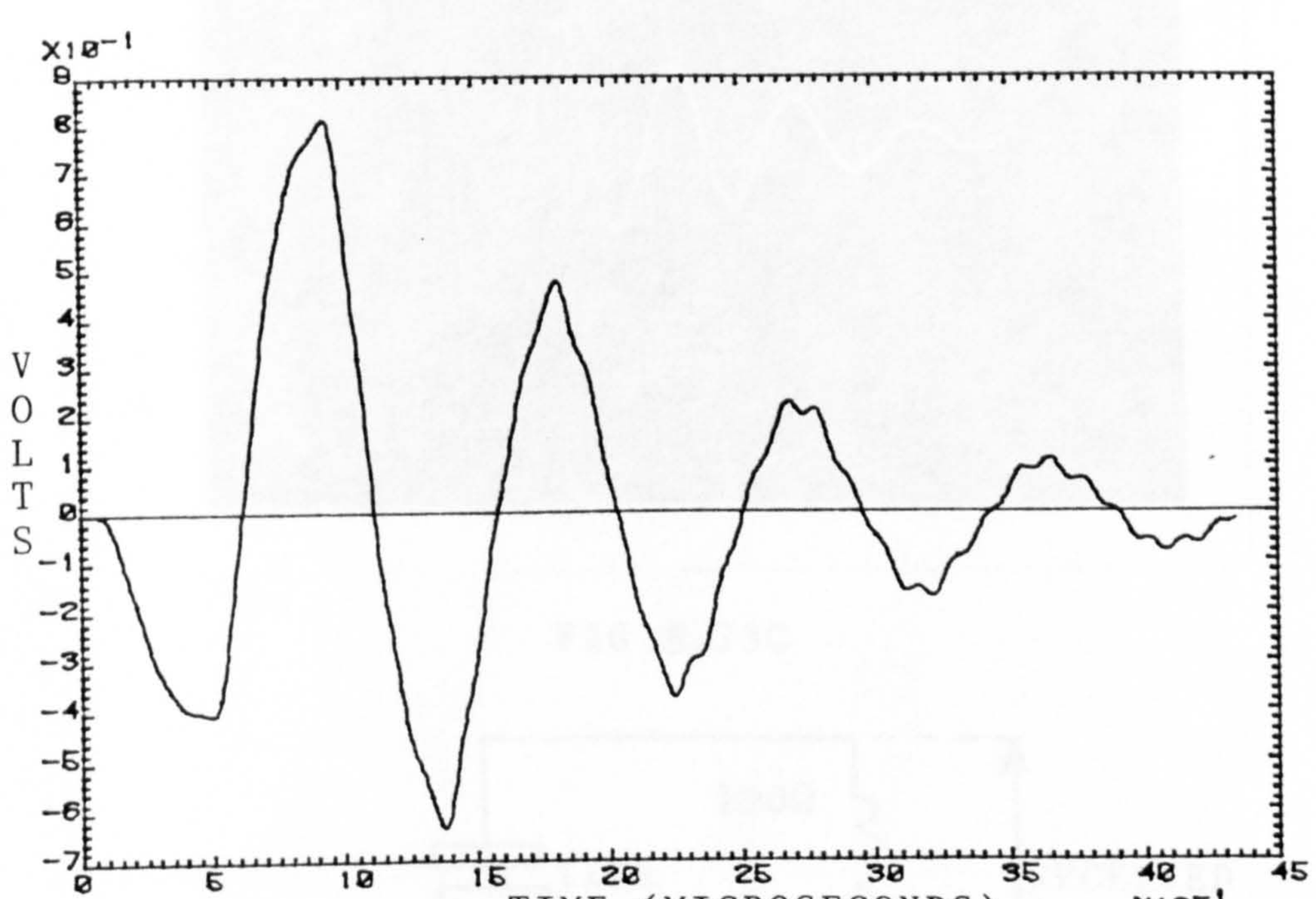

FIG 5.22E

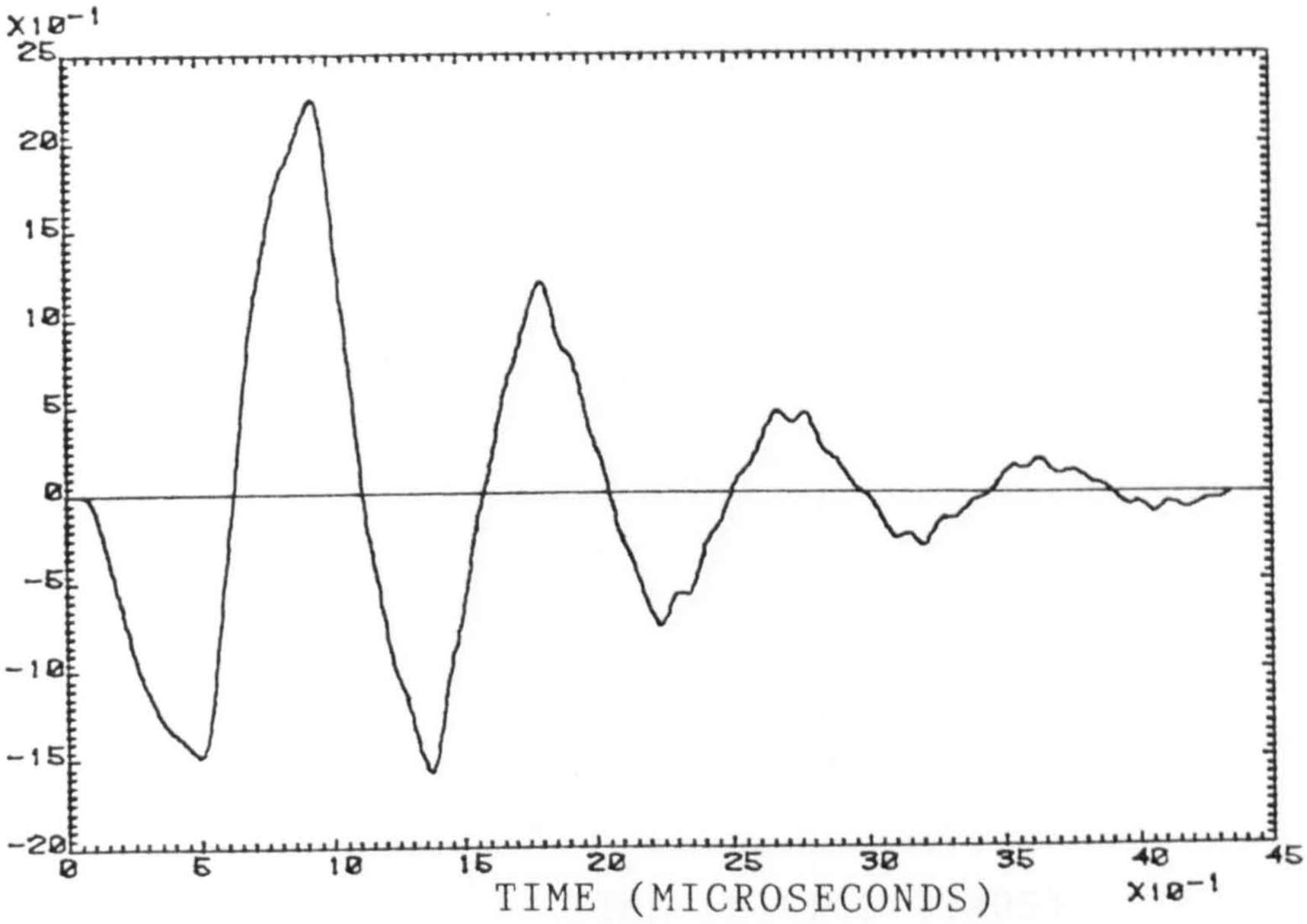

FIG 5.23B

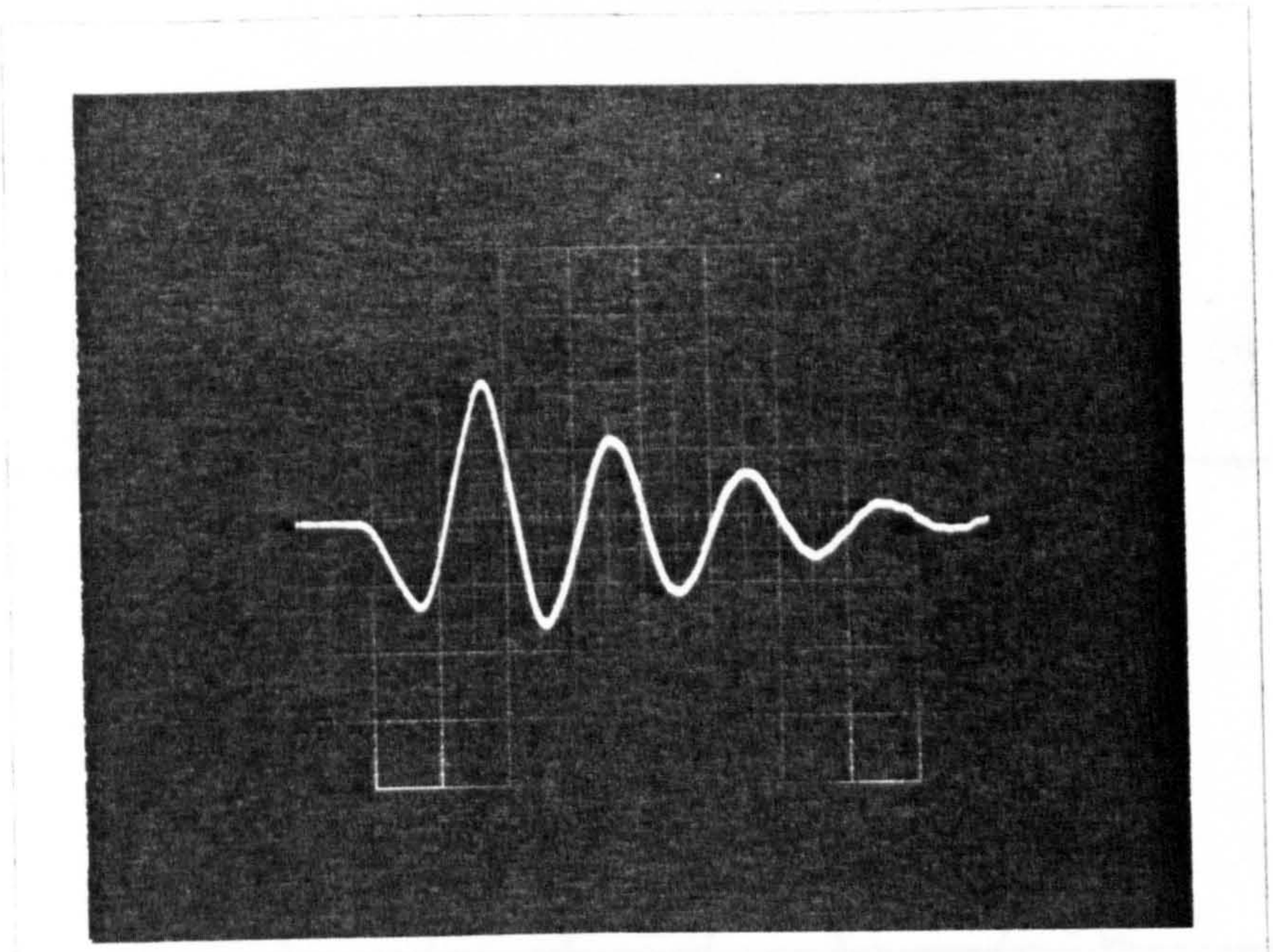

FIG 5.23C

FIG 5.23A

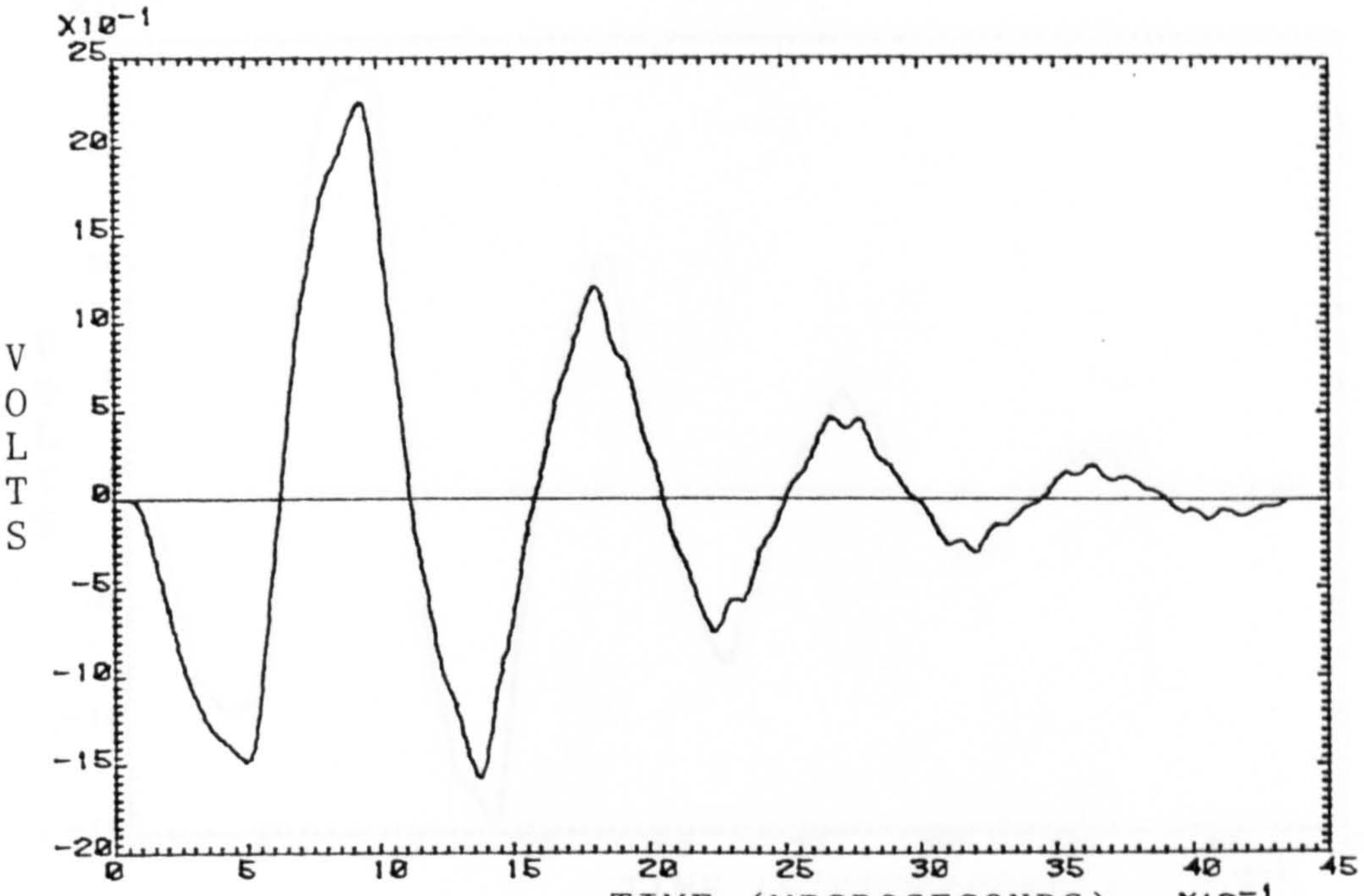

TIME (MICROSECONDS)

FIG 5.23D

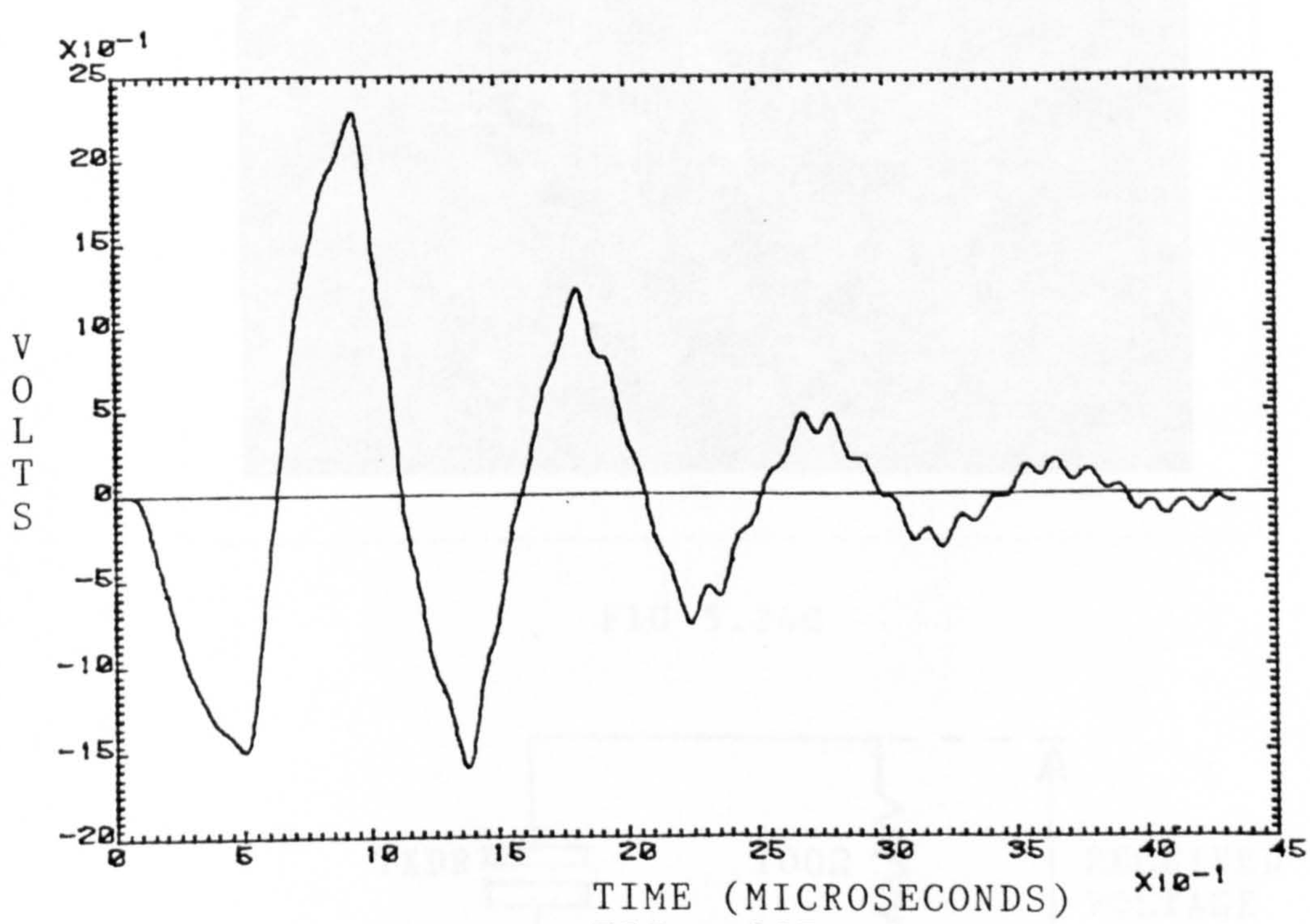

TIME (MICROSECONDS)

FIG 5.23E

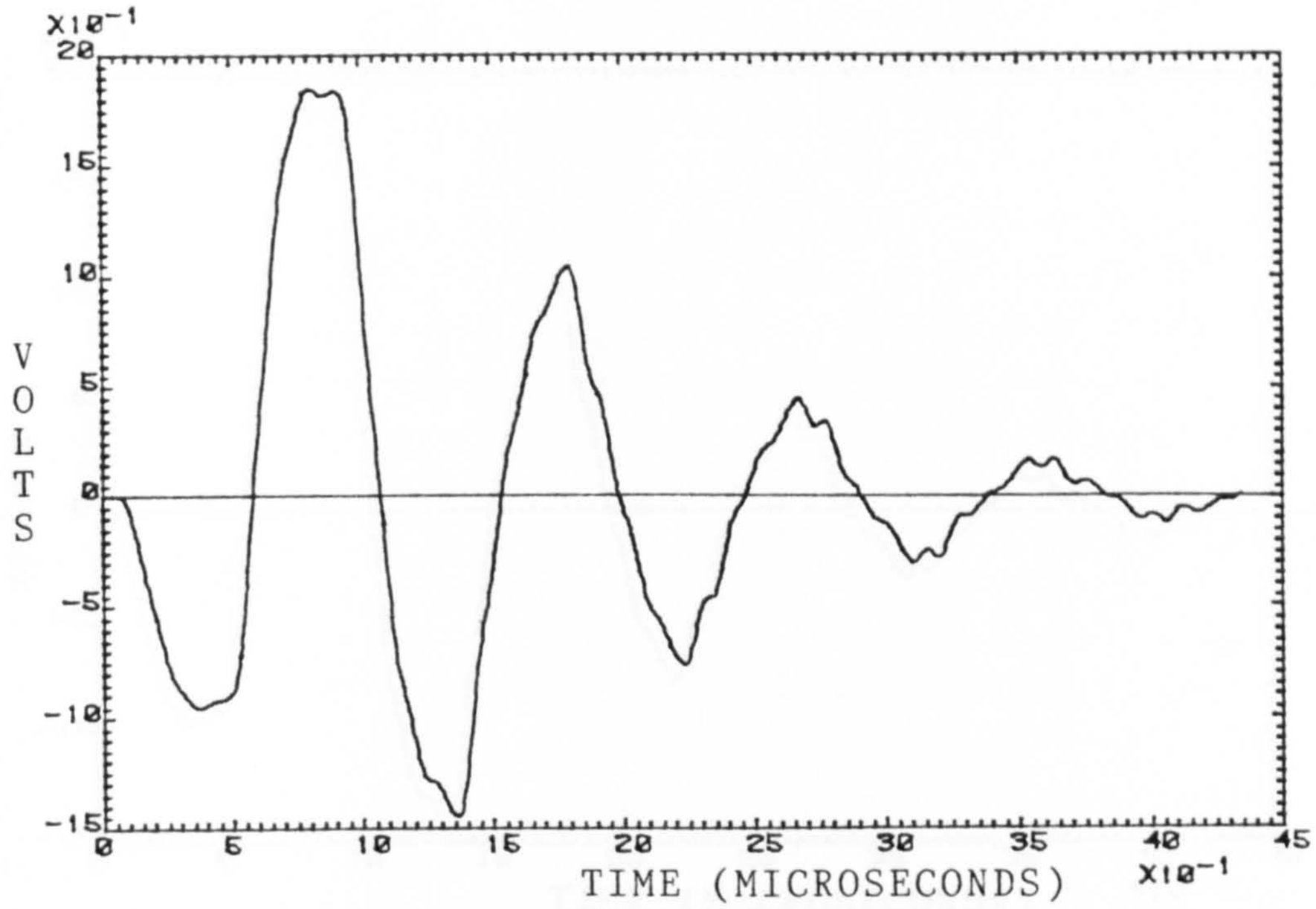

FIG 5.24B

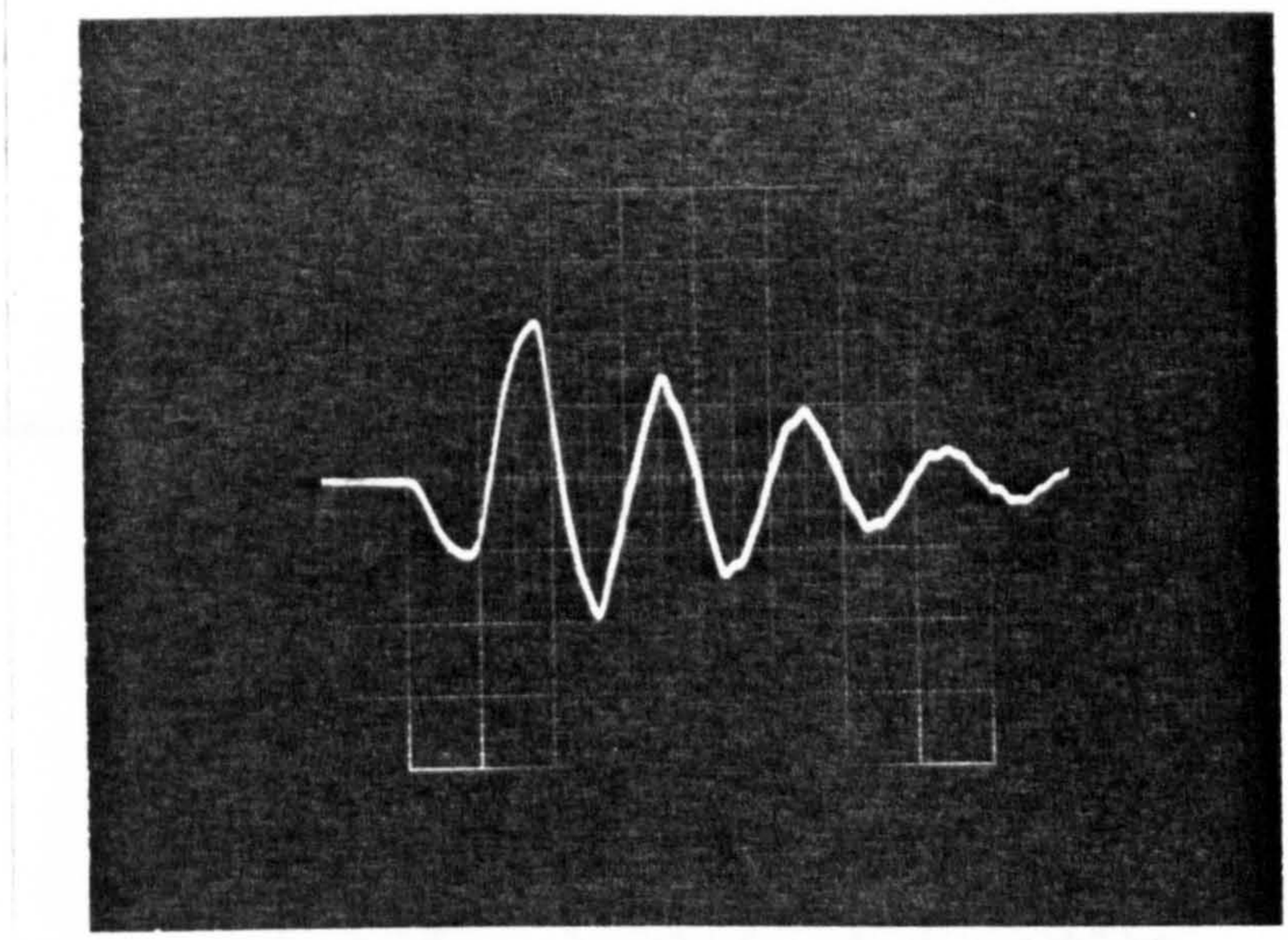

FIG 5.24C

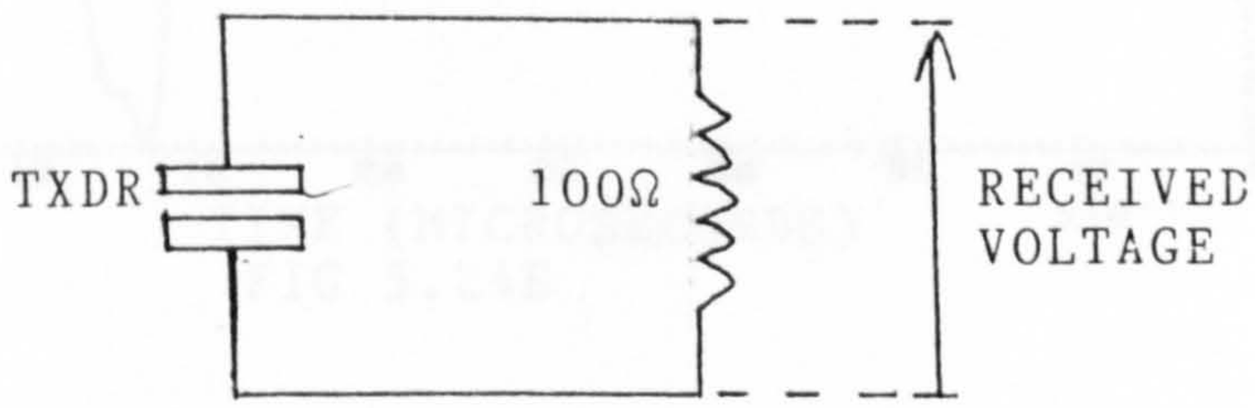

FIG 5.24A

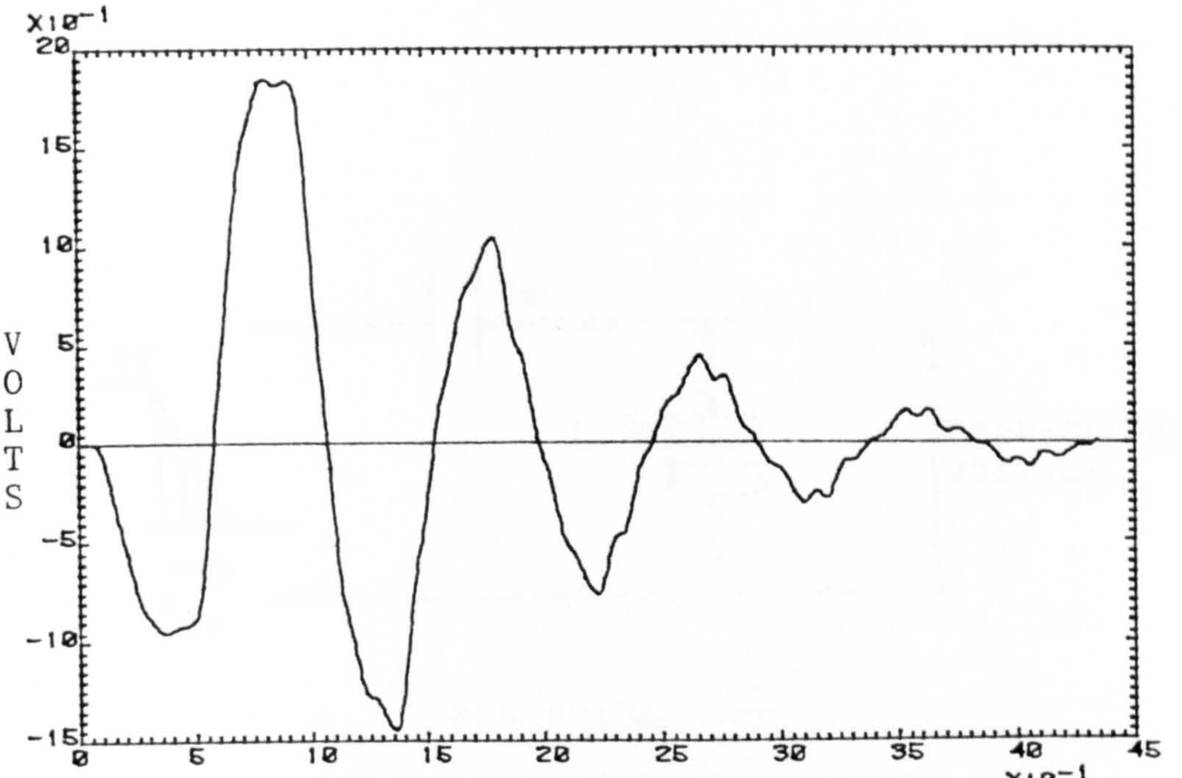

TIME (MICROSECONDS)

FIG 5.24D

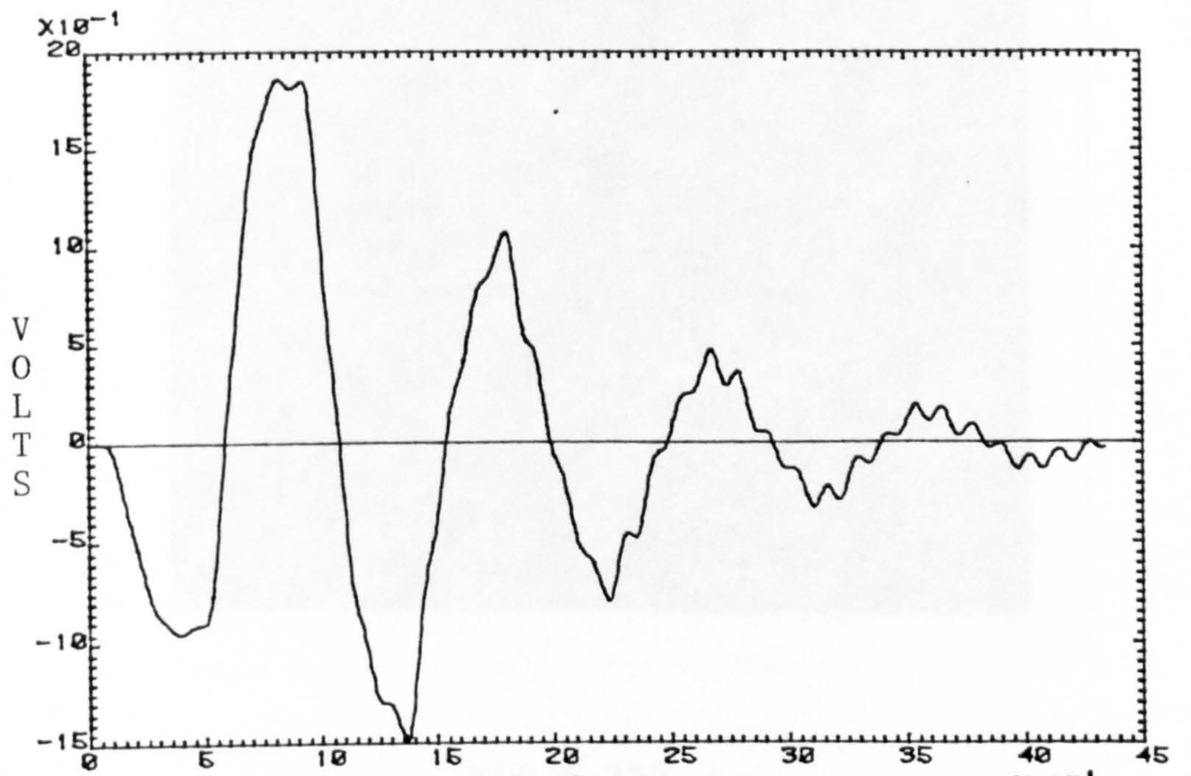

TIME (MICROSECONDS)

FIG 5.24E

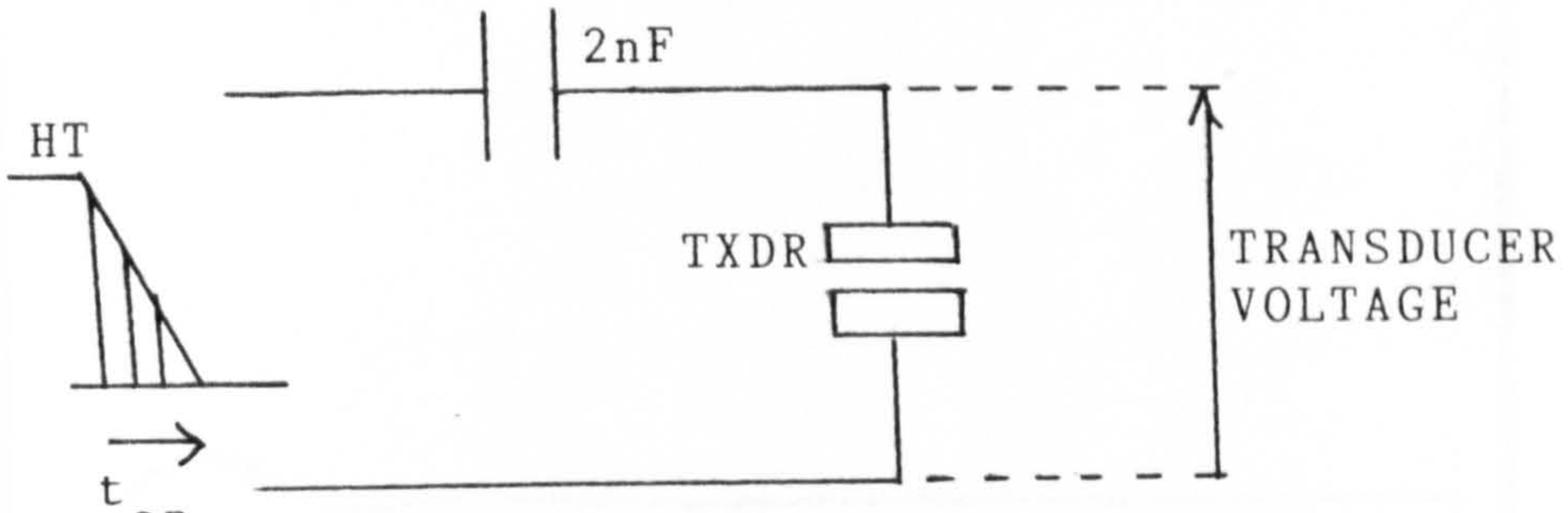

FIG 5.25A

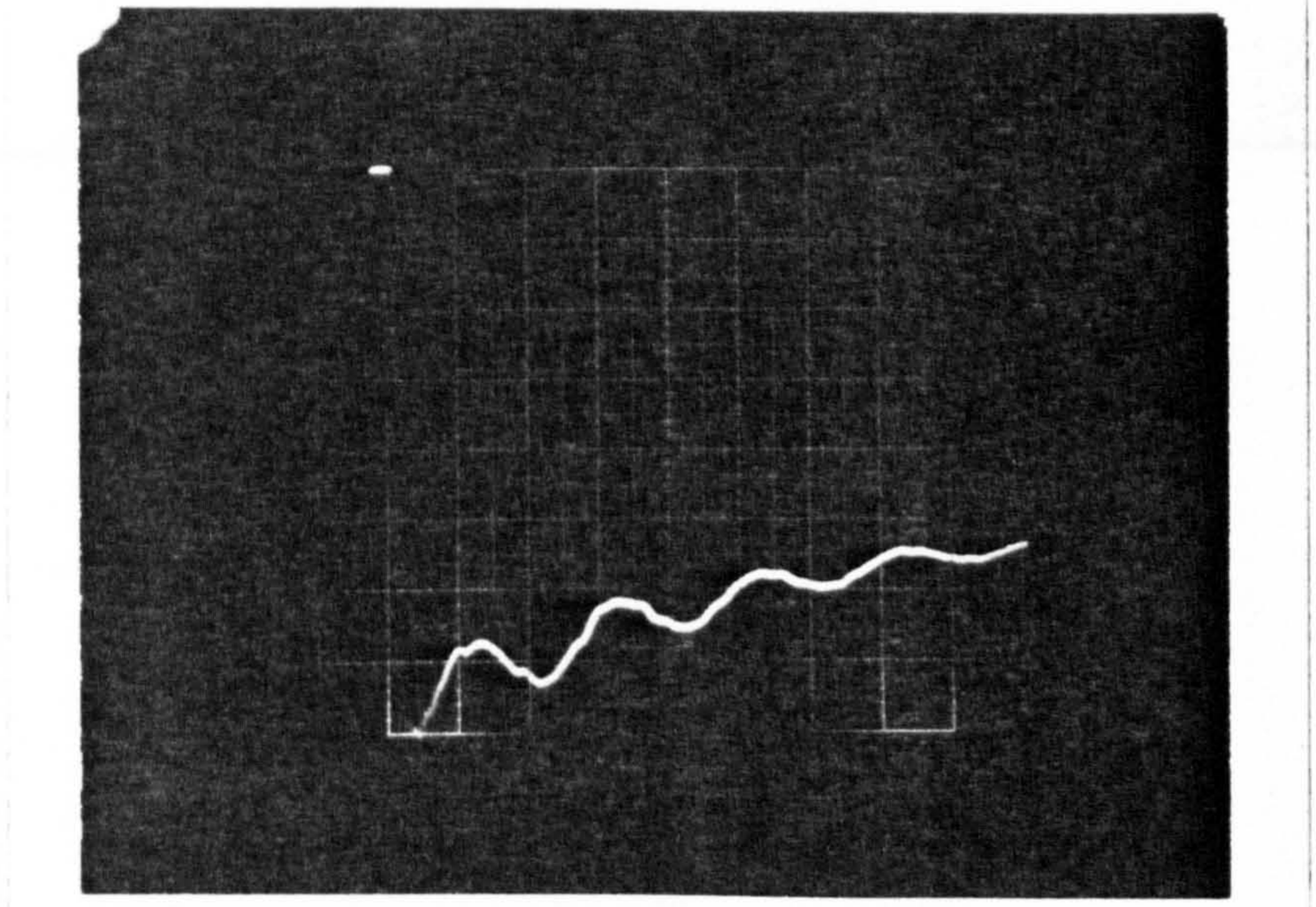

FIG 5.25B

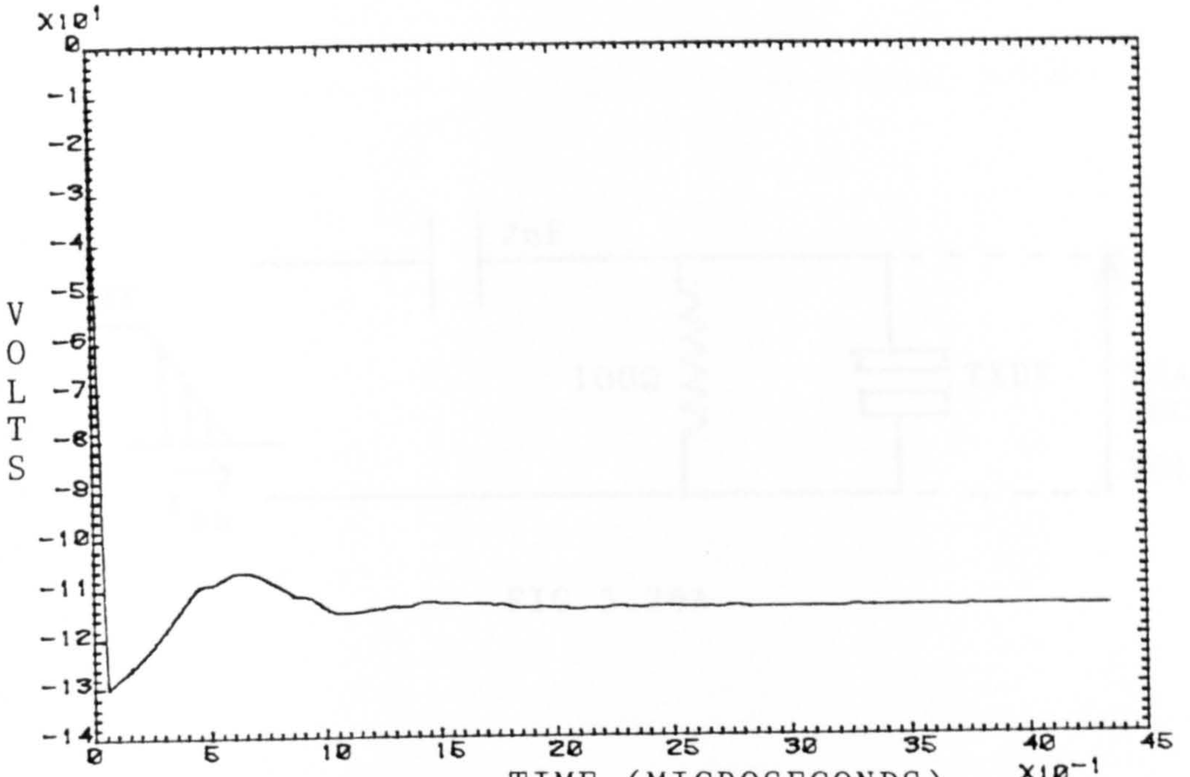

TIME (MICROSECONDS)

FIG 5.25C

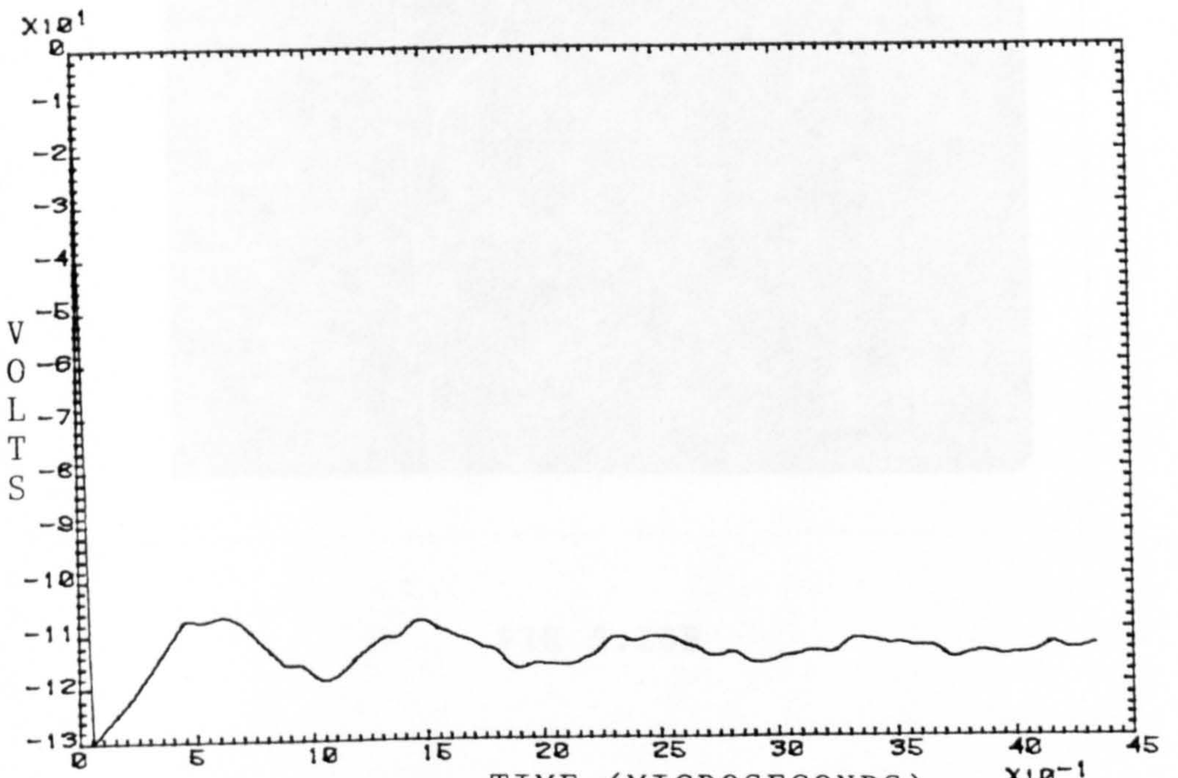

TIME (MICROSECONDS)

FIG 5.25D

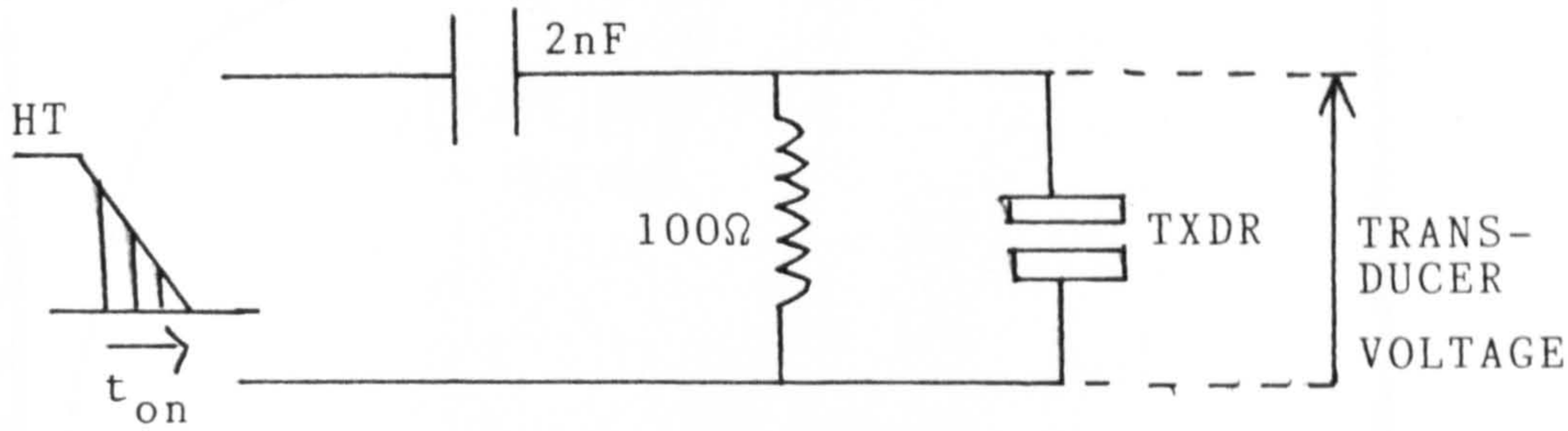

FIG 5.26A

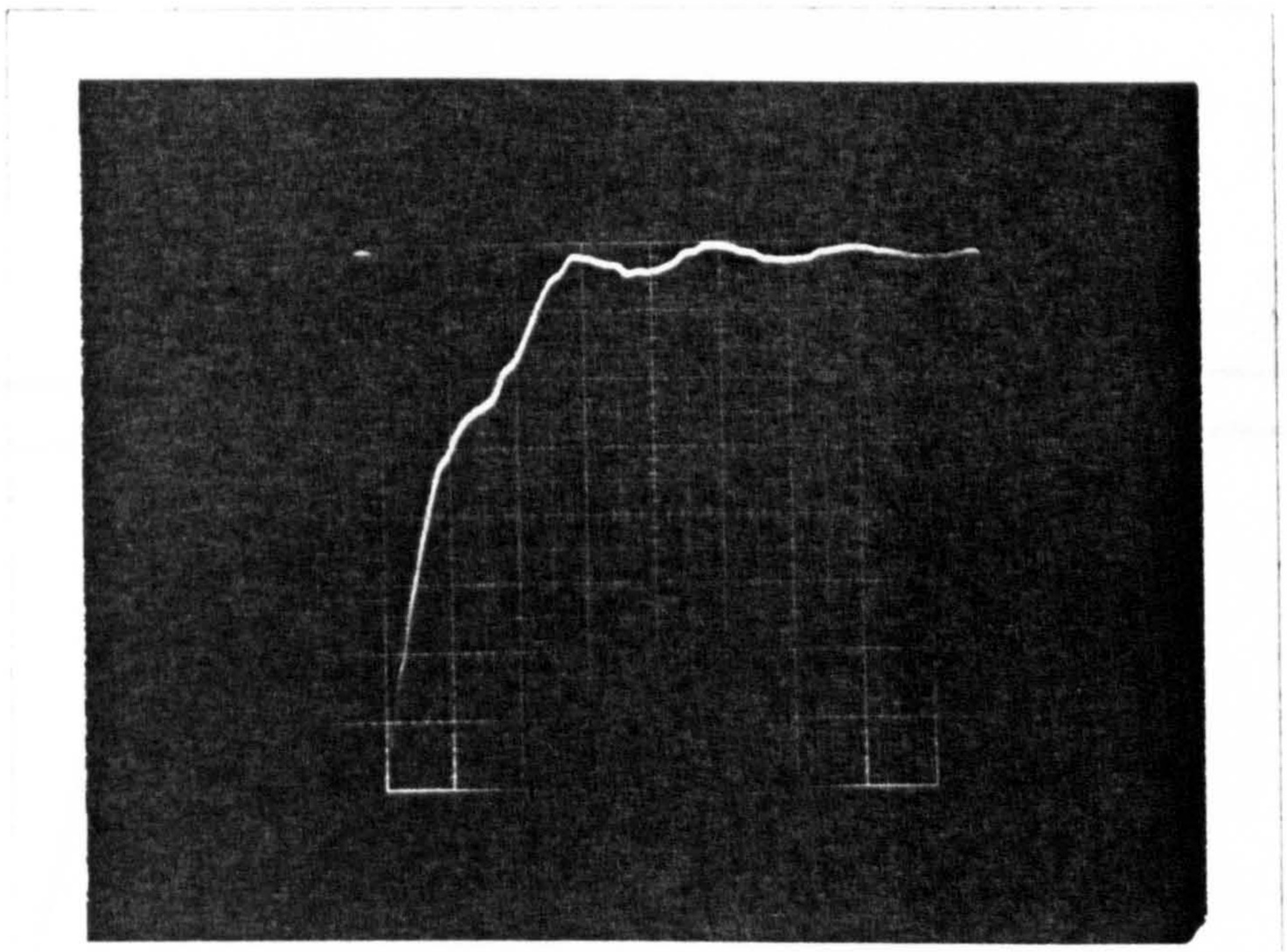

FIG 5.26B

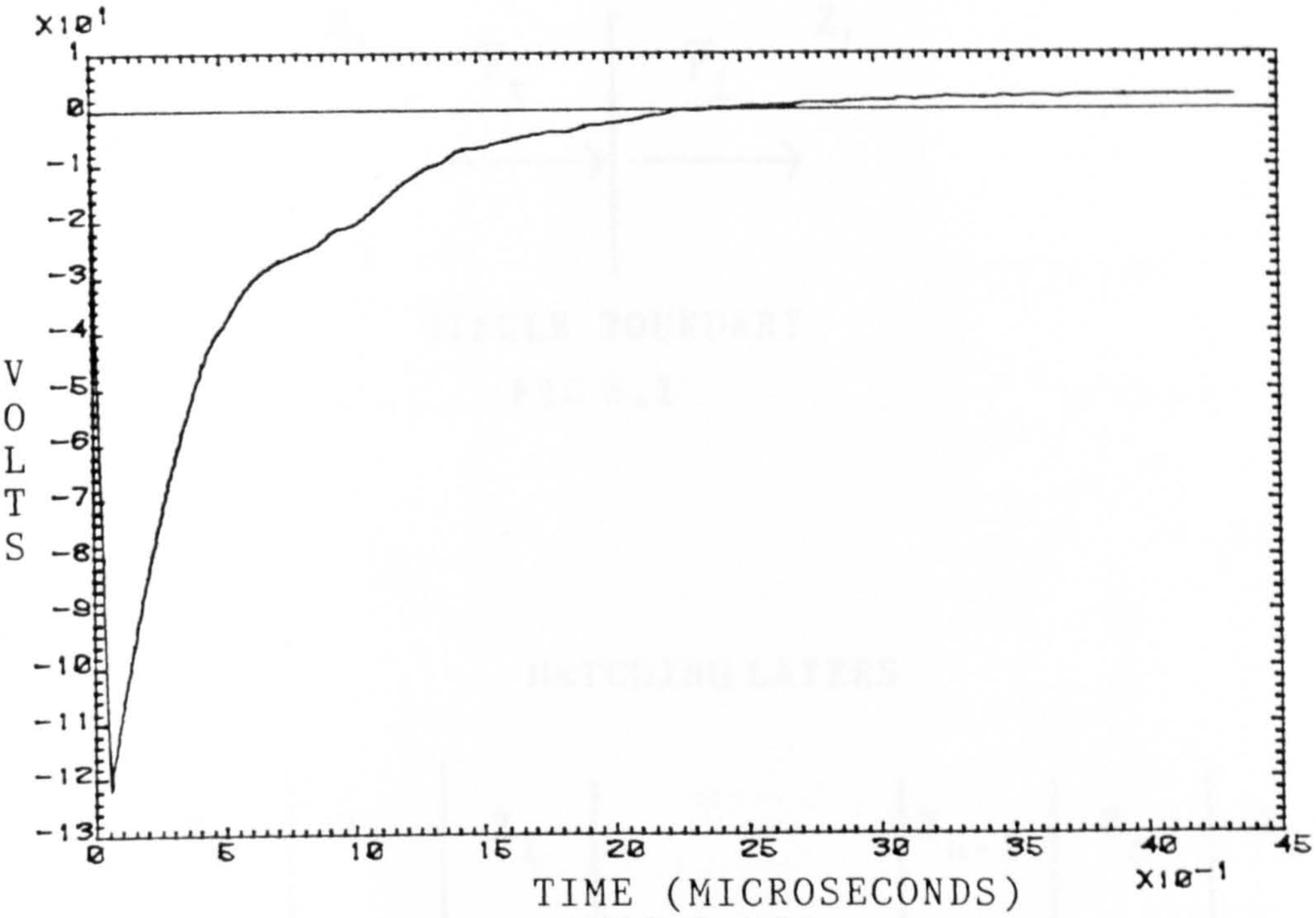

TIME (MICROSECONDS)

FIG 5.26C

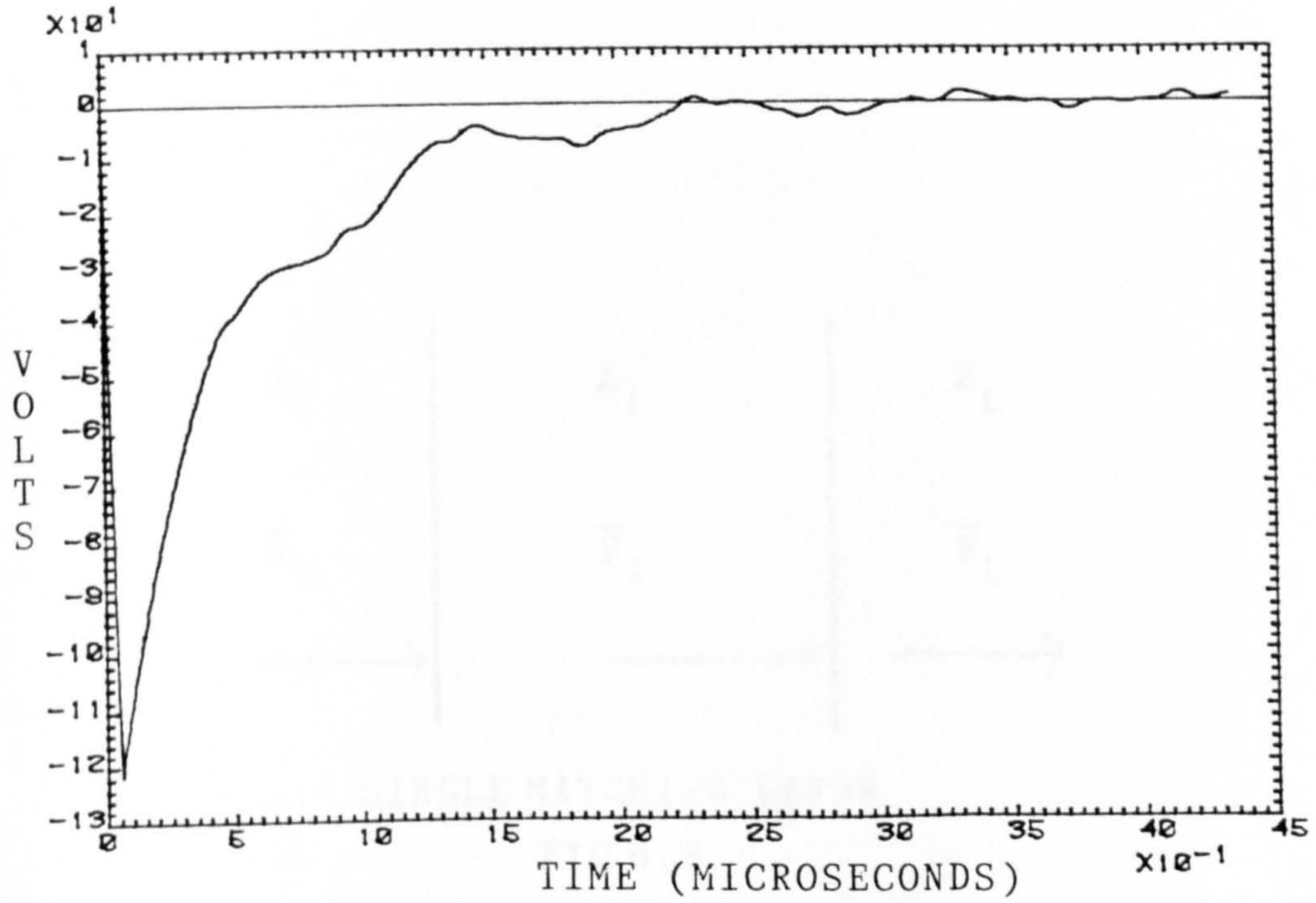

TIME (MICROSECONDS)

FIG 5.26D

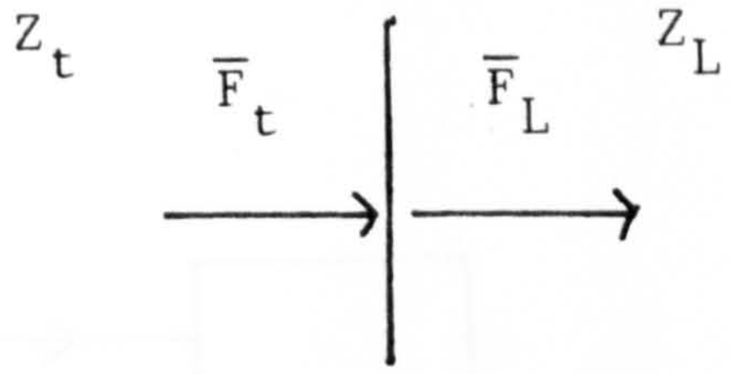

SINGLE BOUNDARY

FIG 6.1

MATCHING LAYERS

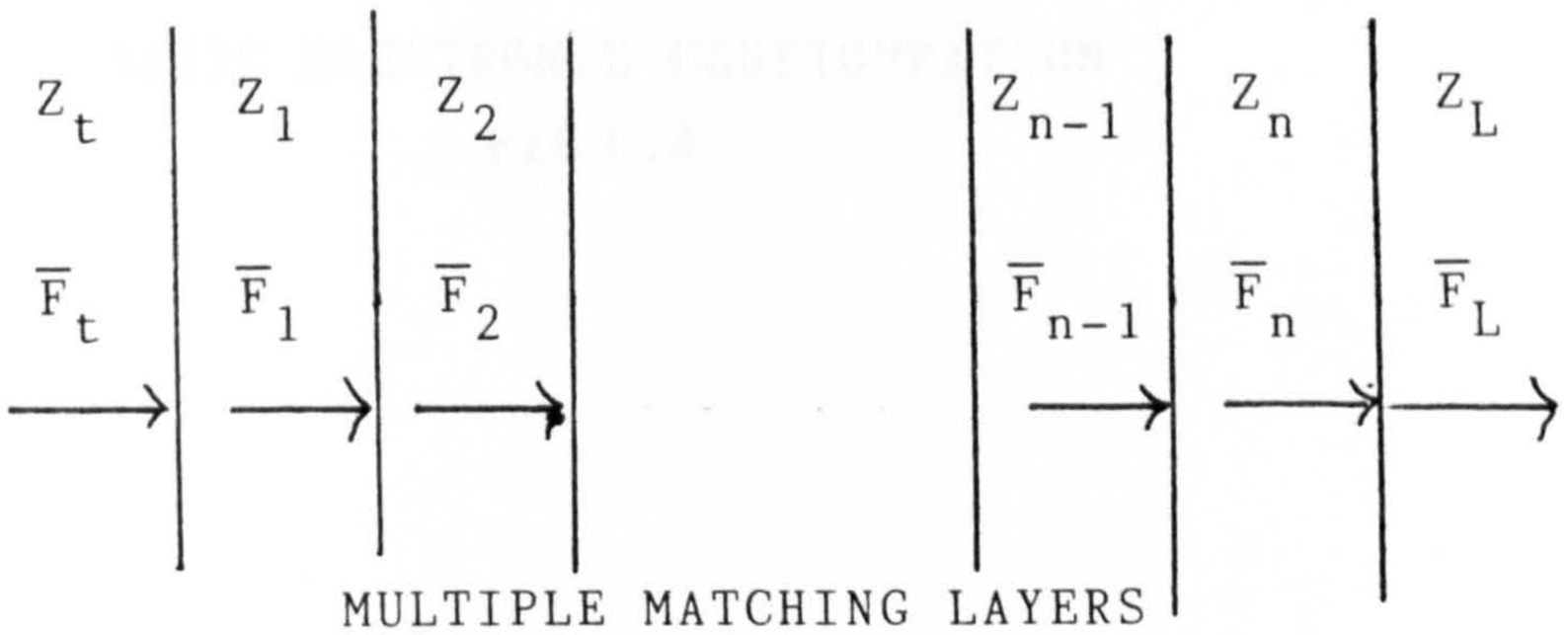

MULTIPLE MATCHING LAYERS

FIG 6.2

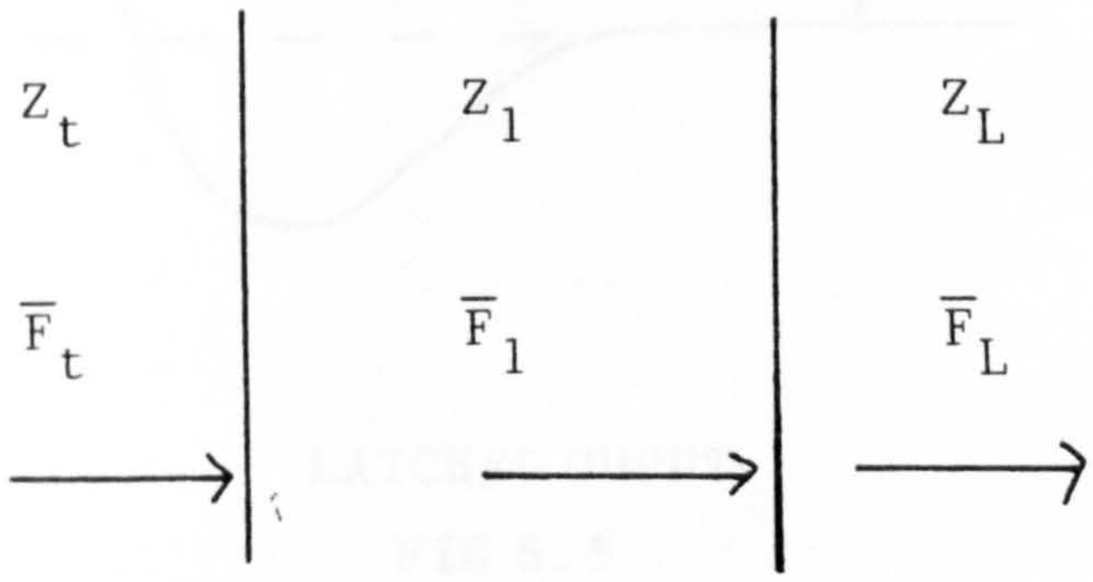

SINGLE MATCHING LAYER

FIG 6.3

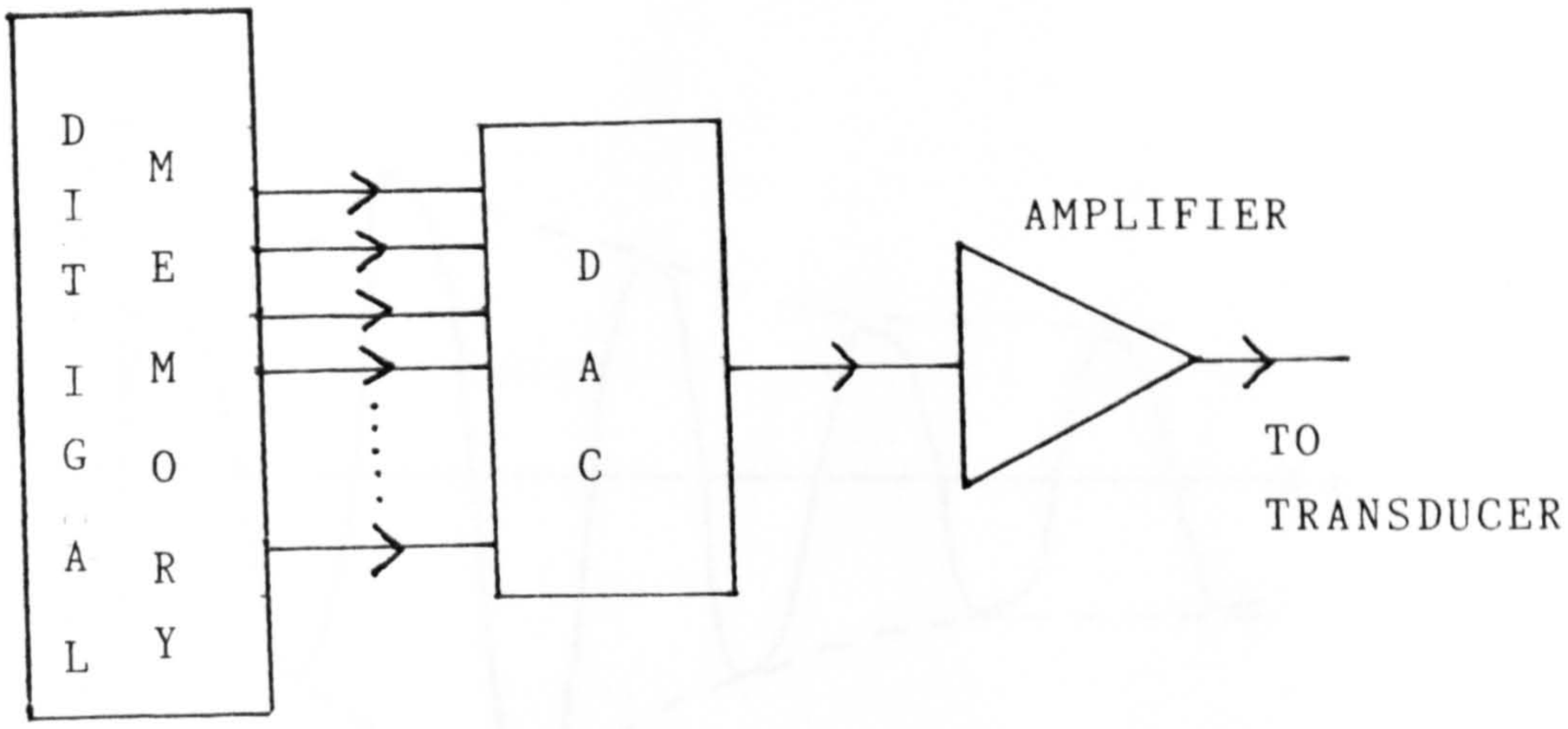

BASIC ELECTRONIC CONFIGURATION

FIG 6.4

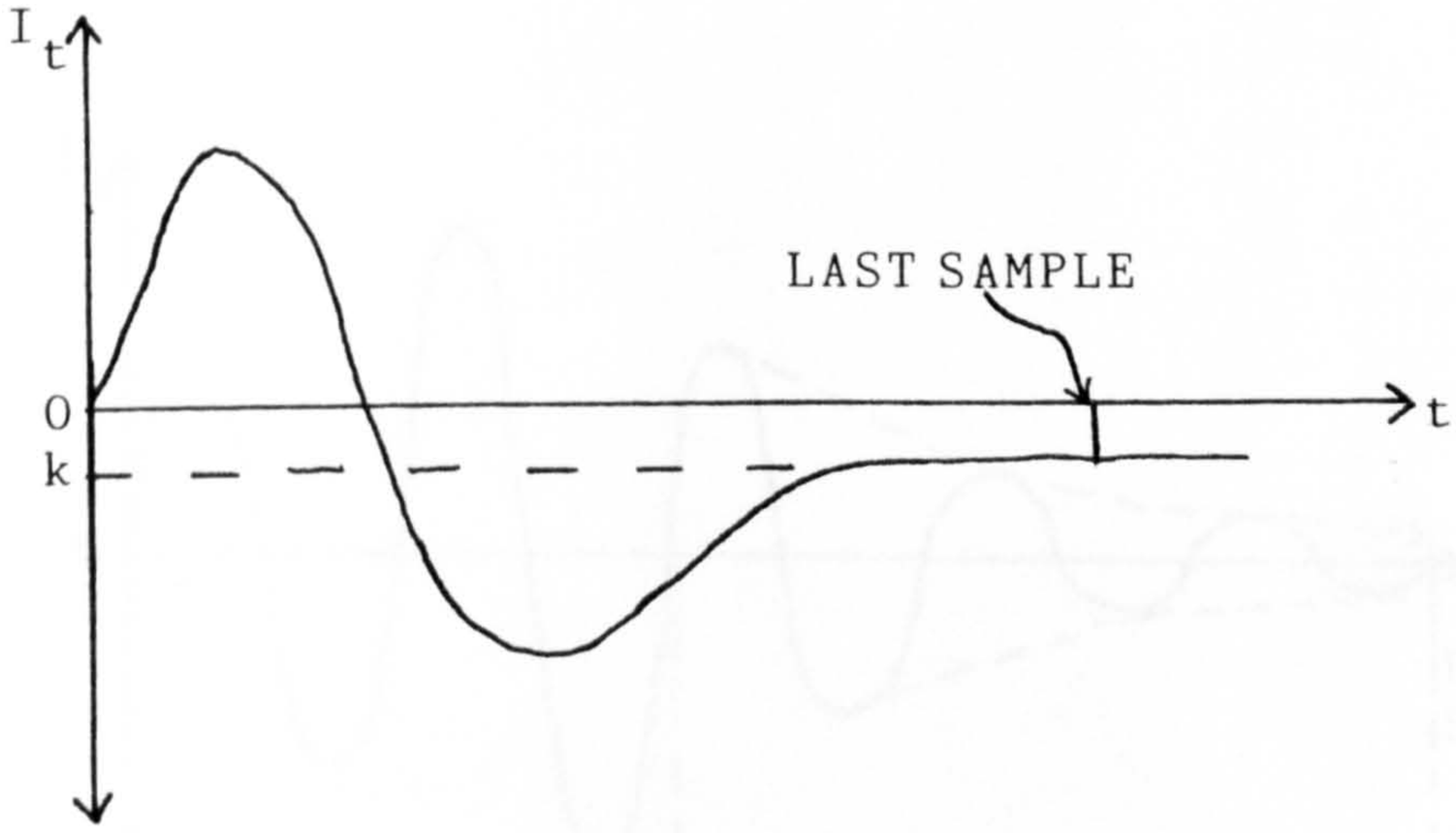

LATCHED OUPUT

FIG 6.5

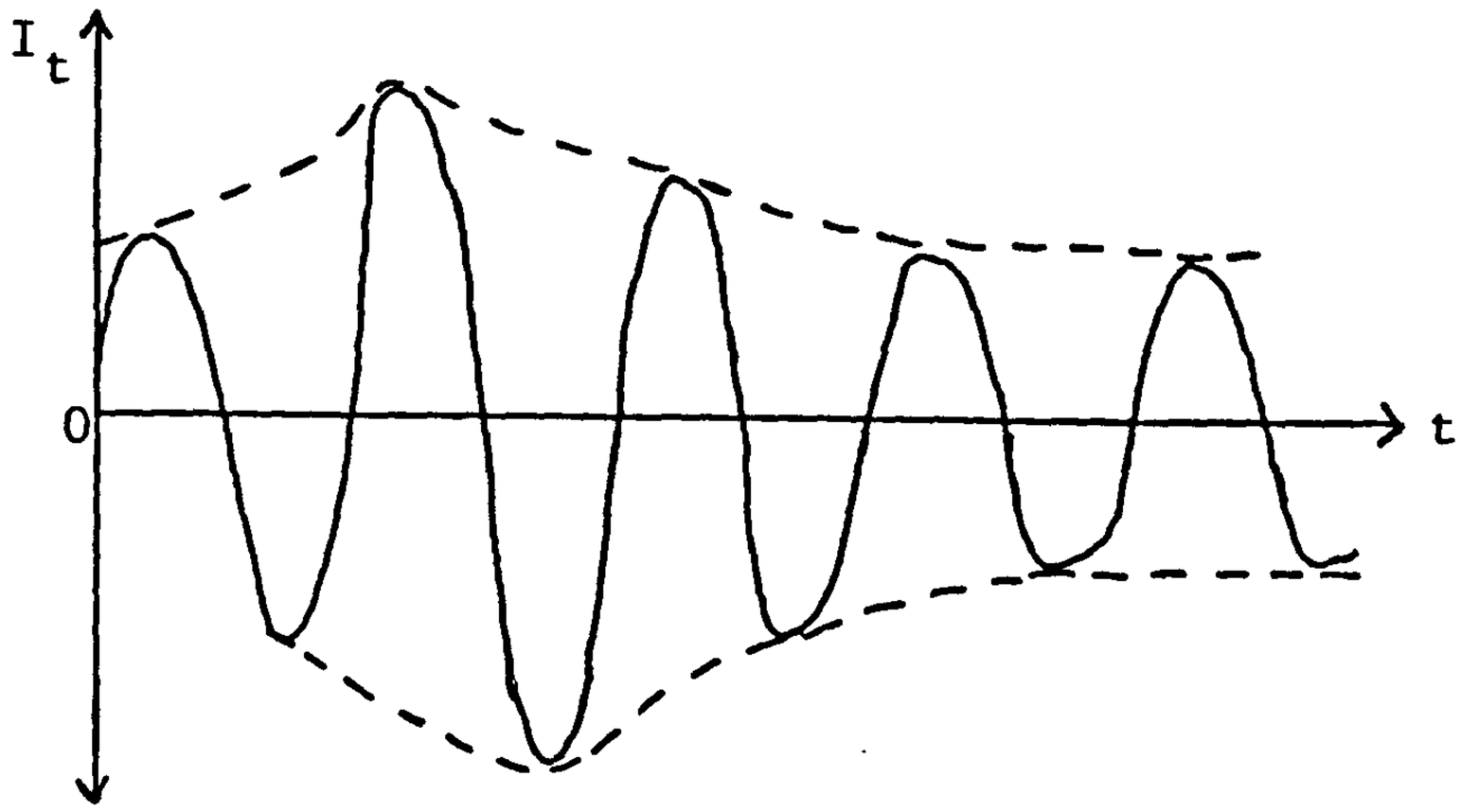

ENVELOPE CONVERGENCE

FIG 6.6

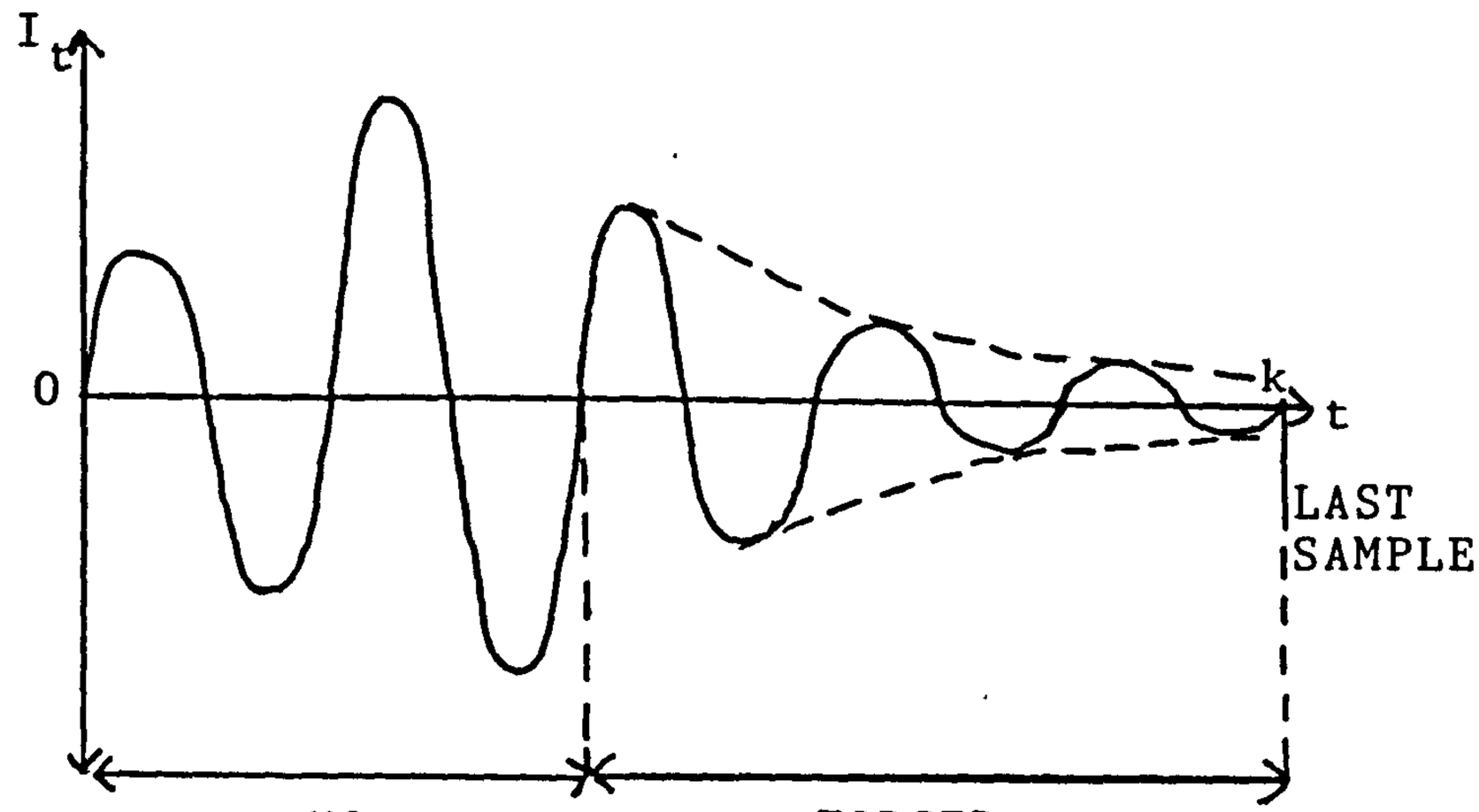

FORCED EXPONENTIAL CONVERGENCE

FIG 6.7

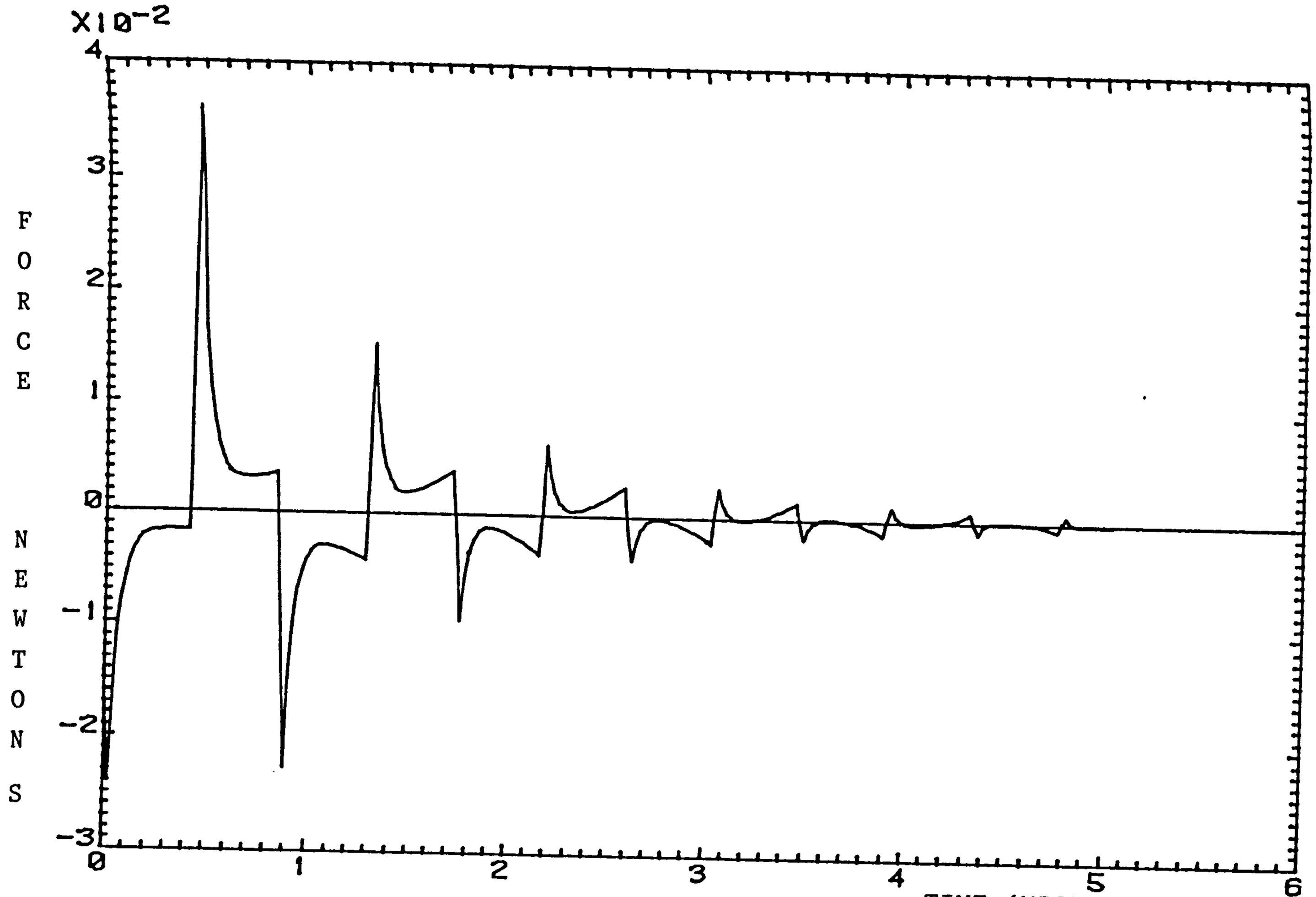

FIG 6.8

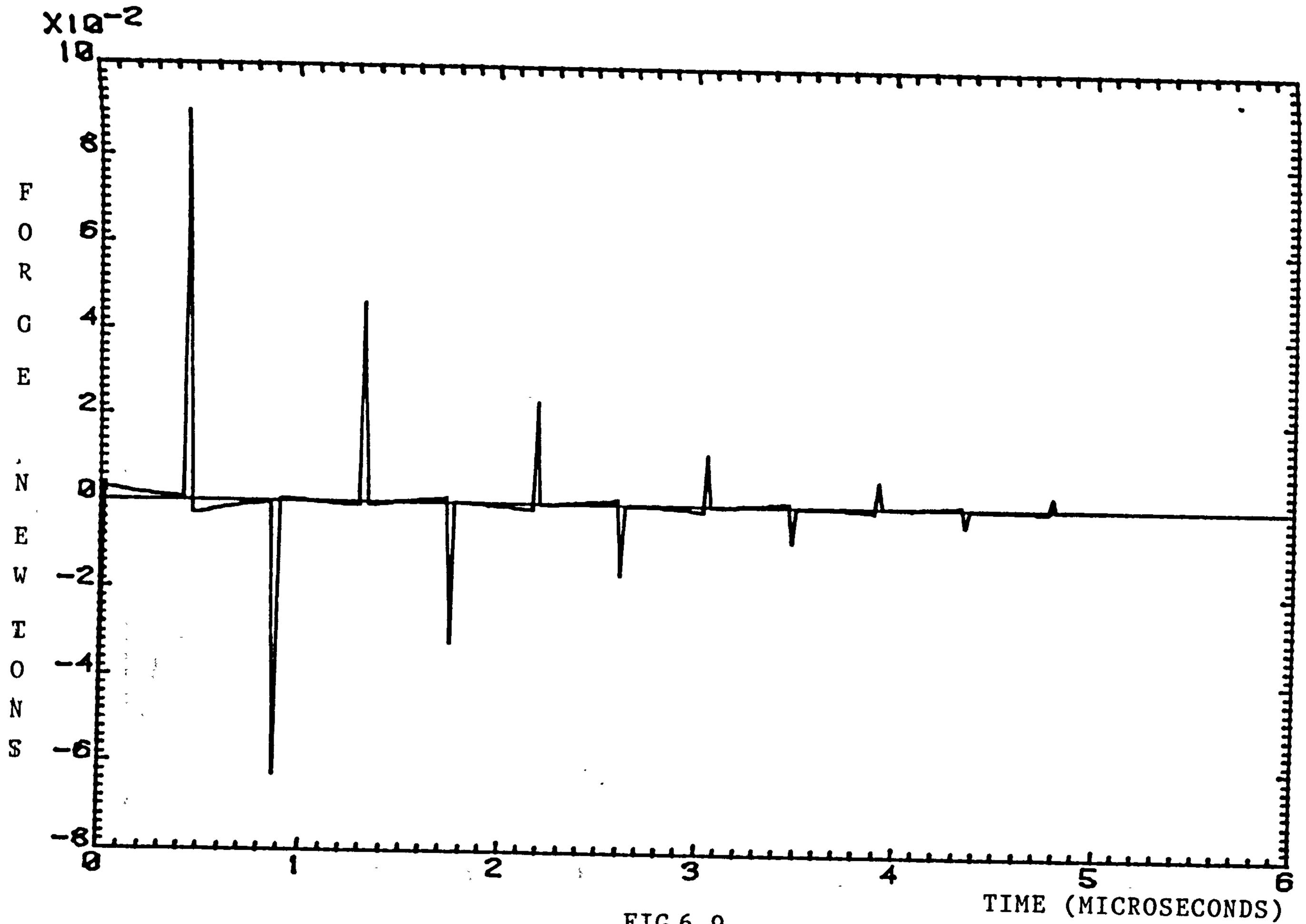
X10-2
10
8
6
4
2
0
-2
-4
-6
-8
FORCE NEWTONS
0
1
2
3
4
5
6
TIME (MICROSECONDS)

FIG 6.9

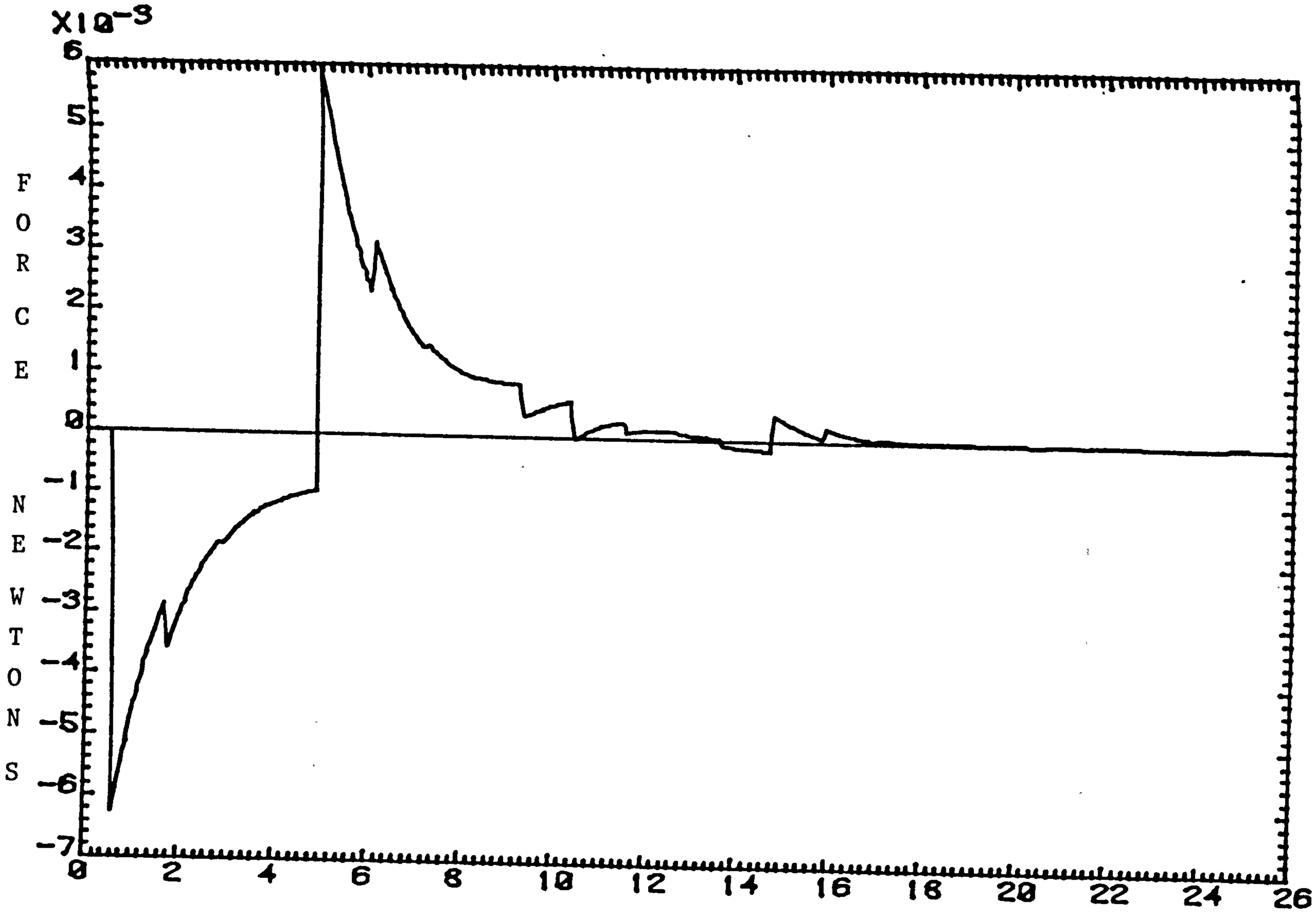
X10-3
6
5
4
3
2
1
0
-1
-2
-3
-4
-5
-6
-7
FORCE
NEWTONS
0
2
4
6
8
10
12
14
16
18
20
22
24
26
TIME (MICROSECONDS)
X10-1

FIG 6.10

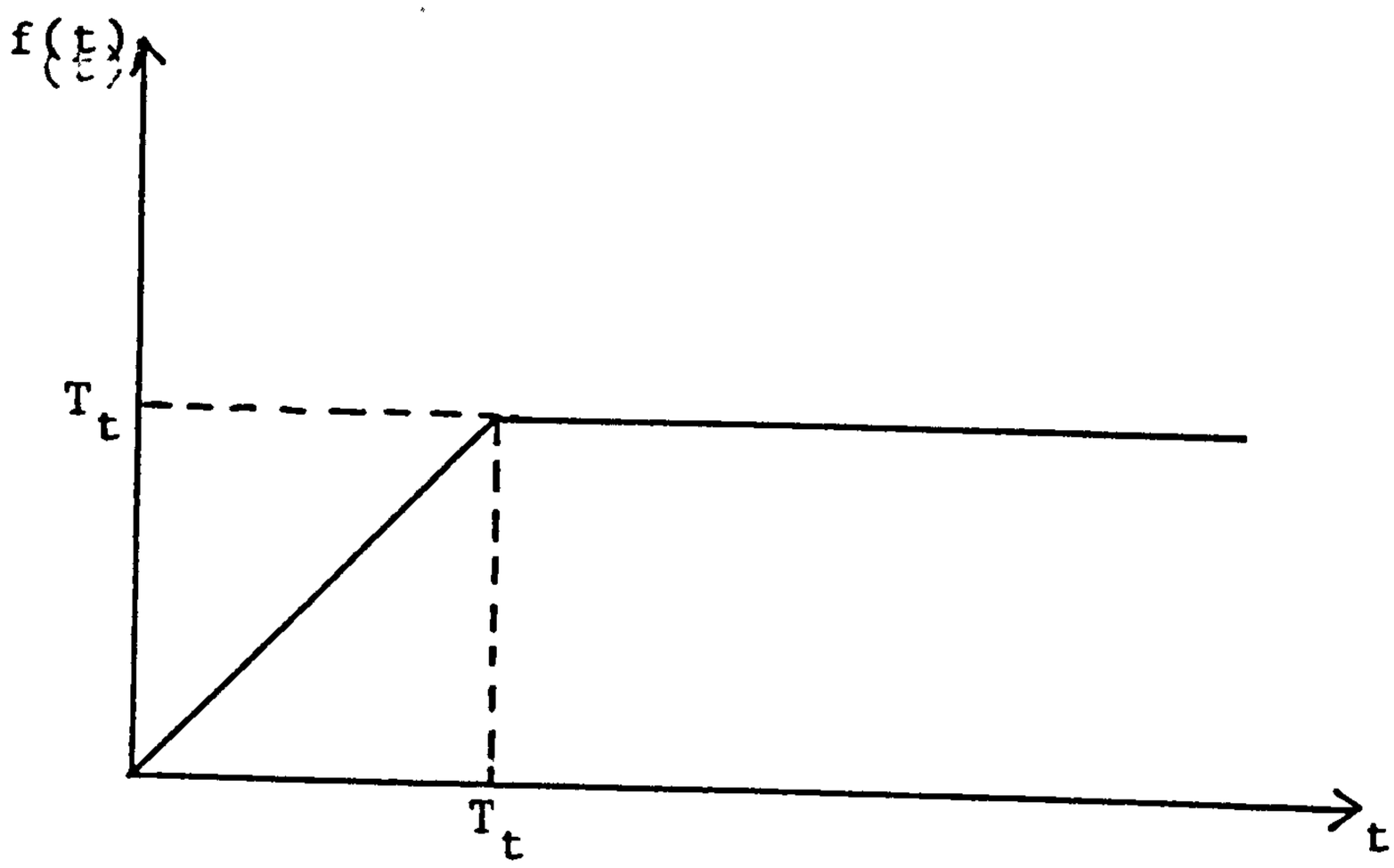

FIG 6.11

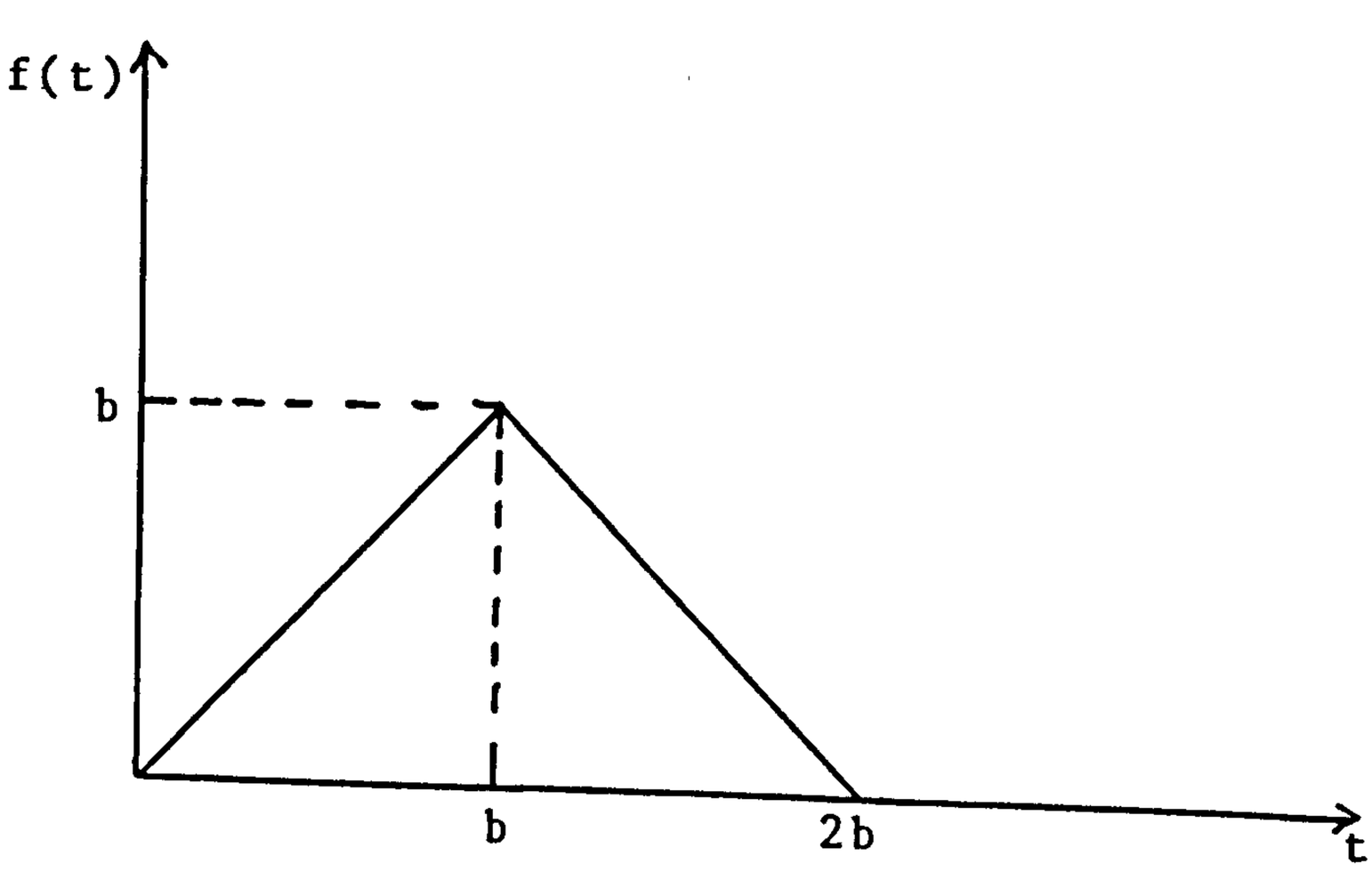

FIG 6.12

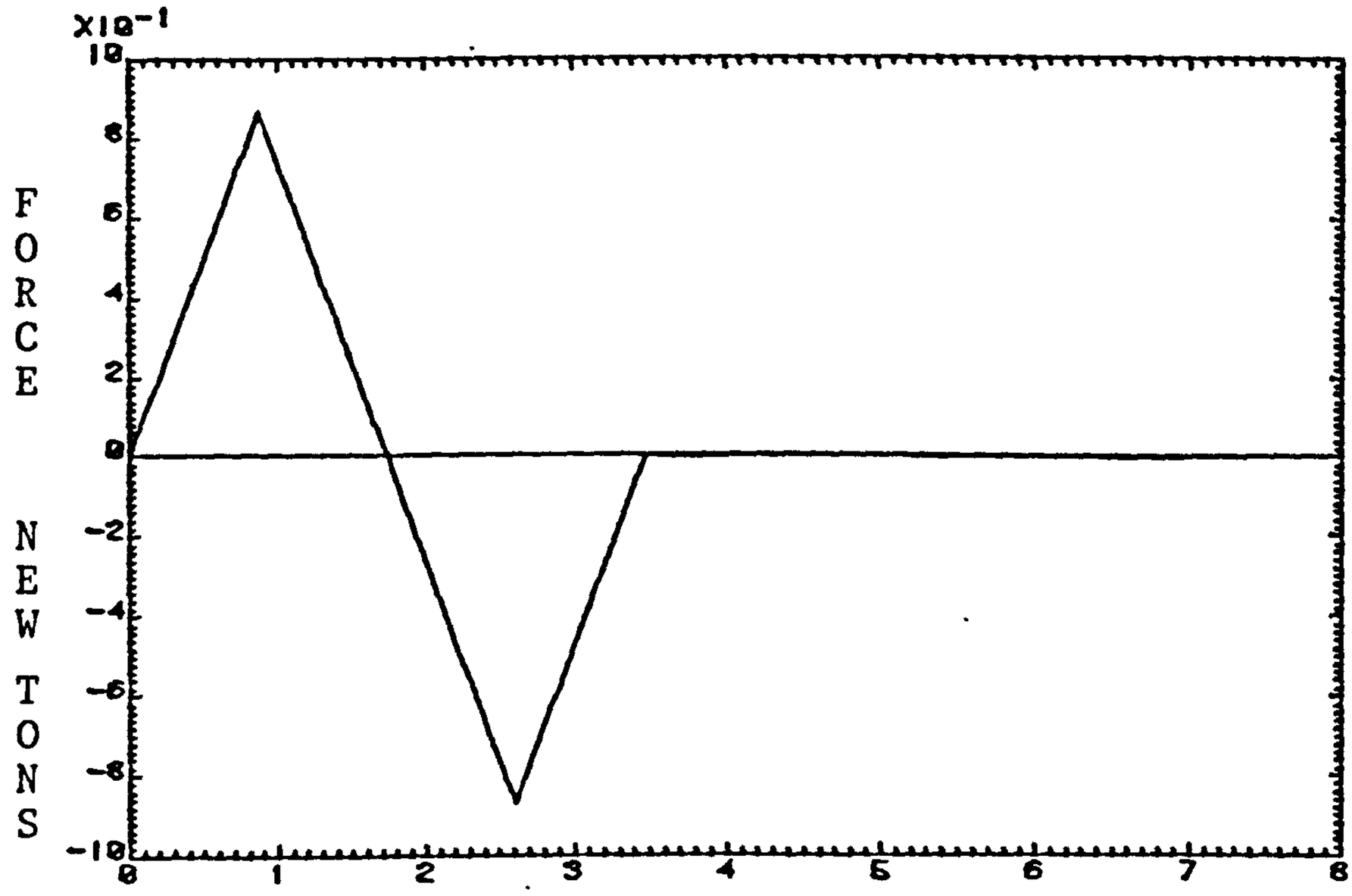

FIG 6.13A

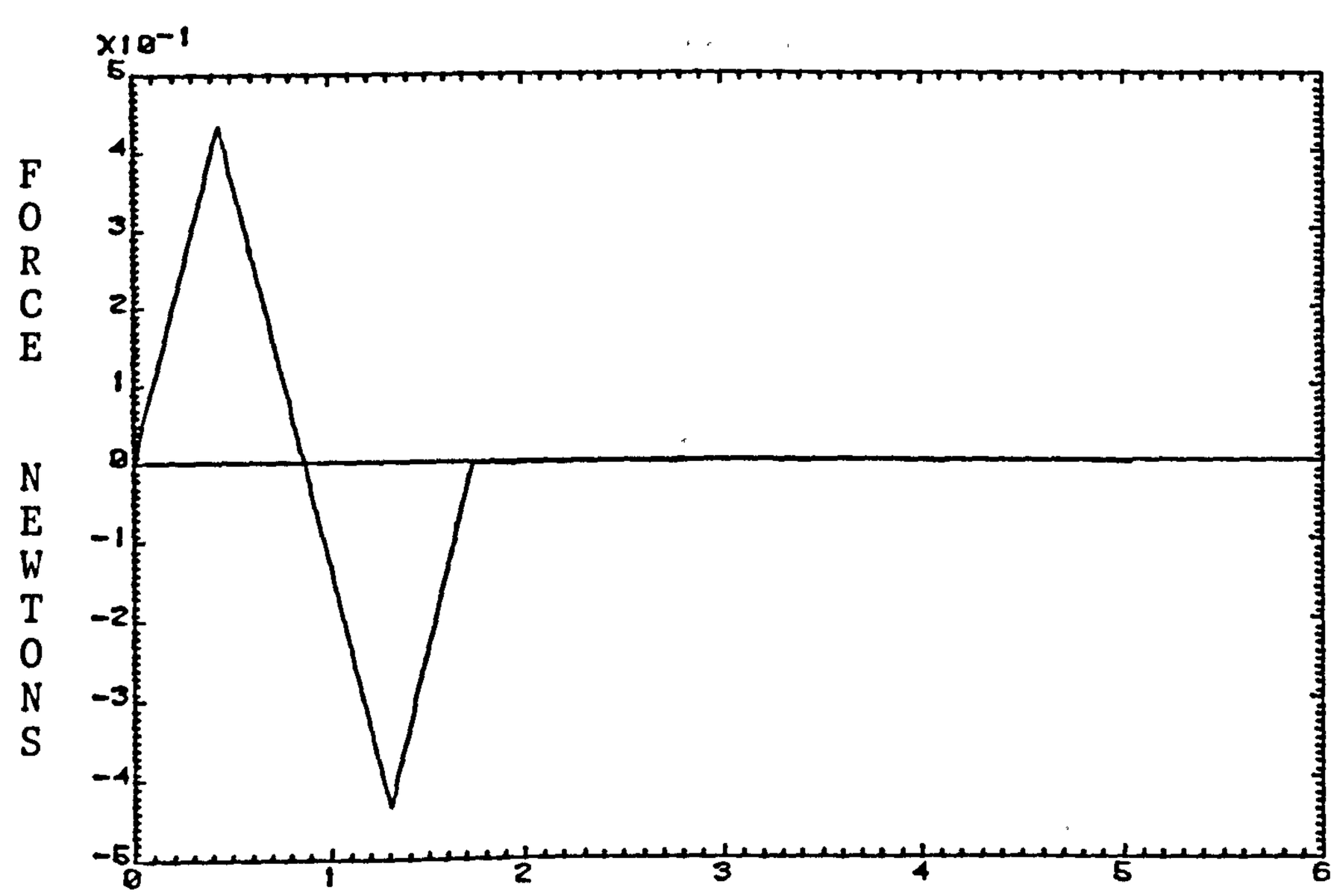

FIG6.13B

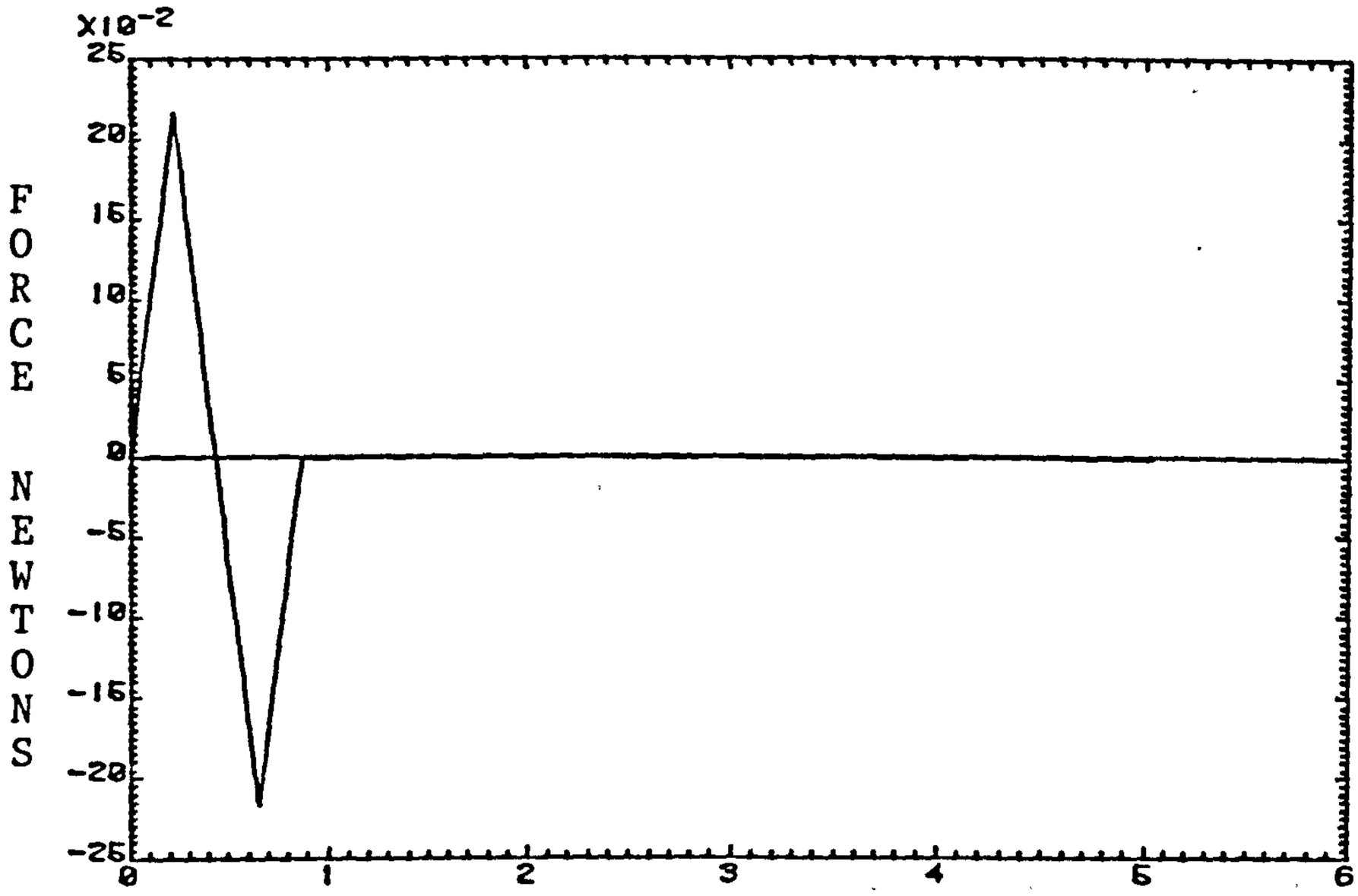

FIG 6.13C

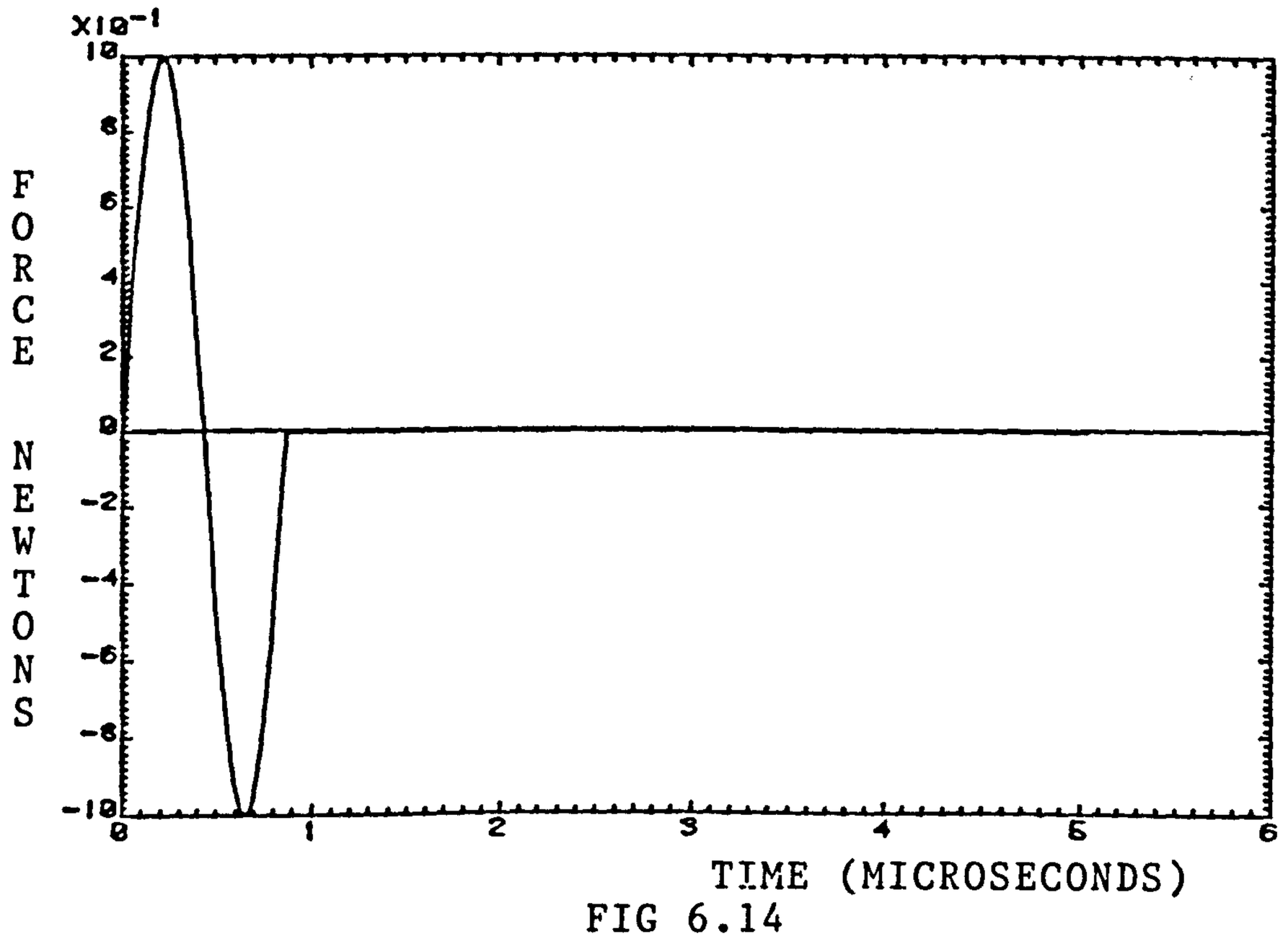

FIG 6.14

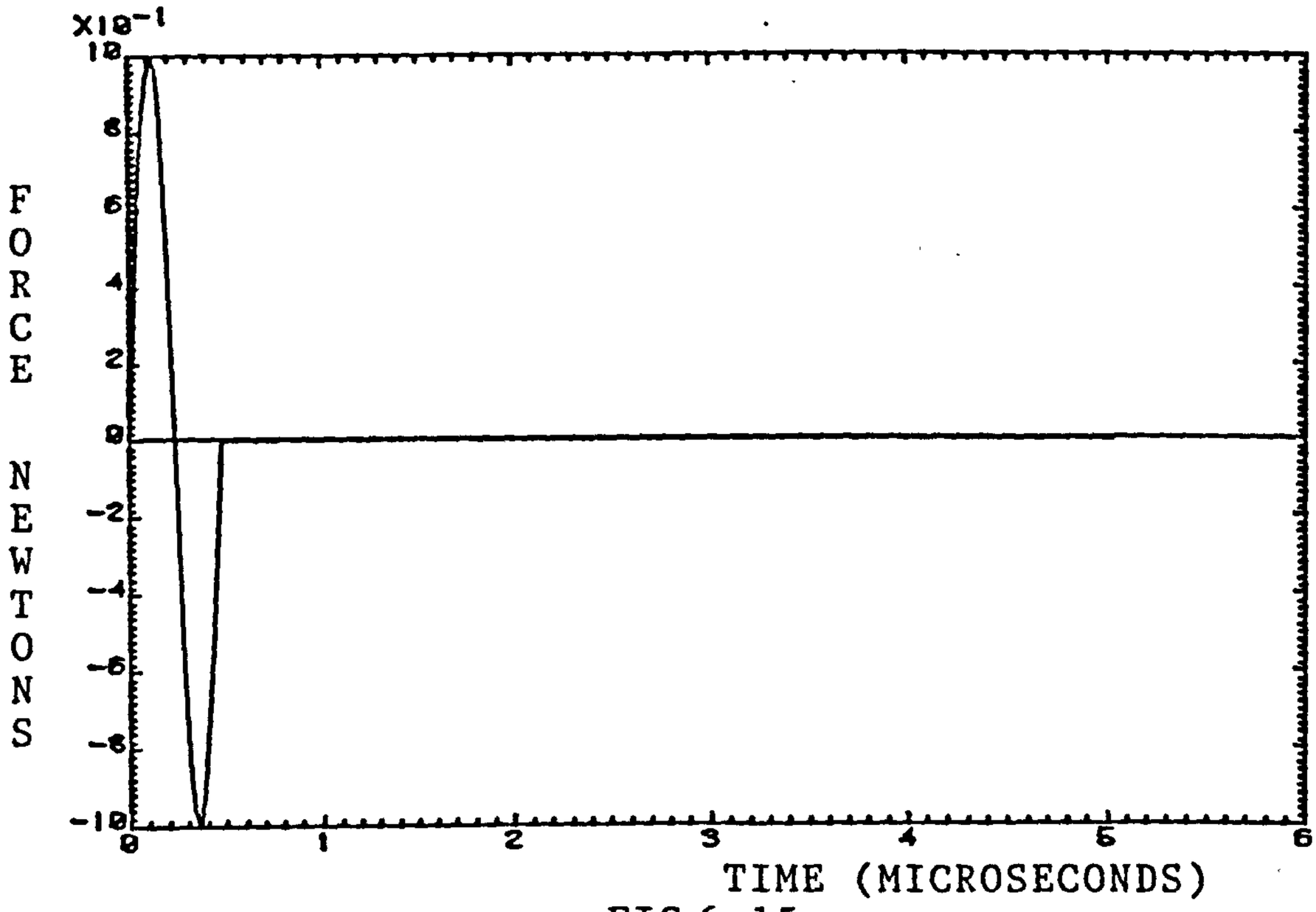

FIG 6.15

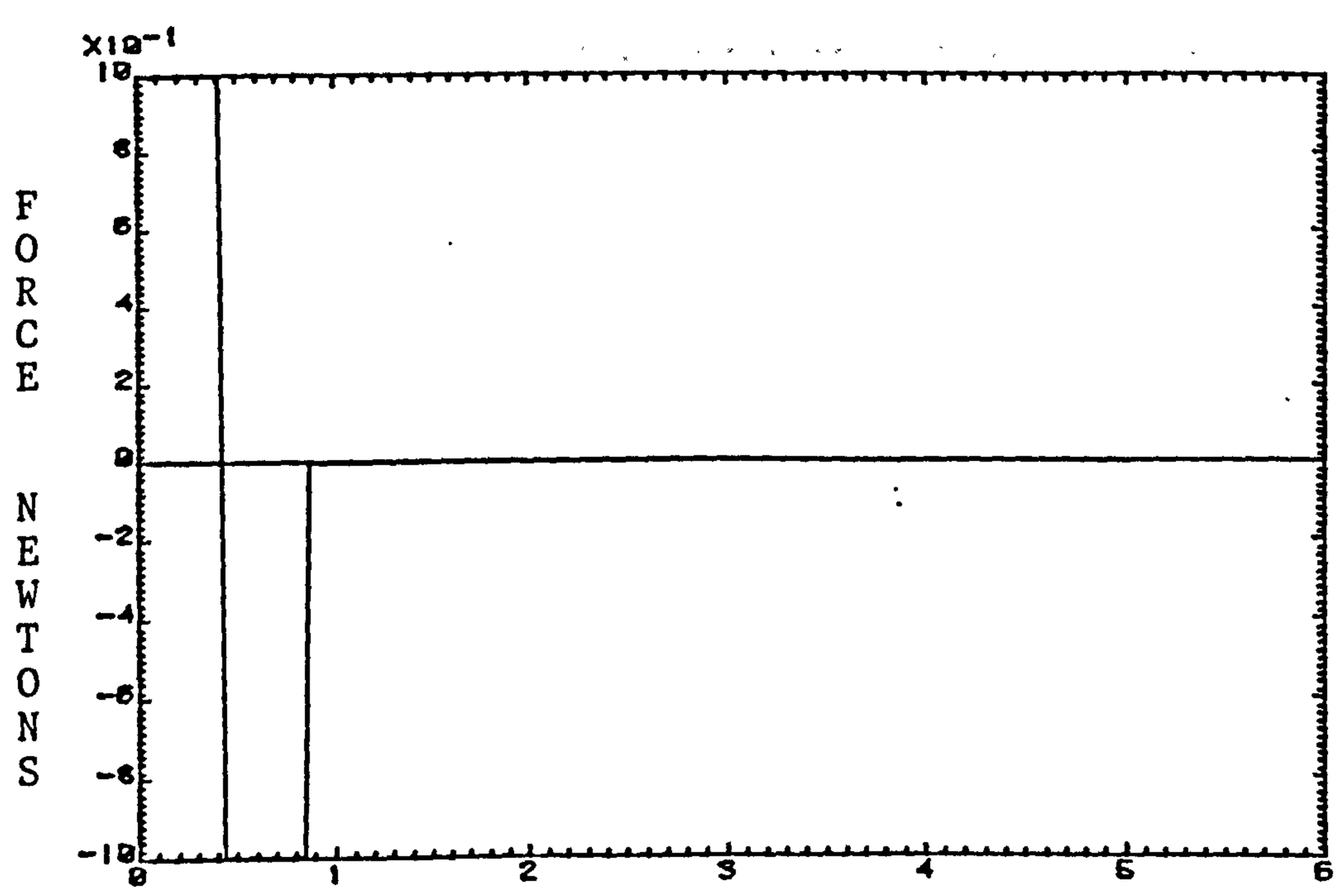

FIG 6.16

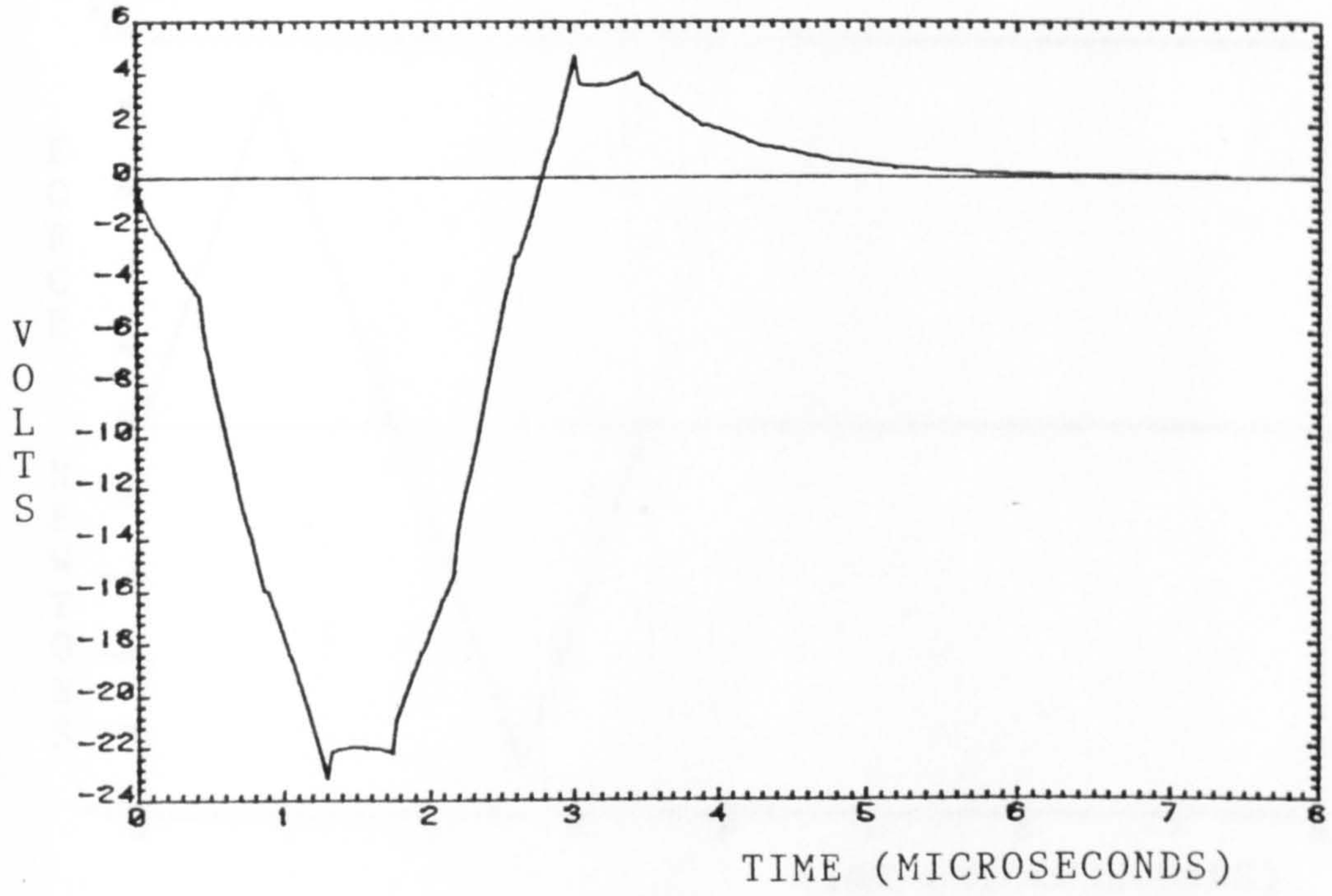

FIG 6.17A

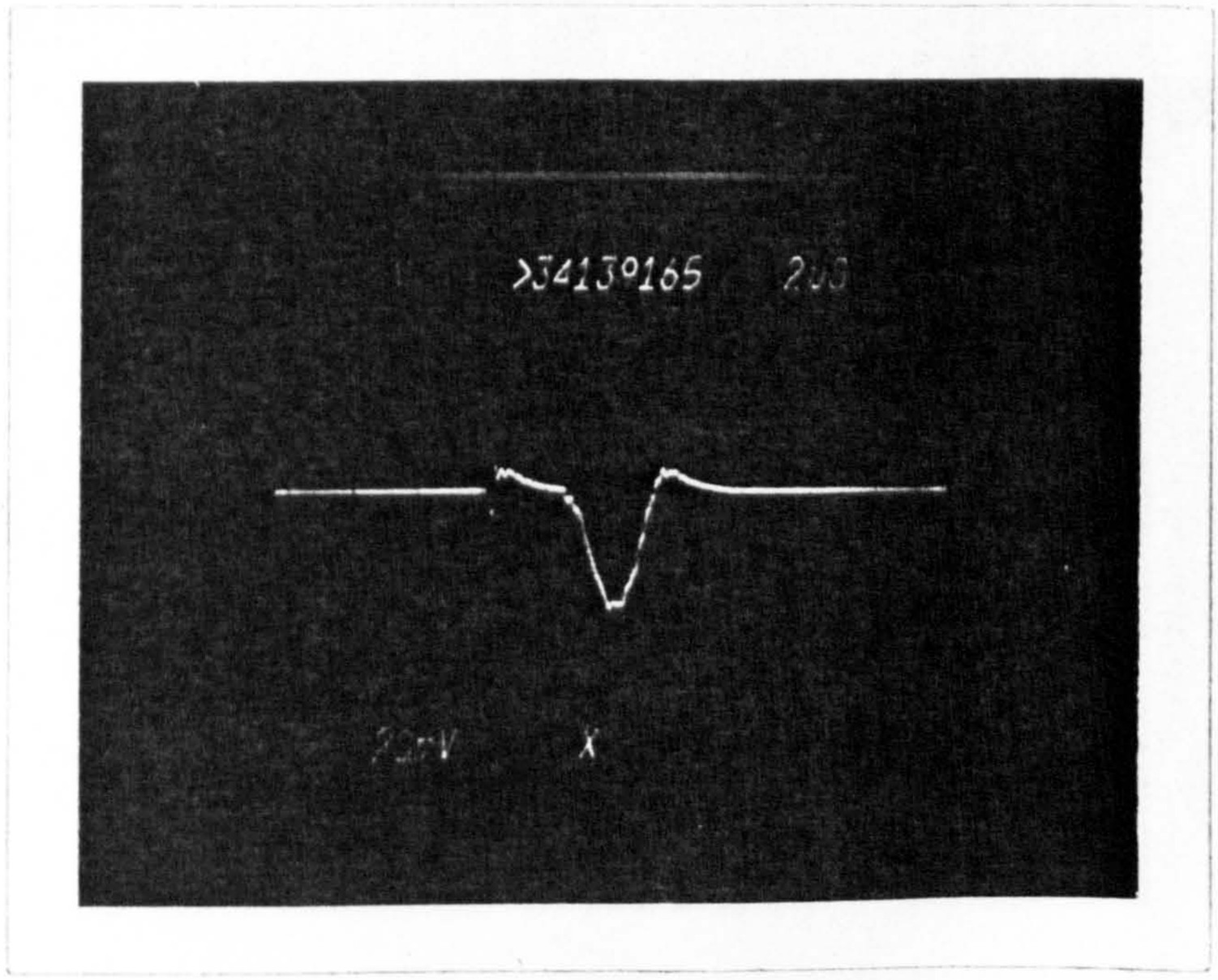

FIG 6.17B

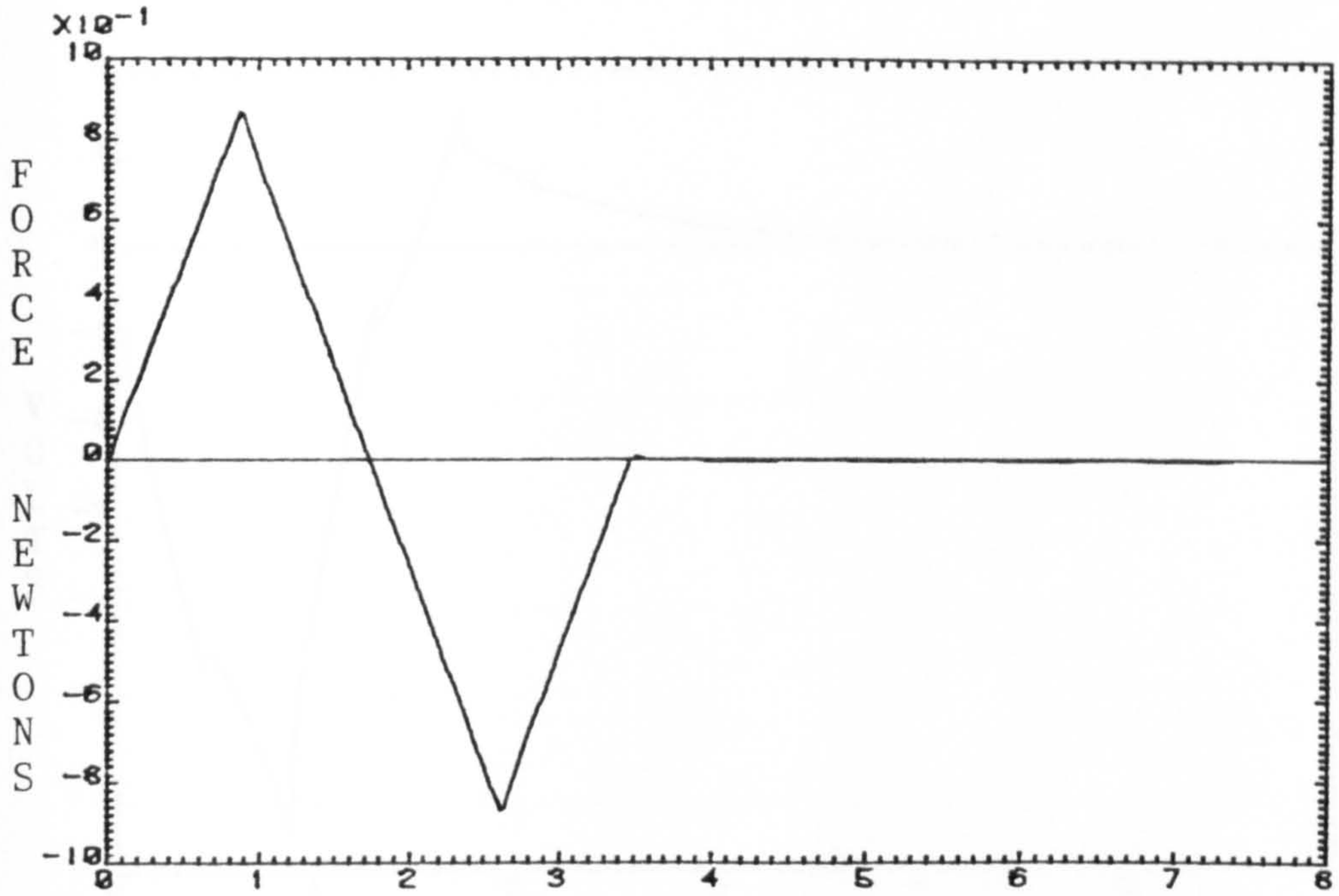

FIG 6.17C

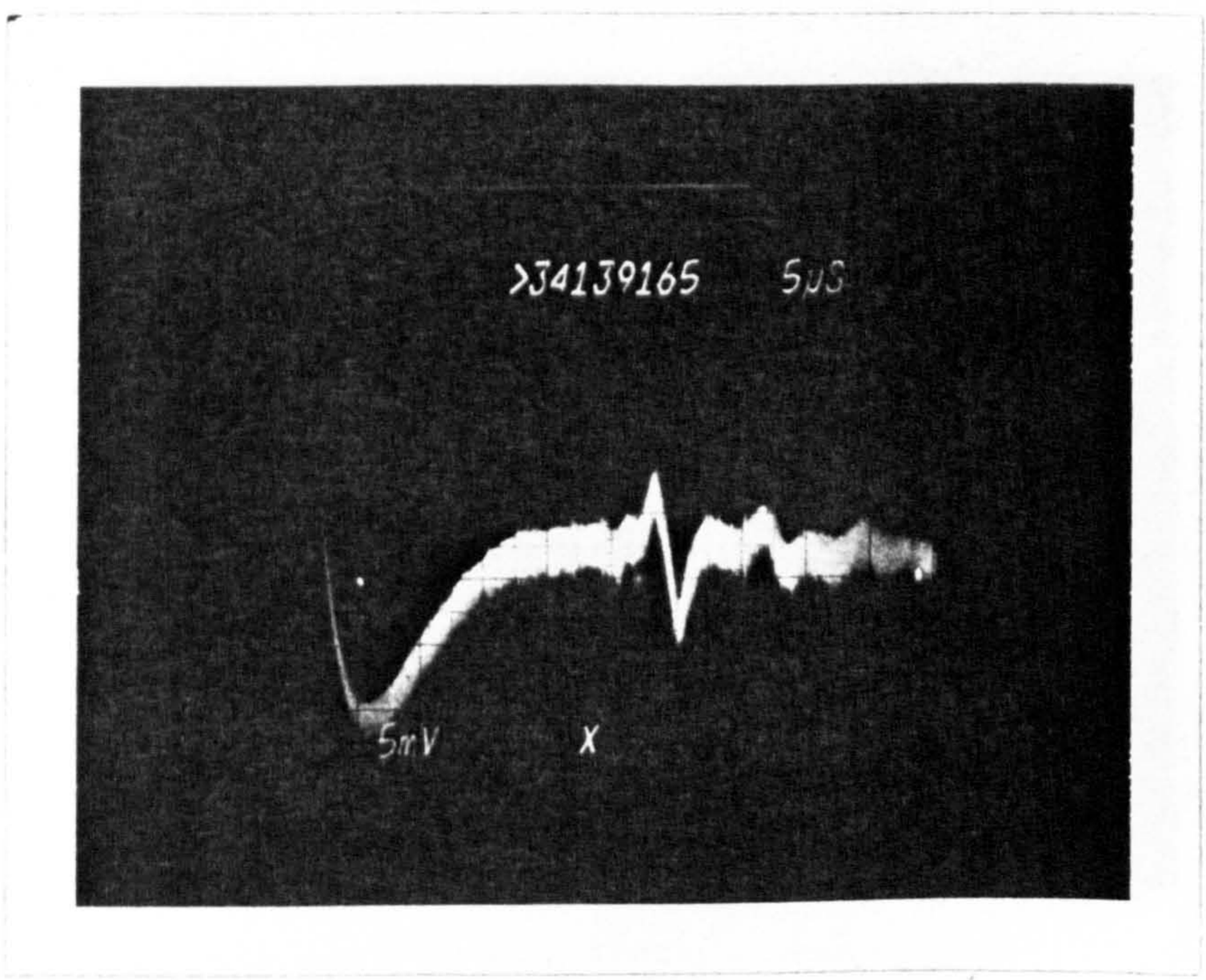

FIG 6.17D

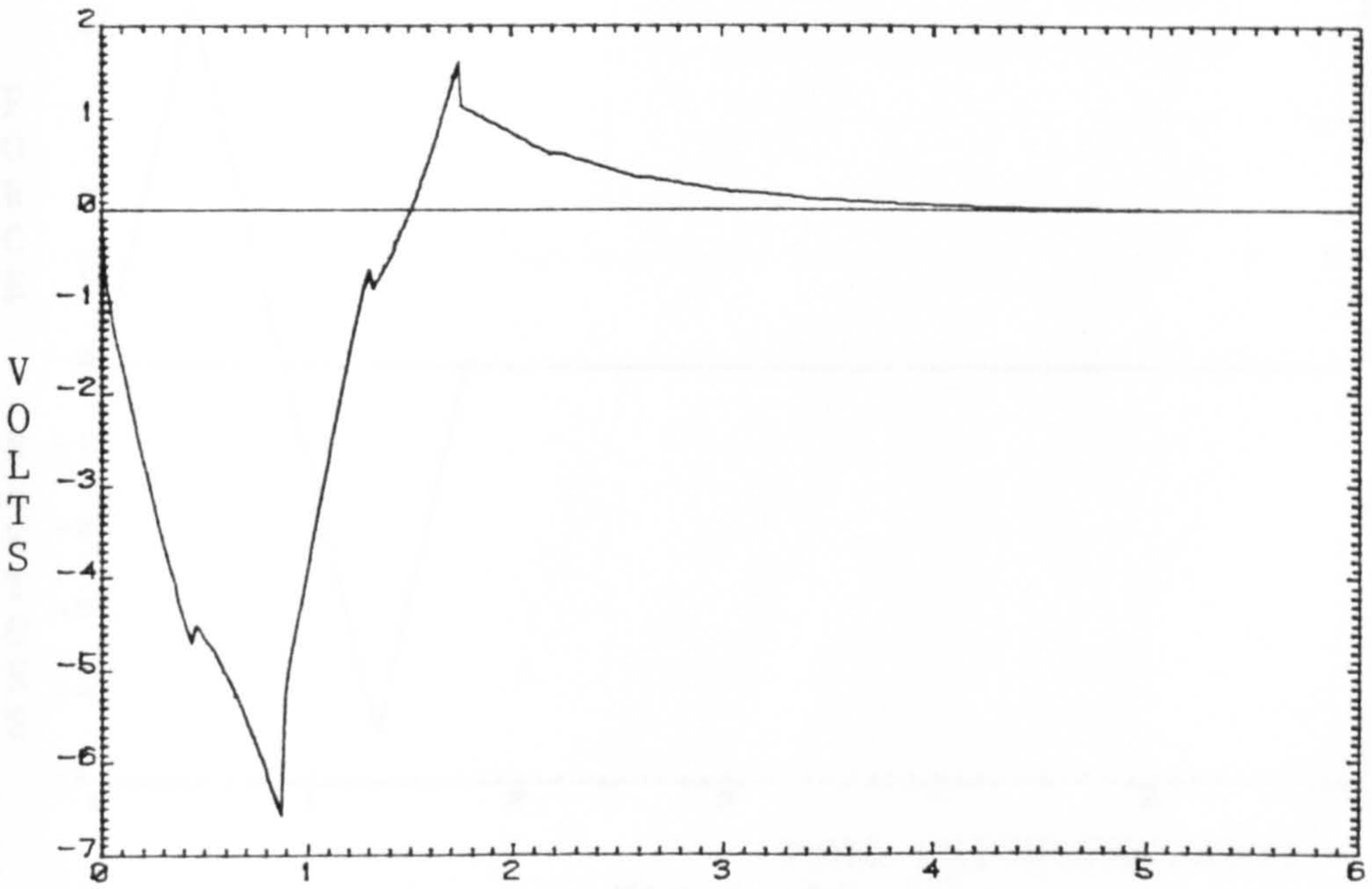

FIG 6.18A

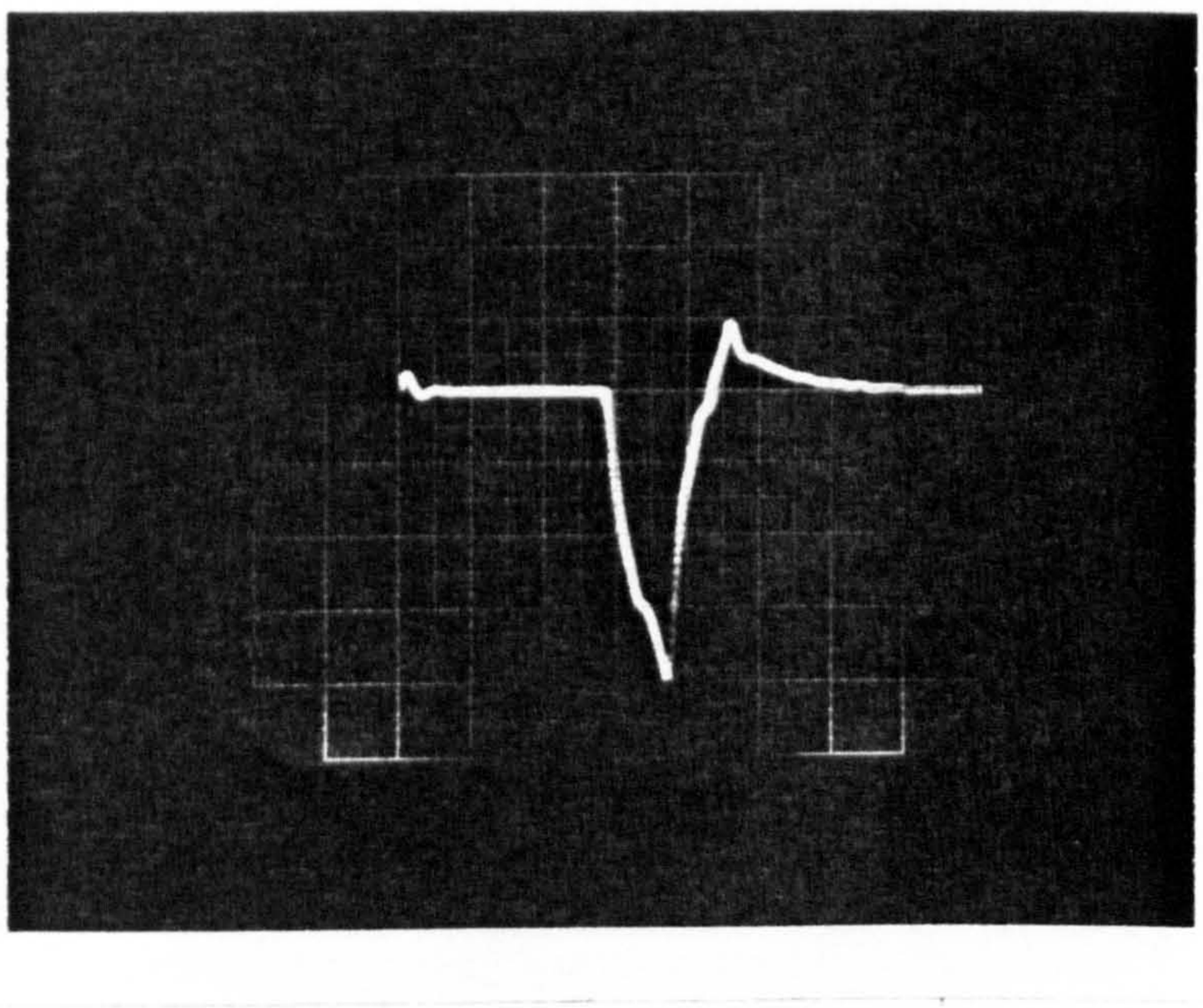

FIG 6.18B

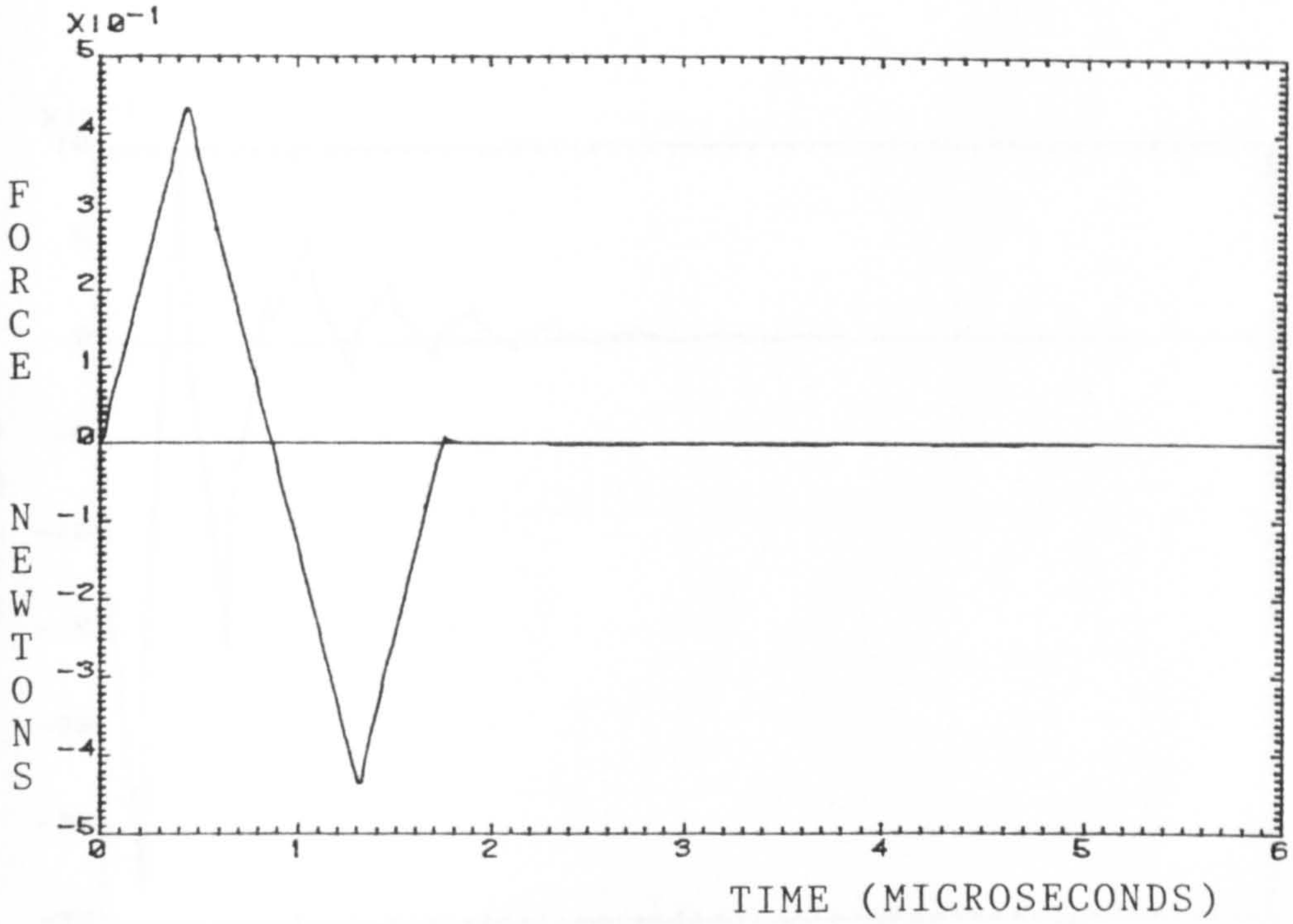

FIG 6.18C

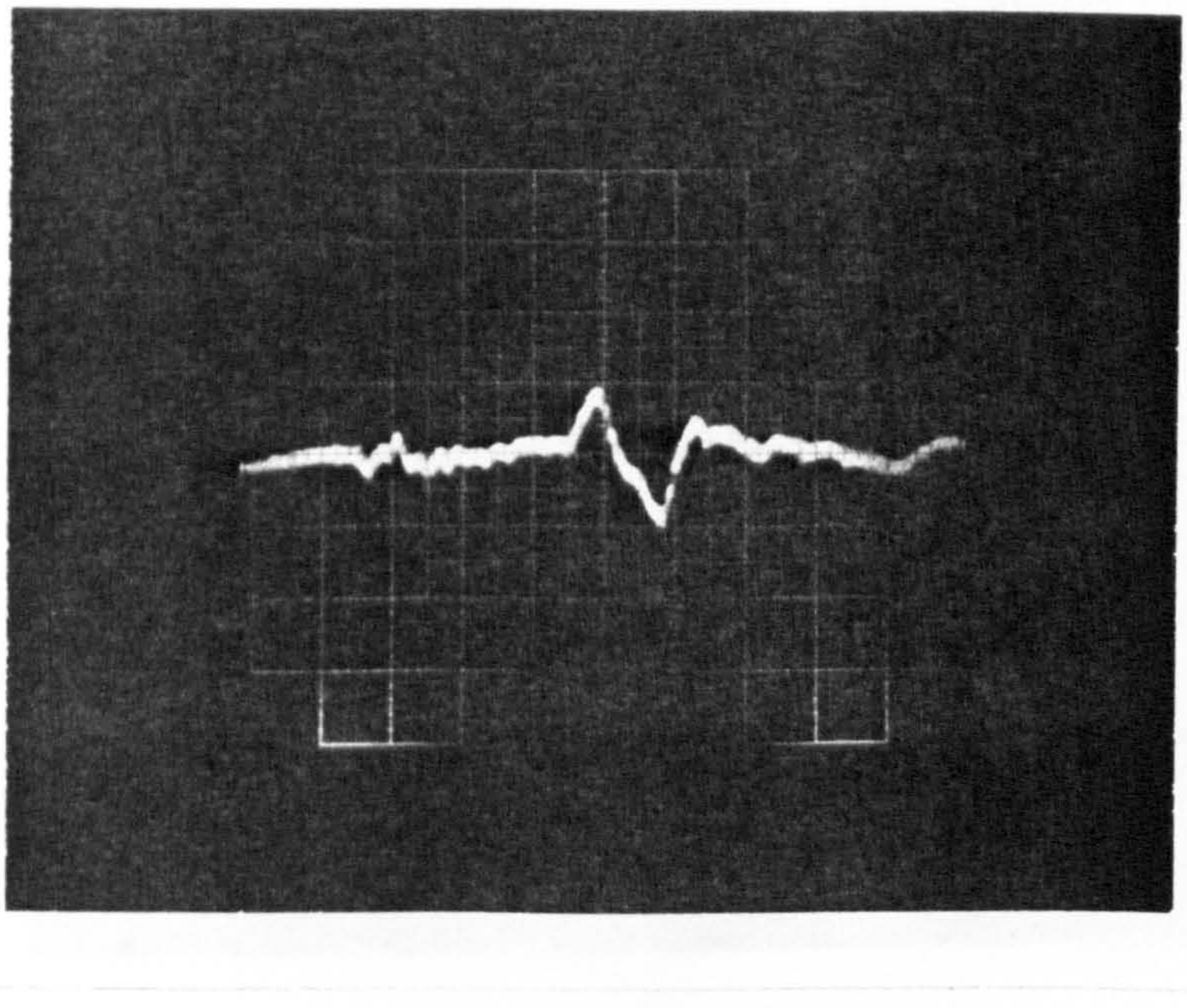

FIG 6.18D

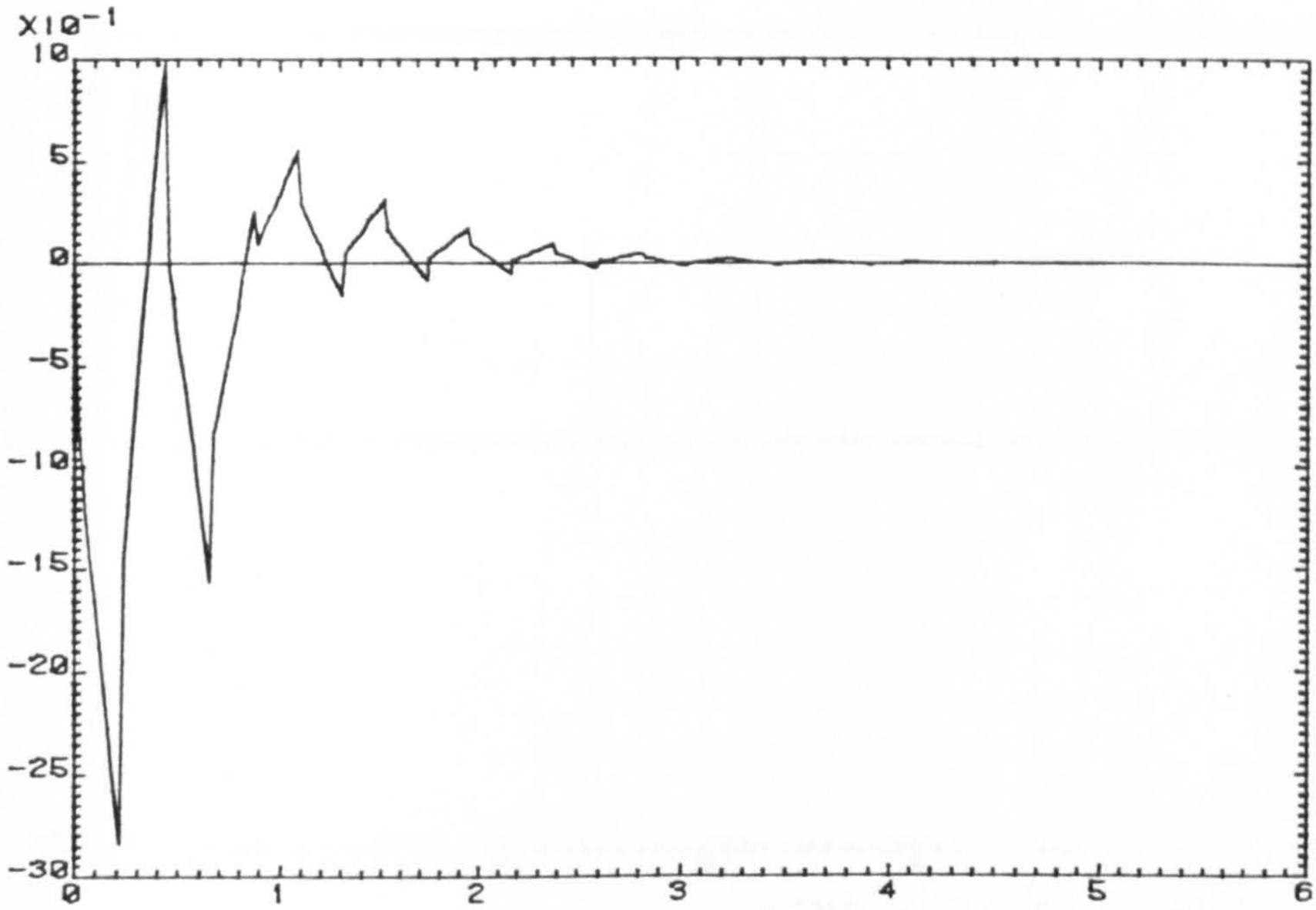

FIG 6.19A

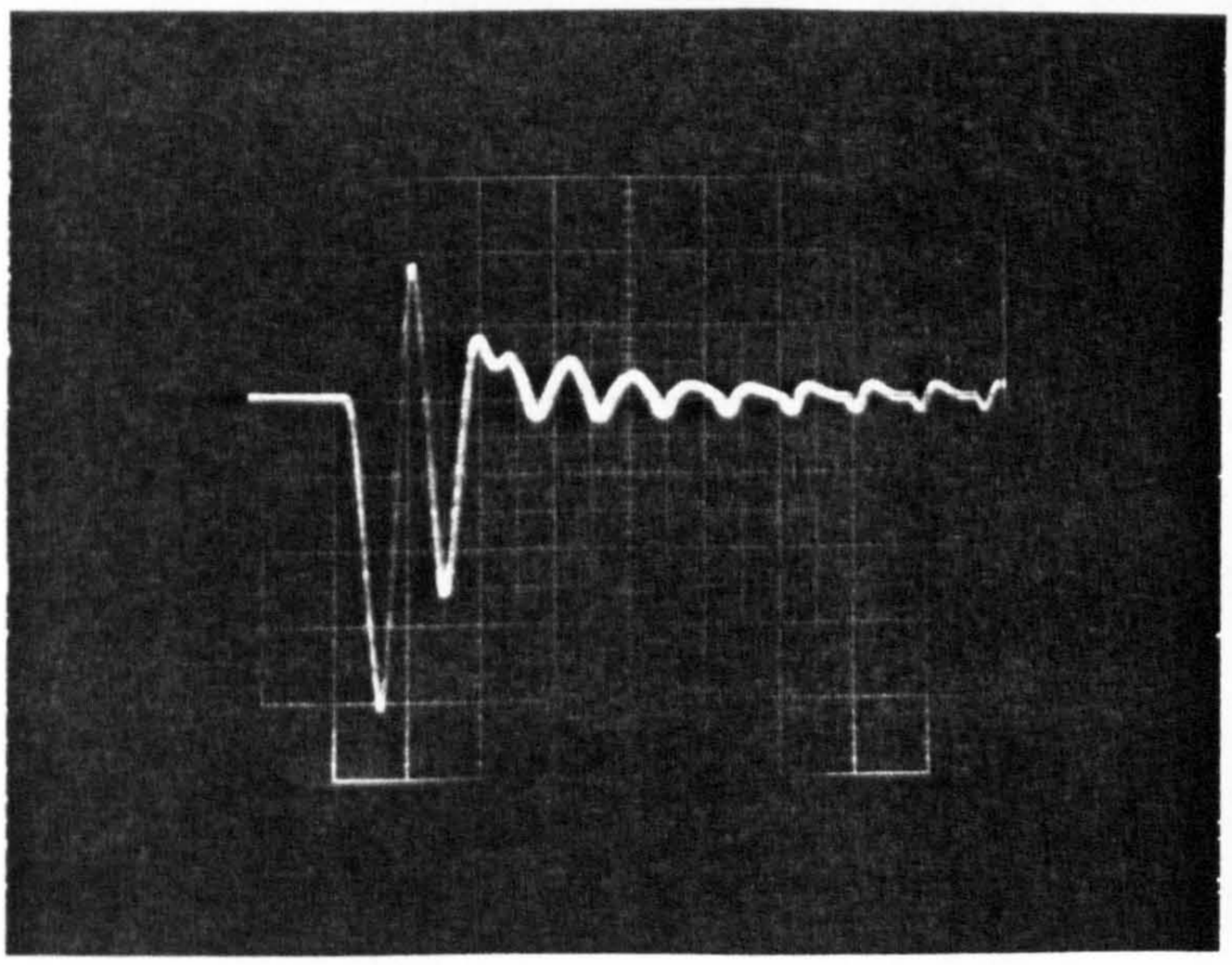

FIG 6.19B

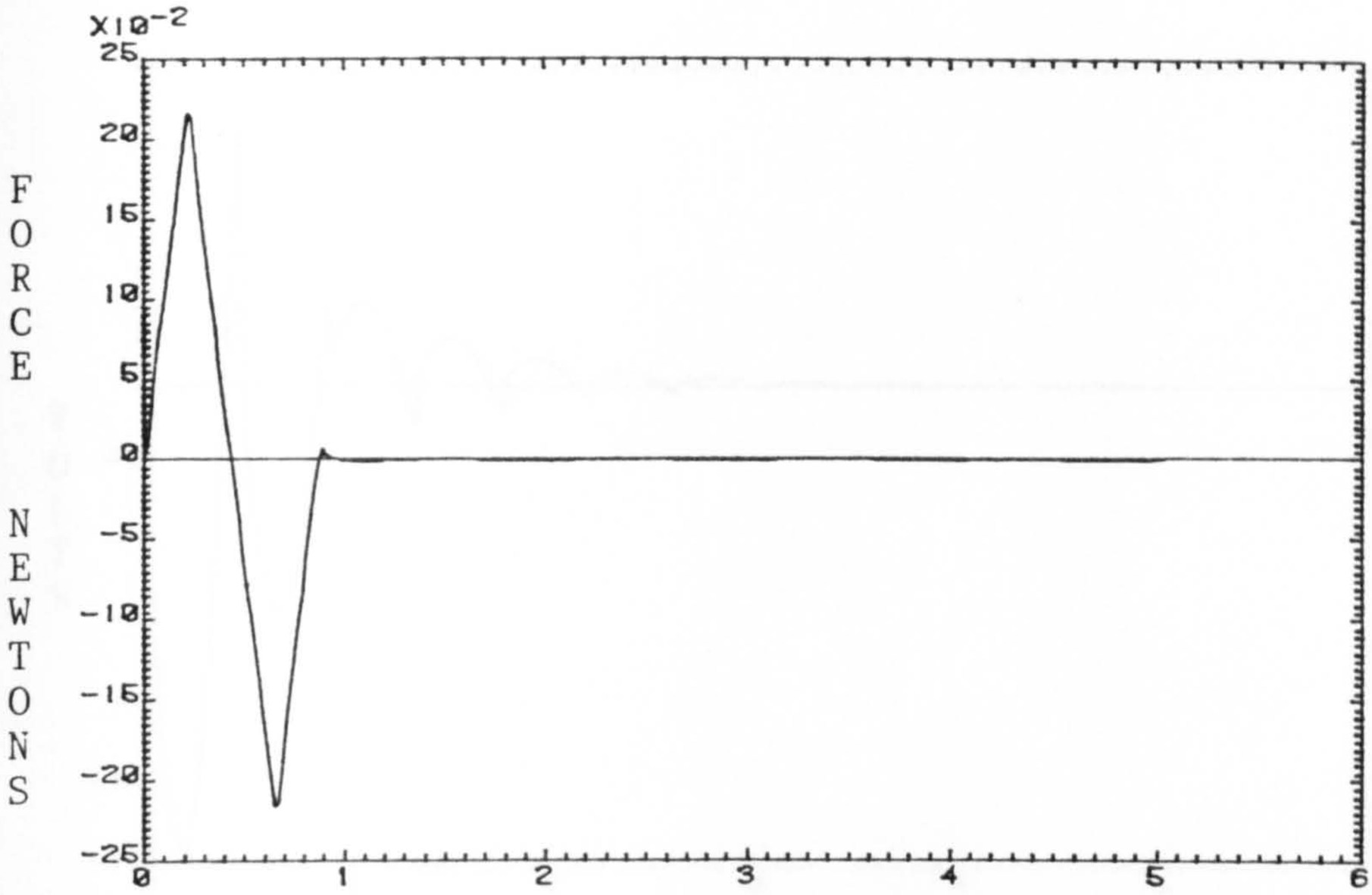

FIG 6.19C

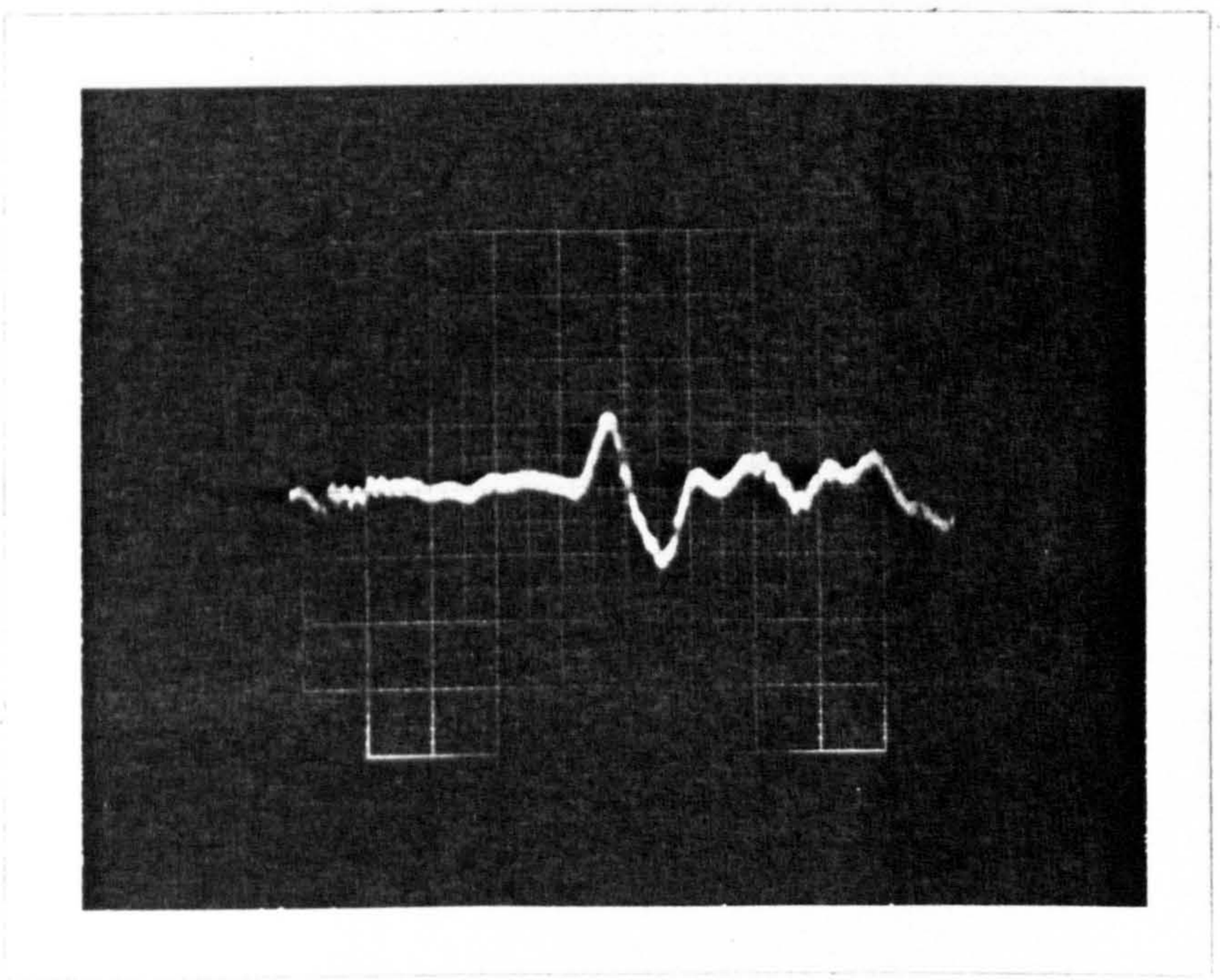

FIG 6.19D

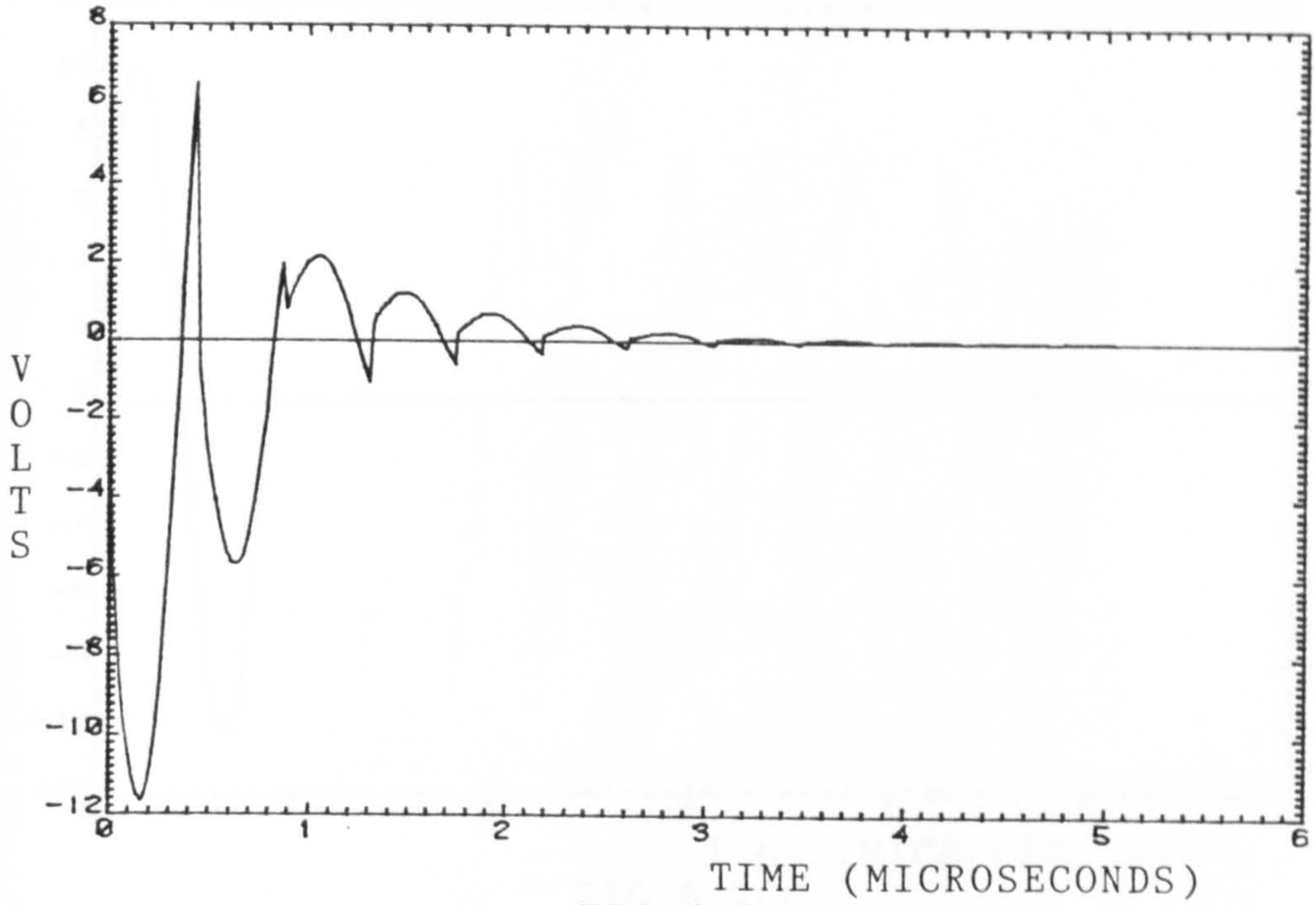

FIG 6.20A

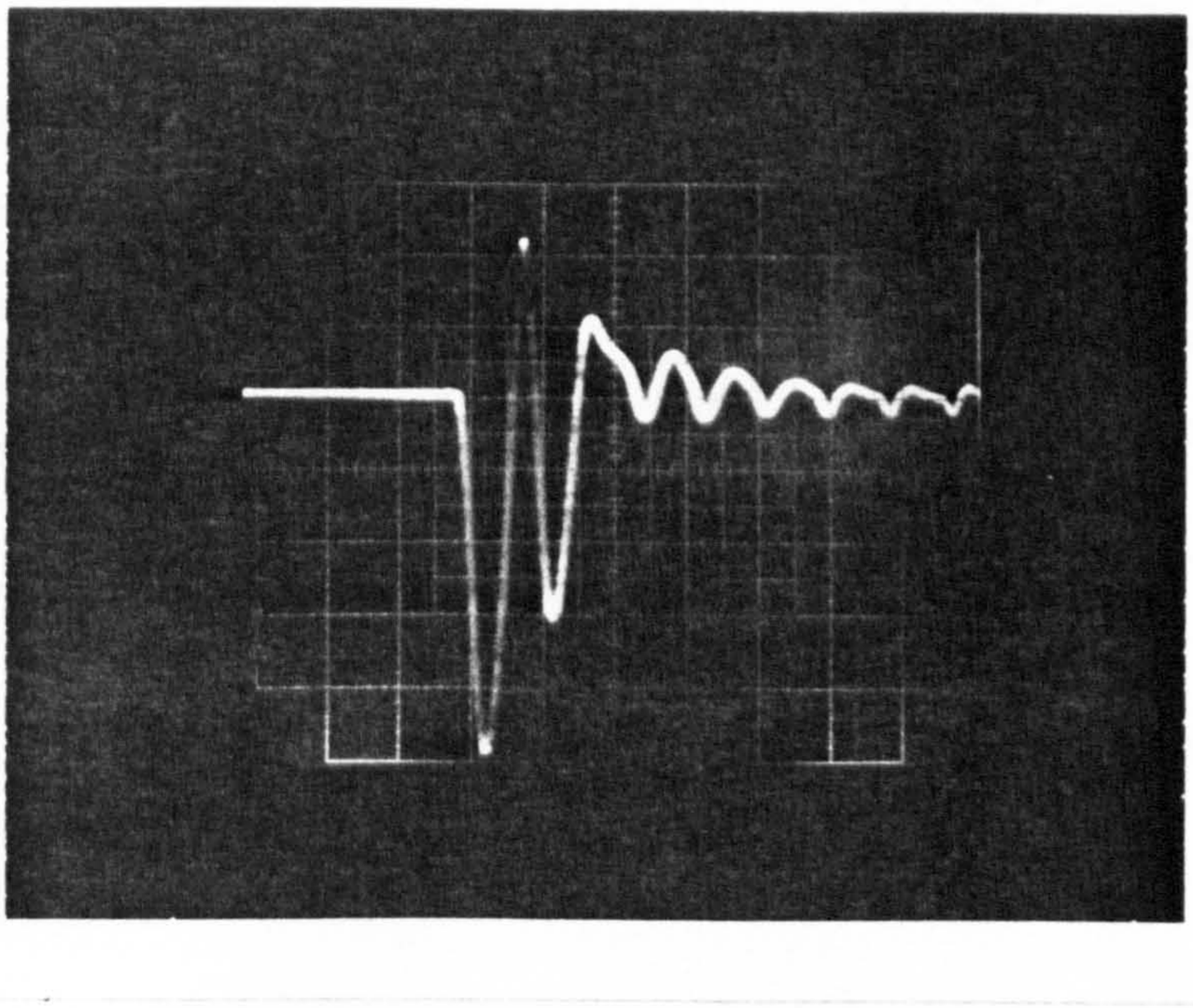

FIG 6.20B

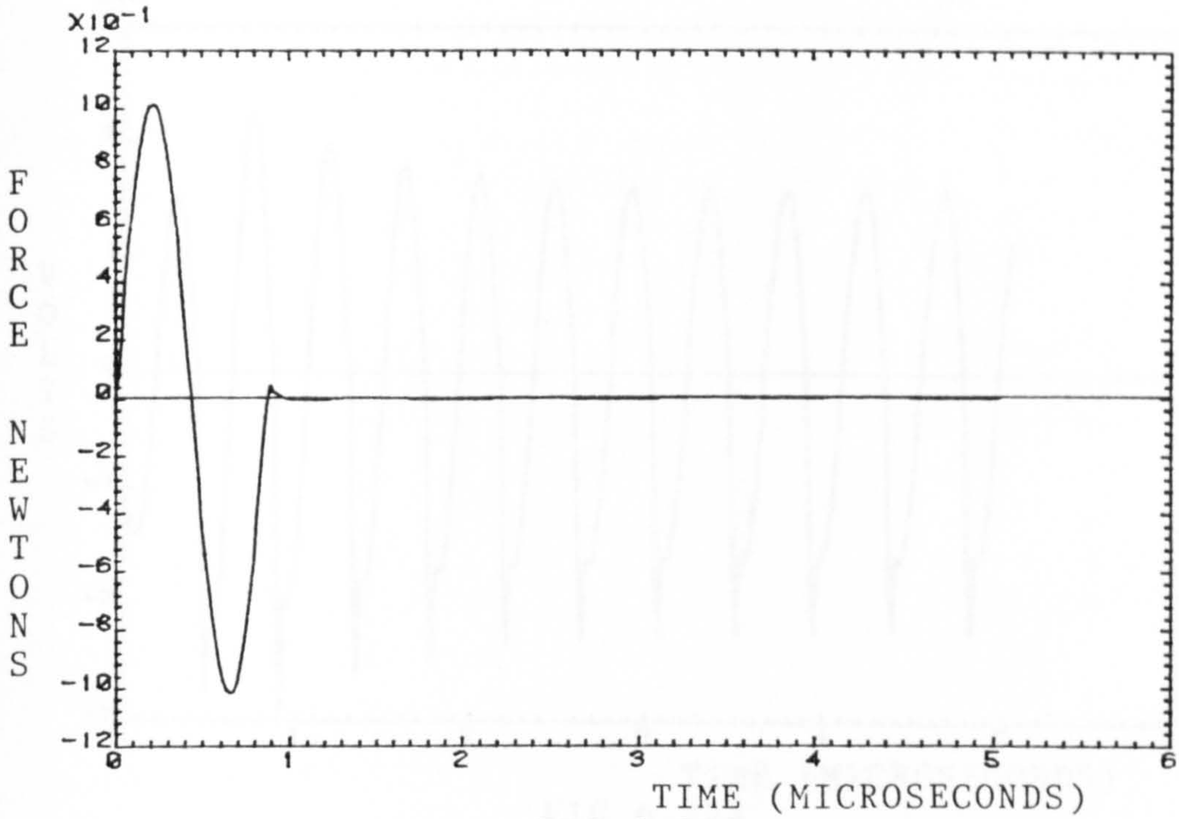

FIG 6.20C

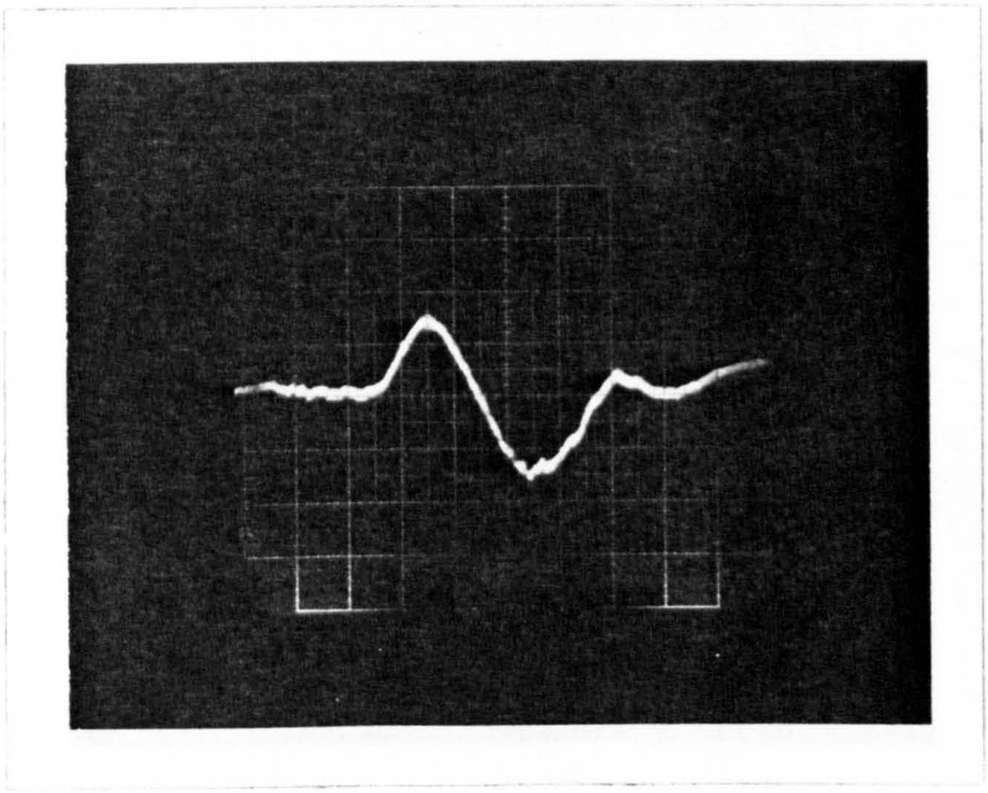

FIG 6.20D

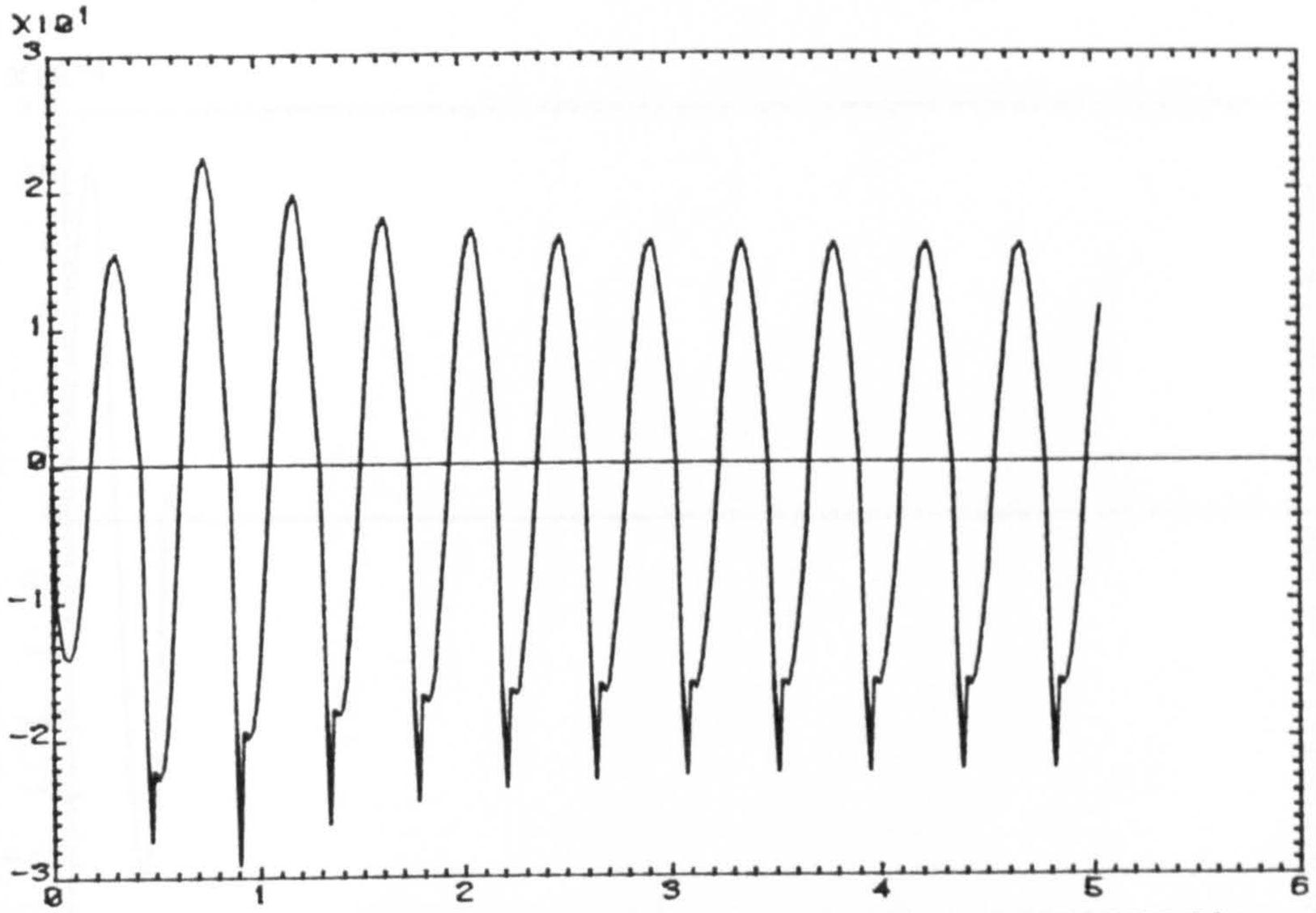

FIG 6.21A

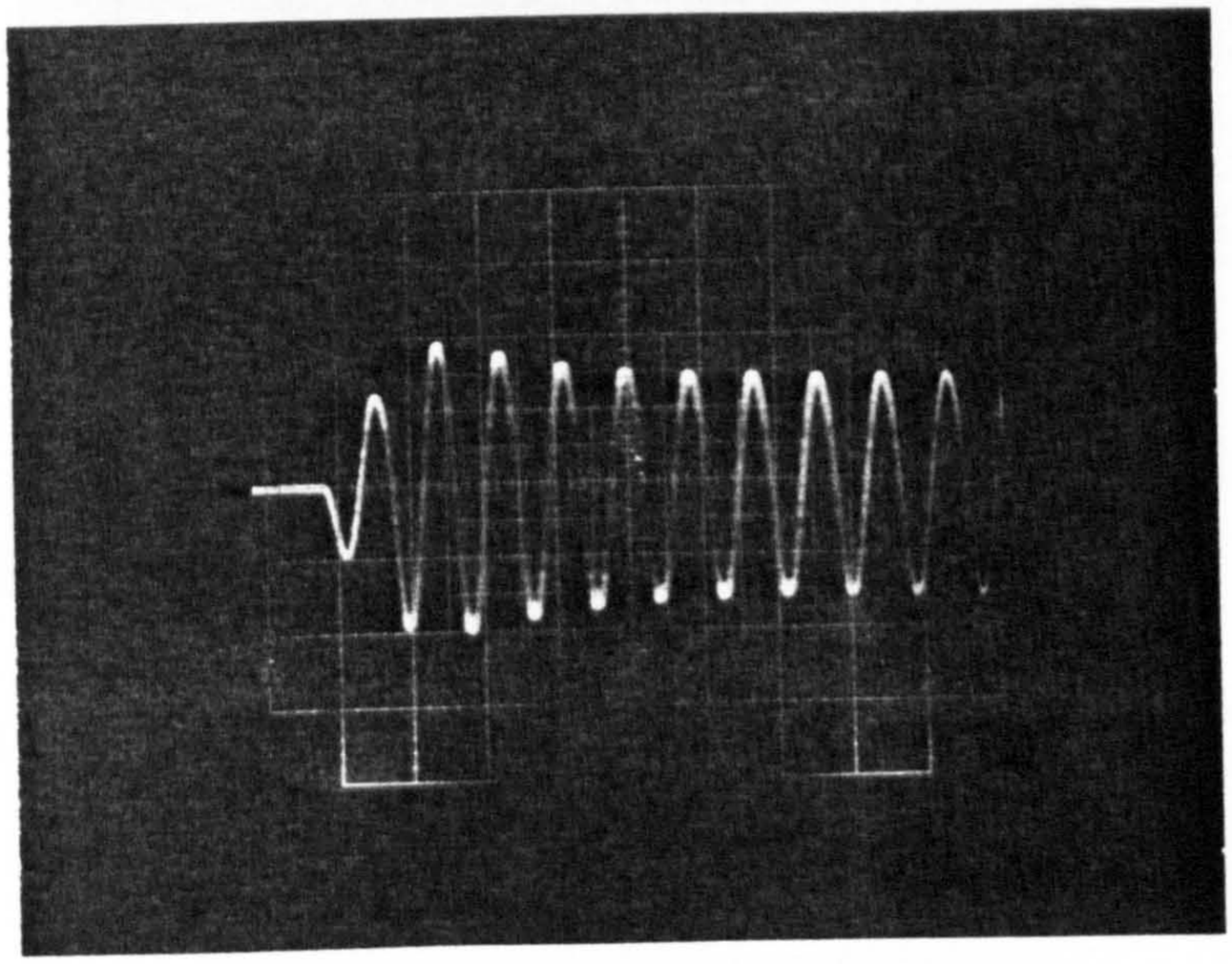

FIG 6.21B

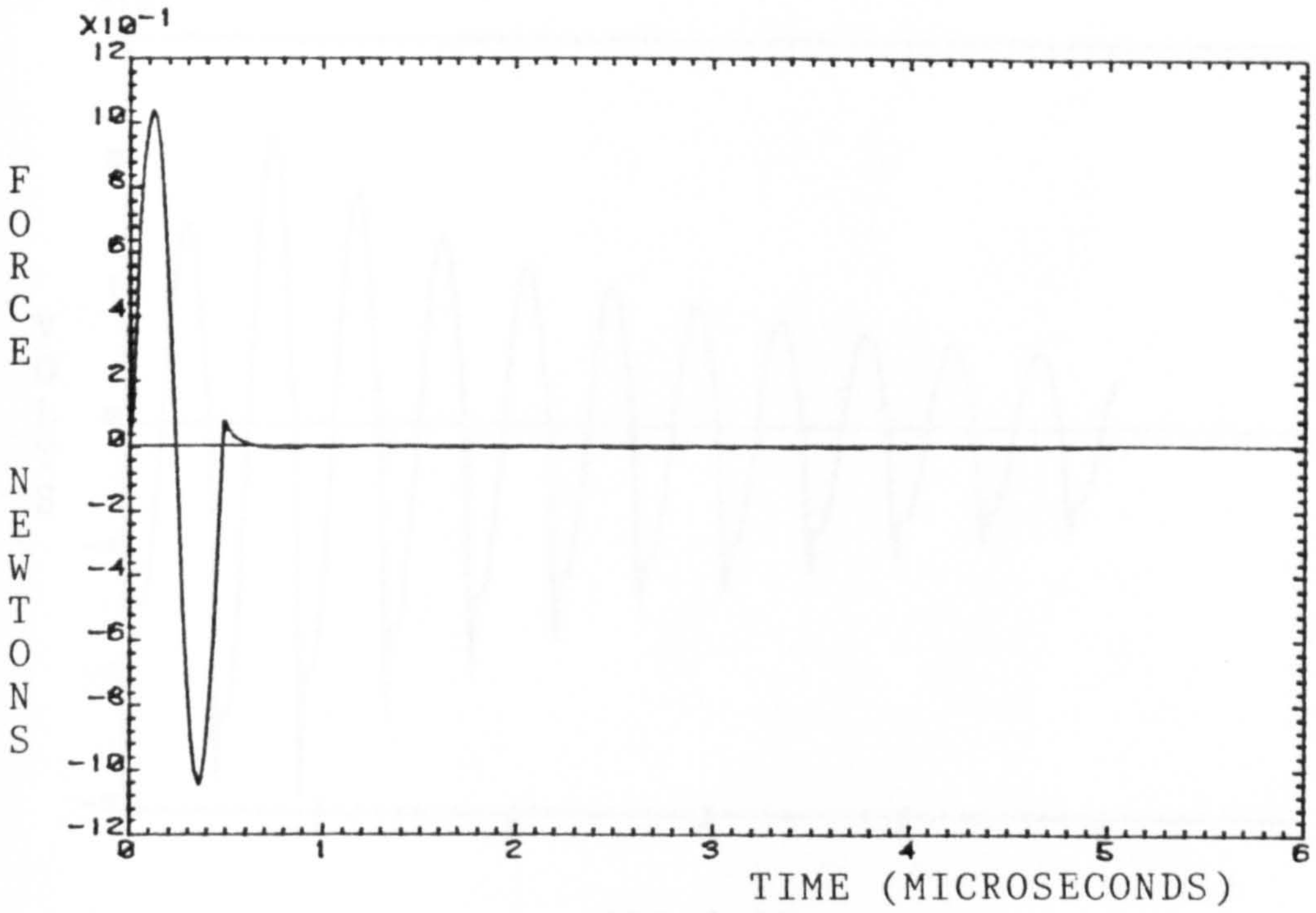

FIG 6.21C

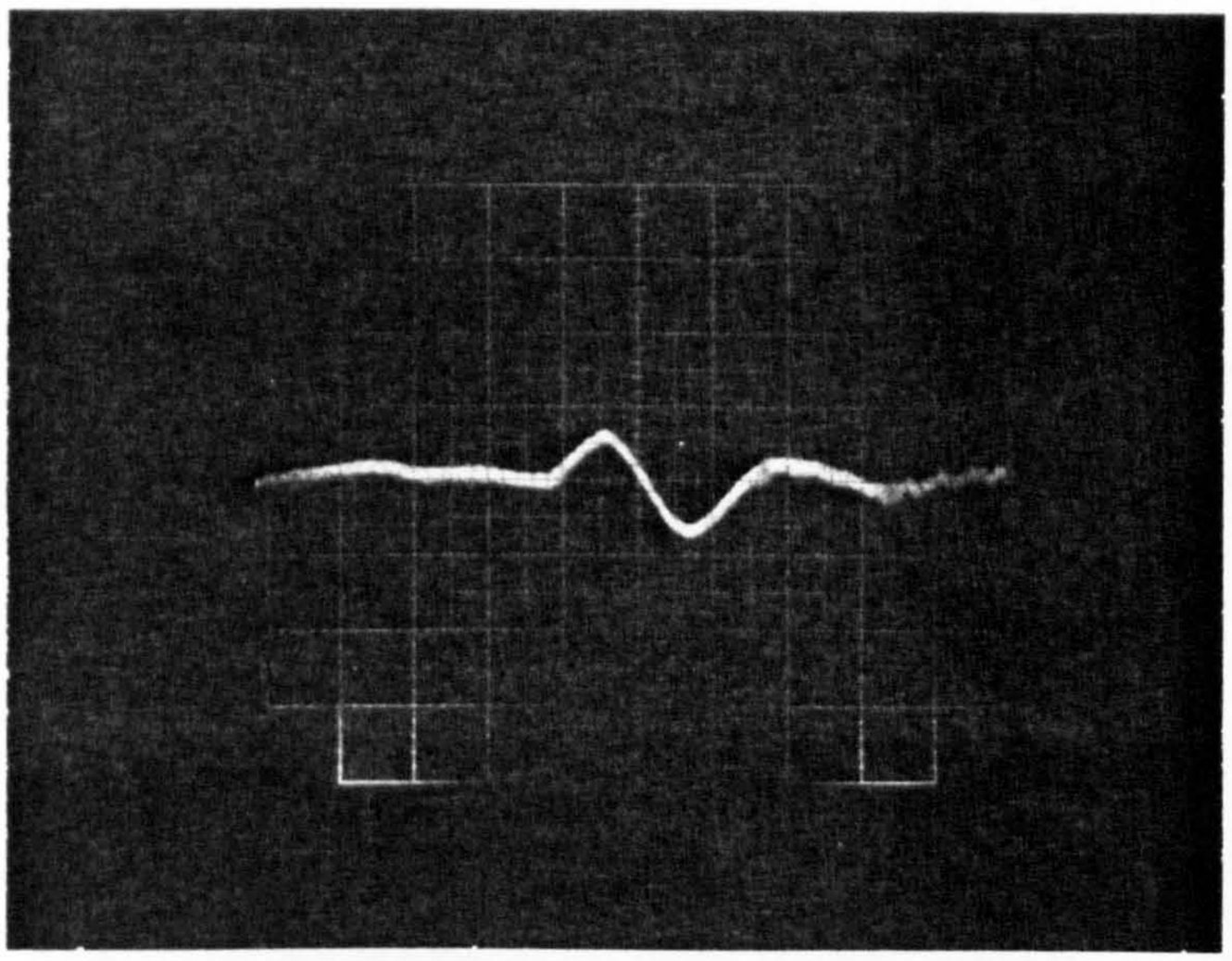

FIG 6.21D

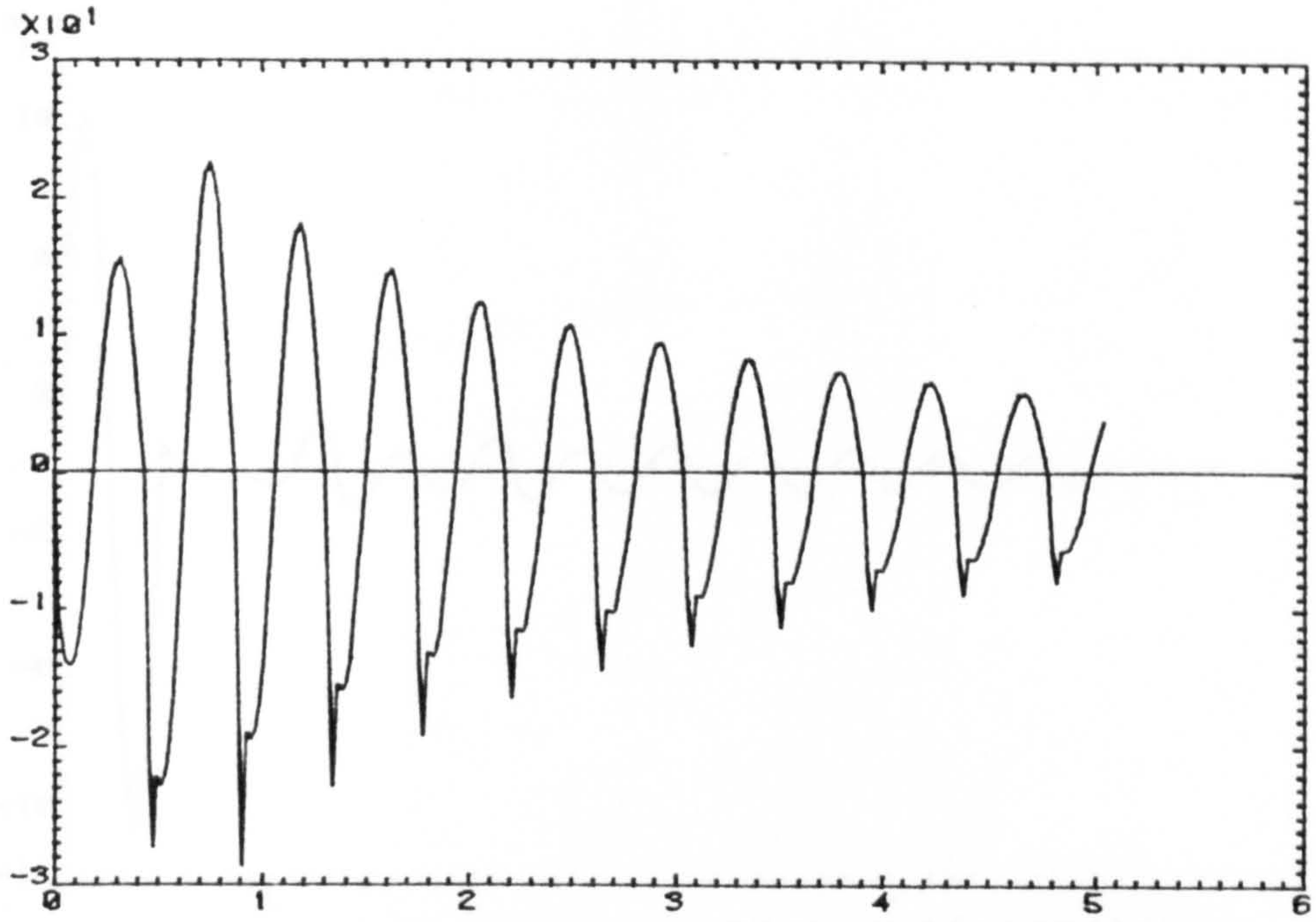

FIG 6.22A

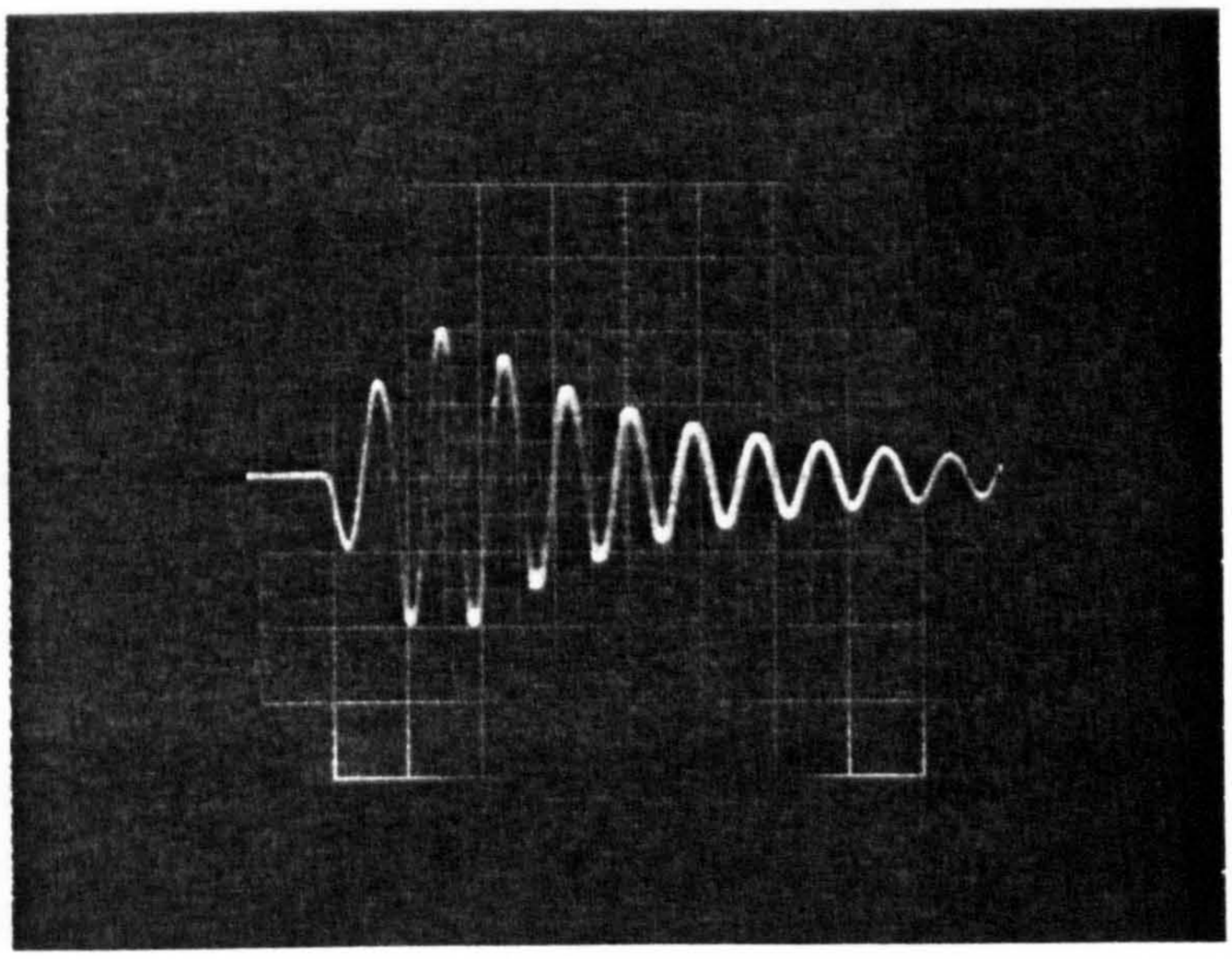

FIG 6.22B

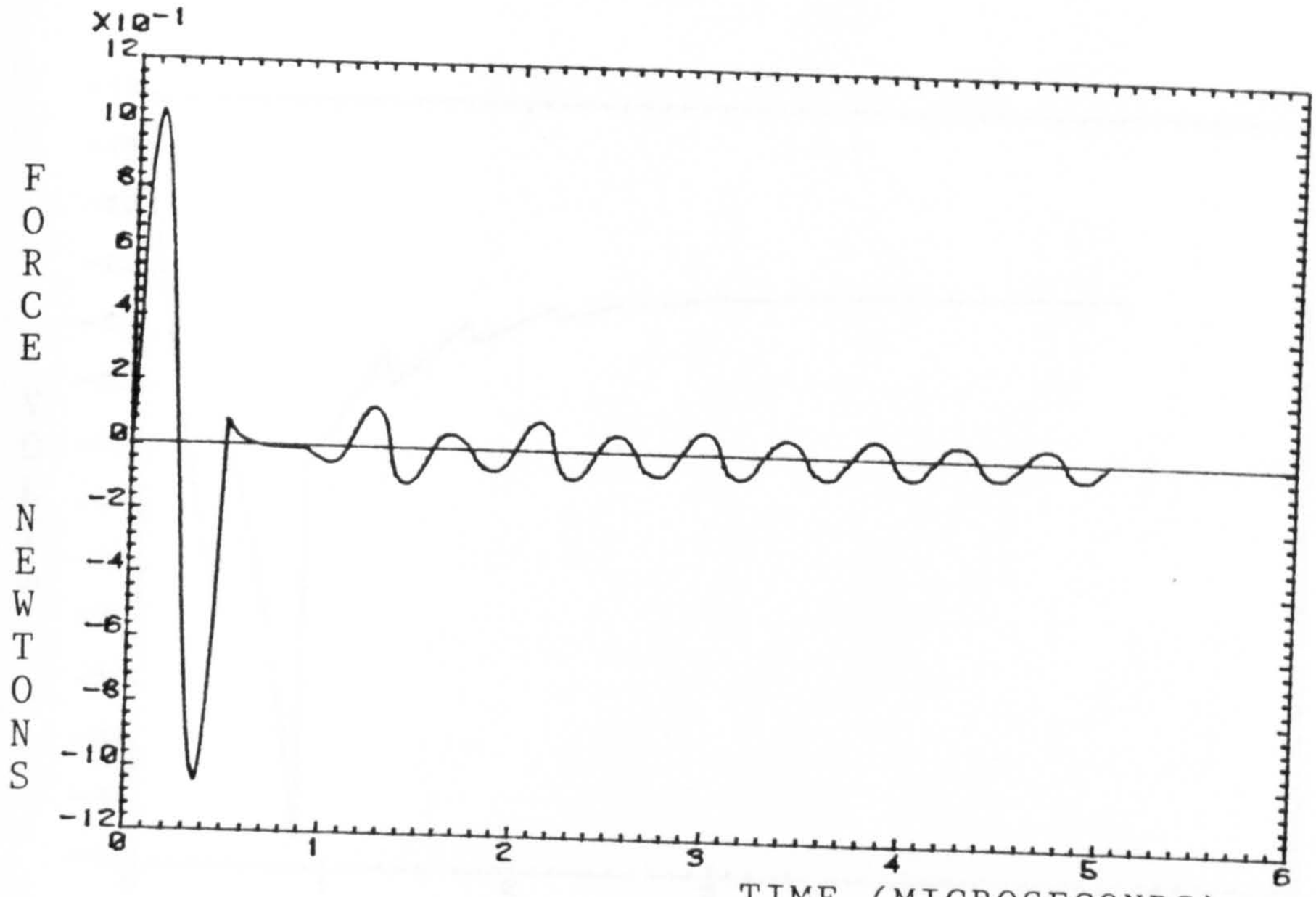

FIG 6.22C

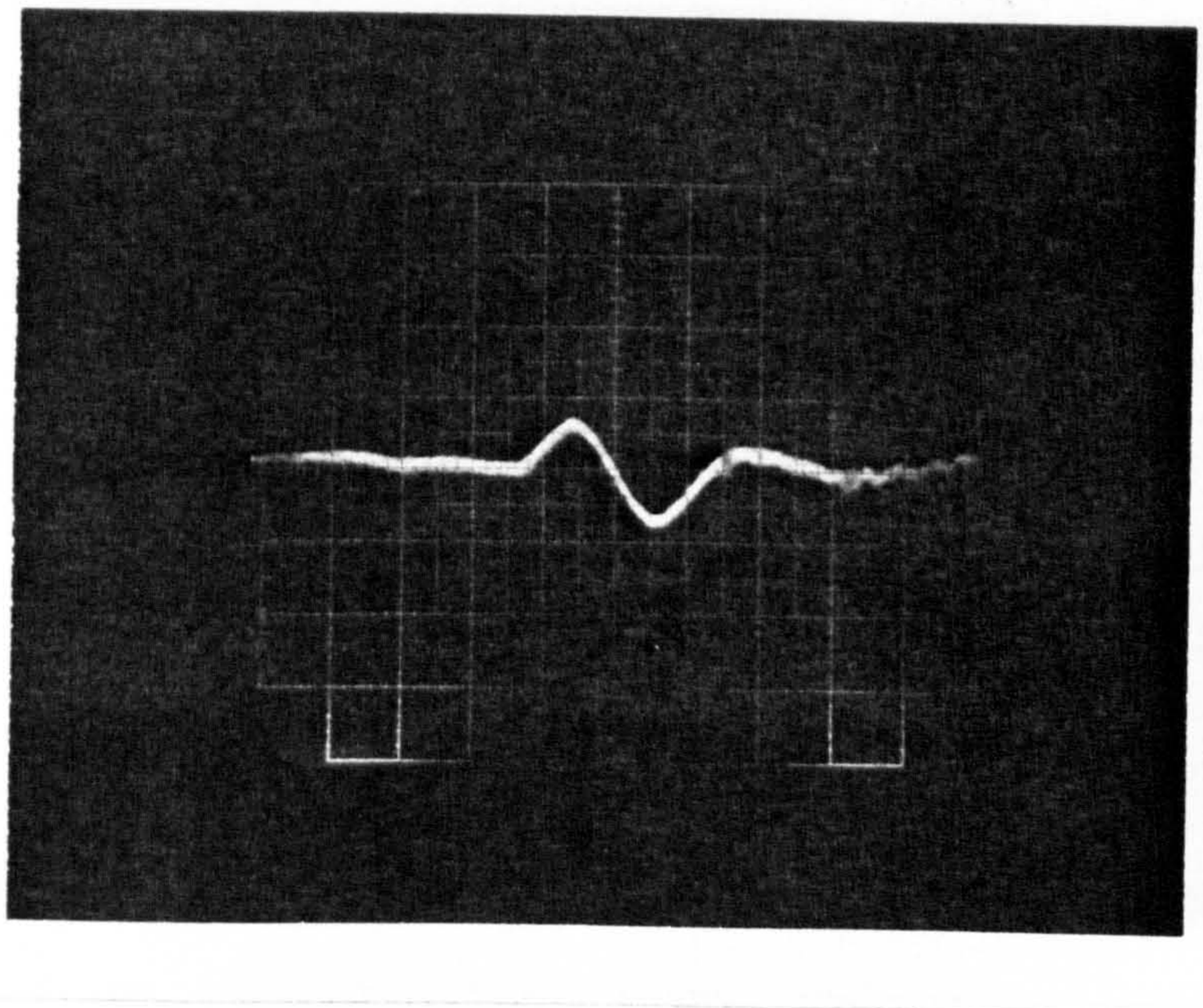

FIG 6.22D

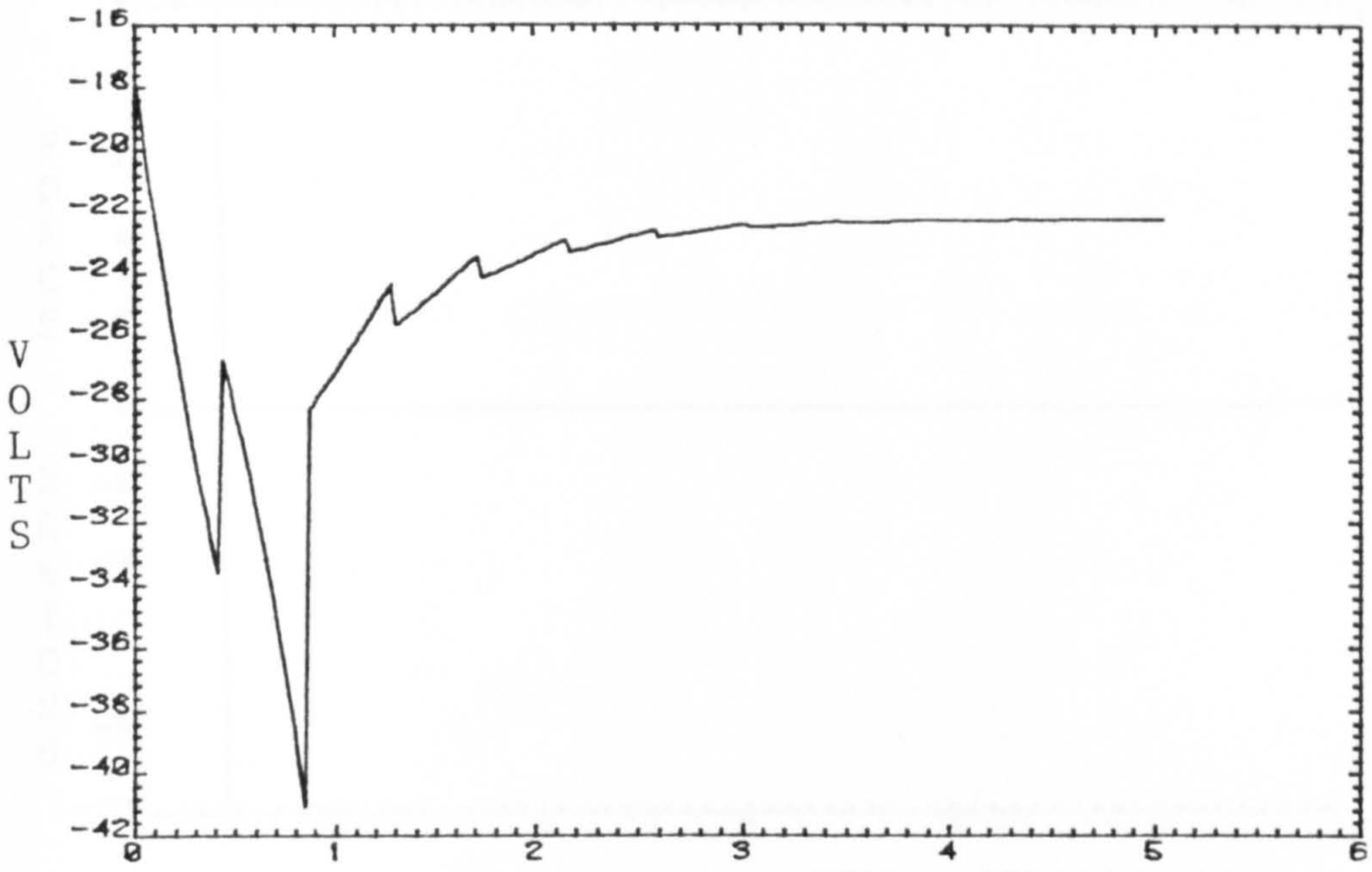

FIG 6.23A

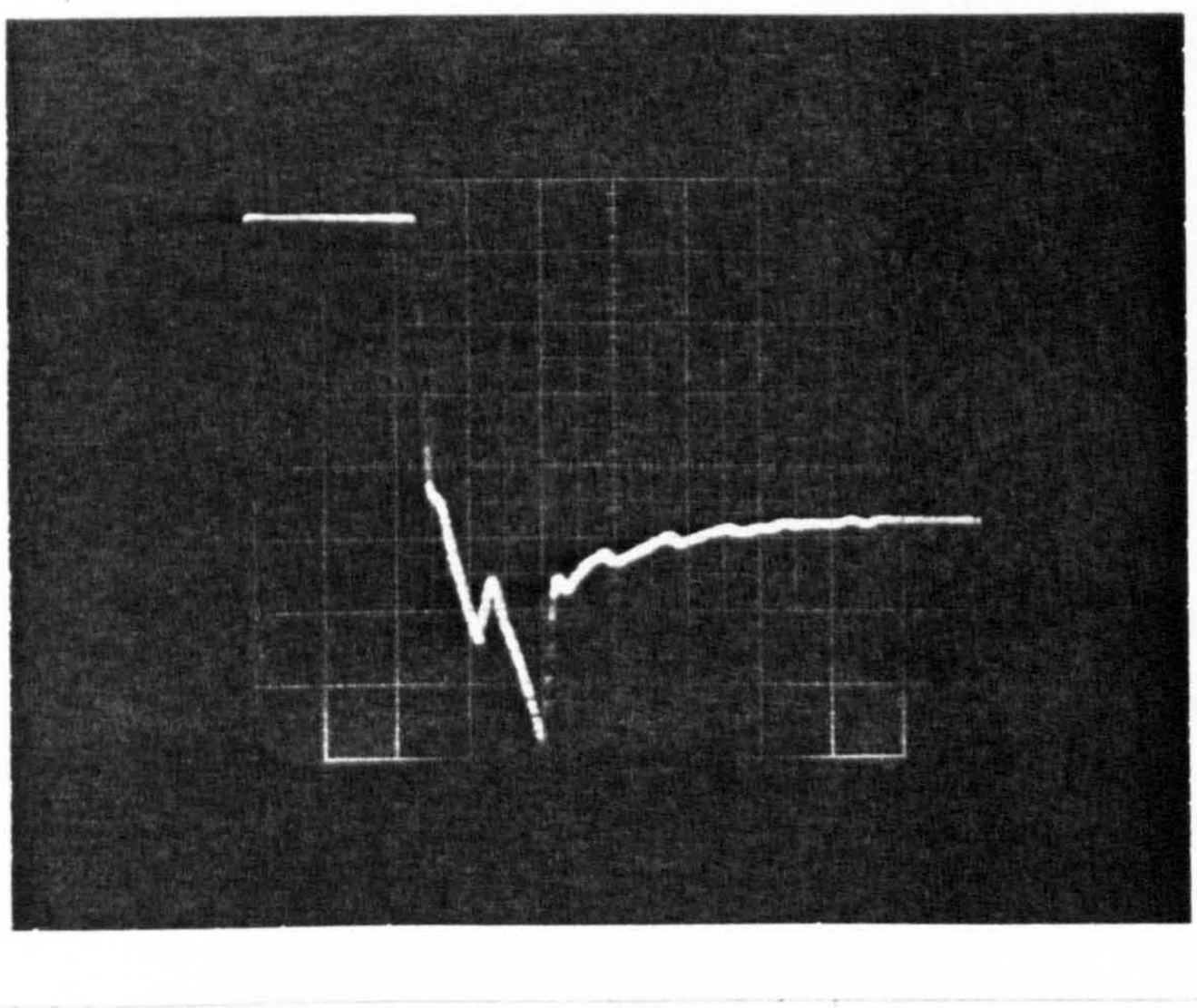

FIG 6.23B

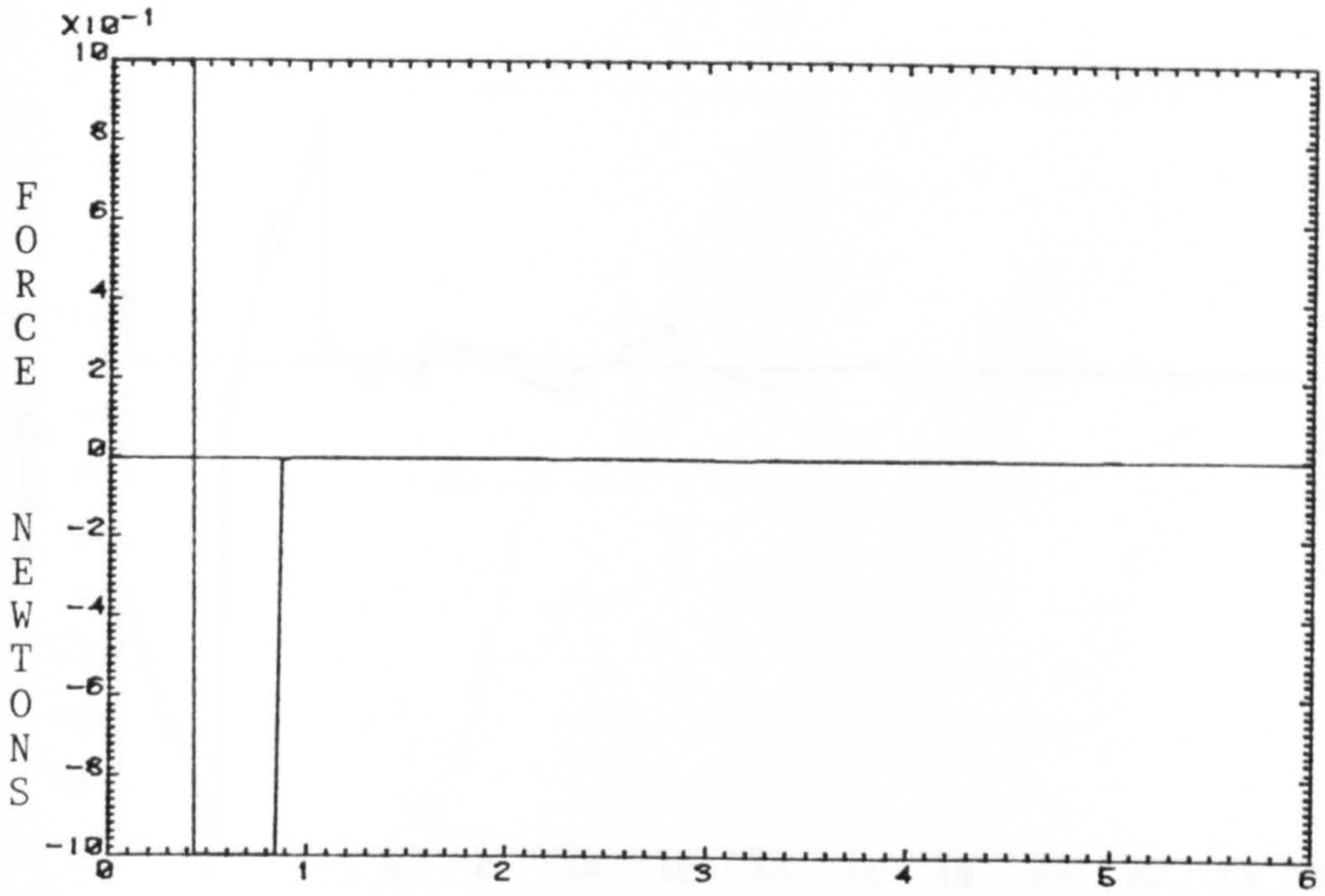

FIG 6.23C

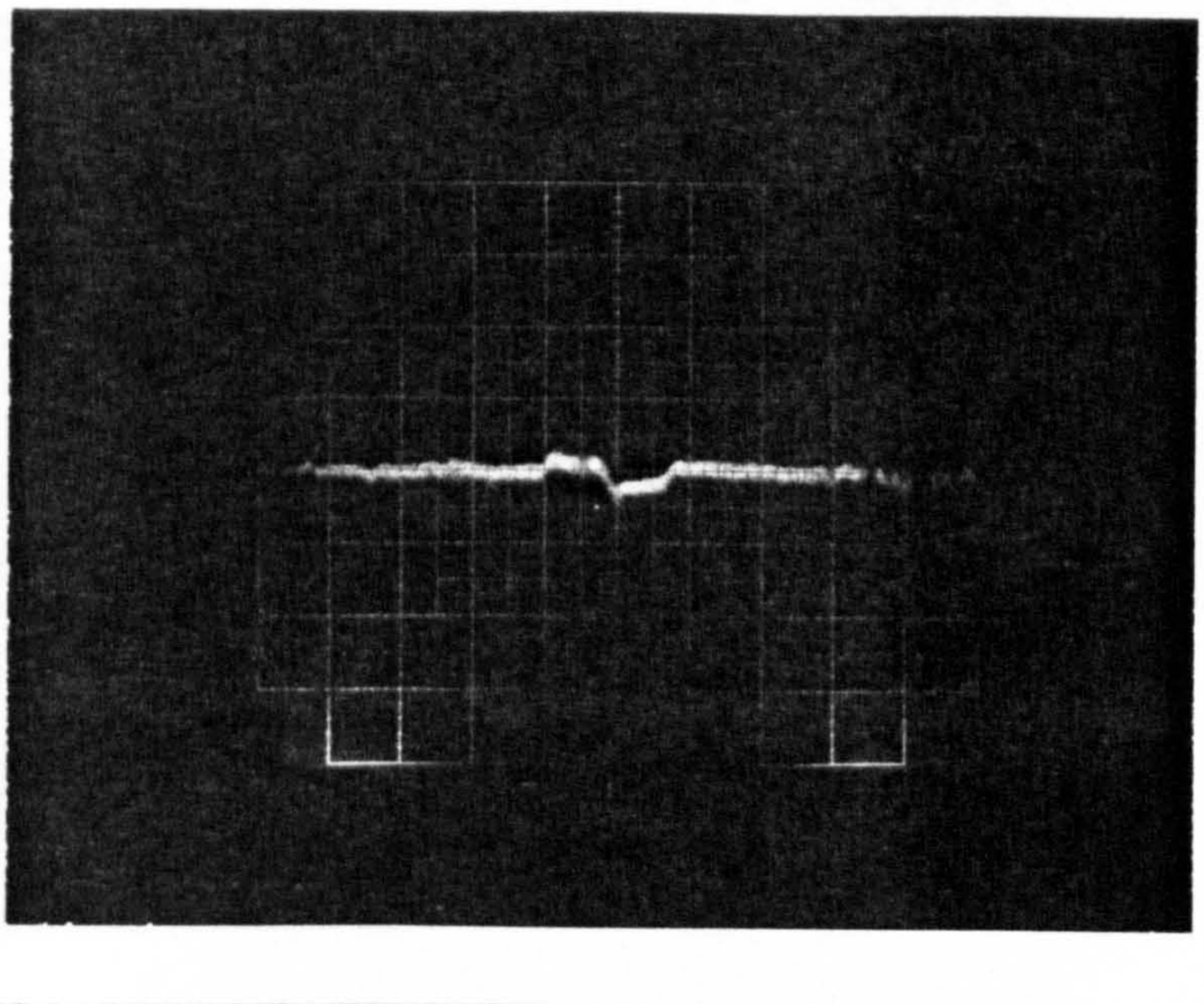

FIG 6.23D

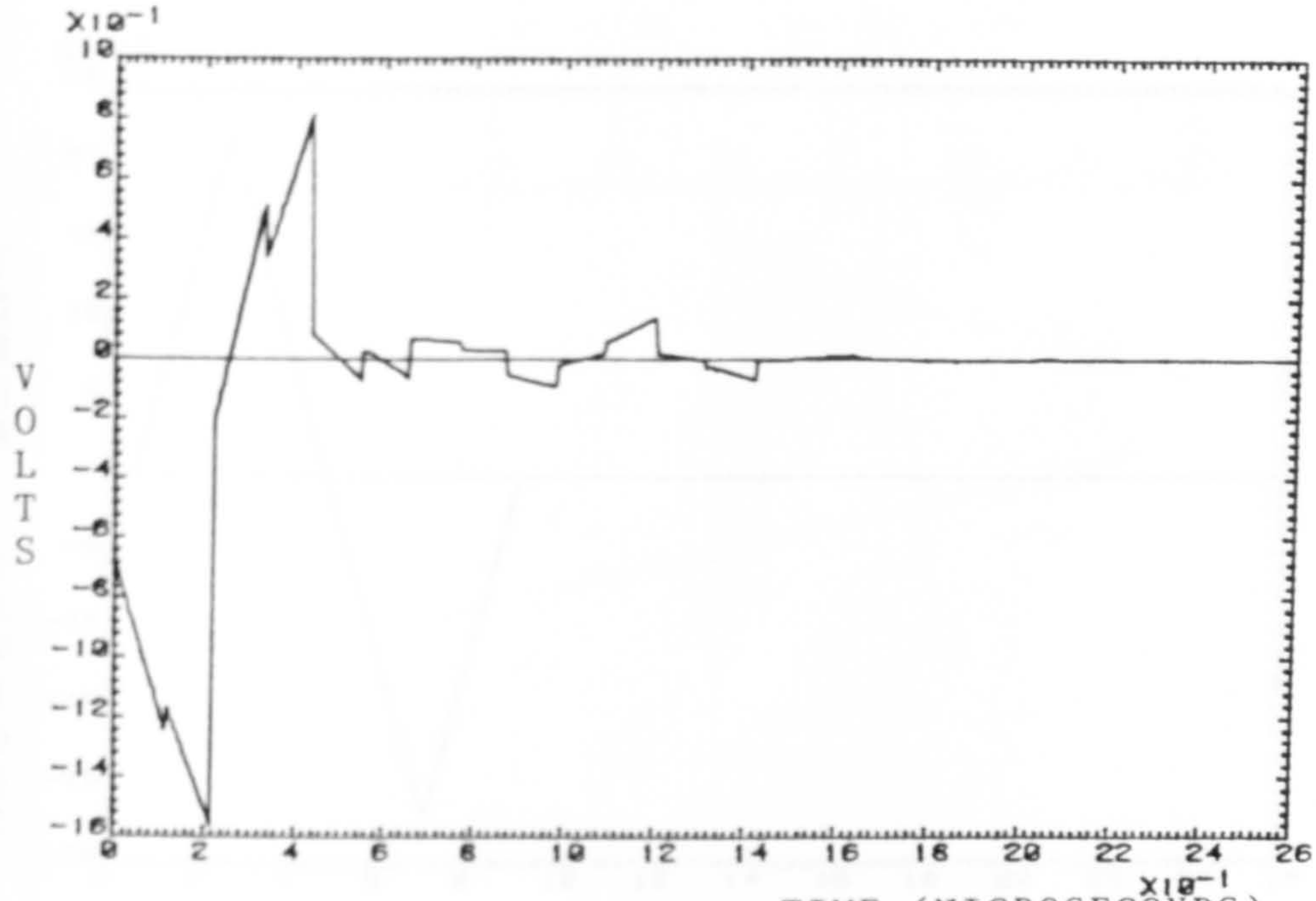

FIG 6.24A

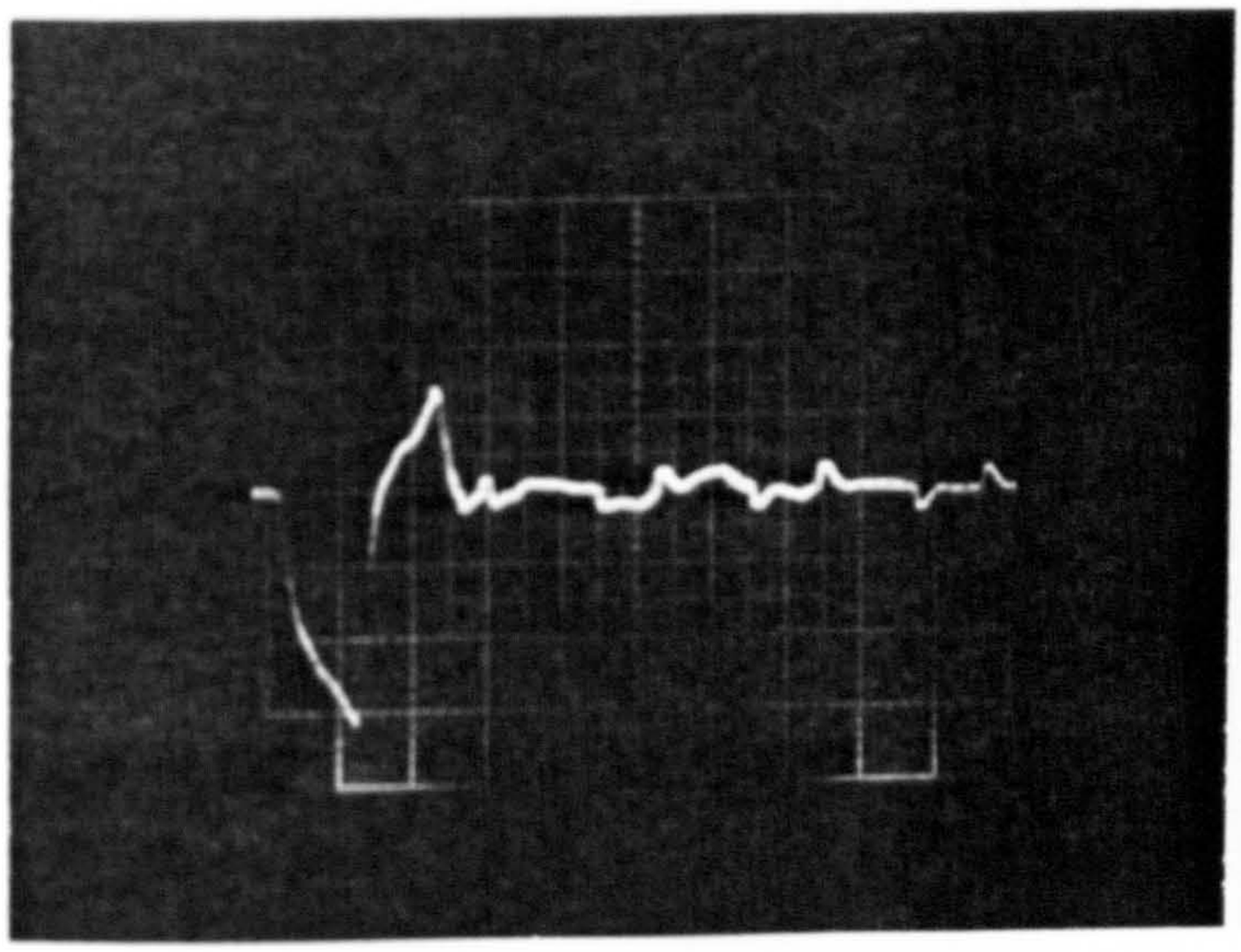

FIG 6.24B

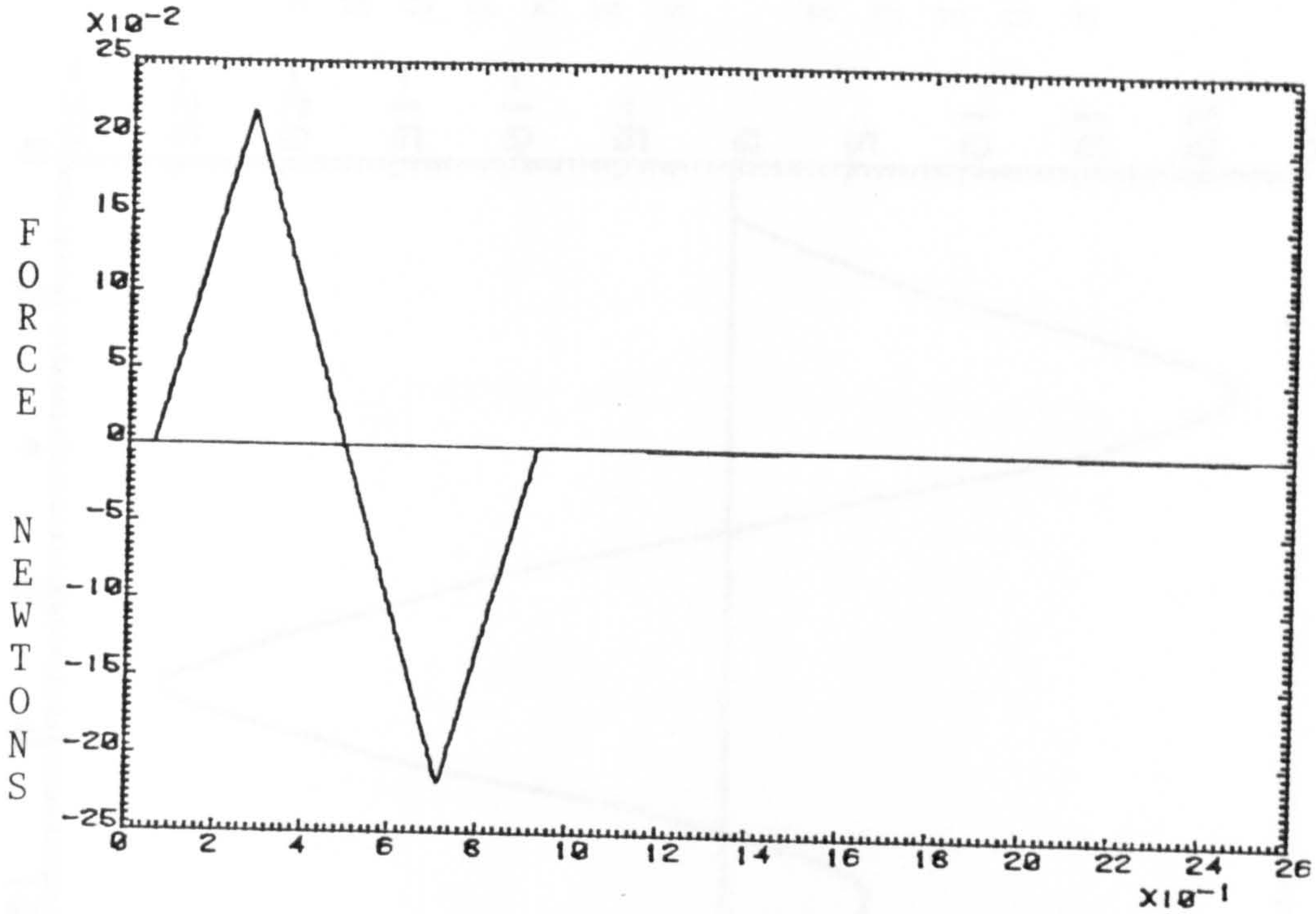

FIG 6.24C

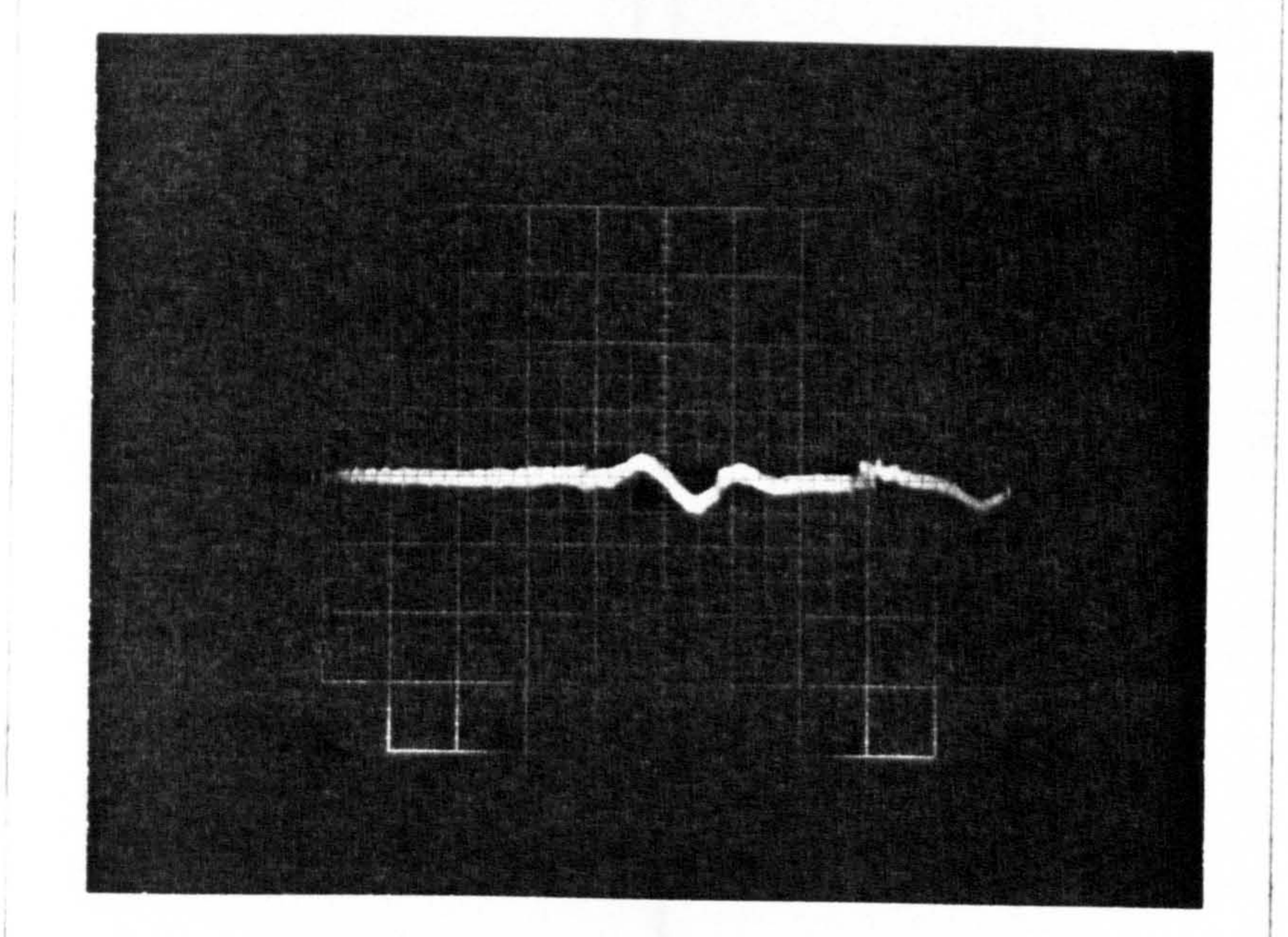

FIG 6.24 D

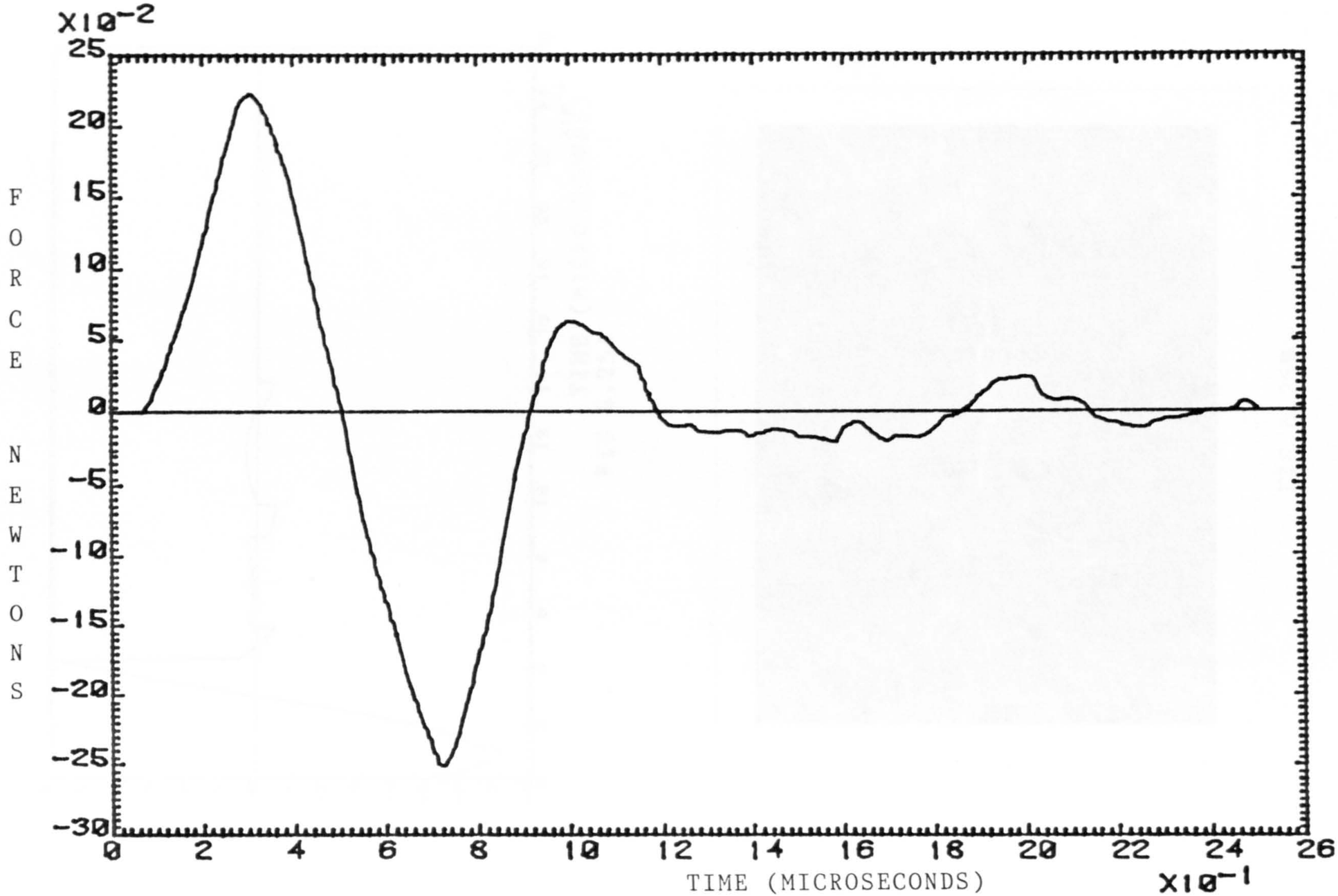
X10-2
25
20
15
10
5
0
-5
-10
-15
-20
-25
-30
FORCE NEWTONS
0
2
4
6
8
10
12
14
16
18
20
22
24
26
TIME (MICROSECONDS)
X10-1

FIG 6.24E

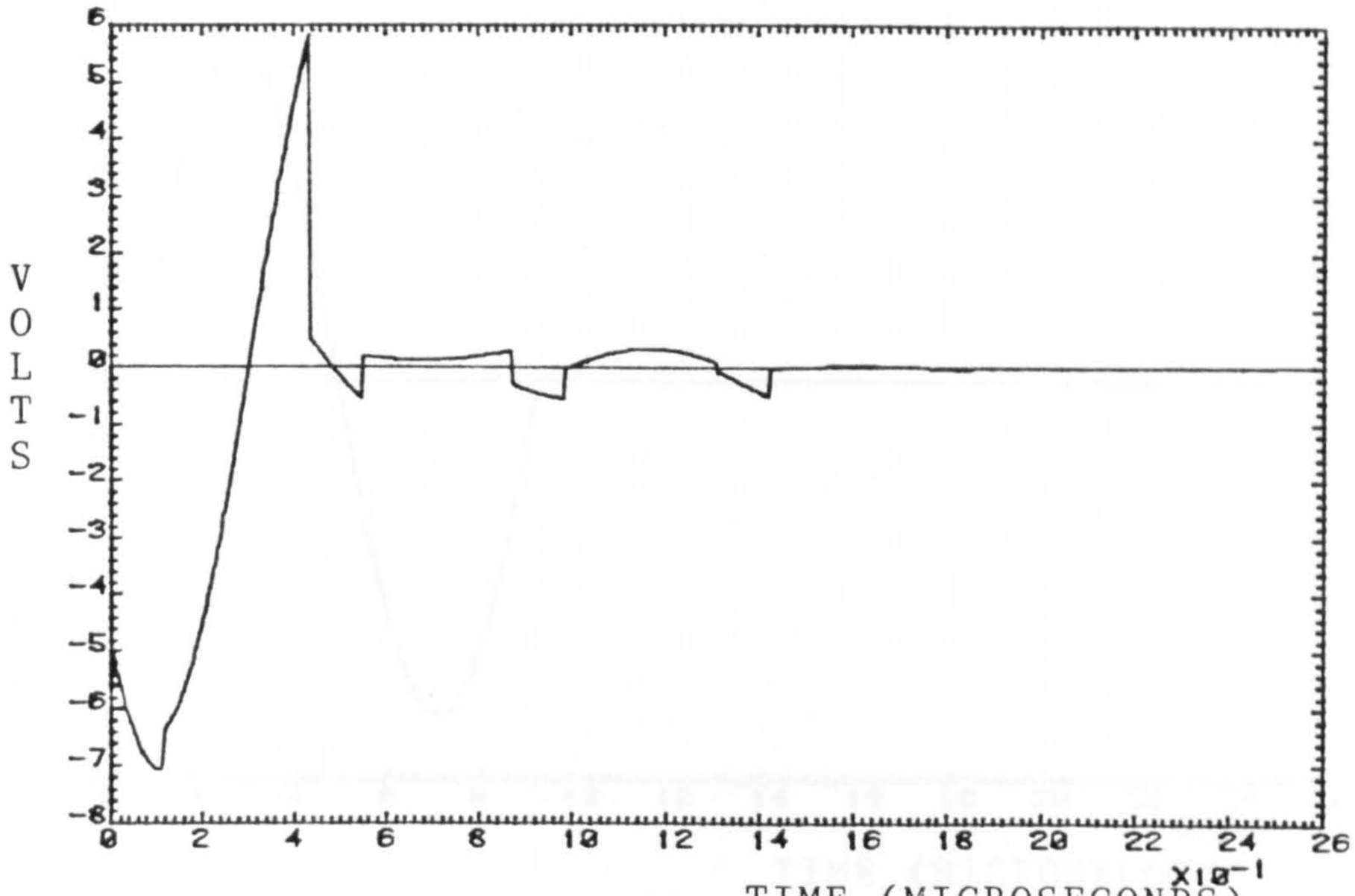

FIG 6.25A

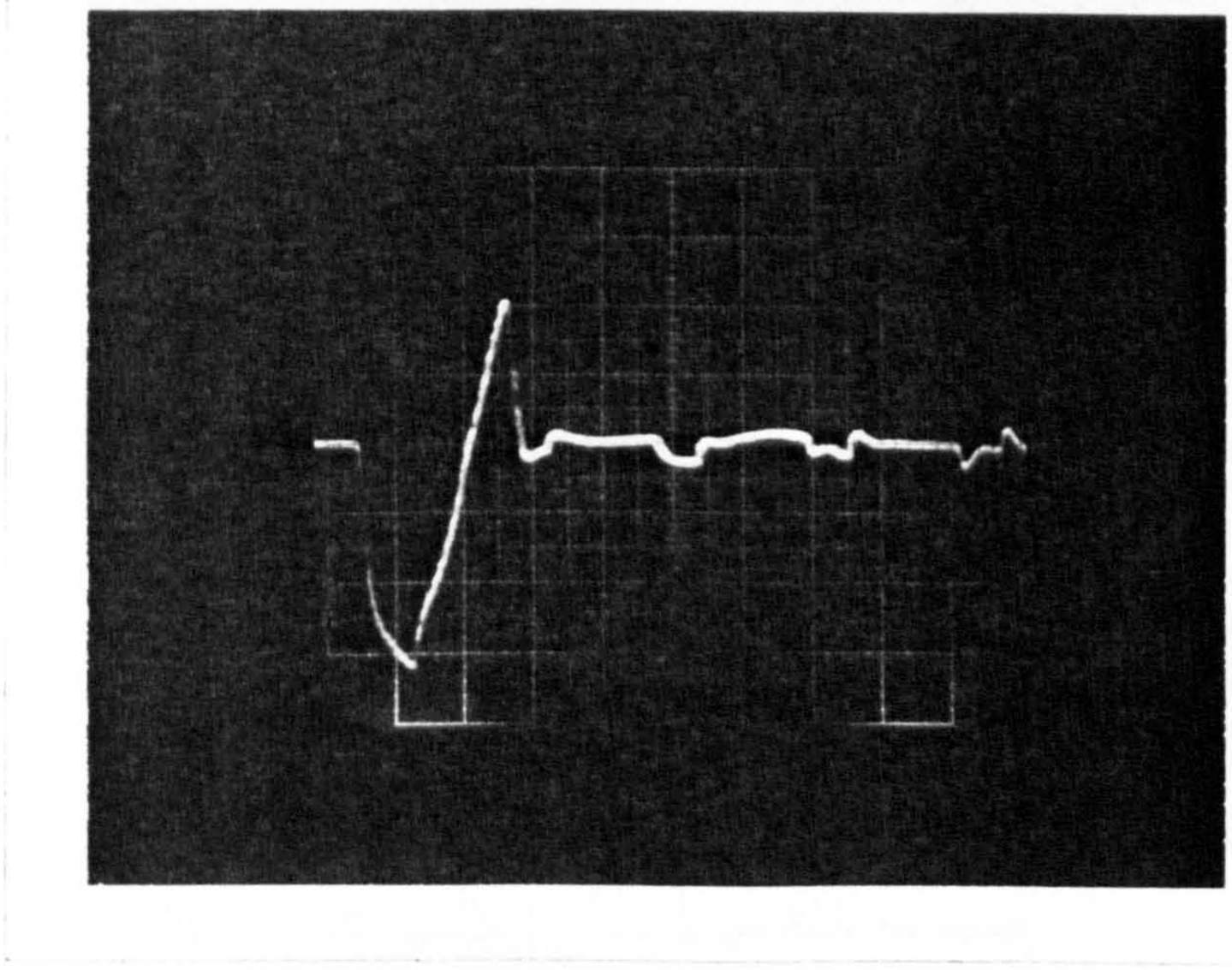

FIG 6.25B

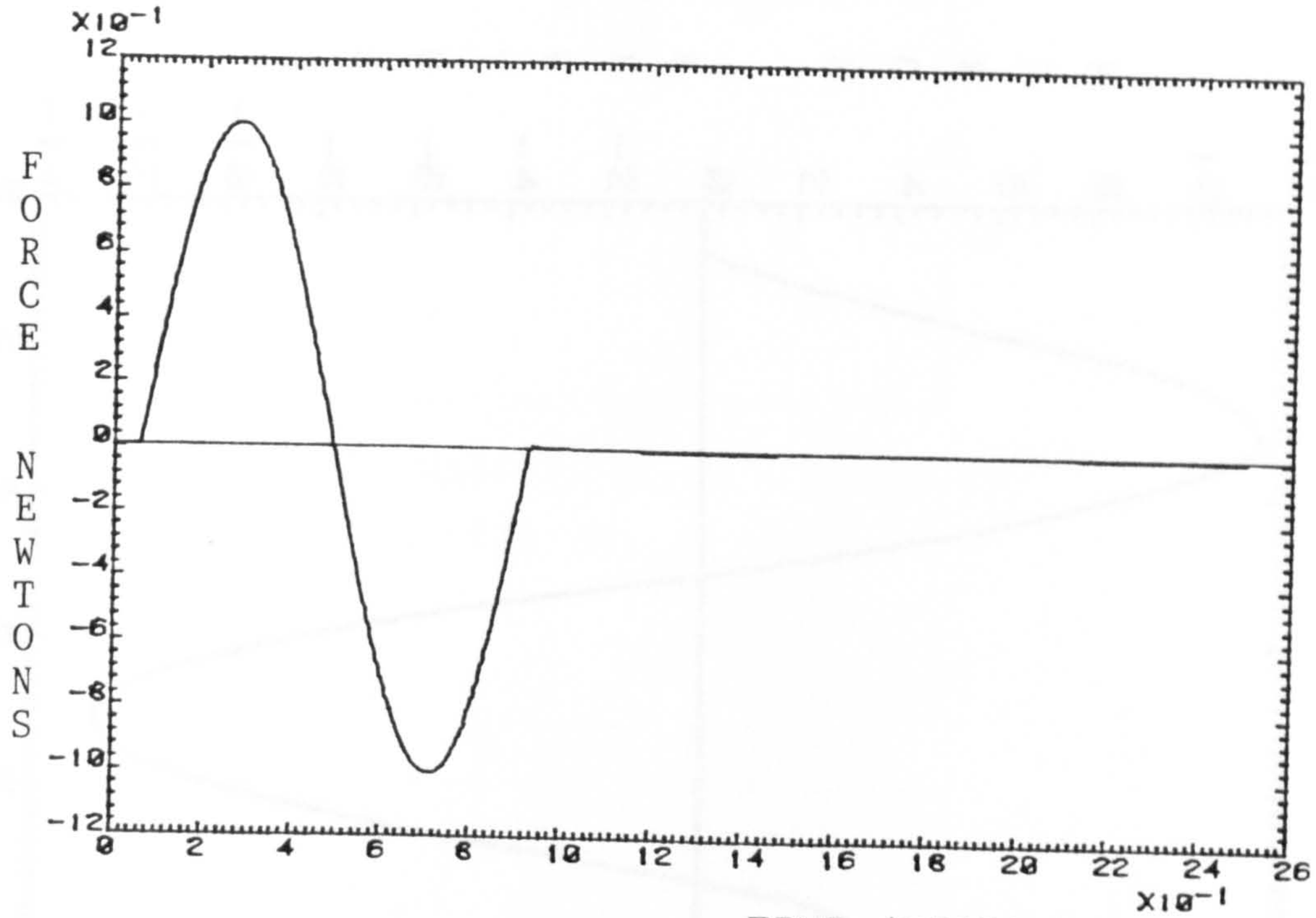

FIG 6.25C

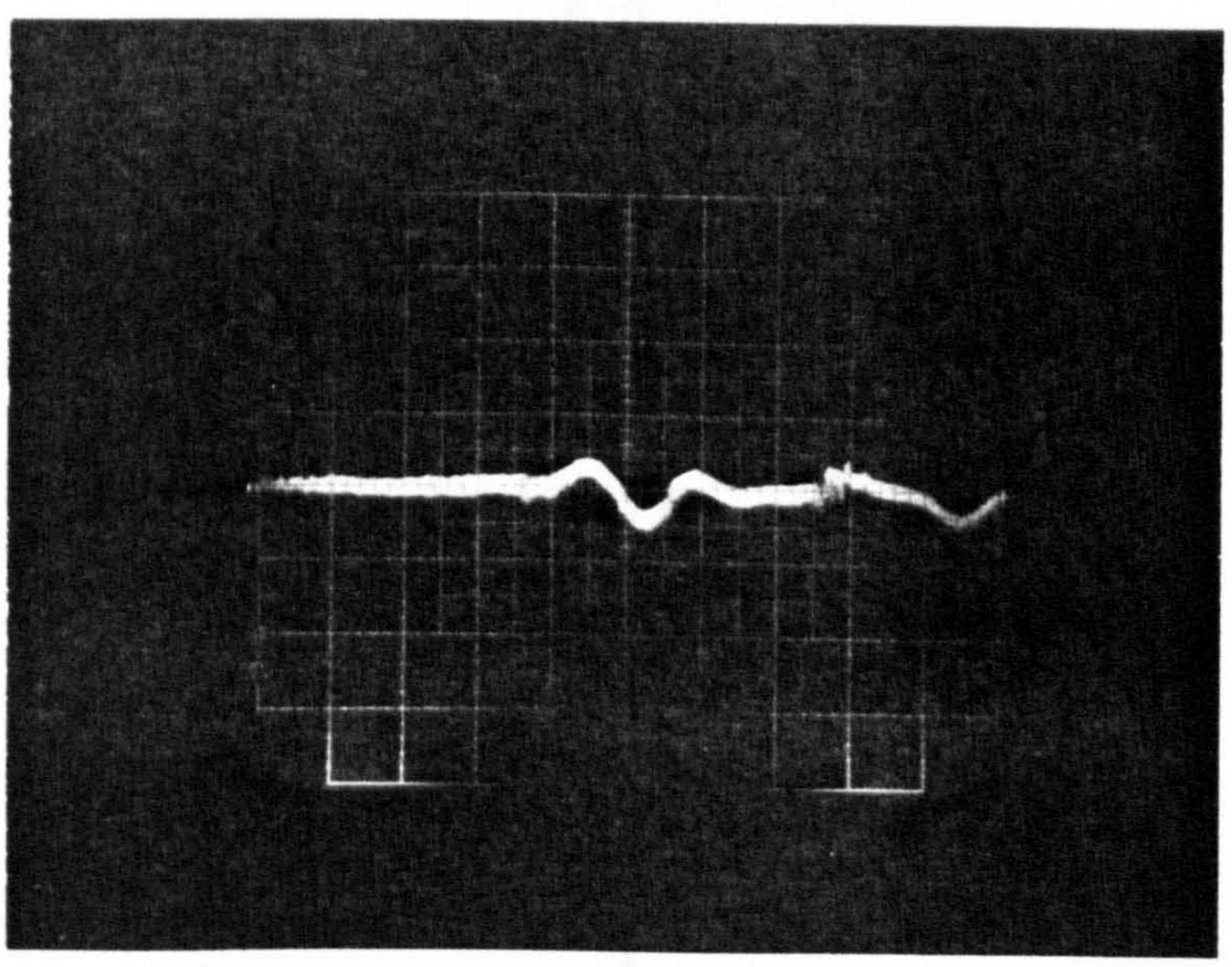

FIG 6.25D

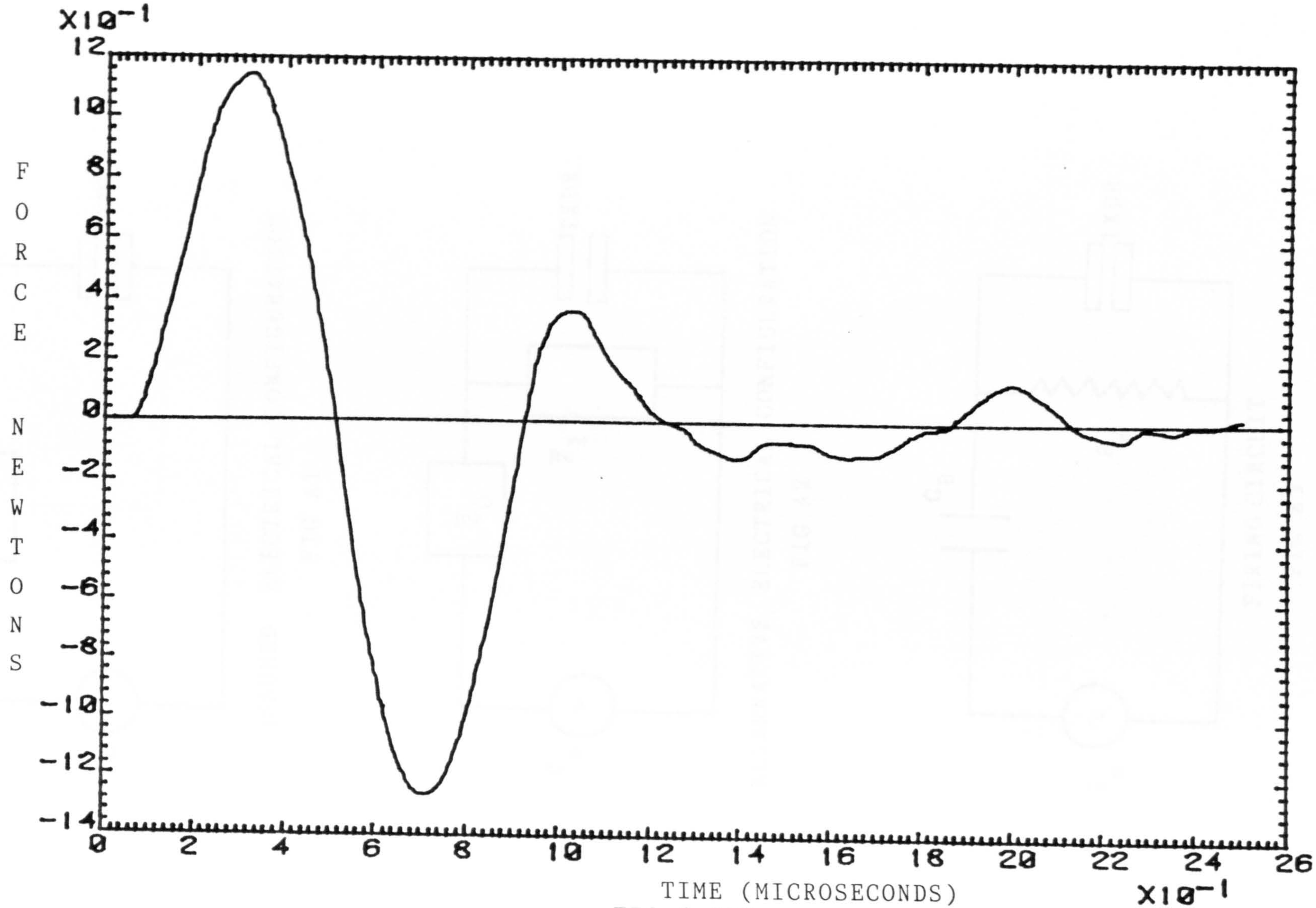
X10⁻¹
12
10
8
6
4
2
0
-2
-4
-6
-8
-10
-12
-14
FORCE NEWTONS
0
2
4
6
8
10
12
14
16
18
20
22
24
26
X10⁻¹
TIME (MICROSECONDS)

FIG 6.25E

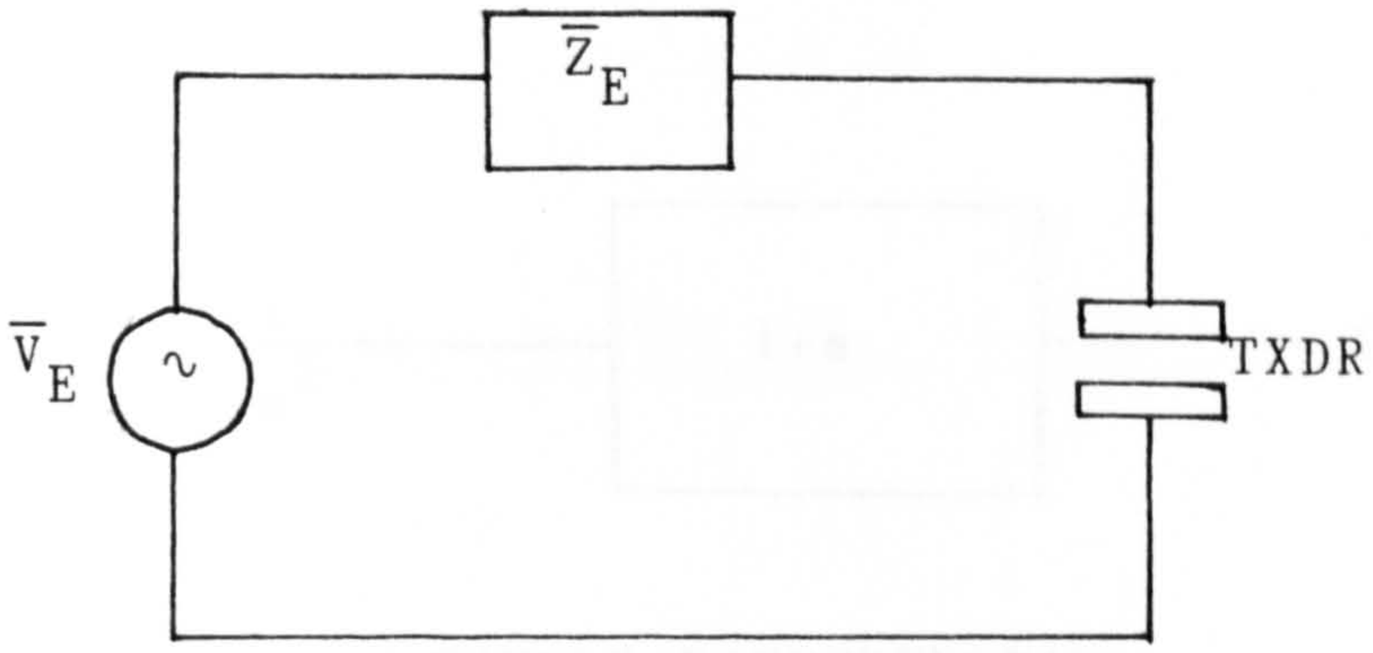

ASSUMED ELECTRICAL CONFIGURATION

FIG A1

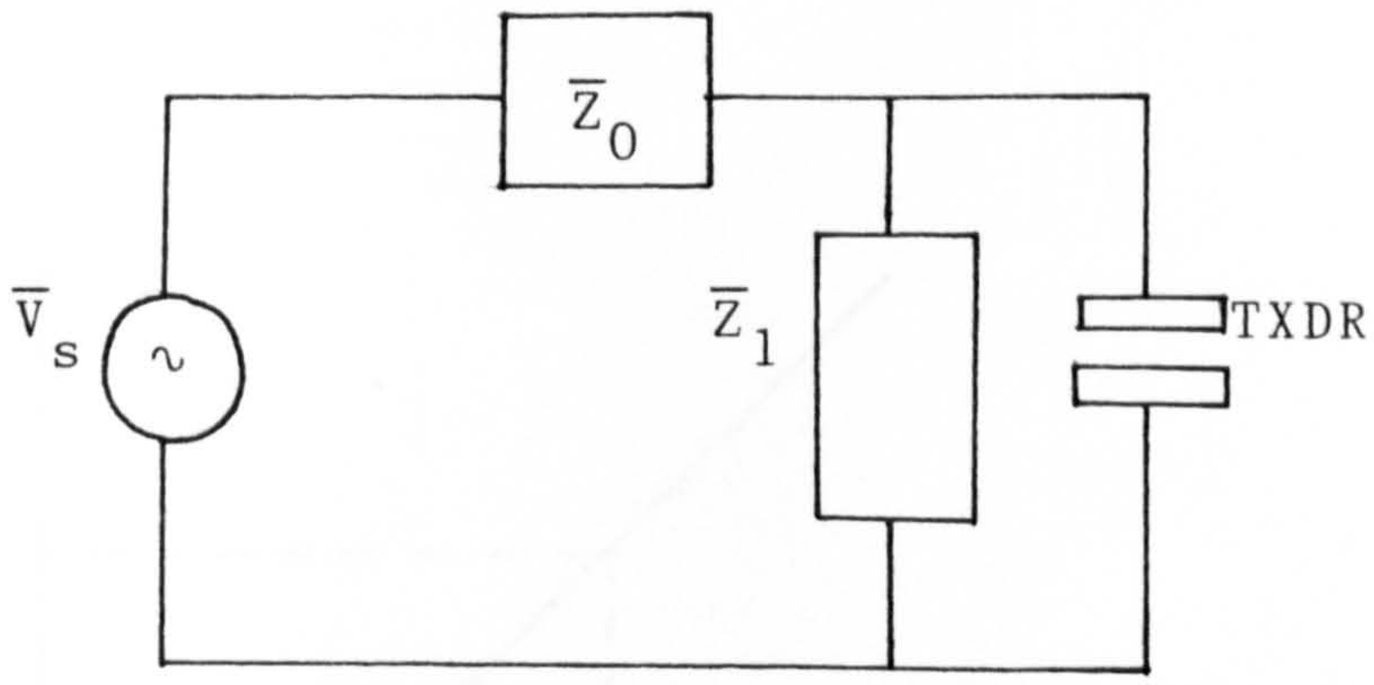

ALTERNATIVE ELECTRICAL CONFIGURATION

FIG A2

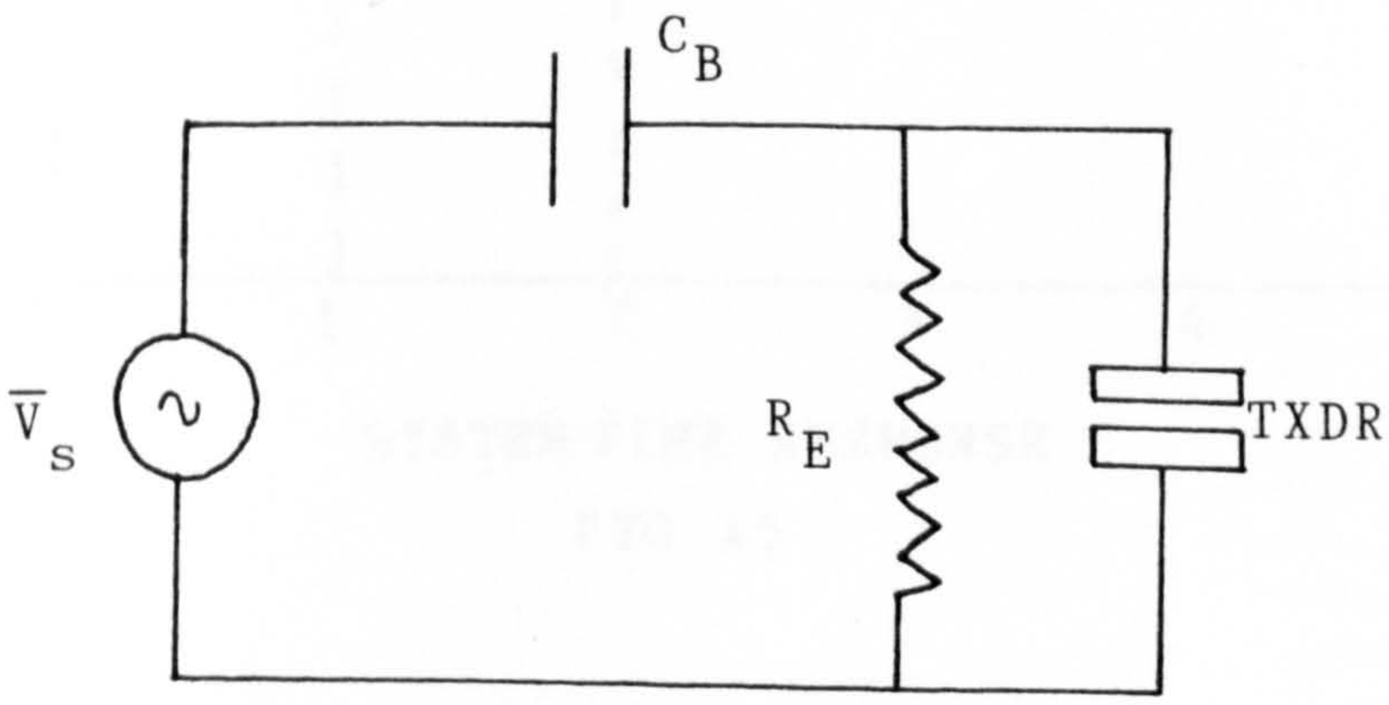

FIRING CIRCUIT

FIG A3

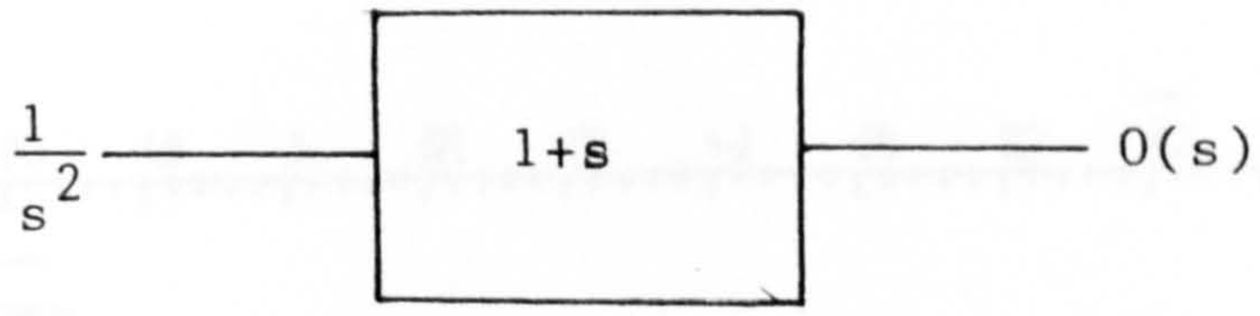

SIMPLE DIFFERENTIAL
SYSTEM
FIG A4

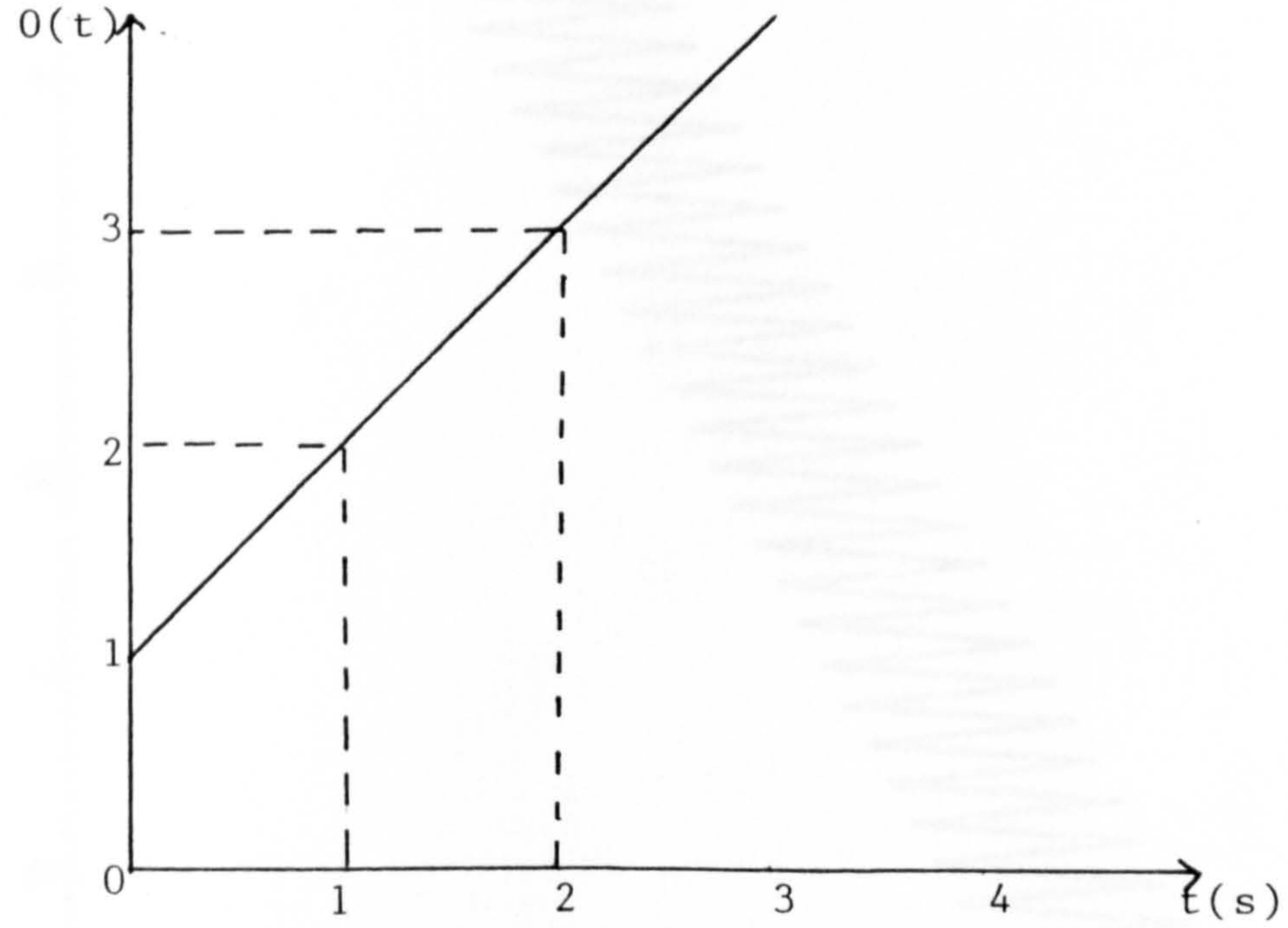

SYSTEM TIME RESPONSE
FIG A5

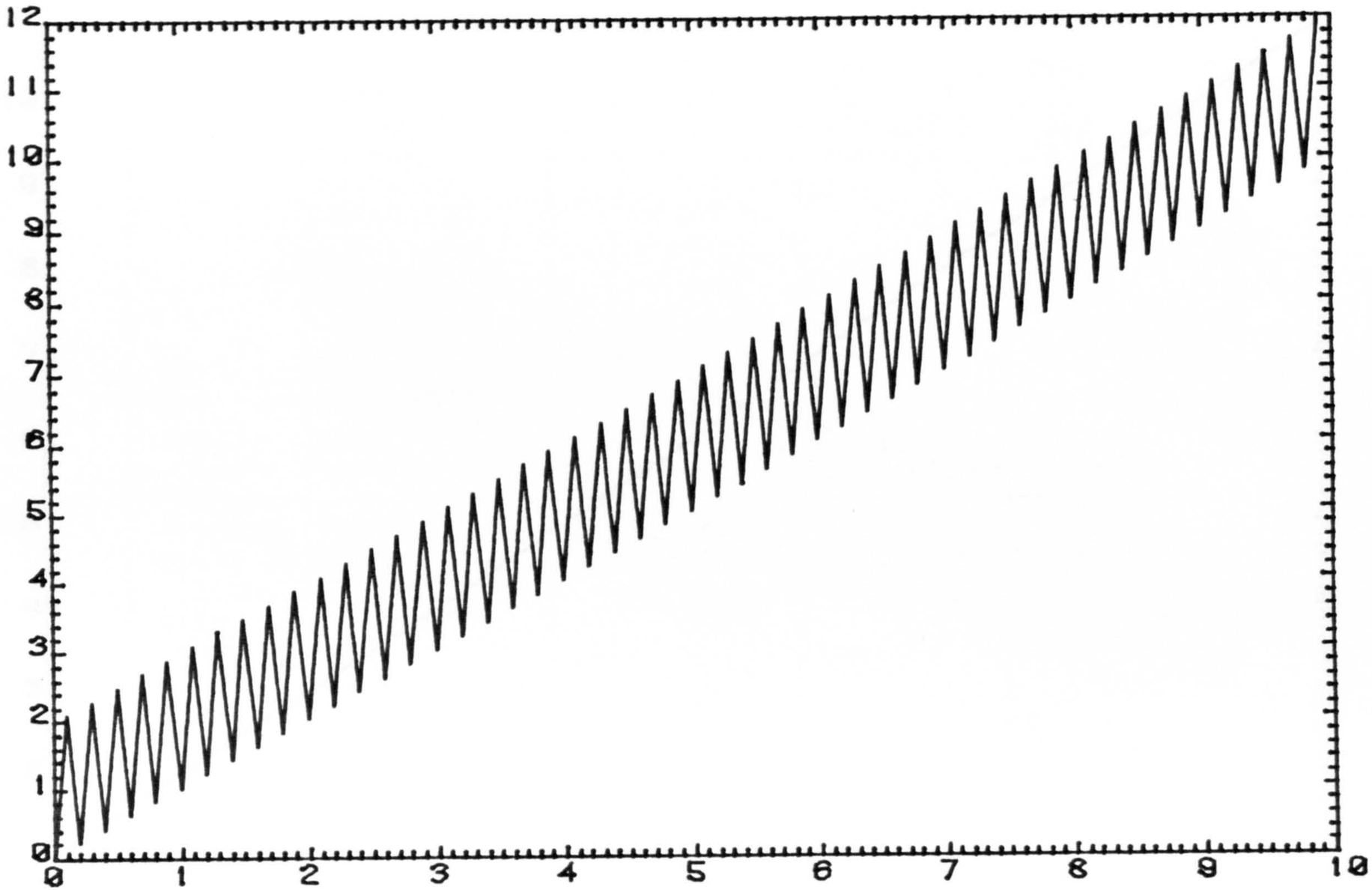

FIG A6

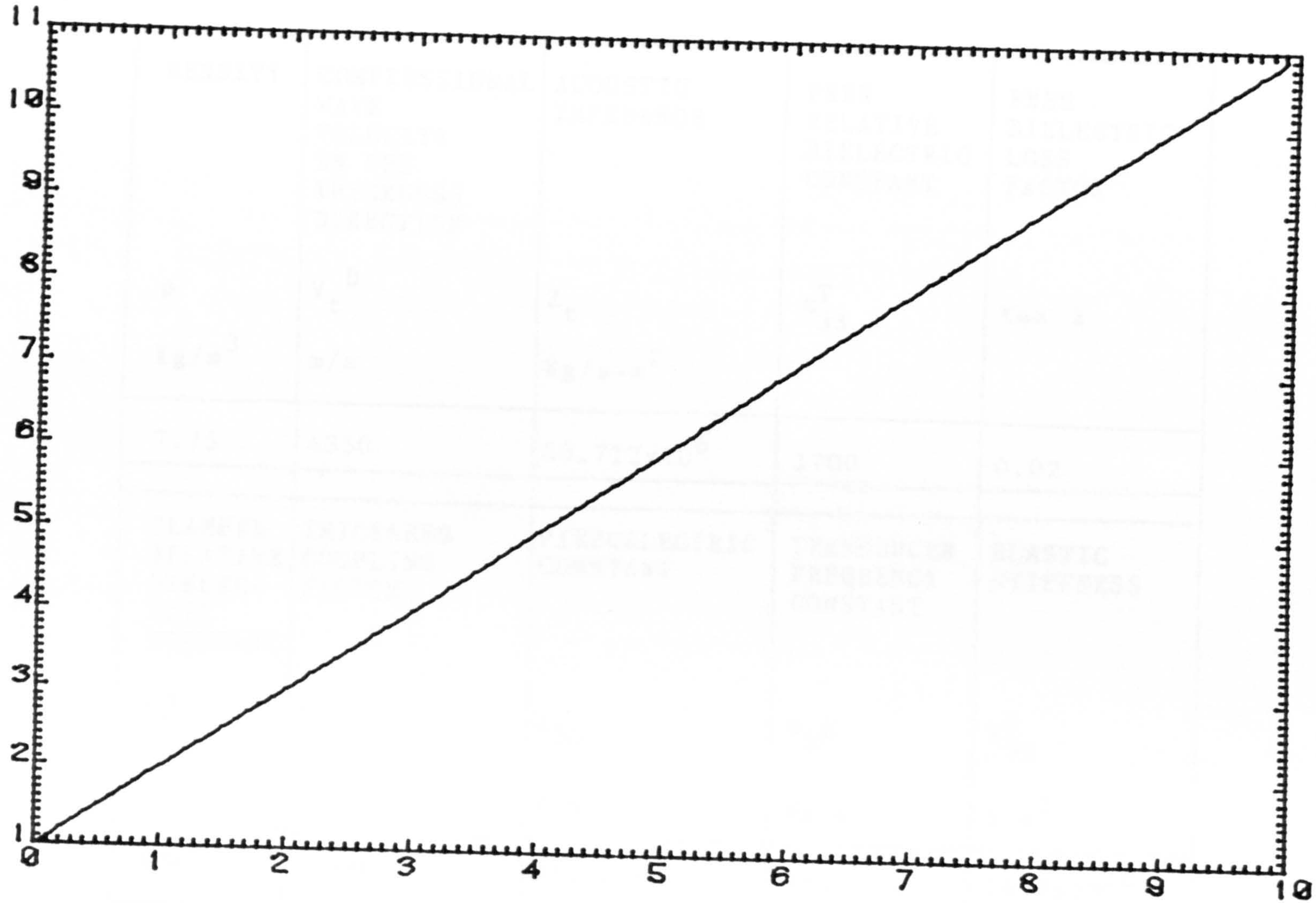

FIG A7

DENSITY ρ Kg/m^3	COMPRESSIONAL WAVE VELOCITY IN THE THICKNESS DIRECTION V_t^D m/s	ACOUSTIC IMPEDANCE Z_t $Kg/s\text{-}m^2$	FREE RELATIVE DIELECTRIC CONSTANT ε_{33}^T	FREE DIELECTRIC LOSS FACTOR tan ∂
7.75	4350	33.712×10^6	1700	0.02

CLAMPED RELATIVE DIELEC-TRIC CONSTANT ε_{33}^S	THICKNESS COUPLING FACTOR k	PIEZOELECTRIC CONSTANT h_{33} V/m	TRANSDUCER FREQUENCY CONSTANT N_3t Hz-m	ELASTIC STIFFNESS Y_{33}^D N/m^2
830	0.486	21.5×10^8	1890	14.7×10^{10}

TABLE 1

CRYSTAL DATA	THICKNESS (mm)	DIAMETER (mm)	MECHANICAL RESONANCE (MHz)	TRANSIT TIME μs	C_t (CALCULATED) nF	C_t (MEASURED) nF
* CERAMIC B	1.87	20.00	1.1508	0.4345	1.221	1.16
CERAMIC D	1.87	19.98	1.145	0.4367	1.221	1.13
CERAMIC E	1.88	19.98	1.150	0.4350	2.75	2.55
VALUES USED FOR SIMULATION	1.87	20	1.15	0.435		B 1.16 D 1.13 E 2.55

* HAYWARD (19)

TABLE B2

TABLE B3

LAYER AND BACKING DATA	ALUMINIUM	LEAD	STEEL	ARALDITE
ACOUSTIC IMPEDANCE ($*10^6 kg/m^2-s$)	(3) 17.5	(3) 27	(3) 45	(4) 2.75
VELOCITY (mm/us)	(3) 6.3	(3) 2.1	(3) 6.1	(4) 2.5
THICKNESS (mm)	2.5 ± 0.02		0.355 ± 0.005	

3 - ENGSMINGER (15)
4 - SILK (58)

NOTE: Data for the silver loaded araldite was not available. It was assumed to have the same properties as ordinary araldite.

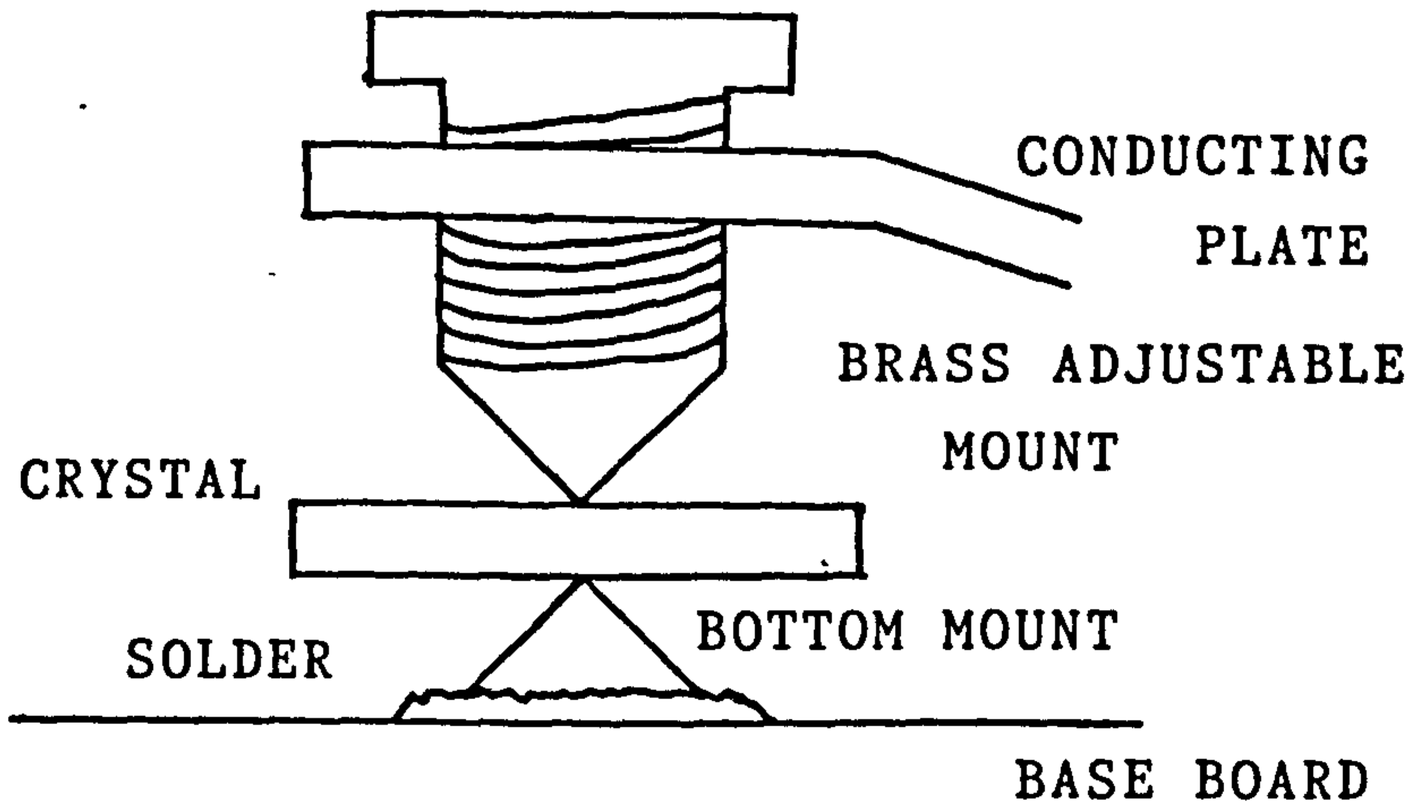

FIG B1

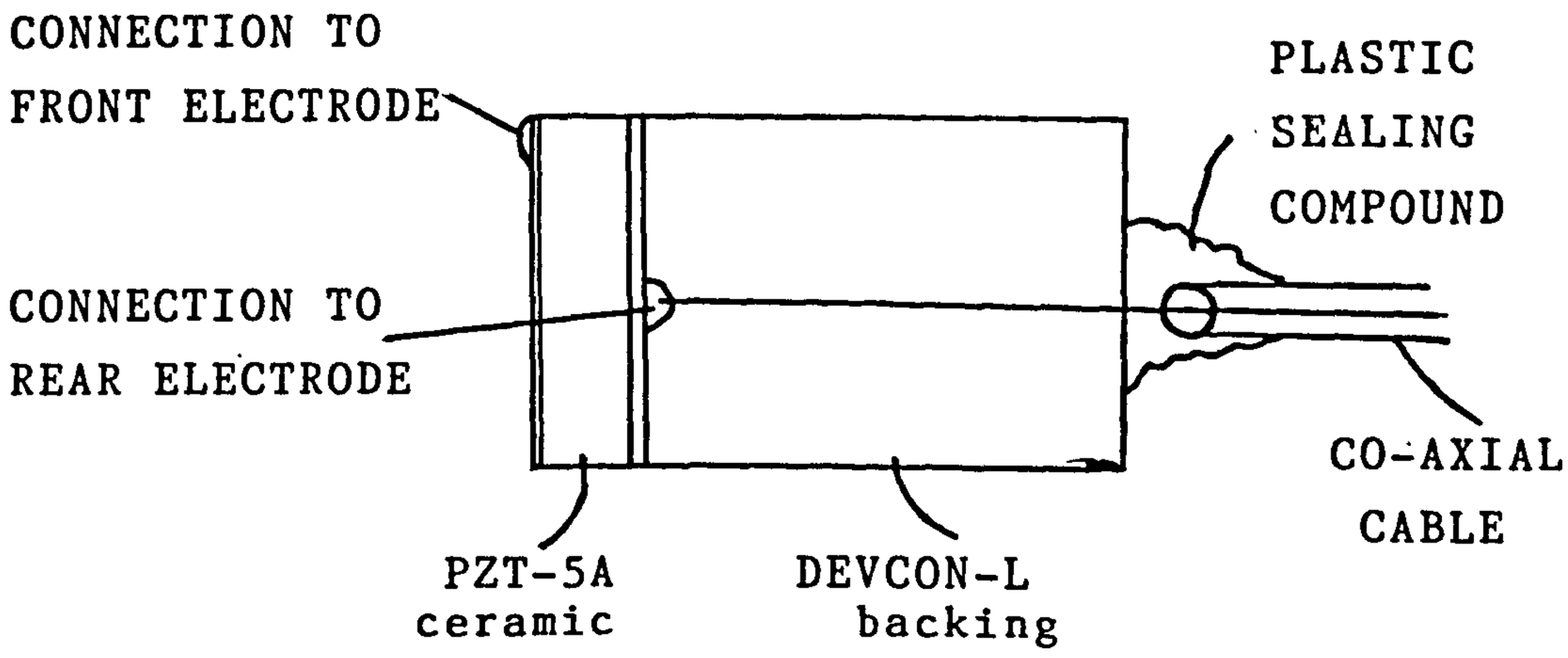

FIG B2

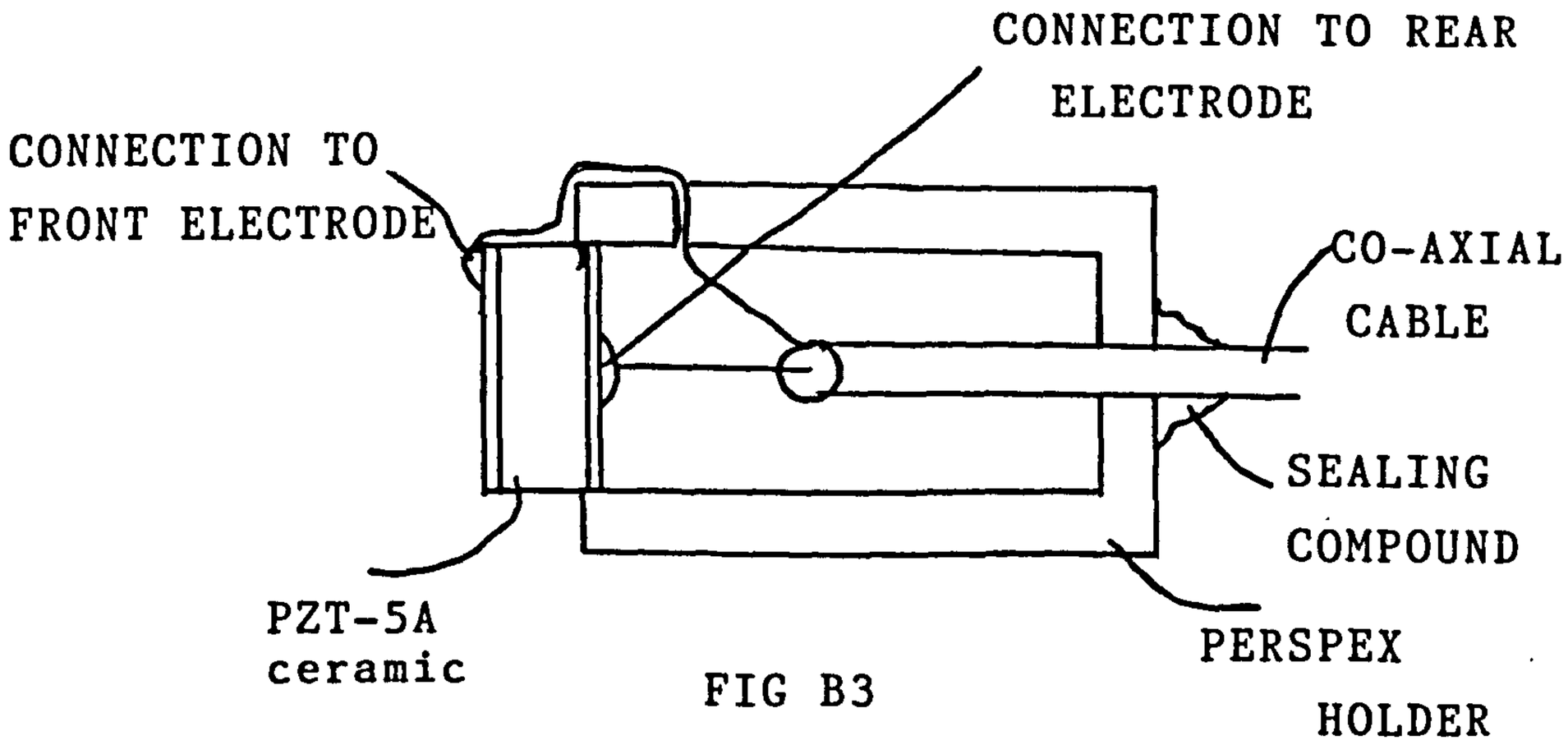

FIG B3

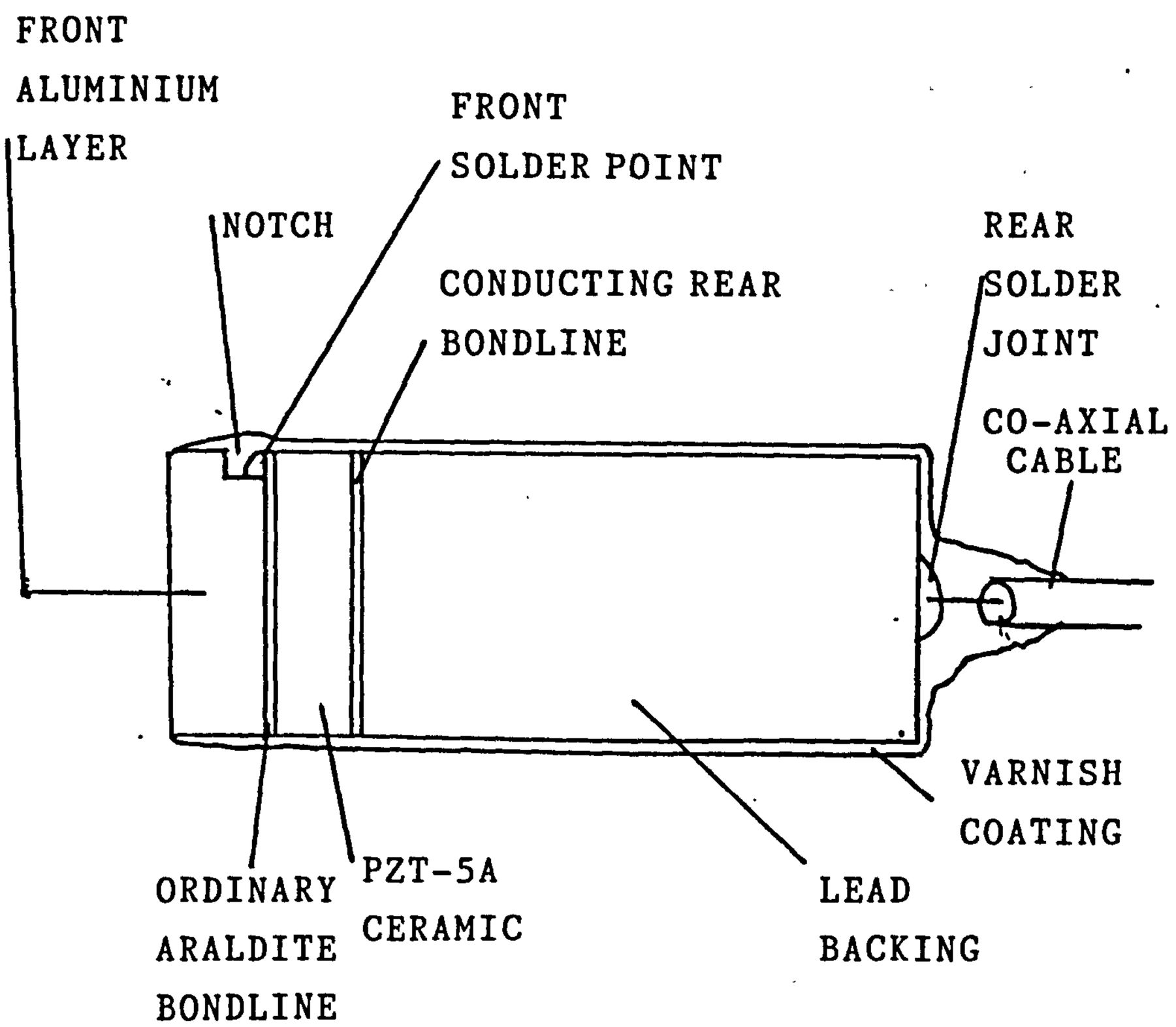
FRONT
ALUMINIUM
LAYER
FRONT
SOLDER POINT
NOTCH
CONDUCTING REAR
BONDLINE
REAR
SOLDER
JOINT
CO-AXIAL
CABLE
VARNISH
COATING
ORDINARY
ARALDITE
BONDLINE
PZT-5A
CERAMIC
LEAD
BACKING

FIG B4

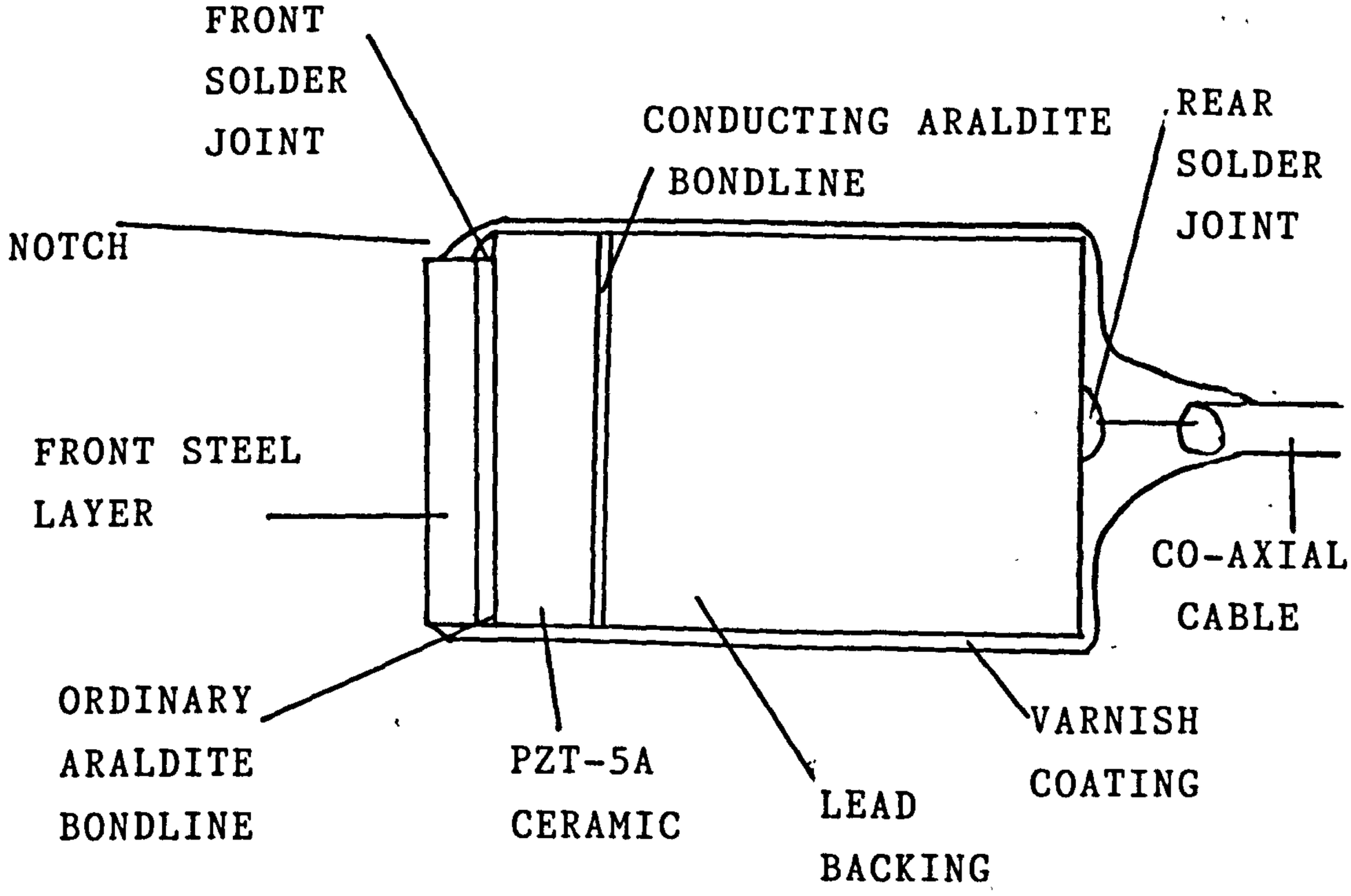
FRONT
SOLDER
JOINT
NOTCH
FRONT STEEL
LAYER
ORDINARY
ARALDITE
BONDLINE
PZT-5A
CERAMIC
CONDUCTING ARALDITE
BONDLINE
REAR
SOLDER
JOINT
CO-AXIAL
CABLE
VARNISH
COATING
LEAD
BACKING

FIG B5

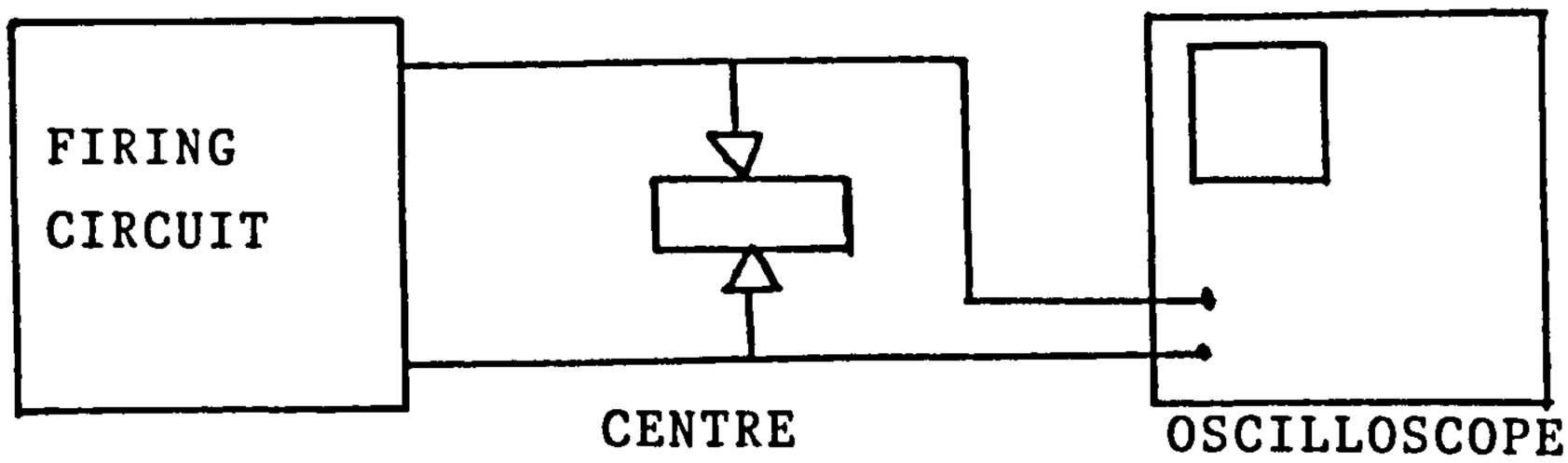

FIG B6

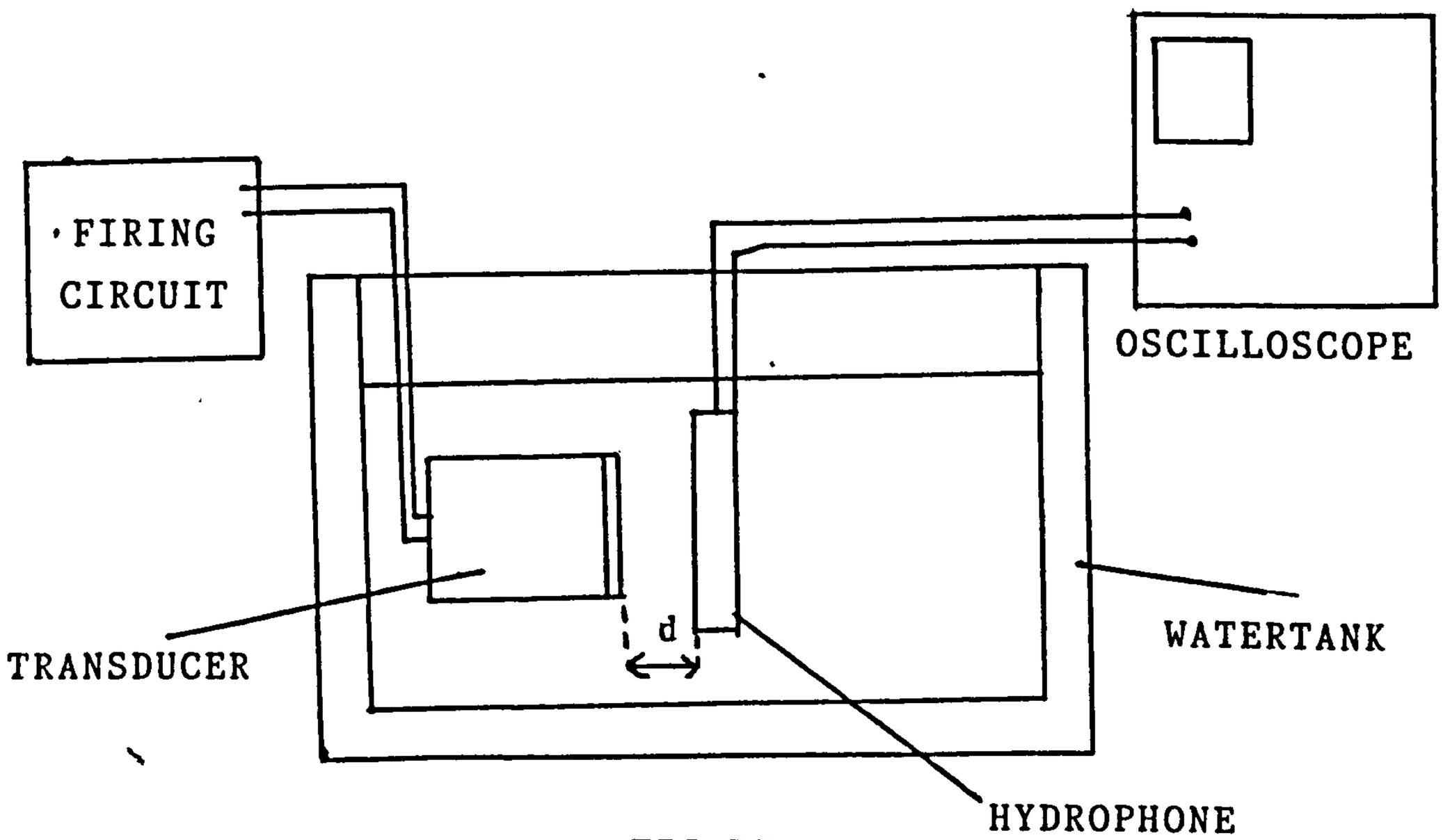

FIG B7

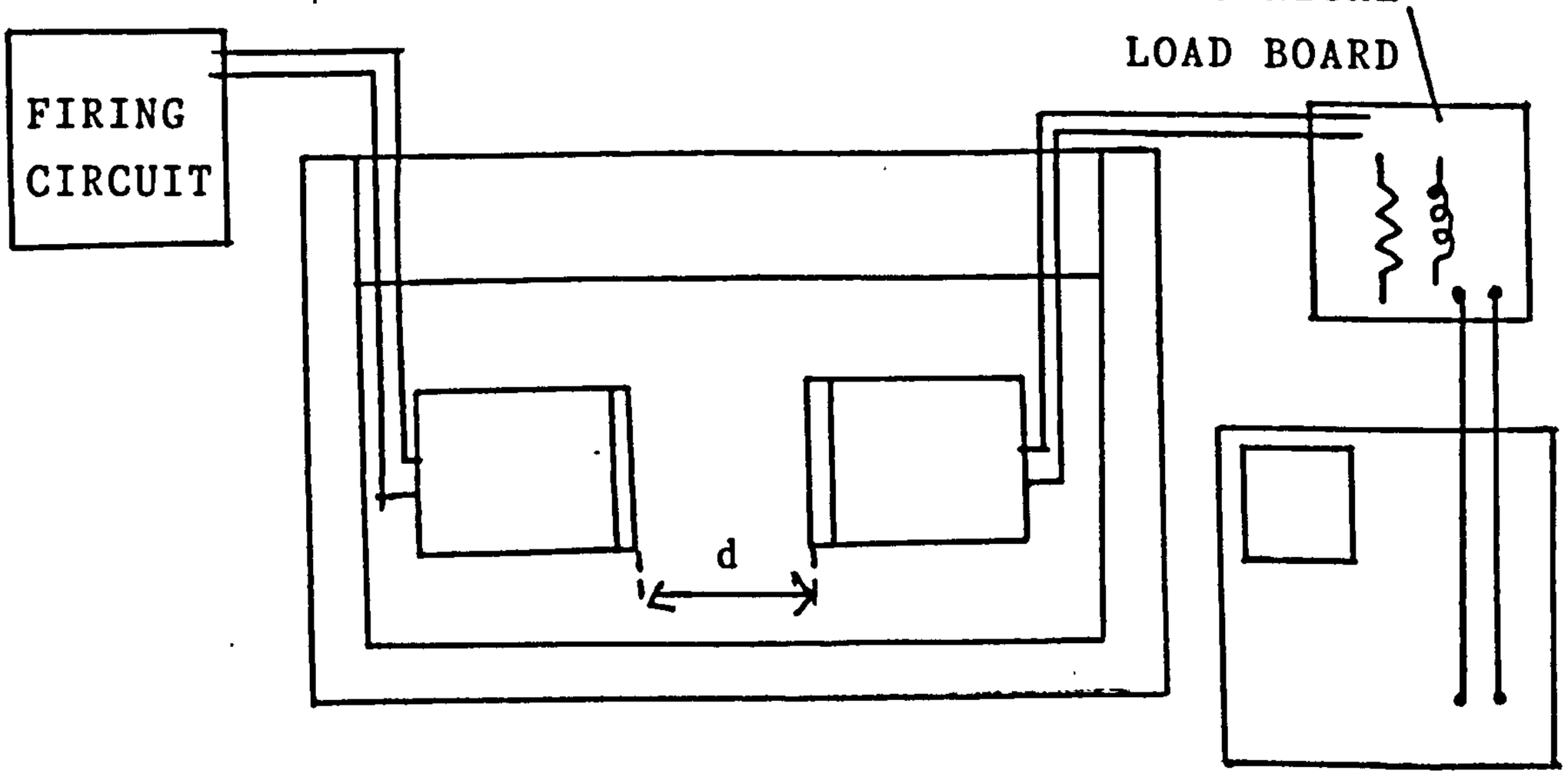

FIG B8

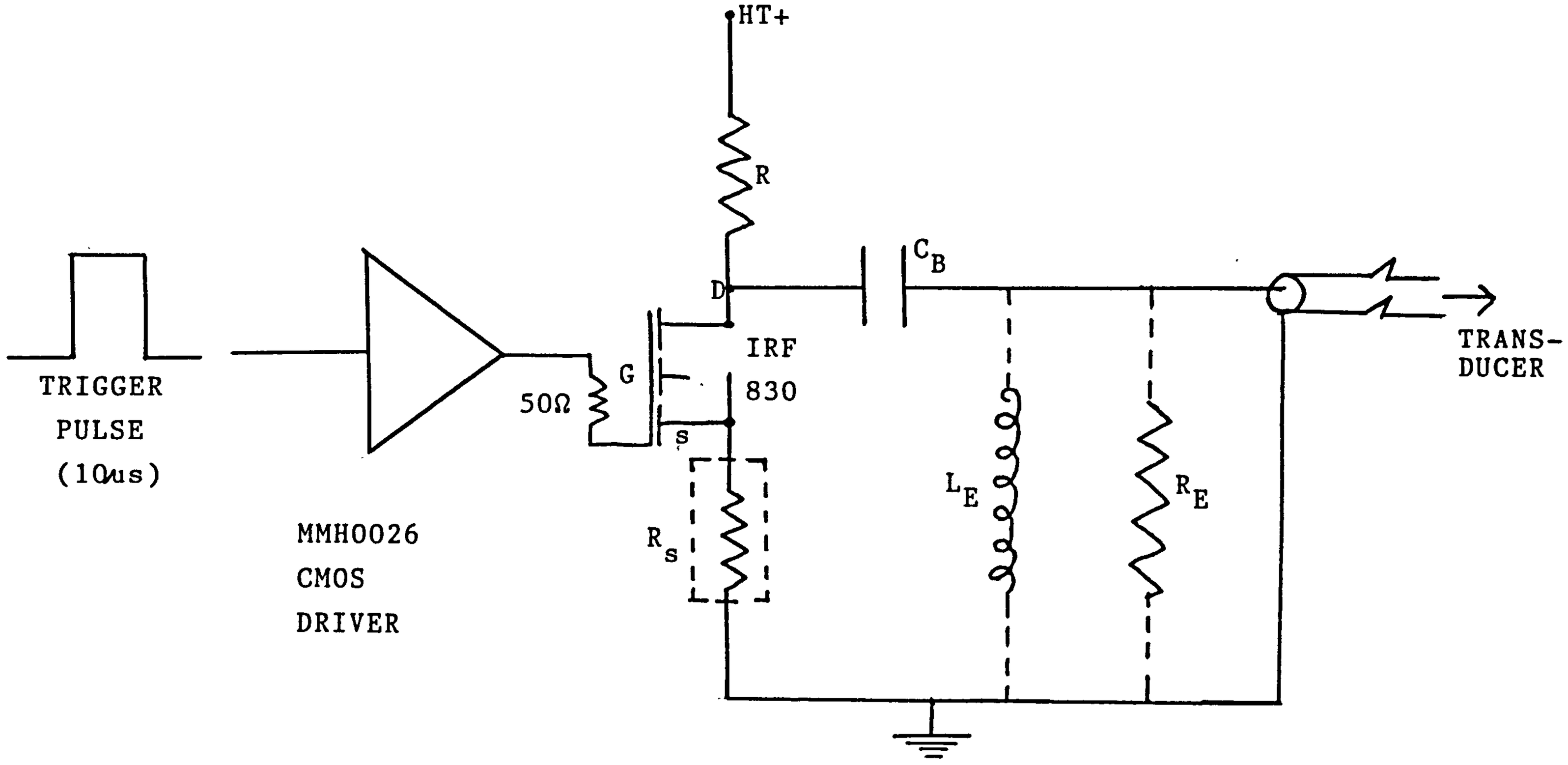
HT+
R
D
C_B
IRF
830
G
50Ω
S
R_S
L_E
R_E
TRANS-
DUCER
TRIGGER
PULSE
(10μs)
MMH0026
CMOS
DRIVER

FIG B9

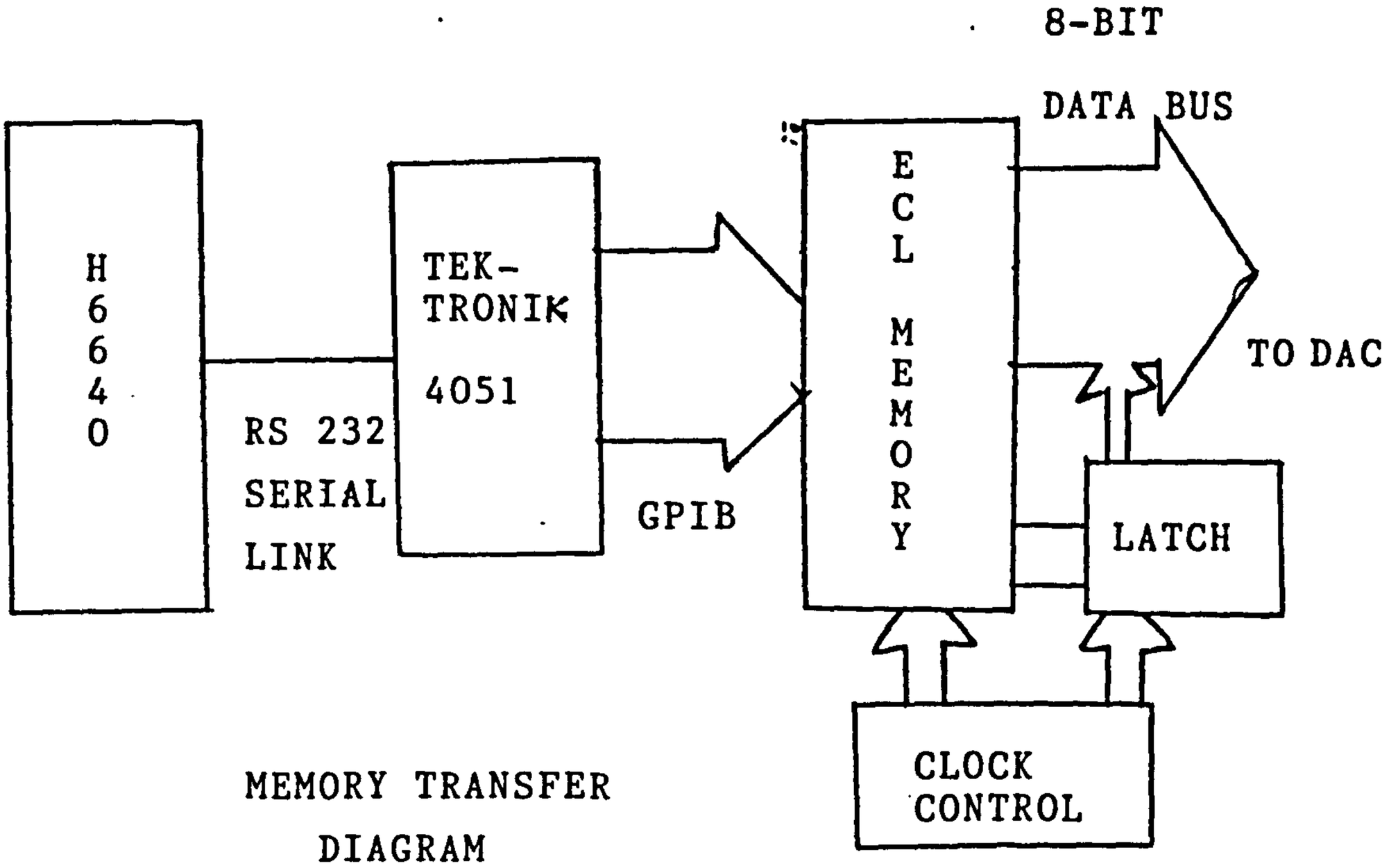

MEMORY TRANSFER
DIAGRAM

FIG B10

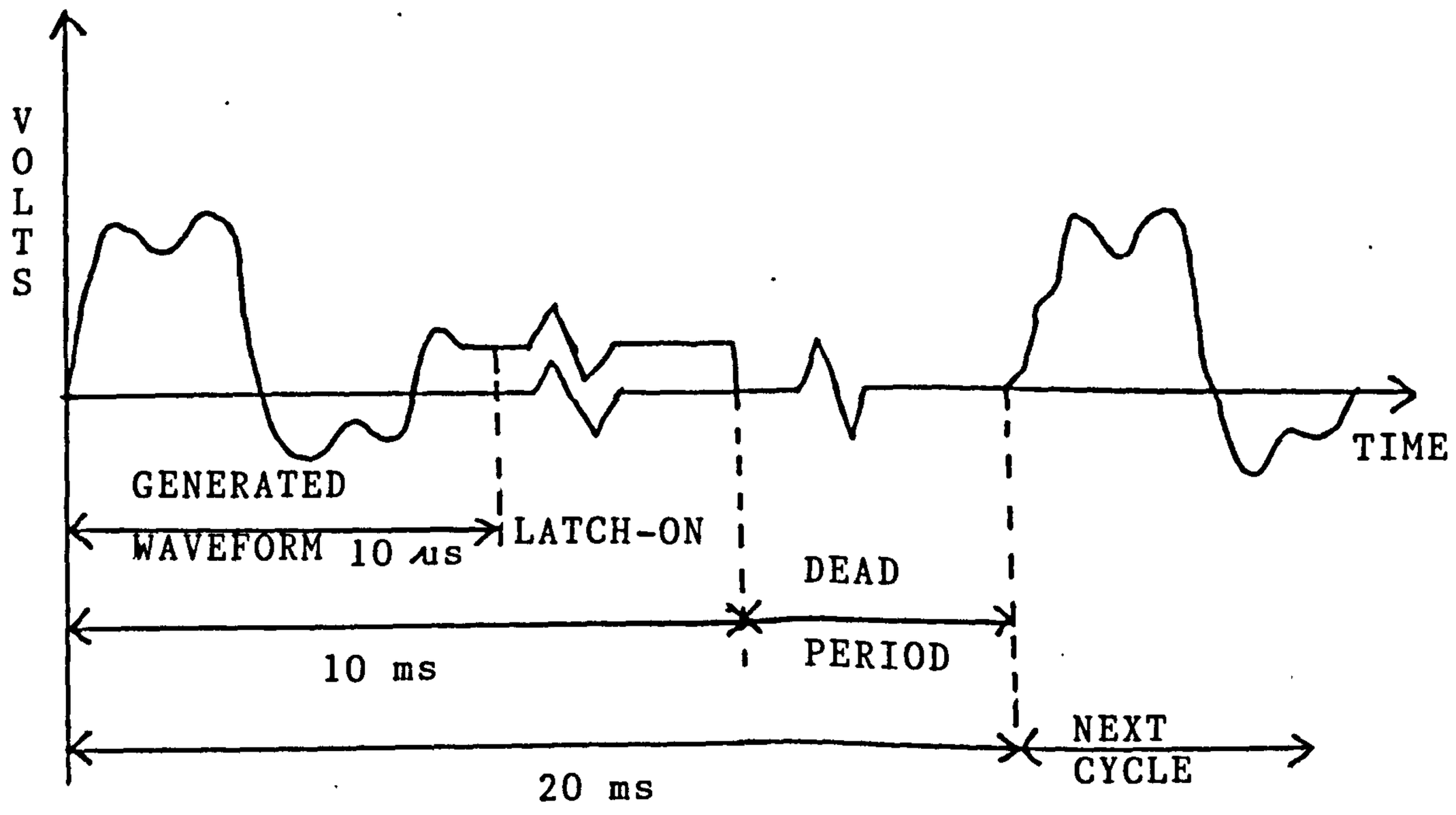

FIG B11

REFRESH CYCLE AND LATCH TIMING DIAGRAM

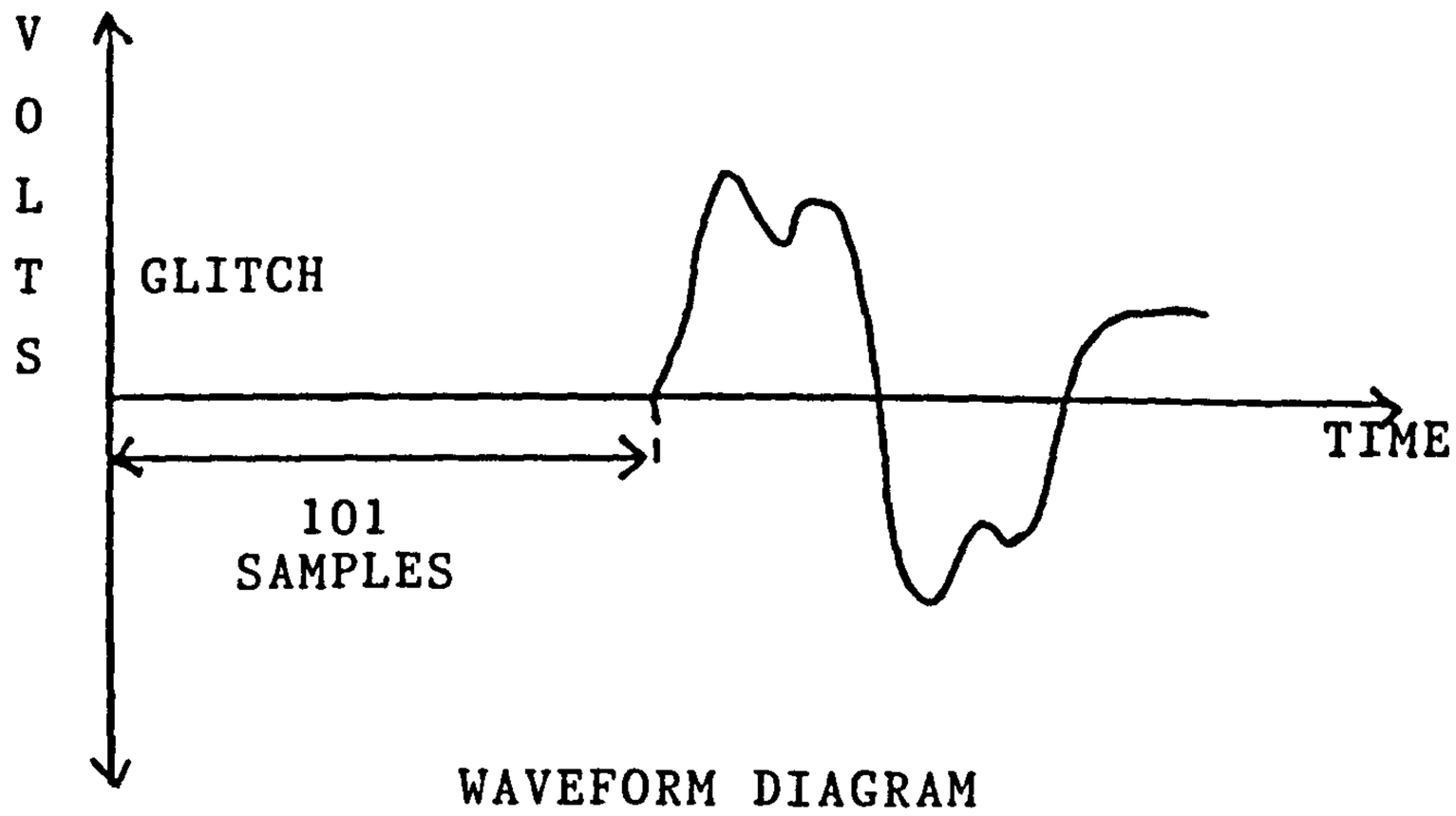

WAVEFORM DIAGRAM

FIG B12

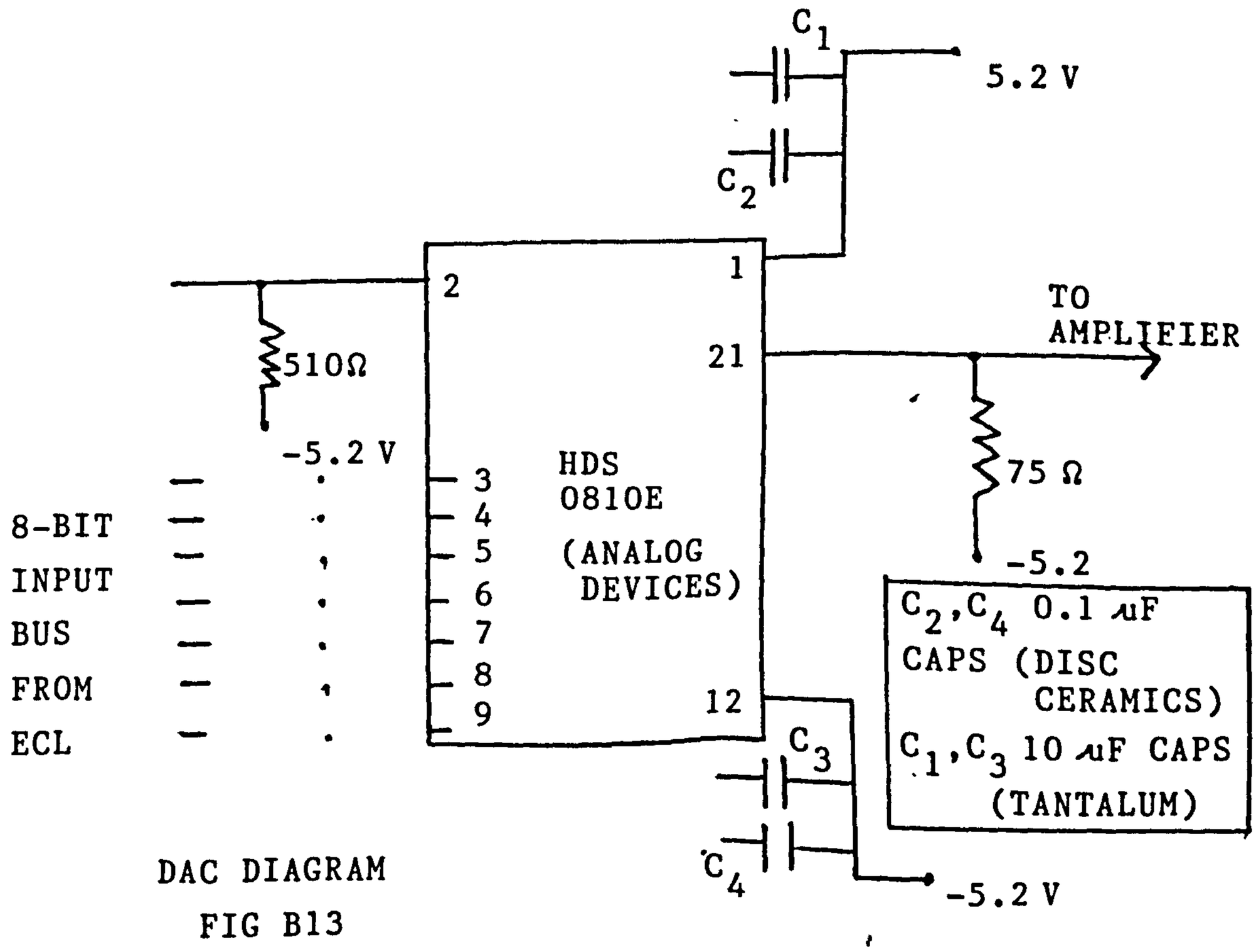

DAC DIAGRAM

FIG B13

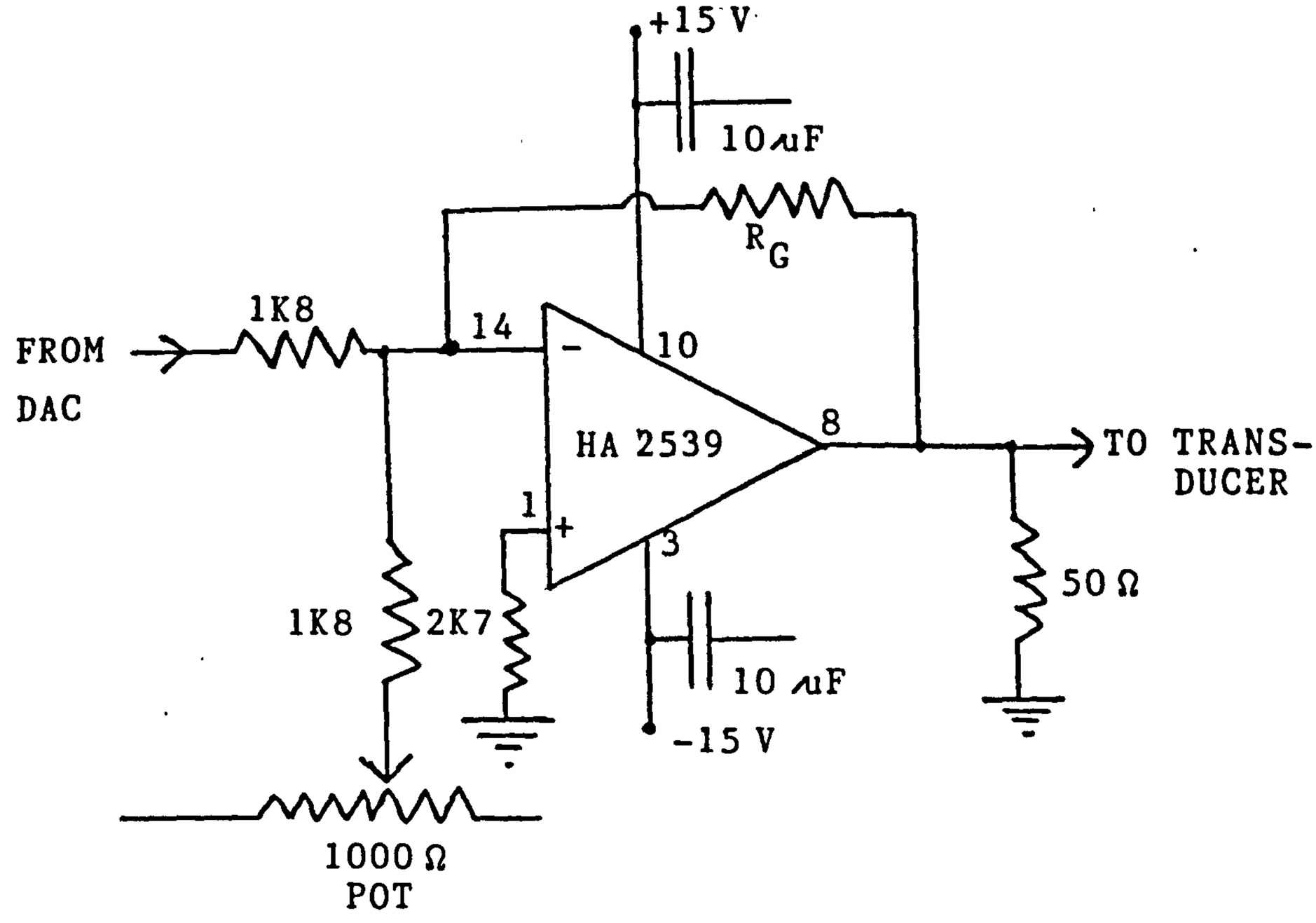

AMPLIFIER CIRCUIT

FIG B14

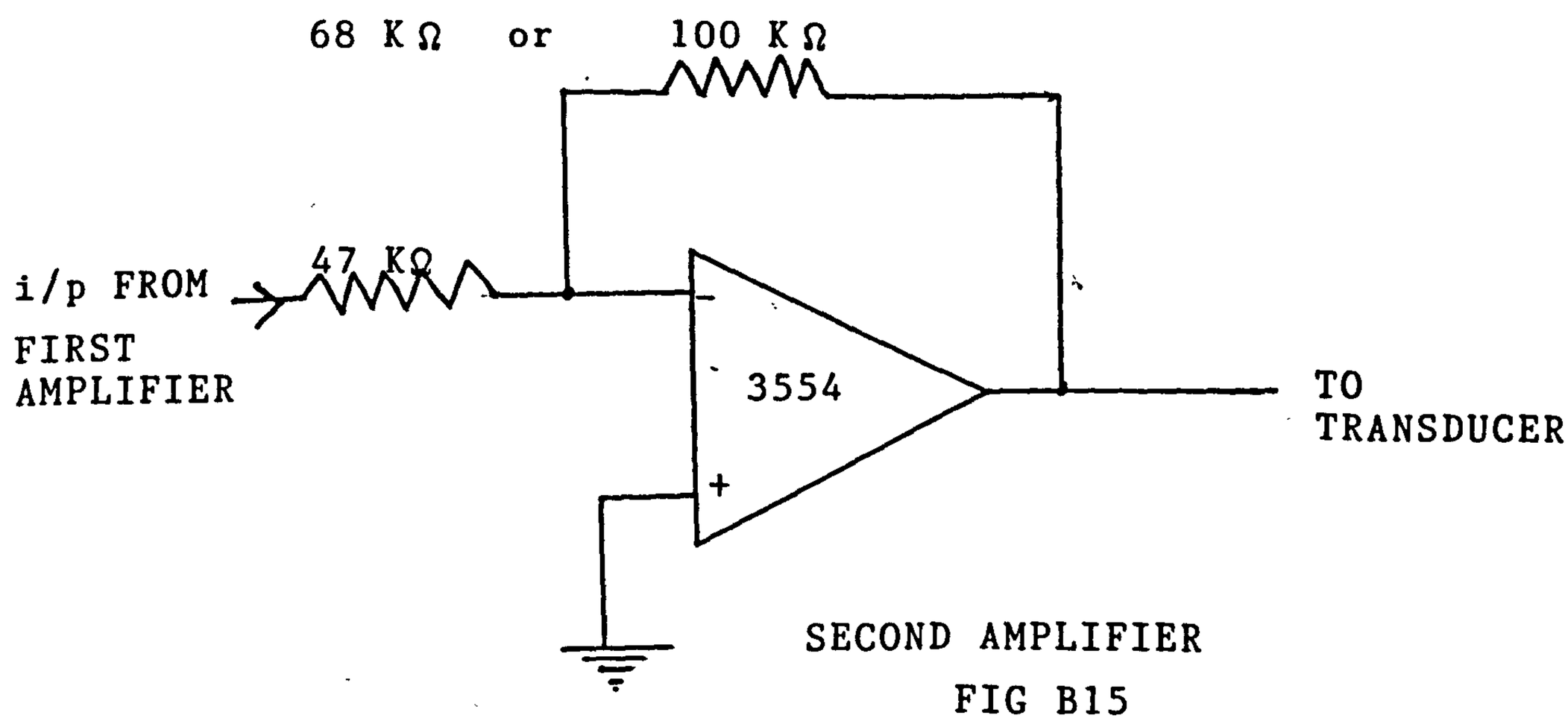

FIG B15

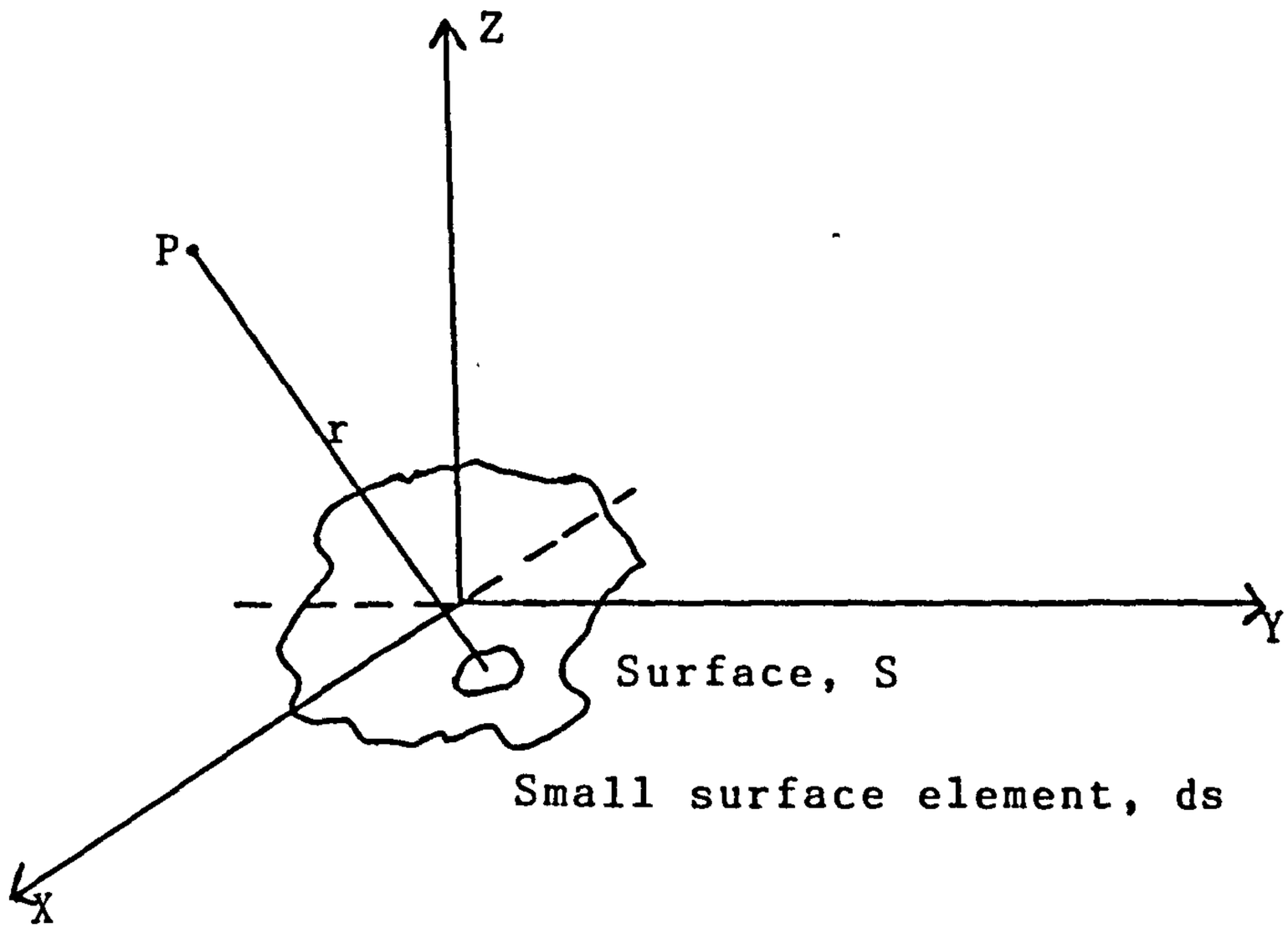
Z
P
r
Y
Surface, S
X
Small surface element, ds

FIG C1

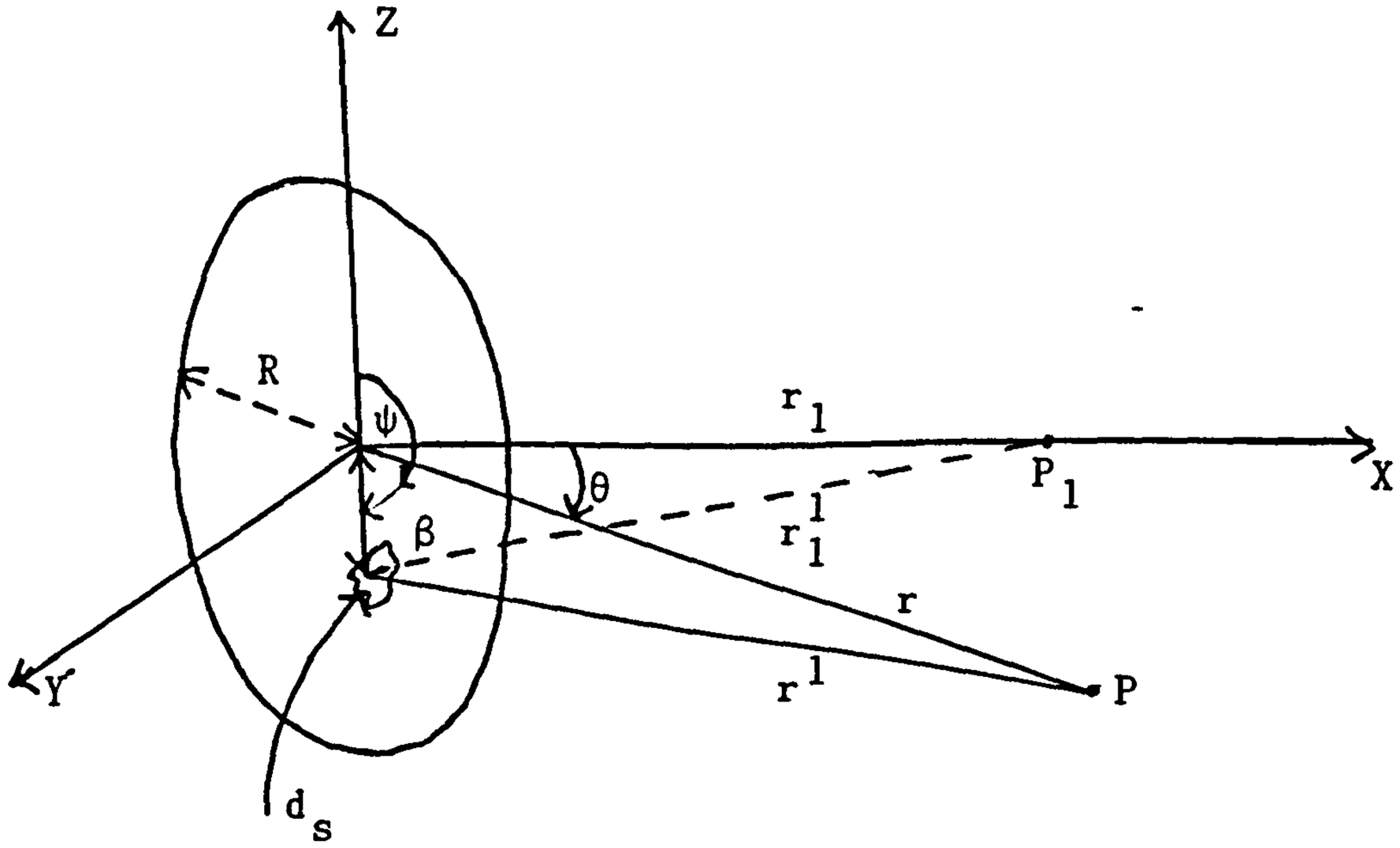
Z
R
ψ
r 1
P 1
X
θ
β
r 1
r
Y
r 1
P
d s

FIG C2

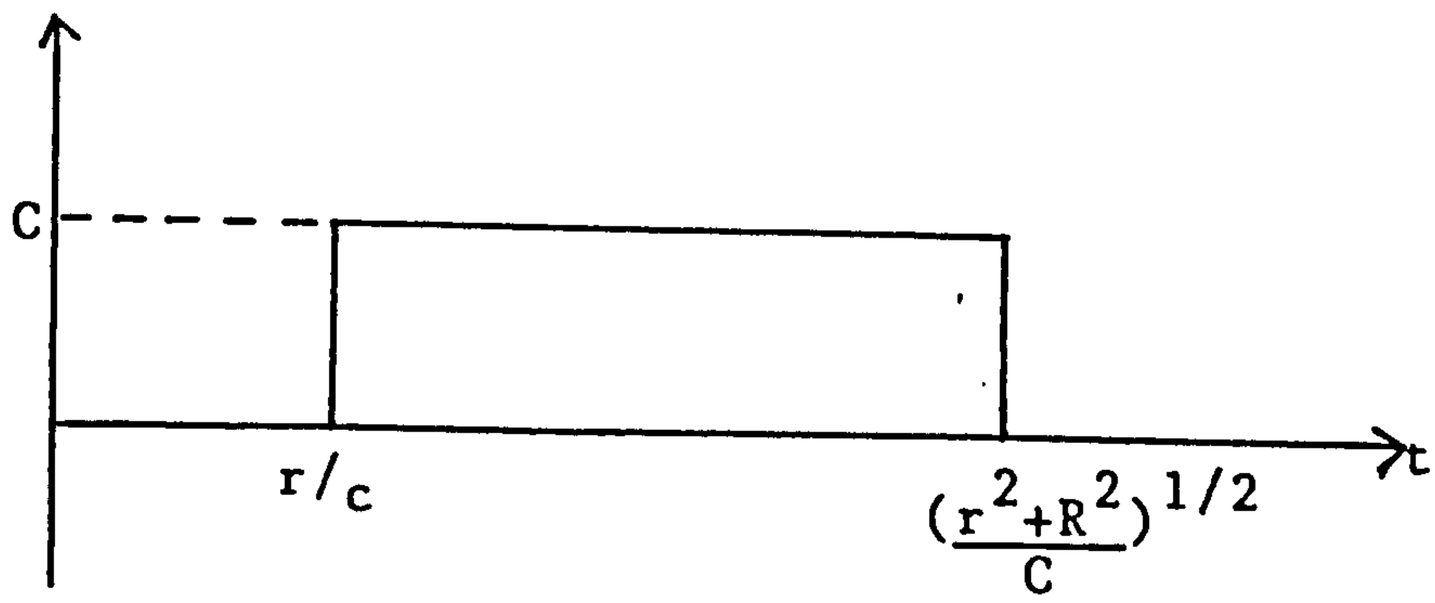

FIG C3

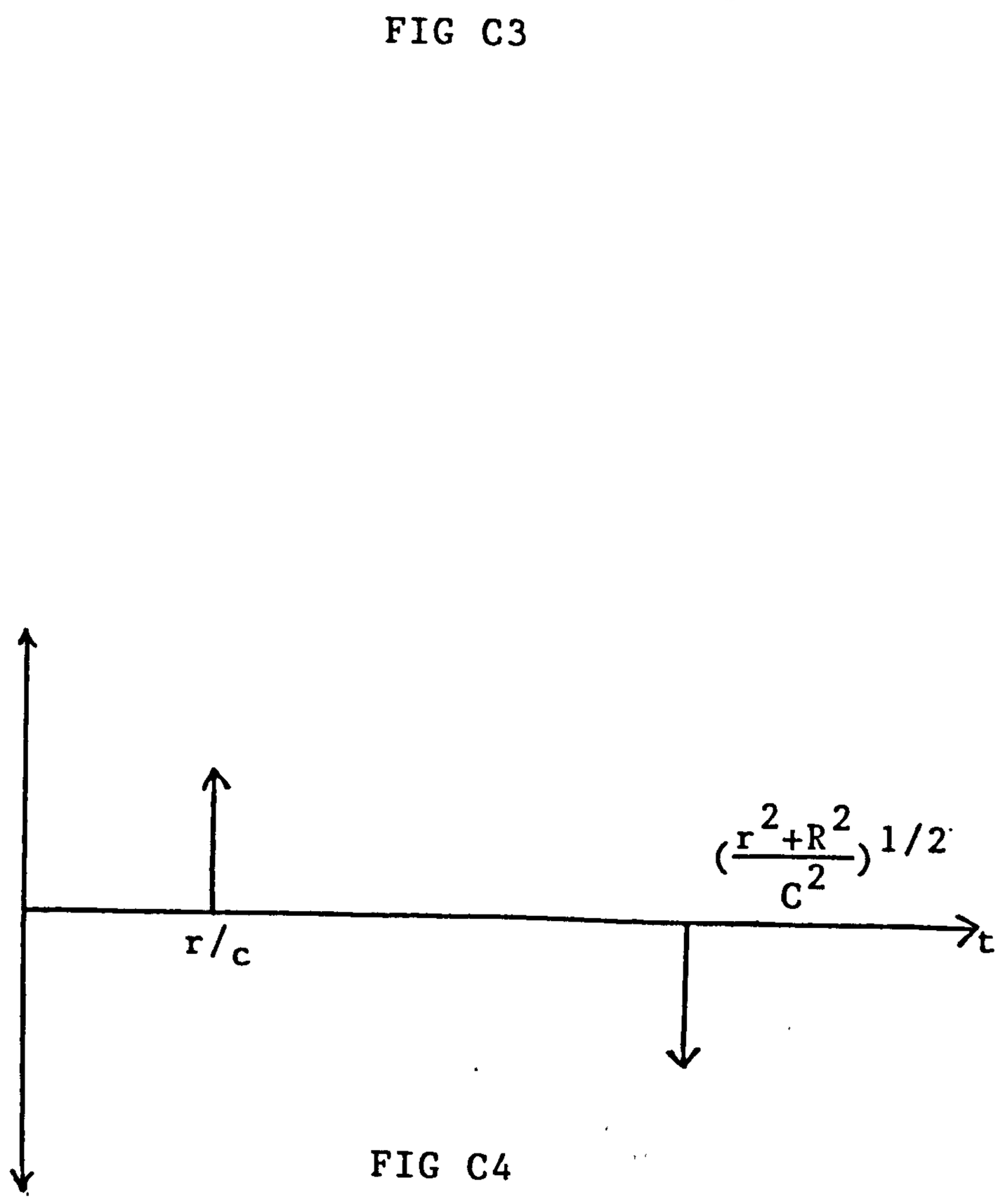

FIG C4